

Title	Spatial and temporal variation of ambient carbonaceous aerosol in Ireland and strategies for effective monitoring of source contributions
Authors	Heffernan, Eimear
Publication date	2022-04
Original Citation	Heffernan, E. 2022. Spatial and temporal variation of ambient carbonaceous aerosol in Ireland and strategies for effective monitoring of source contributions. PhD Thesis, University College Cork.
Type of publication	Doctoral thesis
Rights	© 2022, Eimear Heffernan. - <a href="https://creativecommons.org/licenses/by-nc-nd/4.0/">https://creativecommons.org/licenses/by-nc-nd/4.0/</a>
Download date	2025-07-17 05:08:18
Item downloaded from	<a href="https://hdl.handle.net/10468/13552">https://hdl.handle.net/10468/13552</a>

# **Spatial and Temporal Variation of Ambient Carbonaceous Aerosol in Ireland and Strategies for Effective Monitoring of Source Contributions**

A thesis submitted to

THE NATIONAL UNIVERSITY OF IRELAND, CORK



for the degree of

**DOCTOR OF PHILOSOPHY**

by

**Eimear Heffernan**

Based on research carried out at

School of Chemistry

&

Environmental Research Institute

Supervisor: *Dr Stig Hellebust*

Head of School: *Dr Humphrey Moynihan*

# CONTENTS

---

<b>Declaration</b> .....	<b>v</b>
<b>Dedication</b> .....	<b>vi</b>
<b>Acknowledgements</b> .....	<b>vii</b>
<b>Abstract</b> .....	<b>viii</b>
<b>List of Abbreviations and Acronyms</b> .....	<b>ix</b>
<b>1. Introduction</b> .....	<b>1</b>
<b>1.1 Atmospheric Aerosols</b> .....	<b>2</b>
1.1.1 Sources and Chemical Composition .....	2
1.1.2 Carbonaceous Aerosols .....	4
<b>1.2 Environmental and Health Impacts of Atmospheric Aerosols</b> .....	<b>6</b>
1.2.1 Climate Effects.....	6
1.2.2 Health Effects .....	8
1.2.3 Air Quality Legislation .....	11
<b>1.3 Historical Development of Research into Carbonaceous Aerosol</b> .....	<b>14</b>
<b>1.4 Studies of Carbonaceous Aerosol in Ireland</b> .....	<b>21</b>
<b>1.5 Overview</b> .....	<b>23</b>
1.5.1 Aims of Research .....	23
1.5.2 Overview of Thesis .....	23
<b>2. Instrumentation and Methodology</b> .....	<b>25</b>
<b>2.1 Sampling Sites</b> .....	<b>26</b>
2.1.1 Regional and Urban Background Sites .....	26

2.1.2	Urban Roadside in Dublin City.....	27
2.1.3	Small Town in Rural Ireland.....	27
<b>2.2</b>	<b><i>Field Instrumentation</i></b> .....	<b>32</b>
2.2.1	Ambient Air Sampling by Filter Collection.....	32
2.2.2	Characterisation by Optical Absorption.....	36
2.2.3	Total Carbon Content of Ambient Aerosol.....	47
<b>2.3</b>	<b><i>Off-line Analysis</i></b> .....	<b>52</b>
2.3.1	Determination of Elemental and Organic Carbon Content.....	52
2.3.2	Determination of Ambient Anhydrosugar Concentration.....	57
<b>2.4</b>	<b><i>Data Modelling</i></b> .....	<b>59</b>
2.4.1	Back Trajectory Analysis.....	59
2.4.2	Positive Matrix Factorization.....	59
2.4.3	Meteorological Normalisation .....	60
<b>3.</b>	<b>Carbonaceous Aerosol in Regional and Urban Background Environments in Ireland</b> .....	<b>62</b>
<b>3.1</b>	<b><i>Aims</i></b> .....	<b>63</b>
<b>3.2</b>	<b><i>Methodology</i></b> .....	<b>65</b>
3.2.1	Sampling Sites.....	65
3.2.2	Instrumentation and Analysis.....	73
<b>3.3</b>	<b><i>Results and Discussion</i></b> .....	<b>76</b>
3.3.1	Meteorological Data.....	76
3.3.2	Equivalent Black Carbon .....	81
3.3.3	Elemental Carbon (EC) and Organic Carbon (OC) .....	112
3.3.4	Calculation of Mass Absorption Cross Section .....	125
3.3.5	Levogluconan .....	134

3.3.6	Storm Emma: The Beast from the East.....	148
<b>3.4</b>	<b><i>Conclusions</i></b> .....	<b>160</b>
<b>4.</b>	<b>Carbonaceous Aerosol at an Urban Roadside in Dublin City .....</b>	<b>163</b>
<b>4.1</b>	<b><i>Aims</i></b> .....	<b>164</b>
<b>4.2</b>	<b><i>Methodology</i></b> .....	<b>165</b>
4.2.1	Sampling Site .....	165
4.2.2	Instrumentation and Analysis.....	167
<b>4.3</b>	<b><i>Results and Discussion</i></b> .....	<b>170</b>
4.3.1	Meteorological Data.....	170
4.3.2	Equivalent Black Carbon .....	174
4.3.3	Comparison of Aethalometer Data Measured at Urban Background and Roadside Locations.....	194
4.3.4	Elemental Carbon (EC) and Organic Carbon (OC) .....	207
4.3.5	Calculation of Mass Absorption Cross Section .....	212
4.3.6	Levoglucosan .....	218
4.3.7	On-line Measurement of Carbon Content .....	225
<b>4.4</b>	<b><i>Conclusions</i></b> .....	<b>229</b>
<b>5.</b>	<b>Carbonaceous Aerosol in a Small Town in Rural Ireland .....</b>	<b>231</b>
<b>5.1</b>	<b><i>Aims</i></b> .....	<b>232</b>
<b>5.2</b>	<b><i>Methodology</i></b> .....	<b>234</b>
5.2.1	Sampling Site .....	234
5.2.2	Instrumentation and Analysis.....	237
<b>5.3</b>	<b><i>Results and Discussion</i></b> .....	<b>239</b>
5.3.1	Meteorological Data.....	239
5.3.2	Particulate Matter .....	243

5.3.3	Equivalent Black Carbon .....	247
5.3.4	Elemental Carbon (EC) and Organic Carbon (OC) .....	263
5.3.5	On-line Measurement of Carbon Content .....	274
5.3.6	Comparison of Wintertime Air Quality in 2015, 2020 and 2021 .....	289
<b>5.4</b>	<b><i>Conclusions</i></b> .....	<b>300</b>
<b>6.</b>	<b>Effect of COVID-19 Restrictions on Ambient Air Quality .....</b>	<b>304</b>
<b>6.1</b>	<b><i>COVID-19 (SARS-CoV-2) Pandemic</i></b> .....	<b>305</b>
<b>6.2</b>	<b><i>Particulate Matter</i></b> .....	<b>309</b>
6.2.1	Equivalent Black Carbon .....	313
6.2.2	Carbonaceous Aerosol .....	318
<b>6.3</b>	<b><i>Conclusions</i></b> .....	<b>320</b>
<b>7.</b>	<b>Summary and Perspectives .....</b>	<b>321</b>
<b>7.1</b>	<b><i>Summary</i></b> .....	<b>322</b>
7.1.1	Spatial Variability .....	322
7.1.2	Temporal Variability .....	327
<b>7.2</b>	<b><i>Perspectives</i></b> .....	<b>331</b>
<b>8.</b>	<b>References</b> .....	<b>335</b>

## **DECLARATION**

---

This is to certify that the work I am submitting is my own and has not been submitted for another degree, either at University College Cork or elsewhere. All external references and sources are clearly acknowledged and identified within the contents. I have read and understood the regulations of University College Cork concerning plagiarism and intellectual property.

---

Eimear Heffernan

## DEDICATION

---

Do m'athair: Ní bheidh a leithéid arís ann.

## ACKNOWLEDGEMENTS

---

Funding for this PhD was mainly provided by the College of Science, Engineering and Food Science in University College Cork. Additional funding was provided by the Environmental Protection Agency through a small scale study and the EU COST Action Colossal (CA16109) for research visits to Leibniz Institute for Tropospheric Research (TROPOS) and the National Centre for Scientific Research (NCSR) “Demokritos”, Athens.

To everyone in the CRAC lab, it has been an absolute pleasure to work with you over the past few years. To Dr Stig Hellebust and Prof John Wenger, my sincere thanks. Without your knowledge, expertise, guidance and support, this work would not have been possible. To Paul, Meheal and Niall, you made life in the ERI so enjoyable, but more importantly, you taught me everything I know about soccer and The Simpsons!

To Mom, Dad, Conor and Cían, I couldn't have done this without you. Míle buíochas.

## ABSTRACT

---

The concentration, size and composition of atmospheric aerosols determines their impact on health and climate. These parameters are highly variable and inherently linked with source, seasonality and geographical location. In this study, a suite of instruments was deployed to quantitatively investigate the properties of ambient carbonaceous aerosol at six unique locations around Ireland. Source apportionment analysis was performed for the identification of dominant sources contributing to the ambient carbonaceous aerosol in each environment.

This work serves to highlight the spatial and temporal variability of ambient carbonaceous aerosol in Ireland. Aethalometer data exhibited significant spatial variability of black carbon (BC). The lowest concentrations were recorded at regional background sites, while the highest concentrations were recorded in populous, urban settings. The aethalometer source apportionment model was used to demonstrate spatial variability of contributions from dominant sources. The temporal variability of carbonaceous aerosol was explored through data collected during long-term monitoring campaigns in Dublin and Enniscorthy. Strong seasonal variation in equivalent black carbon (eBC) was evident, particularly in locations strongly influenced by solid fuel burning for residential heating. Furthermore, approximately 40% and 72% of total eBC measured during winter at University College Dublin and Enniscorthy, respectively, was attributed to solid fuel combustion. Strong diurnal trends were observed in each location, however the absolute concentration was seasonally dependent. A pronounced evening peak, attributed to solid fuel combustion emissions, was observed at the majority of sampling sites during the winter months. Urban areas also had a morning peak consistent with rush hour and was attributed to the influence of traffic-related emissions.

Novel data collected at several unique environments as part of three individual long-term monitoring campaigns, demonstrated the ubiquitous nature of carbonaceous aerosol, particularly BC, in Ireland and the associated impact on local air quality. Despite the negative implications on human health, air quality and climate, BC is not regulated or routinely monitored in Ireland. This research outlines the potential benefits of establishing an extensive, national BC monitoring network, including the collection of real-time data to inform vital air pollution mitigation policies.

## LIST OF ABBREVIATIONS AND ACRONYMS

---

AAE	Absorption Ångström Exponent
ACSM	Aerosol Chemical Speciation Monitor
ACTRIS	The Aerosols, Clouds and Trace Gases Research Infrastructure
AEROSOURCE	Source apportionment of airborne pollutants transported to and across Ireland using Aerosol Mass Spectrometry and Positive Matrix Factorisation Techniques
AGL	Above Ground Level
AMS	Aerosol Mass Spectrometer
ATN	Attenuation
ATOFMS	Aerosol Time-of-Flight Mass Spectrometer
AVEC	Attenuation Versus Evolved Carbon
BAM	Beta Attenuation Monitor
BB	Biomass Burning
BC	Black Carbon
BrC	Brown Carbon
BS	Black Smoke
CAFE	Clean Air for Europe
C-CAPS	Centre for Climate and Air Pollution Studies
CCN	Cloud Condensation Nuclei
CCP	Condensation Particle Counter
CEN	European Committee for Standardization
COLOSSAL	Chemical On-Line cOmpoSition and Source Apportionment of fine aerosoL
COST	European Cooperation in Science and Technology

COVID-19	Coronavirus Disease 2019
CP	Carnsore Point Sampling Site
CSO	Central Statistics Office
DART	Dublin Area Rapid Transit
eBC	Equivalent Black Carbon
EC	Elemental Carbon
eEC	Equivalent Elemental Carbon
EMEP	European Monitoring and Evaluation Programme
ENTY	Enniscorthy Sampling Site
eOC	Equivalent Organic Carbon
EPA	Environmental Protection Agency
ESB	Electricity Supply Board
EU	European Union
EUSAAR	European Supersites for Atmospheric Aerosol Research
FF	Fossil Fuel
FID	Flame Ionisation Detector
GC	Gas Chromatography
GDAS	Global Data Assimilation System
HPAEC-PAD	High-Performance Anion-Exchange Chromatography – Pulsed Amperometric Detection
HPLC	High Performance Liquid Chromatography
HPSC	Health Protection Surveillance Centre
HYSPLIT	HYbrid Single-Particle Lagrangian Integrated Trajectory
IC	Ion Chromatography
ICP-MS	Inductively Coupled Plasma – Mass Spectrometry

IMPROVE	Interagency Monitoring of PROtected Visual Environments
IN	Ice Nuclei
IPCC	Intergovernmental Panel on Climate Change
IR	Infrared
LOD	Limit Of Detection
MAAP	Multi Angle Absorption Photometer
MAC	Mass Absorption Cross Section
MDL	Method Detection Limit
MHD	Mace Head Sampling Site
MLN	Malin Head Sampling Site
MS	Mass Spectrometry
NCSR	National Centre for Scientific Research “Demokritos”
ND	No data
NDIR	Non-Dispersive Infrared
NIOSH	National Institute for Occupational Safety and Health
NUIG	National University of Ireland, Galway
OA	Organic Aerosol
OC	Organic Carbon
OECD	Organisation for Economic Co-operation and Development
OPC	Optical Particle Counter
PC	Pyrolysed Carbon
PIXE	Proton Induced X-Ray Emission
POA	Primary Organic Aerosol
PM	Particulate Matter

PMF	Positive Matrix Factorisation
PRS	Pearse Street Sampling Site
PSAP	Particle Soot Absorption Photometer
PTFE	Polytetrafluoroethylene
SAPPHIRE	Source Apportionment of Particulate Matter in Urban and Rural Areas of Ireland
SARS-CoV-2	Severe Acute Respiratory Syndrome Coronavirus-2
SD	Standard Deviation
SF	Solid Fuel
SOA	Secondary Organic Aerosol
SSW	Sudden Stratospheric Warming
STSM	Short Term Scientific Mission
TC	Total Carbon
TCA	Total Carbon Analyzer
TEOM	Tapered Element Oscillating Microbalance
TII	Transport Infrastructure Ireland
Tr	Traffic
TROPOS	Leibniz Institute for Tropospheric Research
UCD	University College Dublin Sampling Site
UNECE	United Nations Economic Commission for Europe
UK	United Kingdom
UP	Ultra-Pure
USA	United States of America
UV	Ultraviolet
VAT	Value Added Tax

VOC	Volatile Organic Compound
WB	Wood Burning
WHO	World Health Organization
XRF	X-Ray Fluorescence

# 1. INTRODUCTION

---

<b>1.1</b>	<b><i>Atmospheric Aerosols</i></b> .....	<b>2</b>
1.1.1	Sources and Chemical Composition .....	2
1.1.2	Carbonaceous Aerosols .....	4
<b>1.2</b>	<b><i>Environmental and Health Impacts of Atmospheric Aerosols</i></b> .....	<b>6</b>
1.2.1	Climate Effects.....	6
1.2.1.1	Direct Effects .....	6
1.2.1.2	Indirect Effects.....	8
1.2.2	Health Effects.....	8
1.2.3	Air Quality Legislation .....	11
<b>1.3</b>	<b><i>Historical Development of Research into Carbonaceous Aerosol</i></b> .....	<b>14</b>
<b>1.4</b>	<b><i>Studies of Carbonaceous Aerosol in Ireland</i></b> .....	<b>21</b>
<b>1.5</b>	<b><i>Overview</i></b> .....	<b>23</b>
1.5.1	Aims of Research .....	23
1.5.2	Overview of Thesis .....	23

## 1.1 ATMOSPHERIC AEROSOLS

---

The suspension of a solid or liquid particle in a gas can be defined as an aerosol (Finlayson-Pitts & Pitts, 2000). The suspension of such particles in the atmosphere are, therefore, referred to as atmospheric aerosols. Particle diameters generally range between  $\sim 0.002 \mu\text{m}$  and  $100 \mu\text{m}$ , however particles in the  $0.002 \mu\text{m}$  to  $10 \mu\text{m}$  size range are most important with regard to atmospheric chemistry and physics (Finlayson-Pitts & Pitts, 2000). Larger particles, comparable in size to fine drizzle or sand, do not remain suspended over lengthy time periods.

Aerosols play an important role in the energy balance of the Earth, the hydrological cycle, atmospheric circulation and the abundance of greenhouse and trace gases (Pöschl, 2005). They also have a strong influence on the health of the human population, causing or exacerbating noncommunicable diseases. Particle concentration, size and chemical composition determine the degree of impact on health and climate. Such parameters are highly variable and are inherently linked with seasonality and geographical location.

### 1.1.1 Sources and Chemical Composition

---

Aerosols have both natural and anthropogenic origins. They can be released directly into the atmosphere, as primary emissions, or formed in the atmosphere as secondary aerosols by chemical or physical processes (Prather et al., 2008; Pöschl, 2005; Tomasi et al., 2017). Sources of natural emissions include sea spray, volcanic eruptions, biological materials, wildfires and wind-driven suspension of soil and mineral dust (Pöschl, 2005). Natural emissions account for  $\sim 98\%$  of particle emissions on a global scale. In terms of total mass, sea spray and mineral dust contribute 84% and 13%, respectively (Viana et al., 2014). Anthropogenic aerosols are composed of numerous organic and inorganic species and usually fall into the sub-micrometre to micrometre size range (Ramanathan et al., 2001). Aerosols derived from anthropogenic activity are usually concentrated in urban environments. Sources include traffic (exhaust emissions, road surface abrasion, brake and tyre wear, particle resuspension from paved roads), industrial activities (power plants, construction) and emissions associated with housing (cooking, domestic heating). Sources of anthropogenic

emissions in rural areas are typically associated with domestic heating (solid fuel combustion) and agricultural activities (Calvo et al., 2013).

Once in the atmosphere, aerosols are subject to physical (e.g., nucleation, condensation) and chemical (e.g., oxidation) transformation and transportation (Figure 1.1). Efficient removal processes, including sedimentation and precipitation, are responsible for residence times of days to weeks, which are much shorter than lifetimes of the main greenhouse gases (Bellouin et al., 2020). The oxidation of primary emitted volatile organic compounds (VOCs) by hydroxyl radicals, nitrate radicals and ozone results in the formation of secondary organic aerosols (SOA). Biogenic VOCs, such as isoprene, terpenes and sesquiterpenes, are well known natural SOA precursors. Anthropogenic precursors include aromatic compounds emitted by fuel combustion, which leads to significant SOA formation in urban areas (Baltensperger et al., 2005; Moise et al., 2015). Given that precursors can undergo numerous degradation processes, the range of possible oxidised products, which may or may not further influence SOA formation, is vast (Hallquist et al., 2009). There is significant uncertainty associated with SOA formation, and thus, its effects on climate and total radiative forcing.

It is widely accepted that both natural and anthropogenic atmospheric aerosols have a strong impact on climate and human health (Pöschl, 2005). Evaluation of chemical composition reveals information about dominant sources, which is of great importance for the development of efficient strategies to counteract adverse effects of atmospheric aerosols.

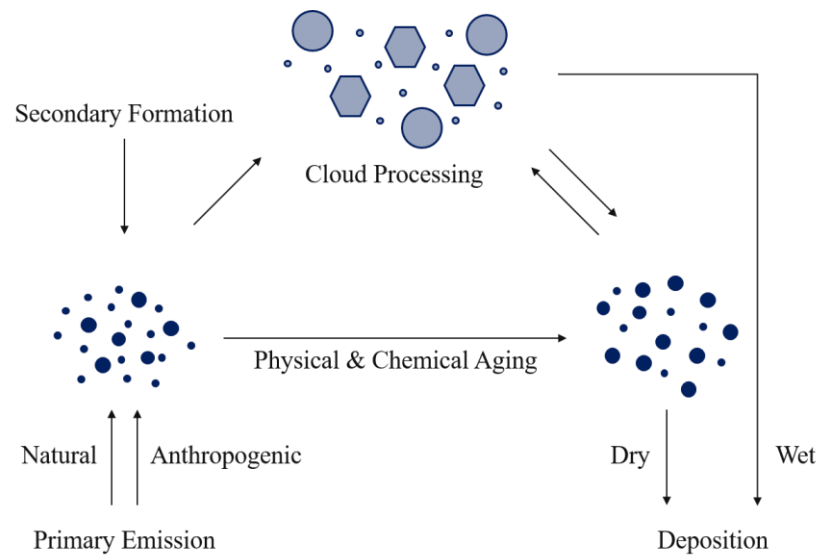


**Figure 1.1** Schematic of the atmospheric cycling of aerosols. Adapted from Pöschl (2005).

### 1.1.2 Carbonaceous Aerosols

Carbonaceous aerosol refers to the fraction of total aerosol containing carbon, consisting predominantly of organic carbon; in which the carbon is bonded to other elements, and black carbon; a light absorbing species produced by the incomplete combustion of biomass and fossil fuels. Black carbon (BC) is similar, but not identical, to elemental carbon (IPCC, 2013; Streets et al., 2004).

There is significant ambiguity in the definition of black carbon. An authoritative review of the topic cites a lack of agreement on terminology that accounts for each of the specific properties, definitions, measurement methods and related uncertainties associated with the species, and therefore, recommends that discrimination be based on method of measurement (Petzold et al., 2013). BC plays an important role in the Earth's climate system by absorbing solar radiation, influencing cloud processes and accelerating the melting of snow and ice. The open burning of forests and savannahs are a major global source of atmospheric BC. Anthropogenic sources (diesel engines, industry, residential heating) contribute a significant additional portion (Bond et al., 2013; Briggs & Long, 2016). The dominant sources of BC and the associated emissions are subject to considerable temporal and regional variability. For example, it is estimated that 60-80% of the BC emissions in Asia and Africa can be attributed to solid fuel combustion in residential settings, while in contrast, 70% of the observed

BC in Europe, North America and Latin America is attributed to emissions from diesel engines (Bond et al., 2013).

Brown carbon (BrC) refers to the fraction of organic aerosol with significant light-absorbing properties. The BrC absorption spectrum demonstrates strong wavelength dependence, with increasingly efficient absorption at lower wavelengths, tending towards the ultraviolet region. The absorption efficiency and spectral dependence of BrC varies with origin (Andreae & Gelencsér, 2006; Feng et al., 2013). Forest fires, biomass burning, domestic solid fuel combustion and biogenic emissions (fungi, plant debris, humic matter) contribute a significant portion of primary BrC. Secondary BrC is attributed to the formation of high molecular weight light-absorbing compounds in atmospheric multi-phase reactions, involving gas-phase, particulate and cloud droplet components (Laskin et al., 2015). Knowledge of the mechanisms and atmospheric transformations associated with BrC is limited, thus increasing the uncertainty in quantifying the effect of BrC.

Organic carbon (OC) contributes significantly to ambient particulate matter concentrations. It is derived from a variety of natural (sea-spray, biogenic emissions) and anthropogenic sources (combustion processes, resuspension of abrasion products, refineries, paints) (Contini et al., 2018; Kuhlbusch et al., 2009; Stockwell et al., 2021). OC can originate from primary sources, through combustion processes or biogenic emissions, or secondary sources, following atmospheric processes, such as the oxidation of biogenic or volatile organic compounds (VOC), which lead to the formation of secondary organic aerosols (SOA). Such processes result in changes to the composition and properties of the organic fraction. Elemental carbon, on the other hand, usually originates exclusively from the incomplete combustion of carbon-containing fuels (Liu et al., 2018). This includes biomass-burning, industrial processes and emissions from diesel engines.

In recent years there has been increased scientific interest in the sources, composition, properties, atmospheric processes and transformations associated with carbonaceous aerosols. Improved knowledge in this area is needed to assess, and ultimately reduce the potential negative impact on climate and human health.

## 1.2 ENVIRONMENTAL AND HEALTH IMPACTS OF ATMOSPHERIC AEROSOLS

---

### 1.2.1 Climate Effects

---

Radiative forcing, as defined by the Intergovernmental Panel on Climate Change (IPCC), is “a measure of the influence a factor has in altering the balance of incoming and outgoing energy in the Earth-atmosphere system and is an index of the importance of the factor as a potential climate change mechanism” (IPCC, 2007a). Positive radiative forcing (i.e. a value larger than zero) has a near-surface warming effect, while negative forcing has a cooling effect (IPCC, 2014). Atmospheric aerosols contribute to both positive and negative radiative forcing, depending on type. A significant fraction of the atmospheric aerosol exerts a dominant cooling effect due to cloud adjustments. This is offset by the warming contribution due to absorption of solar radiation by species such as black carbon (IPCC, 2014). The overall aerosol radiative forcing between 1750 (pre-industrial era) and 2011 is estimated as  $-0.9 \text{ W m}^{-2}$  (range:  $-1.9$  to  $-0.1 \text{ W m}^{-2}$ ) (IPCC, 2014). Thus, a considerable portion of the positive radiative forcing of well-mixed greenhouse gases has been counteracted by the negative radiative forcing of the global mean total aerosol. There are, however, large uncertainties associated with aerosol-driven climate change (Haerter et al., 2009; Lohmann et al., 2010; Stevens, 2015), owing to variability in chemical composition and the diverse temporal and spatial distribution in comparison to greenhouse gases (Bellouin et al., 2020).

The climate effects of atmospheric aerosols can be categorised as direct and indirect effects. The direct effect is associated with the absorption or scattering of solar radiation, in addition to radiation emitted from, or reflected by, the Earth’s surface. Indirect effects are related to the modification of cloud properties (Haywood & Boucher, 2000). Both are influenced by the chemical and physical properties of the aerosol particles (Baltensperger & Prévôt, 2008). Aerosols contribute the largest uncertainty to the total radiative forcing estimate (IPCC, 2013).

#### 1.2.1.1 Direct Effects

---

The direct radiative effect refers to the ability of aerosols to scatter and absorb solar radiation, in addition to radiation emitted from, or reflected by, the Earth’s surface.

The efficiency at which this occurs is dependent on the wavelength of radiation, the distribution of aerosol particle size, shape and refractive index, each of which is determined by chemical composition and mixing state (Bellouin et al., 2020). Dust, nitrate, sulfate, and primary and secondary organic aerosols are estimated to contribute to negative radiative forcing by scattering solar radiation, leading to a net cooling effect on the atmosphere (IPCC, 2013, 2021). Conversely, absorption of radiation by black carbon causes positive radiative forcing of  $+0.11$   $[-0.20$  to  $+0.42]$   $\text{W m}^{-2}$  giving rise to a warming effect (IPCC, 2021). A decrease in solar radiation reaching the ground influences the surface air temperature and the planetary boundary layer height (Jung et al., 2019).

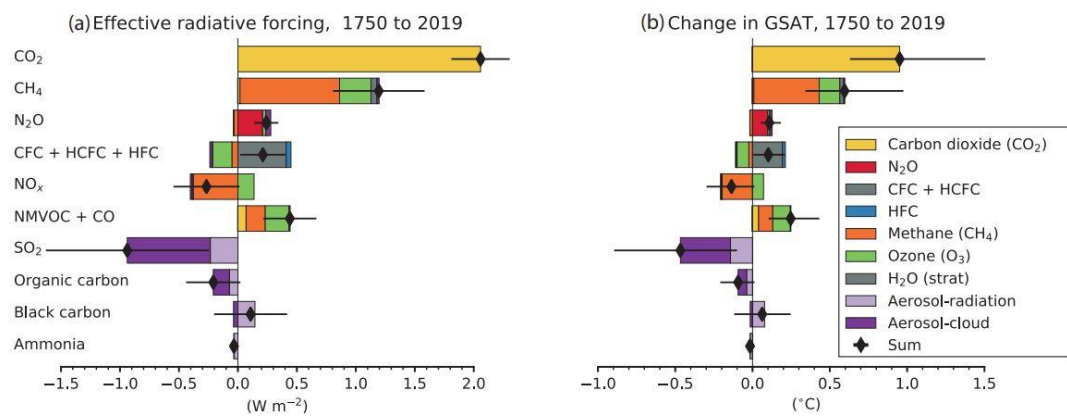


**Figure 1.2** Contribution to effective radiative forcing (a) and global mean surface air temperature (GSAT) change (b) from component emissions between 1750 and 2019 (IPCC, 2021).

### 1.2.1.2 Indirect Effects

The indirect effect refers to the influence of aerosols on cloud microphysics; changing the radiative properties, frequency and lifetimes of clouds. Specifically, the ability of aerosols to act as cloud condensation nuclei (CCN) or ice nuclei (IN). The net positive or negative radiative forcing of a cloud is determined by its physical properties and the CCN population (IPCC, 2013).

The ability of atmospheric particles to act as CCN is dependent on the hydrophilicity of the particle. Increased aerosol concentration forms clouds containing smaller, more numerous water droplets. This induces negative radiative forcing due to increased cloud albedo (Goosse et al. 2008-2010; Levy et al., 2013). Variation in particle type and distribution influences precipitation efficiency. Smaller cloud particles reduce precipitation efficiency, thus prolonging cloud lifetime. Solar absorption by particles containing black carbon, may cause evaporation of cloud droplets by increasing the surrounding air temperature. This is known as a semi-direct effect (Rao & Dey, 2020).

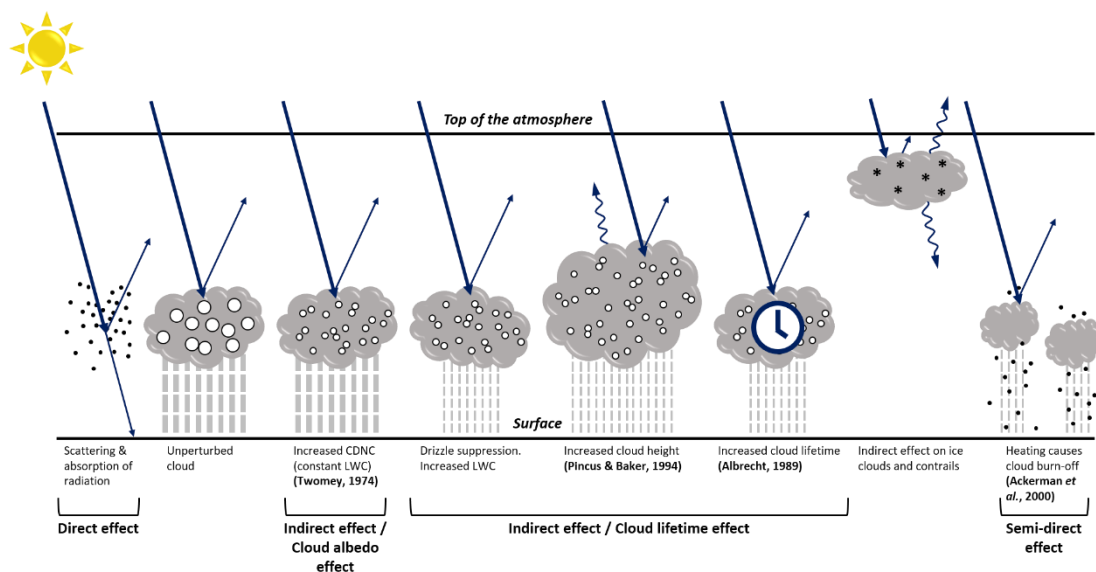
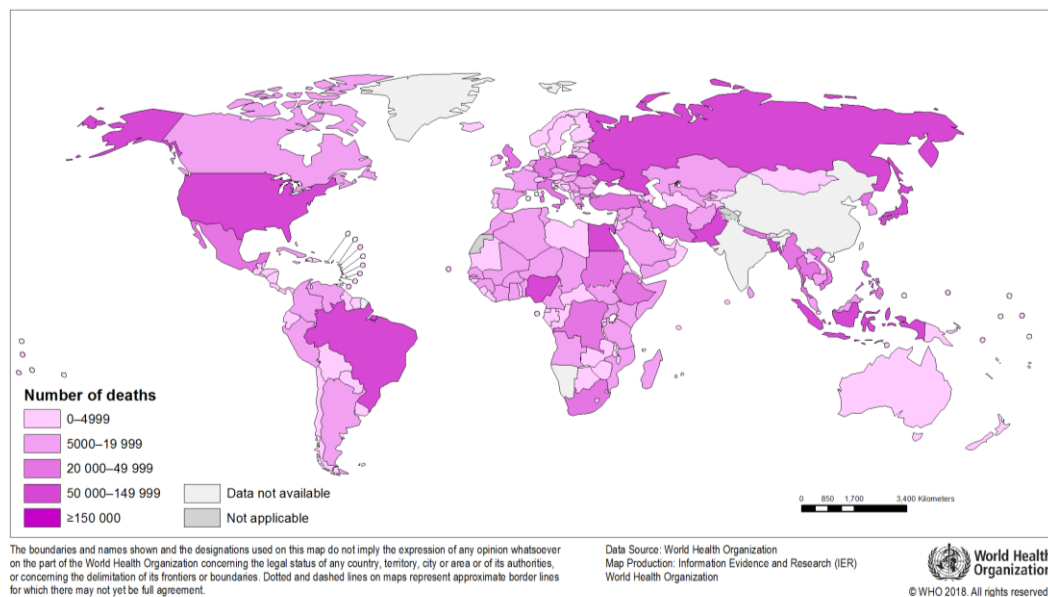


Figure 1.3 Radiative mechanisms. Adapted from IPCC (2007b).

### 1.2.2 Health Effects

According to the World Health Organization (WHO), ambient air pollution is one of the greatest environmental risks to health (World Health Organization, 2019). A report published by the WHO in 2019 stated that 90% of the world's population inhabit areas

where the air is deemed unhealthy to breathe. The report attributes 4.2 million deaths to poor ambient air quality annually (World Health Organization, 2019). Numerous studies have been conducted to demonstrate the positive association between both short- and long-term exposure to particulate matter and increased morbidity and mortality due to respiratory and cardiovascular diseases (Dockery et al., 1993; Fajersztajn et al., 2017; Jakubiak-Lasocka et al., 2014; Lelieveld et al., 2015; Orellano et al., 2020; Pope & Dockery, 2006; Pope III et al., 2002; Sanyal et al., 2018). In 2016, heart disease, stroke and respiratory-related illnesses accounted for 38%, 20% and 43% of the 4.2 million deaths attributed to air pollution, respectively (World Health Organization, 2019). According to the World Cancer Report (2020), air pollution is one of the most important contributors to environmental cancer burden in human populations, causing an estimated 350,167 deaths from lung cancer in 2017 (Wild et al., 2020).



**Figure 1.4** Number of deaths attributed to ambient air pollution in 2016 (World Health Organization, 2021b).

Particulate matter (PM) can enter the human respiratory system via inhalation. The extent to which the particles can penetrate the human respiratory tract is dependent on particle size. Larger particles (5 – 30  $\mu\text{m}$ ) are generally removed in the upper respiratory tract via deposition in the nasopharyngeal region. Smaller particles (1 – 5

$\mu\text{m}$ ) are often deposited in the tracheobronchial region. However, sub-micron ( $< 1 \mu\text{m}$ ) and ultrafine particles ( $< 100 \text{ nm}$ ) can penetrate further into the respiratory system potentially as far as the gas-exchange alveolar region (Bakand et al., 2012; Finlayson-Pitts & Pitts, 2000; Praphawatvet et al., 2020). By crossing the air-blood tissue barrier, these particles can enter the blood and lymphatic circulatory system and reach any organ in the body (Kreyling et al., 2006; Oberdörster et al., 2005). This includes the potential to reach organs such as the brain. A number of studies have previously documented the adverse impact exposure to ambient particulate matter has on cognitive function (Ailshire & Crimmins, 2014; Crinnion, 2017; Shehab & Pope, 2019). In recent years, there is strong evidence for increased risk of Alzheimer's disease, in addition to other forms of dementia, as a result of exposure to air pollution (Kilian & Kitazawa, 2018; Moulton & Yang, 2012; Oudin, 2020).

Although conclusive evidence is limited, exposure to particulate matter and other pollutants during pregnancy, has been associated with pre-term births and low birth weights (Apte et al., 2018; Brauer et al., 2008; Liu et al., 2019; Pedersen et al., 2013). One study showed that a  $5 \mu\text{g m}^{-3}$  increase in  $\text{PM}_{2.5}$  exposure during pregnancy was associated with increased risk of low birth weight at term (Apte et al., 2018), while another observed ambient black carbon particles derived from combustion processes on the foetal side of the placenta (Bové et al., 2019). It is hypothesised that the particles are able to translocate from the mothers lungs to the placenta. A report published by the WHO documented the health implications for children exposed to ambient air pollution, included low birth weight, reduced lung function, impaired mental and motor development, childhood cancers and an increased risk of heart disease, diabetes and stroke in later life (WHO Regional Office for Europe, 2019).

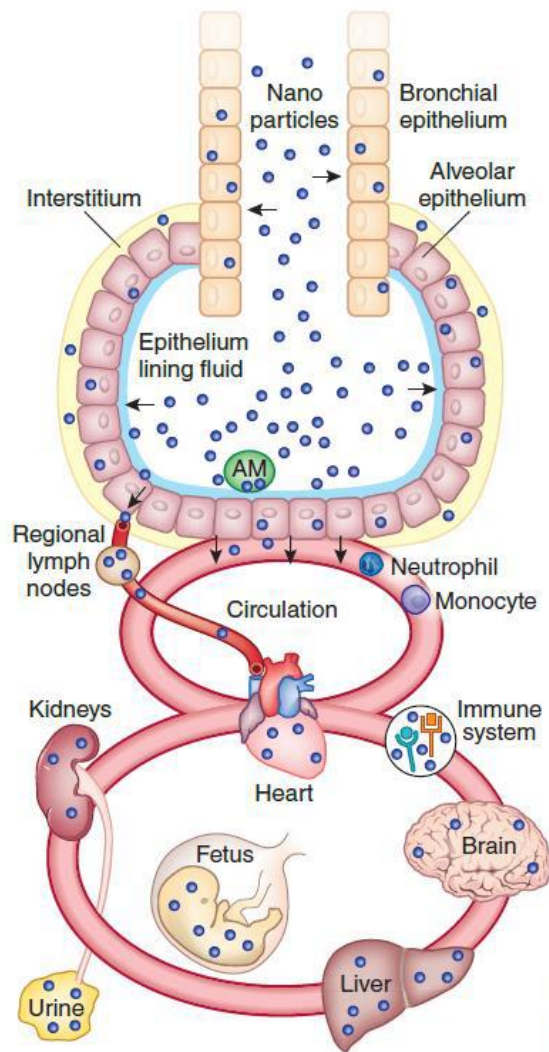


**Figure 1.5** Schematic of the potential deposition sites for particles of diameter less than 100 nm which can enter the bloodstream and be transported throughout the human body, accumulating in various organs (Kreyling et al., 2010).

### 1.2.3 Air Quality Legislation

Regulation and legislation with regard to air pollution effectively limits the climate and human health effects. Health based legislation for particulate matter is based on particle size; PM<sub>10</sub> (PM with a diameter of 10 µm or less) and PM<sub>2.5</sub> (PM with a diameter of 2.5 µm or less). The European Union sets limits for particulate matter pollution for member states in the Clean Air for Europe directive (CAFE – Directive 2008/50/EC). The directive limits PM<sub>10</sub> mass to annual and 24-hour mean values of 40 µg m<sup>-3</sup> and 50 µg m<sup>-3</sup>, and an annual mean concentration of 20 µg m<sup>-3</sup> for PM<sub>2.5</sub>, as of January 2020.

Maintaining currency with new evidence in terms of the negative health implications associated with ambient air quality is crucial to policy makers. As new evidence emerges, air quality guidelines require updating. In 2016, a comprehensive, systematic review of globally conducted studies was undertaken by the WHO in order to update the air quality guidelines originally published in 2005. The aim of the review was to provide evidence, particularly quantitative data, describing the relationship between long-term exposure to PM and mortality (Chen & Hoek, 2020). PICO is a common question frame employed in health sciences research, composed of four elements; population/patient/problem, intervention, comparison and outcome. An adapted version of this conventional question frame was used for the study; PECOS. The intervention (I) component was replaced with exposure (E) corresponding to the concentration of the pollutant of interest, and S was introduced to define the study design of included evidence. The question aimed to estimate the increase in risk of health outcome (O) to any population (P) per unit increase (C) of exposure to ambient concentration of a given air pollutant (E), observed in relevant studies. In brief, ‘what is the lowest concentration that produces a measurable increase in risk?’ (World Health Organization, 2021d). As a result of this study, the WHO updated the recommended guideline limits for both PM<sub>10</sub> and PM<sub>2.5</sub> mass, in addition to ozone (O<sub>3</sub>), nitrogen dioxide (NO<sub>2</sub>) and sulfur dioxide (SO<sub>2</sub>), in September 2021. In order to account for both short-term and long-term exposure to particulate pollution, 24-hour and annual mean guideline limits have been recommended. For PM<sub>10</sub>, the WHO recommends concentration limits of 15 µg m<sup>-3</sup> and 45 µg m<sup>-3</sup> for annual and 24-hour means, respectively. Stringent limits of 5 µg m<sup>-3</sup> and 15 µg m<sup>-3</sup> have been recommended for annual and 24-hour mean values for more damaging PM<sub>2.5</sub> particles (World Health Organization, 2021c). Recommended levels of certain components of PM, including BC and ultrafine particles, could not be presented due to the lack of ‘clear quantitative evidence on independent health effects’, but were, instead, included by means of statement of good practice (World Health Organization, 2021d).

In Ireland, the Air Pollution Act 1987 directs local authorities to implement measures considered necessary to limit or prevent air pollution in their relevant zones. The *Marketing, Sale and Distribution of Fuels Regulations* (1990) prohibited the sale and distribution of bituminous coal in Dublin, initially. It resulted in a significant reduction in black smoke concentration and is associated with improvements in the health of the

population and decrease in premature deaths caused by air pollution (Clancy et al., 2002; Goodman et al., 2009). This regulation has since been extended to cities and towns with populations greater than 10,000. In September 2021, the government announced strict standards for domestic solid fuel to be enforced nationwide by the 2022 heating season. This will include a nationwide ban on burning bituminous coals, limits for the smoke emission rate by manufactured solid fuels and peat briquettes, as well as upper limits for the moisture content of wood (Department of the Environment, Climate and Communications, 2021).

### 1.3 HISTORICAL DEVELOPMENT OF RESEARCH INTO CARBONACEOUS AEROSOL

---

High variability of chemical composition, size, morphology and phase contribute to the large uncertainty associated with measurement and analysis of atmospheric aerosols. A greater understanding of such parameters, in addition to related effects on climate and human health, is vital for the development of effective, and efficient, mitigation strategies. A combined approach is required in order to accurately evaluate the effects that aerosols have on the atmospheric system. This includes (i) field measurements of ambient aerosol; (ii) laboratory studies of the chemical and physical properties of aerosols and their atmospheric processes, and (iii) model analysis that accounts for gas-phase and heterogeneous chemistry, optical properties and photochemical processes (Prather et al., 2008).

There are a number of challenges associated with off-line characterisation and measurement techniques; namely low time resolution, limited capture of real-time changes to ambient conditions and sampling artefacts, both positive and negative. Evaporation of semi-volatile species, reactions between collected particles and gases, and adsorption of gases on filters and/or previously collected particles can occur (Finlayson-Pitts & Pitts, 2000; Lee et al., 2005; Prather et al., 2008; Wilson et al., 2002). This can lead to distorted results, which are not representative of the actual aerosol. These limitations have incentivised the development of reliable and robust on-line techniques for the real-time measurement of atmospheric aerosol.

Smoke and haze associated with anthropogenic activity was exacerbated by the industrial revolution and intensified significantly in the increasingly populous urban centres. In the nineteenth century, characterisation of atmospheric particles began with studies of optical effects of suspended particles and experiments on colour from particle scattering (Hidy, 2019). John Switzer Owens, an Irish physician and environmental engineer hailing from Enniscorthy Co. Wexford, is credited with significant advances in scientific instrumentation used to quantify air pollution during the twentieth century. The deposit gauge (Owens, 1926), a device that captured soot falling from the sky, was developed by the Committee for the Investigation of Atmospheric Pollution, of which Owens was a member. The instrument was deployed at various locations as part of one of the earliest large-scale monitoring networks in

the UK to evaluate the spatial trends in air pollution (Fuller, 2019; Mosley, 2009). As the field progressed, 'Black Smoke' (BS) measurements, based on the degree of optical reflectance, were used for the quantification of air pollution caused by particulate matter. The method was calibrated for domestic coal smoke. It was standardised in the 1960s by the Organisation for Economic Co-operation and Development (OECD) and monitoring networks were deployed for the systematic measurement of the species, as well as sulfur dioxide (Department for Environment, Food & Rural Affairs; Quincey, 2007). Increasing interest in the numerous sources of airborne particles, and their relationship with morbidity and mortality, led to the use of PM<sub>2.5</sub> and PM<sub>10</sub> in the mid-1990s as the accepted measure of particulate matter by academics and regulatory authorities, to encompass the total mass concentration of particles within specific size fractions (Heal & Beverland, 2017).

Particulate matter concentration instrumentation is based on measurement principles, which include gravimetric, optical, microbalance and electrical charge. Gravimetric methods determine the PM mass concentration by weighing the filter, before and after sampling. This is typically an off-line technique (Amaral et al., 2015) used to give average daily concentrations of PM. Tapered element oscillating microbalance (TEOM) and beta attenuation monitors (BAM) also incorporate filter measurements, but can operate on a continuous basis to provide hourly values of mass concentration (Solomon & Sioutas, 2008). Real-time optical measurements of mass concentration are based on the principles of light extinction, absorption and scattering by particles. Such methods provide quantitative information on mass concentration but provide no indication of aerosol composition.

Numerous studies worldwide have reported higher levels of PM mass concentration in winter in comparison with summer months. This is largely attributed to increased biomass burning during the winter heating season (Cheng et al., 2013; Diapouli et al., 2017; Healy et al., 2017; Jeong et al., 2008; Park et al., 2018; Reisen et al., 2013; Saarikoski et al., 2008; Saffari et al., 2013; Yttri et al., 2007; Yttri et al., 2019). In addition, several studies have reported the influence of long range transportation of emissions (ApSimon et al., 2001; Begum et al., 2010; Coz et al., 2009; Healy et al., 2017; Karaca et al., 2009; Salvador et al., 2007; Wang et al., 2015; Zhang et al., 2018). PM mass concentrations vary across Europe. Despite higher mean concentrations in southern Europe, compared to northwest and central regions (Cavalli et al., 2016; Yttri

et al., 2019), similar spatial trends are observed in each region (Glasius et al., 2018; Putaud et al., 2010). In general, levels gradually increase in moving from rural background monitoring sites to kerbside sites in urban settings. Correspondingly, the majority of annual and daily limit exceedances occur in urban and kerbside locations (Putaud et al., 2010). Strong diurnal patterns have also been documented, particularly in cities influenced by high volumes of traffic. These trends are often dependent on dominant sources, combined with variation in seasons, meteorological conditions and boundary layer height. Large contributions from fossil fuels are often observed from 06:00 - 10:00, consistent with morning rush hour traffic, while biomass burning related emissions dominate in the eveningtime (Mousavi et al., 2018; Peralta et al., 2019; Rattigan et al., 2013).

Carbonaceous aerosol represents a significant portion of ambient aerosol; accounting for between 20 and 70% of the total ambient aerosol mass (Cesari et al., 2018; Contini et al., 2018; Jafar & Harrison, 2020; Karanasiou et al., 2015; Ni et al., 2018; Yttri et al., 2009; Yttri et al., 2011). Carbonaceous aerosols can be emitted by both natural and anthropogenic sources, including solid fuel combustion, such as wood and coal burning for residential heating, and fossil fuel combustion, often associated with road traffic. Biogenic, marine biogenic and emissions from forest fires also contribute to carbonaceous aerosol. Total carbon is the term traditionally used to describe the sum of all carbon contained in particles. Total carbon (TC) can be divided into organic carbon (OC) and black carbon (BC) or elemental carbon (EC) fractions (Fuzzi et al., 2006). Discrimination between BC and EC is based on method of measurement. Light absorbing carbonaceous aerosol, which includes black and brown carbon, can affect atmospheric radiative forcing, reduce the albedo of snow and ice and, ultimately, has considerable impact on climate (Liu et al., 2020). Brown clouds, most commonly occurring in Asia, are comprised of both light absorbing and light scattering aerosols and can also contribute to atmospheric solar heating and the cooling of the Earth's surface (Gustafsson et al., 2009; Ramanathan et al., 2007). Numerous adverse health effects, such as heart disease, stroke and respiratory related illnesses, have previously been linked with exposure to elevated concentrations of particulate matter and poor air quality (World Health Organization, 2019). Following widespread recognition of the negative implications on climate and human health linked with carbonaceous aerosol,

the development of modern analytical techniques capable of identification and quantification of carbonaceous fractions of total PM mass became essential.

Quantification of the carbonaceous content of atmospheric aerosols is based on thermal and thermal-optical methods, allowing for determination of total carbon content and the discrimination of elemental (EC) and organic carbon (OC). In conventional thermal methods, filter samples are subjected to increasing temperatures under pure oxygen. Quantification is possible through conversion of evolved carbonaceous vapours to CO<sub>2</sub> by an MnO<sub>2</sub> catalyst, followed by detection of CO<sub>2</sub> by a non-dispersive infrared (NDIR) detector. A significant limitation associated with this method is the evolution of pyrolytic carbon (PC), caused by the charring of organic matter, at higher temperatures, leading to an overestimation of EC (Kuhlbusch et al., 2009). The incorporation of a laser to continuously monitor the filter transmittance in thermal-optical methods corrected for the PC formed during analysis (Birch & Cary, 1996; Huntzicker et al., 1982). Thermal-optical analysis is widely used for discrimination of elemental and organic carbon. This technique involves desorption of OC from a filter at increasing temperatures under an inert pure-helium atmosphere, followed by desorption of EC under an oxidising atmosphere (Wu et al., 2016). Numerous variations of the analytical technique have been published, incorporating modified temperature ramps, residence time and optical measurements (Cavalli et al., 2010; Chow et al., 2007; Chow et al., 1993; NIOSH, 1996; Quincey et al., 2009; Schauer et al., 2003). This analytical technique was initially applied to urban aerosols, particularly targeting diesel soot (Andreae & Gelencsér, 2006).

The distinction between ‘elemental carbon’ and ‘organic carbon’ is not based on molecular structure, but on differences in optical absorption of particles during thermal desorption (Spada & Hyslop, 2018). Accurate distinction of elemental and carbon content can reveal the influence of local sources and long range transportation. EC is produced exclusively during the incomplete combustion of carbon-containing fuels, including fossil fuels and biomass. OC may be primary, as a product of combustion or biogenic emissions, or secondary, as a consequence of atmospheric processes (Jones & Harrison, 2005; Szidat et al., 2009). EC in urban aerosol samples tends to evolve at significantly higher temperatures (550 – 700 °C) compared with aged samples and samples from remote locations (450 – 550 °C) in thermal-optical analyses (Andreae & Gelencsér, 2006). The OC/EC ratio can be used as an indication of dominant fuel types

contributing to the aerosol composition, including biomass burning, coal combustion and vehicle emissions. The ratio estimation is highly dependent on combustion conditions and methods of sampling analysis (Cheng et al., 2011; Ni et al., 2018; Simpson et al., 2007).

Traditionally, filter-based measurements were used to determine the carbonaceous content of ambient aerosol. Such methods can be time consuming and analysis is often carried out off-line, following sample collection. Continuous on-line monitoring of ambient carbonaceous aerosol at high time-resolution can be achieved using the Semi-Continuous OCEC Field Analyzer developed by Sunset Laboratory Inc.

‘Black smoke’ measurements were based on the relationship between the surface particle concentration and reflectance of dark particles within PM, now characterised as black carbon (Heal & Quincey, 2012). The principles of this method are similar to the optical, on-line measurements of black carbon are made using the aethalometer, first developed by Hansen et al. (1984). Both methods rely on the optical properties of sampled particles to determine concentration. Previous publications have demonstrated approaches to deriving a relationship between the methods (Heal & Quincey, 2012; Quincey, 2007). The principle of operation of the aethalometer was based on the continuous measurement of attenuation of light (530 nm) transmitted through a filter as ambient particles were deposited. The current model (AE33, Magee Scientific) features light of seven wavelengths between 370 nm and 950 nm; from the near-UV to near-IR, which are passed through a sample spot of ambient particles collected on an automatically advancing filter tape. The BC concentration is determined by the rate of change of attenuation of light transmitted through the filter, in addition to a pre-selected mass absorption cross section (MAC) value. As a consequence of the incorporation of seven wavelengths, the AE33 aethalometer also has the capacity to carry out source apportionment analysis, evaluating the origins of sampled BC. This analysis is based on the differences in absorption efficiency of particles. Development of this fully automated instrument allowed for collection of detailed description of carbonaceous aerosol composition in real-time, at relatively low cost and has proven to be less labour intensive than previous methods.

The dominant sources of black carbon in European cities are traffic-related and biomass burning emissions (Kutzner et al., 2018). The substantial contribution of

wood burning emissions to PM mass concentration, particularly during the winter heating period, is widely recognised across Europe (Favez et al., 2009; Helin et al., 2018; Herich et al., 2011; Maenhaut et al., 2016; Martinsson et al., 2017; Perrino et al., 2019; Titos et al., 2017; Zhang et al., 2020) and is responsible for frequent exceedances of air quality limits set out by the EU (Crilley et al., 2015). High time-resolution achieved by the aethalometer facilitates detailed diurnal and temporal analysis of carbonaceous aerosol and related contributing sources. Studies have noted higher than expected levels of emissions attributed to biomass burning at the weekends, in comparison to weekdays, suggestive of ‘recreational’ domestic wood burning. This ‘weekend phenomenon’ has been observed in London (Fuller et al., 2014; Jafar & Harrison, 2020) and in Paris (Favez et al., 2009). In each case, the increase in brown carbon (BrC) containing species at weekends is associated with a high prevalence of domestic wood burning.

The most recent addition to the suite of instruments capable of on-line speciation of carbonaceous aerosol with a high time resolution is the Total Carbon Analyzer (TCA-08, Magee Scientific). Determination of total carbon concentration is performed by flash heating the collected sample to 940 °C. The integration of concurrent optical measurements of equivalent black carbon (eBC) allows for the determination of equivalent organic carbon (eOC) content present in the sample. The eBC concentration, measured by the aethalometer, is converted to equivalent elemental carbon (eEC) using a proportionality factor ( $b$ ), thus allowing for accurate quantification of eOC, described in Eqn. 1.1 and Eqn. 1.2 (Rigler et al., 2020).

$$eEC = b \cdot eBC \quad \text{Eqn. 1.1}$$

$$eOC = TC - eEC \quad \text{Eqn. 1.2}$$

By using ambient air as the analytical carrier gas, the requirement of speciality gas supplies is eliminated, simplifying installation. Continuous operation at a high time-resolution allows for reliable capture of real-time changes in aerosol composition, providing a detailed insight into the major contributors and their relative contributions,

while avoiding the labour-intensive filter preparation and analysis associated with conventional analytical techniques.

As a field combination, the multi-wavelength aethalometer and the Total Carbon Analyzer is quite a robust arrangement. The combination of these instruments provides a detailed description of the ambient carbonaceous aerosol in real-time, possibly rendering the conventional thermal-optical method of measuring elemental and organic carbon content obsolete. By employing this method the absolute concentrations of eEC, eOC and TC are obtained. However, in contrast to thermal-optical methods of measurement, the relative volatilities of each fraction of the sampled aerosol observed in thermograms, which can be used to inform a description of the aerosol composition, are not obtained in TCA analysis. Despite widespread recognition of the major role played by black carbon as a positive radiative forcing agent in the atmosphere (Bond & Bergstrom, 2006; IPCC, 2013), it is not a regulated pollutant under U.S., EU or Irish legislation. With the aforementioned combination, it would be possible to routinely monitor ambient levels of BC, while also satisfying the required monitoring of OC and EC.

Complimentary techniques, such as the off-line quantification of levoglucosan, an anhydrosugar commonly used as a biomass burning tracer, and employment of instruments such as an aerosol chemical speciation monitor (ACSM), can provide detailed evidence of contributions to ambient aerosol. Levoglucosan measurements offer an indication of the contribution of wood burning to total solid fuel combustion emissions. Levoglucosan quantification can also be applied in the validation of analysis, such as the aethalometer model, particularly when dominant sources identified in the environment are wood burning and traffic-related emissions.

## 1.4 STUDIES OF CARBONACEOUS AEROSOL IN IRELAND

---

Several studies have been conducted across Ireland to evaluate the ambient atmospheric aerosol in a number of unique environments (Buckley, 2019; Ceburnis et al., 2006; Dall'Osto et al., 2013; Healy et al., 2010; Kourtchev et al., 2011; Lin, 2019; Ovadnevaite et al., 2021; Wenger et al., 2020). Spatial and temporal trends have been identified, with a focus on identification of dominant sources in recent years. Characterisation of the aerosol aids the identification of dominant sources; essential for the development of air pollution mitigation legislation.

Lin et al. (2018) reported the dominance of emissions related to peat and wood burning in a mainly residential area of Dublin, collectively accounting for 61 – 72% of organic aerosol measured in the eveningtime, despite the use of solid fuel as a heat source in only a small portion of households (< 13%). It is estimated that total elimination of wood combustion would result in a 52 - 70% reduction in PM<sub>1</sub> mass concentration. These findings reflect results obtained during a measurement campaign in Galway city where the largest contribution to total ambient organic aerosol was from peat burning (39%), despite the relatively low usage of peat as a primary domestic heating method (Lin et al., 2017). Ovadnevaite et al. (2021) conducted further research into the characterisation of the dominant pollutants influencing air quality in Ireland in the pilot network AEROSOURCE. The study concluded that under polluted conditions, carbonaceous species (e.g. organic matter, black carbon) are dominant, accounting for between 60% and 90% of PM<sub>1</sub>. The authors noted the seasonal variability of emissions from solid fuel burning. Contributions to the total organic aerosol (OA) from coal, peat and wood were greater in winter than in autumn or spring, while the portion of OA attributed to peat and wood were below limits of detection during the summer months. The aerosol composition varied with location; organic matter was the major component of the PM<sub>1</sub> concentration in the residential area of Dublin (> 60%), while black carbon contributed > 50% at a kerbside location in the city centre.

The strong influence of anthropogenic activity on air quality in cities is well documented, however little consideration is given to similar effects experienced by less populated or rural areas. Recently, a comprehensive study (Source Apportionment of Particulate Matter in Urban and Rural Residential Areas of Ireland) conducted by Wenger et al. (2020) reported the significant impact of anthropogenic emissions on

poor air quality in small rural towns in Ireland, predominantly caused by solid fuel combustion for residential heating (Wenger et al., 2020). The SAPPHIRE project consisted of measurement campaigns carried out in the three small towns; Birr, Co. Offaly, Enniscorthy, Co. Wexford and Killarney, Co. Kerry, to determine the chemical composition and the major sources of ambient fine particulate matter (PM<sub>2.5</sub>). At the time legislation was in place to ban the marketing, sale and distribution of bituminous coal in urban areas with populations greater than 15,000, therefore excluding the aforementioned towns. Source apportionment analysis was used to quantify the contribution of residential solid fuel combustion to ambient PM pollution, as well as the amounts contributed by different fuel types (coal, peat and wood). A strong diurnal trend was observed during the wintertime field campaigns; concentrations of PM<sub>2.5</sub> during evening hours were significantly higher than those observed during the day. Average PM<sub>2.5</sub> concentrations of 29.2 µg m<sup>-3</sup>, 15.3 µg m<sup>-3</sup> and 7.9 µg m<sup>-3</sup> were recorded in Enniscorthy (January – February 2015), Killarney (November – December 2014) and Birr (November 2015 – January 2016), respectively. Source apportionment analysis indicated solid fuel combustion as the dominant source of pollution at each location, accounting for 82%, 72% and 60% of total PM<sub>2.5</sub> in Enniscorthy, Killarney and Birr, respectively (Buckley, 2019; Wenger et al., 2020).

Expansion of the nationwide monitoring network, coordinated by the Environmental Protection Agency (EPA), has resulted in increased availability of local PM measurements in real-time, and has heightened awareness of high levels of PM in rural towns, particularly during the winter season. The average hourly PM<sub>2.5</sub> concentration measured across several sampling sites in Dublin was 11.05 µg m<sup>-3</sup> during winter 2019. In contrast, concurrent mean hourly concentrations of 22.72 µg m<sup>-3</sup>, 23.05 µg m<sup>-3</sup>, 24.55 µg m<sup>-3</sup> and 27.04 µg m<sup>-3</sup> were recorded in the rural towns of Macroom, Co. Cork, Tralee, Co. Kerry, Enniscorthy, Co. Wexford and Ennis, Co. Clare, respectively, highlighting the increased levels of PM experienced in areas outside large cities (EPA, 2020).

## 1.5 OVERVIEW

---

### 1.5.1 Aims of Research

---

The overall aims of this study can be summarised as follows:

- Quantify the ambient carbonaceous aerosol at several unique environments around Ireland and identify diurnal, weekday and seasonal patterns in equivalent black carbon.
- Determine the contributions of solid fuel combustion and traffic-related emissions to total equivalent black carbon concentrations and assess the performance of the aethalometer model for the multi-fuel environment in Ireland.
- Compare numerous methods of carbonaceous aerosol measurement and identify the advantages and disadvantages associated with each of the techniques for use in the long-term real-time monitoring of ambient levels of carbonaceous aerosols.
- Provide a consolidated study of spatial and temporal variability of ambient carbonaceous aerosol, and associated sources, in Ireland. This information will extend existing knowledge in the area and inform policies for the targeted reduction of air pollution in an effort to minimise the adverse effects on human health and climate.

### 1.5.2 Overview of Thesis

---

Chapter 1 presents an introduction to atmospheric aerosols, focussing specifically on carbonaceous aerosols; sources, chemical composition and the effects of such aerosols on the planet and human health. Several on-line and off-line methods for the measurement of carbonaceous aerosols are also discussed.

Chapter 2 provides an overview of the principles of operation of the instruments deployed for the research described in this thesis. In addition, the off-line analysis techniques are described.

Chapter 3 provides details of the intensive monitoring campaign that took place between December 2017 and February 2018 at four unique locations in Ireland, which

coincided with the European-wide EMEP/ACTRIS/COLOSSAL intensive measurement period. Source apportionment analysis was performed on real-time equivalent black carbon data collected by the multi-wavelength aethalometer. The results were compared with off-line measurements of elemental and organic carbon concentration and the biomass burning tracer levoglucosan in order to validate the results produced by the aethalometer model.

Chapter 4 provides details of a twelve month measurement campaign at a designated urban roadside site in the centre of Dublin city. The results are used to evaluate the influence of seasonal variation on ambient carbonaceous aerosol concentration at contrasting locations in Dublin; urban background and roadside sites.

Chapter 5 provides details of a measurement campaign that took place in the small town of Enniscorthy, Co. Wexford. The seasonal variability of ambient carbonaceous aerosol is investigated and compared with similar measurements recorded five years previously during the SAPPHIRE campaign. This chapter also evaluates the performance of the newly developed ‘TC-BC’ method employed by the Total Carbon Analyzer in a mixed fuel environment.

Chapter 6 investigates the impact of anthropogenic interventions on ambient aerosol concentrations and composition in the context of the COVID-19 pandemic. The introduction of various restrictions on mobility and social interaction on the basis of public health advice, resulted in a reduction in traffic and thus a shift in contributions to ambient atmospheric aerosol.

Chapter 7 presents a summary of the work presented in the thesis with perspectives, scope for future research and implications for policy making and legislation.

## 2. INSTRUMENTATION AND METHODOLOGY

---

<b>2.1</b>	<b><i>Sampling Sites</i></b> .....	<b>26</b>
2.1.1	Regional and Urban Background Sites .....	26
2.1.2	Urban Roadside in Dublin City .....	27
2.1.3	Small Town in Rural Ireland .....	27
<b>2.2</b>	<b><i>Field Instrumentation</i></b> .....	<b>32</b>
2.2.1	Ambient Air Sampling by Filter Collection .....	32
2.2.1.1	High Volume Air Sampler .....	32
2.2.1.2	Sequential Air Sampler .....	33
2.2.1.3	Filter Preparation .....	34
2.2.1.4	Field Blanks .....	34
2.2.2	Characterisation by Optical Absorption .....	36
2.2.2.1	Calculation of Mass Concentration .....	40
2.2.2.2	Source Apportionment Analysis .....	44
2.2.3	Total Carbon Content of Ambient Aerosol .....	47
2.2.3.1	'TC-BC' Method .....	50
2.2.3.2	Calculation of Proportionality Parameter .....	51
2.2.3.3	Off-line Analysis of Filter Samples .....	51
<b>2.3</b>	<b><i>Off-line Analysis</i></b> .....	<b>52</b>
2.3.1	Determination of Elemental and Organic Carbon Content .....	52
2.3.2	Determination of Ambient Anhydrosugar Concentration .....	57
<b>2.4</b>	<b><i>Data Modelling</i></b> .....	<b>59</b>
2.4.1	Back Trajectory Analysis .....	59
2.4.2	Positive Matrix Factorization .....	59
2.4.3	Meteorological Normalisation .....	60

## 2.1 SAMPLING SITES

---

The locations included in this body of research (Figure 2.1) were selected with the aim of advancing the research by further evaluating the spatial and temporal variability of ambient carbonaceous aerosol by focusing on contrasting environments in Ireland, including remote, coastal, residential and urban environments. A summary of the instruments deployed on-site during each measurement campaign is provided in Table 2.1, Table 2.2 and Table 2.3.

### 2.1.1 Regional and Urban Background Sites

---

Four sites across Ireland were selected for an intensive measurement campaign from December 2017 to February 2018. Carnsore Point, Co. Wexford (CP), Mace Head, Co. Galway (MHD) and Malin Head, Co. Donegal (MLN) were designated as regional background sites, while the monitoring site on the campus of University College Dublin (UCD) was categorised as an urban background site. Site selection allowed for the assessment of spatial variability associated with the composition and concentrations of ambient carbonaceous aerosols during the wintertime, in several unique regional and urban background environments. Dominant sources contributing to total wintertime carbonaceous aerosol were determined using on- and off-line instrumentation deployed at each site (Table 2.1). The data collected throughout this campaign was incorporated into a European-wide intensive measurement campaign, established to test and validate the multi-wavelength aethalometer source apportionment approach in background environments (Fagerli et al., 2019).

The Carnsore Point, Mace Head and Malin Head sites were located on the south-eastern, western and northern coasts of Ireland, respectively. These remote sites were sparsely populated and lacked obvious significant anthropogenic local sources. The coastal location of each of the regional background sampling sites undoubtedly influenced the aerosol composition. The UCD sampling site was situated on the campus of University College Dublin, in a predominantly residential area of Dublin, approximately 4 km from the city centre. A busy arterial route from the city centre (R138) passed 500 m to the east of the site.

### 2.1.2 Urban Roadside in Dublin City

---

A 12-month field campaign was conducted at a monitoring site on Pearse Street, located in Dublin city centre, beginning August 2018. This inner city location was designated as an ‘urban roadside site’. In contrast to the data collected in regional and urban background environments, this measurement campaign provided insights into the seasonal variation of carbonaceous aerosol in an urban environment, dominated by traffic-related emissions. The extent to which traffic emissions influenced the ambient aerosol was evaluated on-line by a multi-wavelength aethalometer.

### 2.1.3 Small Town in Rural Ireland

---

Enniscorthy, Co. Wexford, a small town in the south-east of Ireland, was selected as a sampling location to compliment the data previously collected in contrasting environments. The inclusion of this site broadened the spatial representation of monitoring locations used in this research and serves to provide a more complete picture of ambient carbonaceous aerosol across the range of environments in Ireland.

The ban on the marketing, sale and distribution of bituminous coal was due to be extended nationwide for the 2019 - 2020 heating season. At the outset, the campaign was designed as a continuation of the research carried out by Buckley (2019) and Wenger et al. (2020) in Enniscorthy in 2015 to include seasonally representative measurements and to evaluate the impact of the proposed bituminous coal ban. However, the ban was delayed by the government following threats of legal action by the coal industry. The ban ultimately came into effect for the 2020 - 2021 heating season and measurements during the initial months were captured.

Although the coal ban was not implemented when expected, the instruments were deployed in December 2019 and captured data from the 2019 – 2020 winter heating season. Sampling continued throughout 2020. The onset of the COVID-19 pandemic in Ireland in February 2020 provided an unprecedented measurement opportunity. Instrumentation remained on site until January 2021, capturing the effects of public health measures of varying severity which altered the behaviour and mobility of the population.

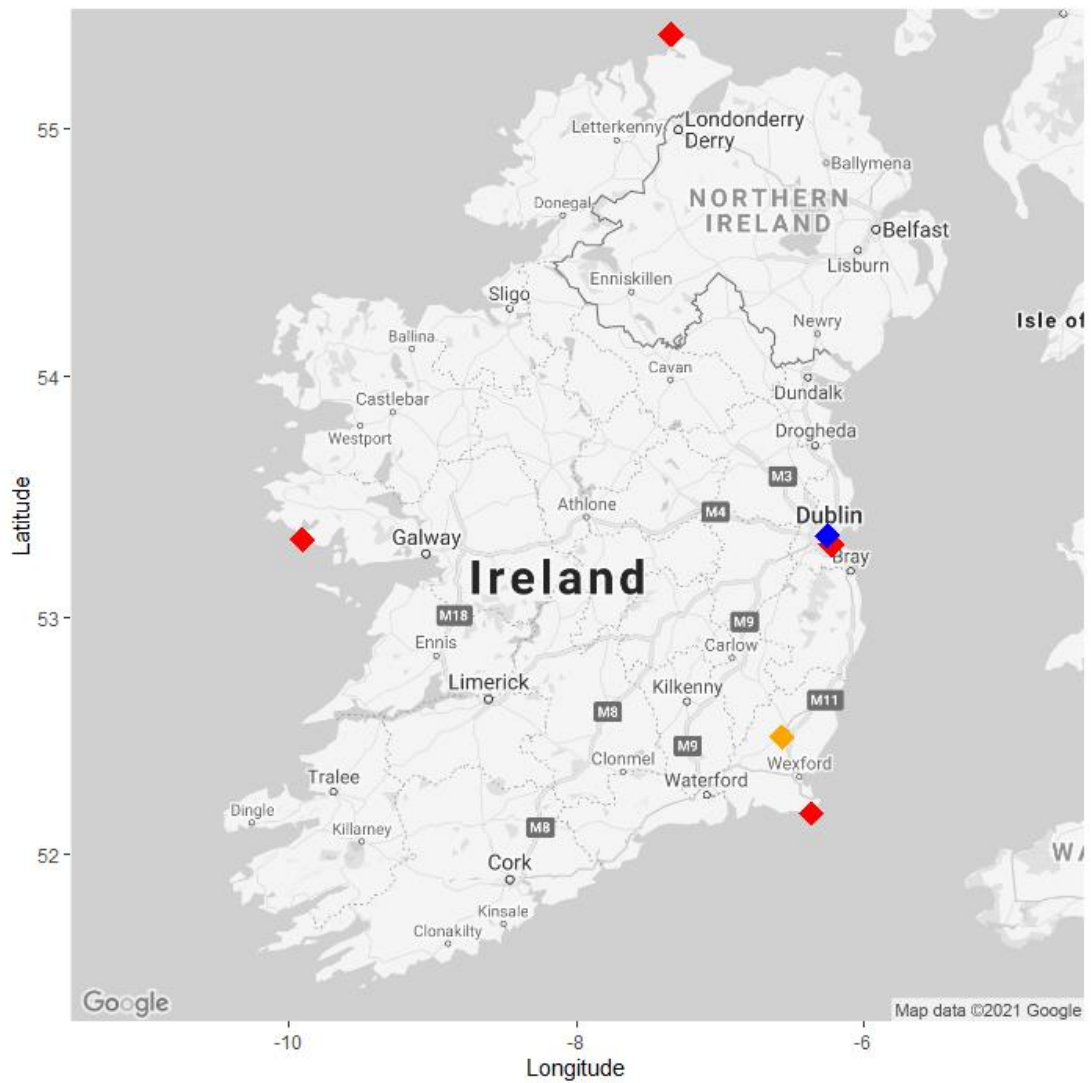


**Figure 2.1** Location of monitoring sites during the background location (red), urban roadside (blue) and rural town (yellow) campaigns.

**Table 2.1** Summary of instrumentation on site during wintertime intensive measurement campaign at background locations.

	<b>Instrument Model</b>	<b>Dates of Operation</b>	<b>Time Basis</b>	<b>Sampling Period</b>	<b>Flow Rate</b> <b>L min<sup>-1</sup></b>
<b>Carnsore Point</b>					
<i>Aethalometer</i>	AE33-S04-00377	01/12/2017 – 04/03/2018	60 s	<i>Continuous</i>	5
<i>Ambient Air Sampler</i>	DIGITEL DHA-80	29/01/2018 – 03/03/2018	24 hr	00:00 – 23:59	500
<b>Mace Head</b>					
<i>Aethalometer</i>	AE33-S05-00500	21/12/2017 – 04/03/2018	60 s	<i>Continuous</i>	5
<i>Ambient Air Sampler</i>	DIGITEL DHA-80	06/12/2017 – 25/02/2018	24 hr	08:00 – 07:59	500
<b>Malin Head</b>					
<i>Aethalometer</i>	AE33-S05-00461	01/12/2017 – 04/03/2018	60 s	<i>Continuous</i>	5
<i>Ambient Air Sampler</i>	DIGITEL DHA-80	18/01/2018 – 04/03/2018	24 hr	00:00 – 23:59	500
<b>University College Dublin</b>					
<i>Aethalometer</i>	AE33-S02-00246	01/12/2017 – 04/03/2018	60 s	<i>Continuous</i>	4
<i>Ambient Air Sampler</i>	Partisol 2025i	21/12/2018 – 25/02/2018	48 hr/24 hr	08:00 – 07:59	16.7

**Table 2.2** Summary of instrumentation on site during the urban roadside campaign.

	Instrument Model	Dates of Operation	Time Basis	Sampling Period	Flow Rate L min <sup>-1</sup>
<b>Pearse Street, Dublin</b>					
<i>Aethalometer</i>	AE33-S02-00246	01/09/2018 – 06/01/2019*	60 s	<i>Continuous</i>	2
		25/01/2019 – 07/04/2019†	60 s	<i>Continuous</i>	2
		21/05/2019 – 31/08/2019	60 s	<i>Continuous</i>	2
<i>Ambient Air Sampler</i>	DIGITEL DHA-80	01/02/2019 – 06/03/2019	12 hr	06:00 – 17:59 18:00 – 07:59	500
<i>Total Carbon Analyzer</i>	TCA-08-S00-00127	22/05/2019 – 21/08/2019	1 hr	<i>Continuous</i>	16.7

\* Aethalometer was removed from the site for an intercomparison study conducted at TROPOS (Cuesta-Mosquera et al., 2020).

† Aethalometer was removed from site for a study conducted by C-CAPS, NUIG.

**Table 2.3** Summary of instrumentation on site during the measurement campaign in a small, rural town.

	<b>Instrument Model</b>	<b>Dates of Operation</b>	<b>Time Basis</b>	<b>Sampling Period</b>	<b>Flow Rate</b> <b>L min<sup>-1</sup></b>
<b>Enniscorthy</b>					
<i>Aethalometer</i>	AE33-S02-00246	01/12/2019 – 20/01/2021	60 s	<i>Continuous</i> 15:00 – 22:59	5
<i>Ambient Air Sampler</i>	DIGITEL DHA-80	03/02/2020 – 23/02/2020	8 hr	23:00 – 06:59 07:00 – 14:59	500
<i>Fine Dust Measurement</i>	Fidas 200	01/12/2019 – 20/01/2021	1 hr	<i>Continuous</i>	5
<i>SO<sub>2</sub> Analyzer</i>	Teledyne API T100	17/01/2020 – 20/01/2021	60 s	<i>Continuous</i>	0.65
<i>Total Carbon Analyzer</i>	TCA-08-S00-00127	01/12/2019 – 20/01/2021	1 hr	<i>Continuous</i>	16.7

## 2.2 FIELD INSTRUMENTATION

---

### 2.2.1 Ambient Air Sampling by Filter Collection

---

Ambient air samples were collected at each monitoring site on quartz fibre filter, using either a high volume air sampler (DHA-80, DIGITEL Elektronik GmbH) or a sequential air sampler (Partisol 2025i, Thermo scientific). Filter samples were subsequently analysed off-line.

#### 2.2.1.1 High Volume Air Sampler

---

A high volume air sampler (DHA-80, DIGITEL Elektronik GmbH) was used for the continuous and autonomous collection of ambient PM<sub>2.5</sub> samples on a pre-set time basis. The sampler was fitted with a PM<sub>2.5</sub> pre-separator to allow for collection of particles of  $\leq 2.5 \mu\text{m}$  on quartz fibre filters ( $d = 150 \text{ mm}$ ), a constant flow rate of  $500 \text{ L min}^{-1}$ . A schematic diagram of the air sampler is shown in Figure 2.2.

Ambient air is sampled through the PM<sub>2.5</sub> inlet (1), which is designed so that particles with an aerodynamic diameter less than  $2.5 \mu\text{m}$  follow the air flow and are collected on a filter, while those with aerodynamic diameters greater than  $2.5 \mu\text{m}$  are accelerated to impact on the grease-trap platform. Using a sampling tube, the ambient air is drawn vertically from top to bottom by a blower (6) through the filter which is placed in the flow chamber (2). In order to guarantee uniform loading of the exposed filter, the upper part of the flow chamber (2) operates like a diffuser with a regular cross section. After the filter, the quantity of transported air is measured and the flow rate is maintained by a buoyancy floater suspended in parallel in a by-pass air stream, which is coupled with a photo-sensor (5a) which optically detects the position of the float (DIGITEL Elektronik GmbH, 2009).

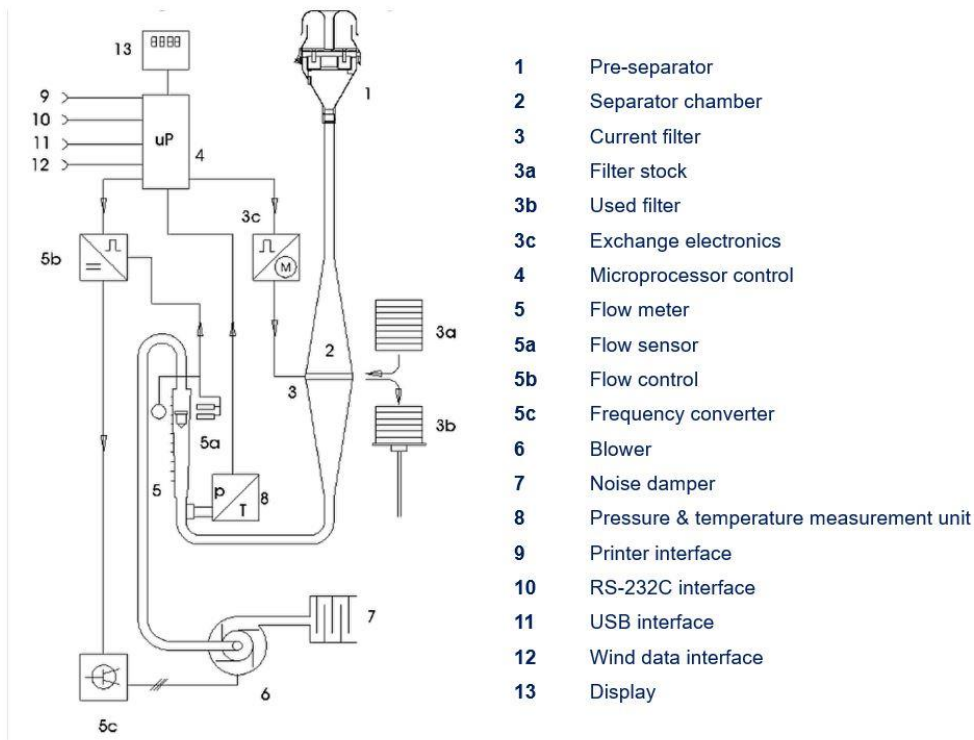


**Figure 2.2** Schematic of DHA-80 high volume air sampler. Adapted from user manual (DIGITEL Elektronik GmbH, 2009).

### 2.2.1.2 Sequential Air Sampler

A sequential air sampler (Partisol 2025i, Thermo Scientific) was used for the continuous collection of PM<sub>2.5</sub> ambient air samples (Figure 2.3). A built-in pump provides the vacuum required to draw the ambient air stream through the sample inlet and through a 47 mm pre-treated filter (PALL Life Sciences, Pallflex®, Tissuquartz). A constant flow rate of 16.7 L min<sup>-1</sup> was maintained throughout the sampling period, using an active, volumetric flow-control system which incorporated a mass flow controller, as well as sensors for measuring ambient temperature and pressure. The quartz fibre filters were contained in reusable cassettes and filter exchange was performed using pneumatic pressure from the sample pump at pre-set time intervals. During this automatic process, a filter cassette was loaded from the supply magazine into the sampling position, while the completed sample was simultaneously transferred to the storage magazine. A field blank was placed in the storage tube before sampling began to assess whether or not sample contamination could be eliminated. The quartz fibre filter designated as ‘field blank’ did not undergo sampling in the instrument.

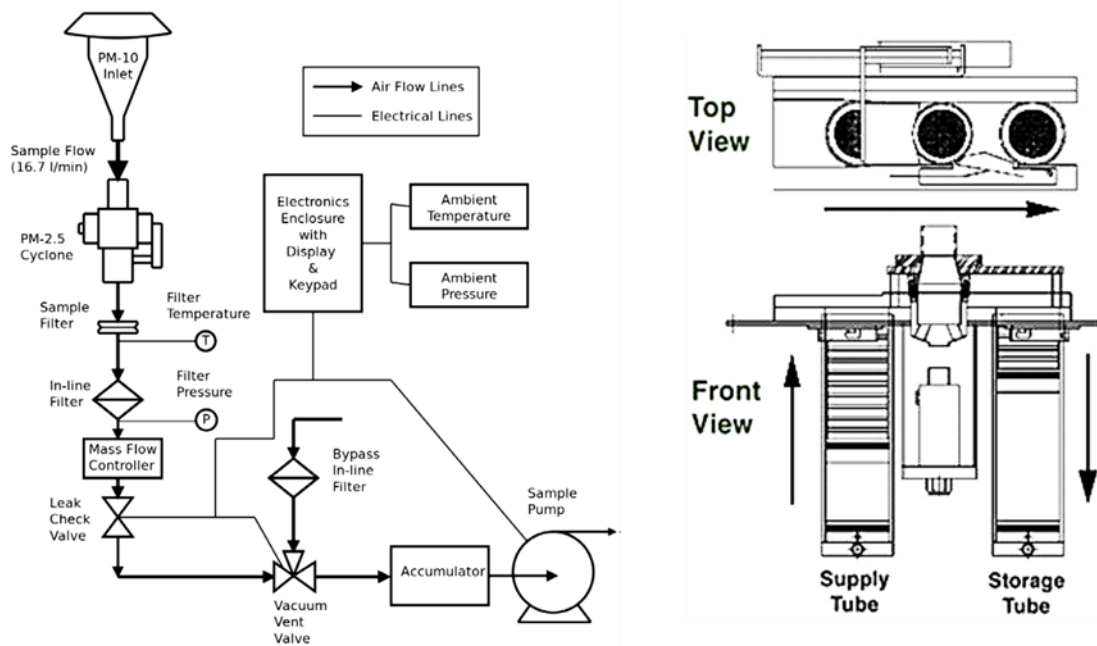


**Figure 2.3** Schematic of Partisol 2025i sequential air sampler (Thermo Scientific, 2015).

### 2.2.1.3 Filter Preparation

Quartz fibre filters (PALL Life Sciences, Pallflex®, Tissuquartz) with diameters of 150 mm and 47 mm were used for sample collection in the high volume air sampler (DHA-80, DIGITEL Elektronik GmbH) and the sequential air sampler (Partisol-2025i, Thermo Scientific), respectively. Prior to sampling, the filters were baked in an oven (Carbolite Furnace, Barloworld Scientific) at 850 °C for 3 hours to remove any possible contaminants (European Committee for Standardization, 2017). After baking, the filters were cooled and then wrapped individually in aluminium foil and stored in a sealed desiccator before transportation to the sampling location.

Following sampling, the filters were removed from the instrument, were again wrapped individually in aluminium foil and placed in a sealed plastic bag to avoid contamination and stored in a freezer at -20 °C for future analysis.

### 2.2.1.4 Field Blanks

Field blanks were treated as described in Section 2.2.1.3. The quartz fibre filters underwent heat treatment and were stored and transported to and from the field in the

same manner as the samples. The field blank was placed in a filter cartridge which was inserted in the lower compartment of the high volume air sampler for the duration of the sampling period. The purpose of the blanks was to monitor for sample contamination by adsorption of volatile compounds from the gas-phase during preparation, transport and analysis. To identify the presence of contaminants, analyses were carried out on field blanks in the same manner as the samples.

## 2.2.2 Characterisation by Optical Absorption

---

A multi-wavelength, dual-spot aethalometer (AE33, Magee Scientific) was used for the measurement of black carbon. The AE33 collects aerosol particles by continuously drawing aerosol-laden ambient air through a spot on the filter tape and subsequently measures the attenuation of light at seven wavelengths which range from near-infrared to the near-ultraviolet regions (370, 470, 520, 590, 660, 880, 950 nm). The instrument measures the transmission of light through a portion of exposed filter tape, and compares it to the transmission through an unloaded spot as a reference area. At low attenuation values, the relationship between attenuation and BC loading is linear. Due to filter saturation, this relationship becomes non-linear at higher values of attenuation, resulting in the underestimation of BC absorption and subsequently the underestimation of eBC concentration (Cuesta-Mosquera et al., 2020; Drinovec et al., 2015). In order to eliminate non-linearities associated with filter based measurements, the aethalometer simultaneously obtains measurements from two sample spots with different rates of accumulation of ambient sample (Drinovec et al., 2015).

The front of the instrument is comprised of two mounts for the filter tape, the optical chamber and the by-pass filter (Figure 2.4). The by-pass filter is utilised during the ‘*Clean Air Test*’ to remove particles from the ambient air stream. The filter tape is made of glass fibres coated with polytetrafluoroethylene (PTFE). The tape material can influence two parameters; optical enhancement factor,  $C$ , and tape tangential leakage factor,  $Z$ . Numerous additional parameters can be adjusted in the ‘General’ section of the ‘Operations’ tab, such as the time base, flow rate, date and time and the maximum attenuation prior to tape advance. A flow diagram of the aethalometer is shown in Figure 2.5.

The aethalometer was regularly maintained as recommended by the manufacturer. Such procedures included checking the sample inlet flow and line tubing, inspecting the optical chamber, flow verification and calibration, and Clean Air, Leakage and ND Optical Filter tests. In addition, the filter tape roll was replaced as necessary. All maintenance procedures strictly adhered to, and were executed periodically as per the user manual (Magee Scientific, 2016).

Inspection and cleaning of the sample inlet, line tubing and optical chamber ensured that the functionality of the instrument was not impaired by obstruction. By removing

any dust or contamination found in the optical chamber, a clear optical path was guaranteed. Verification and calibration of flow and leakage was necessary to ensure that the instrument was running under optimal conditions at the flow rate defined by the user. These procedures were carried out using an external standard flow-meter and the Flow Calibration Pad, supplied as a standard accessory of the instrument. The Clean Air test was performed to verify the stability and performance of the AE33 under dynamic air flow conditions, by removing particles from the ambient air stream as it was drawn through a by-pass cartridge filter, and allowing particle-free air to flow through the analytical system. The Clean Air test was performed manually every 6 months, while the 'Auto Clean Air' test was scheduled to run on a weekly basis on Saturday at 12:00. The 'Neutral Density Optical Filter' test was employed to evaluate the performance of the optical system of the instrument. Four optical elements, comprised of inserts containing Neutral Density glass, were used in the method to assess the response of the optical detectors to varying light intensities from optical sources. If the measured attenuation value of the Neutral Glass element at each wavelength differs by more than 10% from the calibration carried out at the time of manufacturing, the test fails.

The AE33 aethalometer (AE33-S02-00246) used to collect data and perform source apportionment analysis presented in this thesis was included in an intercomparison study of 23 instruments, which aimed to 'determine the unit-to-unit variabilities and their tendencies throughout the spectral range covered by the AE33' (Cuesta-Mosquera et al., 2020). Initial average variability in the measurement of eBC mass concentration reported by the instruments was -2.0% and 0.4% for synthetically generated soot and nigrosin, respectively, prior to calibration of the instruments. Following standardised maintenance, divergence between instruments was -1.0% and 0.5%, respectively. The aethalometer used to perform measurement and analysis presented in this thesis, performed well during the intercomparison study; obtaining adjusted  $r^2$  values  $>0.97$  (ranging from 0.973 to 1) prior to maintenance, indicative of accurate performance in comparison to the measurement of eBC mass concentration by the reference instrument used. Instrument performance improved further following calibration ( $r^2 \geq 0.976$ ).

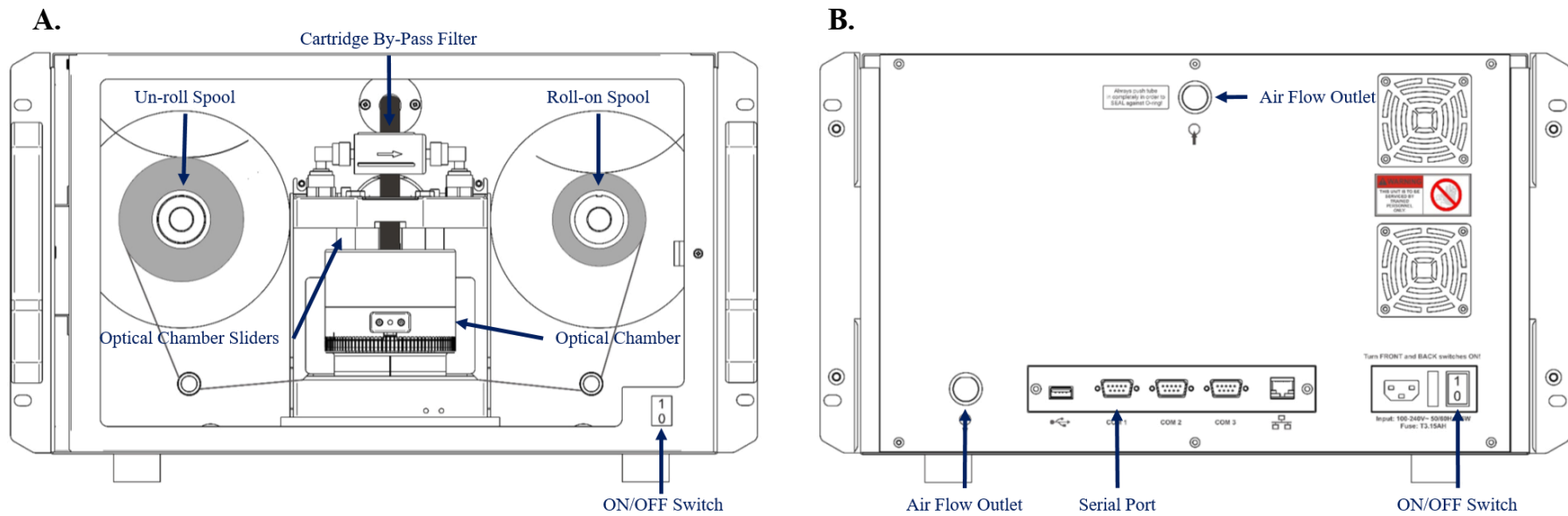


**Figure 2.4** Schematic of front of instrument with door open (A) and rear view (B) of AE33 multi-wavelength aethalometer. Adapted from Magee Scientific (2016).

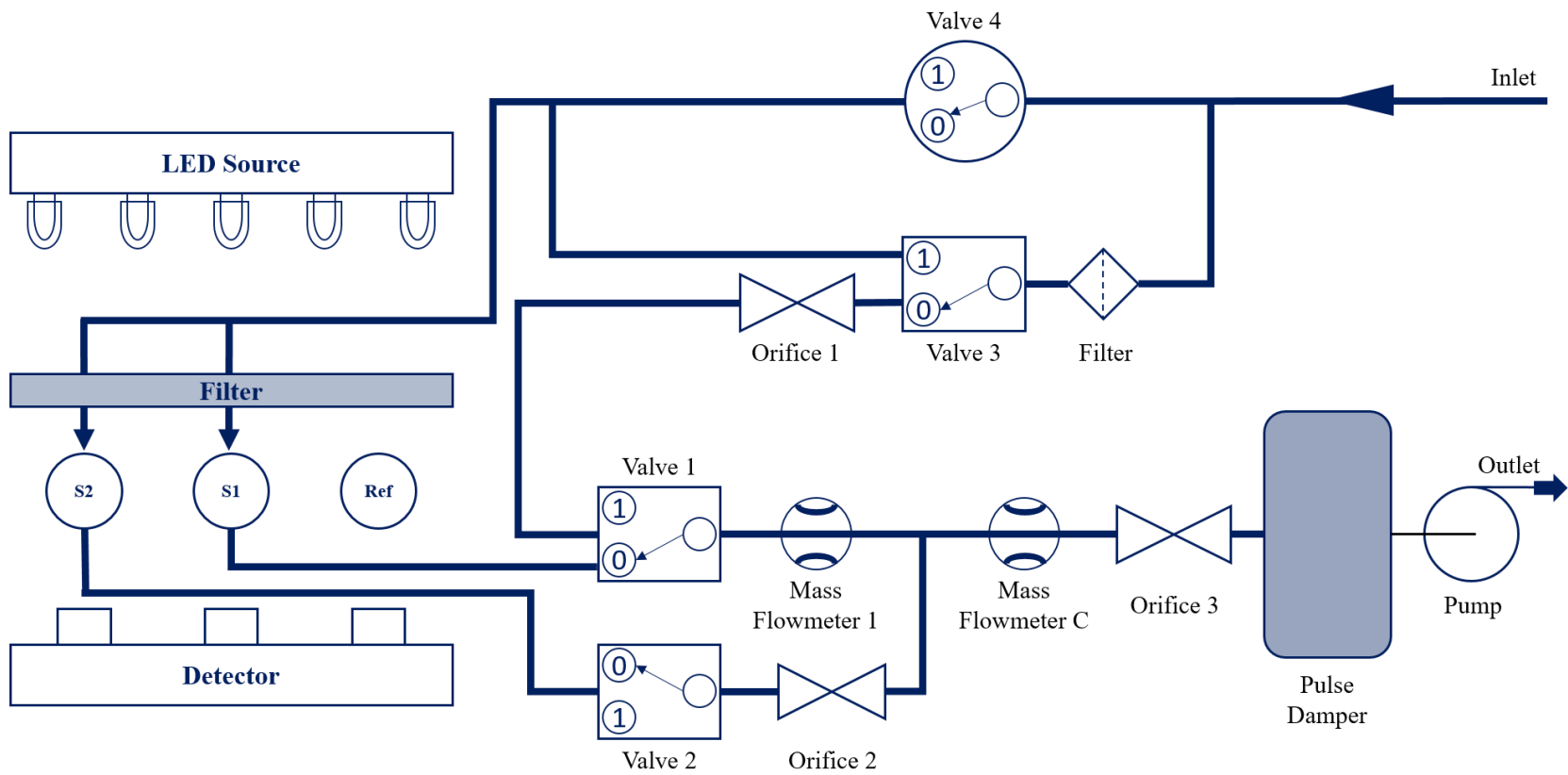


Figure 2.5 Flow diagram of the aethalometer. Adapted from Drinovec et al. (2015).

### 2.2.2.1 Calculation of Mass Concentration

---

A schematic of the measurement of light attenuation is shown in Figure 2.6. The attenuation of light is calculated using the intensity of light passing through both the sample and reference spots on the filter tape using the following equation:

$$ATN \equiv 100 \cdot \ln \left( \frac{I_0}{I_x} \right) \quad \text{Eqn. 2.1}$$

Where  $I_x$  corresponds to the light intensity passing through either sample spot 1 ( $I_1$ ) or 2 ( $I_2$ ), and  $I_0$  corresponds to the light intensity as it passes through the reference spot (Sandradewi, Prévôt, Weingartner et al., 2008). The calculated attenuation ( $ATN$ ) is used to derive an attenuation coefficient ( $b_{atn}$ ):

$$b_{atn} = \frac{S \cdot (\Delta ATN / 100)}{F_{in} \Delta t} \quad \text{Eqn. 2.2}$$

where  $S$  is the spot area,  $\Delta ATN$  is the change in attenuation over time period,  $t$ , and  $F_{in}$  is the flow. This flow can be calculated using the measured flow,  $F_{out}$ , and the leakage factor,  $\zeta$ , which is defined by the user.

$$F_{in} = F_{out} \cdot (1 - \zeta) \quad \text{Eqn. 2.3}$$

The absorption coefficient,  $b_{abs}$ , can be calculated using the attenuation coefficient and the multiple scattering parameter,  $C$  (Weingartner et al., 2003), which is based on the filter material and pre-defined by the user.

$$b_{abs} = \frac{b_{atn}}{C} \quad \text{Eqn. 2.4}$$

With the incorporation of the mass absorption cross section,  $\sigma_{air}$ , which has values set by the manufacturer for each wavelength (Table 2.4), the absorption coefficient can be accurately converted to the equivalent black carbon (eBC) mass concentration:

$$eBC = \frac{b_{abs}}{\sigma_{air}} \quad \text{Eqn. 2.5}$$

The mass absorption cross section (MAC) value relates the absorption efficiency of a particle per unit mass (Bond & Bergstrom, 2006; Knox et al., 2009). Uncoated, freshly emitted BC has a MAC value of  $7.5 \pm 1.2 \text{ m}^2 \text{ g}^{-1}$  at 550 nm (Bond & Bergstrom, 2006). In conjunction with the multiple scattering parameter, the MAC values (Table 2.4) are employed by the AE33 aethalometer to evaluate eBC concentration (Drinovec et al., 2015).

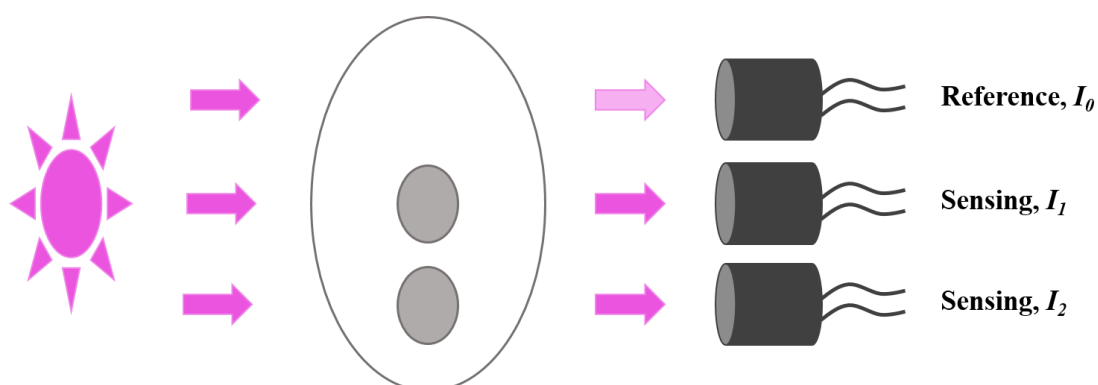


**Figure 2.6** Schematic of measurement of light attenuation. Adapted from Magee Scientific (2016).

The ‘filter loading’ effect is accounted for in the aethalometer by using a ‘real-time loading effect compensation algorithm based on a two parallel spot measurement of optical absorption’ (Drinovec et al., 2015). Briefly, by making two simultaneous measurements, BC1 and BC2, at different degrees of loading,  $ATN1$  and  $ATN2$  respectively, it is possible to eliminate the loading effect. From the two linear equations below, the loading compensation parameter,  $k$ , can be calculated:

$$BC1 = BC \cdot \{1 - k \cdot ATN1\} \quad \text{Eqn. 2.6}$$

$$BC2 = BC \cdot \{1 - k \cdot ATN2\} \quad \text{Eqn. 2.7}$$

The AE33 provides the value of BC extrapolated back to ‘zero loading’ by combining the data according to the above equations. It also provides real-time data on the ‘loading compensation parameter’,  $k$ , providing insights into the nature and composition of sampled aerosol.

A final calculation for the equivalent black carbon mass concentration can be obtained by combining the above equations:

$$eBC = \frac{S \cdot (\Delta ATN / 100)}{F_1(1 - \zeta) \cdot \sigma_{air} \cdot C \cdot (1 - k \cdot ATN_\lambda) \cdot \Delta t} \quad \text{Eqn. 2.8}$$

**Table 2.4** Wavelengths and corresponding mass absorption cross section values employed in calculations.

<b>Channel</b>	<b>Wavelength (nm)</b>	<b>Mass absorption cross section, <math>\sigma_{\text{air}}</math> (<math>\text{m}^2 \text{g}^{-1}</math>)</b>
1	370	18.47
2	470	14.54
3	520	13.14
4	590	11.58
5	660	10.35
6	880	7.77
7	950	7.19

### 2.2.2.2 Source Apportionment Analysis

---

Software developed by the manufacturer is installed on the AE33 aethalometer. This software controls the instrument, provides an accessible interface for the user to control operations and allows for the storage of numerous data parameters. During sampling, the instrument saves parameters to internal memory, which can later be exported as ‘.dat’ files. The principal parameters exported in the ‘.dat’ format are the attenuation measurements for the three spots, the calculated equivalent black carbon mass concentration value for each of the spots and the filter loading correction parameter,  $k$ . A new data file is automatically created each day. Additionally, a log file is created each day in order to record any adjustments made by the user to the operational parameters and to document changes in the status of the instrument.

The instrument performs basic source apportionment analysis on the measured equivalent black carbon mass concentration, based on wavelength dependent absorption efficiency. This model is a linear regression of carbonaceous material with respect to the absorption coefficients at various wavelengths of particles originating from distinct sources (Sandradewi, Prévôt, Szidat et al., 2008). The analysis employs absorption Ångström exponent (AAE) or alpha ( $\alpha$ ) values to differentiate between various sources of equivalent black carbon; biomass burning (eBC<sub>bb</sub>) and fossil fuel related (eBC<sub>ff</sub>) emissions. This exponent can be used to describe the spectral dependence of absorption, where  $b_{abs}$  is the absorption coefficient and  $\lambda$  is the wavelength:

$$b_{abs} \propto \lambda^{-\alpha} \quad \text{Eqn. 2.9}$$

It follows that the  $\alpha$  value is the exponential slope of the regression model for absorption as a function of wavelength (Grange et al., 2020; Moosmüller et al., 2011). Previous studies (Sandradewi, Prévôt, Weingartner et al. (2008) and references therein) have shown that the organic components present in wood smoke tend to absorb strongly in the UV region, while traffic-related emissions result in strong IR absorption, closer to a wavelength of 880 nm. The default values of  $\alpha_{ff} = 1$  and  $\alpha_{bb} = 2$  for fossil fuel related and biomass burning related emissions, respectively, are used in

the on-line analysis. This source apportionment approach will be referred to as the aethalometer model hereafter.

A range of values associated with traffic and wood burning have been quoted in the literature, often ranging between 0.9 – 1.1 and 1.6 – 2.5, respectively (Aas et al., 2017; Buckley, 2019; Crilley et al., 2015). Sandradewi, Prévôt, Szidat et al. (2008) proposed values of 1.10 and 1.86 for traffic and wood burning respectively following a study in an Alpine valley during the winter months, where wood smoke and traffic emissions were the only two sources contributing to ambient PM<sub>1</sub>. More recently, Zotter et al. (2017) recommended the use of 0.9 and 1.68 as the best combination of AAE values for traffic-related and wood burning emissions, respectively.

$$\frac{b_{abs}(470 \text{ nm})_{ff}}{b_{abs}(950 \text{ nm})_{ff}} = \left(\frac{470}{950}\right)^{-\alpha_{ff}} \quad \text{Eqn. 2.10}$$

$$\frac{b_{abs}(470 \text{ nm})_{bb}}{b_{abs}(950 \text{ nm})_{bb}} = \left(\frac{470}{950}\right)^{-\alpha_{bb}} \quad \text{Eqn. 2.11}$$

$$b_{abs}(470 \text{ nm}) = b_{abs}(470 \text{ nm})_{ff} + b_{abs}(470 \text{ nm})_{bb} \quad \text{Eqn. 2.12}$$

$$b_{abs}(950 \text{ nm}) = b_{abs}(950 \text{ nm})_{ff} + b_{abs}(950 \text{ nm})_{bb} \quad \text{Eqn. 2.13}$$

In the above equations,  $b_{abs}(\lambda)$  corresponds to the absorption coefficient,  $\lambda$  corresponds to the wavelength,  $b_{abs}(\lambda)_{ff}$  corresponds to the fossil fuel fraction and  $b_{abs}(\lambda)_{bb}$  corresponds to the biomass burning fraction of the absorption coefficient. The portion of biomass burning,  $BB(\%)$ , is calculated as:

$$BB(\%) = \frac{b_{abs}(950 \text{ nm})_{bb}}{b_{abs}(950 \text{ nm})} \quad \text{Eqn. 2.14}$$

and the biomass burning and fossil fuel related black carbon fractions are calculated as:

$$BC_{bb} = BB \cdot BC$$

*Eqn. 2.15*

$$BC_{ff} = (1 - BB) \cdot BC$$

*Eqn. 2.16*

### 2.2.3 Total Carbon Content of Ambient Aerosol

---

A newly developed instrument, the Total Carbon Analyzer (TCA-08, Magee Scientific) (Rigler et al., 2020) was deployed for the on-line measurement of total, organic and elemental carbon present in ambient aerosol in Pearse Street, Dublin city (May – October 2019) and Enniscorthy, Co. Wexford (December 2019 – January 2021).

This instrument employs thermal methods for the determination of ambient total carbon (TC) concentration. A schematic diagram of the instrument is shown in Figure 2.7. Ambient aerosol is collected on a quartz fibre filter enclosed in a stainless-steel chamber at a flow rate of  $16.7 \text{ L min}^{-1}$  for a specific sampling period, which is user-defined. To allow for continuous sample collection and thermal analysis, the instrument is comprised of two identical channels. Alternation between these two channels is controlled by a system of ball valves. As one channel collects ambient sample on a spot area of  $4.9 \text{ cm}^2$ , the opposite channel proceeds with thermal analysis of the sample collected during the previous sampling period. The analysis duration is 17 minutes. During this time, high powered electrical elements, located above and below the filter, heat the sample almost instantaneously to  $940 \text{ }^\circ\text{C}$ . Due to this ‘flash heating’, the carbonaceous material is combusted efficiently to  $\text{CO}_2$ . The amount of  $\text{CO}_2$  produced is large in comparison to the internal volume of the system. A pulse of short duration, but with a well-defined amplitude over the baseline, is created in the analytical air flow (Rigler et al., 2020). The  $\text{CO}_2$  signal is measured using an absolute, non-dispersive infrared (NDIR) gas analyser (LI-840A  $\text{CO}_2/\text{H}_2\text{O}$  Analyzer, LI-COR Inc., 2016). The concentration of  $\text{CO}_2$  over the baseline is accurately measured and integrated to allow determination of the total carbon content of the collected sample.

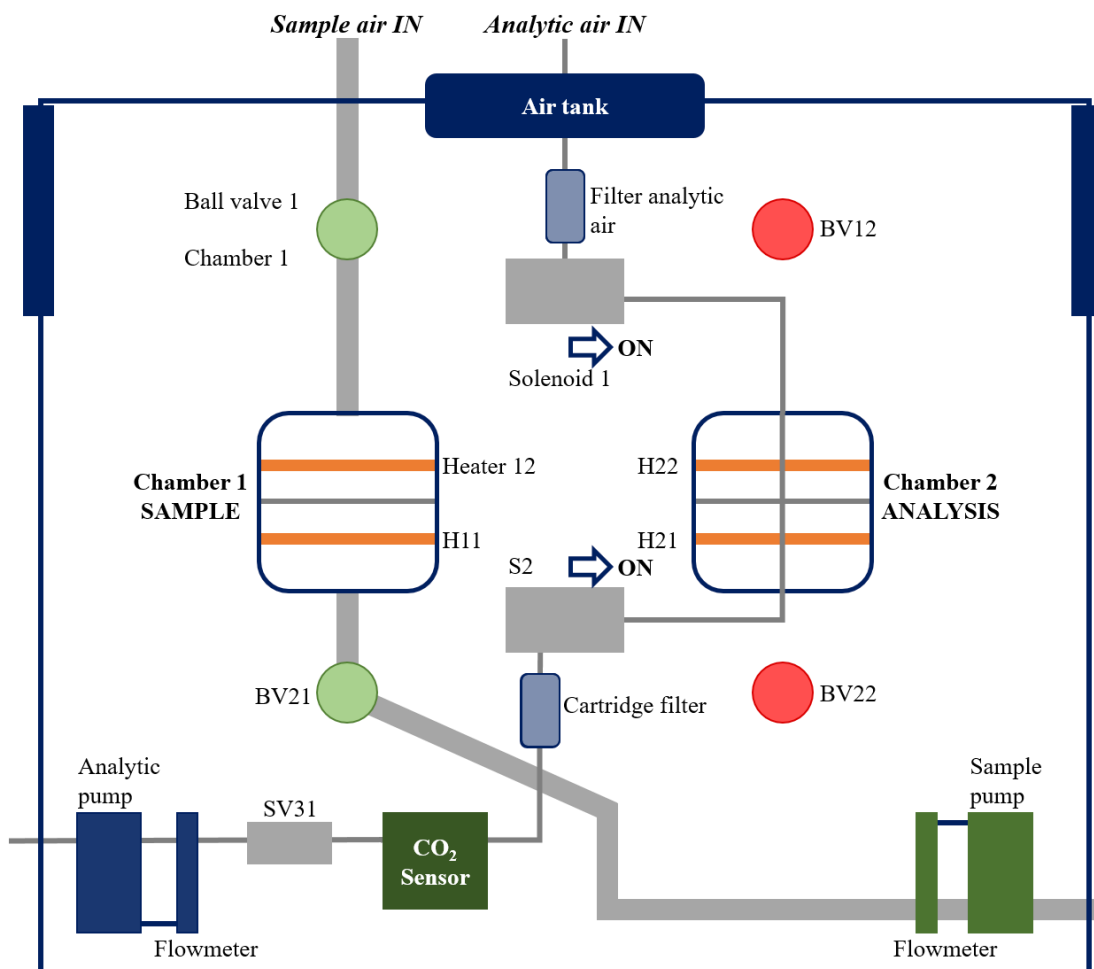
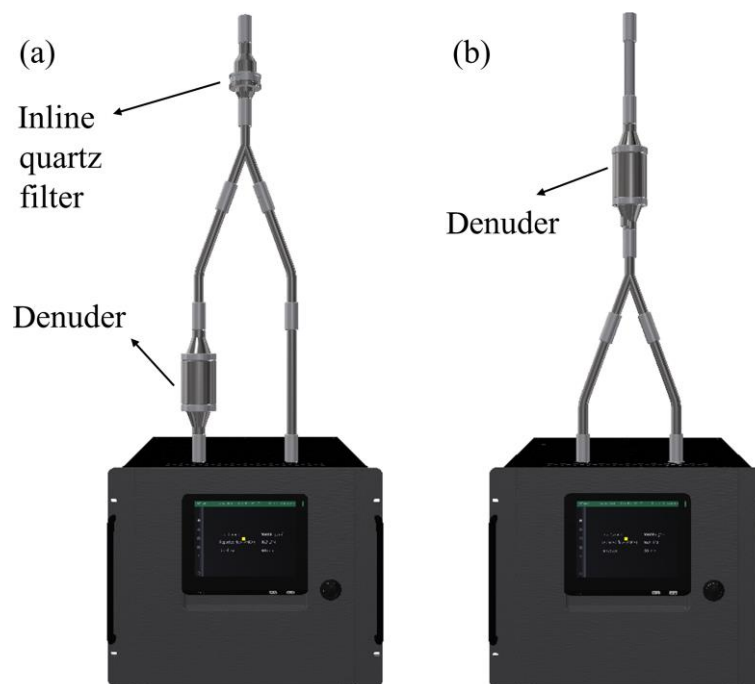


Figure 2.7 Schematic diagram of the TCA-08. Adapted from Rigler et al. (2020).

The use of ambient air as the analytical carrier gas is extremely advantageous as it avoids the need for high-purity compressed gas to be present on site. The air flow of  $0.5 \text{ L min}^{-1}$  is filtered and buffered in an internal volume of 10 L, to account for the ambient fluctuation of  $\text{CO}_2$ . Before flowing through the quartz fibre filter, the air stream flows through an activated charcoal denuder, which traps and removes any organic gases which would otherwise be absorbed by the filter. Over time, the efficiency of the denuder decreases as the surfaces become occupied by the organic species. The efficiency of the denuder,  $E_D$ , is assessed using the configuration shown in Figure 2.8.

$$E_D = \left[ \frac{1}{n} \sum_n \frac{TC_{F,n} - TC_{F+D,n}}{TC_{F,n}} \right] \cdot 100 \quad \text{Eqn. 2.17}$$

In Eqn. 2.17,  $TC_{F+D,n}$  is the  $n$ -th Total Carbon measurement in chamber 1, where the sample airflow passes through the filter above the divider and denuder and  $TC_{F,n}$  is the  $n$ -th Total Carbon measurement in chamber 2, where the sample airflow passes through the filter above the divider only (Magee Scientific, 2018).



**Figure 2.8** TCA-08 setup when (a) performing a denuder efficiency test and (b) sampling (Rigler et al., 2020).

Performing the denuder efficiency test was just one aspect of the quality assurance strategy incorporated into the use of this instrument. Other routine maintenance, calibration and verification procedures employed included quartz filter changes, leakage tests, flow verification and calibration, cleaning procedure, zero verification and carbon calibration. Maintenance activities were carried out in line with procedure and schedule specified in the user manual (Magee Scientific, 2018).

By employing the ‘Quartz filter change procedure’, the instrument automatically checked for leakage and conditioned filters prior to the first sampling period. Regular changing of the filters was recommended to avoid degradation of the filter. The Leakage Test assessed the leakage in chamber flow lines, cartridge filter and CO<sub>2</sub> detector. Determined values below 0.5% were deemed acceptable. Flow verification and calibration was performed using an external flow-meter. The Cleaning Procedure

consisted of running one thermal analysis cycle in order to clean the filter in either Chamber 1 or Chamber 2, as defined by the user. The Zero Verification test was performed to evaluate the reported TC mass on a ‘clean’ filter, by executing one thermal analysis cycle in the preferred chamber. TC mass values below 0.5 µg were acceptable. Carbon calibration was performed by comparing the TC mass content of a dry ambient filter reported by the TCA-08 Offline Procedure and that reported by a calibrated OCEC instrument. The slope of the linear fit was indicative of the Carbon Calibration value.

### 2.2.3.1 ‘TC-BC’ Method

---

Conventional methods of determining the organic and elemental carbon fractions of total measured carbon rely on the volatility of various components of the material, under inert and oxidising atmospheres. However, this recently developed method combines the thermal measurements of total carbon from the TCA-08 with the optical measurements of black carbon from the multi-wavelength AE33 aethalometer (Rigler et al., 2020). The equivalent organic carbon (eOC) portion of the carbonaceous material is defined as:

$$\text{eOC} = \text{TC} - \text{eEC} \quad \text{Eqn. 2.18}$$

where measured black carbon factored by the determined proportionality parameter,  $b$ , is used to determine the equivalent elemental carbon fraction (eEC);

$$\text{eEC} = b \cdot \text{eBC} \quad \text{Eqn. 2.19}$$

The proportionality parameter  $b$  relates the optical measurement of BC and the thermal measurement of EC. As the thermal separation of organic and elemental carbon fractions tend to vary between locations, the  $b$  parameter is site-specific, and is also

largely dependent on the thermal protocol used to determine the EC fraction in traditional OC/EC analytical methods. The default value for  $b$  is 1.

### 2.2.3.2 Calculation of Proportionality Parameter

---

According to Rigler et al. (2020) using an orthogonal regression model without an intercept, the linear relationship between EC and BC is described by slope,  $s$ . The proportionality parameter  $b$  can then be determined (Eqn. 2.20). Unlike the ordinary least squares model which assumes uncertainty applies to only one parameter, the orthogonal regression model minimises the orthogonal distance between the data point and the regression line, taking the uncertainty of both plotted variables into account.

$$b = \frac{1}{s} \qquad \text{Eqn. 2.20}$$

### 2.2.3.3 Off-line Analysis of Filter Samples

---

Ambient aerosol filter samples previously collected by the high volume air sampler can be analysed by the Total Carbon Analyzer in the off-line mode. It is important to have a clean chamber prior to the thermal analysis and new quartz fibre filters must be inserted. The flow chamber should be cleaned by the ‘*Cleaning Procedure*’, followed by the ‘*Zero Verification*’ where one thermal analysis cycle is performed. The mass of total carbon (ng) is determined by completing one full analysis cycle. It is then possible to determine the total carbon concentration (ng cm<sup>-2</sup>) of the filter sample, by entering the punch area prior to starting the analysis.

## 2.3 OFF-LINE ANALYSIS

---

### 2.3.1 Determination of Elemental and Organic Carbon Content

---

The carbonaceous content of ambient samples collected by the high volume air sampler was determined using an OCEC laboratory instrument (Model 5L, Sunset Laboratory Inc.), employing the EUSAAR\_2 protocol (Cavalli et al., 2010).

In this technique, a 1.5 cm<sup>2</sup> punch is taken from the previously exposed filter and placed in the quartz oven. The oven is first purged with helium and the oven temperature is increased according to the temperature ramp set out in the protocol (Table 2.5). During this temperature ramp, the organic compounds and pyrolysis products are thermally desorbed under an inert atmosphere into the oxidising manganese dioxide (MnO<sub>2</sub>) oven. As the carbonaceous material flows through the oxidising MnO<sub>2</sub> oven, it is quantitatively converted to carbon dioxide (CO<sub>2</sub>) gas. Subsequently, the CO<sub>2</sub> gas is carried out of the oven in the helium stream and combined with hydrogen gas. This mixture is finally quantitatively converted to methane as it flows through a heated nickel catalyst, before being measured using a flame ionisation detector (FID). Detailed flow diagrams of the OCEC instrument are shown in Figure 2.9 and Figure 2.10.

The oven is then cooled, and following a switch to an oxidising helium/oxygen carrier gas mixture, the procedure is repeated under an oxidising atmosphere where the elemental carbon is desorbed and enters the oxidising MnO<sub>2</sub> oven. The elemental carbon is detected in the same way as the organic carbon, as evolved CO<sub>2</sub>.

Elemental carbon, exclusively of primary origin, found in ambient air samples is predominantly derived from the incomplete combustion of fossil fuels (Karanasiou et al., 2020). During the initial temperature ramp of this thermal-optical process, charring of the organic carbon can occur, resulting in the formation of elemental carbon on the filter during analysis. This charring is dependent on several factors, including the amount and nature of organic components present and the temperature protocol employed in analysis (Cavalli et al., 2010; Chow et al., 2004; Karanasiou et al., 2015; Sunset Laboratory Inc.). This charring of organic carbon gives rise to an artificially low measurement of organic carbon and an artificially high measurement of elemental carbon. This pyrolysis-induced artefact must be accounted for.

A red light laser is incorporated into the design of the instrument and based on the high light absorbance characteristic of elemental carbon, the pyrolysis-induced artefact may be corrected. The laser passes into the chamber and through the filter as it rests on the sample platform in the oven. The initial transmittance is measured, and as the carbonaceous material is desorbed, the laser transmittance is continuously monitored and decreases with the charring of organic carbon. Under the oxidising atmosphere, when all the elemental carbon has been oxidised off the fibre filter, the laser signal returns to the original background level. Following the analysis, the FID data is reviewed with an overlay of the laser absorbance data. The 'split point' is identified as the point at which the laser transmittance during the oxidising phase equals the initial laser transmittance of the sample pre-analysis. The detection of elemental carbon before this point is categorised as pyrolysed carbon or charred organic carbon. It is, therefore, subtracted from the elemental carbon area and is assigned as organic carbon.

**Table 2.5** The EUSAAR\_2 protocol as described by Cavalli et al. (2010).

<b>Step</b>	<b>Temperature</b>	<b>Duration</b>
	<b>°C</b>	<b>s</b>
He 1	200	120
He 2	300	150
He 3	450	180
He 4	650	180
He/O <sub>2</sub> 1	500	120
He/O <sub>2</sub> 2	550	120
He/O <sub>2</sub> 3	700	70
He/O <sub>2</sub> 4	850	80

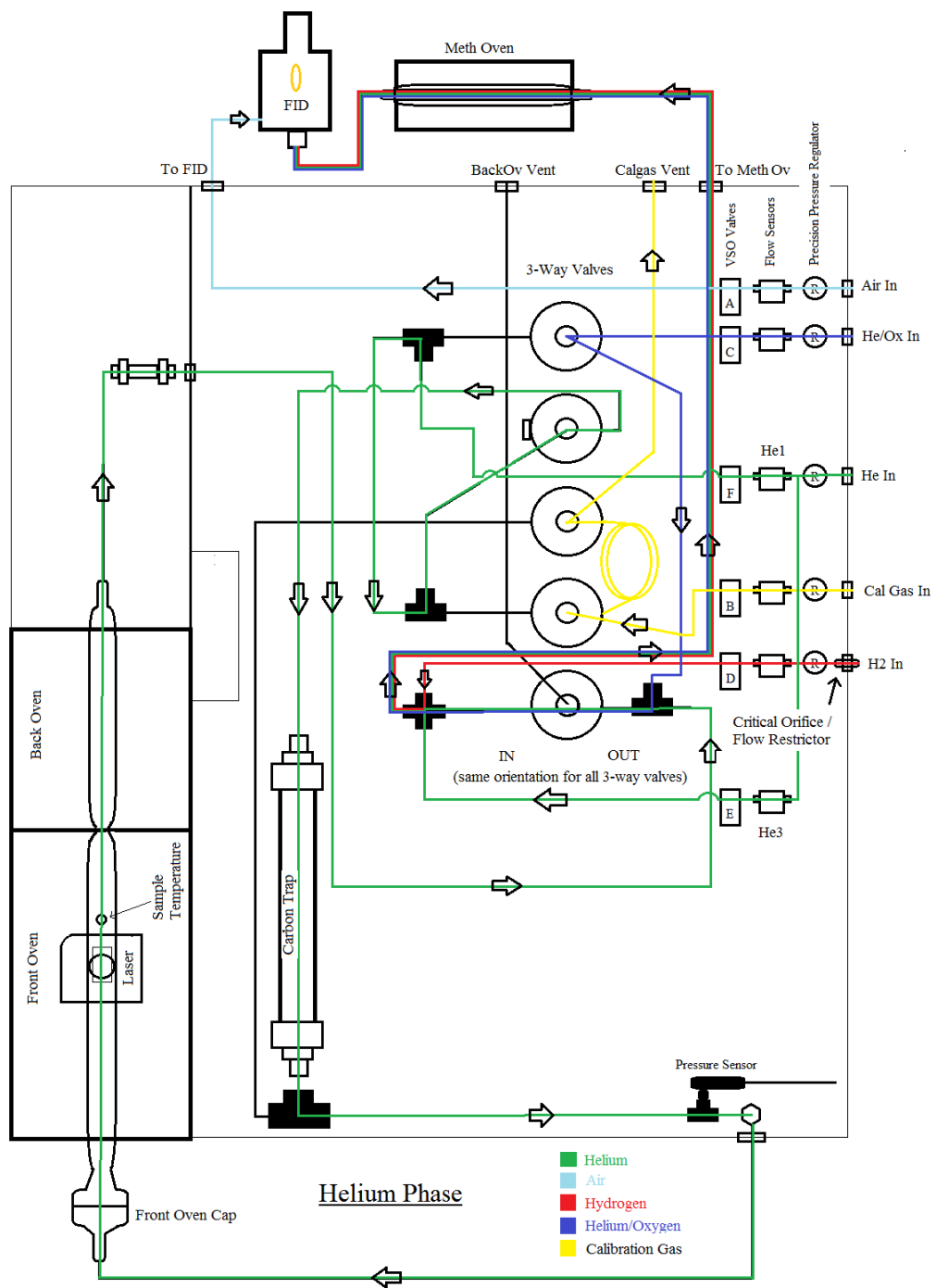
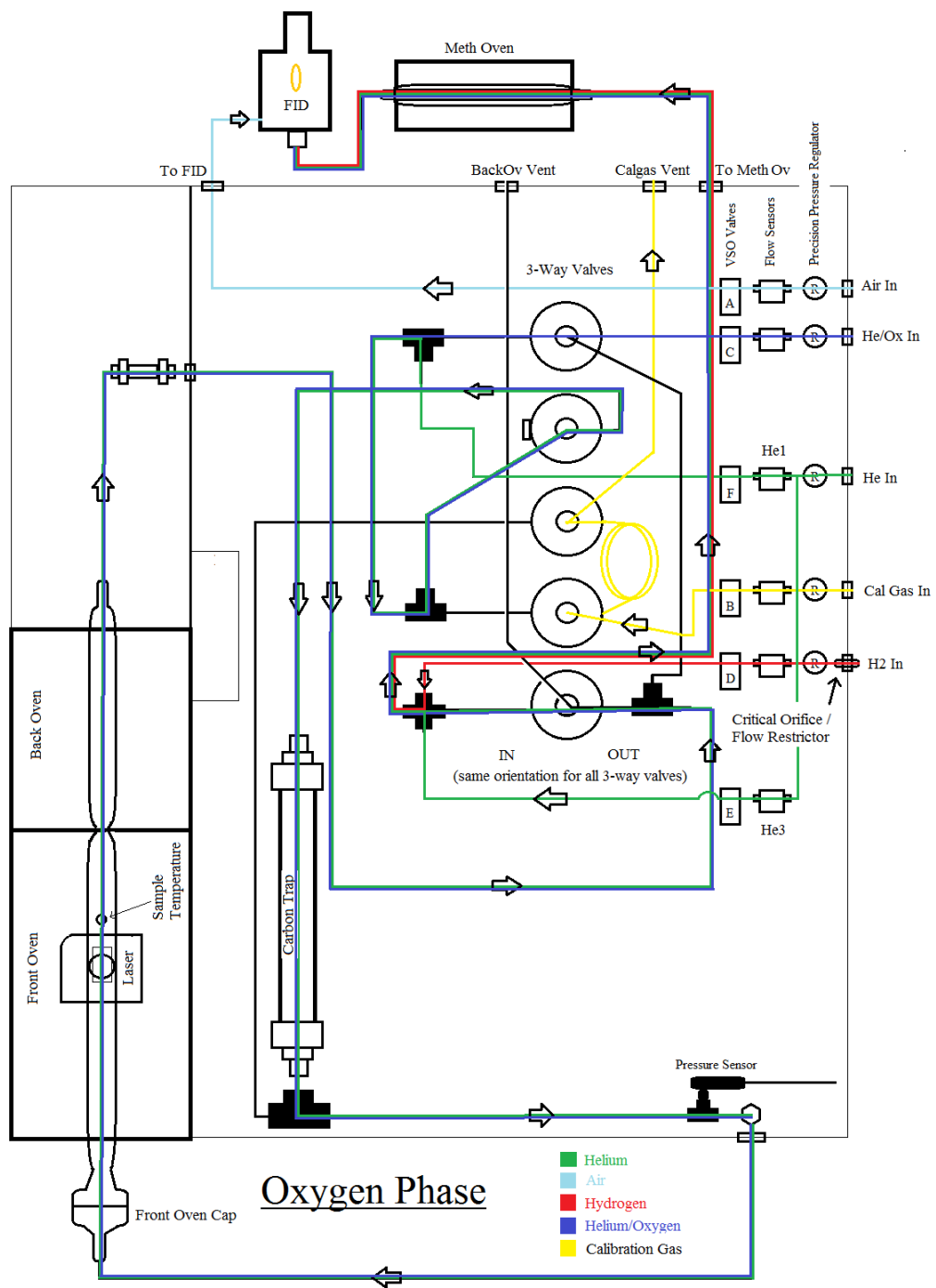


Figure 2.9 Flow diagram of the OCEC instrument under inert conditions (Sunset Laboratory Inc.).



**Figure 2.10** Flow diagram of the OCEC instrument under oxidising conditions (Sunset Laboratory Inc.).

### 2.3.2 Determination of Ambient Anhydrosugar Concentration

Levoglucosan (1,6-anhydro- $\beta$ -D-glucopyranose) is produced from the pyrolysis of cellulose and hemicellulose. Therefore, it can be used as a tracer for biomass burning-derived aerosols. Its isomers; mannosan and galactosan, are also used for the same purpose, although they are often present in much lower concentrations.

Levoglucosan, mannosan and galactosan concentrations were measured using high-performance anion-exchange chromatography coupled with pulsed amperometric detection (HPAEC-PAD) as described by Inuma et al. (2009). This highly selective and sensitive method is convenient for the analysis of levoglucosan in comparison to GC-MS, which is often used. GC-MS analysis of these anhydrosugars can be difficult, due to the polarity of the compounds and the tedious and expensive sample preparation required (Engling et al., 2006; Sullivan et al., 2011). Ion exchange chromatography is a separation technique based on net surface charge. In anion exchange chromatography, a positively charged ion exchange resin is used to separate molecules with a negative surface charge.

The analysis was carried out at the Institute for Tropospheric Research (TROPOS), Leipzig, Germany. Sample preparation consisted of the extraction of a portion of each quartz fibre filter (1.0 cm<sup>2</sup>) in 1 mL ultra-pure (UP) water on a shaker at 420 min<sup>-1</sup> for 120 minutes. The extract was filtered through a syringe filter (0.45  $\mu$ m) to remove any impurities that may have been present.

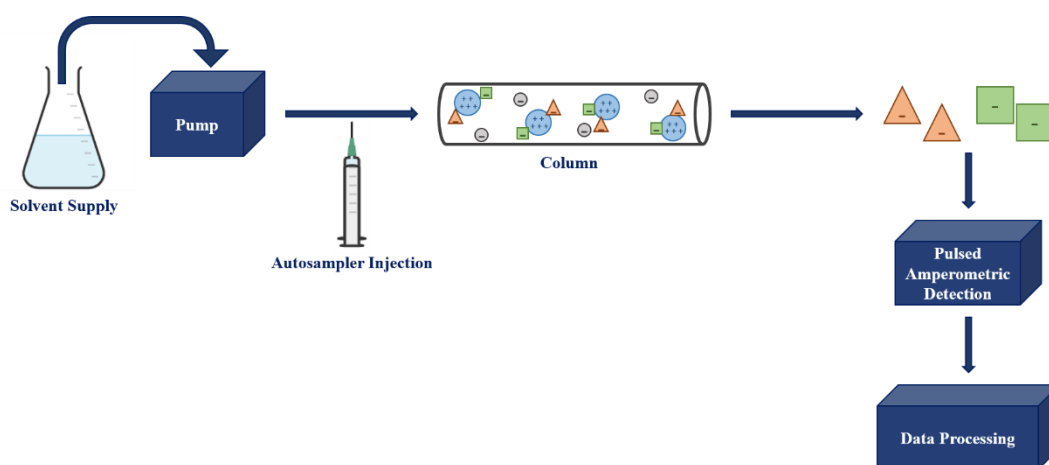


*Figure 2.11 Schematic of general ion exchange chromatography system.*

Analysis was performed using a Dionex ICS-3000 system. Aqueous extracts of filter samples were separated at room temperature on a Dionex CarboPac MA1 column (4 × 250 mm) with a CarboPac MA1 guard column (4 × 50 mm). UP water and 1.0 M sodium hydroxide (NaOH) were used as eluents A and B, respectively, for the separation at a flow rate of 0.4 mL min<sup>-1</sup>. Detection and quantification of the target compound is based on the current generated by the oxidation of the compound at the surface of a gold electrode following application of positive potential (Dionex Technical Note 21).

Analysis of each sample lasted 65 minutes. The autosampler allowed for the continuous analysis of all samples. Six stock solutions containing 11 standards were analysed in conjunction with ambient samples for validation purposes and to evaluate the efficiency of the method. Values ranged from 99% (levoglucosan) to 105% (galactosan). Following pulsed amperometric detection, chromatograms were generated and automatically integrated by the installed software (Dionex Chromeleon Software). It was possible to assess and confirm each chromatogram manually. Finally, a data file, including sample names and the detected concentration (mg L<sup>-1</sup>) of levoglucosan, mannosan and galactosan, as well as a number of other saccharidic tracers, was produced.

## 2.4 DATA MODELLING

---

A variety of data modelling techniques were employed to enhance data analysis and the interpretation of results, namely Back Trajectory Analysis, Positive Matrix Factorization and meteorological normalisation, as outlined below.

### 2.4.1 Back Trajectory Analysis

---

Back trajectory analysis was performed using the Hybrid Single-Particle Lagrangian Integrated Trajectory (HYSPPLIT) model (Draxler & Hess, 1998; Stein et al., 2015) to determine the origin of air masses influencing the sampling sites. The model was run interactively online ([https://www.ready.noaa.gov/HYSPLIT\\_traj.php](https://www.ready.noaa.gov/HYSPLIT_traj.php)) which included meteorological input from the Global Data Assimilation System (GDAS) archive. Back trajectories (72-hour, 48-hour and 24-hour) ending at 500 m above ground level (AGL) at Carnsore Point, Mace Head, Malin Head and University College Dublin were calculated. The output of the model was used to inform source apportionment analysis.

### 2.4.2 Positive Matrix Factorization

---

The Positive Matrix Factorization (PMF) Model is a mathematical receptor model used to analyse environmental sample data. This multi-variate factor analysis tool is often employed in the identification of source types and contributions by reducing a large number of variables in a data set to combinations of species. This dimension reduction can aid in the detection of ‘hidden’ information and explain the variability of the measured variables (Comero et al., 2009). One benefit of the model is the inclusion of known experimental uncertainties as input data, allowing for the individual treatment of matrix elements. In other words, different measurements can be weighted based on their corresponding confidence in the analysis.

The data set can be viewed as a matrix  $X$  of  $i$  by  $j$  dimensions, in which  $i$  number of samples and  $j$  chemical species were measured with uncertainties  $u$ . The aim of the receptor model is to extract source profiles from measured species and temporal trends of source inputs from the temporality of the measured species’ concentrations. The number of factors in the PMF solution,  $p$ , can be determined by the user, based on general guidelines, user-knowledge and location-specific information. The PMF

solution is a solution to Eqn. 2.21, where  $f$  is the species profile of each source,  $g$  is the amount of mass contributed by each factor to each sample and  $e_{ij}$  is the residual for each sample/species (Norris et al., 2014; Paatero, 1997; Paatero & Tapper, 1994).

$$x_{ij} = \sum_{k=1}^p g_{ik} f_{kj} + e_{ij} \quad \text{Eqn. 2.21}$$

The PMF analysis was conducted using EPA Positive Matrix Factorization (PMF) 5.0 (Norris et al., 2014). The model used the off-line measurement of EC and OC fractions of samples collected in Enniscorthy throughout February 2020. The uncertainty associated with the data was calculated using the method detection limit (MDL) and the corresponding method precision, as set out by Norris et al. (2014). The uncertainty ( $unc$ ) was calculated using Eqn. 2.22.

$$Unc = \sqrt{(precision \times concentration)^2 + (0.5 \times MDL)^2} \quad \text{Eqn. 2.22}$$

### 2.4.3 Meteorological Normalisation

---

Meteorological normalisation is a technique employed to investigate the effects of intervention on air quality over a period of time, which controls for weather conditions (Carslaw & Taylor, 2009; Grange et al., 2018). The influence of meteorology can have a significant impact on the concentration of air pollutants, influencing ambient air quality in a given location. Subsequently, trends in pollution concentration, source contribution and the effects of legislation and mitigation strategies can often be difficult to evaluate (Grange & Carslaw, 2019).

The aim of meteorological normalisation is to reduce variability in an air quality time series with statistical modelling. The modelling algorithm employed in the analysis presented in this thesis uses the random forest model (Breiman, 2001), an ensemble decision tree machine learning method. Meteorological normalisation was conducted using the *rmweather* R package (version 0.1.51) (Grange, 2018). The number of trees for the random forest model was fixed at 500, employing *rmweather* function

*'n\_trees'*. The independent variables used were: Unix date (number of seconds since January 1, 1970), Julian day, weekday, hour of the day, maximum air temperature, minimum air temperature, precipitation, atmospheric pressure, wind speed and wind direction.

### 3. CARBONACEOUS AEROSOL IN REGIONAL AND URBAN BACKGROUND ENVIRONMENTS IN IRELAND

---

<b>3.1</b>	<b><i>Aims</i></b> .....	<b>63</b>
<b>3.2</b>	<b><i>Methodology</i></b> .....	<b>65</b>
3.2.1	Sampling Sites.....	65
3.2.2	Instrumentation and Analysis.....	73
<b>3.3</b>	<b><i>Results and Discussion</i></b> .....	<b>76</b>
3.3.1	Meteorological Data.....	76
3.3.2	Equivalent Black Carbon .....	81
3.3.2.1	Temporal Trends.....	81
3.3.2.2	Dependence on Wind Speed and Direction .....	89
3.3.2.3	Diurnal Trends .....	97
3.3.2.4	Delta-C.....	104
3.3.2.5	Source Contribution.....	107
3.3.2.6	Light Absorption of Black Carbon .....	108
3.3.3	Elemental Carbon (EC) and Organic Carbon (OC) .....	112
3.3.4	Calculation of Mass Absorption Cross Section .....	125
3.3.5	Levoglucosan .....	134
3.3.6	Storm Emma: The Beast from the East.....	148
3.3.6.1	Meteorological Conditions .....	148
3.3.6.2	Equivalent Black Carbon.....	152
3.3.6.3	Elemental and Organic Carbon.....	158
3.3.6.4	Levoglucosan .....	159
<b>3.4</b>	<b><i>Conclusions</i></b> .....	<b>160</b>

### 3.1 AIMS

---

Previous research on ambient air quality in Ireland has mainly focused on the comparison and sources of particulate matter in cities and rural towns (Buckley, 2019; Ceburnis et al., 2006; Ovadnevaite et al., 2021; Wenger et al., 2020). However, few studies have investigated the carbonaceous aerosol at background environments across Ireland. In this context, an intensive field campaign was performed in four background environments around Ireland, attempting to characterise the ambient, wintertime carbonaceous aerosol and evaluate the contributing sources in each location. Multi-wavelength aethalometers were deployed, alongside filter sampling equipment, over a period of three months; from December 2017 to February 2018.

With the increasing deployment of the aethalometer across Europe, a field campaign was simultaneously established with the aim of validating the multi-wavelength aethalometer source apportionment approach. The EMEP/ACTRIS/COLOSSAL intensive measurement period took place between December 2017 and February 2018 across Europe, encompassing a variety of monitoring sites, including known low loading areas in Scandinavia and more polluted urban areas in Central Europe. Due to the diversity in environments, ambient samples were expected to differ in both loading and source composition. The field campaign intended to compare on-line measurements of equivalent black carbon attributed to biomass burning ( $eBC_{bb}$ ) and fossil fuel combustion ( $eBC_{ff}$ ), apportioned by the aethalometer model, with off-line filter based measurements of organic (OC) and elemental carbon (EC), and the biomass burning tracer levoglucosan in order to validate the results produced by the aethalometer model. An additional aim of this campaign was to use sophisticated positive matrix factorisation (PMF) analysis to optimise parameter selection in a variety of environments (Aas et al., 2017). In total, 57 monitoring sites across twenty-two countries participated in the field campaign and contributed data (Figure 3.1), including four aforementioned Irish monitoring sites (UNECE, 2020).

The aim of the work presented in this chapter was primarily to evaluate the spatial variability of ambient carbonaceous aerosol, with regard to concentration and major contributing sources, during the winter period. Secondly, off-line measurement techniques were used to quantify elemental, organic and total carbon by thermal-optical methods and levoglucosan by anion-exchange chromatography in order to

assess the functionality of the aethalometer source apportionment model in the Irish environment, within the framework of the EMEP/ACTRIS/COLOSSAL intensive measurement campaign.

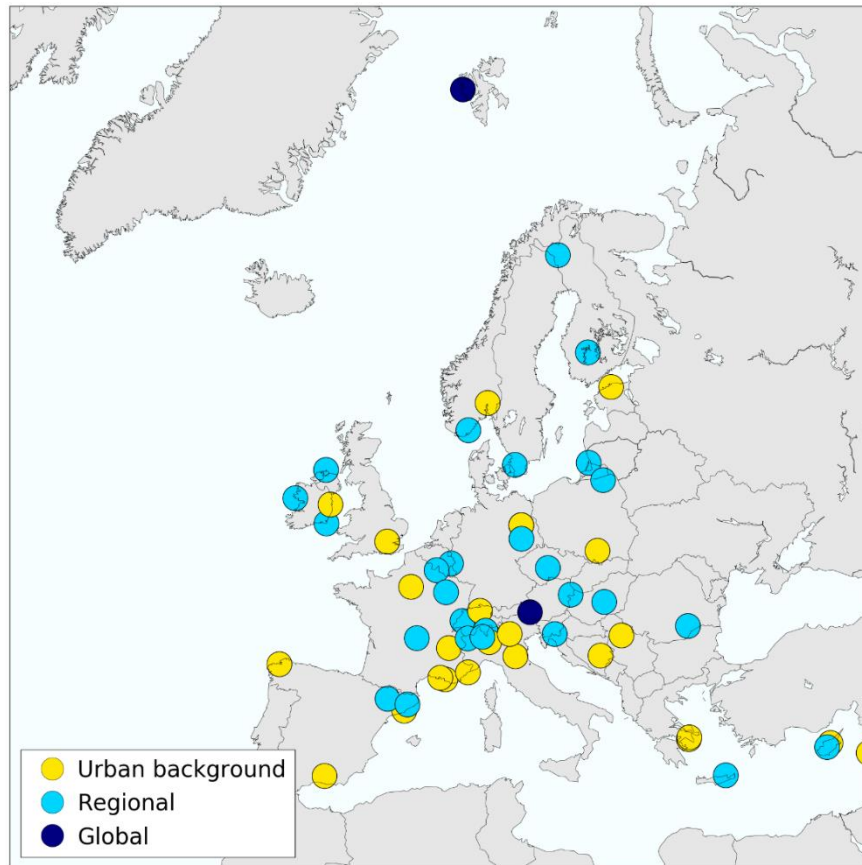


**Figure 3.1** Location of monitoring sites across Europe that contributed to the EMEP/ACTRIS/COLOSSAL intensive measurement field campaign during December 2017 - February 2018 (Colette & Tarasova, 2019).

## 3.2 METHODOLOGY

### 3.2.1 Sampling Sites

Ambient samples were collected at four sites in Ireland during the field campaign (Figure 3.2). The selected sites were Carnsore Point in (Wexford), Mace Head (Galway), Malin Head, (Donegal) and the campus of University College Dublin (Dublin 4). Carnsore Point (CP), Mace Head (MHD) and Malin Head (MLN) were designated as regional background sites, while the University College Dublin (UCD) campus was selected as an urban background monitoring site.

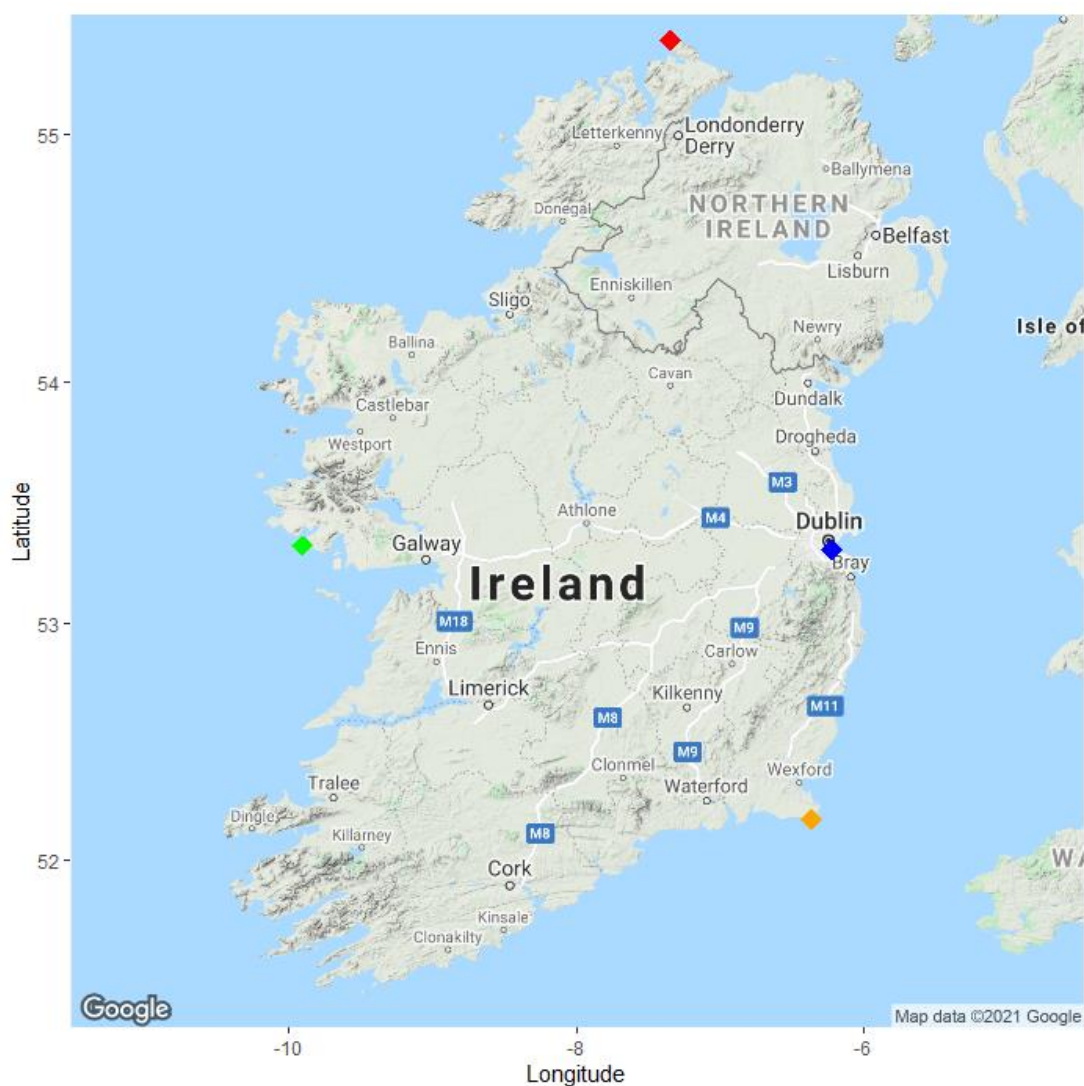


**Figure 3.2** Location of monitoring sites during the wintertime intensive measurement campaign; Carnsore Point (yellow), Mace Head (green), Malin Head (red) and the UCD campus (blue).

Carnsore Point (52° 10' 40.8" N, 6° 21' 54" W) is a headland located on the south east coast of Ireland in County Wexford. There are few dwellings in close proximity to the monitoring site. The monitoring station is situated beside Carnsore Wind Farm, developed by Hibernian Wind Power and is operated in conjunction with the Electricity Supply Board (ESB). Operations at the wind farm, which contains 14 turbines, began in April 2003.

Local meteorological data was obtained from a Met Éireann weather station located in the grounds of Teagasc, Johnstown Castle approximately 16 km northwest of the monitoring site. Meteorological parameters used in the analysis included rainfall (mm), temperature (°C), wind speed ( $\text{m s}^{-1}$ ) and wind direction.

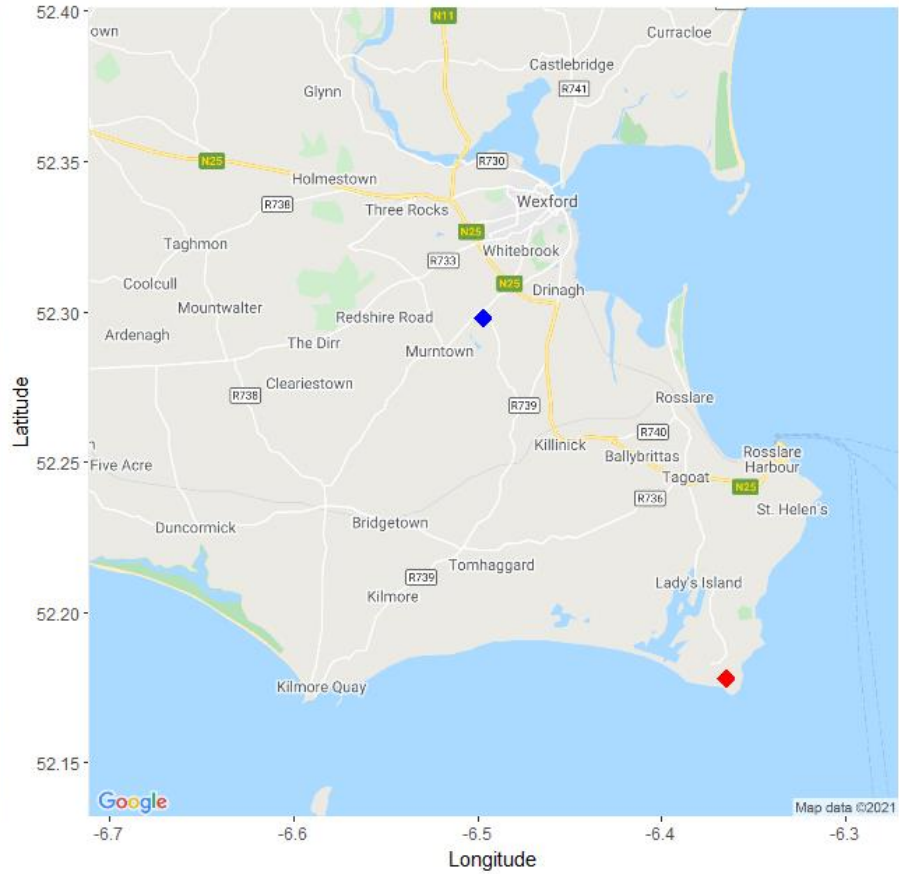
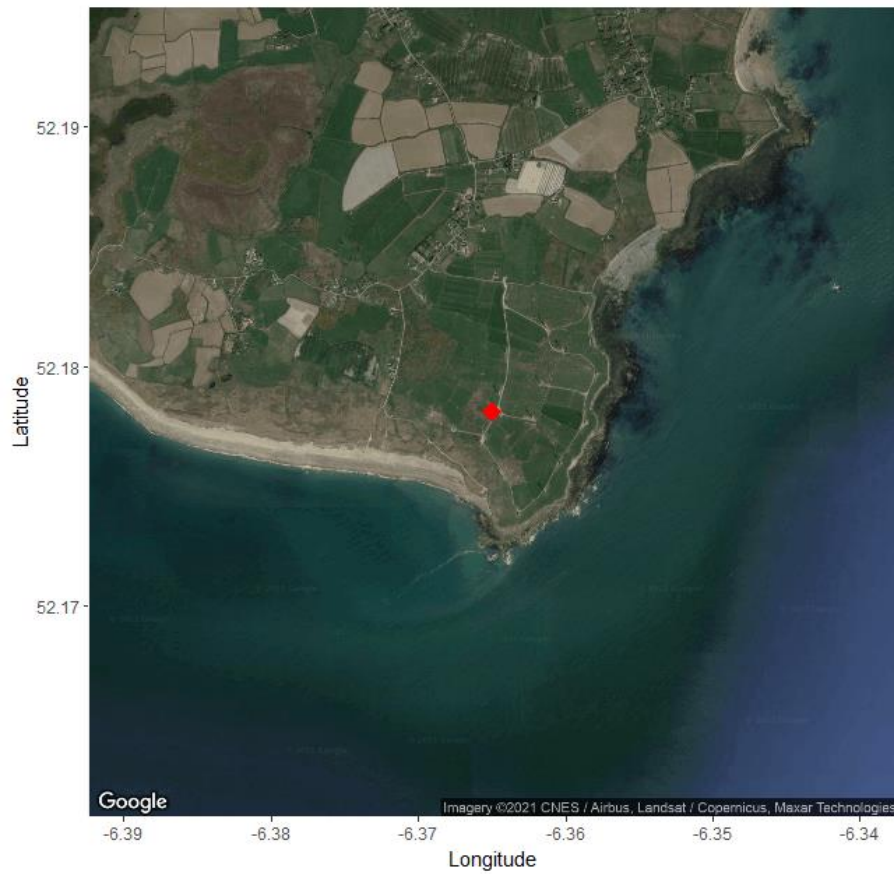


**Figure 3.3** Location of monitoring site (red) at Carnsore Point, Co. Wexford and weather station (blue) at Johnstown Castle, Co. Wexford.

The remote site at Mace Head (53° 19' 33.6" N, 9° 53' 56.4" W) is situated on the west coast of Ireland in County Galway. Due to its exposure to the North Atlantic Ocean, it offers a unique monitoring location in Europe. The monitoring site is approximately 57 km west of Galway city, which has a population of almost 80,000 according to a nationwide census carried out in 2016 (CSO, 2016). The immediate vicinity is sparsely populated. The closest settlements are Roundstone (population ~ 214) and An Cheathrú Rua (population ~ 781) (CSO, 2016), approximately 8 km north-west and 21 km south-east of the monitoring site, respectively. There are a number of off-shore islands to the west of the monitoring site. However these islands are uninhabited.

Filter measurements were collected by a high-volume air sampler (DHA-80, DIGITEL) at a flow rate of 500 L min<sup>-1</sup> which was installed on a 10 m tower adjacent to the shore. Local meteorological data was obtained from a Met Éireann weather station located in the grounds of the monitoring site. Meteorological parameters used in the analysis included rainfall (mm), temperature (°C), wind speed (m s<sup>-1</sup>) and wind direction.

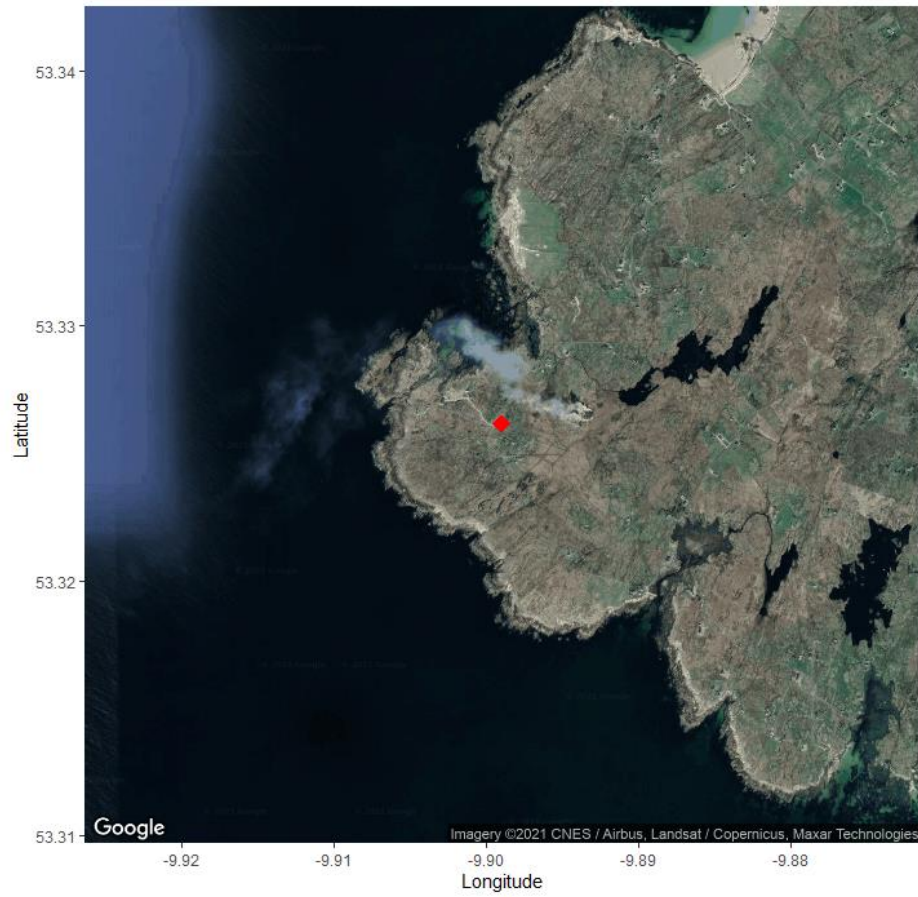


*Figure 3.4 Location of monitoring site at Mace Head, Co. Galway.*

Malin Head (55° 22' 30" N, 7° 20' 34.8" W) in County Donegal was designated as a regional background site for this campaign. The remote site is located on the Inishowen peninsula and is the most northerly point in Ireland. It is a sparsely populated area with the nearest settlements, Culdaff (population ~ 237) and Malin (population ~ 92) (CSO, 2016), approximately 15 and 10 km, respectively, south east of the monitoring site.

Local meteorological data was obtained from a Met Éireann weather station located in the grounds of the monitoring site. Meteorological parameters used in the analysis included rainfall (mm), temperature (°C), wind speed ( $\text{m s}^{-1}$ ) and wind direction.

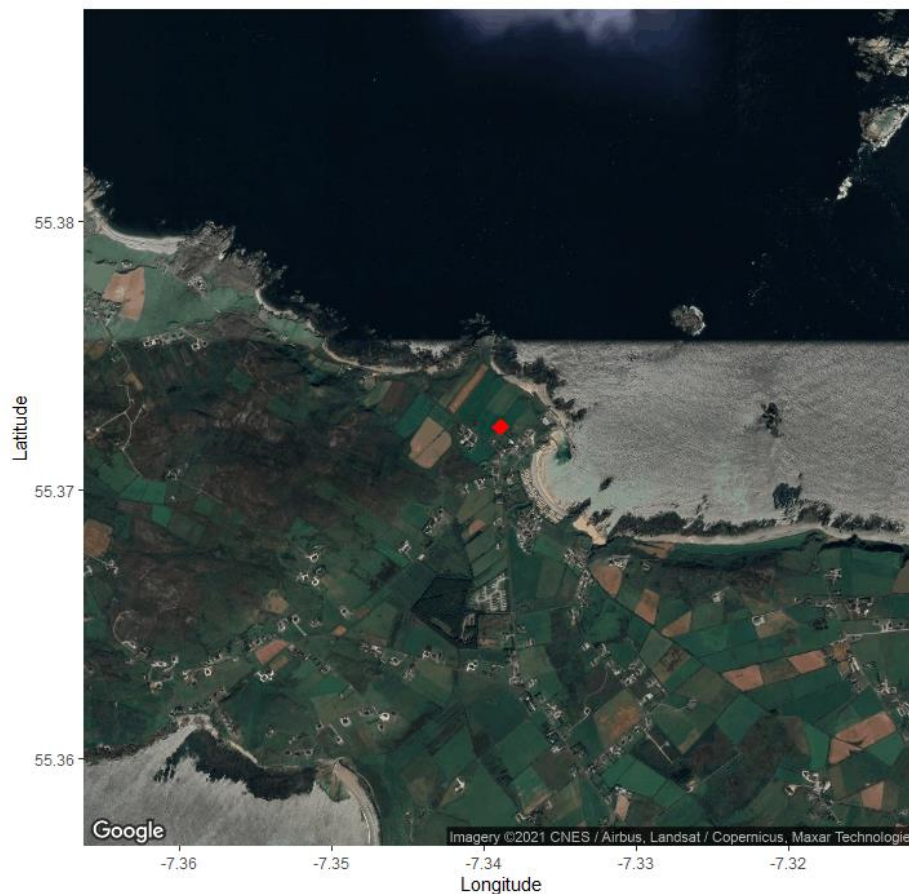


*Figure 3.5 Location of monitoring site at Malin Head, Co. Donegal.*

Sampling of ambient aerosol at an urban background site took place on the campus of University College Dublin (53° 18' 28.8" N, 6° 13' 30" W). Instrumentation was installed in an air-conditioned room on the fourth floor of the north wing of the O'Brien Centre for Science, UCD. The sampling inlet was situated on the roof, approximately 20 m above ground level, and was equipped with a PM<sub>2.5</sub> size selective inlet.

The monitoring site, which is centrally located on the predominantly pedestrianised university campus, is situated 4 km south east of St. Stephen's Green, the heart of Dublin city centre, and approximately 2 km from the coastline of Dublin Bay. Directly to the east of the site (~500 m) is the Stillorgan Road (R138), which develops into the N11 further to the south. This busy route connects Dublin to counties Wicklow and Wexford, and closely passes a variety of significant commuter towns, including Bray and Greystones. It is the only dual-carriageway to pass through the south eastern suburbs of Dublin.

Local meteorological data was obtained from a Met Éireann weather station located in the grounds of Casement Aerodrome, Baldonnell which is approximately 15 km west of the monitoring site. Meteorological parameters used in the analysis included rainfall (mm), temperature (°C), wind speed (m s<sup>-1</sup>) and wind direction.

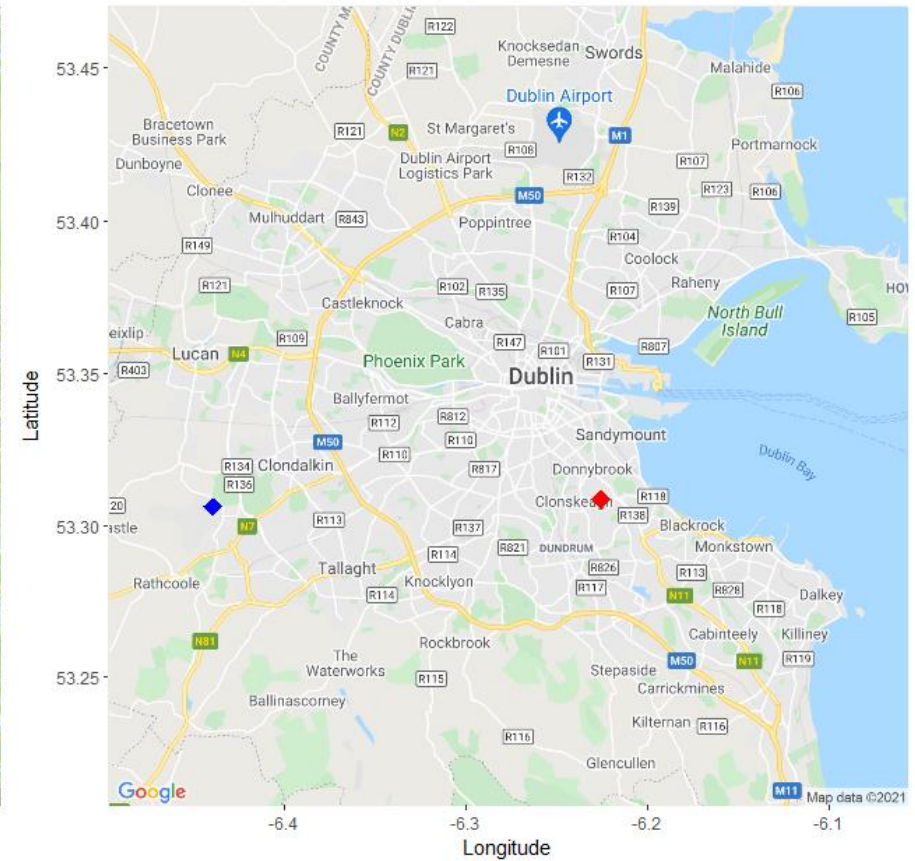


**Figure 3.6** Location of monitoring site on the campus of UCD, Dublin 4 and weather station (blue) at Casement Aerodrome, Co. Dublin.

### 3.2.2 Instrumentation and Analysis

---

The campaign start date was designated as December 1, 2017, however, due to technical difficulties not all instrumentation was on-line at this point. All start dates and data capture percentages are presented in Table 3.1 below. The aethalometer performed well at each sampling site, with stoppages required only for tape advancement and routine maintenance. The operation of ambient filter sampling instrumentation varied. Filter sample collection was continuous throughout the campaign at Carnsore Point and Malin Head. Sample collection was temporarily interrupted at Mace Head and University College Dublin. A number of filter samples collected at Mace Head were damaged and could not be analysed, while filter supply issues interrupted sampling on occasion at UCD.

A multi-wavelength aethalometer was installed at each monitoring site for the full duration of the field campaign, with the exception of Mace Head (Galway) where it was installed on December 21, 2017. The theory of operation of the instrument is outlined in Chapter 2. Source apportionment analysis, based on the aethalometer model developed by Sandradewi, Prévôt, Szidat et al. (2008), was performed by the aethalometer in real-time. The aethalometer employed absorption Ångström exponent ( $\alpha$ ) values of 1 and 2 by default, for the attribution of fossil fuel (eBC<sub>ff</sub>) and biomass burning (eBC<sub>bb</sub>) related emissions, respectively. Based on a comprehensive investigation, the latest, definitive values of 0.9 and 1.68 for the apportionment of eBC<sub>ff</sub> and eBC<sub>bb</sub> related emissions, respectively, were published by Zotter et al. (2017). By comparing the results of eBC source apportionment analysis employing the aethalometer model with <sup>14</sup>C measurements of the fossil fraction of elemental carbon portion of filter samples collected throughout several campaigns in unique locations, an optimal absorption Ångström exponent pair was identified and recommended for use in environments similar to those outlined in the publication; impacted by BC emitted largely by modern road traffic and residential wood burning. These values were applied to analysis completed off-line following the field campaign and will hereafter be referred to as Zotter values. These values are, however, biased towards a continental fuel mixture, which is dominated by wood burning and traffic-related emissions. Therefore, the common nomenclature was adjusted for this study. Source apportioned contributions will be referred to as traffic-related (eBC<sub>Tr</sub>), which incorporates emissions from fossil fuel combustion associated with shipping, an

unnecessary consideration in continental Europe, and solid fuel-related ( $eBC_{SF}$ ) emissions. Despite reference to traffic-related emissions, in environments where coal burning occurs, it is likely that coal will be attributed to this portion of total eBC, as it will appear similar to fossil fuel combustion. ‘Solid fuel’ is used, rather than ‘wood burning’ exclusively, to encompass the variety of fuel types known to influence the Irish environment. A highly oxidised material which absorbs efficiently in the UV region is produced in peat combustion and appears similar to emissions associated with wood burning. It is evident that in a multi-fuel environment, the two source aethalometer model has limited application. Adjustment of the AAE pair to suit the Irish environment was discussed by Buckley (2019), who varied the value of  $\alpha_{SF}$  between 1.5 and 2.2, and  $\alpha_{Tr}$  between 0.9 and 1.1. Optimised pairs for each environment investigated were identified by returning a minimal count of negative values in the splits. Ultimately, it was concluded that, in the absence of AAE values specific to the various fuel types used in Ireland, the best course of action was to employ the accepted AAE pair of 0.9 and 1.68, as recommended by Zotter et al. (2017).

Ambient air samplers facilitated the collection of ambient filter samples which were subsequently analysed to determine elemental, organic and total carbon content, in addition to levoglucosan concentration. Thermal elemental carbon and organic carbon measurements were derived using a thermal-optical analytical technique, which employed the EUSAAR\_2 protocol (Cavalli et al., 2010). Ambient concentrations of levoglucosan, and its isomers, mannosan and galactosan, were determined using anion-exchange chromatographic methods coupled with pulsed amperometric detection, as described by Iinuma et al. (2009).

**Table 3.1** Instrumentation deployed during the wintertime intensive measurement campaign (December 2017 – February 2018).

	<b>Model</b>	<b>Time Resolution</b>	<b>Flow Rate</b> <b>L min<sup>-1</sup></b>	<b>Data Capture</b> <b>%</b>
<b>Carnsore Point</b>				
<i>Aethalometer</i>	AE33-S04-00377	60 s	5	99.94
<i>Ambient Air Sampler</i>	DIGITEL DHA-80	24 hr	500	100
<b>Mace Head</b>				
<i>Aethalometer</i>	AE33-S05-00500	60 s	5	99.06
<i>Ambient Air Sampler</i>	DIGITEL DHA-80	24 hr	500	38
<b>Malin Head</b>				
<i>Aethalometer</i>	AE33-S05-00461	60 s	5	99.88
<i>Ambient Air Sampler</i>	DIGITEL DHA-80	24 hr	500	100
<b>University College Dublin</b>				
<i>Aethalometer</i>	AE33-S02-00246	60 s	4	99.95
<i>Ambient Air Sampler</i>	Partisol 2025i	24 hr 48 hr	16.7	73

### 3.3 RESULTS AND DISCUSSION

---

#### 3.3.1 Meteorological Data

---

The meteorological parameters were obtained from Met Éireann weather stations at Johnstown Castle, Mace Head, Malin Head and Casement Aerodrome as described previously. During the sampling period, temperatures as low as  $-6.2\text{ }^{\circ}\text{C}$  were recorded at Casement Aerodrome, Co. Dublin, while hourly values did not exceed  $14\text{ }^{\circ}\text{C}$  at any of the weather stations. Mean hourly temperatures ranged from  $4.9\text{ }^{\circ}\text{C}$  to  $6.8\text{ }^{\circ}\text{C}$  between December and February, as outlined in Table 3.2 below. The highest hourly wind speeds were recorded at Malin Head, Co. Donegal where hourly wind speeds reached a maximum of  $88.9\text{ km/h}$ . The highest gust recorded at this site was in December 2017 with a speed of  $124.1\text{ km/h}$ , while a gust of  $138.9\text{ km/h}$  was measured at Mace Head in January 2018. Over the entirety of the sampling period a total of  $271.7\text{ mm}$ ,  $395.2\text{ mm}$ ,  $394.9\text{ mm}$  and  $182\text{ mm}$  of rain fell at the weather stations associated with Carnsore Point, Mace Head, Malin Head and the UCD campus, respectively. For Carnsore Point and UCD, this amount of precipitation is within 10% of the mean precipitation for the same period in the preceding decade. However, Malin Head and Mace Head experienced 14% and 22%, respectively, more precipitation than the average value for the sites between 2007 and 2017.

Between February 27 and March 4, 2018 Ireland experienced record low temperatures and significant snowfall as easterly winds swept across the country following sudden stratospheric warming (SSW) events. Due to an exceptionally cold air mass from Siberia, record low temperatures engulfed the country and snow drifts over 2 m were recorded in some locations (Met Éireann, 2019). This extreme event was officially named ‘Storm Emma’ and was commonly referred to as ‘The Beast from the East’. The results discussed in this chapter were obtained between December 1, 2017 and February 25, 2018. It is worth noting that the measurements recorded in late February, which are presented here, may reflect the effects of the approaching severe cold spell and the change in the prevailing wind direction. Measurements continued throughout late February and March, but the results obtained were considerably influenced by this unique weather event. The measurements recorded from February 26, 2018 onwards will be presented in Section 3.3.6.

**Table 3.2** Summary of hourly average meteorological parameters at monitoring sites during the wintertime intensive measurement campaign (December 2017 – February 2018).

	Precipitation (mm)		Temperature (°C)		Wind Speed (m s <sup>-1</sup> )	
	<i>Mean</i>	<i>Range</i>	<i>Mean</i>	<i>Range</i>	<i>Mean</i>	<i>Range</i>
<b>Carnsore Point</b>	0.128	0 – 4.8	5.90	-1.7 – 12.3	5.16	0.51 – 15.43
<b>Mace Head</b>	0.193	0 – 8.4	6.84	-1.4 – 12.2	9.12	0.51 – 23.66
<b>Malin Head</b>	0.189	0 – 7.0	5.93	-1.3 – 12.5	8.96	0.51 – 24.69
<b>University College Dublin</b>	0.086	0 – 5.7	4.93	-6.2 – 13.1	6.10	0.51 – 18.01

The wind rose diagrams in Figure 3.7 describe the frequency of counts for wind direction and wind speeds observed each month during this campaign at the weather stations associated with each monitoring site. The predominant wind direction at each sampling site were westerly and south-westerly. Mace Head and Malin Head experienced the strongest winds, as predicted, owing to their location on the west and north-west coasts of Ireland, as they are most exposed to the strong winds from the North Atlantic Ocean. Carnsore Point and University College Dublin, both situated on the east coast of the country, experienced much lower average wind speeds.

Figure 3.8 illustrates the monthly distribution of recorded temperatures and the measured volumes of precipitation at each of the weather stations during the campaign. The width of the violin plots indicate the frequency of a particular hourly average temperature recorded each month, while the circles expresses whether or not precipitation was recorded, and the amount is represented by the size of the circle. As outlined in Table 3.2, both the minimum (-6.2 °C) and maximum (13.1 °C) temperatures recorded during the sampling period were measured at the weather station associated with the monitoring site at University College Dublin, representative of the largest range in temperatures.

A maximum value of 34.3 mm of rain was recorded over a 24-hour period at Carnsore Point in December 2017. On average, UCD was the driest site with a daily mean of only 2.06 mm of rain. Carnsore Point, Mace Head and Malin Head had mean values of 3.08 mm, 4.63 mm and 4.54 mm, respectively, in a 24-hour period between December 2017 and February 2018.

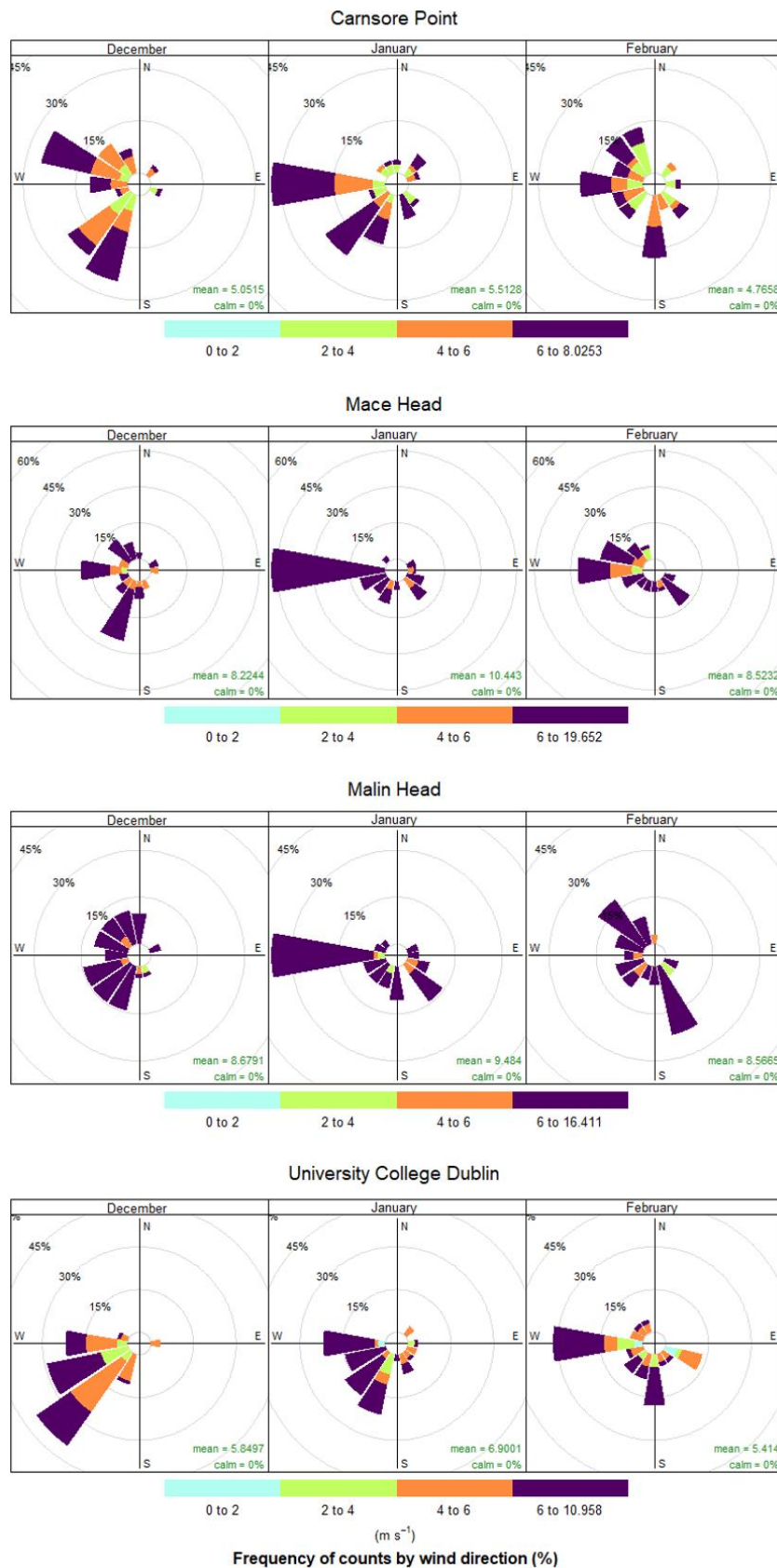


**Figure 3.7** Wind rose plots for Carnsore Point, Mace Head, Malin Head and UCD during the wintertime intensive measurement campaign (December 2017 – February 2018).

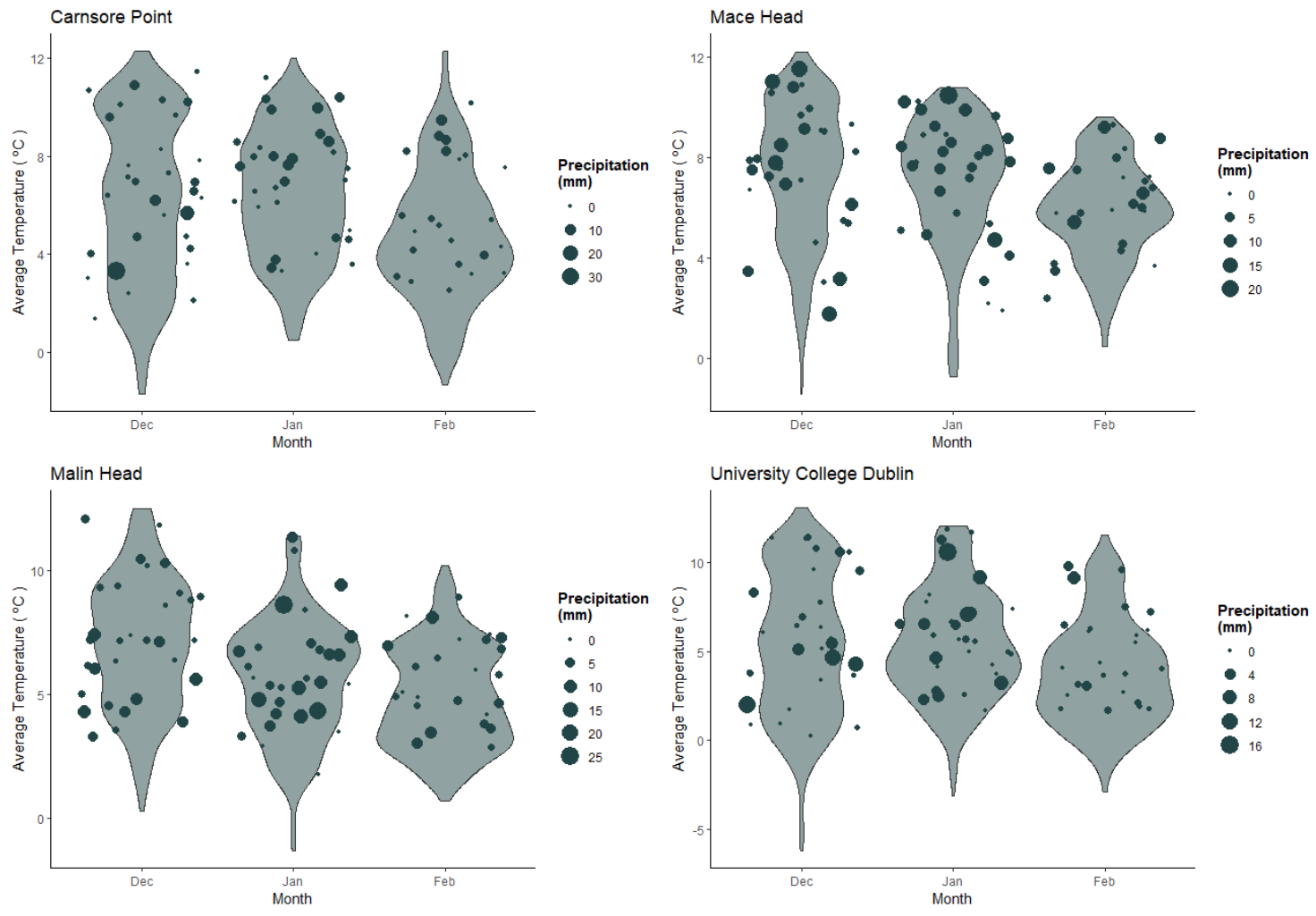


Figure 3.8 Temperature distribution and precipitation recorded during the wintertime intensive measurement campaign (December 2017 – February 2018).

### 3.3.2 Equivalent Black Carbon

---

Black carbon concentrations were measured continuously by multi-wavelength aethalometers at each of the four sites between December 2017 and March 2018. The data capture for each of the instruments employed throughout the campaign (> 99%) is outlined in Table 3.1. Absent data is due to instrument stoppages for routine maintenance while on site.

#### 3.3.2.1 Temporal Trends

---

The highest concentrations of black carbon were observed at the monitoring site on the UCD campus; the only designated urban background site. Black carbon concentrations at UCD, measured at 880 nm (BC6), reached a maximum hourly average value of  $16.62 \mu\text{g m}^{-3}$  in February 2018. The mean hourly average BC6 concentration measured at this site was  $0.78 \mu\text{g m}^{-3}$ . In stark contrast, a maximum hourly average BC6 concentration of  $2.91 \mu\text{g m}^{-3}$  was observed at Mace Head, where a mean hourly value of  $0.12 \mu\text{g m}^{-3}$  was measured throughout the winter period. Mean hourly average BC6 concentrations of  $0.27 \mu\text{g m}^{-3}$  and  $0.28 \mu\text{g m}^{-3}$  were recorded at Carnsore Point and Malin Head, respectively. Table 3.3 includes the hourly average and 60 second measurement range of equivalent black carbon (eBC) and black carbon measured at 880 nm (BC6) recorded at each monitoring site. Table 3.3 also provides a summary of the mean and standard deviation of eBC and BC6, based on the hourly average concentrations.

As mentioned in Chapter 2, a Clean Air test was set to run automatically at midday every Saturday for the duration of the campaign. This test is used to assess the stability and performance of the multi-wavelength aethalometer under air flow conditions. As particle-free air flows through the system during this test, it is possible to determine the range of uncertainty within the instrument using the values recorded. Between December 1, 2017 and February 25, 2018 the test was run 13 times at each site, with the exception of Mace Head where it was run only 10 times, as continuous monitoring began on December 21, 2017 at this location. Despite a small number of outliers, the measurements recorded during the 60 second intervals typically tended towards zero, as anticipated. Mean black carbon values of  $0.12 \mu\text{g m}^{-3}$ ,  $0.09 \mu\text{g m}^{-3}$ ,  $0.09 \mu\text{g m}^{-3}$  and

0.41  $\mu\text{g m}^{-3}$  were recorded at a wavelength of 880 nm during automatic Clean Air tests at Carnsore Point, Mace Head, Malin Head and University College Dublin, respectively. Minimum values of ambient eBC and BC6 provided in Table 3.3 are negative values at each site. However, following comparison with the range of values observed during the Clean Air test each of the hourly average concentrations recorded were within acceptable limits.

**Table 3.3** Mean and standard deviation of hourly average concentrations of equivalent black carbon (eBC) and black carbon (BC6) measured at each site (December 2017 – February 2018). Maximum and minimum values of equivalent black carbon and black carbon measured at 880 nm are also included.

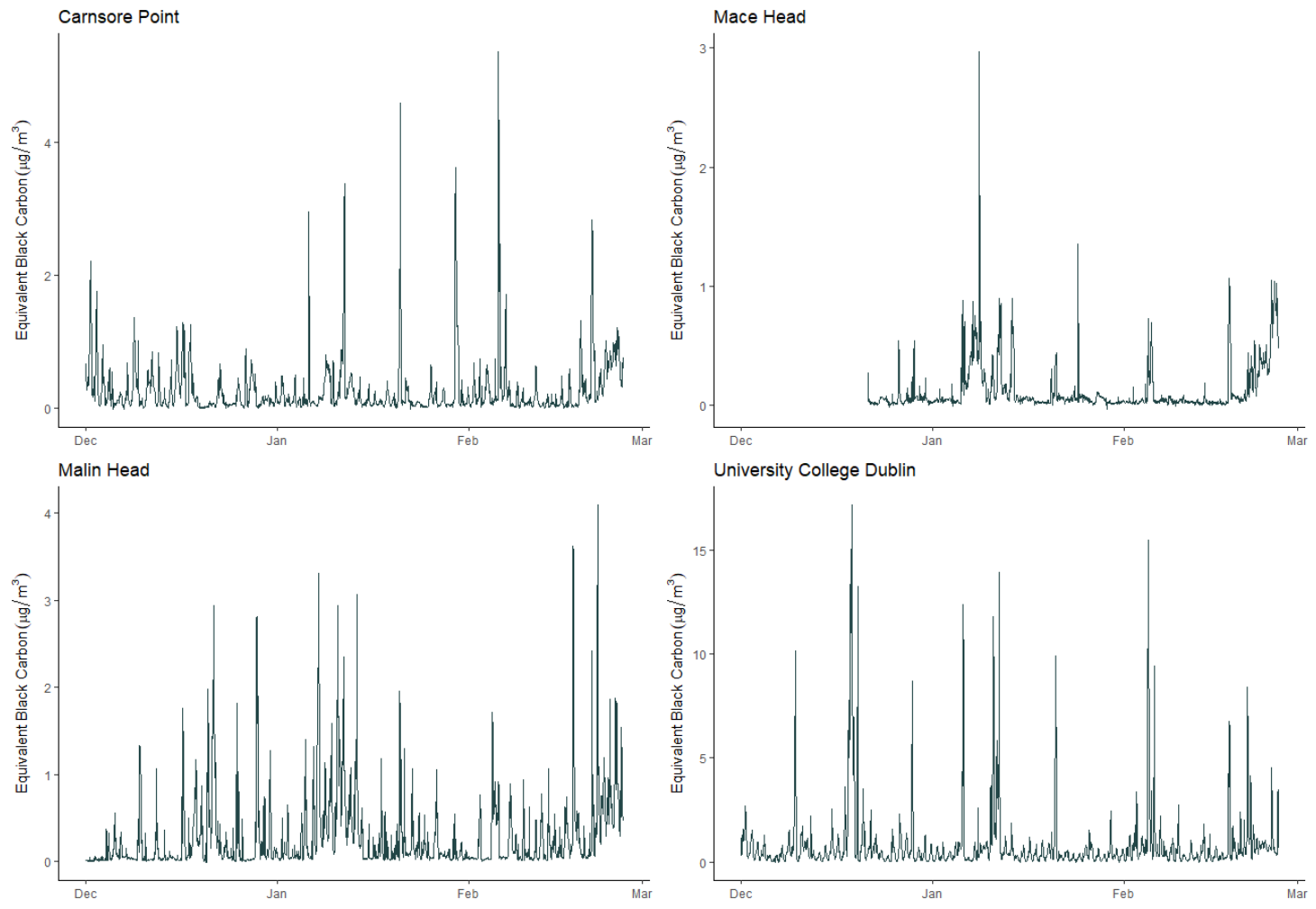
	Equivalent Black Carbon, eBC ( $\mu\text{g m}^{-3}$ )		
	<i>Mean <math>\pm</math> SD</i>	<i>Range</i>	
		<i>Hourly Average Measurement</i>	<i>60 Second Measurement</i>
<b>Carnsore Point</b>	0.27 $\pm$ 0.43	-0.01 – 5.36	-1.70 – 32.79
<b>Mace Head</b>	0.12 $\pm$ 0.21	-0.04 – 2.97	-1.53 – 78.36
<b>Malin Head</b>	0.28 $\pm$ 0.43	-0.01 – 4.10	-1.30 – 31.45
<b>University College Dublin</b>	0.80 $\pm$ 1.62	-0.03 – 17.18	-8.81 – 1096.51
	Black Carbon, BC6 ( $\mu\text{g m}^{-3}$ )		
	<i>Mean <math>\pm</math> SD</i>	<i>Range</i>	
		<i>Hourly Average Measurement</i>	<i>60 Second Measurement</i>
<b>Carnsore Point</b>	0.27 $\pm$ 0.42	-0.03 – 5.29	-1.54 – 31.97
<b>Mace Head</b>	0.12 $\pm$ 0.21	-0.03 – 2.91	-1.56 – 72.18
<b>Malin Head</b>	0.28 $\pm$ 0.42	-0.03 – 4.01	-1.38 – 30.69
<b>University College Dublin</b>	0.78 $\pm$ 1.59	-0.03 – 16.62	-6.85 – 1022.50

Table 3.3 shows a wide range of concentrations at each site throughout the campaign. Mace Head experienced the lowest hourly average ambient concentrations of eBC. A number of significant spikes in concentration were observed on the same dates at each site, most likely due to shared weather events and air masses. A noticeable increase in eBC was observed towards the end of February during the final six days of measurements (February 20 – 25, 2018) at Carnsore Point, Mace Head and Malin Head, however this was not the case at the UCD sampling site (Figure 3.9). During this time period, the mean eBC concentration increased by more than 145%, 360% and 200% at Carnsore Point, Mace Head and Malin Head, respectively. The average concentration recorded at UCD during these six days, though not as considerable as at the other monitoring sites, increased by 25% above the mean concentration of the preceding 11 weeks. This notable increase in eBC concentration coincides with the change in prevailing winds and the arrival of a severely cold air mass from Siberia, resulting in Storm Emma.

A number of pollution events occurred throughout the sampling period illustrated by the temporal profile of recorded equivalent black carbon (Figure 3.9). Several of the events recorded coincided with similar events at other sites, such as on January 20, February 5 and that towards the end of February 2018, as previously discussed. Others were more localised events. In early December 2017, large concentrations of eBC, relative to the entirety of the sampling period, were measured at Carnsore Point, while an increase in concentration was not recorded at the other monitoring sites during the corresponding period. Similarly, at the end of January, Carnsore Point again experienced a significant increase in eBC. On both occasions, the pollution event appeared to be exclusive to that location. During December 17 – 21, 2017 UCD experienced an event which caused an increase in eBC concentrations, including a maximum hourly average in excess of  $17 \mu\text{g m}^{-3}$ . During this time period, Carnsore Point, also located on the east coast of Ireland and approximately 126 km south of Dublin, did not experience such a significant increase in observed concentrations. A slight increase to  $1.26 \mu\text{g m}^{-3}$  was recorded at midnight on December 18 at Carnsore Point, however concentrations had returned to a base level of  $0.15 \mu\text{g m}^{-3}$  by 21:00 that evening.

The Zotter parameters, ( $\alpha_{\text{Tr}} = 0.9$ ,  $\alpha_{\text{SF}} = 1.68$ ) were applied to the data recorded at each site to generate a temporal profile of eBC attributed to solid fuel combustion and

traffic-related emissions (Figure 3.10). It is evident that negative values occurred, most notably in Mace Head and University College Dublin where the lowest and highest respective concentrations of eBC were recorded, leading to uncertainty over the precision of the source apportionment aethalometer model in these environments. At extremely low concentrations of ambient eBC, such as those observed at Mace Head, it appears that the model begins to collapse and no longer accurately apportions measured black carbon to the appropriate sources.



**Figure 3.9** Temporal trends of total equivalent black carbon observed at the monitoring sites during the wintertime intensive measurement campaign (December 2017 – February 2018).

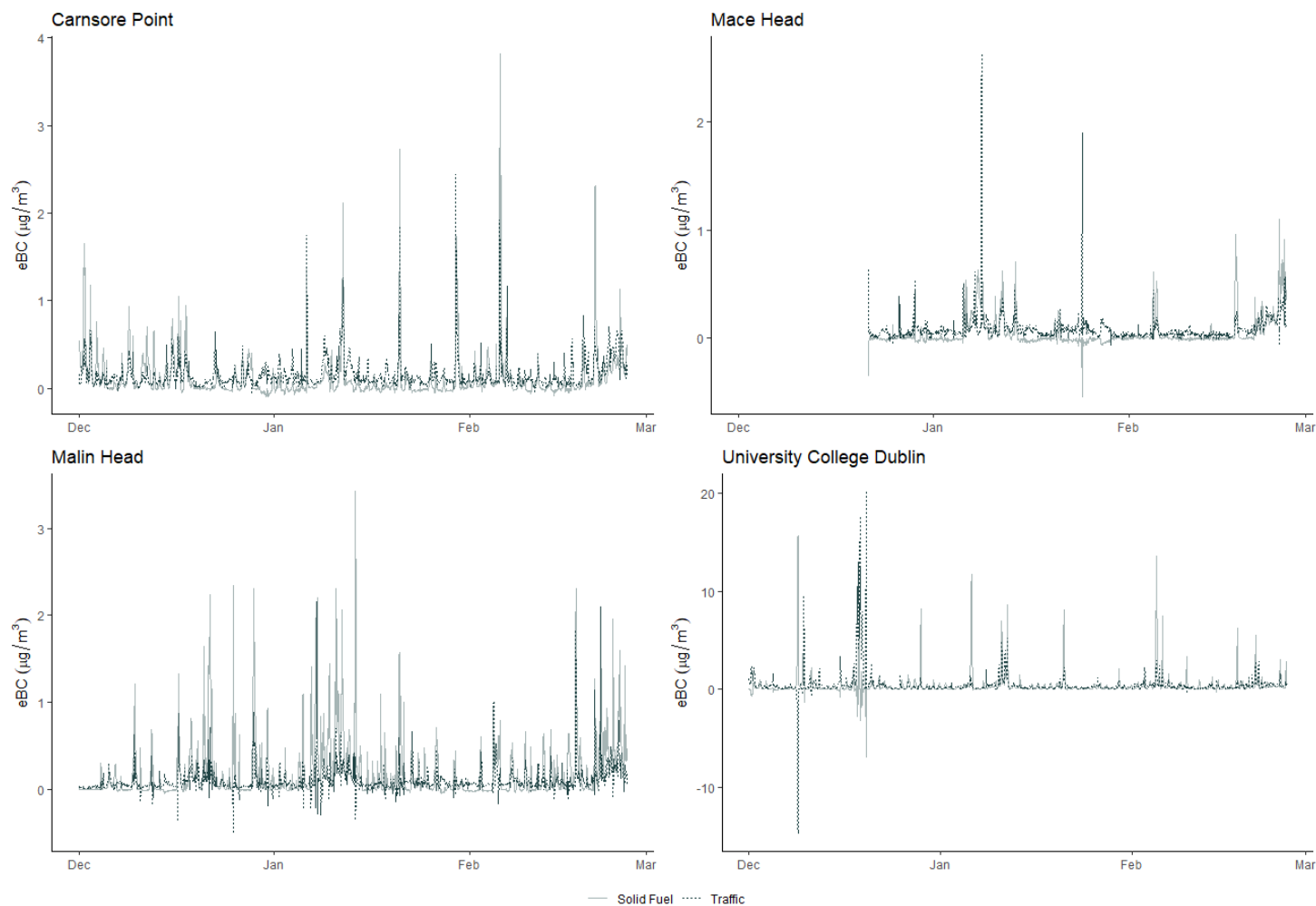


**Figure 3.10** Temporal trend of hourly average  $eBC_{SF}$  and  $eBC_{Tr}$  observed at Carnsore Point, Mace Head, Malin Head and UCD during the wintertime intensive measurement campaign (December 2017 – February 2018).

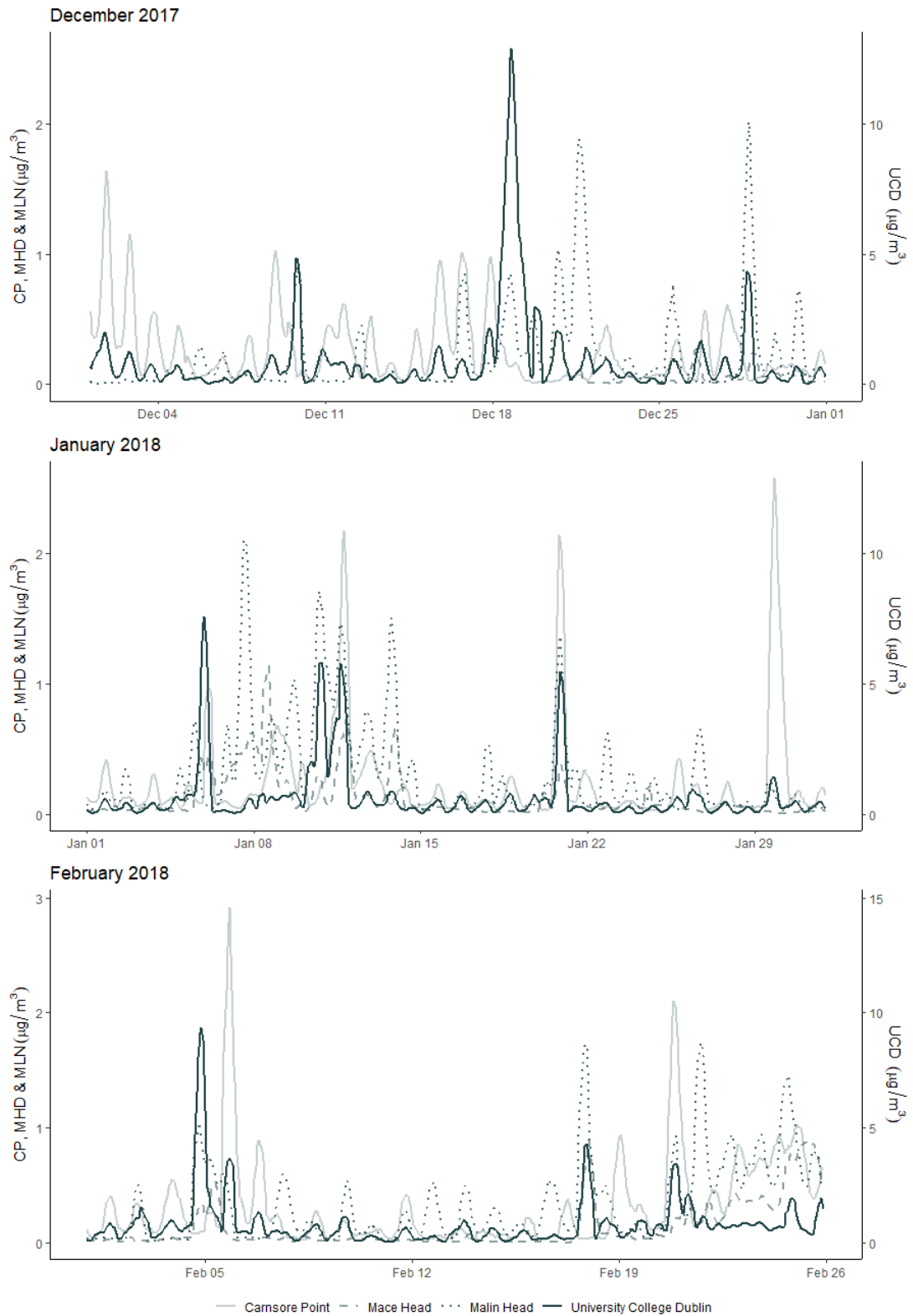


**Figure 3.11** Rolling average (24-hour) of eBC concentration by month (December 2017 – February 2018) at each sampling site.

### 3.3.2.2 *Dependence on Wind Speed and Direction*

---

Wind speed and direction had a pronounced effect on the ambient concentration of black carbon. Figure 3.12, a calendar plot produced using the *Openair* package (Carslaw & Ropkins, 2012) developed using the *R* computer language, illustrates the daily average BC<sub>6</sub> concentration by its colour. The daily average wind direction is represented by the direction of the arrow, while the length of the arrow tail depicts the strength of the wind on a particular day; the longer the arrow, the greater the wind speed. It is clear that on days when ambient concentrations of BC<sub>6</sub> were highest, the wind speeds were at their lowest. This was true for each sampling site. It is worth noting that although each calendar plot has its own scale, concentrations of black carbon were comparable ( $\sim 1 \mu\text{g m}^{-3}$ ) at each site towards the end of February. The easterly air mass had a pronounced effect at the Carnsore Point, Mace Head and Malin Head sampling sites, while at UCD the aerosol carried by the incoming air mass was comparable to background levels, and thus the effects were less prominent.

The dependence of black carbon concentration on wind speed is confirmed further by Figure 3.13. These plots demonstrate that maximum concentrations were observed at minimum wind speeds. The plots also indicate the wind direction with the greatest influence on concentrations at each site. It is unsurprising that the highest concentrations of eBC measured at Mace Head and Malin Head come from the east and south-east, respectively, due to their geographical location. Pollution measured at these sites commonly originates on the land mass of Ireland. It is difficult to extricate the origin of the strongest influential sources at the urban background monitoring site on the campus of UCD, as it is surrounded by pollution sources in all directions. The results observed at Carnsore Point were noteworthy. Due to its geographical location in the south-east of Ireland, it was expected that the majority of equivalent black carbon would come from the north-west; across the landmass. However, comparable concentrations were also detected from the south-east; the seaward direction.

Elevated eBC concentrations originating in the east are most pronounced at all monitoring sites in the month of February (Figure 3.14). Augmentation of the measured concentration is undoubtedly a consequence of the arrival of Siberian air mass which travelled across continental Europe before reaching Irish shores.

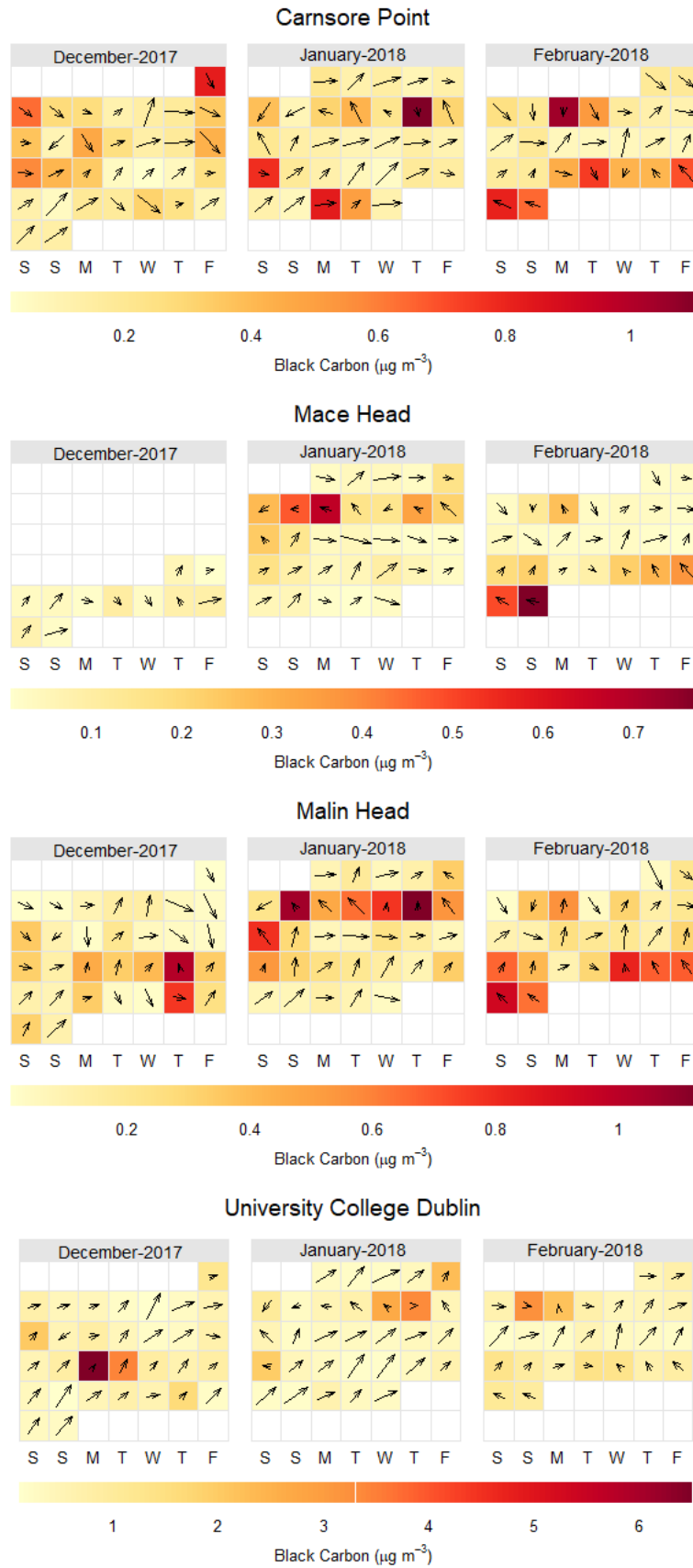


**Figure 3.12** Calendar plots describing the effect of wind speed and direction on BC6 concentration measured at each site.

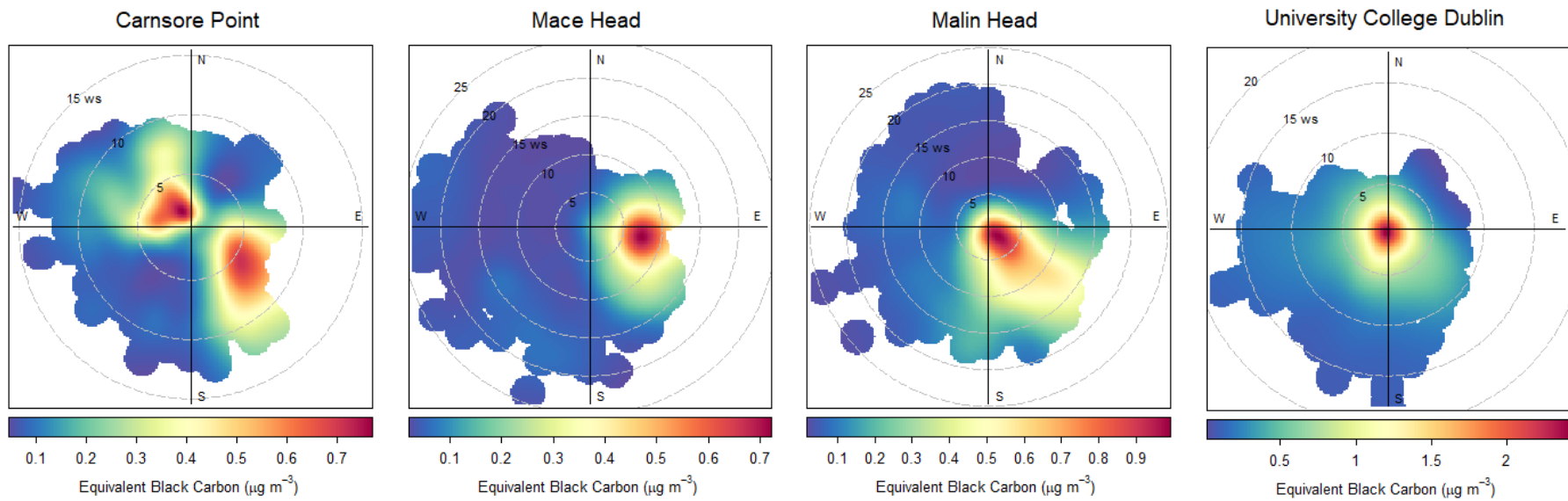


**Figure 3.13** Polar plots describing the wind dependence of mean eBC concentrations during the wintertime intensive measurement campaign (December 2017 – February 2018).

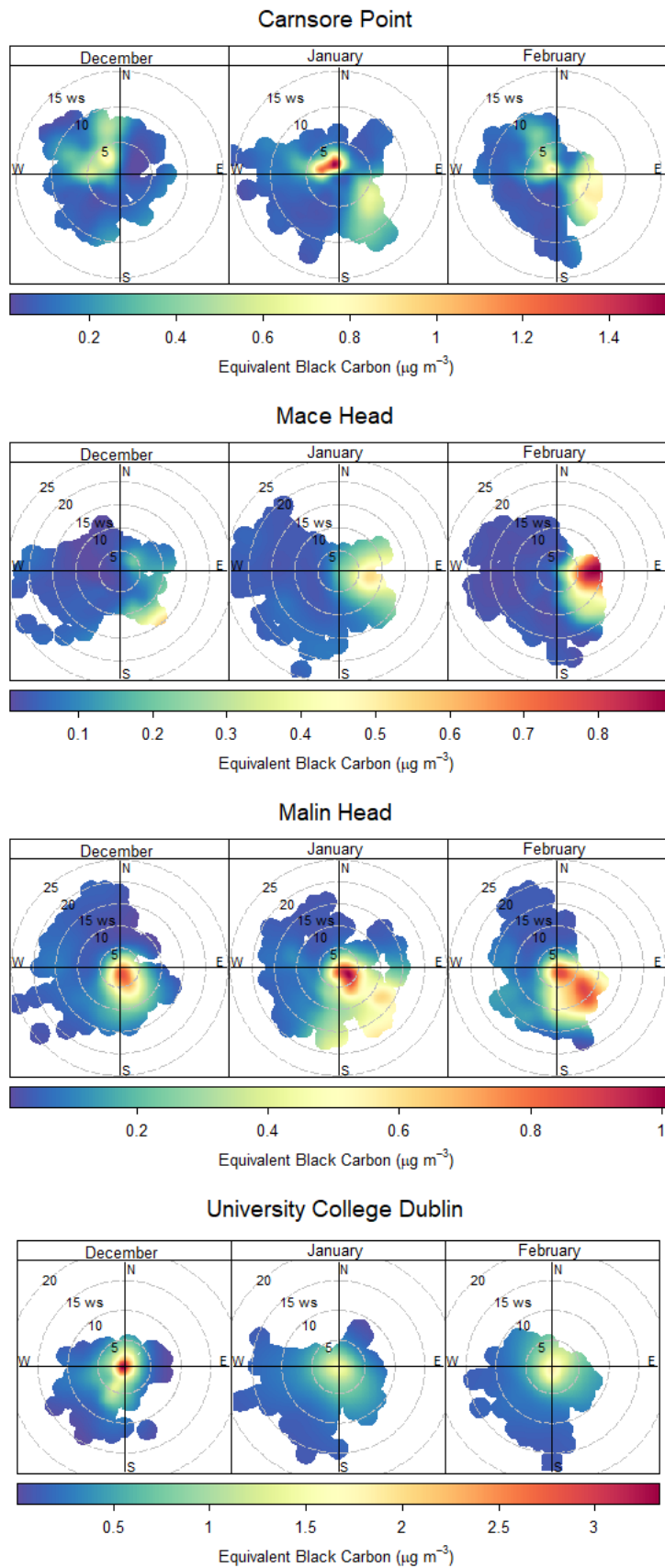


**Figure 3.14** Polar plots describing the monthly wind dependence of mean eBC concentrations during the wintertime intensive measurement campaign (December 2017 – February 2018).

Figure 3.13 demonstrates comparable eBC concentrations originating to the north-west and south-east of the Carnsore Point monitoring site when averaged over the duration of the sampling period. Using the absorption Ångström exponents of 0.9 and 1.68, the measured eBC was split into traffic and solid fuel combustion related sources, respectively (Figure 3.15). It was evident that emissions related to the combustion of solid fuels, most likely due to domestic heating came from north-west of the site; Wexford county and possibly further afield, while the emissions associated with traffic or transportation vehicles originated largely in the south-east, suggesting that shipping routes in the Celtic Sea between Rosslare, the UK and continental Europe contributed significantly to the ambient eBC concentrations measured at Carnsore Point. Presumably, continental air masses from Europe also contributed to the measurements at this location. Figure 3.15 also exhibits increased concentrations of eBC attributed to traffic-related emissions to the west of Mace Head. Although lower than those recorded to the east of the site, the concentrations from the seaward side are significant.

Back trajectory analysis was performed using HYSPLIT modelling to identify and further investigate the air masses influencing the sampling site during notable periods of increased ambient eBC concentration originating to the south-east of the Carnsore Point sampling site. On December 18, 2017 although a south-easterly wind was recorded at the site, the air mass had originated in North America 72 hours previously, before travelling across Ireland from the north-west and finally arriving at the monitoring site from a south-easterly direction (Figure 3.16 Top). In this case, presumably the increased concentrations can be attributed to emission sources in Ireland, and possibly long-range transportation from further afield. In contrast, the air mass influencing measurements on January 8, 2018 had two interesting components. One air mass moved across Europe and Great Britain after tracking south from the Arctic Circle 48 hours previously, while another originated in the Atlantic and moved north across Spain and France, prior to colliding with the air mass from the north and tracking west towards Ireland (Figure 3.16 Middle). Later that month on January 20 (Figure 3.16 Bottom), easterly winds from North America arrived at Carnsore Point from a south-easterly direction.

The observations made at Carnsore Point and Mace Head highlight the important question of whether or not the current two-source aethalometer model can correctly

attribute influential sources. Two possible explanations for the observations made at these monitoring sites are proposed:

- The aethalometer model correctly assigns the fossil fuel combustion emissions which are mainly related to shipping. Figure 3.15 shows that a significant portion of measured  $eBC_{Tr}$  was from the seaward direction; to the south east of Carnsore Point and to the west of Mace Head. This scenario would be more plausible at Carnsore Point than at Mace Head due to the proximity of commercial shipping lanes.
- In clean environments where extremely low concentrations are observed, the absorption Ångström exponents measured by the aethalometer are biased towards  $\sim 1$ . Both monitoring sites experienced relatively low concentrations of eBC throughout the sampling period; mean hourly averages did not exceed  $0.3 \mu\text{g m}^{-3}$  in either location. Absorption coefficients below the limit of detection of the aethalometer can result in negative values of eBC in pristine environments, often arising from instrument noise and uncertainties (Asmi et al., 2021; Backman et al., 2017).

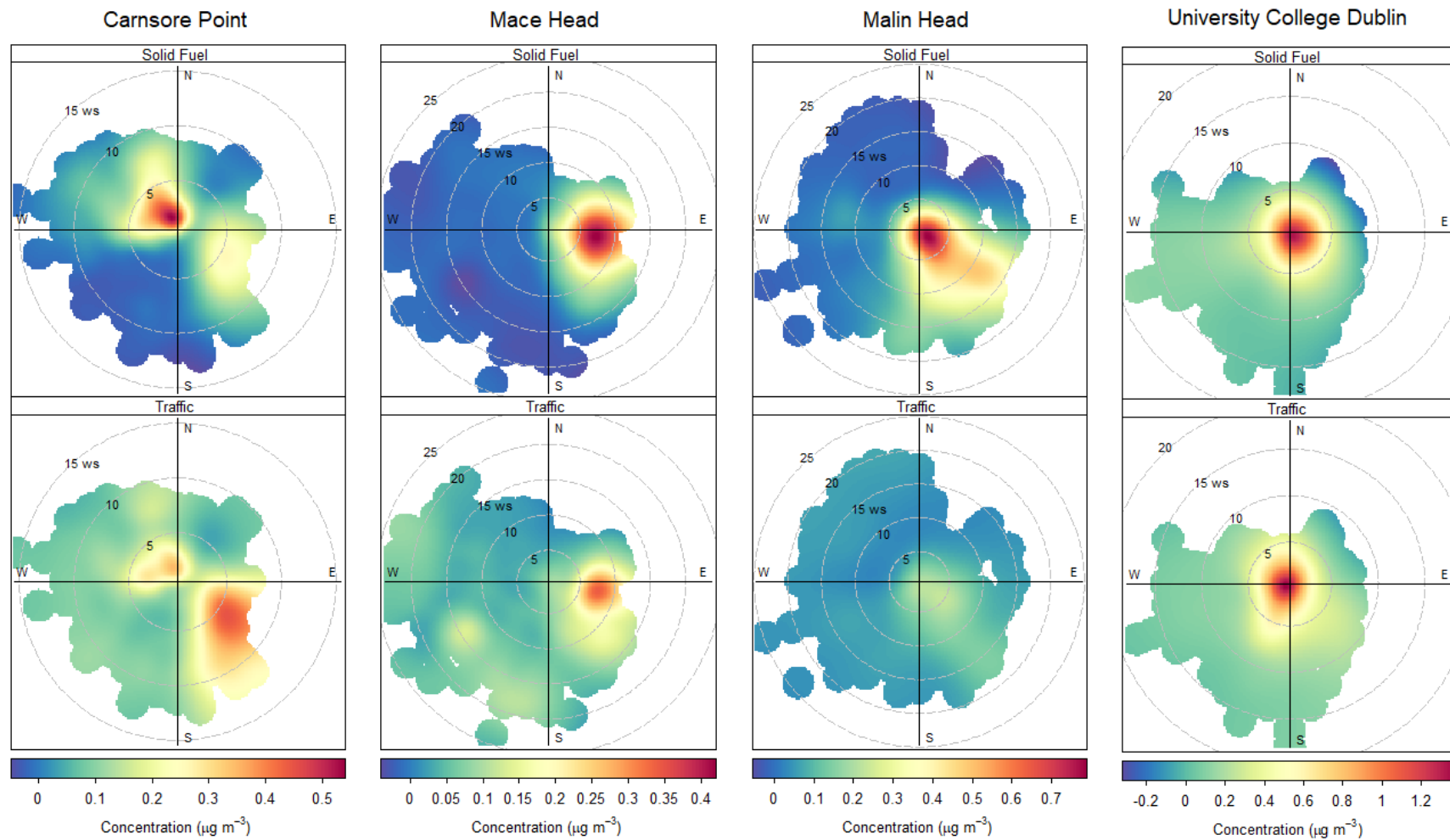


**Figure 3.15** Polar plots describing the wind dependence of  $eBC_{SF}$  and  $eBC_T$  concentrations at each sampling site during the wintertime intensive measurement campaign (December 2017 – February 2018).

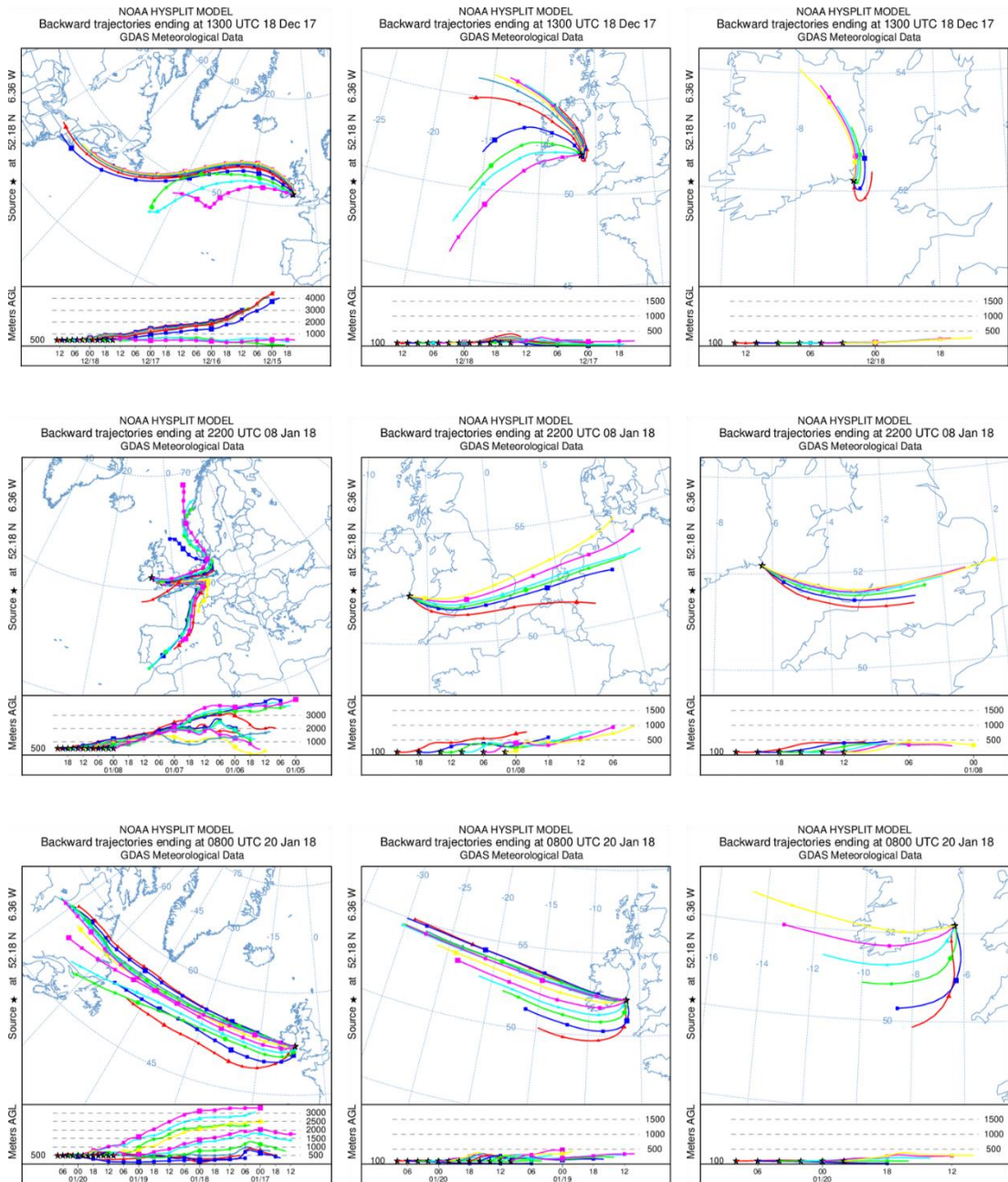


**Figure 3.16** Back trajectories performed using the HYSPLIT model ending at 500 m above ground level at the Carnsore Point sampling site; 72-hour (left), 24-hour (centre) and 12-hour (right).

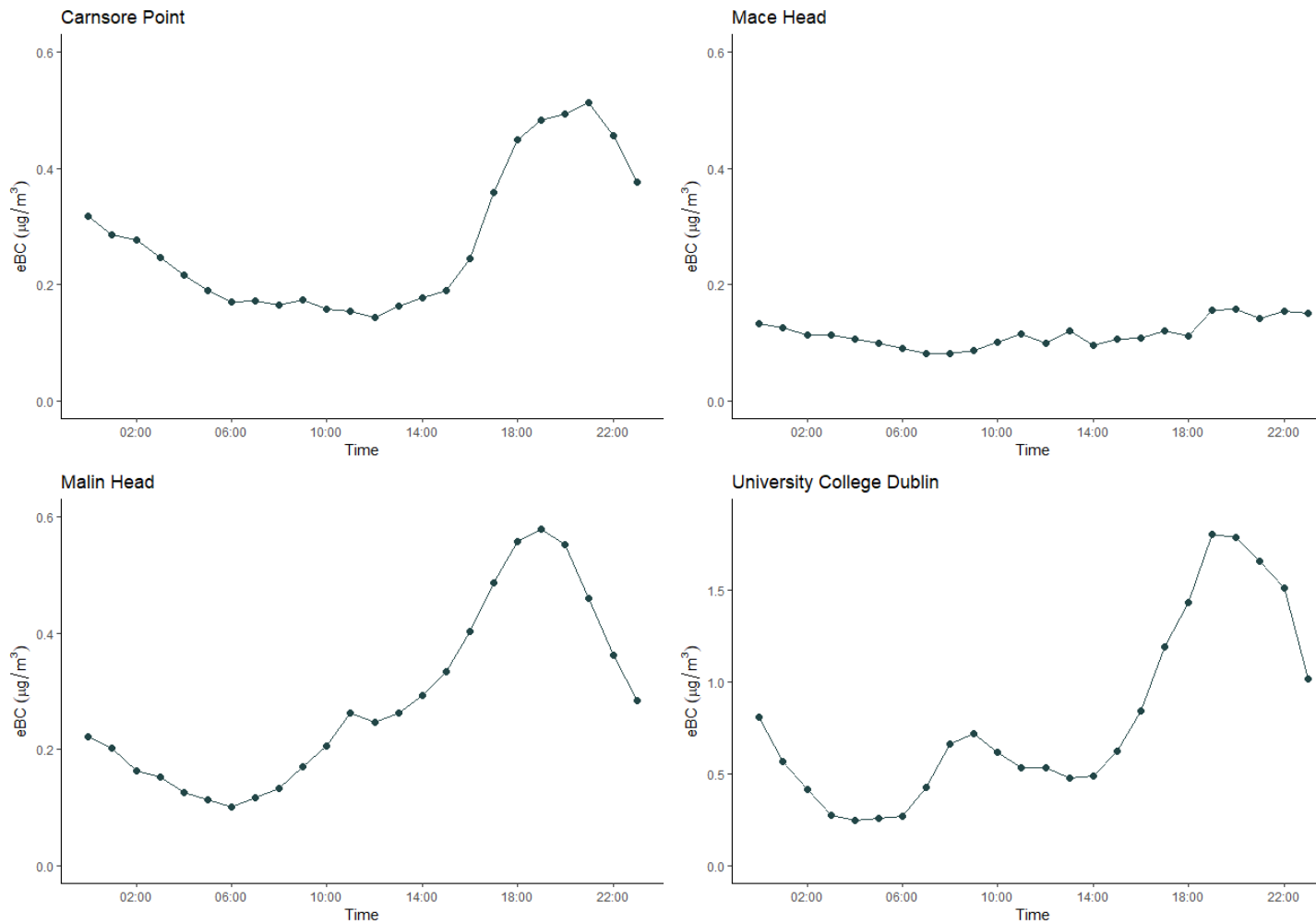
### 3.3.2.3 Diurnal Trends

---

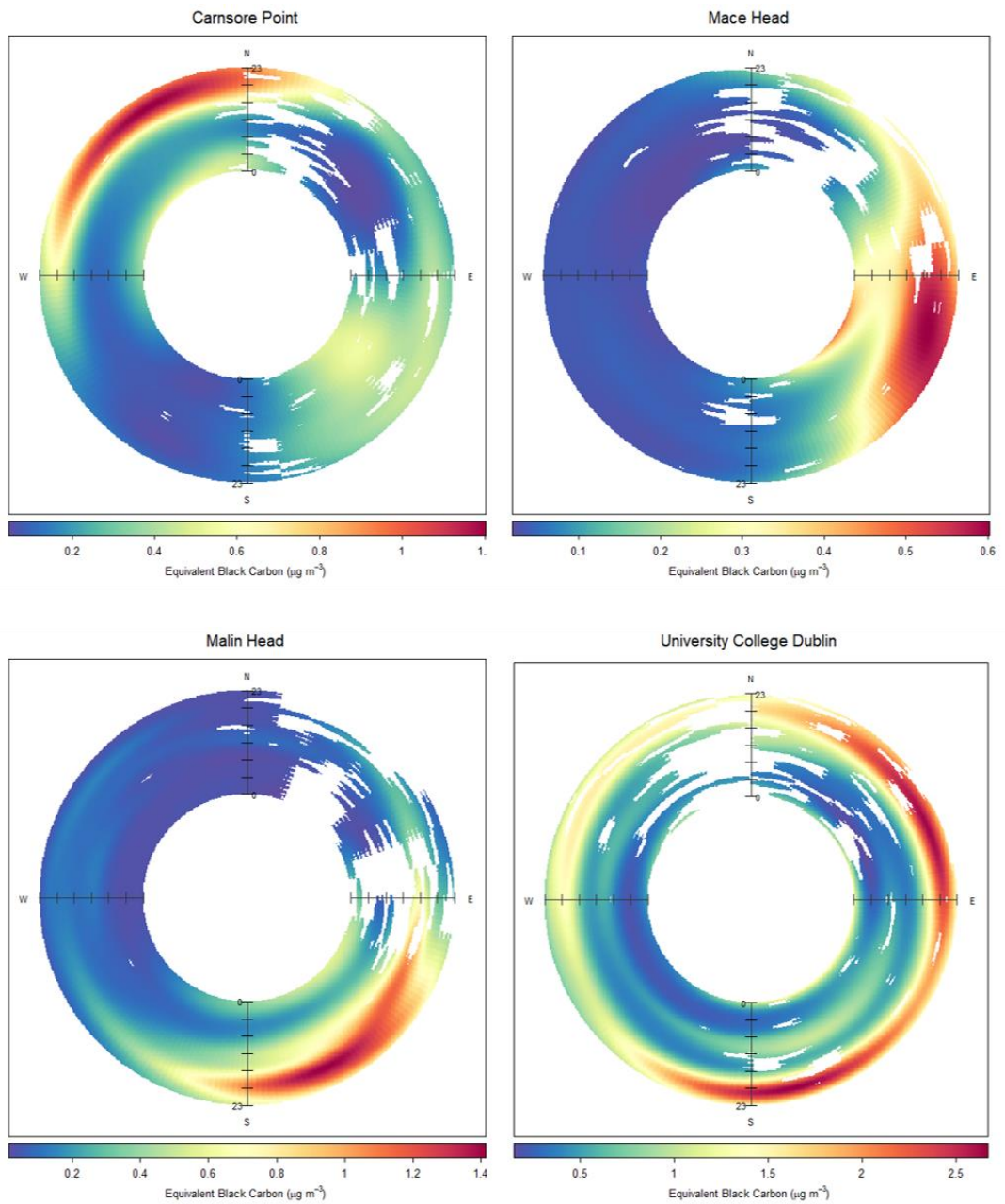
The diurnal profiles of hourly average eBC concentrations in Carnsore Point, Mace Head, Malin Head and UCD are illustrated in Figure 3.17. Although concentrations vary, a similar pattern was observed at each of the sites with the exception of Mace Head. There was a significant increase in eBC concentrations in the afternoon and eveningtime from approximately 14:00 onwards. Mean concentrations reached a maximum at 19:00 in both Dublin and Malin Head and at 21:00 in Carnsore Point.

Figure 3.18 illustrates the pronounced trend observed for concentrations of eBC and the direction from which the pollution comes as a function of the hour of the day, averaged over the entire sampling period. As expected for each site, the majority of measured eBC originated across the land mass; to the north-west of Carnsore Point, to the east of Mace Head, to the south east of Malin Head and predominantly to the south and east of the monitoring site at UCD, situated in a densely populated residential area. At each site, maximum concentrations were observed in the eveningtime indicating that solid fuel combustion for domestic heating was a major contributor to the total increase in eBC concentrations.

Interestingly, similar to Figure 3.13, increased concentrations were observed from the north-west and the south-east of the monitoring site at Carnsore Point. However, Figure 3.18 explains this observation further. Slightly increased concentrations in the south-east were observed throughout the day, while the amplified concentrations to the northwest of the site were observed in the evening, between 19:00 and midnight. This indicated variation in diurnal trends associated with differing sources, specifically the significant impact of solid fuel combustion for domestic heating on the ambient conditions in the eveningtime.



**Figure 3.17** Average diurnal profile of total eBC measured at each monitoring site throughout the wintertime intensive measurement campaign (December 2017 – February 2018).



**Figure 3.18** Mean eBC concentrations as a function of wind direction and time of day during the wintertime intensive measurement campaign (December 2017 – February 2018).

Mace Head consistently experienced extremely low concentrations of eBC. The mean concentration recorded during the sampling period was  $0.12 \mu\text{g m}^{-3}$  (Table 3.3). Owing to the remote location of the site and the absence of significant local emissions, it is unsurprising that a strong diurnal pattern was not observed. Figure 3.17 attempts to establish an average diurnal trend at the site, ranging between  $0.08 \mu\text{g m}^{-3}$  and  $0.16 \mu\text{g m}^{-3}$  over the entire sampling period. The trend was investigated further to account for the influence of wind direction on the diurnal pattern (Figure 3.19). On days when wind was blowing onshore (53 days), mean concentrations were at a minimum, ranging between  $0.04 \mu\text{g m}^{-3}$  and  $0.1 \mu\text{g m}^{-3}$ . There was a slight increase in the eveningtime, but it was, at most, an increase of  $0.06 \mu\text{g m}^{-3}$ . The observations on days when wind was blowing from an easterly direction (14 days) across the land mass, could not be described as a ‘pattern’, but it is evident that concentrations recorded on these days were slightly elevated ( $0.22 \mu\text{g m}^{-3} - 0.45 \mu\text{g m}^{-3}$ ) in comparison to those observed on days with a westerly wind.

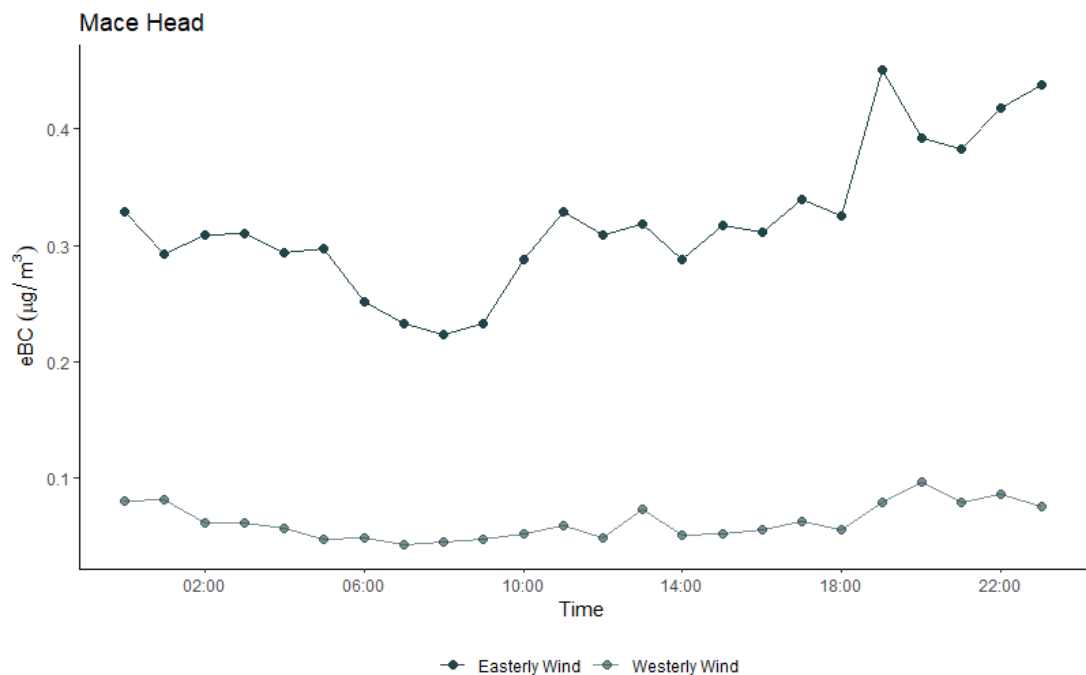


**Figure 3.19** Average diurnal profile of eBC concentrations measured at Mace Head as a function of daily wind direction.

The diurnal trend of the eBC attributed to solid fuel combustion and traffic-related emissions was also considered (Figure 3.20 and Figure 3.21). An increase in eBC attributed to traffic at the UCD site was observed during peak rush hour in the morning and evening times. Though the concentrations attributed to traffic may vary from day to day, the daily morning and evening peaks will reflect the traffic levels and are thus expected to be comparable in size.

Due to the extremely low concentration of total eBC recorded at Mace Head, accurate distinction between sources was difficult to achieve. Minimal emissions caused by localised solid fuel burning were observed, however such contributions were extremely wind dependent. Traffic-related emissions were not expected to contribute significantly to the total eBC concentration, due to the remote location of the site and relatively large distance from urban areas and roadways.

The substantial increase in evening time concentration of eBC was significantly influenced by solid fuel combustion emissions at the Carnsore Point and Malin Head sampling sites. Minor increases in the eBC concentration was attributed to traffic-related emissions at both sampling sites, however, the peaks were only observed during the evening hours. It is possible that the increase in concentration was exaggerated by a change in the boundary layer caused by decreasing temperatures in the evening time. However, it is also possible that the source apportionment model could not accurately attribute dominant sources in a mixed fuel environment, as previously discussed, and that this increase was, in fact, due to coal combustion for domestic heating. The aethalometer model was originally developed to quantitatively determine the contributions of wood burning and fossil fuel combustion emissions to particulate matter mass concentration (Sandradewi, Prévôt, Szidat et al., 2008). The mixed fuel environment in Ireland, which also includes coal and peat, may limit the application of the model. This supports the premise that the application of a single pair of AAE values is inappropriate for accurate source apportionment in different environments and presents an argument for the development of site-specific absorption Ångström exponents.

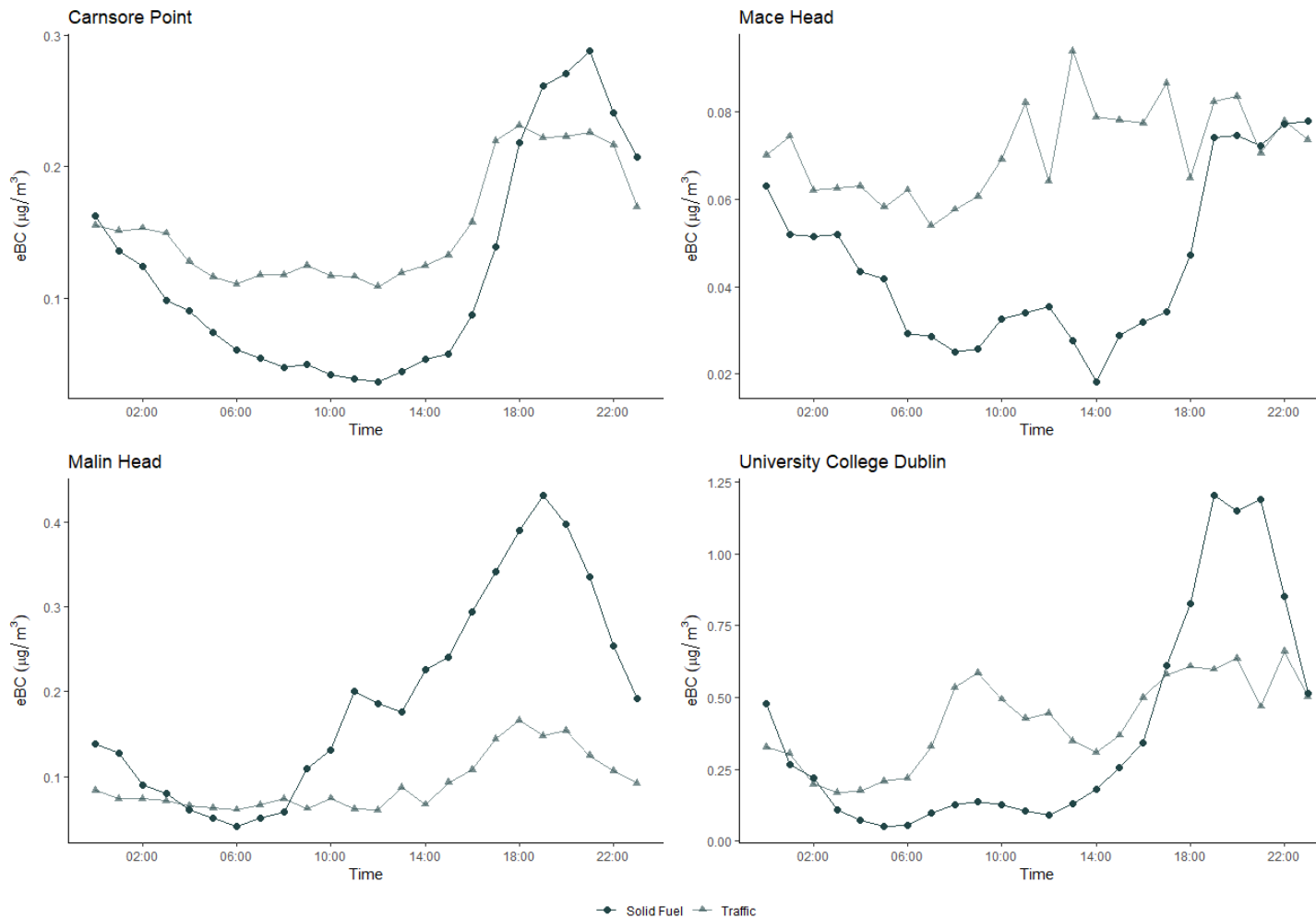


**Figure 3.20** Average diurnal profile of eBC attributed to solid fuel combustion and traffic-related emissions at each sampling site during the intensive wintertime measurement campaign (December 2017 – February 2018).

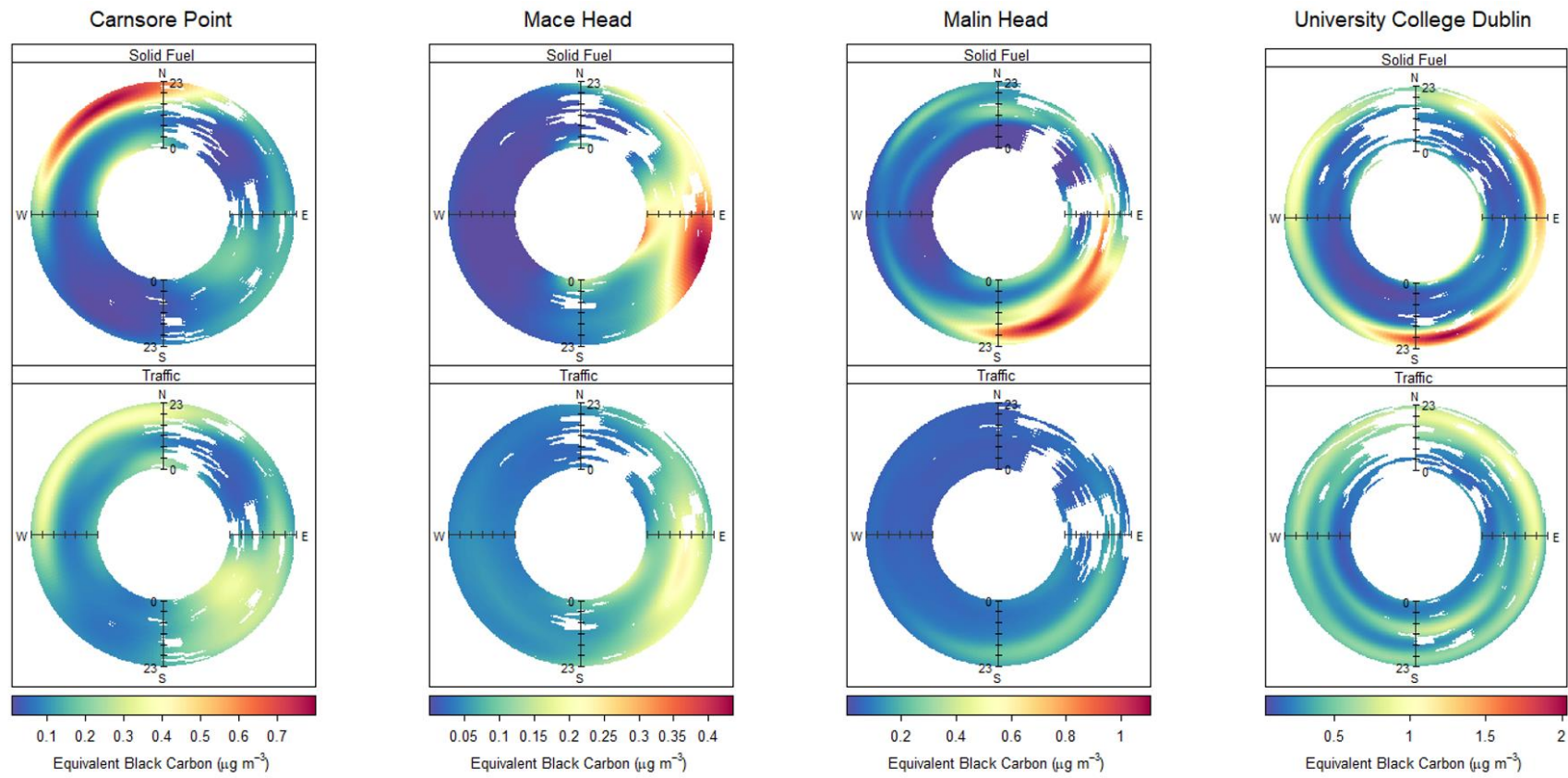


**Figure 3.21** Average diurnal trend of eBC attributed to solid fuel combustion and traffic-related emissions, as a function of origin, at each sampling site during the intensive wintertime measurement campaign (December 2017 – February 2018).

#### 3.3.2.4 *Delta-C*

---

Optical absorption at 370 nm is enhanced in the organic components of wood smoke, relative to the absorption of such components at 880 nm. By investigating the difference in concentrations measured by the aethalometer in these channels, BC1 and BC6, respectively, the ‘Delta-C’ ( $\Delta C$ ) value can be determined (Allen et al., 2004; Wang et al., 2012). Allen et al. (2004) noted that the  $\Delta C$  value can be used as an indicator for the presence of wood smoke, but not as a quantitative measurement. The diurnal profiles of  $\Delta C$  illustrated in Figure 3.22, further substantiate the significant influence of solid fuel combustion related emissions to the ambient eBC concentration in the eveningtime at the locations under consideration.

Significant increases in concentration were observed from 14:00 onwards at Carnsore Point, Malin Head and on the UCD campus, consistent with the aethalometer model output. Mean concentrations increased marginally at the Mace Head sampling site in the evening, however there was little variation throughout the day and total concentrations were extremely low. The total eBC and  $\Delta C$  diurnal patterns were similar at both Carnsore Point and Malin Head, suggesting that wood burning strongly influenced total eBC levels. At the UCD sampling site the absence of a morningtime traffic peak was obvious in the  $\Delta C$  diurnal profile, while the large increase observed during the evening indicates that wood combustion strongly influenced this site, in agreement with the aethalometer model output.

The relationship between  $\Delta C$  and the eBC attributed to solid fuel and traffic-related emissions is examined in Figure 3.23. As both sets of measurements were derived from the aethalometer data, a strong correlation between the parameters was expected. However, by investigating the correlation between  $\Delta C$  and  $eBC_{SF}$  and  $\Delta C$  and  $eBC_{Tr}$ , the effectiveness of the application of Zotter values to differentiate between the sources can be examined. There was excellent agreement between  $\Delta C$  and  $eBC_{SF}$  ( $r^2 > 0.93$ ), while the correlation between  $\Delta C$  and  $eBC_{Tr}$  was much weaker ( $r^2 < 0.33$ ). As the  $\Delta C$  value is indicative of the presence of wood burning related particles, the linear regression models confirm that wood burning emissions were correctly attributed to  $eBC_{SF}$ , using an AAE of 1.68. However, the analysis does not provide further insight into the suitability of the Zotter value pair in a mixed fuel environment as it does not account for peat and coal combustion emissions.

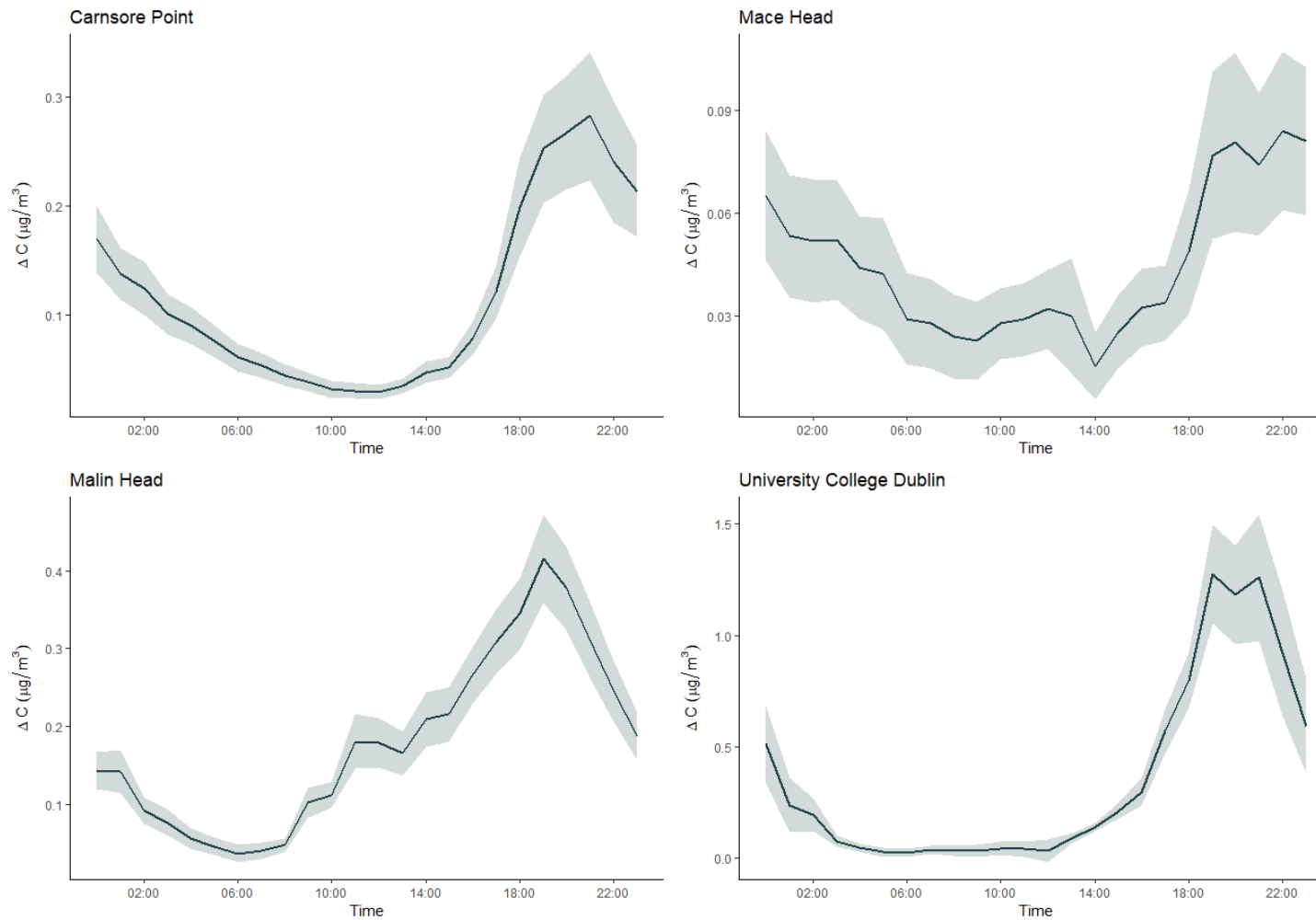


**Figure 3.22** Average diurnal profile of  $\Delta C$  parameter measured at each site during the wintertime intensive measurement campaign (December 2017 – February 2018).  $\Delta C$  is the difference in concentration measured at wavelengths 370 nm and 880 nm.

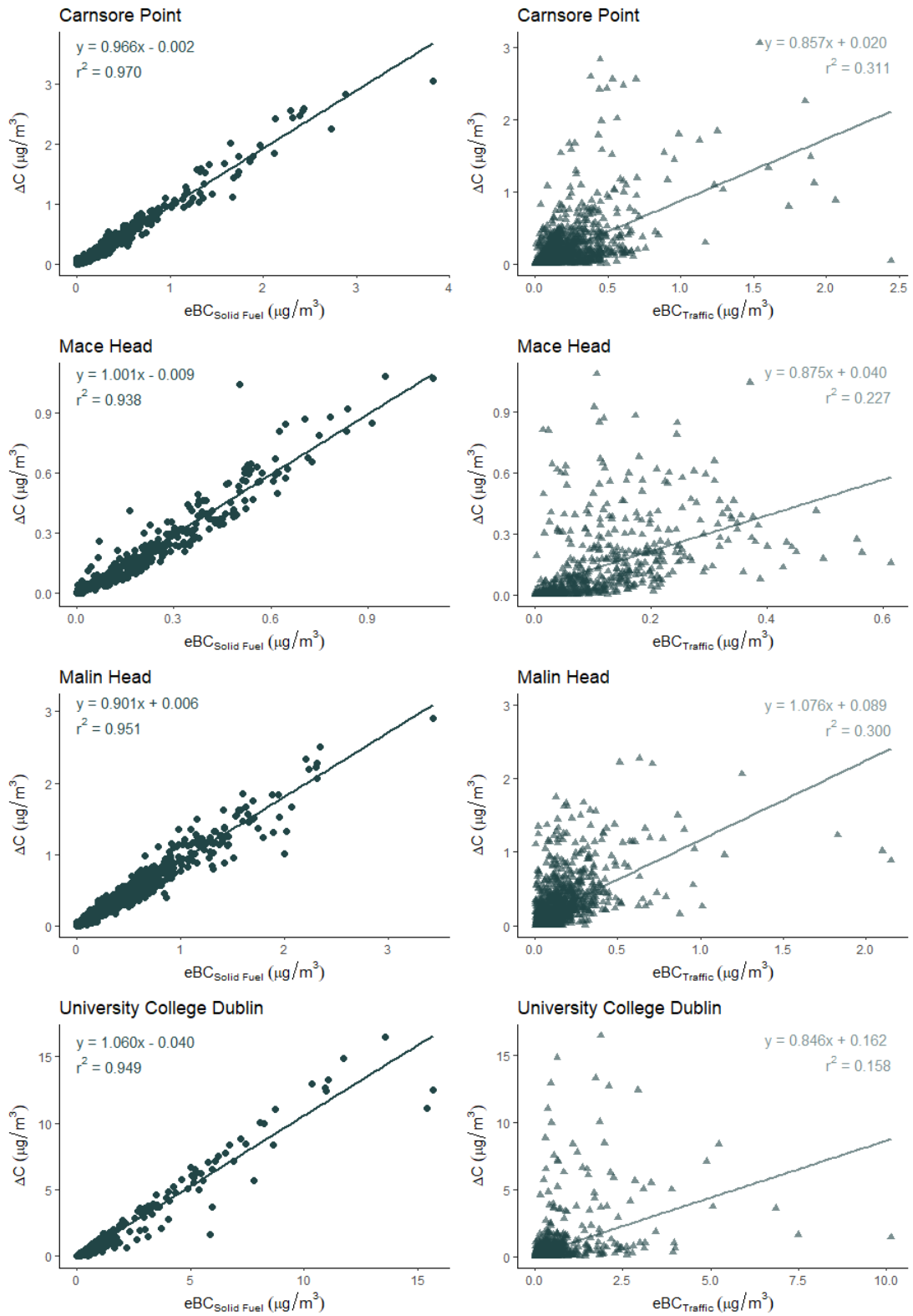


**Figure 3.23** Correlation between  $\Delta C$  and  $e\text{BC}_{\text{SF}}$  and  $e\text{BC}_{\text{Tr}}$  at each of the sampling sites involved in the intensive measurement campaign (December 2017 – February 2018).

### 3.3.2.5 Source Contribution

---

Source contribution to total ambient eBC concentration was spatially and temporally variable. Figure 3.24 illustrates the mean eBC attributed to traffic-related and solid fuel combustion emissions as a percentage of the total measured eBC, following the application of AAE values of 0.9 and 1.68, respectively. According to the aethalometer model, eBC<sub>Tr</sub> accounted for a large percentage of total monthly eBC at Carnsore Point ( $\bar{x}$  = 83.6%), Malin Head ( $\bar{x}$  = 69.7%) and UCD campus ( $\bar{x}$  = 59.5%). Conversely, 11% of the total eBC was attributed to eBC<sub>Tr</sub> at Mace Head.

It is interesting that despite an absence of major local sources at Carnsore Point, traffic-related emissions contributed a higher percentage to the total eBC concentration (83.6%) than at the UCD monitoring site (59.5%), which is located in a well populated residential area, approximately 500 m from one of the main road arteries into Dublin city. Again, the accuracy of the source apportionment model is open to question. It does not seem credible that, on average over the three month period, almost 84% of the measured eBC at Carnsore Point could be derived from traffic-related emissions. Rosslare Harbour is approximately 8 km north of the sampling site, however during the sampling period northerly winds were rarely recorded. Thus, is it unlikely that the harbour is the source of the emissions. It is plausible that the use of inappropriate AAEs has resulted in the incorrect assignment of measured eBC to traffic-related emissions, primarily due to the mixture of solid fuels used. Coal burning for residential heating may have contributed to the large portion of total eBC efficiently absorbed in the near-IR region, resulting in an over-estimation of 'traffic-related' contributions, which would explain the increase in 'eBC<sub>Tr</sub>' in the eveningtime at Carnsore Point and Malin Head (Figure 3.20). The overall low percentage of eBC attributed to traffic at Mace Head implies a regional contribution from traffic sources, not from any particular direction. The air masses influencing conditions at Mace Head were presumably less continental than at any other location.

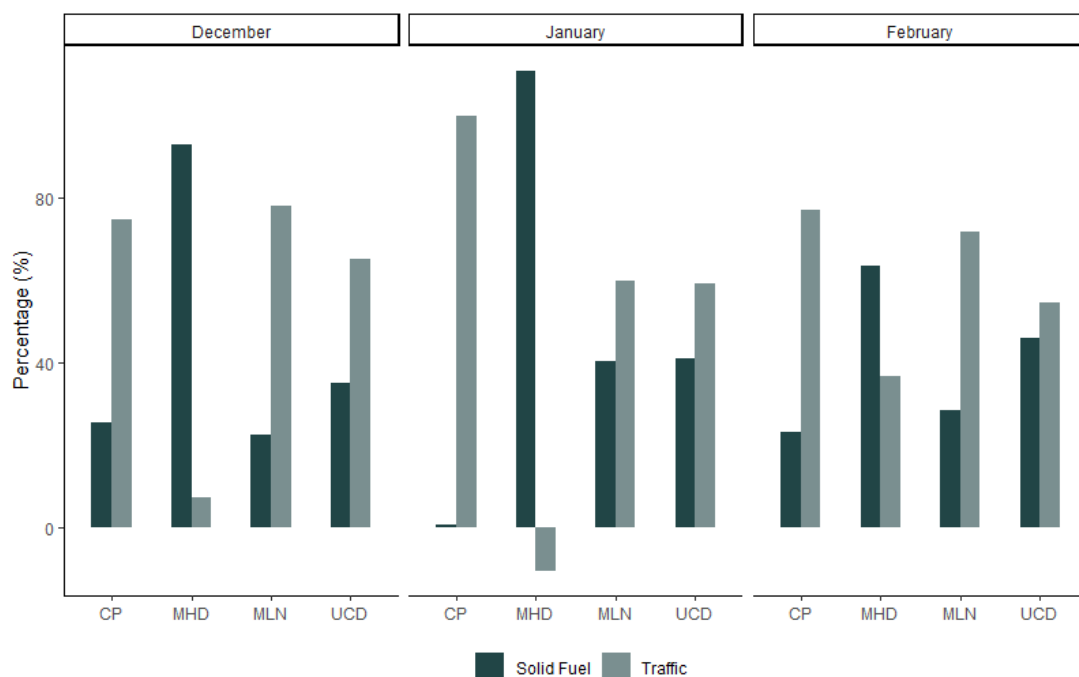


**Figure 3.24** Average monthly percentage source contributions measured at Carnsore Point (CP), Mace Head (MHD), Malin Head (MLN) and University College Dublin (UCD) between December 2017 and February 2018.

### 3.3.2.6 Light Absorption of Black Carbon

Further investigation into source apportionment of measured eBC involved examination of the absorption Ångström exponents calculated by the aethalometer (60 s). Figure 3.25 demonstrates the average aethalometer absorption dependence on wavelengths for the four Irish monitoring sites involved in the measurement campaign, normalised to the absorption recorded at a wavelength of 950 nm. The site at Malin Head appears to have had the strongest absorption in the UV region, likely due to wood burning and solid fuel combustion related emissions. In contrast, the aerosol sampled at Mace Head absorbs less efficiently in the ultra-violet region, in contrast to the previous estimation of 89% of total eBC attributed to solid fuel related emissions, on average across the entire sampling period (Figure 3.24). There is little variation ( $2.133 \times 10^{-6} \text{ m}^{-1}$ ) in the absolute mean absorbance in the UV and IR regions at this sampling site.

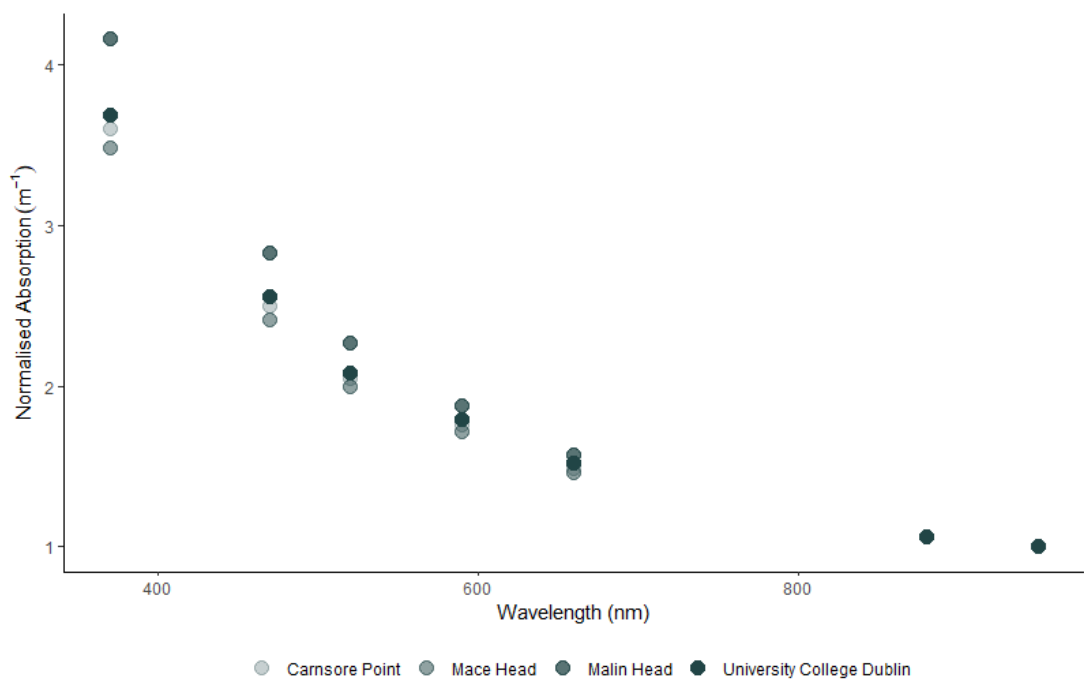


**Figure 3.25** Normalised aethalometer absorption dependence on wavelengths for each of the monitoring sites involved in the measurement campaign (December 2017 – February 2018).

Absorption Ångström exponents were calculated by curve fitting of the values for  $b_{abs}$  at wavelengths 470, 520, 590, 660, 880 and 950 nm with exponential regression models of absorption measurements. The frequency distribution of AAE values at each monitoring site for the entire monitoring campaign are shown in Figure 3.26. The distribution of these values in a locality gives an indication of the predominant sources of eBC in that location. Examining the calculated AAE emphasised some interesting results. It was observed that the most frequently measured values of the AAE were between 1.3 and 1.5. However, the distribution at the three regional background locations differed significantly in comparison to the distribution observed at UCD. A narrow range of AAE values was derived from the aethalometer measurements collected at UCD centred around 1.3, with two adjacent peaks. This indicates an environment with two major source types; solid fuel burning, likely encompassing contributions from wood and peat, and traffic-related sources, which potentially includes coal combustion emissions. The regional background sites have a similar peak value, however, the distributions are much broader. The location of the peak is indicative of consistent influence from solid fuel related sources. The wide variation in values, and the absence of a defined peak at the lower range of distribution, suggests

inconsistent contributions from traffic-related or fossil fuel combustion sources. These findings highlight that the variation in calculated AAE values is dependent on local sources. This suggests that application of one pair of AAE values may not be appropriate for use across a range of sampling environments, as the use of an incorrect AAE pair will lead to inaccurate source apportionment. Furthermore, the distributions show that in clean environments there was a low range of AAE values. This implies a strong influence from fossil fuel combustion, however in reality it is a feature of low BC concentrations. Despite the assignment of an overwhelming portion of total eBC to solid fuel combustion emissions at Mace Head ( $\bar{x} = 89\%$ ), the frequency distribution exhibits AAE values biased towards  $\sim 1$  ( $\bar{x} = 0.88$ ), indicating a fossil fuel dominant environment. In an environment dominated by eBC<sub>SF</sub>, an AAE closer to 1.68 would be expected. This reinforces the hypothesis that the model collapses at extremely low concentrations, such as those measured at Mace Head.

In a similar study, Grange et al. (2020) noted sites which are exposed to wood burning emissions have a tail that extends beyond 1.68, while the AAE distribution at traffic dominated sites contain only a small component beyond 1.68. The AAE distribution at both Mace Head and Malin Head extends beyond the  $\alpha_{SF}$  value of 1.68, while the distribution at Carnsore Point and UCD rarely continues further than 1.68. Grange et al. (2020) also concluded that bi-modal distribution indicates exposure to additional sources, possibly fresh wood smoke emitted close to the monitoring site and detected prior to the occurrence of any type of chemical processing. Bi-modal distribution was identified at each of the sites analysed in the current study (Figure 3.26), suggesting that aged wood smoke is not the only source present at each site. This validates the use of nomenclature *SF* rather than *wb*, to account for both wood and peat combustion. However, the use of coal for domestic heating causes complications and, due to its composition, it is possibly assigned to the eBC<sub>Tr</sub> portion of total eBC. Thus, application of the current two source aethalometer model, does not account for all solid fuel types in the eBC<sub>SF</sub> category.

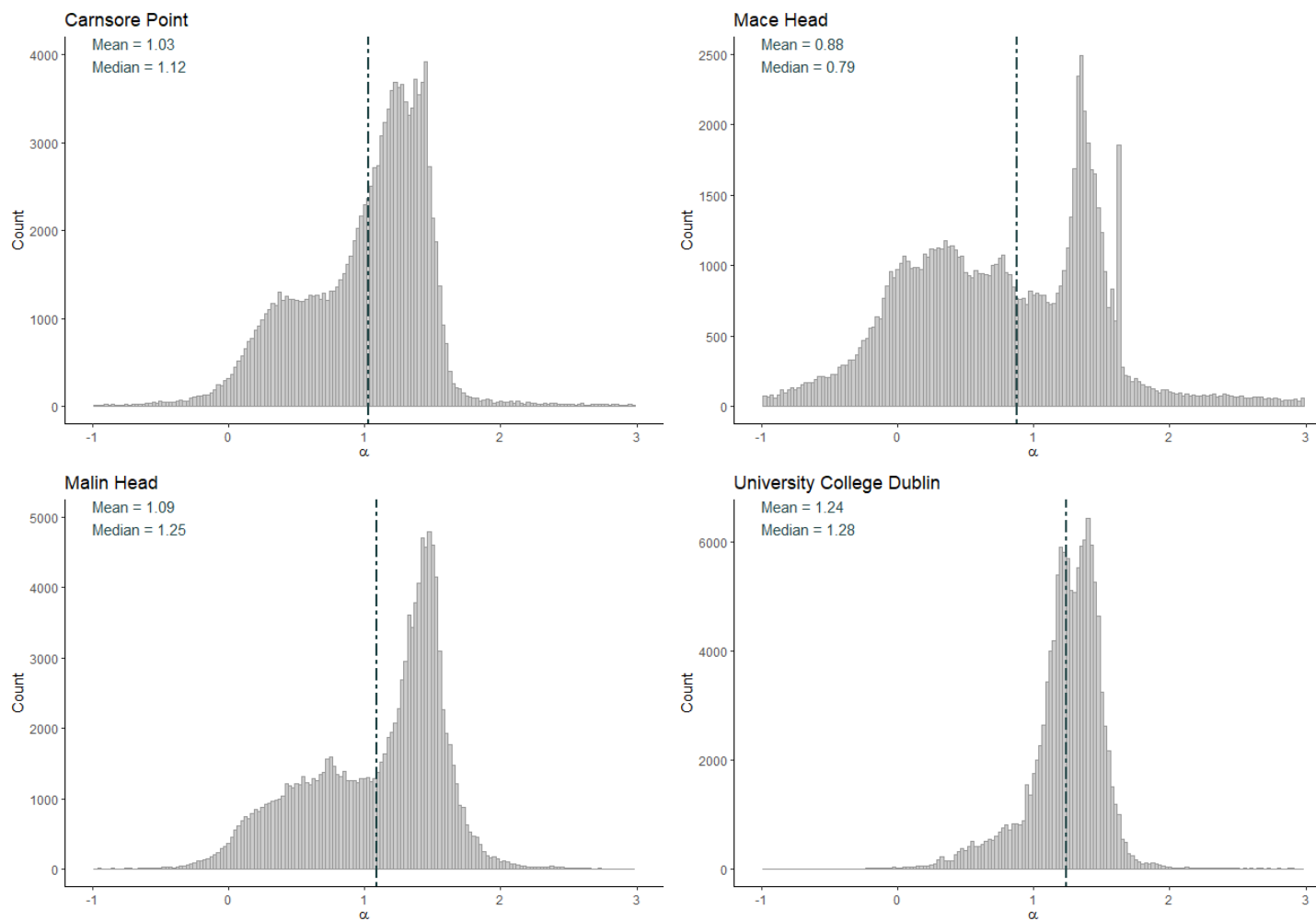


**Figure 3.26** Frequency distribution of calculated absorption Ångström exponents at each monitoring site (December 2017 – February 2018), between wavelengths 470 nm and 950 nm.

### 3.3.3 Elemental Carbon (EC) and Organic Carbon (OC)

---

The temporal profiles of organic, elemental and total carbon concentrations recorded at Carnsore Point, Mace Head, Malin Head and UCD sampling sites are shown in Figure 3.28. A summary of the range and mean concentrations is provided in Table 3.4 below. The highest concentrations were regularly recorded at UCD, where the maximum ambient 24-hour TC concentration was  $16.6 \mu\text{g m}^{-3}$ , of which  $1.7 \mu\text{g m}^{-3}$  and  $14.9 \mu\text{g m}^{-3}$  was attributed to elemental and organic carbon, respectively.

The highest percentage of organic carbon was observed at Mace Head, Co. Galway, however the absolute concentrations recorded were considerably less than at any other monitoring site. Due to the sparsely populated, remote location of Mace Head, it is unlikely that the OC content can be attributed exclusively to solid fuel combustion. This is confirmed by Figure 3.30, which illustrates a poor correlation between organic carbon and  $\text{eBC}_{\text{SF}}$  ( $r^2 = 0.15$ ). In contrast, there was a strong correlation between these two parameters at the other sampling sites, particularly at Carnsore Point ( $r^2 > 0.94$ ). During the winter months, it is unlikely that the dominant source at any site is biogenic emissions from terrestrial vegetation. However, it is reasonable to speculate that the organic carbon content is influenced by marine biogenic sources at Carnsore Point, Mace Head and Malin Head (O'Dowd et al., 2004; Yoon et al., 2007).

The mean and range of absolute EC and OC concentrations recorded at each sampling site are illustrated in Figure 3.27. EC accounted for quite a low percentage of the total carbon content measured at each site (range: 2.8% – 14.1%). There was little variation in the absolute EC concentrations measured at Carnsore Point, Malin Head and UCD, contradicting the broad range of contributions from  $\text{eBC}_{\text{Tr}}$  according to the aethalometer source apportionment model.

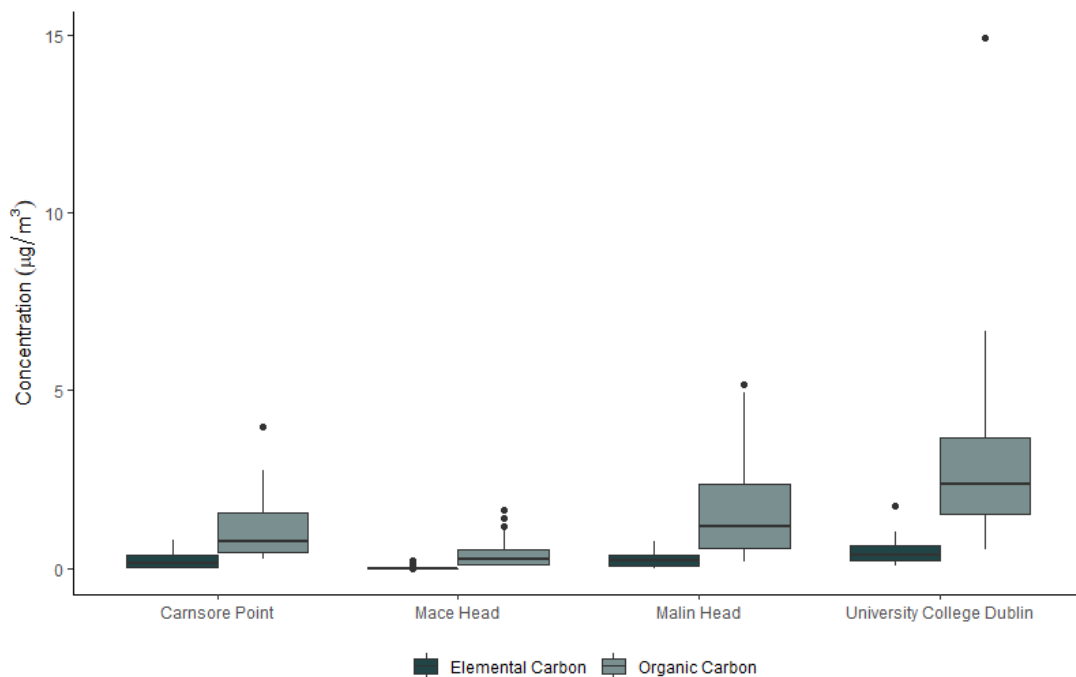


**Figure 3.27** Boxplot of absolute EC and OC concentrations recorded at each of the monitoring sites involved in the intensive measurement campaign (December 2017 – February 2018).

The small proportion of EC challenges the assertion provided by the aethalometer data which suggests the majority of eBC carbon measured should be attributed to traffic-related emissions at Carnsore Point, Malin Head and UCD. Primary organic aerosol (POA) and black carbon contribute a significant proportion of carbonaceous particulate matter in Europe, which is consistent with the large fraction of diesel powered vehicles, in comparison to environments dominated by gasoline powered vehicles where SOA dominates the carbonaceous fraction of PM (Platt et al., 2017). Similar to other European member states, the Irish market is dominated by diesel-powered vehicles. In 2017, 60% of the national fleet was powered by diesel, 38.7% powered by gasoline and the remaining vehicles were either electric or hybrid (plug-in/gasoline) (O'Connell, 2019). Subsequently, if such a high proportion of the eBC measured at the sampling sites originated from traffic-related emissions, as indicated by the aethalometer model, a greater proportion of thermally measured EC content would be anticipated.

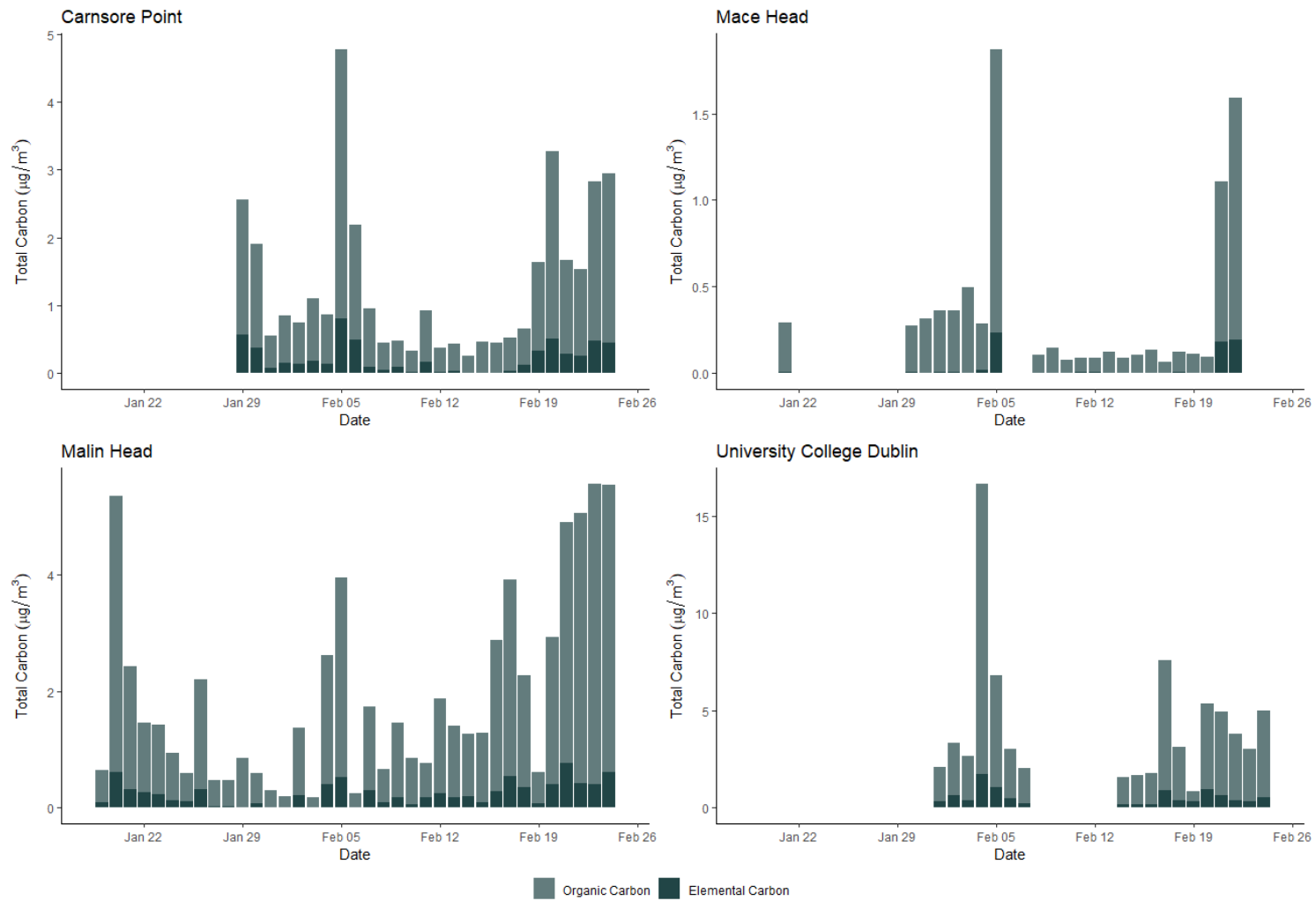
The temporal trends of eBC and TC measurements are shown in Figure 3.29. Good agreement between the two parameters was observed; both the eBC and TC follow a similar trend and significant increases were recorded on the same days. Correlation

between the two parameters was greatest at Carnsore Point ( $r^2 = 0.96$ ) and Malin Head ( $r^2 = 0.92$ ), where filter samples were collected on a 24-hour basis between midnight and 23:59. Over the entire sampling period, an  $r^2$  value of 0.59 was determined for these parameters at the urban background site; UCD. However, this value improves significantly ( $r^2 = 0.96$ ) when the month of February is isolated and analysed. During February 2018, filter samples were collected at 24-hour intervals, between 08:00 and 07:59. Previously, from December 21, 2017 to January 19, 2018, filter samples were collected on a 48-hour basis at this site. In order to compare the two parameters, the measured eBC was averaged over the corresponding sampling period of ambient aerosol. Averaging the 60 second measurements over a 48-hour period in such a complex environment with several probable sources, potentially concealed significant variation in ambient concentration, ultimately reducing the correlation between parameters. The correlation between eBC and TC recorded at Mace Head was also weak ( $r^2 < 0.3$ ). Although similar trends were observed at this monitoring site, the relationship between the measured concentration values is poor. This suggests that a large fraction of the OC was unrelated to the measured black carbon, thus indicating contribution from additional sources, potentially marine biogenic sources.

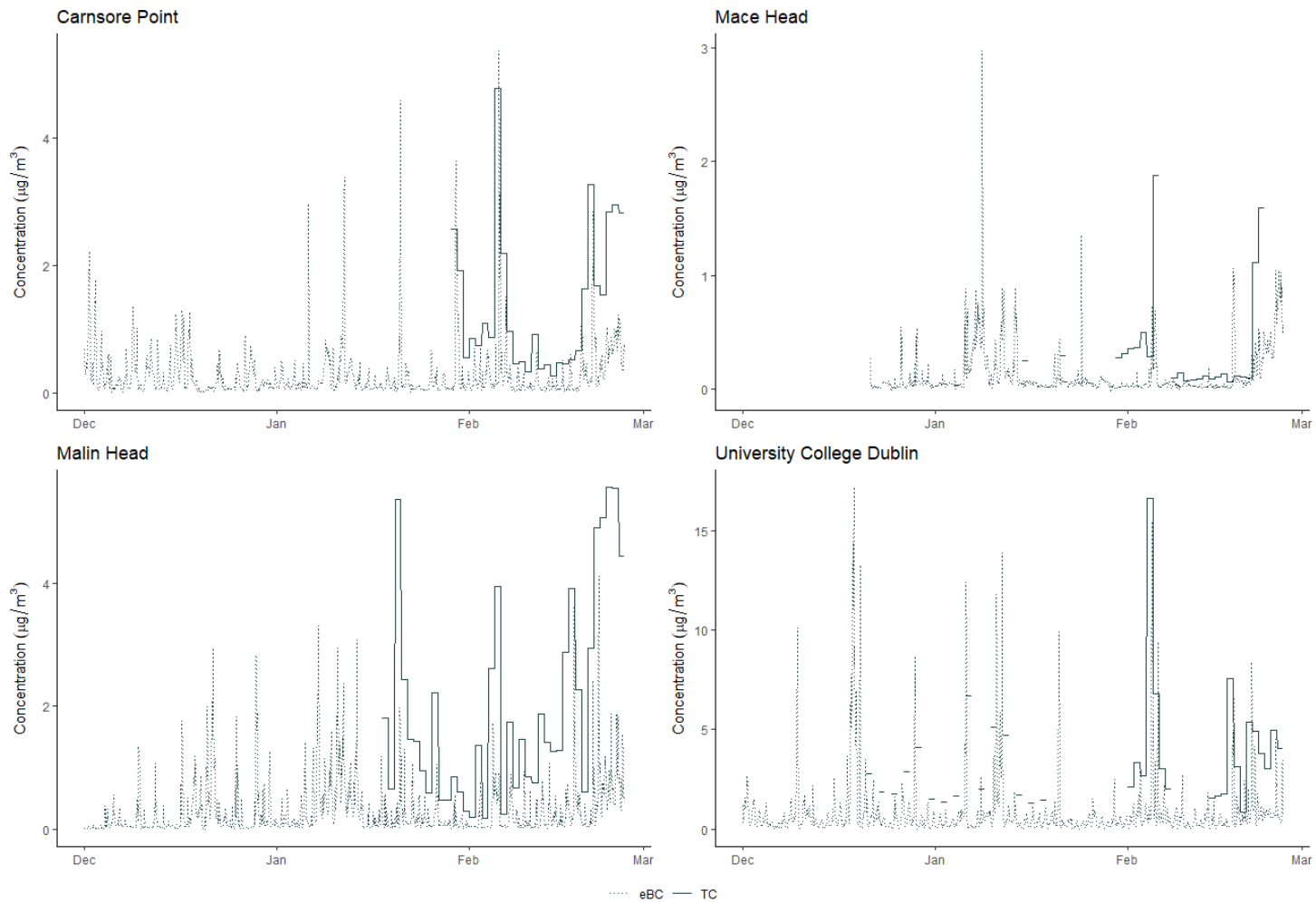
An increase in TC, common to all sampling sites, was observed in early February 2018 (04/02/2018 – 05/02/2018). Measured eBC concentrations increased correspondingly. This coincided with a period of low wind speed, particularly on the east coast. At Mace Head and Malin Head, the increase in pollutants also coincided with a change in wind direction; a southerly wind was recorded on February 5, 2017, in contrast to the northerly wind recorded during the preceding days. In late February 2017 (20/02/2018 – 24/02/2017), TC again increased significantly at Carnsore Point, Mace Head and Malin Head, again corresponding with an increase in ambient eBC. Wind speeds were somewhat lower during this event, however the change in prevailing wind from westerly to easterly was of most significance. This event was recorded in the days prior to the arrival of the ‘Beast from the East’ on February 27, 2017.

**Table 3.4** Summary of measured EC, OC and TC measured at each sampling site involved in the wintertime measurement campaign (December 2017 – February 2018).

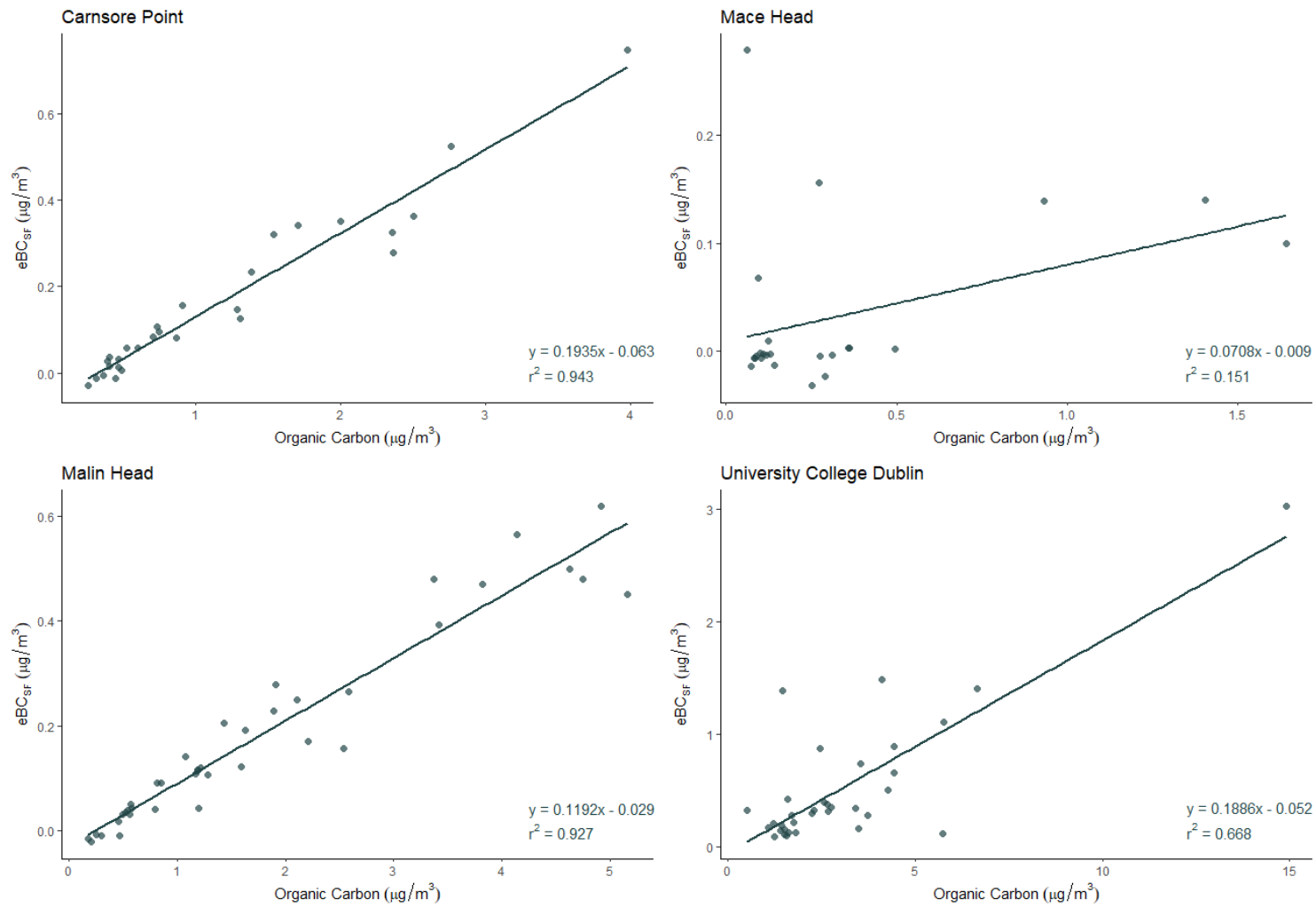
	<b>Carnsore Point</b>	<b>Mace Head</b>	<b>Malin Head</b>	<b>University College Dublin</b>
<b>Organic Carbon (<math>\mu\text{g m}^{-3}</math>)</b>				
<i>Mean <math>\pm</math> SD</i>	1.15 $\pm$ 0.93	0.42 $\pm$ 0.42	1.74 $\pm$ 1.47	3.05 $\pm$ 2.57
<i>Range</i>	0.26 – 3.97	0.06 – 1.64	0.18 – 5.16	0.53 – 14.90
<b>Elemental Carbon (<math>\mu\text{g m}^{-3}</math>)</b>				
<i>Mean <math>\pm</math> SD</i>	0.23 $\pm$ 0.21	0.03 $\pm$ 0.07	0.25 $\pm$ 0.20	0.49 $\pm$ 0.36
<i>Range</i>	0.00 – 0.80	0.00 – 0.23	0.00 – 0.77	0.08 – 1.75
<b>Total Carbon (<math>\mu\text{g m}^{-3}</math>)</b>				
<i>Mean <math>\pm</math> SD</i>	1.38 $\pm$ 1.14	0.45 $\pm$ 0.48	1.99 $\pm$ 1.66	3.54 $\pm$ 2.90
<i>Range</i>	0.26 – 4.78	0.06 – 1.87	0.18 – 5.55	0.87 – 16.64
<b>OC/EC Ratio</b>	4.2	5.1	6.5	6.4
<b>EC/TC (%)</b>	13.6	2.8	11.4	14.1
<b>OC/TC (%)</b>	86.4	97.2	88.6	85.9



**Figure 3.28** Temporal trends of EC, OC and TC measured at each monitoring site during the overlapping sampling period (January 18 – February 25, 2018).



**Figure 3.29** Comparison of temporal profiles of thermal TC and optical eBC measured at each of the sampling sites involved in the intensive measurement campaign (December 2017 – February 2018).



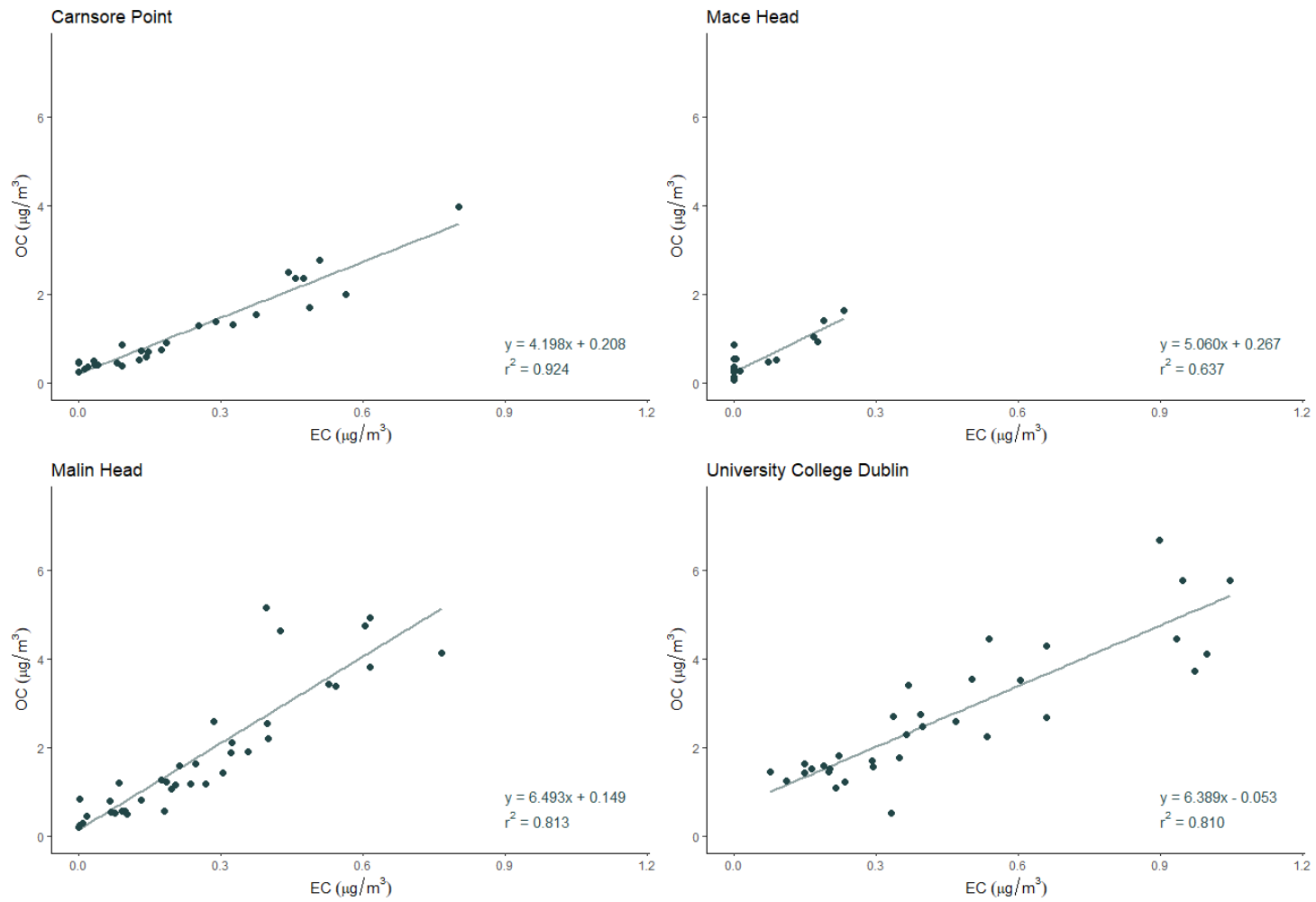
**Figure 3.30** Comparison of eBC<sub>SF</sub> and OC measured at each of the sampling sites involved in the intensive measurement campaign (December 2017 – February 2018).

Table 3.4 includes the OC/EC ratio values obtained for each site during this field campaign. The OC/EC ratio can vary widely with location and seasonality. It is often used to investigate the processes leading to the formation of secondary organic aerosols and examine the influence of sources contributing to ambient conditions. The ratio is commonly used to differentiate between solid fuel types used in combustion in a given region. Ni et al. (2018) noted the effect that combustion conditions (eg. flaming versus smouldering) can have on the ratio, in addition to the impact that thermal protocols used in the analysis of elemental and organic carbon content can have. Ni et al. (2018) selected OC/EC ratio values of  $2.38 \pm 0.44$  and  $5 \pm 2$  to indicate the presence of coal and wood burning emissions, respectively. Grieshop et al. (2009) also noted the effect that combustion conditions could have on the OC/EC ratio (1.1 - 13) in a controlled study of the atmospheric aging of wood smoke. A wide range (1 - 20) in the OC/EC ratio attributed to biomass burning was used in the study presented by Gilardoni et al. (2011).

Numerous studies have been carried out across Europe investigating the OC/EC ratio. Generally, lower values are recorded at polluted sites, while higher ratios are recorded at more remote sites (Karanasiou et al., 2020). Despite noting the uncertainty associated with the OC/EC ratio of wood burning, Simpson et al. (2007) suggested a mean European ratio of 2.1 for wood burning, considering ratios previously reported for several combustion methods. Pio et al. (2011) compiled a wide range of OC/EC ratios from a number of urban, rural and remote sites, predominantly in Spain, Portugal and the UK, concluding that the OC/EC ratio obtained is dependent on the location and major sources of OC. Recently, Mbengue et al. (2018) reported a mean OC/EC ratio of  $5.05 \pm 2.59$  over a measurement period of four years in Czechia. The study notes the seasonal fluctuation, with the mean value significantly higher during the summer months. A study carried out by Karanasiou et al. (2020) at two sites in northern Spain reported OC/EC ratios of 0.7 – 8.1 (traffic dominated site) and 1.8 – 12.8 (regional background site).

Previous studies carried out in small Irish towns reported average values of between 3.8 and 6.3 in Killarney, Co. Kerry and Birr, Co. Offaly, respectively (Buckley, 2019). The study concluded that the ambient carbonaceous aerosol was likely influenced by both coal and biomass burning in Killarney, and dominated by biomass burning in Birr. Ceburnis et al. (2006) noted clear seasonal differences in OC/EC ratios between

winter and summer, ranging from 0.4 to 5.5 and 1.0 to 30.0, respectively, across four various environments. The OC/EC ratio recorded during the current field campaign ranged from 4.2 (Carnsore Point) to 6.5 (Malin Head) (Figure 3.31). Based on the review carried out by Ni et al. (2018), such values are strongly indicative of biomass burning.



**Figure 3.31** Measured concentration of organic carbon versus elemental carbon at each sampling site involved in the intensive measurement campaign (December 2017 – February 2018).

There was a strong correlation between the optically measured BC (880 nm) and the thermally measured EC and OC in the samples collected at Carnsore Point and Malin Head ( $r^2 > 0.87$ ). A weaker correlation was observed between these parameters at UCD ( $r^2 \approx 0.57$ ), where, due to the quantity and wide range of sources, the ambient environment is more complex. A correlation between the parameters could not be established for the samples collected at Mace Head, owing to the small number of viable samples, most of which contained extremely low concentrations. A similar trend in correlation is observed in the comparison of total eBC versus thermally measured EC and OC (Figure 3.32).

BC is almost exclusively of primary origin, produced during the incomplete combustion of fossil fuel or biomass burning, whereas OC can be emitted directly to the atmosphere, or formed as a secondary species (Grivas et al., 2012; Pio et al., 2011; Viidanoja et al., 2002). In samples containing organic carbon that could not be attributed to black carbon (samples with poor correlation between OC and BC), it is possible that the organic components of the samples can be attributed to biogenic, marine biogenic, terrestrial vegetation, or agricultural emissions or atmospheric processes, such as aging or oxidation, in which case they could be classified as secondary organic aerosols. Further analysis is required to confirm this, and to ascertain the origin.

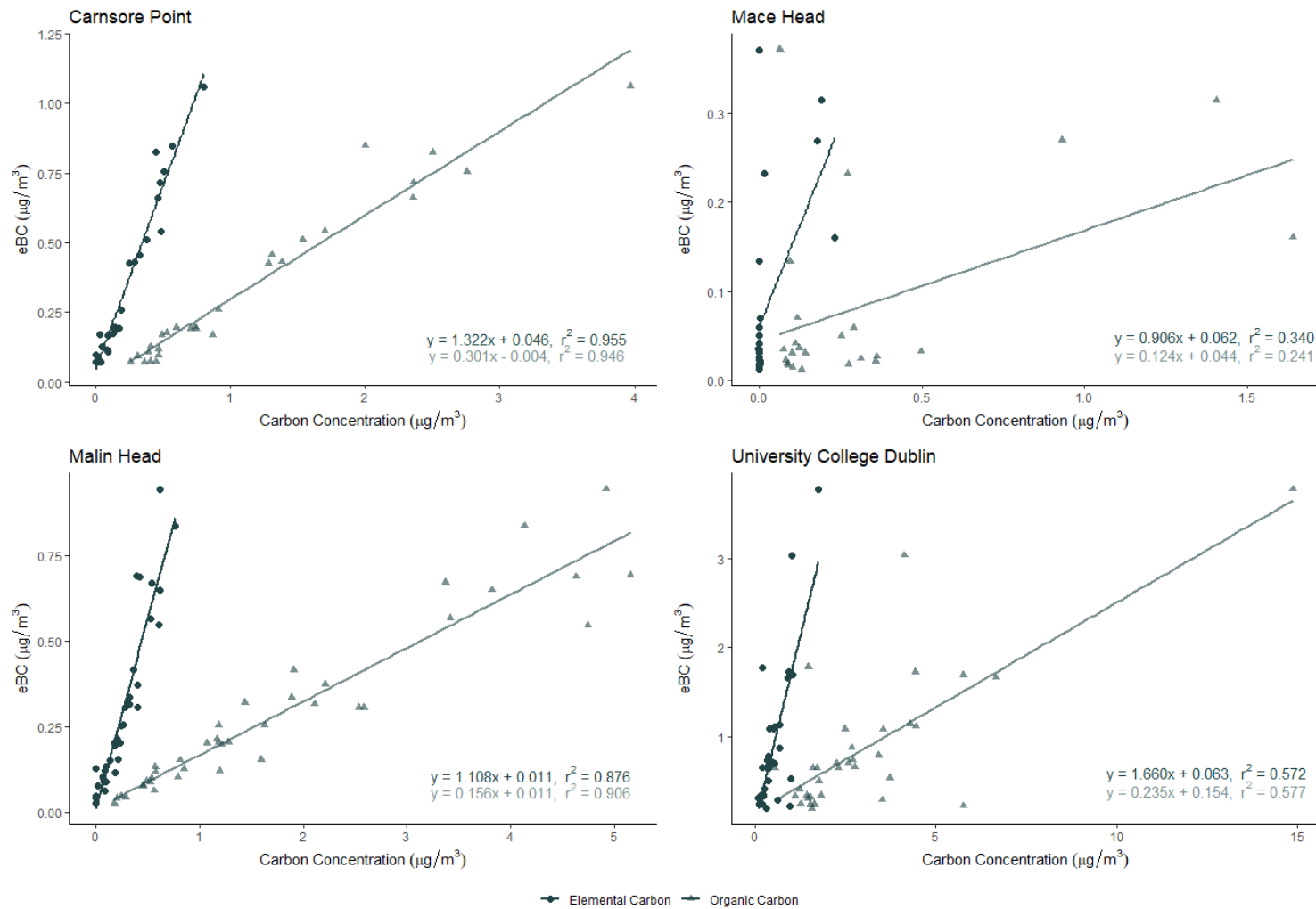


**Figure 3.32** Optical eBC versus thermal EC and OC measured at each of the monitoring sites involved in the field campaign (December 2017 – February 2018).

OC was also compared with  $\Delta C$  values, derived from aethalometer measurements, as described in Section 3.3.2.4. Different techniques were used to measure these two parameters, and the measurements were recorded at different time resolutions. The aethalometer data was averaged to match the sampling period of the OC samples. There was good agreement between  $\Delta C$  and OC at Carnsore Point and Malin Head where  $r^2$  values of 0.89 and 0.90 were obtained, respectively. A weaker correlation was observed at UCD ( $r^2 = 0.67$ ), where there was a much greater spread of values, while a correlation between the parameters measured at Mace Head could not be established.

As the  $\Delta C$  value can be used as a qualitative tracer for wood burning, a strong correlation with thermally derived OC indicates that the majority of the organic carbon detected in the ambient samples may be attributed to wood combustion, further supporting the hypothesis that SOA, biogenic or marine emissions may have had considerable influence on OC concentration sampled at UCD.

### 3.3.4 Calculation of Mass Absorption Cross Section

---

Light absorption by black carbon (BC) can be described by the “absorption coefficient” ( $b_{abs}$ ,  $m^{-1}$ ). BC absorption per mass is described by the term ‘mass absorption cross-section’ (MAC) (Knox et al., 2009). The MAC value is influenced by the coating that builds up on BC, which can act as a lens and focus light into the core of the BC particle (Bergstrom et al., 1982; Knox et al., 2009). At a wavelength of 550 nm, the measured MAC value of freshly emitted black carbon has quite a narrow range;  $7.5 \pm 1.2 m^2 g^{-1}$  (Bond et al., 2013). The MAC value is highly dependent on the mixing state of black carbon and other chemical processes. The ‘mixing state’ defines the distribution of various particle species among particles; externally mixed particles contain a single individual species, while internally mixed particles contain multiple species. Consequently, light absorption by the black carbon particle can be influenced (Yuan et al., 2021). Water is a component of mixed aerosols and its uptake can increase the size of a particle, thus affecting BC absorption. A significant increase in BC absorption at increased humidity has previously been reported (Bond et al., 2013; Mikhailov et al., 2006). Due to the coastal location of each of the sites involved in this field campaign, the relative humidity is high. The mean hourly relative humidity during the sampling period ranged between 81.7% (Malin Head) and 86.7% (University College Dublin). This must be taken into account when analysing the calculated MAC values.

The types of coatings on BC particles vary with source composition. Therefore, MAC values are spatially and temporally variable. In a previous study MAC values of between  $8.34 m^2 g^{-1}$  and  $11.1 m^2 g^{-1}$  were calculated for three small towns in Ireland (Buckley, 2019). Zanatta et al. (2016) provided a range of MAC values from numerous monitoring sites and environments across Europe in a comprehensive review, and concluded that at a wavelength of 637 nm a MAC value of  $10.0 m^2 g^{-1}$  can be considered representative of the mixed boundary layer at European background sites. Similarly, Pandolfi et al. (2014) noted a mean MAC value (637 nm) of  $10.90 m^2 g^{-1}$  at a high-altitude monitoring site in the western Mediterranean basin.

The site-specific MAC value is estimated for each of the sampling sites during the field campaign, using methods described by Knox et al. (2009), in Eqn. 3.1 and Eqn. 3.2 below.

$$BC = \frac{b_{abs}(\lambda)}{MAC(\lambda)} \quad \text{Eqn. 3.1}$$

$$MAC_{true} [m^2 \cdot g^{-1}] = \frac{b_{abs} [m^{-1}]}{EC [g \cdot m^{-3}]} \quad \text{Eqn. 3.2}$$

This method employs the absorption coefficient ( $b_{abs}$ ), calculated using the aethalometer measurements, and the EC content measured thermally off-line by the Sunset OCEC Laboratory Instrument.

BC6 is measured on-line by the aethalometer at a wavelength of 880 nm, with an assumed MAC value of  $7.77 \text{ m}^2 \text{ g}^{-1}$ . The thermal EC concentration is measured off-line by the Sunset OCEC Laboratory Instrument. This instrument has an integrated laser with a nominal wavelength range between 655 and 660 nm. In order to compare the two techniques as accurately as possible, the site-specific MAC value was also estimated using the absorption coefficient derived from the aethalometer measurements from the 660 nm channel (BC5), by applying an assumed MAC value of  $10.35 \text{ m}^2 \text{ g}^{-1}$ . The site-specific MAC estimations are provided in Table 3.5 below. A higher calculated MAC value is obtained when the absorption coefficient of the 660 nm aethalometer channel is employed, in comparison to that of the 880 nm channel.

Thermal EC was determined by analysis of filter samples which were collected on a 24-hour time basis. The aethalometer data was averaged to correspond to the correct time period. The MAC was derived from the slope of the linear regression of absorption coefficient versus the thermal EC (Figure 3.33). The correlation between the parameters varied spatially; the  $r^2$  value at both Carnsore Point ( $n = 28$ ) and Malin Head ( $n = 39$ ) was greater than 0.8, demonstrating good agreement between the AE33 and OCEC instruments. The correlation between the parameters was poor at the Mace Head ( $n = 24$ ,  $r^2 = 0.33$ ) and UCD ( $n = 34$ ,  $r^2 = 0.57$ ) monitoring sites. The concentrations recorded at UCD range widely. This variability undoubtedly influenced the regression outputs.

The estimates of  $10.09 \text{ m}^2 \text{ g}^{-1}$ ,  $6.96 \text{ m}^2 \text{ g}^{-1}$ ,  $8.50 \text{ m}^2 \text{ g}^{-1}$  and  $12.64 \text{ m}^2 \text{ g}^{-1}$  for Carnsore Point, Mace Head, Malin Head and UCD, respectively, were all in close proximity to values previously determined at a number of sites in Ireland, during winter (Buckley, 2019) and across Europe (Zanatta et al., 2016).

It is important to acknowledge the variety in MAC values ascertained for each location. The largest site-specific MAC value calculated was obtained from measurements collected at University College Dublin. This site also had the highest mean concentration of TC of the four sites involved in the campaign, and a larger OC/EC ratio (6.4) than both Carnsore Point and Mace Head. Conversely, Carnsore Point, which had the next largest calculated MAC value ( $10.09 \text{ m}^2 \text{ g}^{-1}$ ), had the lowest OC/EC ratio (4.2) of the monitoring sites.

It is evident that the contribution of EC played an important role in the calculation of individual site-specific MAC values. The largest proportion of EC was measured at UCD, which subsequently influenced the calculation of the largest MAC value. The trend is consistent for MAC values calculated using absorption coefficient values derived from the 660 nm and 880 nm aethalometer channels at Carnsore Point, Malin Head and Mace Head; decreased elemental carbon contribution resulted in lower calculated MAC values.

**Table 3.5** Site-specific mass absorption cross-section estimation (December 2017 – February 2018).

	Calculated MAC, $\sigma$ ( $\text{m}^2 \text{ g}^{-1}$ )	
	880 nm Channel	660 nm Channel
<b>Carnsore Point</b>	10.1	14.9
<b>Mace Head</b>	7.0	10.2
<b>Malin Head</b>	8.5	12.8
<b>University College Dublin</b>	12.6	18.7

By employing the optimised site-specific MAC value, the slope of the linear regression of optical black carbon (880 nm) versus thermal EC was improved; the value approached unity. This was the predicted outcome as the optical black carbon is calculated using Eqn. 3.3.

$$BC = \frac{b_{abs}}{\sigma_{true}} \quad \text{Eqn. 3.3}$$

However, due to the nature of the method employed in obtaining a true site-specific mass absorption cross-section estimate, the re-calculation of optical BC is circular, and could continue to be improved.

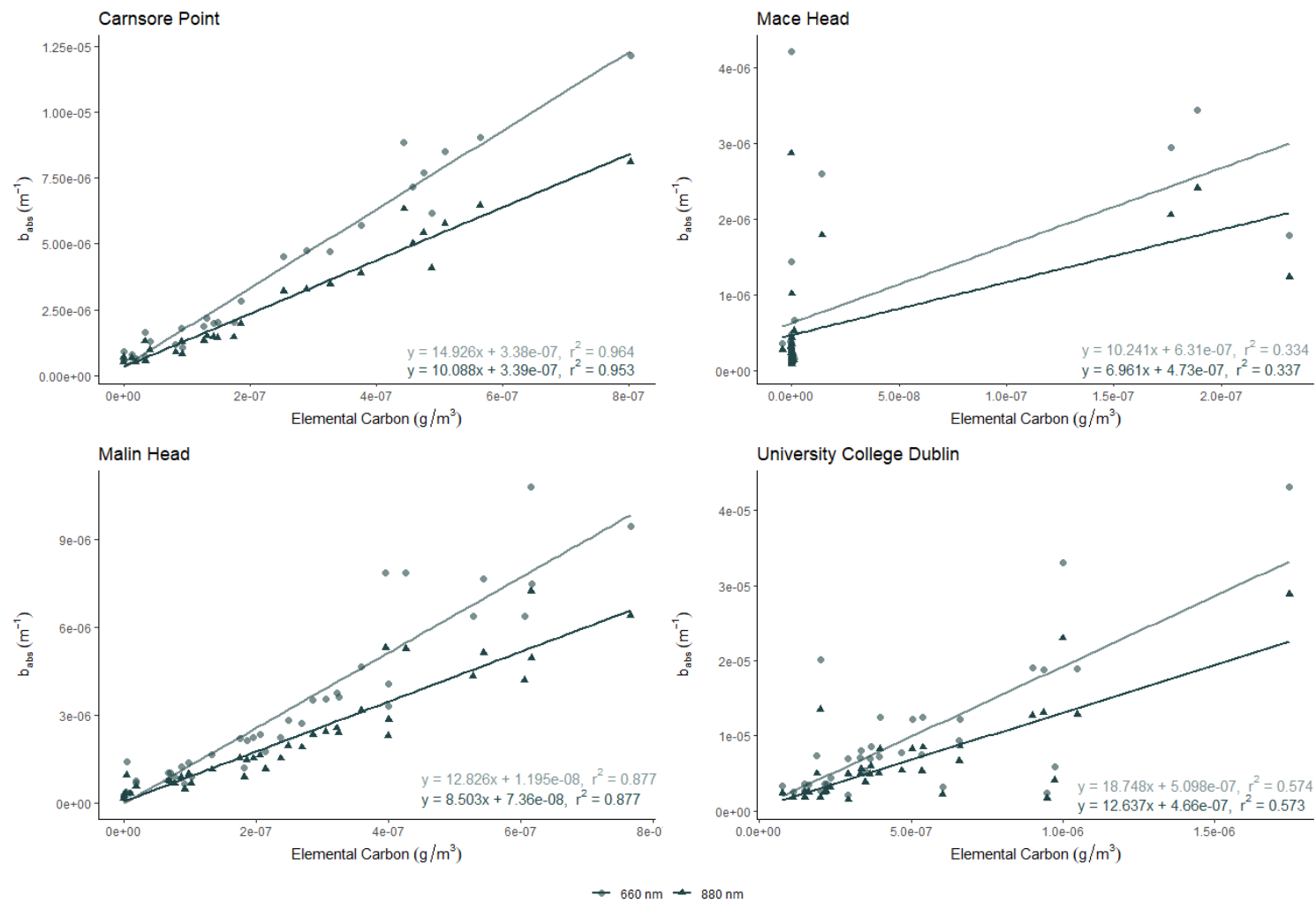


Figure 3.33 Estimation of site-specific MAC value using absorption coefficients calculated at 660 nm and 880 nm.

Another method of calculating the MAC was presented by Nicolosi et al. (2018) who proposed a novel method for representing thermal-optical organic and elemental carbon in the ‘Attenuation Versus Evolved Carbon (AVEC) plot’. By employing this method, the behavior of the sample under analysis can be visually represented, rather than focusing solely on the instrument output, as in a thermogram. It also allows for the amount of organic, elemental and pyrolysed carbon to be estimated directly from the plot. The y-axis of the plot represents the optical attenuation, while the x-axis denotes the amount of carbon evolved from the sample. Therefore, it is possible, in principle, to obtain a value for the MAC of the material evolved from the filter in the oxygenated phase of the thermal-optical analysis, in units of  $\text{cm}^2 \mu\text{g}^{-1}$ . The gradient of this section of the curve is given by Eqn. 3.4.

$$\sigma = \frac{\Delta \text{Attenuation}}{\Delta \text{Carbon evolved}} \quad \text{Eqn. 3.4}$$

The study outlines how artefacts, such as the shadowing effect and multiple scattering effects, must be considered. The shadowing effect may underestimate the calculated attenuation. This effect is caused by large quantities of particles collected on a filter, often at roadside sites. In contrast, the measured attenuation may be overestimated when scattered light is not detected due to the distance between sample and detector. Accounting for such possible artefacts, Nicolosi et al. (2018) reported estimated MAC values of  $35 \pm 14 \text{ m}^2 \text{ g}^{-1}$  in roadside samples,  $42 \pm 8 \text{ m}^2 \text{ g}^{-1}$  in urban samples and  $45 \pm 10 \text{ m}^2 \text{ g}^{-1}$  in rural samples. Spatial variability in calculated values is evident.

A summary of the estimates of mass absorption cross-section of the particles leaving the filter at each monitoring site in this field campaign is provided in Table 3.6. The MAC calculated using samples collected at UCD ( $n = 31$ ) had a mean value of  $39.48 \text{ m}^2 \text{ g}^{-1}$ . This value was similar to that observed by Nicolosi et al. (2018) in the analysis of urban samples. The mean value calculated for Carnsore Point ( $54.36 \text{ m}^2 \text{ g}^{-1}$ ) and Mace Head ( $48.38 \text{ m}^2 \text{ g}^{-1}$ ) were both within the range reported for rural samples by Nicolosi et al. (2018). Malin Head had the largest MAC value estimate, with a mean of  $67.30 \text{ m}^2 \text{ g}^{-1}$ . The range of MAC values calculated by this method was quite broad at each site, indicating contribution from a variety of sources to the ambient aerosol.

**Table 3.6** Estimation of mass absorption cross section as described by Nicolosi et al. (2018).

	Calculated MAC, $\sigma$		
	n	Mean ( $\text{m}^2 \text{g}^{-1}$ )	Range ( $\text{m}^2 \text{g}^{-1}$ )
<b>Carnsore Point</b>	24	54.36	24.87 – 147.17
<b>Mace Head</b>	7	48.38	32.35 – 69.90
<b>Malin Head</b>	34	67.30	26.66 – 184.84
<b>University College Dublin</b>	31	39.48	23.32 – 133.96

This method of estimating the site-specific mass absorption cross section may be beneficial if few viable samples are collected during a sampling period, as it allows for the MAC value to be obtained from a single sample, whereas the method presented by Knox et al. (2009) requires a number of samples to estimate the MAC over time. The time series of AVEC plots shown in Figure 3.35 illustrates the temporal variability associated with MAC value, along with spatial variability.

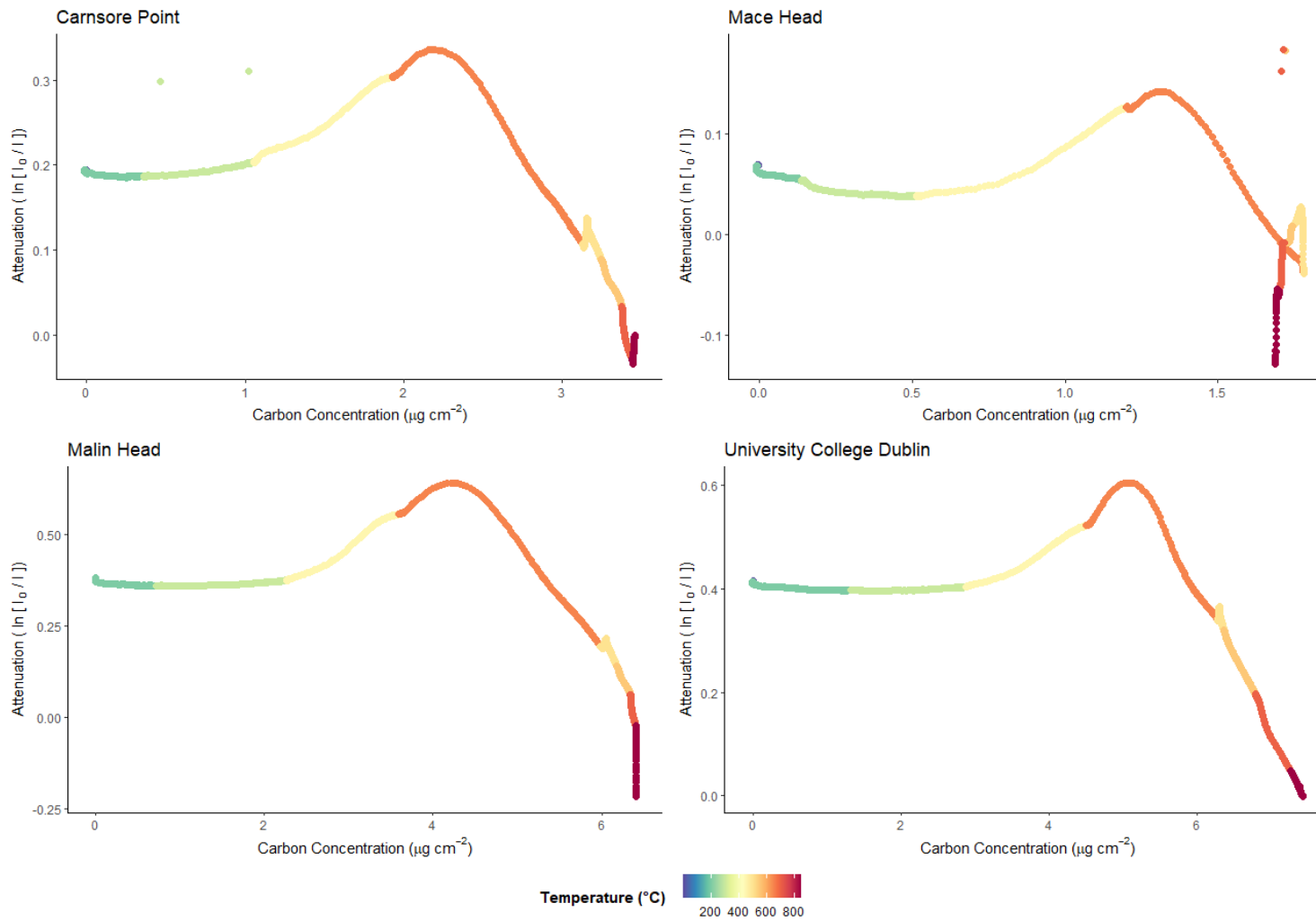


Figure 3.34 AVEC plots of samples collected at each sampling site on February 2, 2018

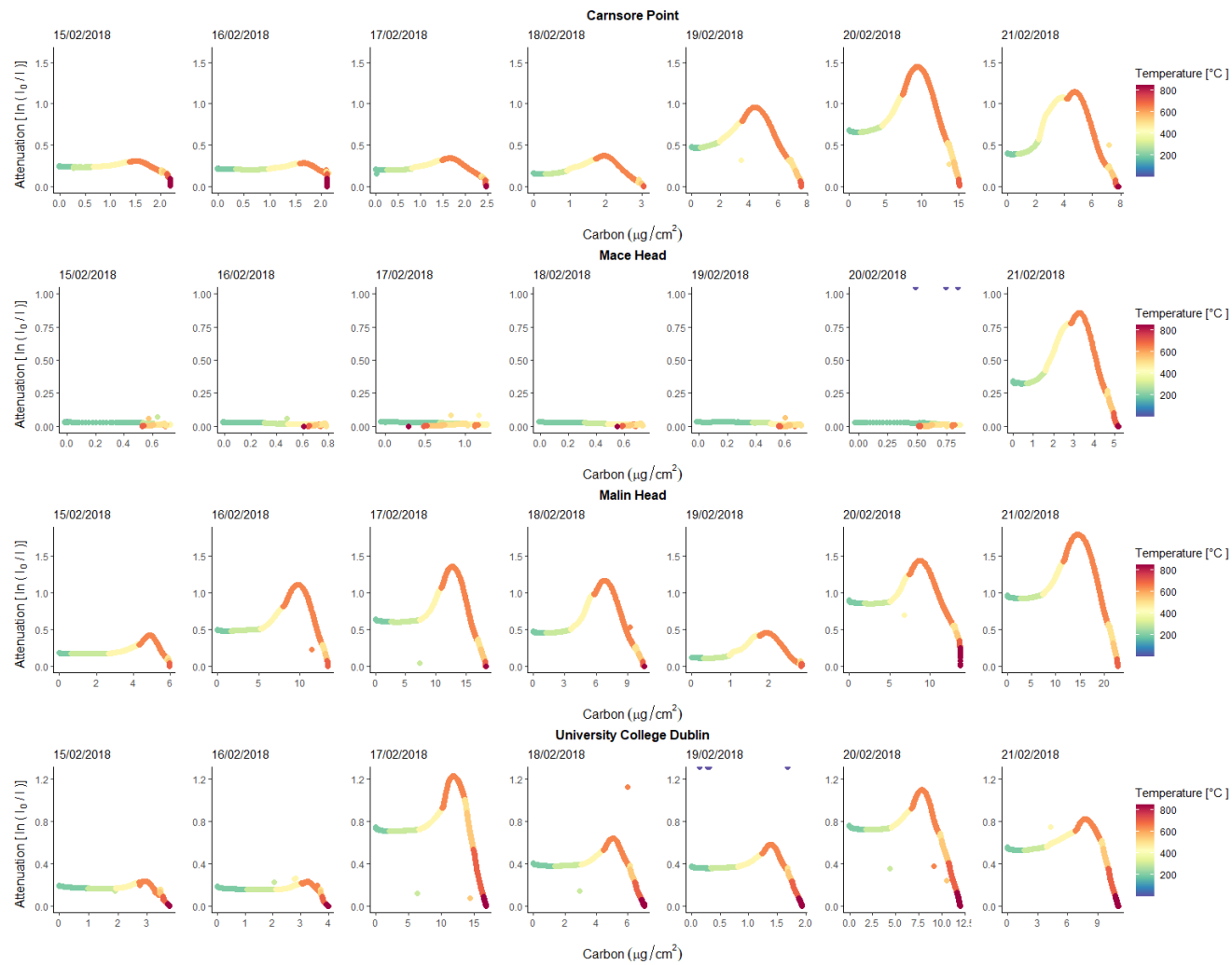


Figure 3.35 Time series of AVEC plots constructed using filter samples collected at each sampling site (February 2 - 21, 2018, inclusive).

### 3.3.5 Levoglucosan

---

Levoglucosan was detected in the majority of samples analysed (81%). This ranged from levoglucosan detection in 100% of the samples collected at University College Dublin to 30% of the samples collected at Mace Head. Galactosan was detected in only 37% of the total samples. According to Figure 3.24 solid fuel was almost exclusively the source of equivalent black carbon in Mace Head, yet only 30% of the samples analysed contained levoglucosan. This result is most likely due to extremely low concentrations resulting in a lack of material on the filters. Table 3.7 gives an overview of the detection of the relevant anhydrosugars, and their respective concentrations, in samples collected at each of the four sites between December 2017 and February 2018. A number of field blanks were collected at each site during the monitoring period. Neither levoglucosan, mannosan or galactosan were detected in the analysis of the field blanks.

Ambient samples were collected over a 24-hour period between 00:00 and 23:59 at Carnsore Point and Malin Head and between 08:00 and 07:59 at Mace Head. Between December 21, 2017 and January 19 2018, samples were collected on a 48-hour basis at the site in UCD and on a 24-hour basis from February 1, 2019 onwards (08:00 - 07:59). The highest ambient concentrations of each of the target anhydrosugars; levoglucosan ( $1090.05 \text{ ng m}^{-3}$ ), mannosan ( $195.75 \text{ ng m}^{-3}$ ) and galactosan ( $34.87 \text{ ng m}^{-3}$ ), were observed at UCD in early February (04/02/2018). The lowest ambient concentration of levoglucosan ( $0.49 \text{ ng m}^{-3}$ ) was recorded at Mace Head, while the minimum values of mannosan ( $0.53 \text{ ng m}^{-3}$ ) and galactosan ( $0.74 \text{ ng m}^{-3}$ ) were recorded at Malin Head and Carnsore Point, respectively. The limit of detection (LOD) for each of the sugars was set out by Iinuma et al. (2009) as  $0.5 \text{ ng m}^{-3}$ ,  $0.3 \text{ ng m}^{-3}$  and  $0.8 \text{ ng m}^{-3}$  for levoglucosan, mannosan and galactosan, respectively, for samples collected at  $500 \text{ L min}^{-1}$  over a 24-hour period. The method provided a positive result for only one sample below the LOD of levoglucosan and one sample below the LOD of galactosan in samples collected during the current field campaign. However, the results obtained below the LOD can be considered accurate as field blanks never produced a positive concentration result.

The mean concentration of levoglucosan recorded at UCD over the entire sampling period was  $149.26 \text{ ng m}^{-3}$ . This is comparable to measurements from central London ( $160 \pm 17 \text{ ng m}^{-3}$ ) reported by Fuller et al. (2014). Mean concentrations observed at

the other locations were significantly lower, ranging from 15.22 ng m<sup>-3</sup> at Mace Head to 43.42 ng m<sup>-3</sup> at Malin Head. Table 3.7 sets out the minimum, maximum and mean concentrations of levoglucosan, mannosan and galactosan recorded at each of the monitoring sites.

**Table 3.7** Summary of anhydrosugar concentration detected in samples collected at each of the monitoring sites involved in the intensive measurement campaign (December 2017 – February 2018).

	<b>Carnsore Point</b>	<b>Mace Head</b>	<b>Malin Head</b>	<b>University College Dublin</b>
<b>Sample Number</b>	<b>28</b>	<b>30</b>	<b>39</b>	<b>34</b>
<b>Levogluconan (ng m<sup>-3</sup>)</b>				
<i>Detection (%)</i>	96.4	30.0	92.3	100.0
<i>Mean ± SD</i>	40.31 ± 40.75	15.22 ± 16.83	43.42 ± 42.99	149.26 ± 196.16
<i>Range</i>	2.55 – 149.25	0.49 – 37.84	0.79 – 151.72	33.05 – 1090.05
<b>Mannosan (ng m<sup>-3</sup>)</b>				
<i>Detection (%)</i>	92.9	16.7	82.1	100.0
<i>Mean ± SD</i>	8.42 ± 8.71	4.34 ± 2.21	8.07 ± 6.87	25.57 ± 34.96
<i>Range</i>	0.64 – 34.14	0.72 – 6.23	0.53 – 25.97	4.89 – 195.75
<b>Galactosan (ng m<sup>-3</sup>)</b>				
<i>Detection (%)</i>	42.9	3.3	38.5	61.8
<i>Mean ± SD</i>	3.57 ± 2.57	1.23 ± ND	4.44 ± 2.42	7.51 ± 7.38
<i>Range</i>	0.74 – 8.25	1.23 – 1.23	1.30 – 9.08	1.87 – 34.87

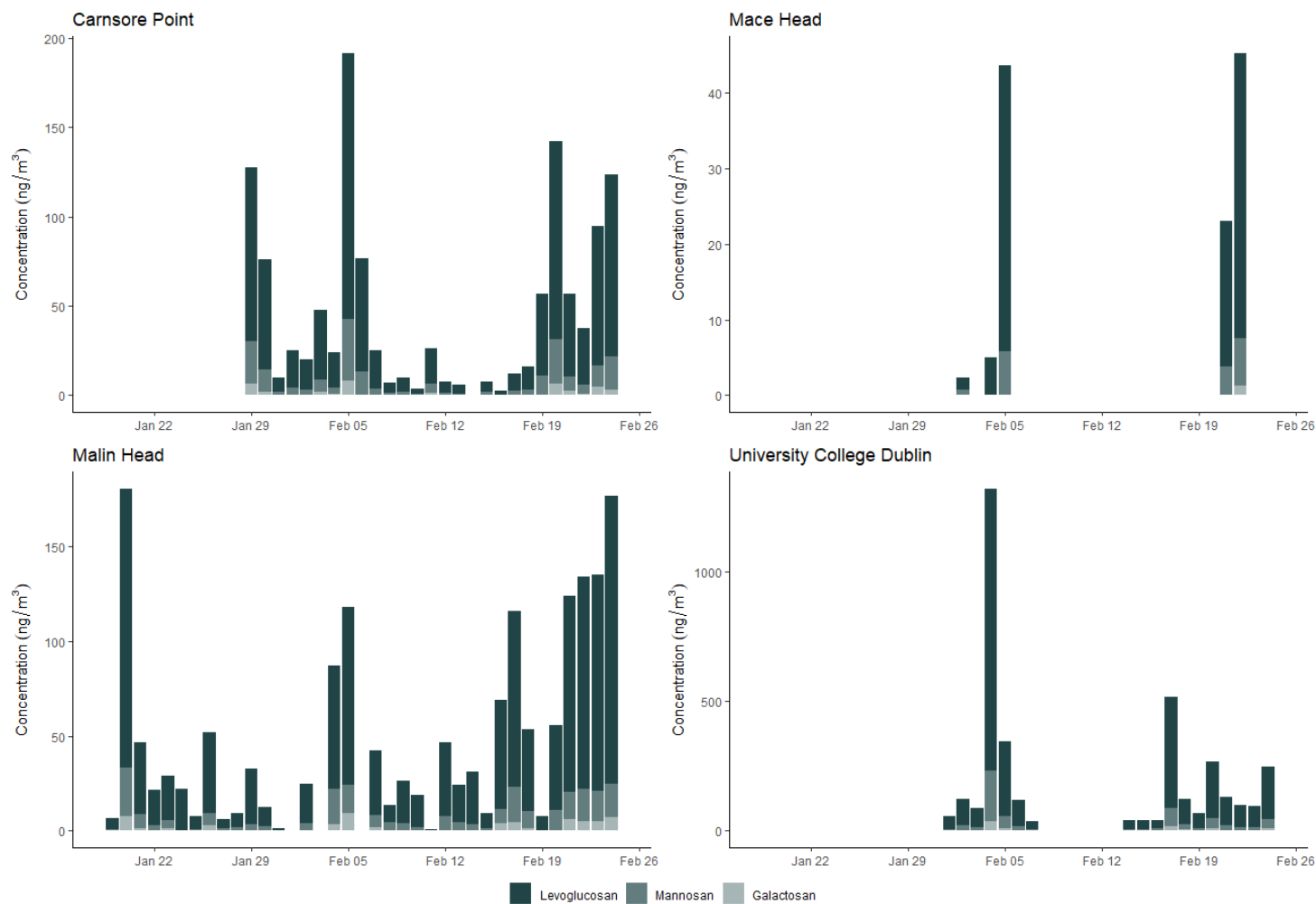


**Figure 3.36** Temporal profiles of levoglucosan, mannosan and galactosan measured at each of the monitoring sites involved in the intensive measurement campaign (December 2017 – February 2018).

The correlation between the three isomers at each of the sites varied slightly. The strongest correlation was observed at UCD ( $r^2 > 0.96$ ), while a lower degree of correlation was recorded at Malin Head ( $r^2 > 0.71$ ). A high degree of correlation indicated that each of the isomers originate from a common source. These observations are illustrated in Figure 3.37.

The ratio of levoglucosan to mannosan can be used to distinguish between types of wood used in combustion. Previous studies have concluded that, in general, softwood, such as pine and spruce, give a lower levoglucosan to mannosan ratio than hardwood, such as ash and oak. Reported ratios for softwoods range between 3.9 and 4.7, while ratio values of up to 25 have been determined for hardwood (Fine et al., 2004a, 2004b; Kourtchev et al., 2011; Schmidl et al., 2008). The levoglucosan/mannosan ratios obtained for peat ( $8.58 \pm 0.03$ ) and bituminous coal ( $3.11 \pm 0.01$ ) have also been reported in a study conducted by Kourtchev et al. (2011). A summary of the mean ratios obtained at each of the monitoring sites involved in the current campaign is provided in Table 3.8. Little spatial variation in levoglucosan to mannosan (L/M) ratio was observed, while a wider range in levoglucosan to galactosan (L/G) ratio was recorded. The lowest average L/M ratio recorded at Carnsore Point ( $4.9 \pm 0.9$ ) is consistent with previous speculation that coal burning contributed to total ambient aerosol at this location, particularly in the eveningtimes.

*Table 3.8 Mean calculated ratio of levoglucosan to its isomers; mannosan and galactosan.*

	Ratio (Mean $\pm$ SD)	
	L/M	L/G
<b>Carnsore Point</b>	$4.9 \pm 0.9$	$23.1 \pm 8.2$
<b>Mace Head</b>	$5.3 \pm 1.8$	$30.7^\ddagger$
<b>Malin Head</b>	$6.0 \pm 2.0$	$19.6 \pm 5.4$
<b>University College Dublin</b>	$6.0 \pm 0.6$	$24.5 \pm 5.7$

$^\ddagger$  Standard deviation could not be determined due to the limited number of samples in which the anhydrosugar was detected.

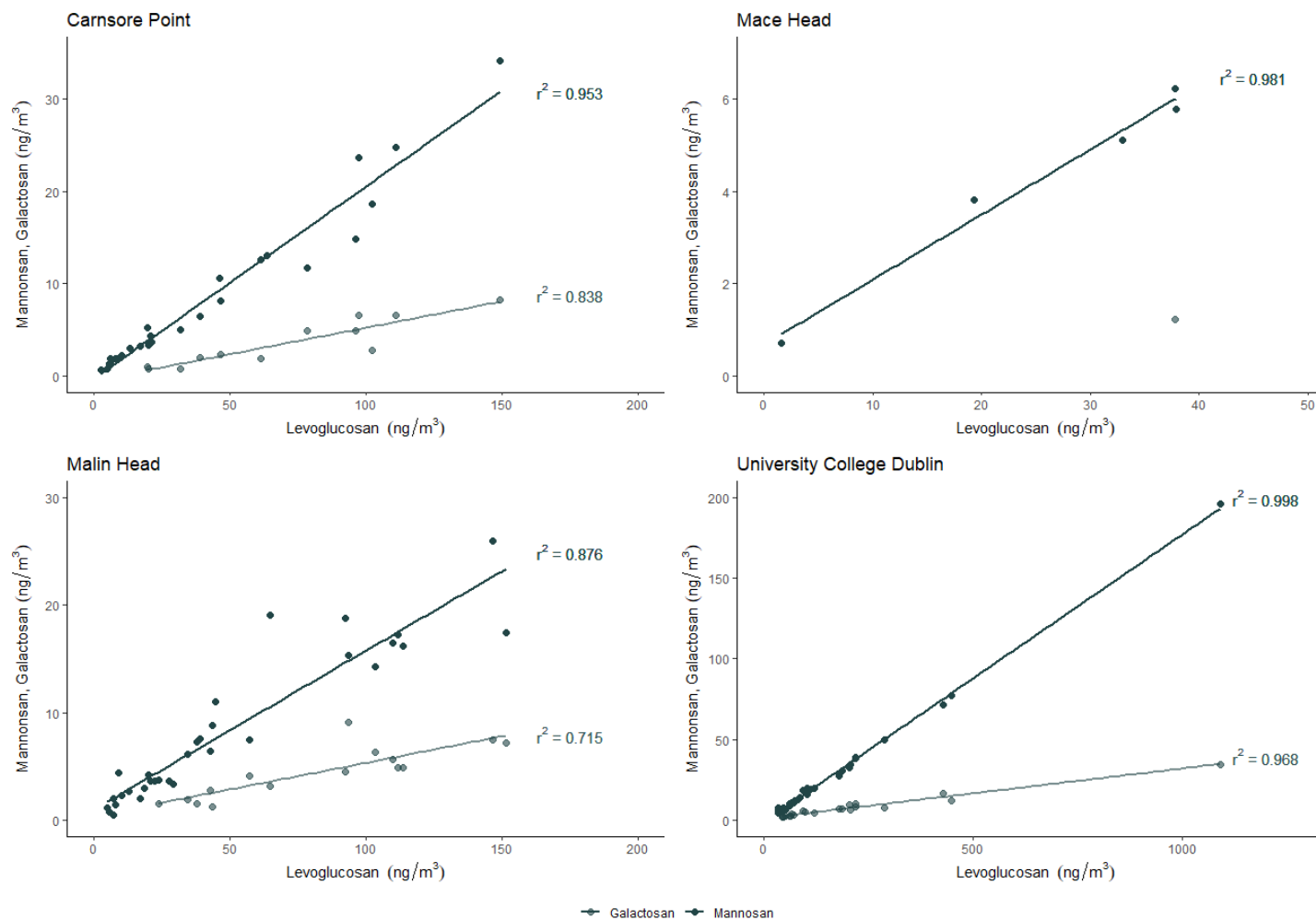


**Figure 3.37** Scatter plot of the concentrations of mannosan and galactosan versus levoglucosan collected at each of the monitoring sites involved in the intensive measurement campaign (December 2017 – February 2018).

Levoglucosan concentrations, determined using filter samples collected over a 24-hour period throughout the field campaign, were compared to a number of parameters derived from the aethalometer data. For an accurate comparison, the aethalometer data was averaged over the corresponding time period for each site. Concentrations of levoglucosan, and its isomers, were extremely low in ambient samples collected at Mace Head. Levoglucosan was detected in only nine samples. Analysis and output of reliable results was difficult with such a small sample size.

The relationships between levoglucosan and BC<sub>6</sub> (880 nm), eBC, eBC<sub>SF</sub> and eBC<sub>Tr</sub> at Carnsore Point, Malin Head and University College Dublin, respectively, were investigated. Similar results were observed at all three sites; strong correlation was observed between levoglucosan and eBC<sub>SF</sub>, while the relationship between levoglucosan and eBC<sub>Tr</sub> was quite weak, as predicted (Figure 3.39). The strongest relationship between levoglucosan and eBC<sub>SF</sub> was measured at Carnsore Point ( $r^2 = 0.95$ ). This site also had the strongest correlation between levoglucosan and BC<sub>6</sub> (880 nm) and total eBC.

It is interesting to note that at Carnsore Point levoglucosan appeared to have a stronger correlation with BC<sub>6</sub> and total eBC than with eBC<sub>SF</sub>. This is inconsistent with observations made at other monitoring sites and may provide further support for the assertion that the measured eBC is sometimes incorrectly assigned to sources by the aethalometer model, particularly at this monitoring site. It is possible that the high absorption efficiency in the IR region of primary emissions derived from coal burning, which contains levoglucosan, caused the particles to appear similar to traffic-related emissions in the context of the aethalometer model, ultimately leading to an overestimation of eBC<sub>Tr</sub>.

The correlation between levoglucosan and the calculated AAE was also examined (Figure 3.38). Levoglucosan concentrations increased with AAE, but the relationship was not linear. Levoglucosan concentrations at Carnsore Point and Malin Head were very low when the corresponding AAE was <1.2 and increased sharply with AAE thereafter. The concentration of levoglucosan samples collected at UCD, a more complex environment, also appeared to increase with increasing AAE. However AAE averaged over the corresponding time period of these samples ranged between 1.19 and 1.42. The results detected were consistent with anticipated observations. Increased

concentrations of levoglucosan correspond to enhanced contributions from wood and peat combustion, which ultimately results in an average AAE tending towards 1.68. In instances where lower AAE values are recorded, the environment is generally dominated by fossil fuel combustion emissions, presumably containing little to no significant quantities of levoglucosan.

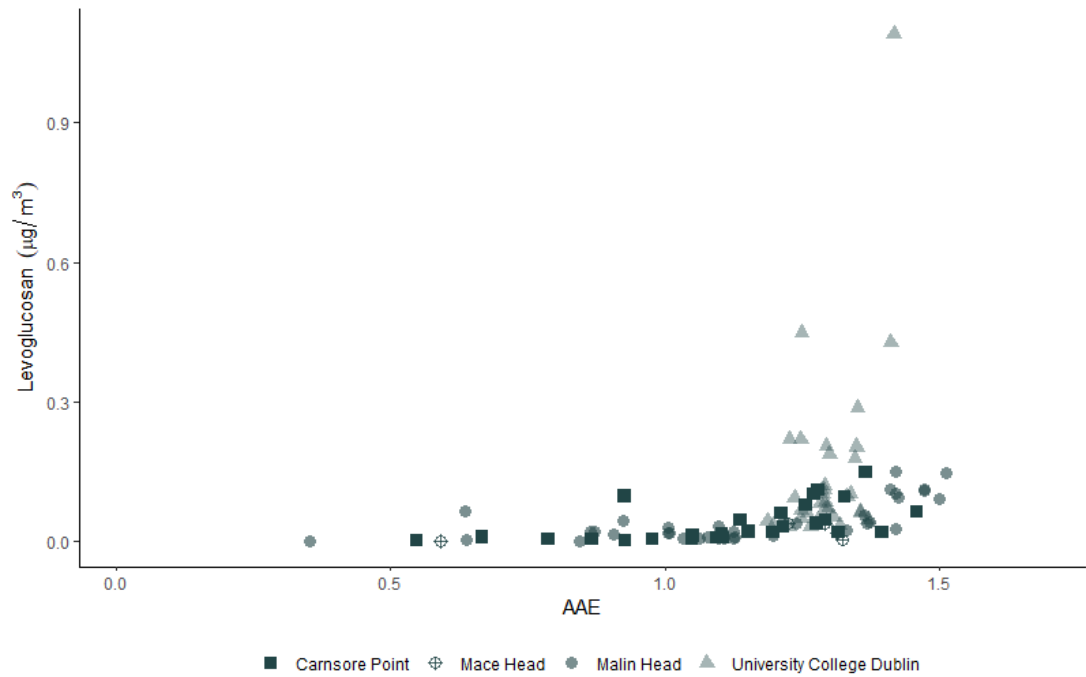


**Figure 3.38** Levoglucosan concentration versus AAE derived from aethalometer output.

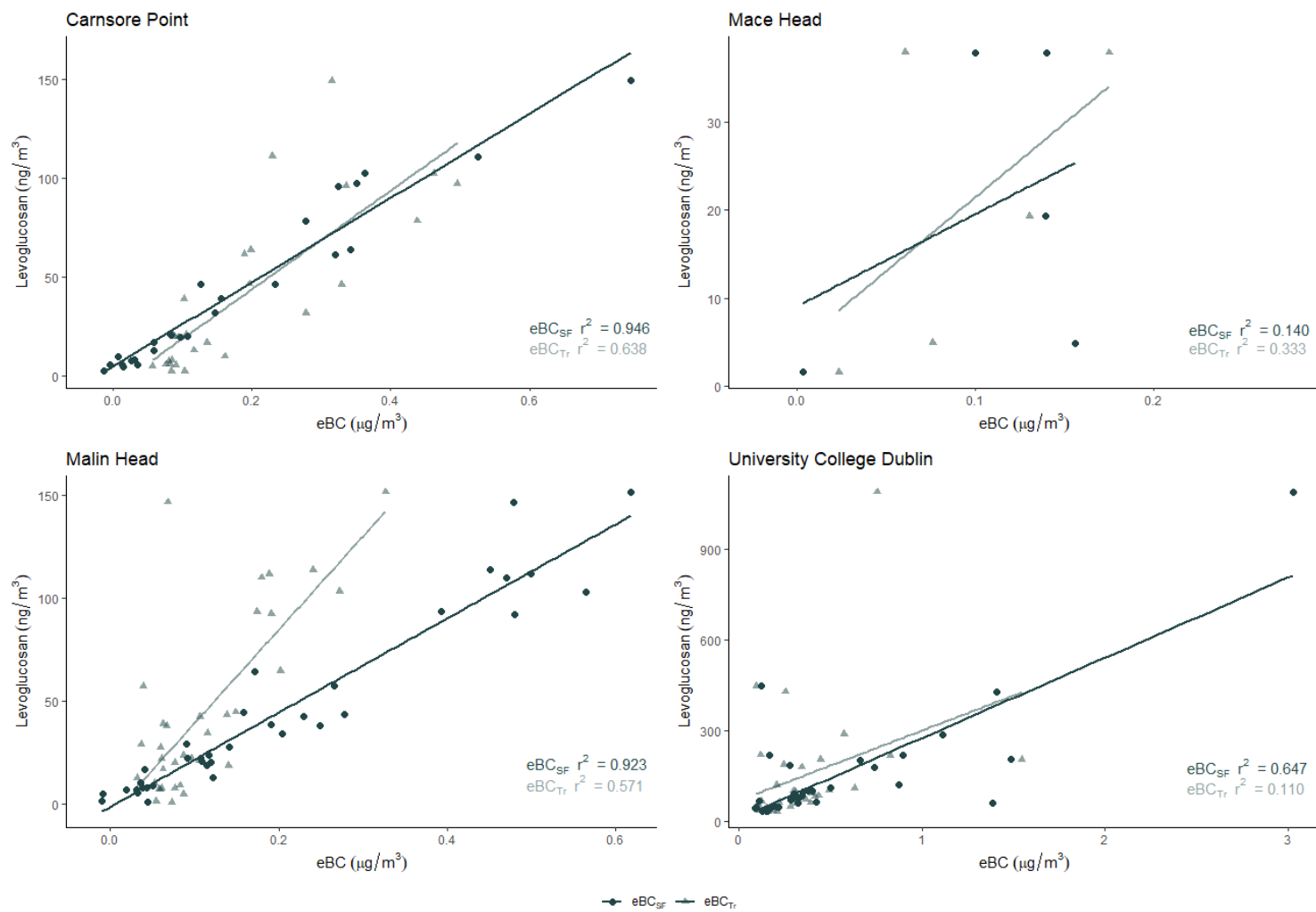


Figure 3.39 Levoglucosan concentrations versus eBC<sub>SF</sub> and eBC<sub>Tr</sub> concentrations measured at each sampling site (December 2017 – February 2018).

The measured levoglucosan concentrations ( $\text{ng m}^{-3}$ ) follow a similar trend to the EC and OC concentrations ( $\mu\text{g m}^{-3}$ ), illustrated by Figure 3.40. The fractions of OC and EC correspond to the carbon evolved (OC1 – EC4) during each step of the temperature protocol (EUSAAR\_2). The pyrolysed carbon (PC) exists due to the formation of elemental carbon caused by charring of organic carbon during the initial, inert phase. The artificially low measurement of OC and falsely high measurement of EC is identified and corrected for by continuously monitoring the laser transmittance, as described in Chapter 2. When stacked, these fractions amount to the total carbon measured in each sample.

Levoglucosan was detected on very few samples collected at Mace Head, Co. Galway. Only 30% of the filter samples (30) collected contained levoglucosan concentrations high enough to be detected, including 3 samples with concentrations lower than the limit of detection reported by Iinuma et al. (2009) for this method. For this reason, the analysis of the Mace Head data is excluded from Figure 3.40 below.

The organic fraction desorbed during the inert phase of the analysis protocol at  $650\text{ }^{\circ}\text{C}$  (OC4) appeared to increase substantially with levoglucosan at Carnsore Point, Mace Head and Malin Head. OC2, which desorbs at  $300\text{ }^{\circ}\text{C}$  under the inert atmosphere, increased most significantly with levoglucosan in the samples collected at UCD. This indicates that a higher proportion of the organic content of the samples collected at UCD was more volatile than those collected elsewhere, suggesting measurement of fresh, less oxidised emissions. A higher proportion of the OC4 fraction at other locations indicates a stronger influence of aged emissions. No obvious association between levoglucosan and EC was observed.

The levoglucosan to OC ratio was also investigated. A similar mean ratio was recorded at Carnsore Point ( $37.7\ \mu\text{g mg}^{-1}$ ), Malin Head ( $40.4\ \mu\text{g mg}^{-1}$ ) and University College Dublin ( $45.2\ \mu\text{g mg}^{-1}$ ), however a much lower ratio was observed at Mace Head ( $14.4\ \mu\text{g mg}^{-1}$ ). Kourtchev et al. (2011) reported levoglucosan/organic carbon ratios derived from a number of fuel types, ranging from  $1.84 \pm 0.03\ \mu\text{g mg}^{-1}$  (smokeless coal) to  $235.59 \pm 1.73\ \mu\text{g mg}^{-1}$  (ash wood) The ratio obtained for Mace Head indicates that bituminous coal ( $12.41 \pm 0.17\ \mu\text{g mg}^{-1}$ ) was the dominant source, however the extremely low concentrations of both OC and levoglucosan must be accounted for.

This monitoring site also experienced high wind speeds and was constantly influenced by clean air masses from the North Atlantic.

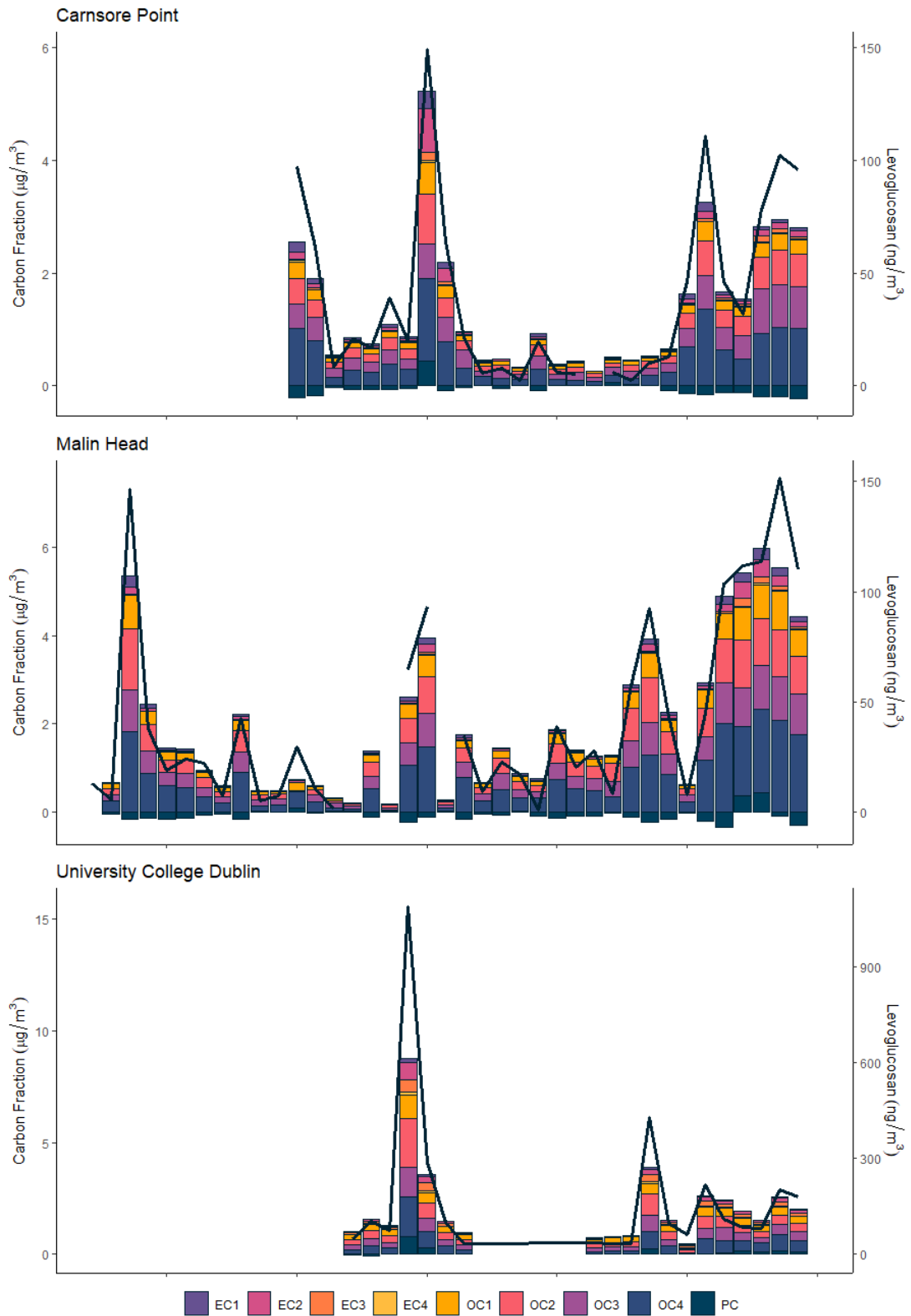


**Figure 3.40** EC and OC fractions with corresponding levoglucosan concentration for samples collected at Carnsore Point, Malin Head and University College Dublin (January – February 2018).

The presence of levoglucosan in ambient PM indicates wood burning in the locality. Assuming that levoglucosan is only emitted during this specific process, it is expected that levoglucosan will not be detected during periods when there are no contributions from wood burning. Therefore, as described by Fuller et al. (2014), the regression of levoglucosan concentrations against the estimated  $b_{abs}(wood\ burning)$  is expected to yield a zero intercept; the line passing through the origin. It follows that an appropriate site-specific Ångström exponent for black carbon attributed to traffic-related emissions ( $\alpha_{Tr}$ ) can be calculated.  $\alpha_{wb}$  was set to a value of 1.68, a value widely accepted as the absorption Ångström exponent for black carbon attributed to biomass burning, while a range of values (0.8 – 1.2) were employed in steps of 0.1 as  $\alpha_{Tr}$  in a series of tests. Fuller et al. (2014) concluded that the mean values of  $b_{abs}(wb)(370\ nm)$  were more sensitive to changes in  $\alpha_{wb}$  for  $\alpha_{Tr}$  values  $< 1$ , but became insensitive to changes in  $\alpha_{wb}$  for  $\alpha_{Tr}$  values greater than 1.2. In a similar study, Diapouli et al. (2017) calculated an optimal  $\alpha_{Tr}$  value of 1.03.

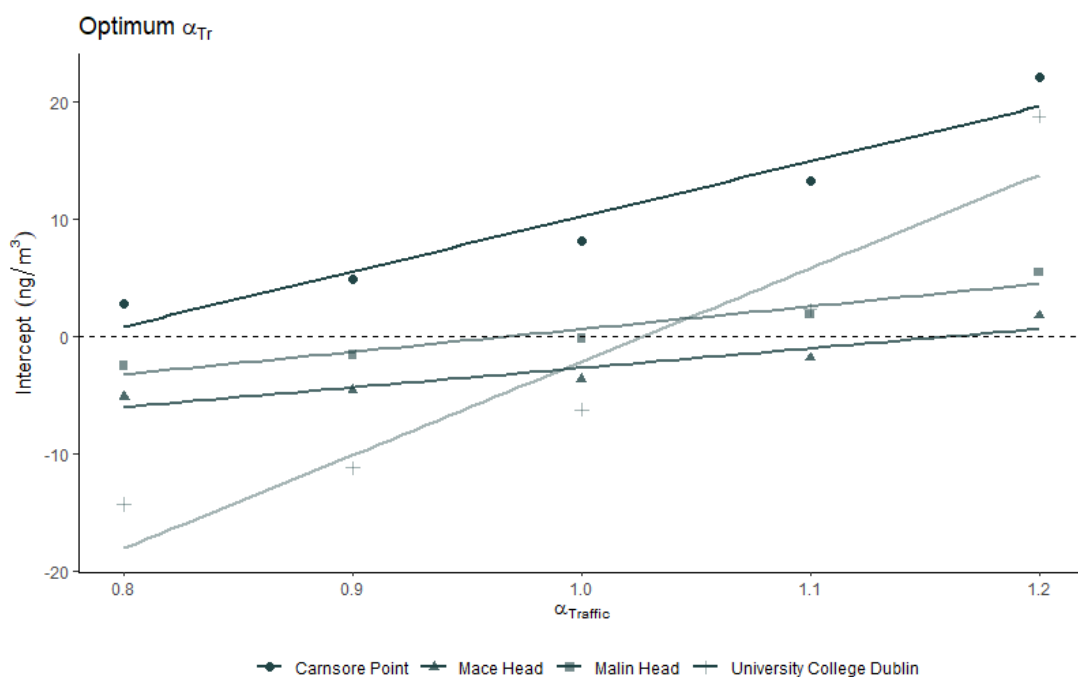


**Figure 3.41** Values of the intercept of the linear regression of levoglucosan concentrations over corresponding mean  $b_{abs}$ , calculated for different  $\alpha_{Tr}$  values.

Figure 3.41 illustrates the individual intercepts determined for the various values of  $\alpha_{Tr}$ , and subsequently the deduced optimum values of  $\alpha_{Tr}$  for each of the four sites. Table 3.9 provides a summary of the optimum absorption Ångström exponents for

attributing black carbon to traffic-related emissions and the related  $r^2$  values obtained ( $0.88 \leq r^2 \leq 0.93$ ). The calculated Pearson coefficient suggests strong correlation, positively confirming the use of this methodology. The optimum  $\alpha_{Tr}$  values calculated for Mace Head, Malin Head and UCD are quite similar, with a mean value of 1.05. The  $\alpha_{Tr}$  value calculated for Carnsore Point is more than 10% smaller than  $\alpha_{Tr}$  values recommended by both Sandradewi, Prévôt, Szidat et al. (2008) ( $\alpha_{Tr} = 1.1$ ) and Zotter et al. (2017) ( $\alpha_{Tr} = 0.9$ ) This confirms the observations made previously that the measurement and assignment of traffic-related emissions may not be entirely accurate at this site. Measurements at the site may not be influenced solely by local sources, including coal combustion, but could also be affected by long range transportation from Europe.

*Table 3.9 Summary of optimum values calculated for  $\alpha_{Tr}$ .*

	<b>Optimum <math>\alpha_{Tr}</math> Value</b>	<b><math>r^2</math></b>
<b>Carnsore Point</b>	0.80	0.93
<b>Mace Head</b>	1.14	0.89
<b>Malin Head</b>	0.97	0.93
<b>University College Dublin</b>	1.02	0.90

In previous studies, this method assumes only two sources of black carbon; traffic-related and wood combustion emissions. But how appropriate is this in an Irish context where a variety of solid fuels are used in combustion for domestic heating? Kourtchev et al. (2011) attributed the presence of levoglucosan to the combustion of wood, peat, bituminous and smokeless coal, further validating the terminology used throughout the analysis presented; ‘solid fuel’ rather than ‘wood burning’, exclusively.

### 3.3.6 Storm Emma: The Beast from the East

---

Sometimes nature provides unusual experimental conditions. Storm Emma in 2018 is one such example. In early spring 2018, Ireland experienced record low temperatures and widespread snowfall. Unusual easterly winds swept across the country, in marked contrast with the predominant south-westerly winds. This section will investigate the impact of this natural meteorological event on ambient air quality; whether it resulted in an increase or decrease in levels of monitored pollutants at Carnsore Point, Mace Head, Malin Head or University College Dublin and if it influenced the ambient aerosol composition.

#### 3.3.6.1 *Meteorological Conditions*

---

Between February 27 and March 4, 2018 Ireland experienced record low temperatures and significant snowfall as easterly winds swept across the country following sudden stratospheric warming (SSW) events. Due to an exceptionally cold air mass from Siberia, record low temperatures engulfed the country and snow drifts over 2 m were recorded in some locations. Prevailing winds in Ireland are south westerly, usually bringing clean air masses from across the Atlantic Ocean, however this easterly wind carried air masses from Siberia and across Europe and Great Britain and was commonly referred to as ‘The Beast from the East’. Simultaneously, a depression named ‘Emma’ tracked northwards from the Bay of Biscay with its associated frontal systems. This resulted in further low temperatures and widespread snowfall during the early days of March 2018 (Met Éireann, 2019). The impacts of Storm Emma and ‘The Beast from the East’ were widespread; disrupting farming, travel, power, communication and numerous other services.

HYSPLIT modelling was used to construct Figure 3.44 which illustrates the 168-hour back trajectory of air masses influencing the four Irish monitoring sites on February 18 and February 25, 2018. A clean air mass from the North Atlantic Ocean reached Ireland at midnight on February 18, and one week later, by midnight on February 25, Ireland was experiencing the effects of an air mass that had travelled across Europe, resulting in unusually low temperatures and increased concentrations of eBC.

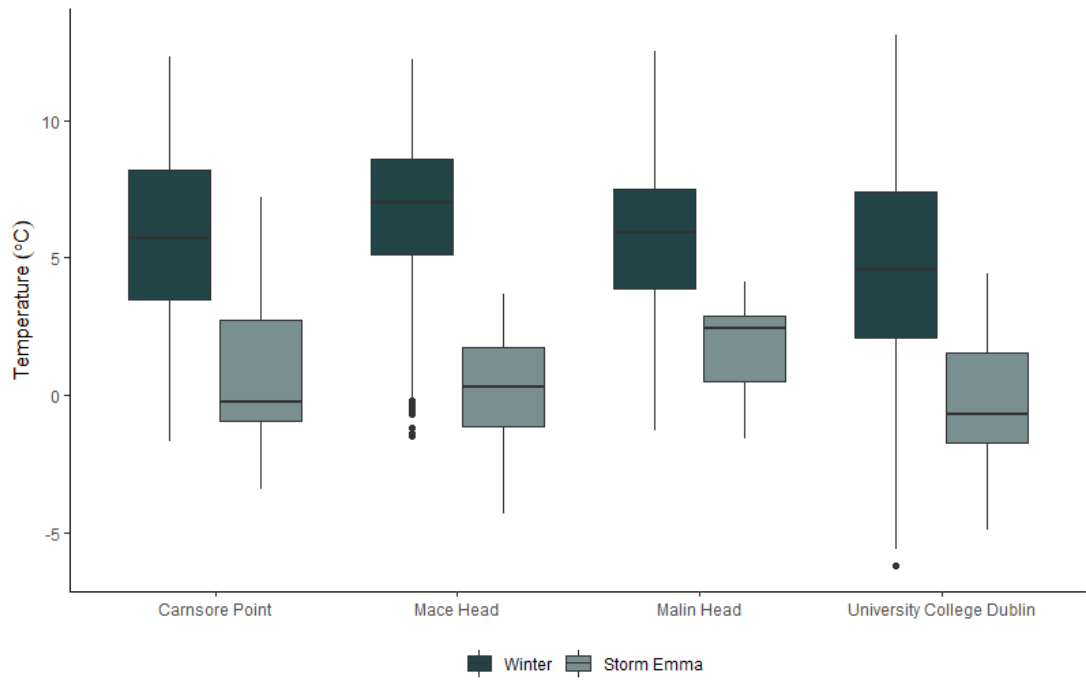


**Figure 3.42** Comparison of ambient temperatures recorded at each sampling site throughout the winter (December 1, 2017 - February 25, 2018) and during Storm Emma (February 28, - March 4, 2018).

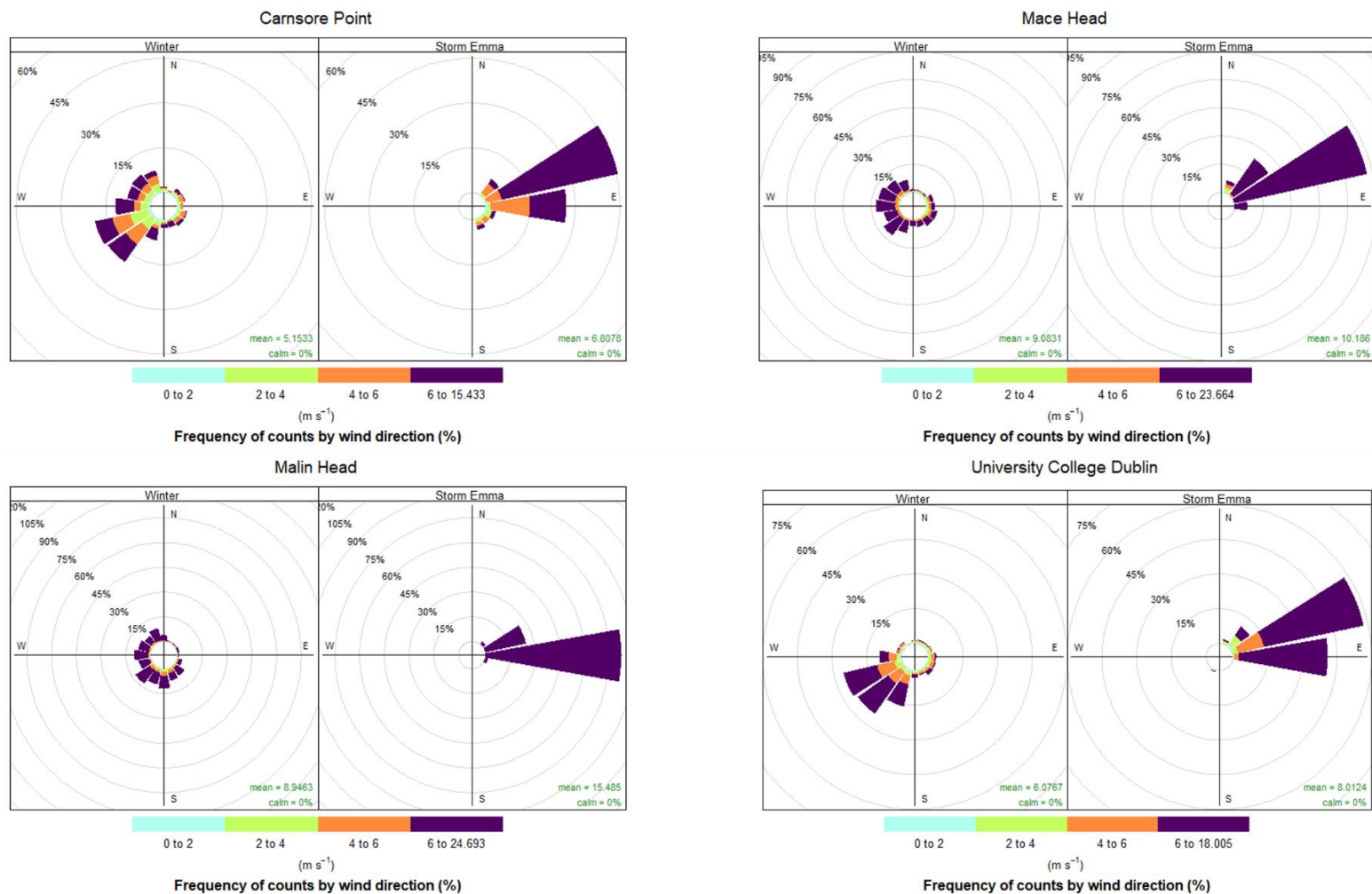


**Figure 3.43** Windrose plots comparing the wind speed and wind direction recorded at each sampling site throughout the winter (December 1, 2017 - February 25, 2018) and during Storm Emma (February 28, - March 4, 2018).

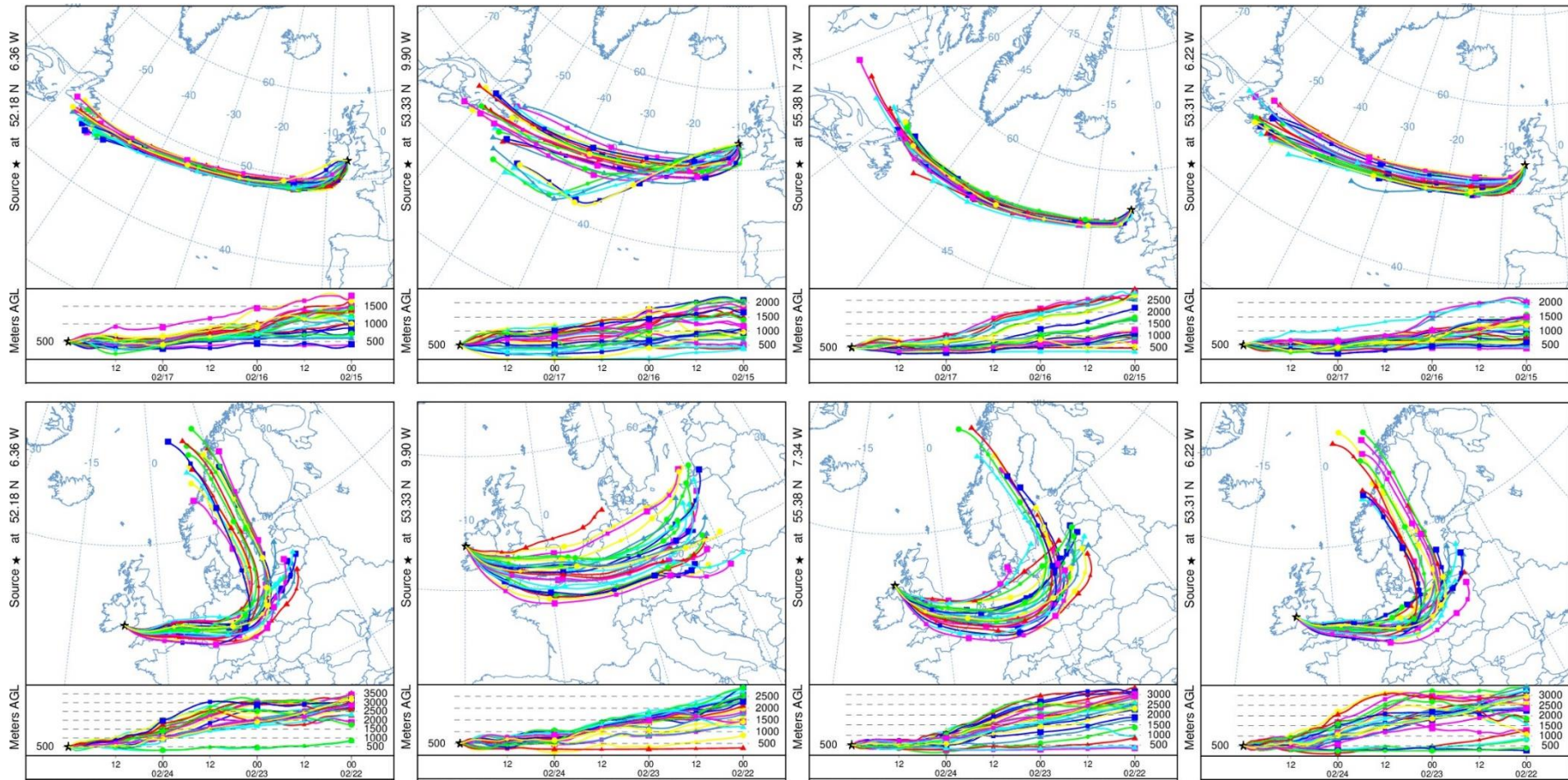


Figure 3.44 HYSPLIT back trajectories of air masses influencing monitoring sites on February 18 (top) and February 25 (bottom), 2018.

### 3.3.6.2 Equivalent Black Carbon

---

Multi-wavelength aethalometers were deployed at each monitoring site for the continuous measurement of equivalent black carbon between December 2017 and March 2018. This allowed for data capture throughout the winter (01/12/2017 – 25/02/2018) and the unprecedented severe conditions experienced during Storm Emma (26/02/2018 – 04/03/2018). Mean hourly average concentrations of eBC increased significantly under storm conditions at each location (Figure 3.45, Table 3.10). This severe weather event also influenced the composition of the ambient aerosol. Application of the Zotter parameters ( $\alpha_{Tr} = 0.9$  and  $\alpha_{SF} = 1.68$ ) allowed for the source apportionment of the total measured eBC. Contributions from traffic-related and solid fuel combustion emissions to total eBC varied. The storm conditions did not have comparable effects on the contribution of the dominant sources at each location (Table 3.10). Despite a slightly stronger influence from solid fuel burning emissions at Malin Head and University College Dublin during the storm, compared to general wintertime conditions, a significant difference was observed at Carnsore Point, where the percentage contribution increased from 16.7% to 40.0%. In contrast, the percentage contribution of eBC<sub>SF</sub> to total eBC decreased at Mace Head during Storm Emma. This is likely due to a drastic change in aerosol composition at this location. Clean air masses from the Atlantic Ocean usually dominate the ambient conditions at Mace Head, with little influence from local solid fuel combustion emissions. However, the easterly winds carried an air mass composed of a mix of fresh and aged particles, with numerous sources across Europe, the UK and Ireland, resulting in unusual aerosol composition at Mace Head. The impact of a change in predominant wind direction on local air quality was most evident at this sampling site.

To further investigate the effect of this unusual easterly wind on the ambient aerosol composition, the frequency distribution of calculated AAEs derived from aethalometer measurements was examined. Throughout the initial sampling period (December 1, 2017 – February 25, 2018) the range of AAE values obtained was quite broad at each location, with the exception of UCD, indicative of a mixed aerosol composition. In contrast, particularly at Carnsore Point (Figure 3.46) and Mace Head (Figure 3.47), a narrow frequency distribution was observed in measurements recorded during Storm Emma, suggesting fewer influential sources. At Malin Head (Figure 3.48) a bi-modal distribution was obtained during the Storm period, similar to the previous months.

Despite the similarities in bi-modal distribution, the most frequent AAEs were shifted towards 1 and above during Storm Emma. Although a narrow distribution of AAEs was recorded at UCD throughout the winter, the distribution narrowed further (1.1 – 1.4) in data collected during Storm Emma at this location (Figure 3.49).

**Table 3.10** Summary of hourly average eBC concentrations at regional and urban background locations, representative of ambient conditions during wintertime and during Storm Emma. Contributions from solid fuel combustion related emissions to total eBC are included.

	Winter		Storm Emma	
	<i>Mean</i>	<i>Range</i>	<i>Mean</i>	<i>Range</i>
<b>Equivalent Black Carbon (<math>\mu\text{g m}^{-3}</math>)</b>				
<b>Carnsore Point</b>	0.27	0.00 – 5.36	0.42	0.04 – 0.94
<b>Mace Head</b>	0.14	0.00 – 8.87	0.50	0.05 – 1.78
<b>Mal in Head</b>	0.29	0.00 – 4.10	0.31	0.03 – 1.67
<b>University College Dublin</b>	0.79	0.00 – 17.18	1.02	0.03 – 10.78
<b>eBC<sub>SF</sub>/eBC<sub>Total</sub> (%)</b>				
<b>Carnsore Point</b>	16.7	-	40.0	-
<b>Mace Head</b>	91.0	-	61.3	-
<b>Malin Head</b>	31.3	-	34.8	-
<b>University College Dublin</b>	40.4	-	45.7	-

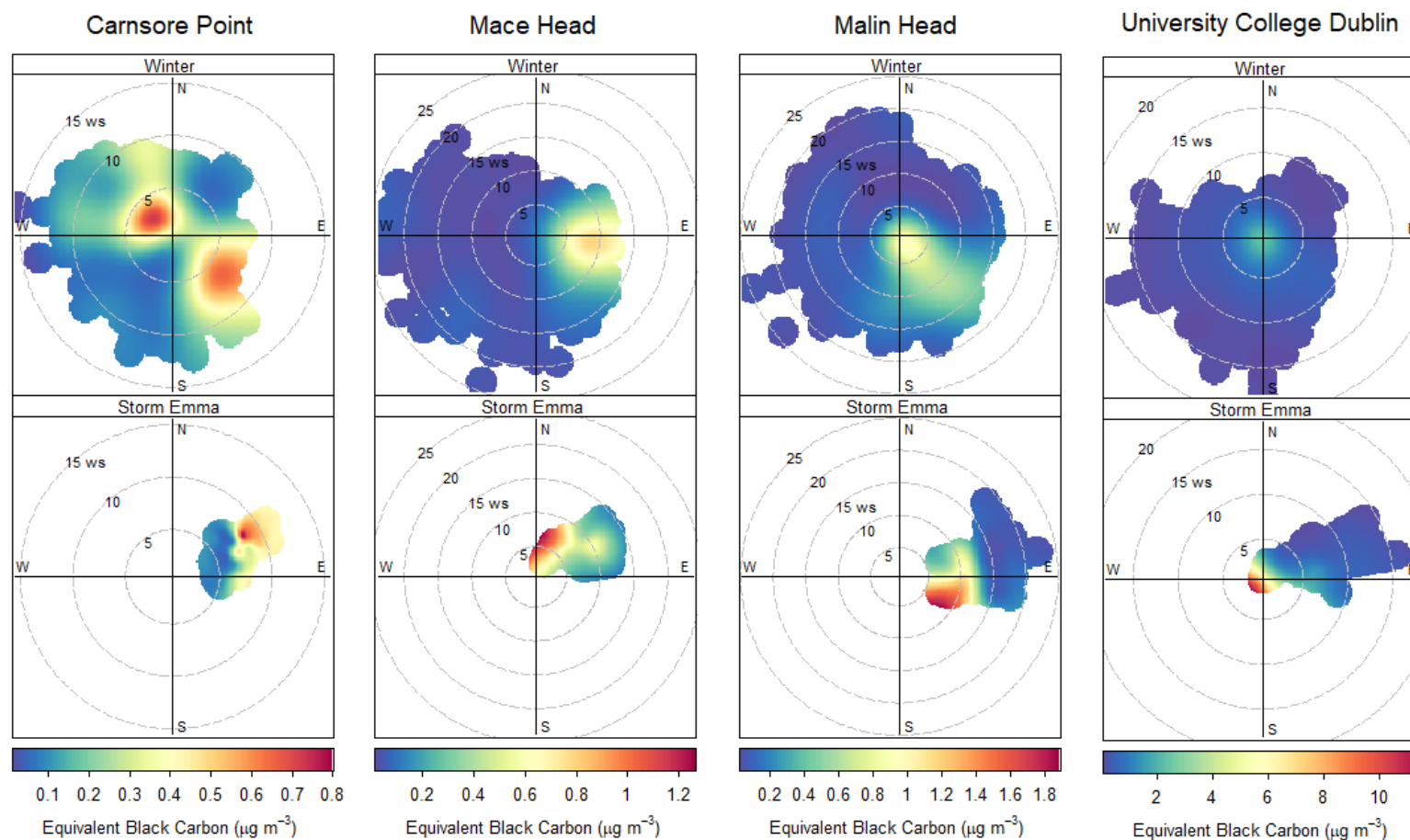


**Figure 3.45** Polar plots depicting the wind-dependence of equivalent black carbon measured throughout the winter (December 2017 - February 2018) and during Storm Emma (February 28, 2018 - March 4, 2018).

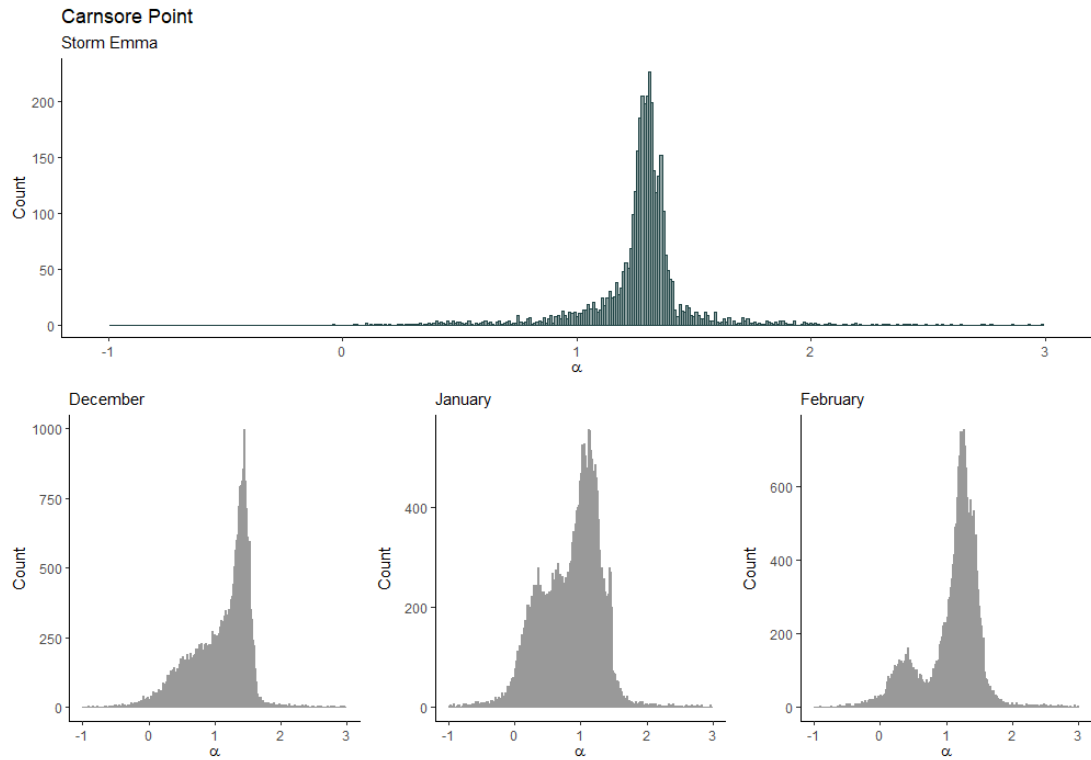


**Figure 3.46** Frequency distribution of the AAE recorded at Carnsore Point throughout the winter months and during Storm Emma.

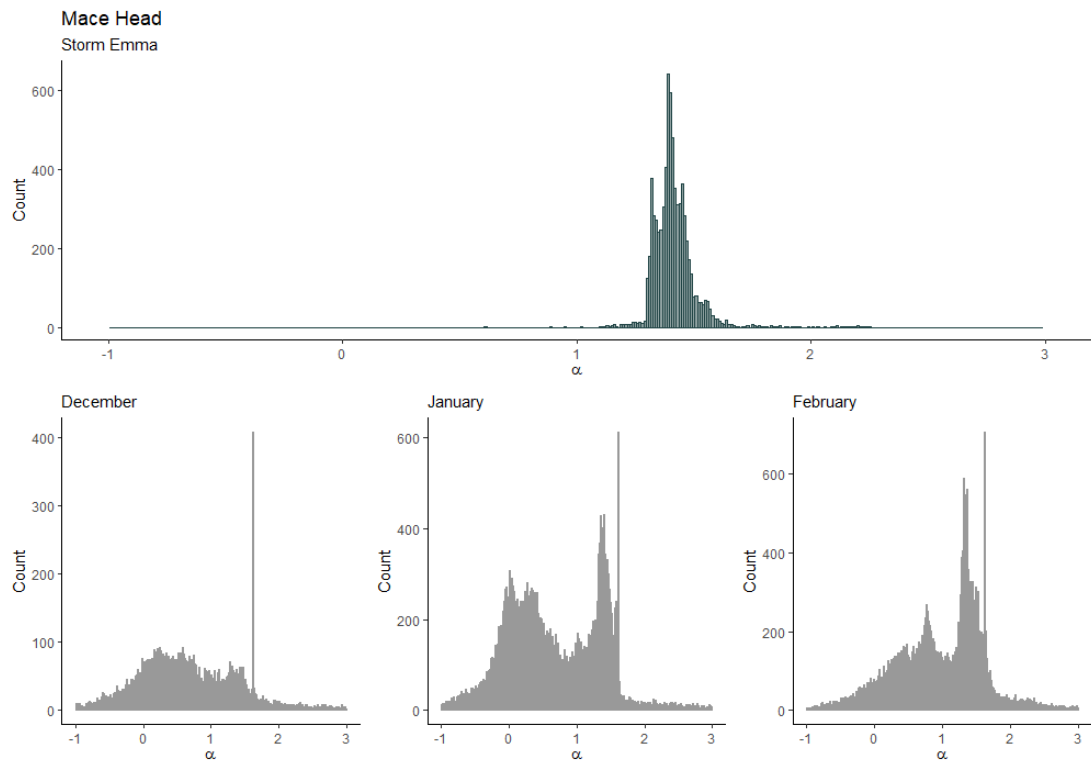


**Figure 3.47** Frequency distribution of the AAE recorded at Mace Head throughout the winter months and during Storm Emma.

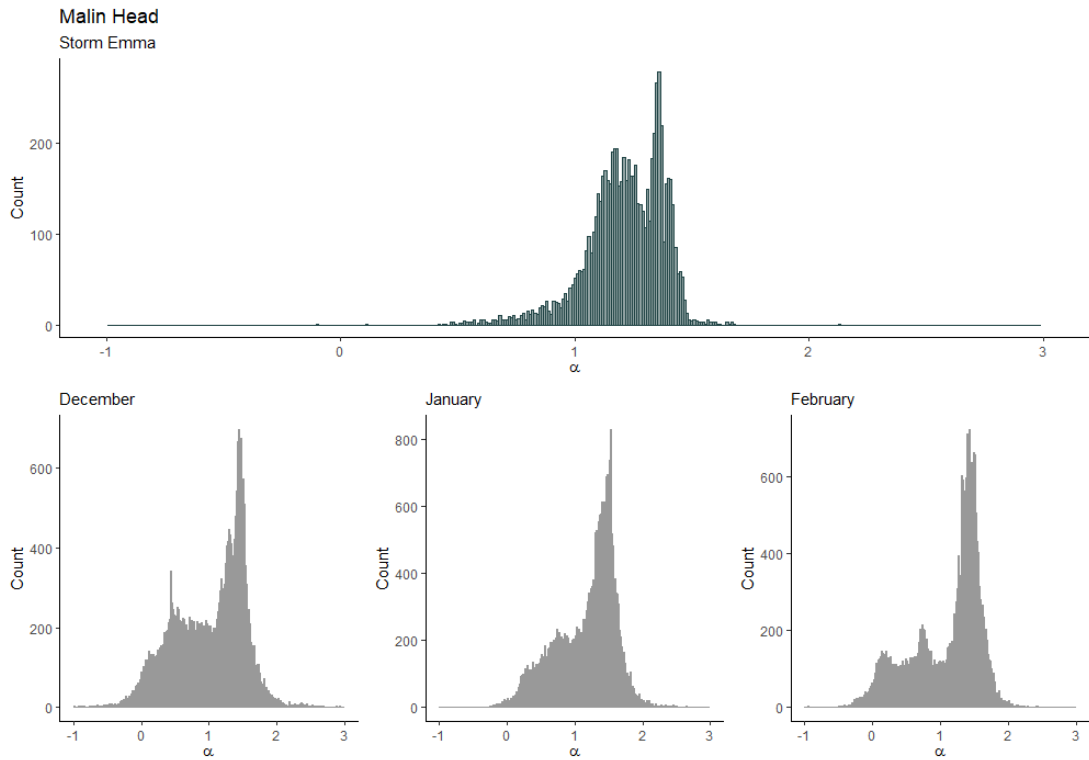


**Figure 3.48** Frequency distribution of the AAE recorded at Malin Head throughout the winter months and during Storm Emma.

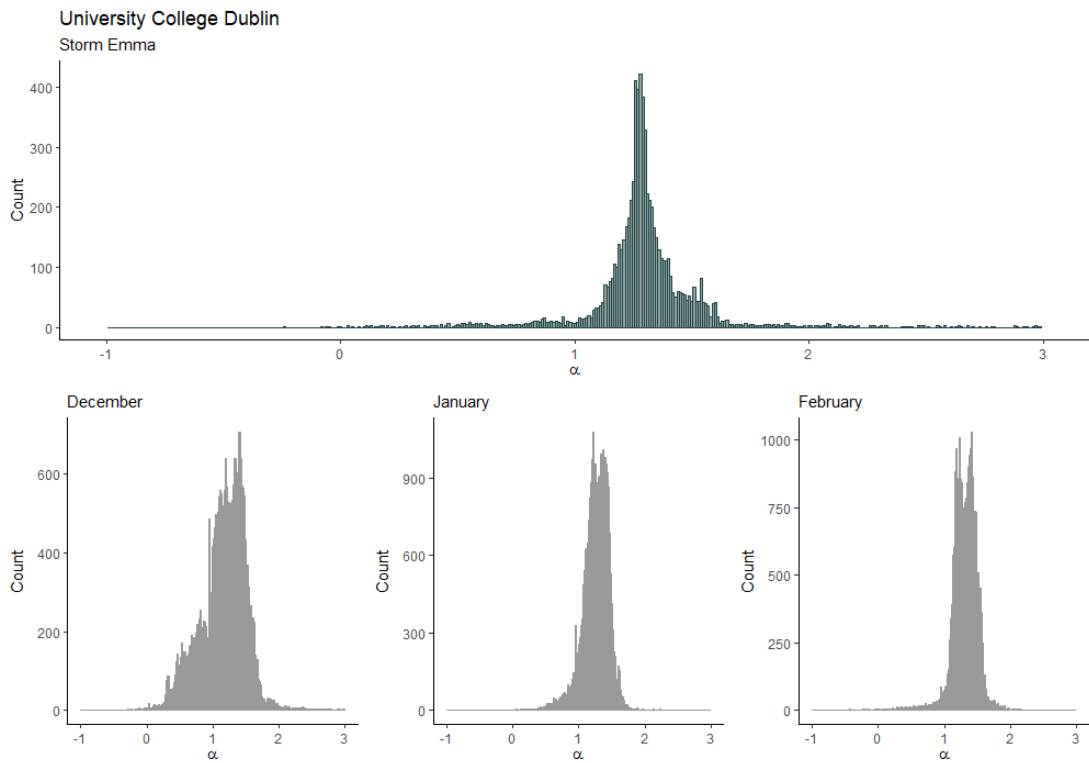


**Figure 3.49** Frequency distribution of the AAE recorded at University College Dublin throughout the winter months and during Storm Emma.

### 3.3.6.3 Elemental and Organic Carbon

The elemental and organic content of the ambient filter samples was determined off-line using an OCEC Laboratory Instrument (Sunset Laboratory Inc.) which employed the EUSAAR\_2 protocol. This analysis was limited by the number of 24-hour filter samples collected during the storm period; 4 and 5 samples were collected at Carnsore Point and Malin Head, respectively.

The mean concentration of both EC and OC content measured in samples collected at Carnsore Point increased during Storm Emma in comparison to the samples collected previously during the winter period. The opposite was true for the samples collected at Malin Head (Table 3.11). The variation in mean OC/EC ratios during the two periods at both locations provides evidence of a change in aerosol composition.

**Table 3.11** Comparison of carbon content measured on filter samples collected at Carnsore Point and Malin Head during the winter period and Storm Emma.

	Winter	Storm Emma
<b>Carnsore Point (<math>\mu\text{g m}^{-3}</math>)</b>		
<b>Elemental Carbon</b>	0.25	0.53
<b>Organic Carbon</b>	1.23	2.11
<b>Total Carbon</b>	1.48	2.64
<b>OC/EC Ratio</b>	7.01	4.64
<b>Malin Head (<math>\mu\text{g m}^{-3}</math>)</b>		
<b>Elemental Carbon</b>	0.28	0.19
<b>Organic Carbon</b>	1.94	1.53
<b>Total Carbon</b>	2.22	1.72
<b>OC/EC Ratio</b>	8.79	9.60

### 3.3.6.4 Levoglucosan

A summary of the levoglucosan concentration present in filter samples collected at Carnsore Point and Malin Head is provided in Table 3.12. The mean concentration did not vary significantly between winter (40.4 ng m<sup>-3</sup>) and Storm Emma (43.3 ng m<sup>-3</sup>) at Carnsore Point, however a significant reduction in average levoglucosan concentration was observed at Malin Head, decreasing from 44.6 ng m<sup>-3</sup> in winter to 24.4 ng m<sup>-3</sup> during Storm Emma, indicative of a reduced contribution from biomass burning to local ambient aerosol. The ratio of levoglucosan to mannosan can be used to discriminate between types of wood used in biomass burning. There is little difference between the ratios obtained in samples collected during the winter and during Storm Emma at either location, indicating little, if any, change in the fuel type used locally.

**Table 3.12** Comparison of the mean concentration of levoglucosan and its isomers measured on filter samples collected at Carnsore Point and Malin Head during the winter period and Storm Emma.

	Winter	Storm Emma
<b>Carnsore Point (ng m<sup>-3</sup>)</b>		
<b>Levoglucosan</b>	40.4	43.3
<b>Mannosan</b>	8.4	10.9
<b>Galactosan</b>	3.6	4.2
<b>Levoglucosan/Mannosan</b>	5.0	5.4
<b>Malin Head (ng m<sup>-3</sup>)</b>		
<b>Levoglucosan</b>	44.6	24.4
<b>Mannosan</b>	8.2	4.7
<b>Galactosan</b>	4.6	2.4
<b>Levoglucosan/Mannosan</b>	6.0	5.8

### 3.4 CONCLUSIONS

---

A multi-wavelength aethalometer (AE33, Magee Scientific) and an ambient air sampler were deployed at Carnsore Point, Mace Head, Malin Head and on the campus of University College Dublin over a 3 month period, which coincided with a wider European intensive measurement campaign, between December 2017 and February 2018. While the aethalometers measured continuously during the sampling period, filter samples were collected for off-line analysis on a 24-hour and 48-hour time basis. The number of viable filter samples collected at each site ranged from 28 to 49, with a number of field blanks also collected for each site.

When compared with meteorological parameters, obtained online from the Met Éireann database, it is clear that equivalent black carbon concentrations were strongly dependent on wind speeds; increased concentrations were observed during periods of low wind speed (Figure 3.12). Spatial variation was observed in eBC concentrations. UCD experienced the highest levels of eBC, while the opposite was true for the sampling site at Mace Head, a pristine monitoring location strongly influenced by clean, North Atlantic air masses. Application of the aethalometer source apportionment model indicated that the burning of solid fuels played a significant role in the ambient conditions and contributed a significant portion of the total eBC concentrations, particularly in the evening times during the winter season as illustrated by Figure 3.20 and Figure 3.21. This was confirmed by the diurnal profile of  $\Delta C$  measurements, also derived from the aethalometer data (Figure 3.22).

Off-line analysis of filter samples indicated that, on average, OC accounted for over 85% of the total carbon measured at each site, while temporal increases and decreases in levoglucosan concentrations followed a similar profile to both measured eBC and TC. Spatial variability in OC/EC ratios was indicative of unique dominant sources in each locality. The filter samples were used to investigate the comparison of thermally determined EC and the absorption coefficient of optically measured BC, which was used to estimate optimised MAC values, specific to each monitoring site. Although the aethalometer employs a default MAC value of  $7.77 \text{ m}^2 \text{ g}^{-1}$  in the 880 nm channel, optimised MAC values of  $10.09 \text{ m}^2 \text{ g}^{-1}$ ,  $6.96 \text{ m}^2 \text{ g}^{-1}$ ,  $8.50 \text{ m}^2 \text{ g}^{-1}$  and  $12.64 \text{ m}^2 \text{ g}^{-1}$  were derived for Carnsore Point, Mace Head, Malin Head and UCD, respectively. The evaluation of the levoglucosan concentrations in the filter samples also allowed for the

estimation of optimum site-specific absorption Ångström exponents for use in the aethalometer model to calculate the contribution of traffic-related emissions to the total eBC concentration.

Analysis has highlighted the significant effect that wind direction can have on local aerosol composition and air quality. A significant increase in ambient concentration of equivalent black carbon was observed during Storm Emma at each of the monitoring locations, strongly influenced by the change in wind direction, indicative of an increase in transported aerosol from the continent. The change in wind direction also impacted the local aerosol composition, as indicated by the percentage contribution of solid fuel burning emissions to total eBC, in addition to the variation in OC/EC ratio. Analysis of EC, OC and levoglucosan concentration was limited by the number of filters collected. Further detailed chemical analysis of the filter samples is required to thoroughly investigate the change in aerosol composition associated with Storm Emma, including the assessment of the effects of long range transportation from Europe.

Despite the overall consistency in temporal trends of the data recorded during the field campaign, a number of instances were identified where the accuracy of the two-source aethalometer model was questioned. Firstly, the temporal profile of eBC attributed to solid fuel and traffic-related emissions is shown in Figure 3.10. Analysis was performed by employing AAEs proposed by Zotter et al. (2017) of 1.68 and 0.9, respectively. The analysis produced negative values of both  $eBC_{SF}$  and  $eBC_{Tr}$  at different sites. At Mace Head, negative values of  $eBC_{SF}$  and  $eBC_{Tr}$  were observed, whereas negative values of  $eBC_{Tr}$  were obtained for measurements at Malin Head. Furthermore, negative values of  $eBC_{SF}$  and  $eBC_{Tr}$  were ascertained during separate periods at the UCD sampling site. Generally, these negative splits occurred during periods of high ambient concentrations of total eBC, relative to the average levels. When investigated further, the measurements during these periods of interest exhibited increased absorption across all seven wavelengths, in comparison to the mean absorption recorded throughout the entire sampling period. In relatively clean background environments, the aethalometer model appeared to collapse and failed to accurately apportion ambient eBC, with the calculated AAEs tending towards 1.

Secondly, the average monthly percentage eBC attributed to traffic-related emissions at both Carnsore Point and Malin Head, both regional background sites, was greater than the portion attributed to vehicular emissions at UCD, an urban background site. Carnsore Point was also the only monitoring site where the correlation between levoglucosan and total BC<sub>6</sub> and total eBC was greater than the correlation with eBC<sub>SF</sub>. This was unexpected. This could be due to the wide variety of fuels used in the absence of legislation restricting fuel types in the local areas surrounding Carnsore Point and Malin Head. In contrast, the legal ban on the sale and distribution of bituminous coal restricts the solid fuel combustion in the vicinity of the UCD sampling site. Despite the fact that the use of wood and peat is unregulated across the country, such fuels may be more readily available in some rural areas, and hence, may have a greater influence on the ambient aerosol. It is possible that the influence of these additional emission sources caused a portion of the eBC to be incorrectly assigned as traffic-related contributions. Kourtchev et al. (2011) demonstrated that levoglucosan is not exclusively related to wood burning, but can also be emitted in combustion of coal and peat, albeit in relatively smaller quantities. A strong influence from coal combustion emissions is plausible at both Carnsore Point and Malin Head, where an increase in eBC<sub>Tr</sub> was observed in the eveningtime. Increased absorption in the IR region, due to coal burning, would explain the increased contributions from ‘traffic-related’ sources.

Generally, studies investigating the aethalometer source apportionment model have been conducted in regions with two major sources of carbonaceous aerosol; namely wood burning and fossil fuel emissions from traffic. In Ireland, this is not the case and the multi-fuel environment should be accounted for in the further development of the aethalometer model to ensure more accurate source apportionment in future. In order to achieve this, additional on-site instrumentation, supplemented by detailed source emission profiling, is required to allow for the optimisation of parameters employed in the source apportionment model. Adjusting the naming convention to attribute fossil fuel combustion emissions to total eBC (eBC<sub>ff</sub>), contributions from road traffic, shipping and coal burning would be accounted for. However, in the context of source apportionment for targeted mitigation strategies, such nomenclature may not be sufficiently specific.

## 4. CARBONACEOUS AEROSOL AT AN URBAN ROADSIDE IN DUBLIN CITY

---

<b>4.1</b>	<b><i>Aims</i></b> .....	<b>164</b>
<b>4.2</b>	<b><i>Methodology</i></b> .....	<b>165</b>
4.2.1	Sampling Site .....	165
4.2.2	Instrumentation and Analysis.....	167
<b>4.3</b>	<b><i>Results and Discussion</i></b> .....	<b>170</b>
4.3.1	Meteorological Data.....	170
4.3.2	Equivalent Black Carbon .....	174
4.3.2.1	Temporal Trends.....	174
4.3.2.2	Dependence on Wind Speed and Direction .....	179
4.3.2.3	Diurnal Trends .....	182
4.3.2.4	Source Contribution.....	185
4.3.2.5	Light Absorption of Black Carbon .....	190
4.3.2.6	Delta-C.....	193
4.3.3	Comparison of Aethalometer Data Measured at Urban Background and Roadside Locations.....	194
4.3.3.1	Temporal Trends of eBC .....	194
4.3.3.2	Source Contribution.....	200
4.3.4	Elemental Carbon (EC) and Organic Carbon (OC) .....	207
4.3.5	Calculation of Mass Absorption Cross Section .....	212
4.3.6	Levoglucosan .....	218
4.3.7	On-line Measurement of Carbon Content .....	225
<b>4.4</b>	<b><i>Conclusions</i></b> .....	<b>229</b>

## 4.1 AIMS

---

Dublin, the capital city of the Republic of Ireland, has a population of over 1.1 million people (city and suburbs) accounting for almost 25% of the total population of the Republic of Ireland, according to the 2016 census. A total of 422,404 workers inhabit Dublin city and suburbs, 382,002 of which also worked in the city. Approximately 40,400 people work outside the urban area, while an additional 130,447 workers make the commute to the city from outside its limits each day. This results in a daytime working population of 512,449 in the capital city (CSO, 2016). With such a vast number of people travelling to and from the city each day for work alone, there is a high level of traffic throughout the city, including private vehicles, heavy and light goods vehicles and public transport.

In order to assess air quality in a traffic-dominated part of Dublin, a multi-season air quality monitoring campaign was conducted at a location on Pearse Street in the city centre from September 2018 to August 2019. This traffic dominated site was selected to provide a contrast to the urban residential environment around the University College Dublin (UCD) campus, located approximately 5 km to the south east, where similar measurements had previously taken place (September 2017 – August 2018). A portion of results from the measurement campaign at UCD during Winter 2017-2018 are outlined in Chapter 3, in the framework of the intensive measurement period established by EMEP/ACTRIS/COLOSSAL.

A variety of instrumental methods for measuring and characterising carbonaceous aerosols were employed to investigate the diurnal, temporal and seasonal variations in this high density traffic area. The data will be used to identify and quantify the main contributing sources of carbonaceous PM in Dublin city centre. It can also be used to assess the potential for improvement in air quality in the city centre with the implementation of traffic restriction measures and the incorporation of hybrid and electric vehicles in the Dublin Bus fleet, which currently has more than 1000 diesel buses in operation (Dublin Bus, 2021).

## 4.2 METHODOLOGY

---

### 4.2.1 Sampling Site

---

Sampling of ambient aerosol took place at an urban roadside location on Pearse Street (53° 20' 42.3" N, 6° 15' 15.3" W) in the centre of Dublin city. Instrumentation was installed in an air conditioned basement of a building, property of Trinity College Dublin. The instrumentation included a multi-wavelength aethalometer (AE33, Magee Scientific), a high volume air sampler (DHA-80, DIGITEL) and the recently developed Total Carbon Analyzer (TCA-08, Magee Scientific). The sampling inlet was situated at ground level and was equipped with a PM<sub>2.5</sub> size selective inlet.

The monitoring site was situated on the R802, a main road through Dublin city centre from the Grand Canal Dock to O'Connell Bridge which has a constant flow of traffic for most of the day. The site is situated on almost 20 cross-city and radial bus routes, serving north, south and west of the city centre and the greater Dublin area, while also incorporating large commuter towns in counties Kildare and Meath. The majority of the buses run throughout the day, seven days a week. The DART (Dublin Area Rapid Transport) train line runs close to the site, less than 200 m away. Directly to the south of the site is the campus of Trinity College Dublin which is predominantly pedestrianised. To the north of the site is the River Liffey (~300 m), which runs through the heart of Dublin, while Dublin Port is approximately 3 km east of the site.

Meteorological data was obtained from a Met Éireann weather station located in the grounds of Casement Aerodrome, Baldonnell which is approximately 14 km south west of the monitoring site. Meteorological parameters used in the analysis included rainfall (mm), temperature (°C), wind direction and wind speed (m s<sup>-1</sup>).

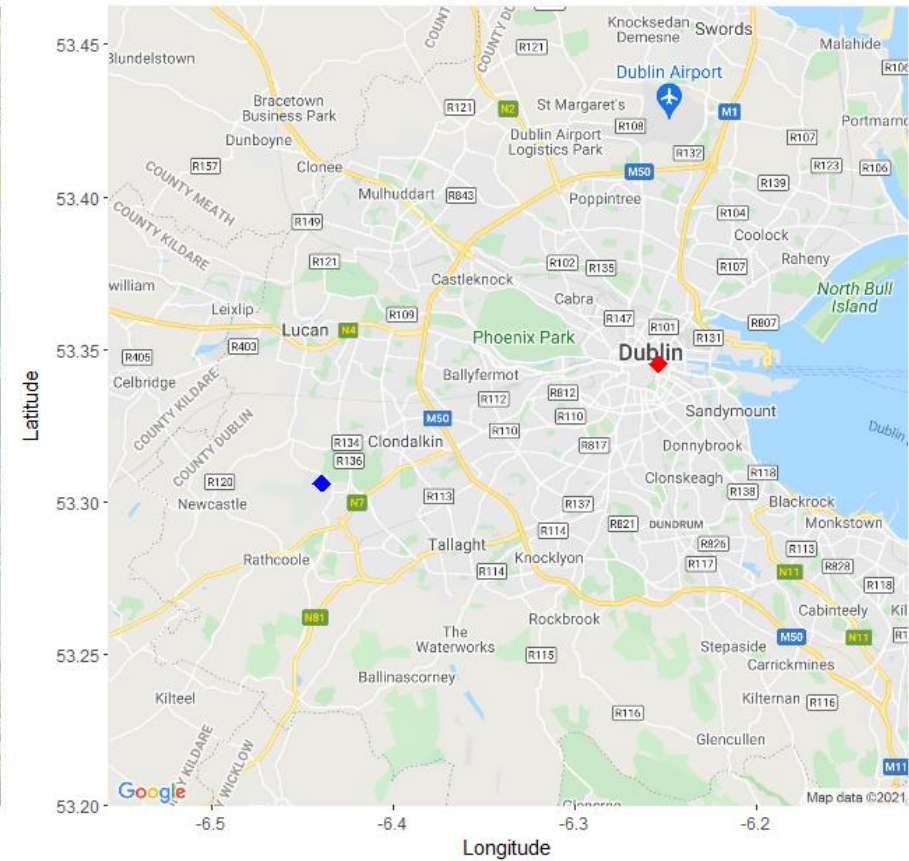


**Figure 4.1** Location of monitoring site (red) on Pearse Street and weather station (blue) at Casement Aerodrome.

#### 4.2.2 Instrumentation and Analysis

---

A number of instruments were installed at the monitoring site over the course of this twelve month monitoring campaign which began in September 2018. The ‘dual spot’, multi-wavelength aethalometer ran continuously throughout the sampling period apart from two occasions when it was removed from the monitoring site in order to participate in an inter-comparison study (TROPOS, Leipzig, January 2019) and fuel combustion experiments carried out by colleagues from National University of Ireland, Galway (NUIG) (April – May 2019). Ambient equivalent black carbon concentration was determined on a continuous basis and source apportionment was conducted using the aethalometer model for source apportionment of carbonaceous aerosol (Sandradewi, Prévôt, Szidat et al., 2008), and the model parameters (AAE values of 0.9 and 1.68) developed by Zotter et al. (2017). This analysis allowed for the contributions of traffic-related and solid fuel combustion related emissions, respectively, to the total measured eBC to be estimated. A detailed description of the instrument and the aethalometer model for source apportionment is provided in Chapter 2.

Filter sample collection began in February 2019, with the initial intention of collecting 12-hour samples (06:00 – 17:59 and 18:00 – 05:59) for the entire month. However, due to technical difficulties the instrument was non-operational during February 13 - 20 February, inclusive, and so filter sample collection was extended until March 5, 2019. Following collection, filter samples underwent thermal-optical analysis (Cavalli et al., 2010) to assess the elemental, organic and total carbon content, and anion-exchange chromatography methods (Iinuma et al., 2009) to determine levoglucosan concentrations present in ambient samples.

The Total Carbon Analyzer (TCA-08), provided by Aerosol d.o.o. (Ljubljana, Slovenia), was installed on site in May 2019. This recently developed instrument allowed for the continuous measurement and thermal analysis of equivalent elemental and organic carbon. The TCA-08 uses ambient air as analytical carrier gas and therefore eliminates the need for gas supplies. A detailed description of the operating principles of the instrument is provided in Chapter 2. Briefly, ambient aerosol samples are collected on a 47 mm quartz fibre filter at a flow rate of 16.7 L min<sup>-1</sup>. The sampling period is defined by the user. The instrument has two identical sampling and analysis

channels, allowing for the continuous monitoring. While one channel collects the sample, the other channel analyses the sample collected during the previous period. The sample collected on the filter is heated, almost instantaneously, resulting in the combustion of all carbonaceous material into CO<sub>2</sub>. The CO<sub>2</sub> concentration is measured by a sensitive detector, providing the total carbon content of the sample. The ‘TC-BC’ method employs the thermally measured total carbon and the optically measured black carbon concentration provided by the co-located AE33 aethalometer to determine the organic carbon content of the sample, using Eqn. 4.1 below.

$$OC = TC - b \cdot BC \qquad \text{Eqn. 4.1}$$

A proportionality parameter ( $b$ ) is employed to relate the optical measurement of black carbon (BC) to the thermally measured elemental carbon (EC). The default value of  $b$  is 1, however the variability of the value depends on seasonality and location. The parameter can be estimated by comparing the measurements made by the Total Carbon Analyzer and the conventional thermal OC/EC analysis. The value of  $b$  is dependent on the thermal protocol used in the conventional OC/EC analysis (Rigler et al., 2020).

**Table 4.1** Dates of instrumentation operation and percentage data capture.

		Dates of Operation	Data Capture %
<b>Aethalometer</b>	AE33	01/09/2018 – 06/01/2019 <sup>§</sup>	99.38
		25/01/2019 – 07/04/2019 <sup>**</sup>	99.32
		21/05/2019 – 31/08/2019	82.04
<b>Ambient Air Sampler</b>	DHA-80	01/02/2019 – 06/03/2019	76.9
<b>Total Carbon Analyzer</b>	TCA-08	22/05/2019 – 21/08/2019	95.1

<sup>§</sup> Aethalometer was removed from the site for an intercomparison study conducted at TROPOS (Cuesta-Mosquera et al., 2020).

<sup>\*\*</sup> Aethalometer was removed from the site for a study conducted by C-CAPS, NUIG.

## 4.3 RESULTS AND DISCUSSION

---

### 4.3.1 Meteorological Data

---

Meteorological data was obtained from the Met Éireann weather station at Casement Aerodrome (53° 18' 21.6" N, 6° 26' 20.4" W), approximately 14 km south-west of the sampling site. A summary of the meteorological parameters investigated in this study is presented in Table 4.2. Maximum temperatures were recorded during the summer months (June, July and August), while a minimum temperature of -3.7 °C was recorded in October 2018 and February 2019. The greatest range in hourly average temperatures was observed in October 2018 ( $-3.7 \leq ^\circ\text{C} \leq 19.4$ ).

High wind speeds generally originated from a westerly and south-westerly direction, the predominant wind direction in Ireland. There were occasions, however, when high wind speeds originated to the east of the weather station, most notably in November 2018, April and June 2019 (Figure 4.4). Wind speeds were lowest during summer months.

A number of storms occurred during the sampling period; Storms Ali and Bronagh (September 19 – 21, 2018), Storm Callum (October 11 – 13, 2018), Storm Diana (November 28, 2018), Storm Deirdre (December 15 – 16, 2018), Storm Erik (February 8 – 9, 2019), Storm Freya (March 3 – 4, 2019), Storm Gareth (March 10 – 16, 2019) and Storm Hannah (April 26 – 27, 2019).

**Table 4.2** Hourly average meteorological parameters recorded at Casement Aerodrome.

	Precipitation (mm)		Temperature (°C)		Wind Speed (m s <sup>-1</sup> )	
	<i>Mean</i>	<i>Range</i>	<i>Mean</i>	<i>Range</i>	<i>Mean</i>	<i>Range</i>
<b>Sep 2018</b>	0.05	0 - 3.4	12.43	1.2 – 22.5	5.16	0 - 18.52
<b>Oct 2018</b>	0.08	0 - 4.6	9.66	-3.7 – 19.4	4.81	0 -15.95
<b>Nov 2018</b>	0.15	0 - 6.7	8.48	-0.1 – 14.5	5.48	0 - 16.98
<b>Dec 2018</b>	0.12	0 - 3.7	8.06	0.8 – 13.0	5.80	0 - 16.46
<b>Jan 2019</b>	0.04	0 - 2.3	5.46	-2.5 – 10.9	4.84	0 - 11.83
<b>Feb 2019</b>	0.03	0 - 1.4	7.60	-3.7 – 17.1	6.19	0 - 17.49
<b>Mar 2019</b>	0.12	0 - 3.9	7.09	-1.7 – 16.2	6.44	0 - 15.43
<b>Apr 2019</b>	0.10	0 - 5.3	8.72	-1.5 – 21.1	4.27	0 - 14.40
<b>May 2019</b>	0.04	0 - 2.9	11.03	-0.9 – 21.1	3.65	0 - 10.80
<b>Jun 2019</b>	0.13	0 - 7.7	12.80	5.4 – 24.5	4.27	0 - 13.18
<b>Jul 2019</b>	0.06	0 - 11.6	16.30	7.2 – 24.5	3.94	0 - 12.35
<b>Aug 2019</b>	0.15	0 - 11.0	15.51	7.3 – 24.6	5.32	0 - 11.83

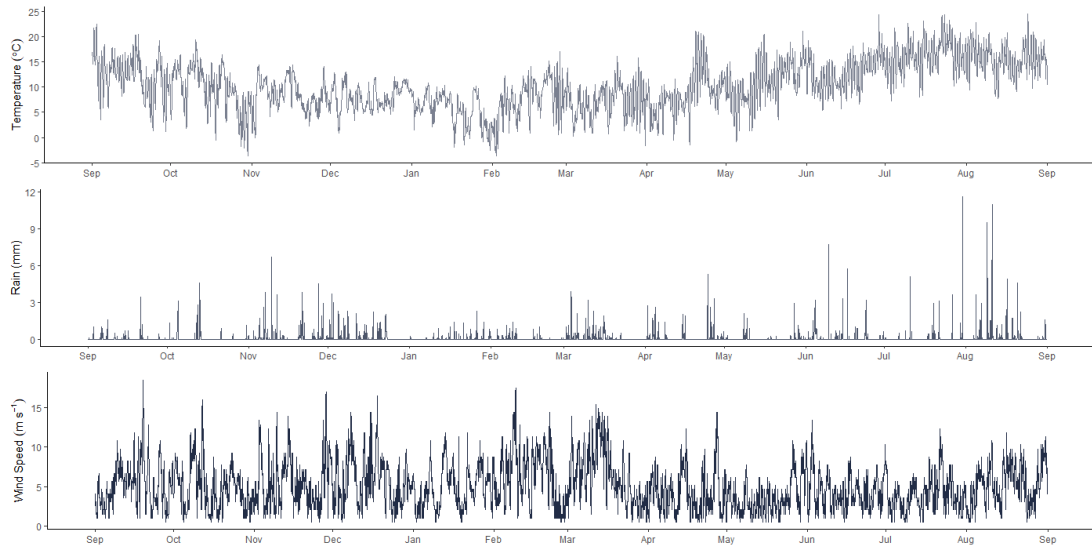


**Figure 4.2** Temporal profiles of meteorological parameters recorded at Casement Aerodrome during the field campaign, September 1, 2018 – August 31, 2019.

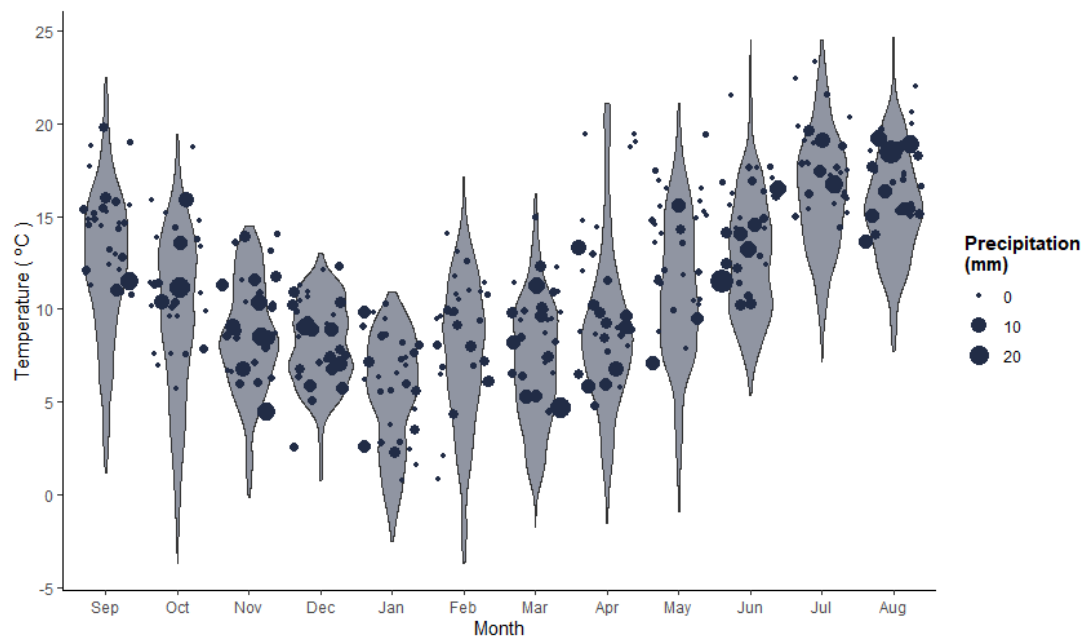


**Figure 4.3** Temperature distribution and precipitation recorded at Casement Aerodrome during the field campaign, September 1, 2018 – August 31, 2019.

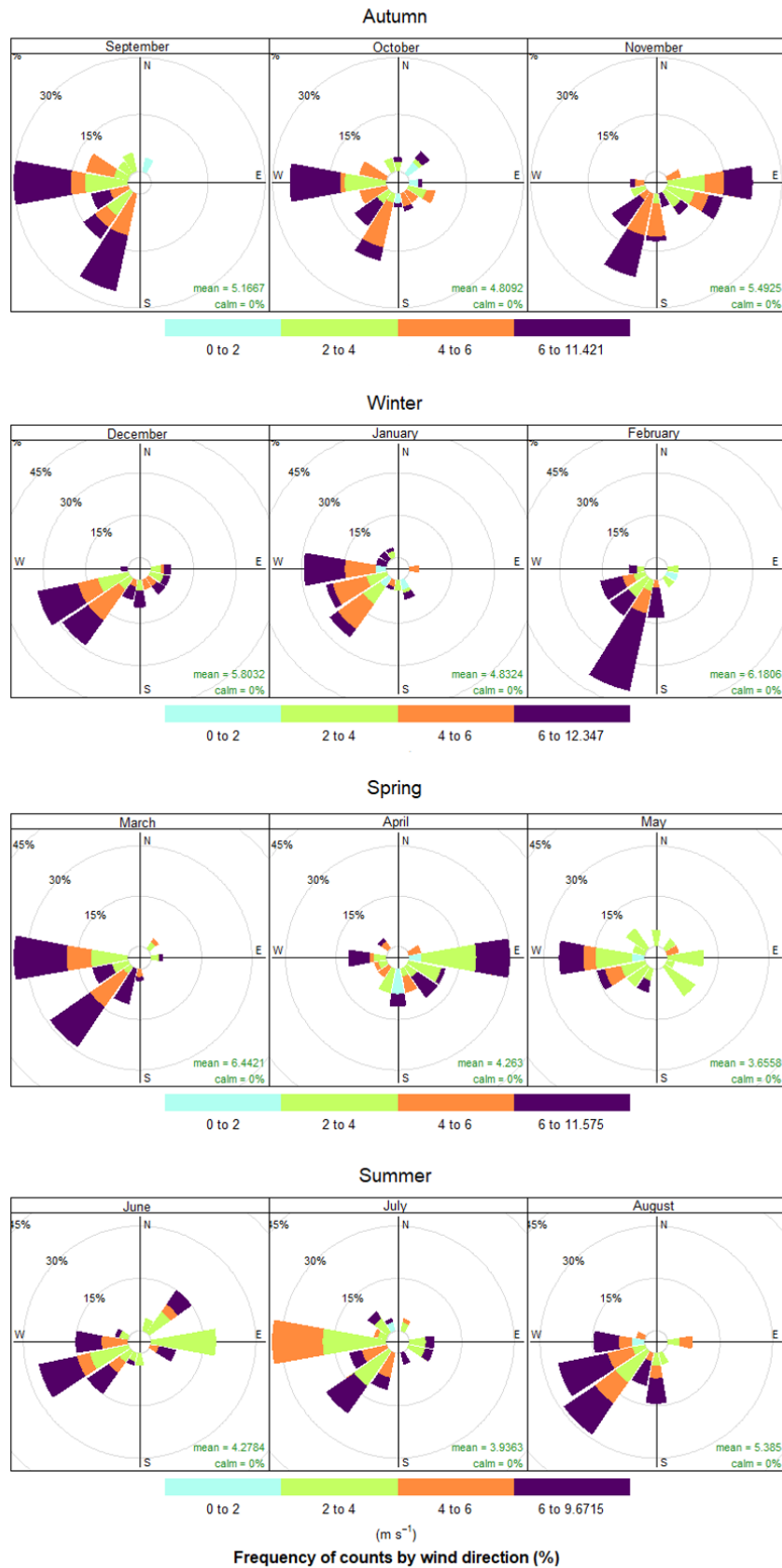


*Figure 4.4* Wind rose distribution showing wind speed as a function of direction recorded at Casement Aerodrome during the urban roadside campaign (September 2018 - August 2019).

### 4.3.2 Equivalent Black Carbon

---

The multi-wavelength aethalometer was employed for the measurement of black carbon at Pearse Street, an urban roadside monitoring site. Following installation of the aethalometer, sampling began on September 1, 2018. As previously stated, the aethalometer was removed from the sampling site on two occasions during January 2019 and April 2019. The data capture of the instrument, while on site, was 92.8%. In general, omitted data during the time period is due to routine maintenance and calibration of the instrument such as tape changes and clean air tests which were run every Saturday at 12:00. Sampling was interrupted for a time during the summer (21/06/2019 – 08/07/2019, inclusive) when the sample inlet became blocked following intensive street cleaning carried out by Dublin City Council. The inaccurate data recorded during this period has been removed from the analysis presented in this chapter. Analysis presented in this chapter is based on sampling on dates outlined in Table 4.3.

#### 4.3.2.1 Temporal Trends

---

A temporal profile of the equivalent black carbon measured at Pearse Street during the year-long monitoring campaign is illustrated by Figure 4.5. The highest equivalent black carbon concentrations were observed during the autumn and winter seasons, when maximum hourly averages of  $38.76 \mu\text{g m}^{-3}$  and  $27.58 \mu\text{g m}^{-3}$  were recorded in October and December 2018, respectively. The lowest concentrations of equivalent black carbon were measured between March and August, during which time maximum concentrations did not exceed  $15 \mu\text{g m}^{-3}$ .

Zotter values ( $\alpha_{\text{Tr}} = 0.9$ ,  $\alpha_{\text{SF}} = 1.68$ ) were applied to attribute equivalent black carbon to traffic-related and solid fuel combustion sources. Table 4.3 provides a summary of the mean monthly contribution from each major source. Interestingly, the contribution from solid fuel is relatively consistent throughout the year; a mean contribution of 22.5% attributed to solid fuel emissions, ranging from 18.26% (July 2019) to 27.61% (January 2019), despite the expectation of a significant decrease in contribution from this source during the warmer, summer months. This presents the question of whether the model is correctly assigning solid fuel emission contributions, albeit significantly

more than anticipated, or is the model incorrectly apportioning compounds that absorb efficiently in the near-ultraviolet region to solid fuel combustion emissions? Despite the distinct environment types, a similar issue was highlighted in Chapter 3 in the analysis of data collected at rural locations.

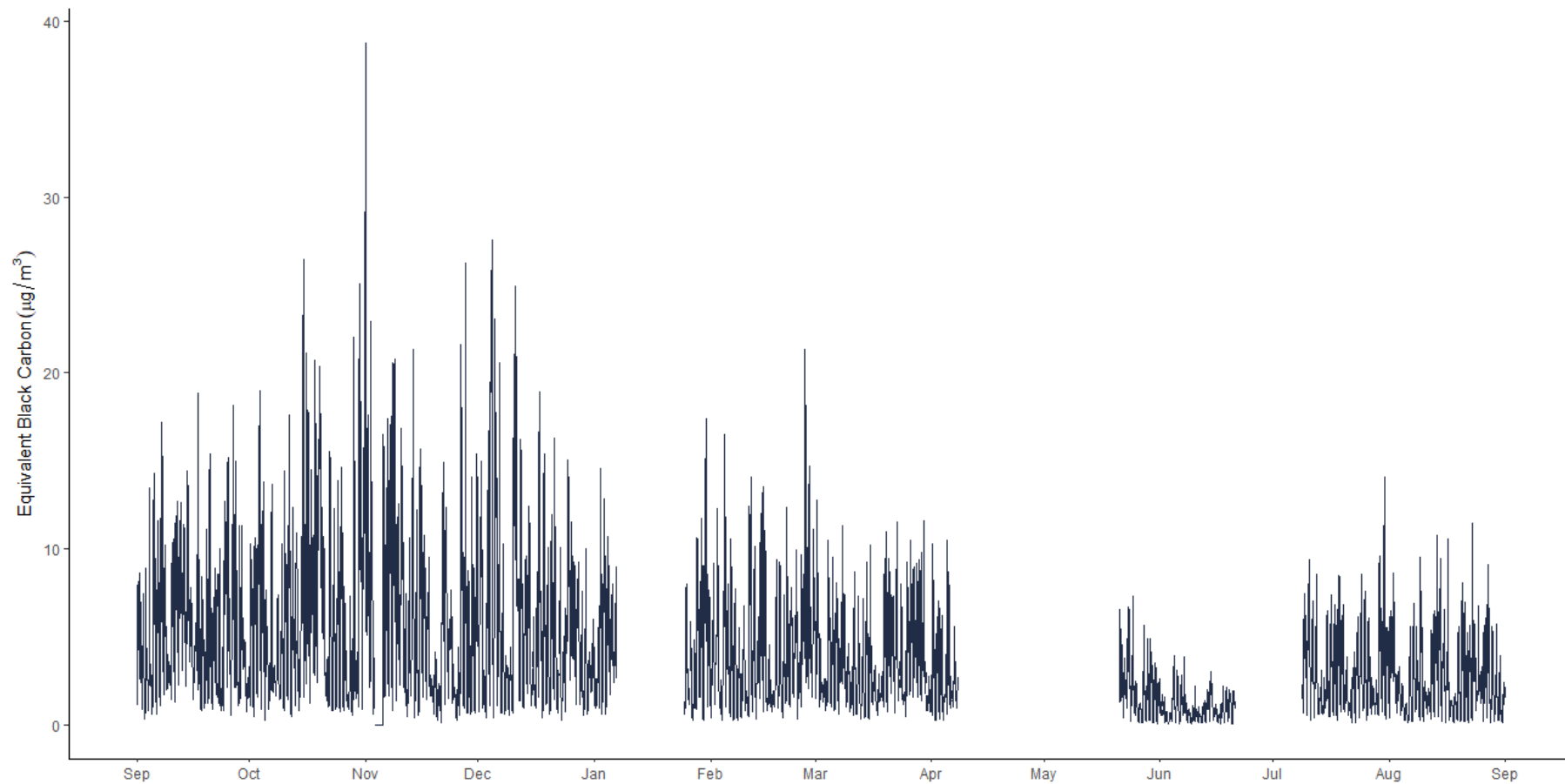


**Figure 4.5** Temporal profile of equivalent black carbon measured at Pearse Street (September 2018 – August 2019).

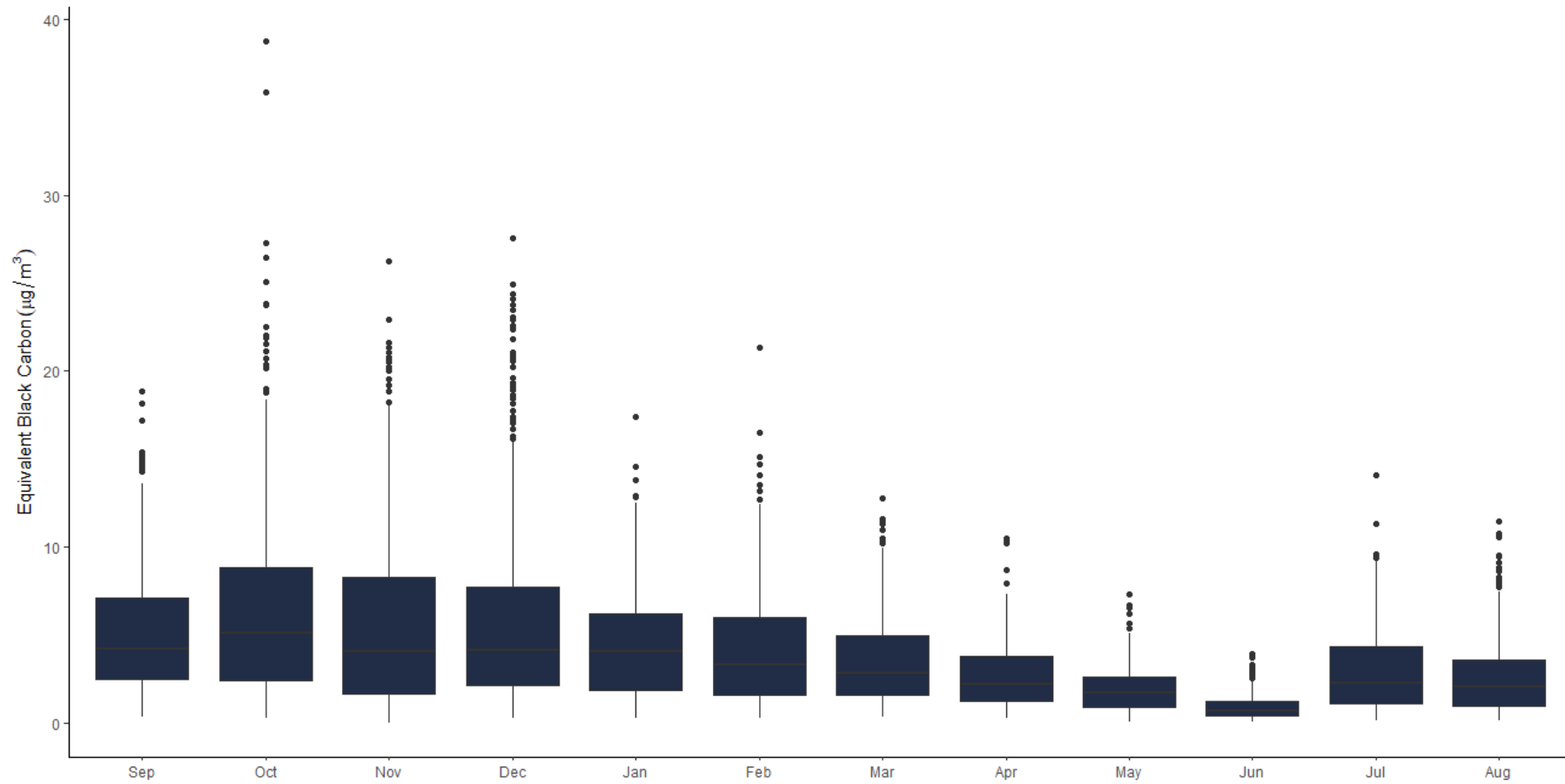


**Figure 4.6** Distribution of equivalent black carbon measured monthly at Pearse Street (September 2018 – August 2019). Analysis is based on 13, 7, 11, 20 and 23 days in January, April, May, June and July 2019, respectively.

**Table 4.3** Summary of hourly average eBC measured at Pearse Street (September 2018 - August 2019).

	# Days Analysed	Equivalent Black Carbon ( $\mu\text{g m}^{-3}$ )			eBC <sub>SF</sub>	eBC <sub>Tr</sub>
		<i>Mean ± SD</i>	<i>Minimum</i>	<i>Maximum</i>	%	%
<b>Sep 2018</b>	30	5.11 ± 3.41	0.29	18.82	20.32	79.68
<b>Oct 2018</b>	31	6.37 ± 5.15	0.24	38.76	22.08	77.92
<b>Nov 2018</b>	30	5.45 ± 4.84	0.00	26.24	22.83	77.17
<b>Dec 2018</b>	31	5.69 ± 4.93	0.25	27.58	26.76	73.24
<b>Jan 2019</b>	13	4.47 ± 3.17	0.24	17.37	27.61	72.39
<b>Feb 2019</b>	28	4.17 ± 3.15	0.22	21.31	24.75	75.25
<b>Mar 2019</b>	31	3.48 ± 2.40	0.33	12.77	21.74	78.26
<b>Apr 2019</b>	7	2.70 ± 2.07	0.22	10.47	26.04	73.96
<b>May 2019</b>	11	1.92 ± 1.40	0.07	7.28	21.46	78.54
<b>Jun 2019</b>	20	0.87 ± 0.70	0.04	3.93	20.85	79.15
<b>Jul 2019</b>	23	2.86 ± 2.18	0.14	14.09	18.26	81.74
<b>Aug 2019</b>	31	2.49 ± 1.97	0.09	11.47	20.64	79.36

#### 4.3.2.2 *Dependence on Wind Speed and Direction*

---

The relationship between ambient eBC concentration, wind speed and wind direction is highlighted in Figure 4.8. South westerly winds prevailed for over 60% of the total sampling period, followed by south easterly winds which were recorded on 20% of sampling days. Figure 4.8 demonstrates the influence of the south easterly and south westerly winds on the ambient concentration of eBC, most notably in autumn and winter. Tall buildings line both the north and south sides of this street, which combined with the positioning of the sample inlet at ground level, may limit the influence that wind speed and direction had on this particular dataset.

The meteorological data (maximum and minimum temperatures, precipitation, wind speed and wind direction) recorded at Casement Aerodrome and Dublin Airport weather stations, approximately 14 km south west and 9 km north of the sampling site, respectively, are compared in Figure 4.7. Daily weather patterns were similar ( $0.56 \leq r^2 \leq 0.97$ ) at both stations and meteorological data used in the analysis provided was recorded at Casement Aerodrome, Baldonnell, Co. Dublin. This data is indicative of the weather experienced by the greater Dublin area and represents the general conditions at the sampling site for the duration of the field campaign. Despite local variation in rainfall, wind speed and direction are of greatest significance in this investigation of carbonaceous aerosols. South westerly and south easterly winds, the predominant wind directions at this site, presumably have the greatest effect on background levels of air pollution as they carry emissions from other parts of the city, across suburbs and the greater Dublin area, to the sampling site.

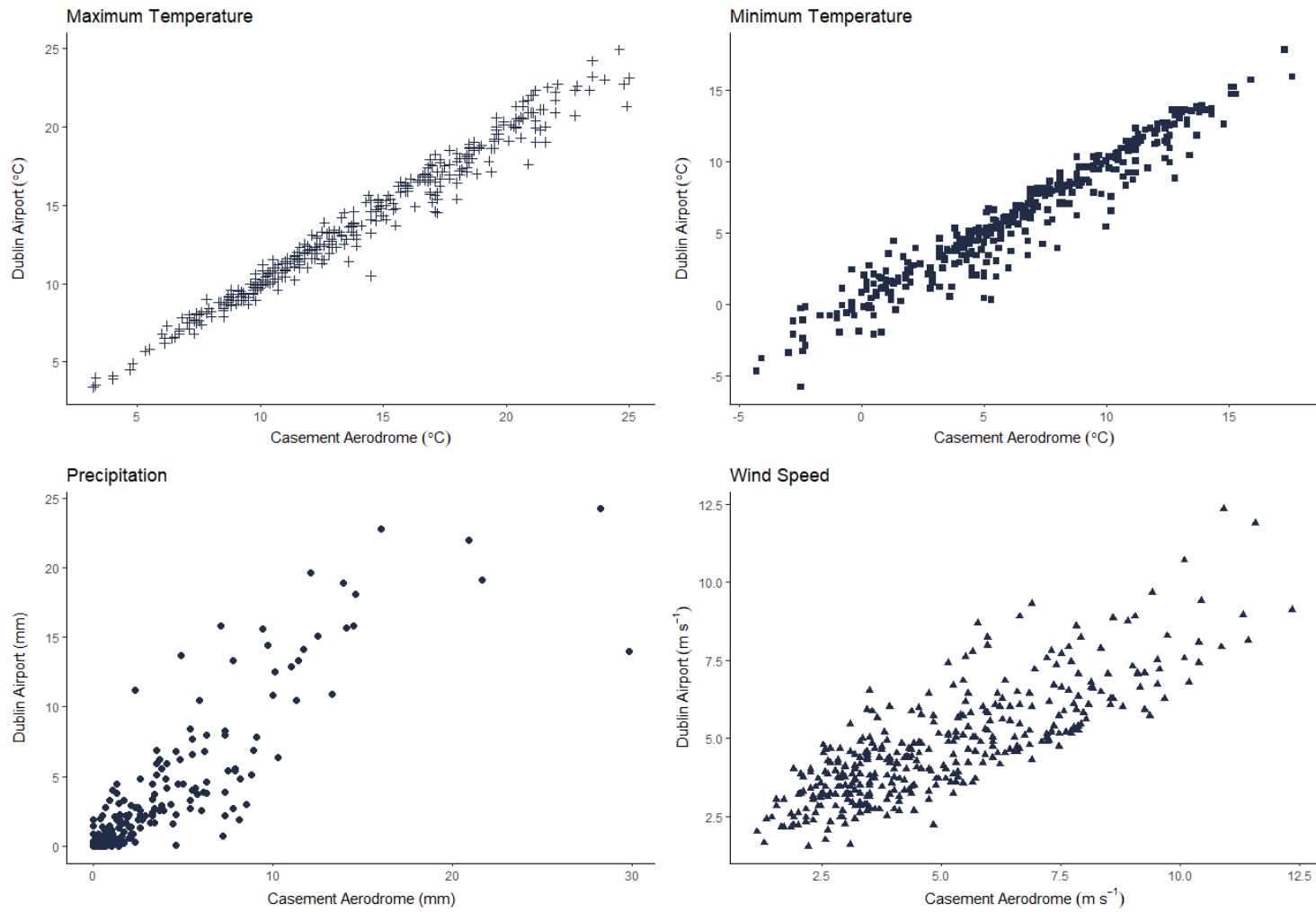


**Figure 4.7** Comparison of weather data recorded at Casement Aerodrome and Dublin Airport (September 2018 - August 2019).

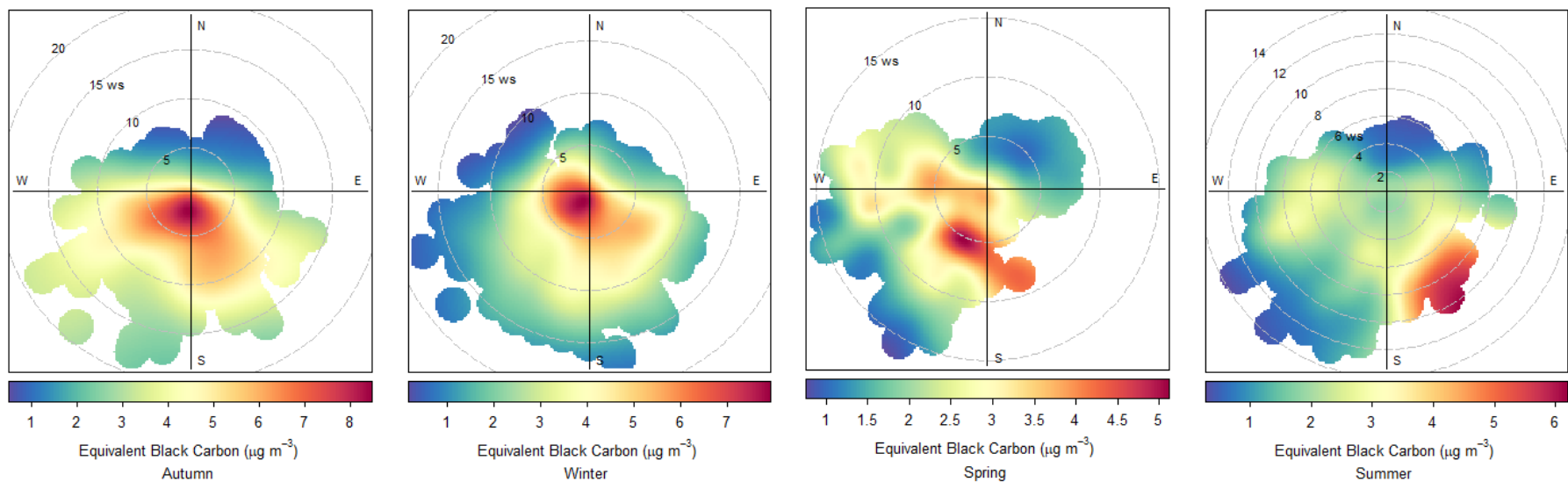


**Figure 4.8** Seasonal polar plots describing the dependence of eBC concentration on wind speed and direction at Pearse Street (September 2018 – August 2019). Autumn, winter, spring and summer analyses were based on 91, 72, 49 and 74 days sampling, respectively.

#### 4.3.2.3 Diurnal Trends

---

The diurnal pattern of eBC concentration observed at this urban roadside location is shown for each season in Figure 4.9. Large peaks were observed in the morning and evening times, corresponding to rush hour traffic. Generally, these peaks were equivalent in spring, summer and autumn. During the winter months, however, the magnitude of the evening peak was larger than that observed in the morning time, thus indicating a secondary source contributing to total ambient concentration; most likely increased solid fuel combustion emissions associated with domestic heating.

Significant variation in weekday and weekend diurnal trends was also observed, particularly during the summer months. Throughout the year, the lack of traffic-related peaks during morning and evening rush hours is evident on Saturdays and Sundays. Mean hourly average eBC concentrations were reduced by approximately 45% at the weekends in autumn (42%), winter (45%) and spring (47%). Ambient concentrations were dramatically reduced by 56% at the weekends during the summer months. This provides further indication that domestic solid fuel burning plays a significant role in total concentration during the typically colder seasons, irrespective of the day of the week. In its absence during the summer months, a greater decrease in eBC concentrations was evident at the weekend when typical weekday commuter traffic was non-existent. Without the contribution from commuter traffic at the weekends, evening time increases in concentrations due to solid fuel combustion emissions were clearly defined in the diurnal profile determined for the winter season.

Figure 4.10 also illustrates the seasonal variation in observed diurnal trends. The plots allow for the visualisation of the diurnal trend of pollutant concentration as a function of wind direction. The analyses show that the concentrations were dominated by southerly winds, but concentrations were seasonally dependent. The intense red colour highlights the amplified levels of eBC during morning and evening rush hours. This trend was constant throughout the entire sampling period.

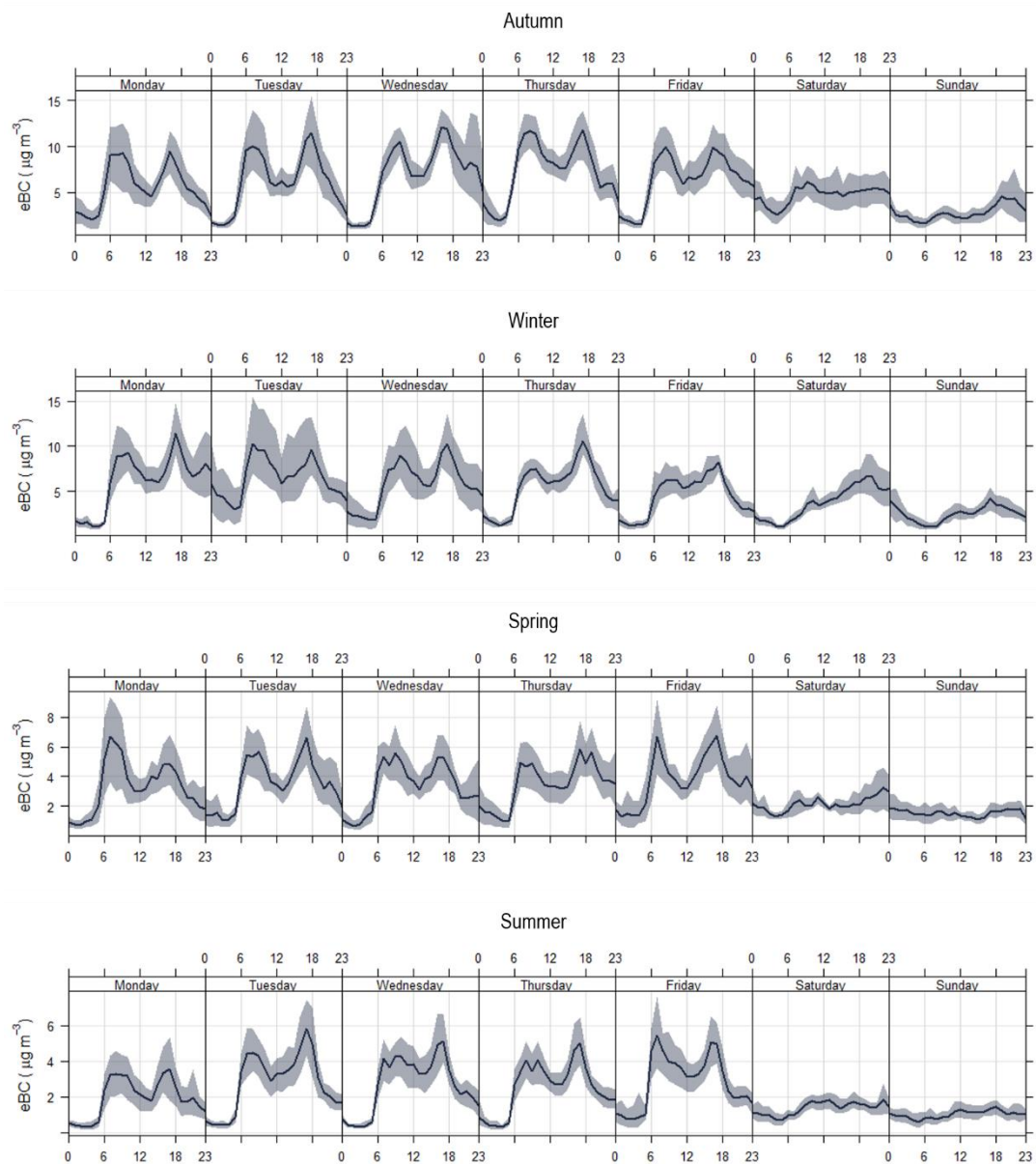


**Figure 4.9** Seasonal variation in diurnal patterns of eBC concentrations recorded at Pearse Street (September 2018 – August 2019). Autumn, winter, spring and summer analyses were based on 91, 72, 49 and 74 days sampling, respectively.

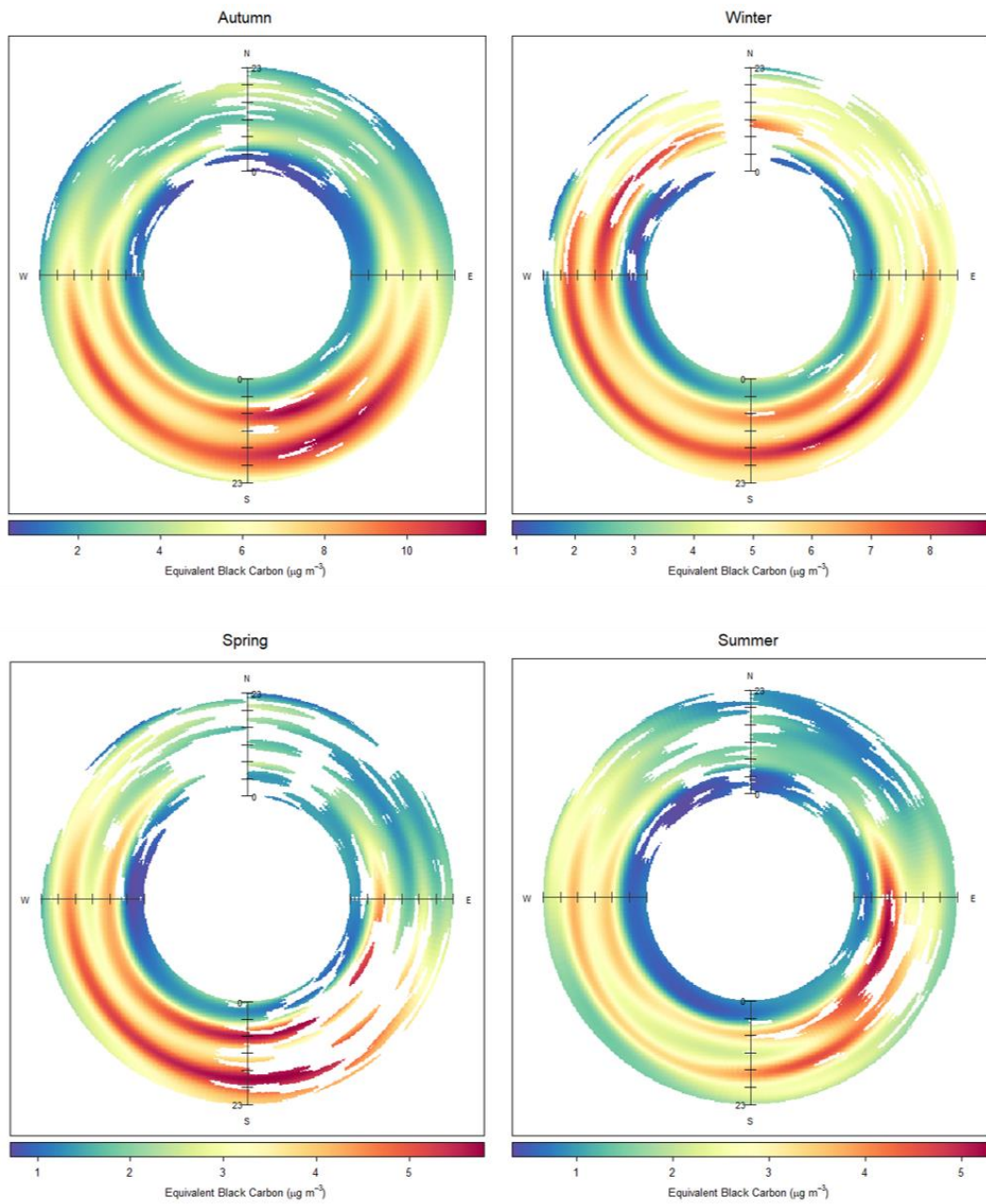


**Figure 4.10** Seasonal diurnal trend of mean eBC as a function of wind direction, recorded at Pearse Street (September 2018 – August 2019). Autumn, winter, spring and summer analyses were based on 91, 72, 49 and 74 days sampling, respectively.

#### 4.3.2.4 Source Contribution

---

In order to distinguish the dominant sources contributing to the total ambient eBC concentrations, the Zotter parameters ( $\alpha_{SF} = 1.68$ ,  $\alpha_{Tr} = 0.9$ ) were applied to the data. This allowed for the source apportionment of solid fuel combustion and traffic-related emissions. As expected at an urban roadside monitoring site with a high volume of traffic and few residential dwellings in close proximity, traffic-related emissions were the dominant source each month. The average contribution from solid fuel combustion was 22.5%, ranging from 18.3% in July 2019 to 27.6% January 2019 (Table 4.3).

Clear seasonal variation in both traffic and solid fuel burning related emissions was observed (Figure 4.11). The lowest concentrations of both traffic and solid fuel combustion sources were measured between March and August 2019 coinciding with increasingly warm temperatures. The highest concentrations from traffic sources were observed between September and December 2018. Simultaneously, solid fuel burning emissions were also greatest during this period. During the colder months, elevated ambient concentrations attributed to solid fuel combustion were expected, however consistent emissions from traffic sources were expected throughout the year. This increase in autumn and winter was likely a consequence of reduced pollution dispersion due to lower boundary layer heights during the cold period. Similar findings were reported in a two year study previously conducted in Dublin between August 2016 and August 2018 (Buckley, 2019). Previous studies have also noted the effect low temperatures can have on emission factors associated with vehicle emissions. An exponential increase in particulate matter emissions with decreasing ambient temperature has been reported in the literature. This distinct increase in emissions is exaggerated during engine ignition under cold conditions due to inefficient combustion and catalytic operation (Chan et al., 2013; Clairotte et al., 2013; Nam et al., 2010; Yusuf & Inambao, 2019). In addition, semi-volatile species exhibit greater partitioning to the particle phase at lower temperatures (Ranjan et al., 2012).

The distinct dominance of traffic-related emissions is illustrated by the source apportioned seasonal diurnal trends in Figure 4.12. The prevailing winds recorded throughout the sampling period were south westerly and south easterly, however it is unclear to what extent the winds influenced the measured concentrations due to the central location of the monitoring site in Dublin city. Figure 4.12 shows the impact of

morning and evening rush hour on the ambient concentration attributed to traffic sources. The significant influence of traffic-related emissions was corroborated by temporal trends in  $\text{NO}_x$  concentrations; often used as a tracer for traffic emissions. Figure 4.13 depicts the seasonal diurnal trend observed for both  $\text{eBC}_{\text{Tr}}$  and  $\text{NO}_x$ . Similarities between the diurnal trends of  $\text{eBC}_{\text{Tr}}$  and  $\text{NO}_x$  were observed, in terms of both concentration and direction of origin throughout the monitoring campaign, but particularly in autumn and winter.  $\text{NO}_x$  measurements were provided by Dr Darius Ceburnis of NUIG, as presented by Lin et al. (2020). Interestingly, a similar pattern was observed in concentrations assigned to solid fuel combustion, albeit a lower magnitude. Solid fuel emissions are usually associated with increased levels of pollution in the evening times, and although low boundary layer heights may impact the dispersion, it is unlikely that peaks of solid fuel burning emissions played a significant role in the ambient concentration at a time that coincided with morning rush hour. Both petrol and diesel vehicles emit compounds that are important secondary organic aerosol (SOA) precursors (Gentner et al., 2017; Platt et al., 2013; Sundvor et al., 2012). Sundvor et al. (2012) reported that organic aerosols are often formed following photooxidation of such precursors. The light absorbing fraction of organic matter is termed brown carbon (BrC) and is usually associated with biomass burning emissions (Andreae & Gelencsér, 2006; Saleh et al., 2014). It is possible that the traffic-derived formation of secondary organic aerosol may have been incorrectly apportioned to solid fuel combustion emissions by the aethalometer due to efficient absorbance in the near-ultraviolet range. This might also explain the consistency in percentage contribution of black carbon attributed to solid fuel combustion emissions. Reduced contributions from solid fuel were expected during the summer months when temperatures were at their highest and residential heating is not required. If the aethalometer model incorrectly assigned secondary organic compounds produced by precursors emitted by vehicles, this could account for consistent contributions of so-called ‘solid fuel combustion’ all year round. If this is the case, it can be assumed that this also occurs during the winter months in periods of actual solid fuel burning, therefore presenting the requirement of separation and correct apportionment of the sources.

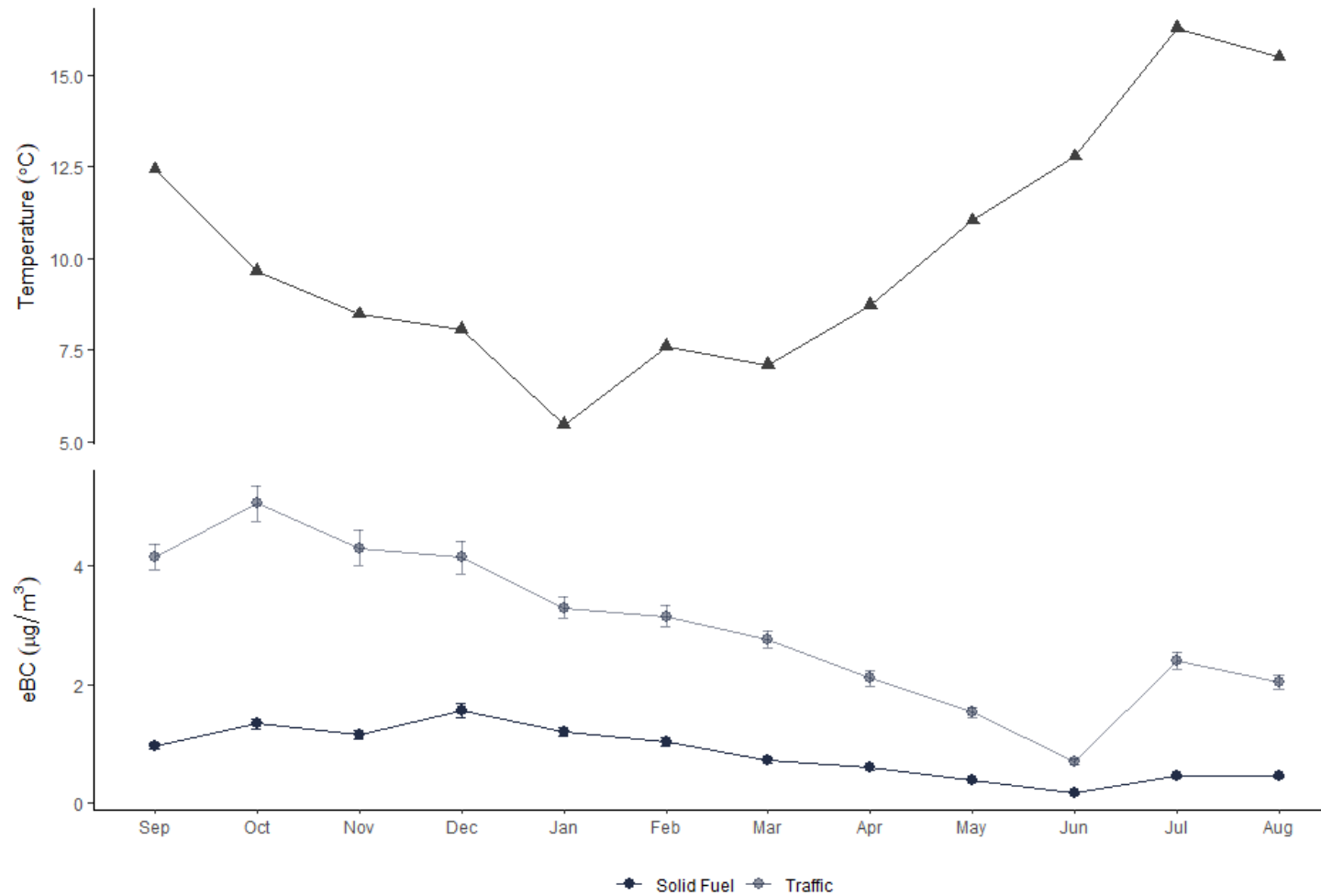


**Figure 4.11** Mean concentration of  $eBC_{SF}$  and  $eBC_{Tr}$  with 95% confidence interval recorded at Pearse Street (September 2018 – August 2019), in addition to mean monthly ambient temperature. Autumn, winter, spring and summer analyses of  $eBC$  concentrations were based on 91, 72, 49 and 74 days sampling, respectively.

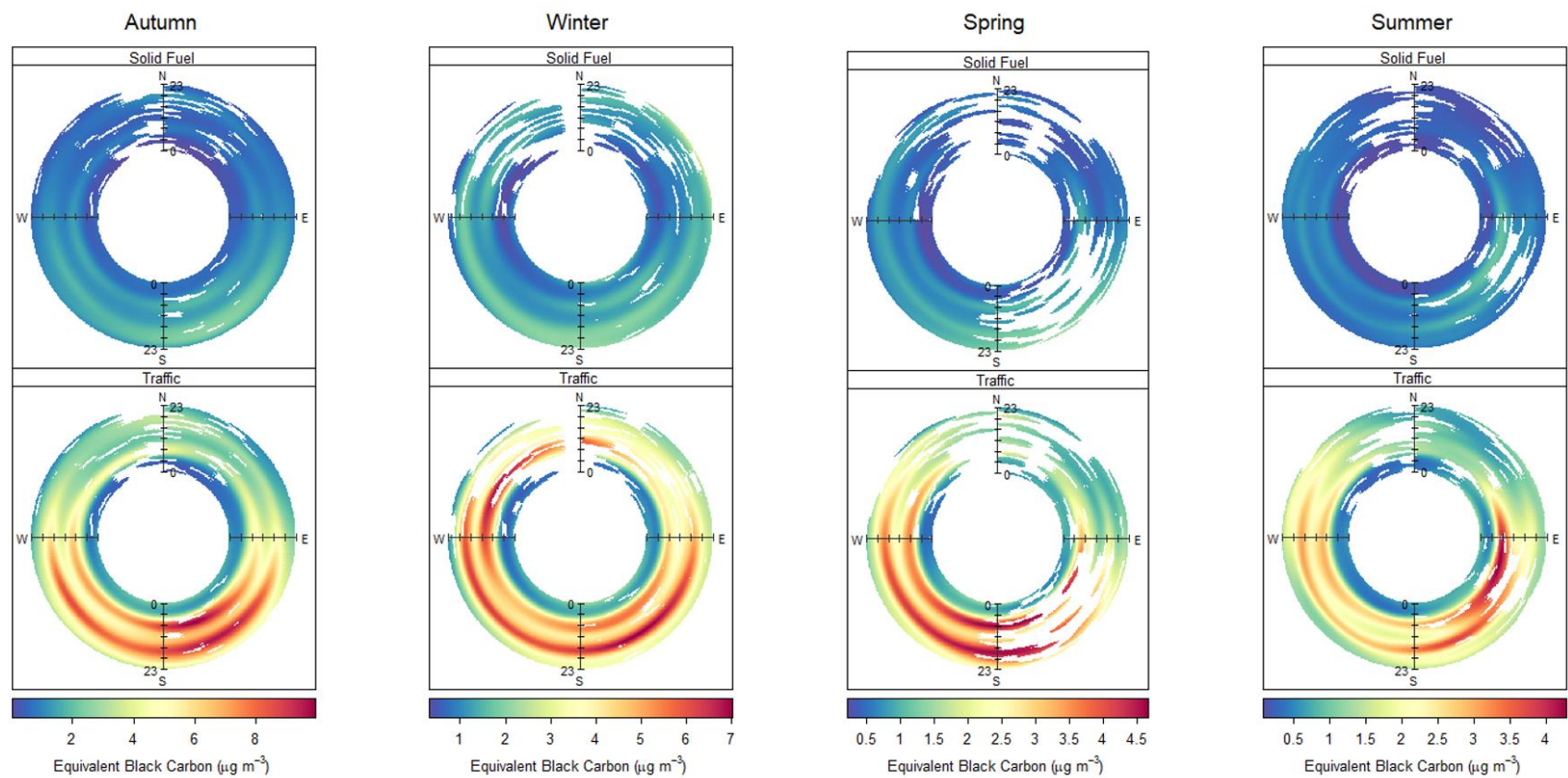


**Figure 4.12** Seasonal diurnal trend of eBC attributed to solid fuel and traffic-related emissions measured at Pearse Street (September 2018 – August 2019). Autumn, winter, spring and summer analyses of eBC concentrations were based on 91, 72, 49 and 74 days sampling, respectively.

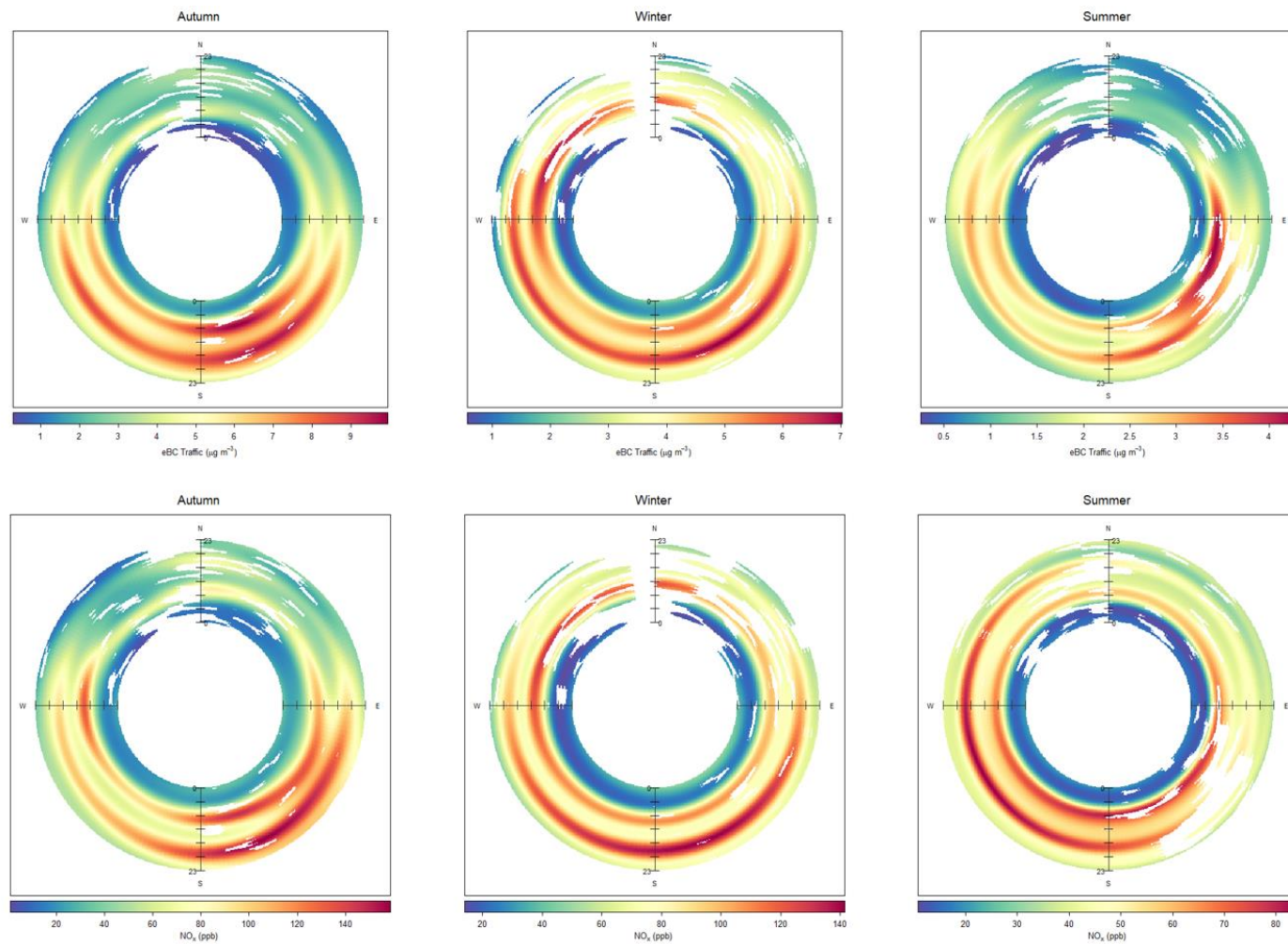


**Figure 4.13** Seasonal diurnal trend of eBC attributed to traffic-related equivalent black carbon emissions (top) and  $\text{NO}_x$  (bottom) measured at Pearse Street (September 2018 - February 2019 and June - August 2019).

#### 4.3.2.5 Light Absorption of Black Carbon

Absorption of black carbon particles attributed to solid fuel burning emissions is highly efficient in the ultraviolet region, whereas black carbon associated with traffic emissions absorbs most efficiently in the near-infrared region. This explains the significant difference in absorbance in the near-ultraviolet region between seasons when solid fuel contributions fluctuate, primarily depending on ambient temperatures (Figure 4.14). The highest absorbance in the near-UV region was recorded during the autumn and winter, while the absorbance at smaller wavelengths was much lower during the summer, when solid fuel burning was at a minimum. A curve, demonstrating the variation in absorbance by the ambient aerosol was quite apparent during the autumn and winter season, indicating the significant impact of solid fuel combustion. The curve was flattened substantially during the summer months, when the impact of solid fuel burning was less.

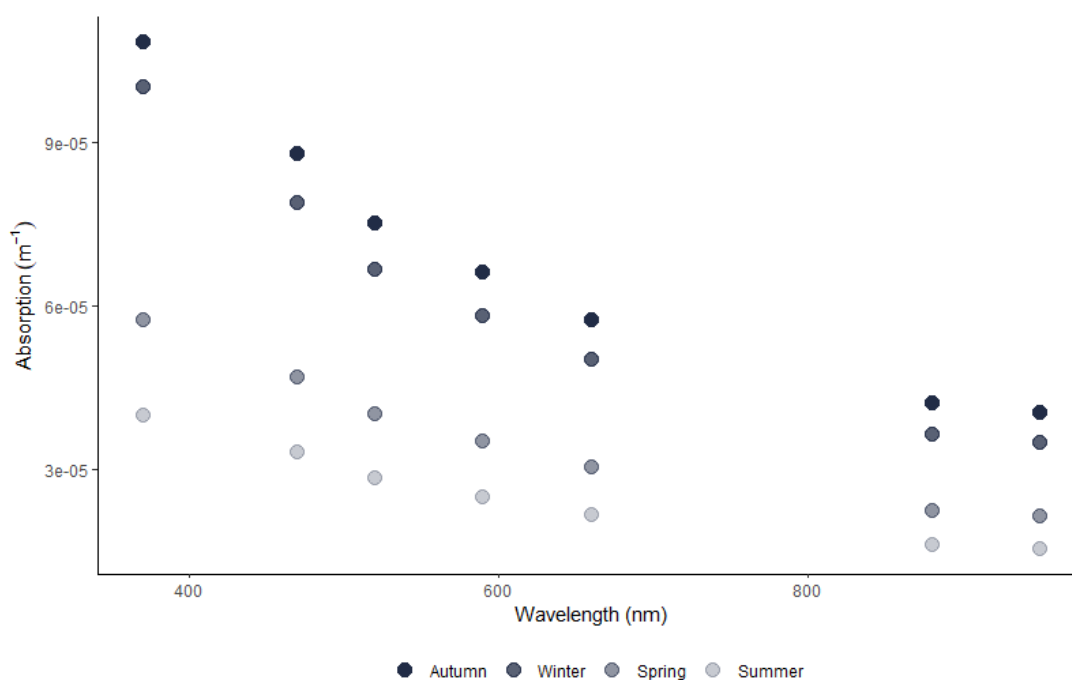


**Figure 4.14** Average seasonal absorbance of black carbon measured at each wavelength. Measurements were recorded at Pearse Street between September 2018 and August 2019. Autumn, winter, spring and summer analyses were based on 91, 72, 49 and 74 days sampling, respectively.

The frequency distribution of the calculated absorption Ångström exponents were also examined. The AAEs were determined by the curve fitting wavelengths 470, 520, 590,

660, 880 and 950 nm with exponential regression models of 60 second measurements (Figure 4.15). The overall narrow distribution is indicative of an environment strongly influenced by one major source. The mean AAE, represented by the vertical blue line, was relatively constant throughout the year; 1.11, 1.09, 1.11 and 1.14 in spring, summer, autumn and winter, respectively; the expected outcome at a traffic dominated sampling site such as this. The mean value was lowest during the summer ( $\alpha \sim 1.09$ ) and highest during winter, reflecting the relative contribution of solid fuel emissions in these seasons. During winter, the distribution of AAE values show a shoulder skewed towards higher values, due to increased contributions from solid fuel and biomass burning. The hourly average AAE calculated during December, January and February ranged between 0.75 and 1.58. The median AAE calculated during spring, summer, autumn and winter were 1.10, 1.08, 1.10 and 1.12, respectively.

The calculated AAE was also investigated during ‘traffic’ hours in morning rush hour (05:00 – 09:59) and during typical ‘solid fuel burning’ hours in the eveningtime (19:00 – 00:59) in both summer and winter. During the summer months there was little variation observed in mean AAE during the two time periods, 1.08 (traffic hours) and 1.11 (solid fuel burning hours). However, over the winter period the variation was greater; ranging from 1.10 during the morning rush hour and 1.19 in the eveningtime when solid fuel burning was more prevalent. Despite the monitoring site being dominated by traffic-related emissions, the impact of solid fuel burning during the colder months was evident.

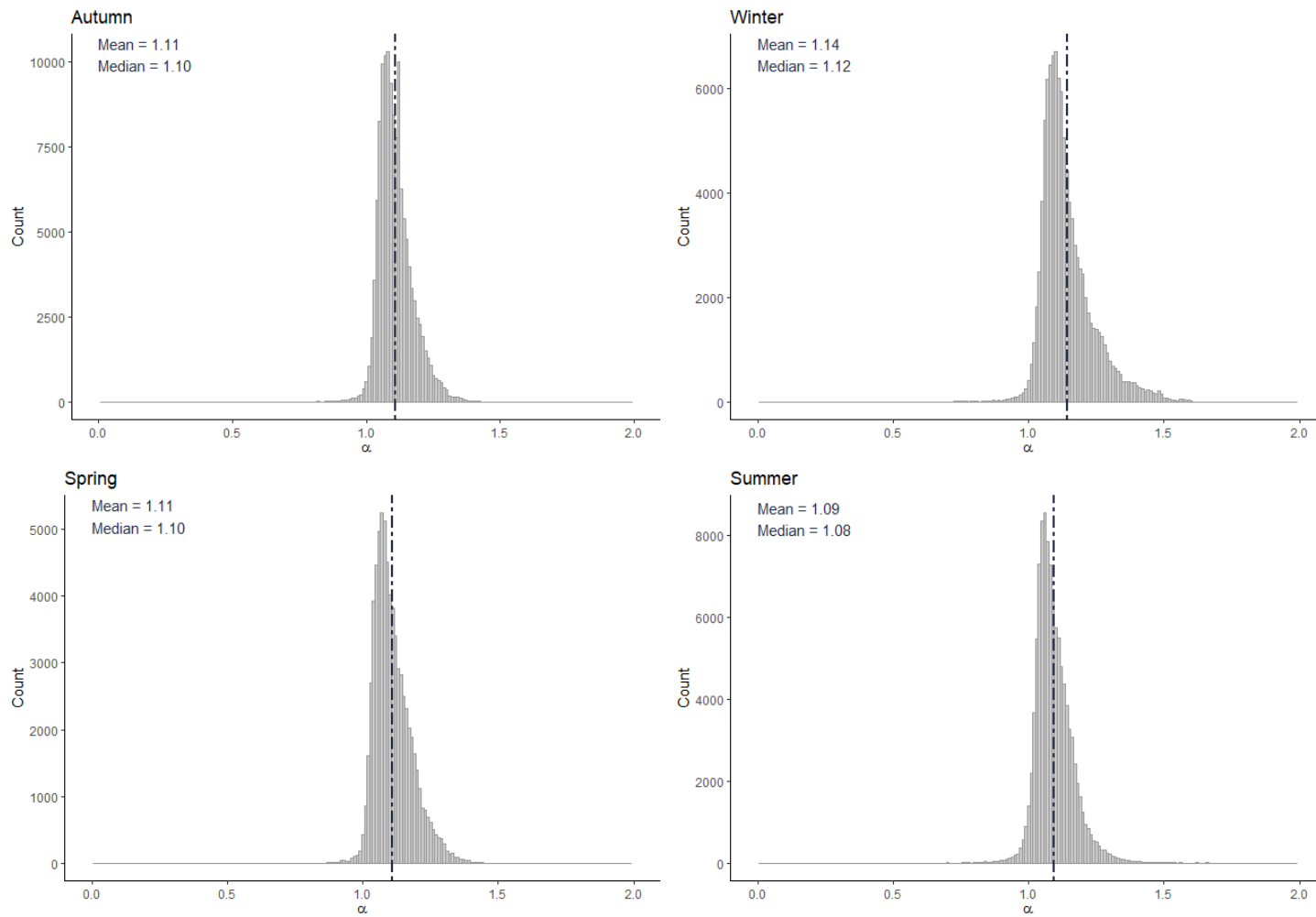


**Figure 4.15** Seasonal frequency distribution of calculated AAE recorded at Pearse Street (September 2018 - August 2019). Mean AAE is represented by the dashed line. Autumn, winter, spring and summer analyses were based on 91, 72, 49 and 74 days sampling, respectively.

#### 4.3.2.6 Delta-C

The delta-C ( $\Delta C$ ) parameter can be calculated using the aethalometer measurements of black carbon at 370 nm and 880 nm. It is indicative of the proportion of total eBC assigned to solid fuel burning related particles, due to enhanced optical absorption at 370 nm as outlined in Section 3.3.2.4. Thus, it can be used to assess the validity of AAE values employed in the source apportionment model. The average diurnal trend of  $\Delta C$  observed in both summer and winter at Pearse Street is shown in Figure 4.16. The trends confirm previous assertions that solid fuel burning was prevalent during the colder, winter period, with increased emissions in the eveningtime. Conversely, a well-defined trend was not observed during the summer months, despite the assignment of approximately 20% of total eBC to solid fuel combustion emissions by the aethalometer model. It is possible that due to an overall decrease in the level of eBC during the summer months, in addition to the assumed absence of solid fuel combustion for home heating, the values of  $\Delta C$  presented can be attributed to background levels of UV absorbing species in ambient aerosol, including aged and oxidised compounds.

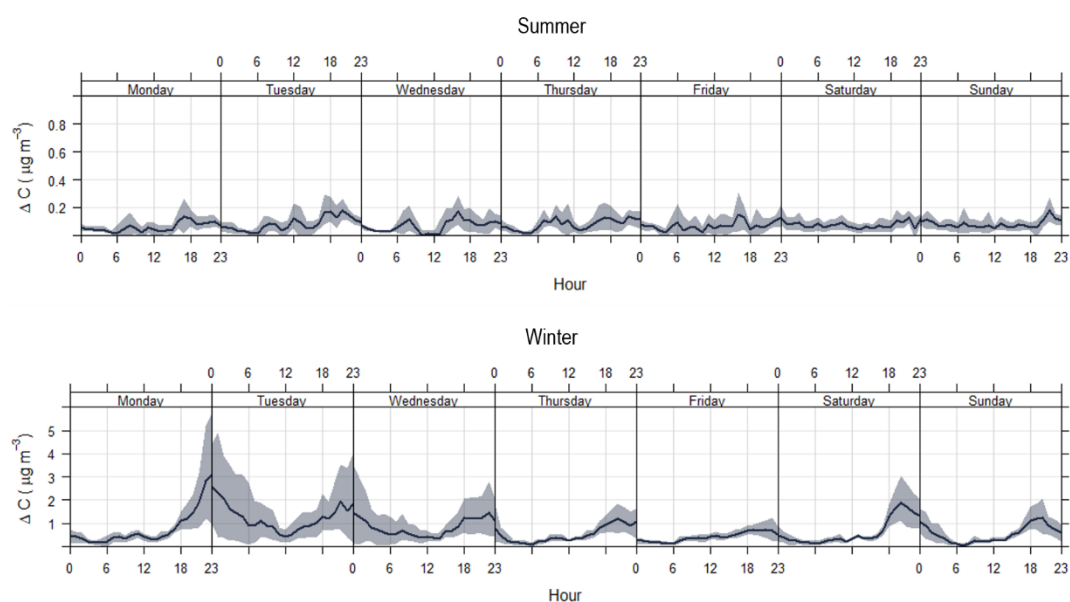


**Figure 4.16** Seasonal variation in diurnal trend of  $\Delta C$  parameter recorded at Pearse Street (September 2018 – August 2019). Winter and summer analyses of  $\Delta C$  were based on 72 and 74 days sampling, respectively.

### 4.3.3 Comparison of Aethalometer Data Measured at Urban Background and Roadside Locations

---

The aethalometer data collected at the urban roadside monitoring site on Pearse Street in Dublin city centre (September 2018 – August 2019) was compared with data previously collected on the campus of University College Dublin (September 2017 – August 2018), an urban background site located in a primarily residential area approximately 5 km southeast of Pearse Street. These two environments were expected to yield contrasting results, both quantitative and qualitative.

#### 4.3.3.1 Temporal Trends of eBC

---

Despite a significant difference in the absolute concentrations recorded at the monitoring sites, comparable seasonality was observed at both sampling sites; lowest concentrations recorded during summer months, while the highest seasonal mean concentration was recorded during winter and autumn at Pearse Street and University College Dublin, respectively (Figure 4.17). There was less variation in the range of daily average concentrations recorded each season at UCD. eBC concentrations generally ranged between  $0 \mu\text{g m}^{-3}$  and  $1 \mu\text{g m}^{-3}$ , and exceeded  $1 \mu\text{g m}^{-3}$  on approximately 50 occasions. In contrast, a wide range of daily average eBC concentrations were recorded at Pearse Street throughout the twelve month sampling period ( $0 \mu\text{g m}^{-3} \leq \text{eBC} < 15 \mu\text{g m}^{-3}$ ). The seasonal trend of eBC measured at University College Dublin is concealed by the wide range of concentrations measured at Pearse Street throughout the twelve month field campaign (Figure 4.18, Figure 4.19). Table 4.4 provides a summary of the hourly average eBC measured at both sampling sites.

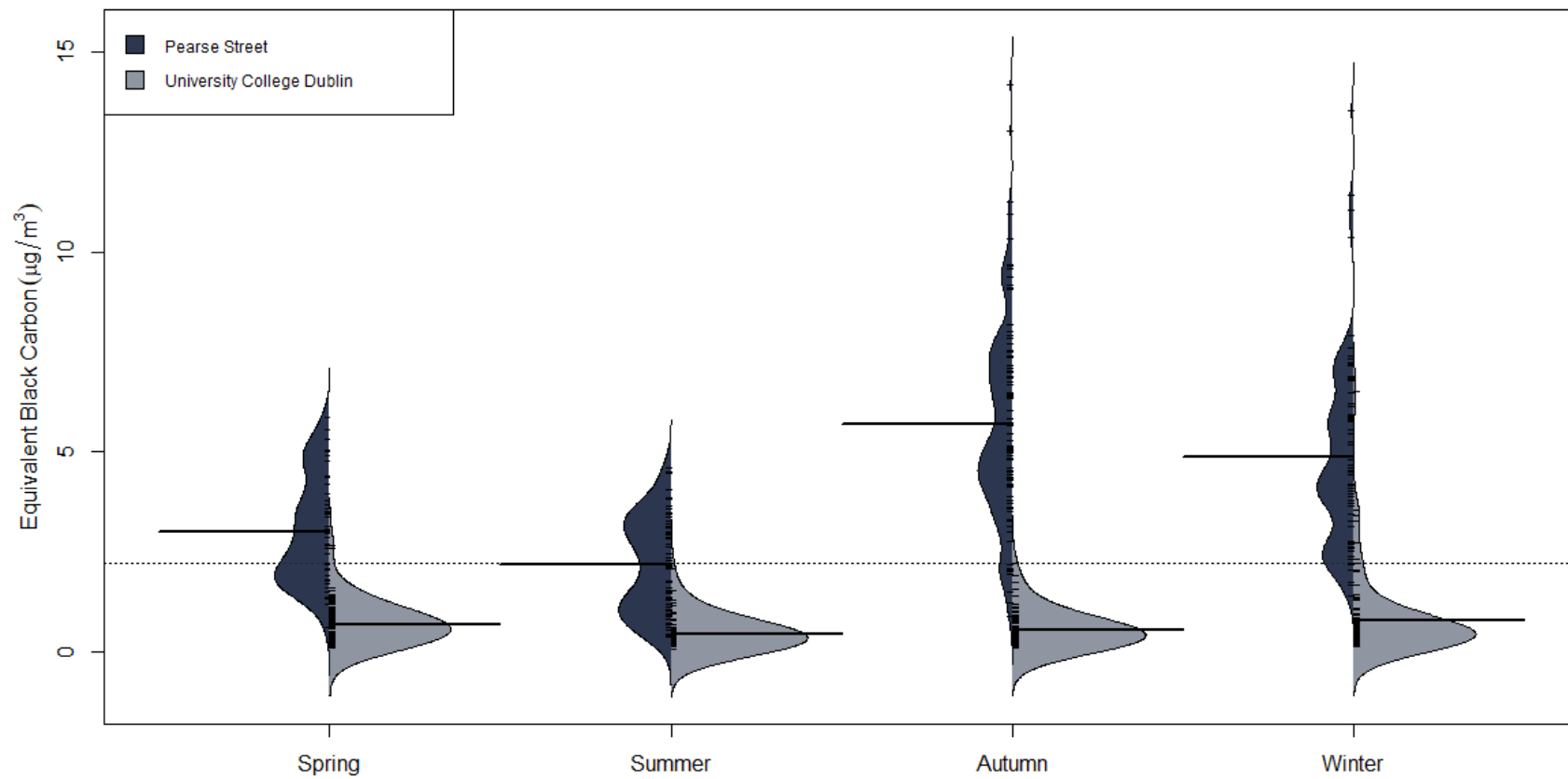


**Figure 4.17** Seasonal distribution of daily average eBC concentrations measured at Pearse Street (September 2018 – August 2019) and University College Dublin (September 2017 – August 2018). Analysis at Pearse Street was based on 49, 74, 91 and 72 sampling days in spring, summer, autumn and winter, respectively.

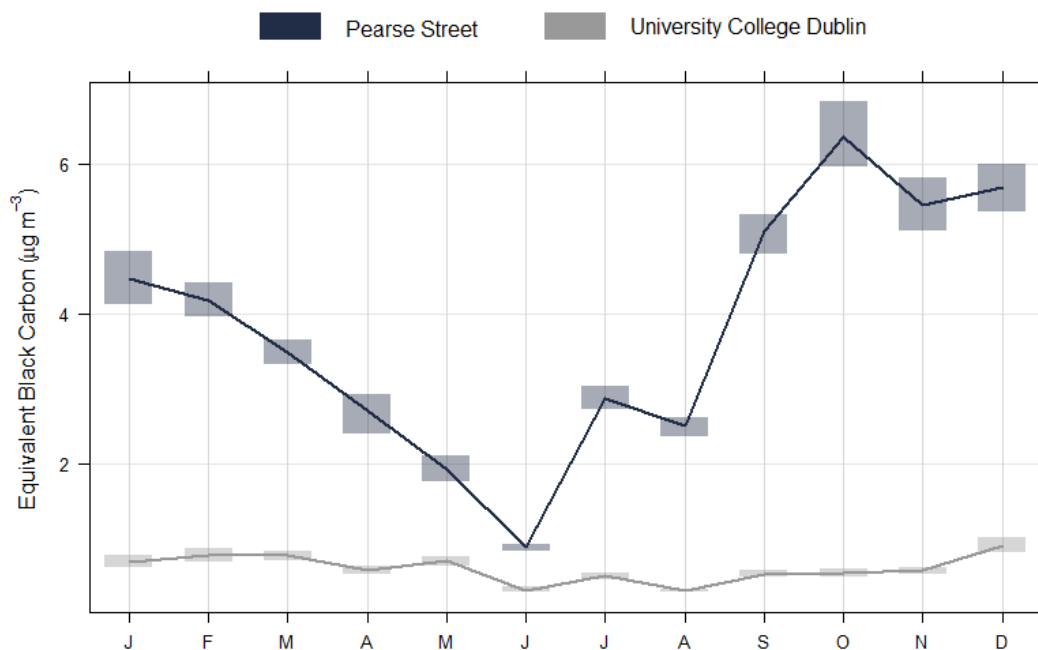


**Figure 4.18** Average monthly eBC concentrations measured at Pearse Street (September 2018 – August 2019) and University College Dublin (September 2017 – August 2018). The shaded regions represent the 95% confidence interval in the calculated mean values. Analysis represents 13, 7, 11, 20 and 23 days of sampling in January, April, May, June and July 2019 at Pearse Street and 20 days of sampling in August at UCD.

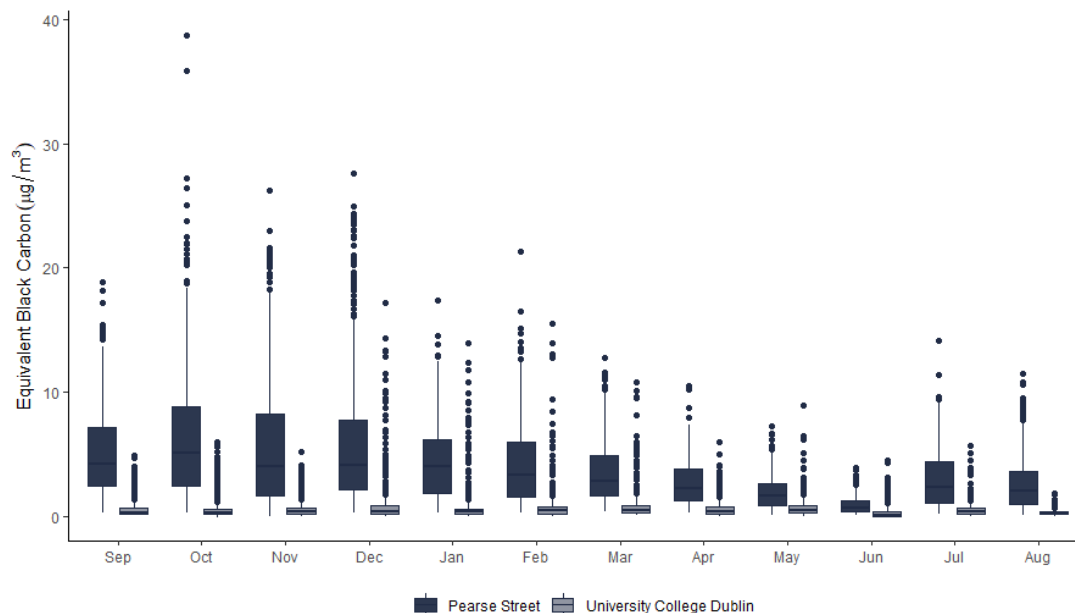


**Figure 4.19** Distribution of eBC measured at Pearse Street (September 2018 - August 2019) and University College Dublin (September 2017 - August 2018). Analysis represents 13, 7, 11, 20 and 23 days of sampling in January, April, May, June and July 2019 at Pearse Street and 20 days of sampling in August at UCD.

**Table 4.4** Mean hourly average eBC concentration measured each month at Pearse Street (September 2018 – August 2019) and on the campus of University College Dublin (September 2017 – August 2019).

<b>Equivalent Black Carbon Concentration (<math>\mu\text{g m}^{-3}</math>)</b>				
	<b>Pearse Street</b>		<b>University College Dublin</b>	
	<i>Mean</i>	<i>Range</i>	<i>Mean</i>	<i>Range</i>
<b>Sep</b>	5.11	0.29 – 18.82	0.52	0.01 – 4.87
<b>Oct</b>	6.37	0.24 – 38.76	0.54	0 – 5.94
<b>Nov</b>	5.45	0 – 26.24	0.57	0 – 5.17
<b>Dec</b>	5.69	0.25 – 27.58	0.90	0 – 17.18
<b>Jan</b>	4.47 <sup>††</sup>	0.24 – 17.37	0.67	0 – 13.90
<b>Feb</b>	4.17	0.22 – 21.32	0.78	0 – 15.46
<b>Mar</b>	3.48	0.33 – 12.77	0.77	0.02 – 10.78
<b>Apr</b>	2.70 <sup>‡‡</sup>	0.23 – 10.47	0.58	0 – 5.92
<b>May</b>	1.93 <sup>§§</sup>	0.07 – 7.28	0.70	0 – 8.91
<b>Jun</b>	0.88 <sup>***</sup>	0.04 – 3.93	0.31	0 – 4.46
<b>Jul</b>	2.86 <sup>†††</sup>	0.14 – 14.09	0.49	0 – 5.68
<b>Aug</b>	2.49	0.09 – 11.47	0.29 <sup>‡‡‡</sup>	0.01 -1.85

<sup>††</sup> Analysis is based on 13 days of sampling at Pearse Street (urban roadside) in January 2019.

<sup>‡‡</sup> Analysis is based on 7 days of sampling at Pearse Street (urban roadside) in April 2019.

<sup>§§</sup> Analysis is based on 11 days of sampling at Pearse Street (urban roadside) in May 2019.

<sup>\*\*\*</sup> Analysis is based on 20 days of sampling at Pearse Street (urban roadside) in June 2019.

<sup>†††</sup> Analysis is based on 23 days of sampling at Pearse Street (urban roadside) in July 2019.

<sup>‡‡‡</sup> Analysis is based on 20 days of sampling at UCD (Urban background) in August 2018.

Diurnal profiles and absolute concentrations of eBC were temporally and spatially variable (Figure 4.20). A clear diurnal trend was observed at both Pearse Street and University College Dublin during the winter season (December, January, February). There were strong peaks in the morning and evening times at both locations, predominantly due to commuter traffic. These peaks were generally comparable at Pearse Street, suggesting that the increased concentrations were due exclusively to traffic, while the evening peak observed at UCD was larger than that recorded in the morning, indicating additional contributions from a source other than traffic; most likely solid fuel combustion. A similar trend was observed at both locations on Saturdays and Sundays in winter, where a traffic-related peak was not apparent in the morning, while a strong peak was observed in the evening, presumably due to emissions from solid fuel burning. The contribution from solid fuel can be concealed by large traffic-related emissions during the week.

Average concentrations were substantially decreased at both locations during the summer months (June, July, August). Hourly average concentrations recorded at UCD showed little variation throughout the day and rarely exceeded  $1 \mu\text{g m}^{-3}$ . Conversely, a strong diurnal profile was observed at Pearse Street where, although concentrations were reduced compared to those measured during the winter, similar trends were observed in both seasons. During the summer months there were traffic-related peaks at regular intervals from Monday to Friday which coincide with rush hour. Such peaks were not present on Saturdays and Sundays. Background levels of approximately  $1 \mu\text{g m}^{-3}$  were recorded over the weekends.

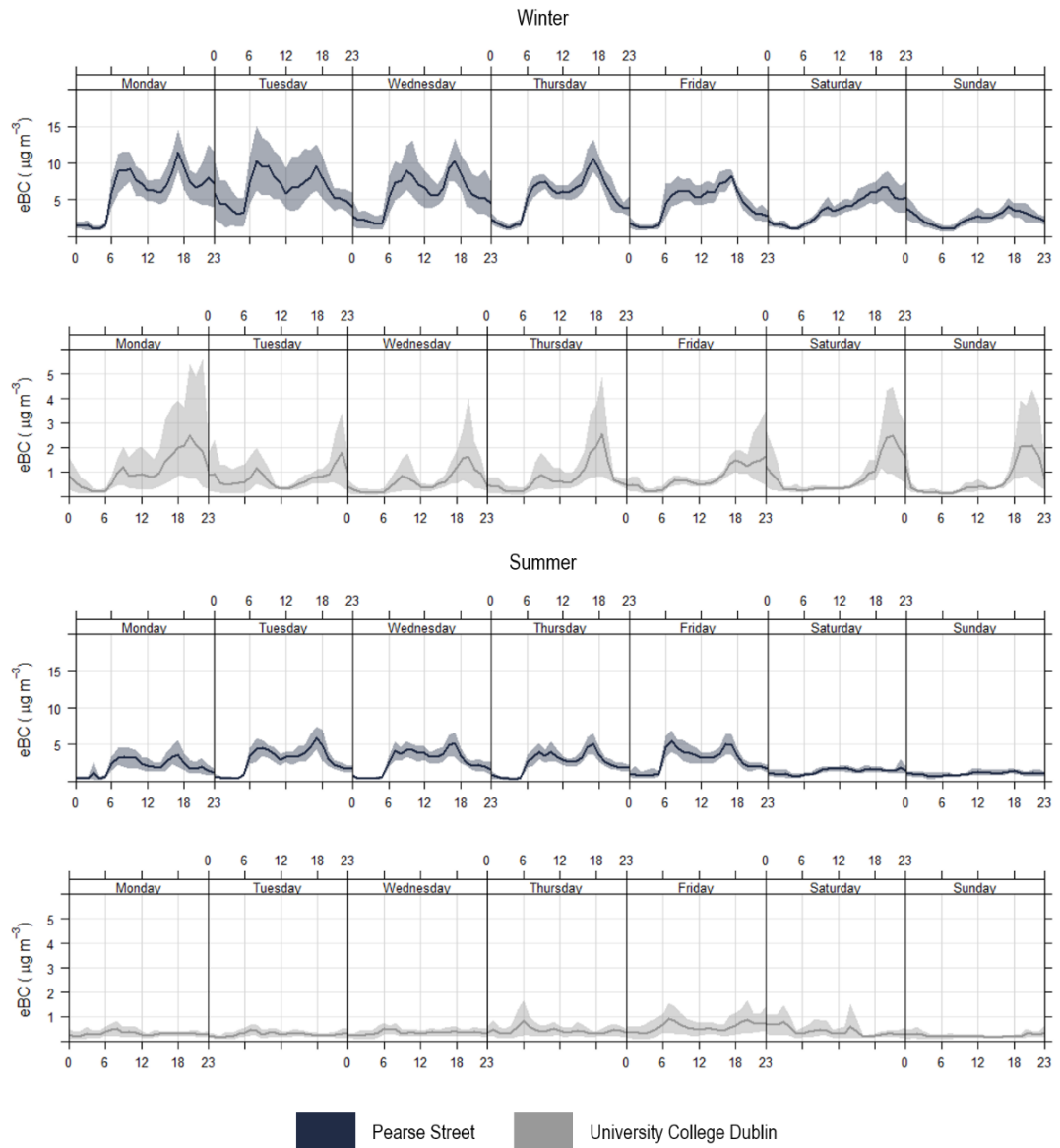


**Figure 4.20** Weekday variation in diurnal trends of eBC concentration measured during winter and summer at Pearse Street (September 2018 – August 2019) and University College Dublin (September 2017 – August 2018).

#### 4.3.3.2 *Source Contribution*

---

The average monthly concentration of black carbon attributed to solid fuel combustion and traffic-related emissions measured at Pearse Street and University College Dublin are illustrated in Figure 4.21. Traffic-related emissions were the dominant source of black carbon at both Pearse Street and UCD, however solid fuel combustion contributed a significant percentage of the total eBC concentration measured at UCD, particularly during winter and spring when ambient temperatures were quite low. The absolute concentrations must be considered carefully in this comparison of sampling sites; despite a higher percentage contribution of solid fuel related emissions at UCD, the absolute concentration was substantially reduced relative to measurements made at Pearse Street. The annual mean hourly average concentration of eBC attributed to solid fuel and traffic-related emissions were  $0.27 \mu\text{g m}^{-3}$  and  $0.33 \mu\text{g m}^{-3}$ , respectively, at University College Dublin (September 2017 – August 2018), in contrast to mean annual values of  $0.90 \mu\text{g m}^{-3}$  and  $3.20 \mu\text{g m}^{-3}$  measured at Pearse Street (September 2018 – August 2019).

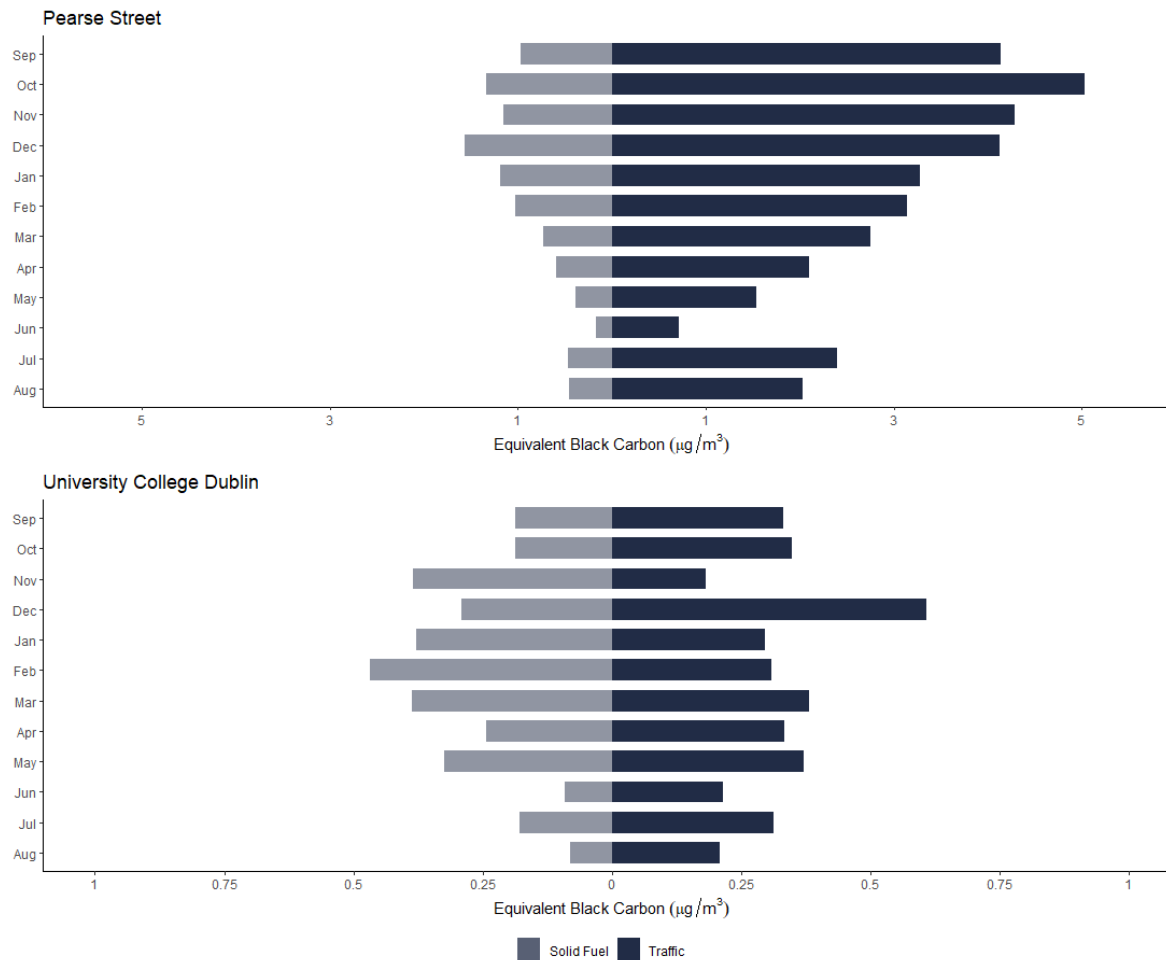


**Figure 4.21** Mean hourly average concentration of equivalent black carbon attributed to solid fuel and traffic-related emissions at Pearse Street (September 2018 – August 2019) and University College Dublin (September 2017 – August 2018). Analysis represents 13, 7, 11, 20 and 23 days of sampling in January, April, May, June and July 2019 at Pearse Street and 20 days of sampling in August at UCD.

The variation in source contribution at the sampling sites was investigated further by comparing the absorption Ångström exponent, which tended towards unity in environments dominated by traffic-related emissions and was higher when emissions were more influenced by solid fuel combustion. Little seasonal variability was observed at Pearse Street ( $\bar{x} = 1.11$ ). In contrast, the AAE recorded at UCD fluctuated considerably from month to month, revealing the impact that different sources had on the composition of ambient aerosol. At this sampling site, a mean hourly average AAE of 1.21 was recorded. The distribution of AAEs recorded each month at Pearse Street and UCD is shown in Figure 4.22.

Figure 4.23 illustrates the distribution of AAE recorded at Pearse Street and UCD during winter and summer. Although the mean AAE recorded at Pearse Street decreased slightly during the summer months, relative to winter months, the distribution throughout the year was quite narrow and uniform, indicative of one major source. There is significant variation in the distribution of AAE observed at UCD during the twelve month period. Bi-modal distribution was observed in both seasons, suggestive of contribution from multiple sources to the ambient aerosol. Although bi-modal, a narrow distribution of AAE was observed during the summer in contrast to winter. During wintertime, larger AAEs were recorded at UCD, in comparison to those recorded during the summer months, as there was greater influence from solid fuel combustion emissions, significantly increasing the AAE. Higher values of AAE are also indicative of aged or oxidised aerosol, which absorbs more strongly in the UV region.

The AAE diurnal trend at both sampling sites was also examined (Figure 4.24). During the summer months, little variation was observed in the AAE at each sampling site, however the values were consistently higher at UCD than at Pearse Street. The AAE tends to drift upwards slightly in the eveningtime during the summer months at both locations. Significant solid fuel combustion is unlikely at this time of year, however organic processing of aerosols throughout the day may result in increased absorption efficiency in the UV region and thus increase the observed AAE. Conversely, during the winter months, there was significant variation in AAE throughout the day. During the winter at Pearse Street, the AAE was lowest during the day when the ambient aerosol was dominated by traffic emissions. An increased AAE was observed overnight, during which time it is likely that solid fuel contributions increased. Despite

an increase in AAE at night, a narrow range of mean values were observed throughout the day; between 1.097 and 1.119 (08:00 – 16:00). Similarly, the AAE was much greater in the eveningtime at UCD during the winter months when solid fuel combustion related emissions were the dominant contributor, however the range in values was much greater. Mean values of less than 1.11 were observed between 05:00 and 09:00 in the morning, while values increased to almost 1.45 at 21:00 in the evening. It is interesting to note the similarity in AAE (~ 1.1) during the wintertime at 09:00. This intersection suggests a dominance of similar sources at both locations at this time. It is likely attributed to traffic-related emissions at peak rush hour; it is one of the lowest AAE values at University College Dublin, while it is typical of the AAE observed throughout the day at Pearse Street. It also corresponds to the time of day when the practice of solid fuel combustion is least common.

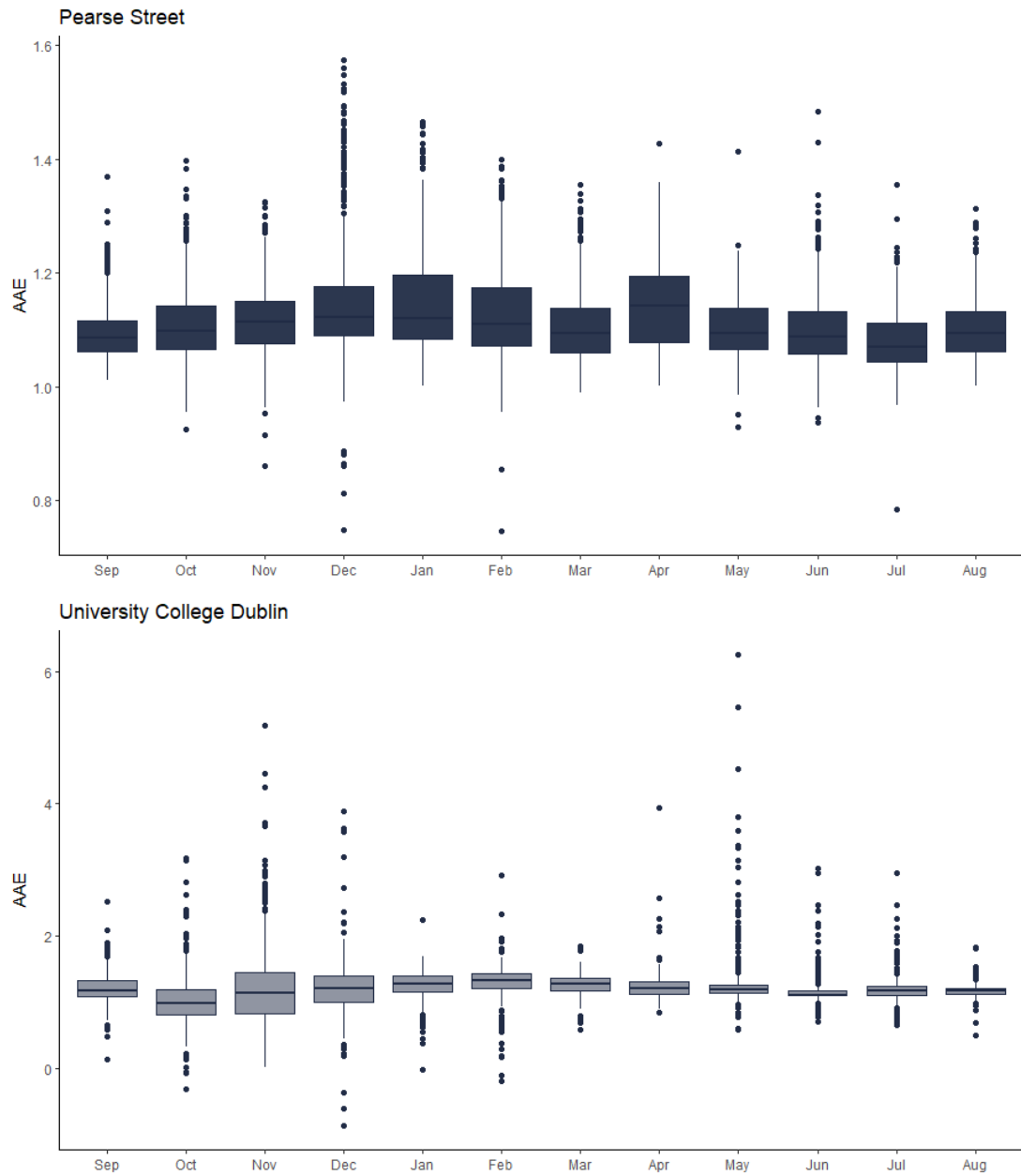


**Figure 4.22** Distribution of monthly absorption Angström exponent recorded at Pearse Street (September 2018 - August 2019) and UCD (September 2017 - August 2018). Analysis represents 13, 7, 11, 20 and 23 days of sampling in January, April, May, June and July 2019 at Pearse Street and 20 days of sampling in August at UCD.

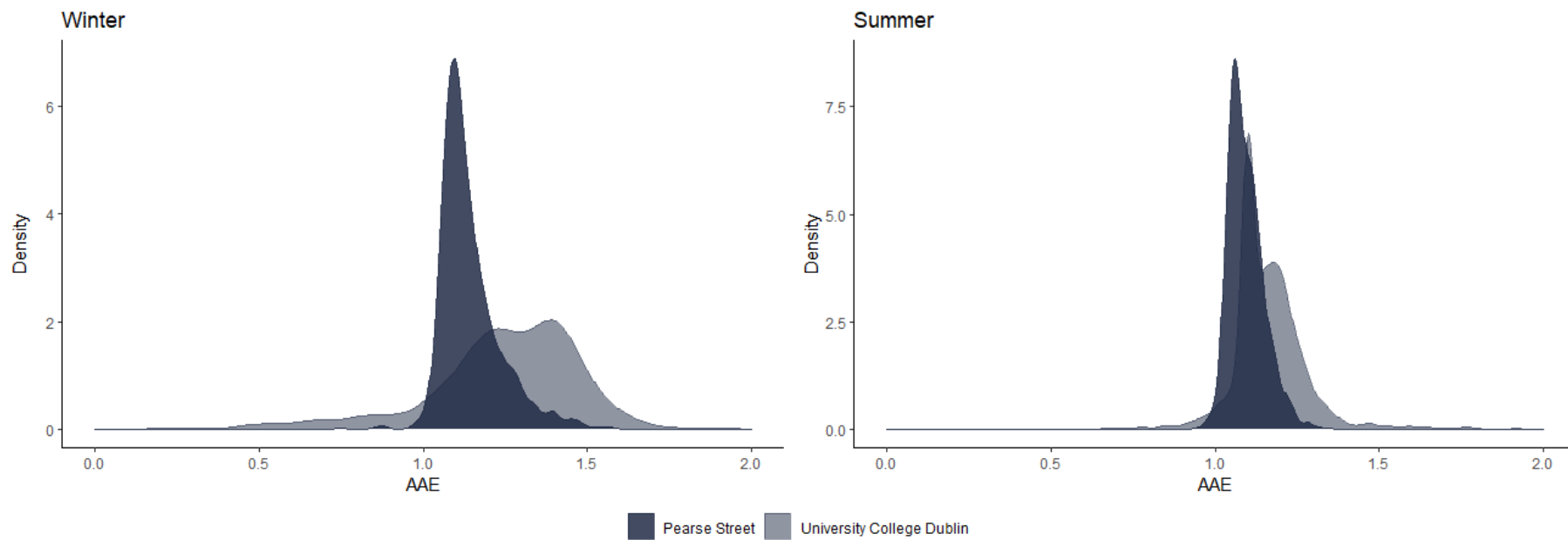


**Figure 4.23** Distribution of absorption Ångström exponent calculated for Pearse Street (September 2018 – August 2019) and University College Dublin (September 2017 – August 2018) during summer and winter.

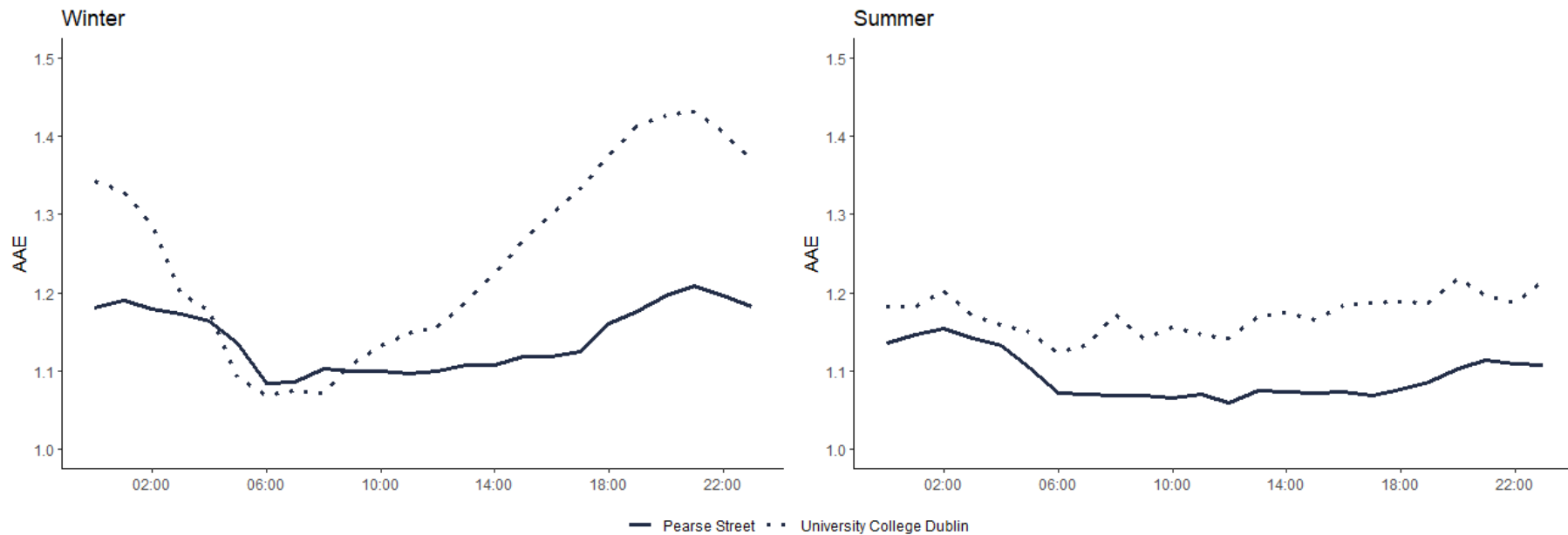


**Figure 4.24** Mean diurnal profile of absorption Ångström exponent recorded during summer and winter at Pearse Street (urban roadside, September 2018 – August 2019) and University College Dublin (urban background, September 2017 – August 2018).

#### 4.3.4 Elemental Carbon (EC) and Organic Carbon (OC)

---

The EUSAAR\_2 protocol was employed to determine the elemental, organic and total carbon content in the filter samples collected at Pearse Street throughout February and March 2019. In total, 50 samples and three field blanks were analysed. A summary of the carbon concentrations measured are provided in Table 4.5. Little variation was observed in the mean total carbon concentrations of  $7.80 \mu\text{g m}^{-3}$  and  $7.35 \mu\text{g m}^{-3}$ , measured during the day and nighttime, respectively. However, organic carbon dominated the total carbon content measured overnight, greater than 65% on average, corresponding to increased levels of solid fuel burning and atmospheric processing. Roughly equivalent contributions from EC (47.7%) and OC (52.3%) were detected in filter samples collected during daytime hours (06:00 – 05:59). There was a greater distribution in the range of values of OC concentration measured in samples collected at nighttime, in comparison to EC content. This subsequently led to similar observations in total carbon concentration (Figure 4.25, Figure 4.26).

Three field blank filter punches ( $1.5 \text{ cm}^2$ ) were analysed using the EUSAAR\_2 protocol (Cavalli et al., 2010). The total carbon content measured on field blanks did not exceed  $1.4 \mu\text{g cm}^{-2}$ . Carbon detected in field blanks was attributed to OC by the EUSAAR\_2 protocol. This is most likely due to the adsorption of semi-volatile organic compounds from the gas phase.

The organic carbon/elemental carbon (OC/EC) ratio was lowest during the day when comparable contributions from OC and EC were observed. The OC/EC ratio of filter samples collected during the day ranged between 0.64 and 2.72, with a mean value of 1.20 (Figure 4.27). The mean ratio increased to approximately 2 in samples collected overnight, between 18:00 and 05:59. OC/EC ratios ranging between 0.44 and 1.45 were published for vehicle emissions specific to China by Ni et al. (2018). Pio et al. (2011) reported an increase in OC/EC ratio in rural and remote settings comparative to urban locations. This was attributed to the strong influence of local emissions in urban settings, while regional and long range transported secondary OC had a greater impact on the OC/EC ratio in rural locations. A mean ratio of 7.15 was obtained from 24-hour (08:00 – 07:59) samples collected the previous year, over 21 days in the month of February 2018, at University College Dublin. This larger ratio indicated contribution from additional sources at this urban residential sampling site; most likely

solid fuel combustion emissions given the residential setting and time of year. The position of the sampling inlets may also have affected the determination of the ratio. At Pearse Street, the inlet was located at ground level, almost directly in line with vehicle exhausts resulting in the exclusive measurement of traffic-related emissions. In contrast, the sample inlet at University College Dublin was located approximately 20 m above ground levels leading to measurement of mixed and diluted aerosol; presumably more representative of the ambient conditions.

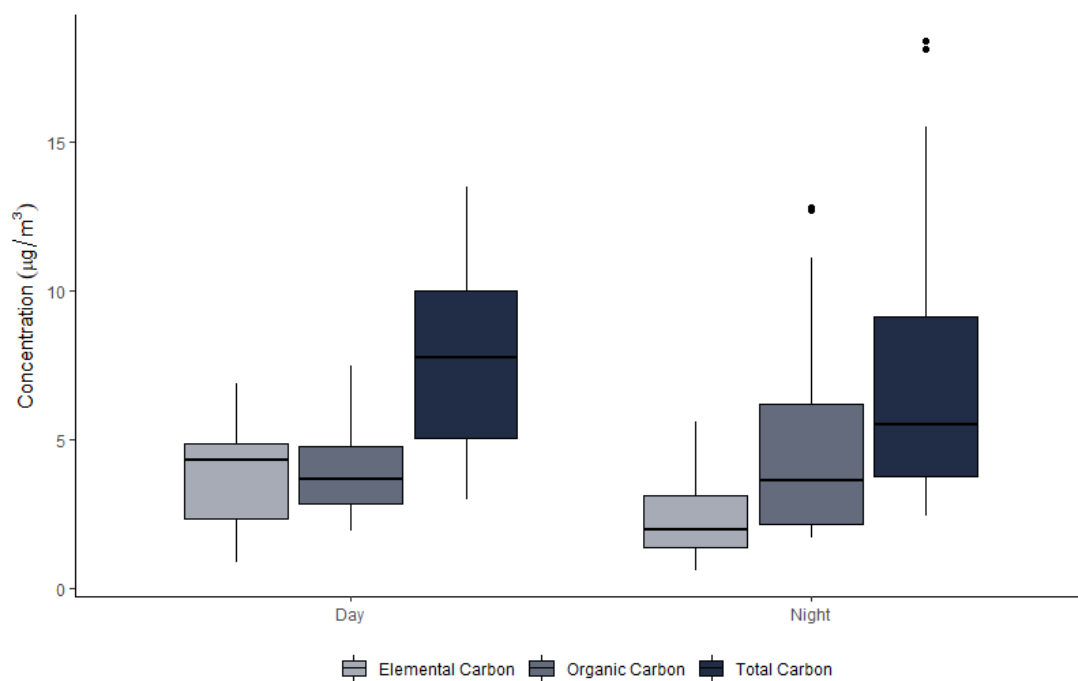


**Figure 4.25** Distribution of elemental, organic and total carbon concentration measured in twelve-hour filter samples collected at Pearse Street between February and March, 2019.

**Table 4.5** Summary of elemental, organic and total carbon content on filter samples collected during daytime (06:00 – 17:59) and nighttime (18:00 – 05:59) between February 1 and March 5, 2019. Concentrations were determined using the EUSAAR\_2 protocol.

		Mean ± SD	Minimum	Maximum
<b>Elemental Carbon (<math>\mu\text{g m}^{-3}</math>)</b>	<i>Daytime</i>	3.85 ± 1.77	0.89	6.87
	<i>Nighttime</i>	2.44 ± 1.43	0.62	5.59
<b>Organic Carbon (<math>\mu\text{g m}^{-3}</math>)</b>	<i>Daytime</i>	3.95 ± 1.59	1.93	7.49
	<i>Nighttime</i>	4.91 ± 3.48	1.73	12.77
<b>Total Carbon (<math>\mu\text{g m}^{-3}</math>)</b>	<i>Daytime</i>	7.80 ± 3.10	3.01	13.48
	<i>Nighttime</i>	7.35 ± 4.83	2.43	18.36
<b>OC/EC Ratio</b>	<i>Daytime</i>	1.21 ± 0.55	0.64	2.72
	<i>Nighttime</i>	2.04 ± 0.74	0.85	3.90

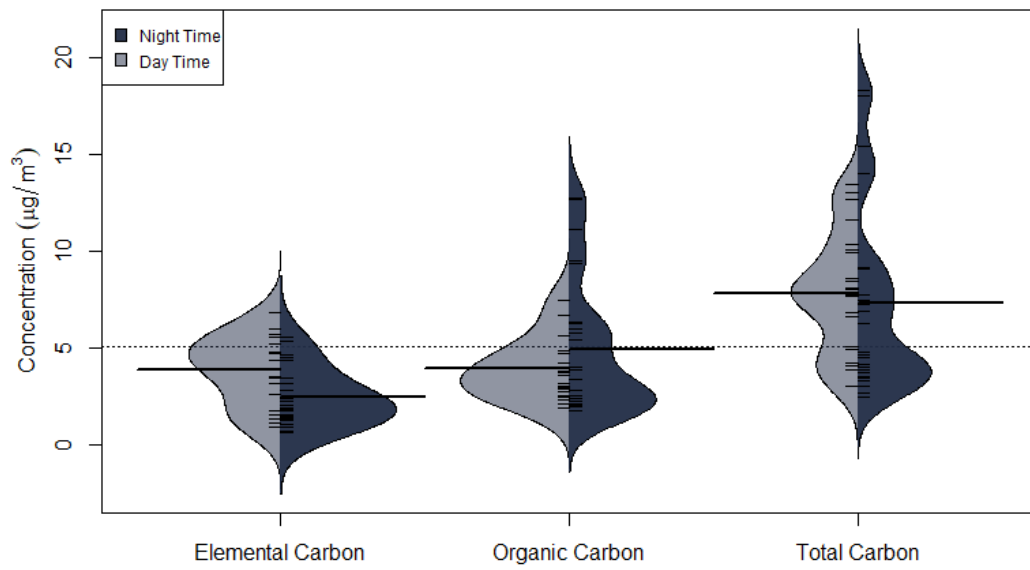


**Figure 4.26** Distribution of elemental, organic and total carbon measured in twelve hours filter samples collected at Pearse Street (February - March 2019).

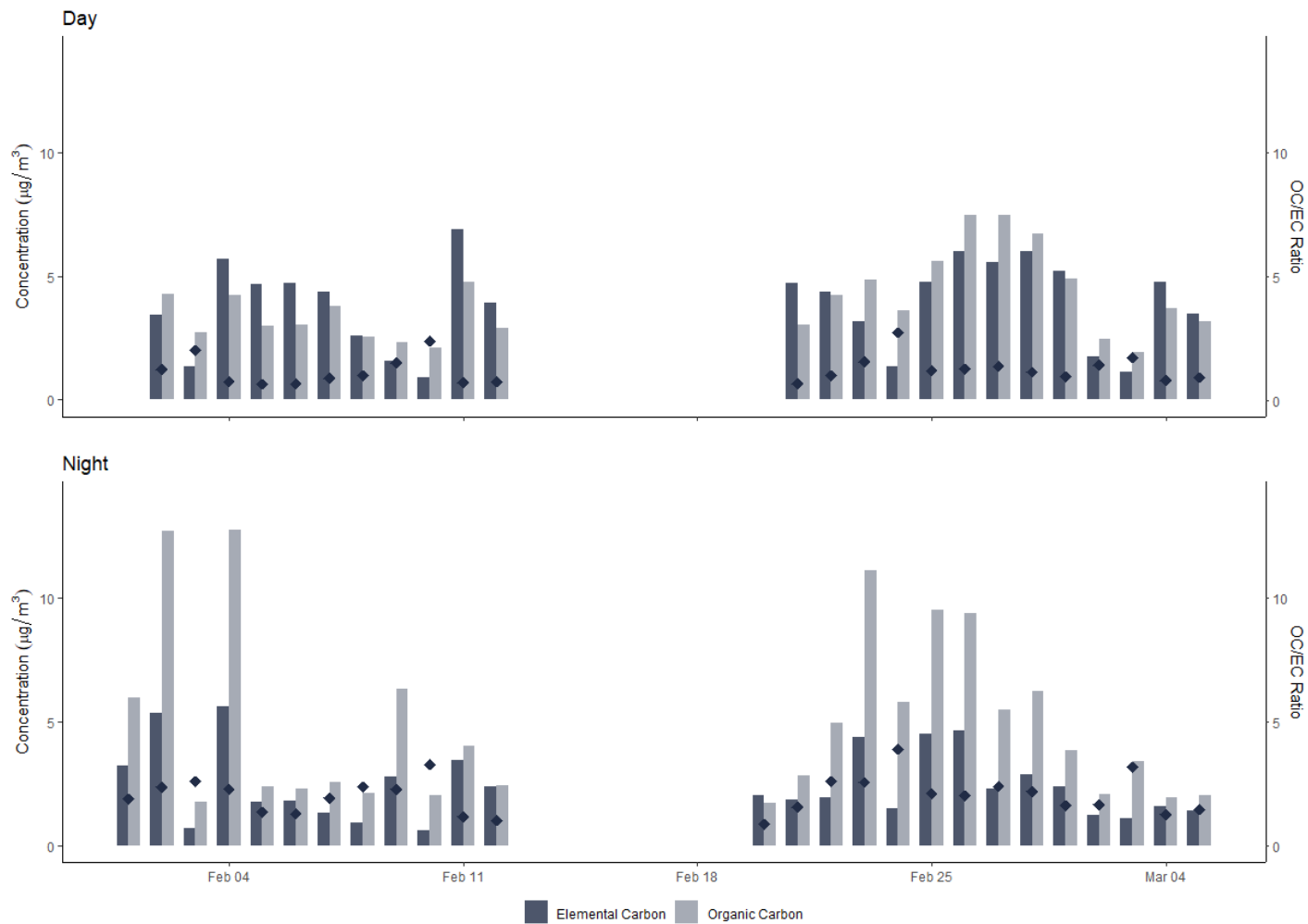


**Figure 4.27** Barplot of elemental and organic carbon with corresponding OC/EC ratio (point) measured at Pearse Street during the day (06:00 – 17:59) and night (18:00 – 05:59) in February and March 2019.

#### 4.3.5 Calculation of Mass Absorption Cross Section

The regression of equivalent black carbon measured optically by the aethalometer versus the thermally measured EC and OC is shown in Figure 4.28. There was excellent correlation between the eBC and EC ( $r^2 = 0.985$ ). It is important to note the variation in techniques used to determine concentration and also the differing time period over which samples were collected. Accordingly, the aethalometer data (60 s timebase) was averaged over the corresponding 12-hour sampling period of filter samples for this analysis.

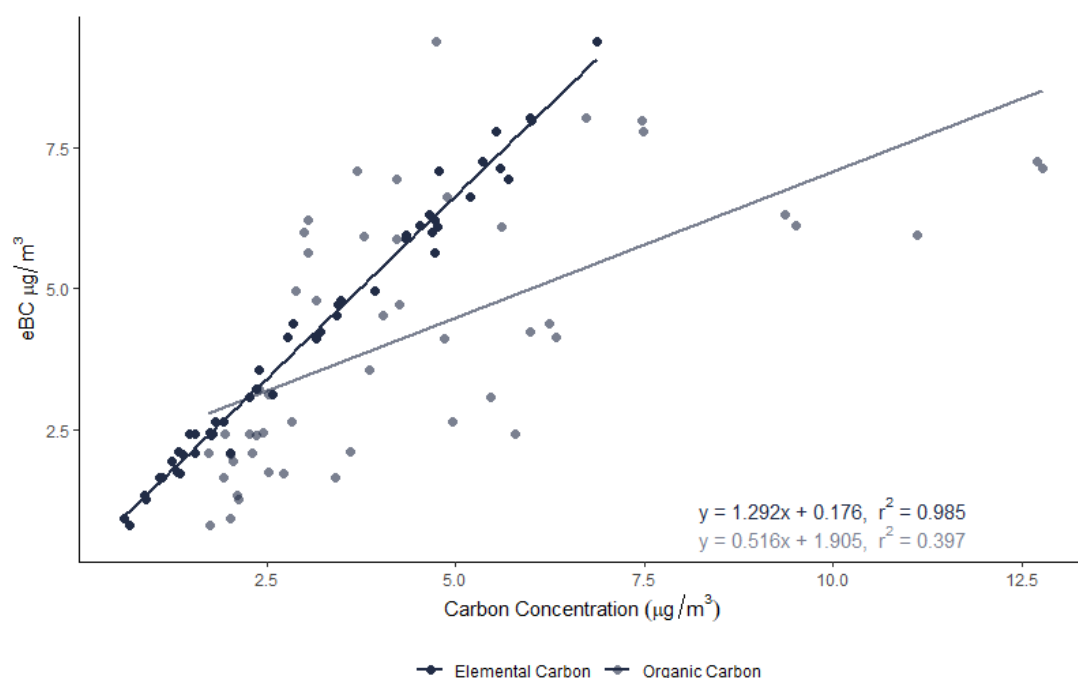


**Figure 4.28** Optically derived equivalent black carbon versus thermally measured elemental and organic carbon measured at Pearse Street (February – March 2019).

In contrast to the absorption coefficient of black carbon ( $b_{abs}$ ) which is a measure of the light absorbed by black carbon per volume in which the BC exists, the mass absorption cross section (MAC) is used to describe the absorbance of light per mass (Knox et al., 2009). The MAC value is dependent on the mixing state, particle age and, subsequently, the coatings that may have accumulated. The ‘mixing state’ defines the distribution of various particle species among particles; externally mixed particles contain a single individual species, while internally mixed particles contain multiple

species. Bond et al. (2013) reported that freshly generated black carbon possesses a MAC value of  $7.5 \pm 1.2 \text{ m}^2 \text{ g}^{-1}$  at 550 nm and increases significantly as internal mixing occurs. The mass absorption cross section was calculated for the monitoring site located on Pearse Street by investigating the regression of the thermally derived EC concentration versus the absorption coefficient of the optically measured black carbon (Figure 4.29). The absorption coefficient ( $b_{abs}$ ) was calculated using the default MAC value ( $\sigma_{air}$ ) employed by the aethalometer in each relevant channel (Eqn. 4.2). The site-specific mass absorption cross section value was determined at a range of wavelengths between 370 and 950 nm (Table 4.6).

$$BC = \frac{b_{abs}}{\sigma_{air}} \quad \text{Eqn. 4.2}$$

The sampling inlet was installed at ground level on Pearse Street and the site was surrounded by tall buildings creating a canyon-like effect which can cause pollutants to become trapped with little dispersion (Lin et al., 2020). Due to the positioning and location of the sampling inlet, it is likely that freshly emitted particles were a major component of the sampled aerosol. The adjusted values calculated were, on average, 32% greater than the default values. The MAC value determined for a wavelength of 880 nm ( $9.68 \text{ m}^2 \text{ g}^{-1}$ ) was lower than that calculated at the urban residential monitoring site located on the campus of University College Dublin ( $12.64 \text{ m}^2 \text{ g}^{-1}$ ) over a similar time period one year previous (February 2018). A comparison of MAC values for daytime and nighttime samples was also carried out (Table 4.6, Figure 4.30). At 880 nm, values of  $9.74 \text{ m}^2 \text{ g}^{-1}$  and  $9.83 \text{ m}^2 \text{ g}^{-1}$  were determined for daytime and nighttime, respectively, both significantly greater than the default value of  $7.77 \text{ m}^2 \text{ g}^{-1}$ . These values are similar to the range ( $10.70 - 11.45 \text{ m}^2 \text{ g}^{-1}$ ) previously reported by Healy et al. (2017) at near-road sites using similar methodology. A wider variation in MAC values was observed at shorter wavelengths, while values converged at higher wavelengths, likely due to aging and atmospheric processing of particles throughout the day.

**Table 4.6** Mass absorption cross-section values calculated for samples collected at Pearse Street, Dublin (February–March 2019).

<b>Wavelength (nm)</b>	<b>Mass Absorption Cross Section (m<sup>2</sup> g<sup>-1</sup>)</b>			
	<i>AE33 Default</i>	<i>Site-Specific</i>	<i>Day</i>	<i>Night</i>
<b>370</b>	18.47	25.64	24.03	32.36
<b>470</b>	14.54	20.61	20.02	23.46
<b>520</b>	13.14	17.45	17.17	19.14
<b>590</b>	11.58	15.25	15.11	16.37
<b>660</b>	10.35	13.20	13.15	13.89
<b>880</b>	7.77	9.68	9.74	9.83
<b>950</b>	7.19	9.29	9.36	9.37

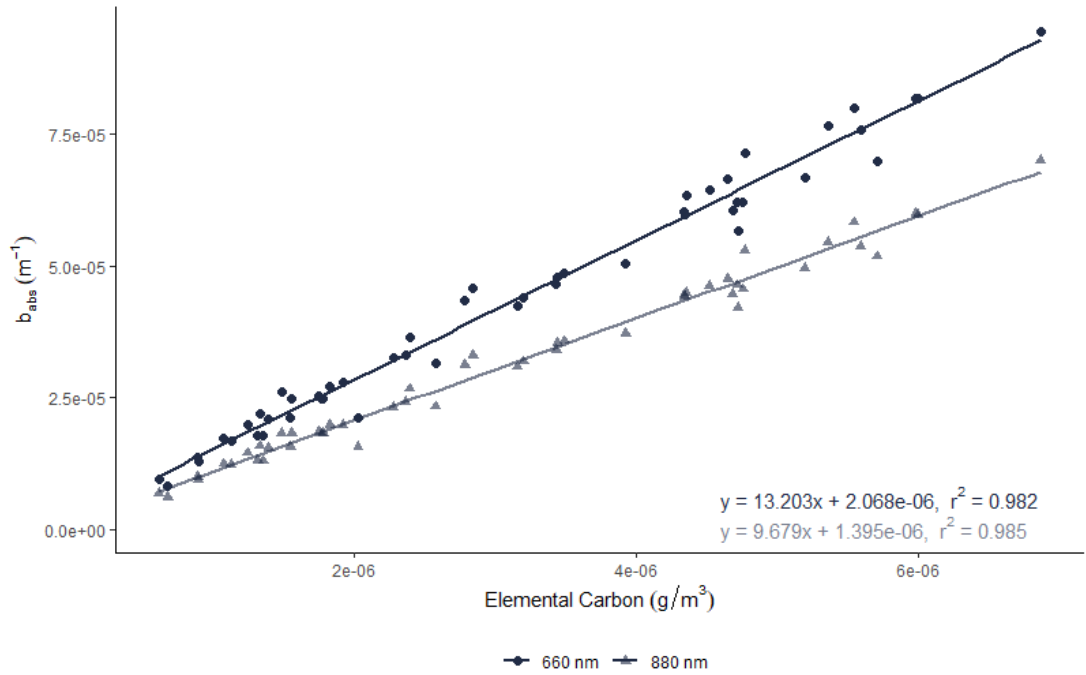


**Figure 4.29** Calculation of site-specific MAC using *e*BC, optically derived at wavelengths of 660 nm and 880 nm, and EC concentration derived thermally from filter samples collected at Pearse Street (February - March 2019).

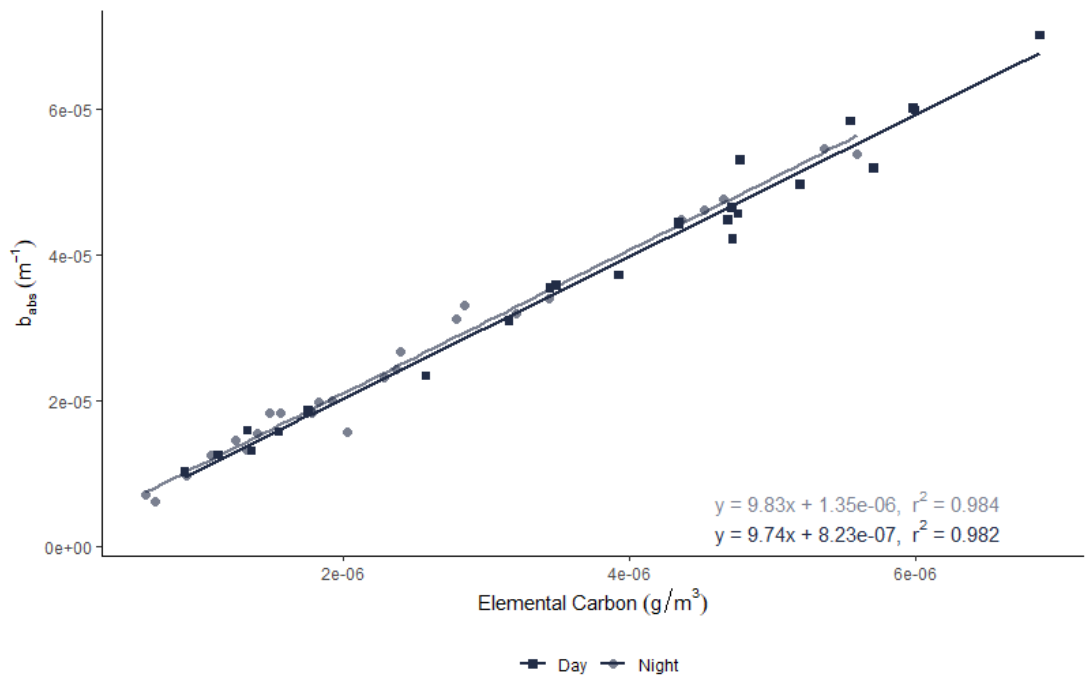


**Figure 4.30** Calculation of daytime and nighttime MAC values at 880 nm from ambient samples collected at Pearse Street (February – March 2019).

Table 4.7 provides a summary of mean monthly hourly average equivalent black carbon concentration estimated using the adjusted site-specific mass absorption cross section values at wavelengths 370, 470, 520, 590, 660, 880 and 950 nm. The table also includes the mean percentage contribution of solid fuel combustion and traffic-related emissions to total ambient black carbon measurements. The application of the adjusted MAC value did not affect mean monthly concentration of total equivalent black carbon, however, it did influence the calculation of the AAE and subsequently, the proportion of equivalent black carbon attributed to solid fuel combustion and traffic-related emissions. The mean monthly percentage of eBC<sub>SF</sub> increased from 22.5%, using instrumental default values, to 36.4% following the introduction of the adjusted MAC values. This value seemed quite high for the environment in which this sampling site was situated, with a consistently high volume of traffic with few residential buildings in the vicinity. The adjusted MAC values, which were applied to the entire, twelve month aethalometer dataset, were determined using thermally analysed filter samples collected in February 2019. Determination of MAC values using samples collected continuously throughout a measurement campaign or during periods representative of each season would be preferable and would yield more accurate source apportionment analysis.

**Table 4.7** Summary of  $eBC_{SF}$  and  $eBC_{Tr}$  calculated using adjusted, site-specific MAC value.

	Equivalent Black Carbon ( $\mu\text{g m}^{-3}$ )	$eBC_{SF}$	$eBC_{Tr}$
	<i>Mean <math>\pm</math> SD</i>	%	%
<b>Sep 2018</b>	5.11 $\pm$ 3.41	35.51	64.49
<b>Oct 2018</b>	6.37 $\pm$ 5.15	37.44	62.59
<b>Nov 2018</b>	5.45 $\pm$ 4.84	38.25	61.75
<b>Dec 2018</b>	5.69 $\pm$ 4.93	42.56	57.44
<b>Jan 2019</b>	4.53 $\pm$ 3.20	43.28	56.72
<b>Feb 2019</b>	4.17 $\pm$ 3.15	40.37	59.63
<b>Mar 2019</b>	3.48 $\pm$ 2.40	37.06	62.94
<b>Apr 2019</b>	2.69 $\pm$ 2.07	41.80	58.20
<b>May 2019</b>	1.92 $\pm$ 1.40	36.76	63.24
<b>Jun 2019</b>	0.70 $\pm$ 0.65	33.47	66.53
<b>Jul 2019</b>	2.27 $\pm$ 2.27	23.33	76.67
<b>Aug 2019</b>	2.49 $\pm$ 1.97	35.85	64.15

#### 4.3.6 Levoglucosan

---

Levoglucosan (1,6-anhydro- $\beta$ -D-glucopyranose), and its isomers mannosan (1,6-anhydro- $\beta$ -D-mannopyranose) and galactosan (1,6-anhydro- $\beta$ -D-galactopyranose), were analysed using anion-exchange chromatographic methods outlined by Iinuma et al. (2009). Of the 28 samples analysed, 13 were collected during the day (06:00 – 17:59) and 15 were collected overnight (18:00 – 05:59) between February 1 and 28, 2019. Levoglucosan was detected in all analysed samples, while mannosan and galactosan was detected in 96% and 50%, respectively, of the samples analysed. The single field blank did not produce a positive concentration result.

Extremely high ambient concentrations of levoglucosan were recorded at the sampling site during February 2019. Due to the type of roadside environment in a central location, such high levels of levoglucosan were unexpected. In the samples analysed, levoglucosan concentrations ranged from 15.51 ng m<sup>-3</sup> to 877.74 ng m<sup>-3</sup>, with mean concentrations of 68.56 ng m<sup>-3</sup> and 265.01 ng m<sup>-3</sup> measured in samples collected during the daytime and nighttime, respectively. Significantly lower ambient concentrations of both mannosan and galactosan were measured; between 2.74 ng m<sup>-3</sup> (nighttime) and 152.35 ng m<sup>-3</sup> (nighttime) and 3.25 ng m<sup>-3</sup> (daytime) and 44.40 ng m<sup>-3</sup> (nighttime), respectively. Maximum concentrations recorded at this sampling site exceeded maximum values reported by Fuller et al. (2014) in a study of ambient wintertime concentrations at five urban background monitoring sites across London.

The increased concentrations of levoglucosan and its isomers measured at nighttime during the month of February indicated a strong influence of solid fuel combustion, for residential heating (Figure 4.31). The mean levoglucosan concentration overnight, measured between 18:00 and 05:59, was almost four times greater than mean concentrations measured during the day (06:00 – 17:59).

**Table 4.8** Summary of concentration of levoglucosan, mannosan and galactosan measured at Pearse Street, Dublin (February 2019) during daytime (06:00 – 17:59) and nighttime (18:00 – 05:59).

		Mean $\pm$ SD	Minimum	Maximum
<b>Levoglucosan (ng m<sup>-3</sup>)</b>	<i>Daytime</i>	68.56 $\pm$ 46.62	15.51	155.13
	<i>Nighttime</i>	265.01 $\pm$ 273.81	22.31	877.74
<b>Mannosan (ng m<sup>-3</sup>)</b>	<i>Daytime</i>	11.04 $\pm$ 6.99	3.50	23.55
	<i>Nighttime</i>	45.78 $\pm$ 50.22	2.74	152.35
<b>Galactosan (ng m<sup>-3</sup>)</b>	<i>Daytime</i>	5.42 $\pm$ 2.01	3.25	7.35
	<i>Nighttime</i>	19.12 $\pm$ 14.45	5.30	44.40

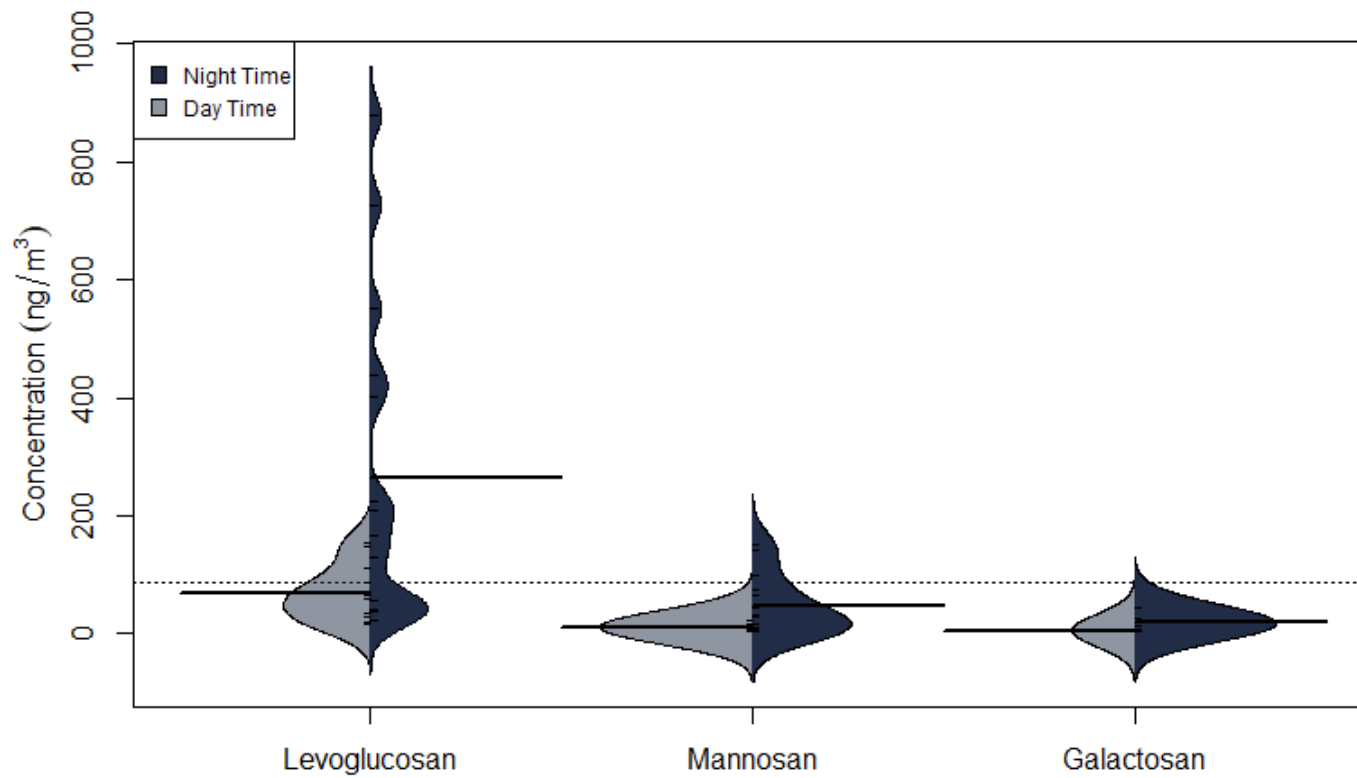


**Figure 4.31** Distribution of levoglucosan, mannosan and galactosan concentrations measured during the day and night at Pearse Street, Dublin (February 2019).

A strong correlation between the three isomers was observed ( $r^2 > 0.95$ ), indicating that the levoglucosan, mannosan and galactosan present in the ambient aerosol originated from a common source (Figure 4.32). The ratio of levoglucosan to mannosan can be used to distinguish between types of solid fuels used in combustion. The ratio measured at the sampling site on Pearse Street ranged from 3.63 to 9.01, resulting in a mean ratio of 6.44 ( $n = 27$ ). This is similar to the mean ratio obtained at the UCD site during the previous winter ( $mean = 6.02, n = 34$ ), despite the larger range of ratio values observed at Pearse Street in a smaller sample set. This suggested that although ambient concentrations measured at Pearse Street are much larger than those measured in the urban residential setting of University College Dublin, similar fuel types were used for combustion in both locations.

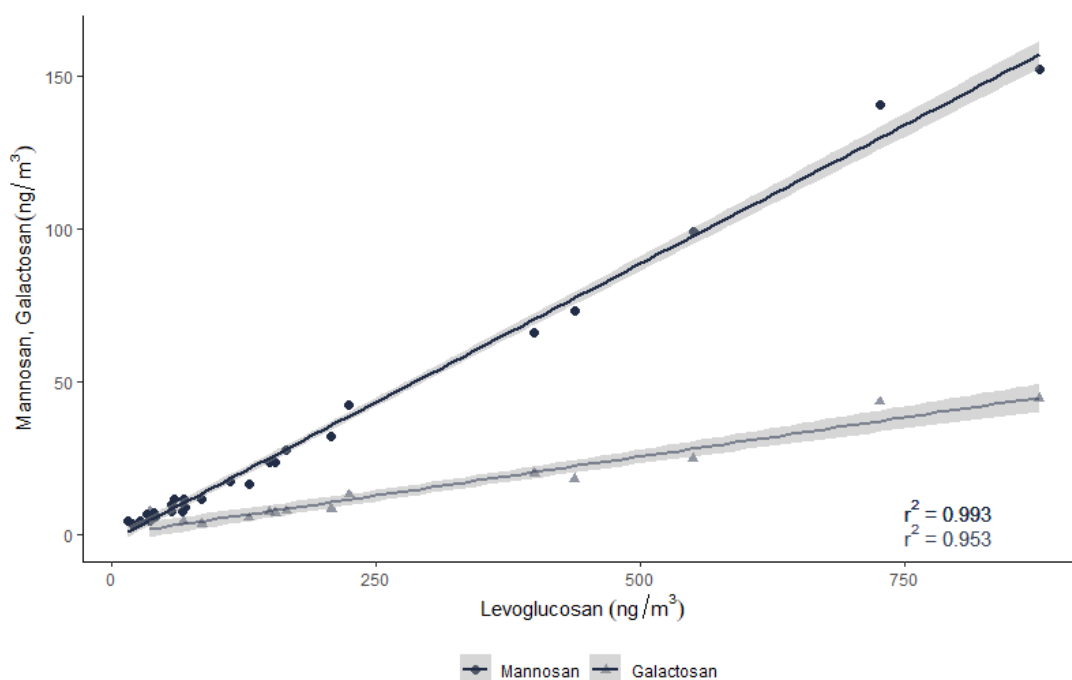


**Figure 4.32** Correlation between levoglucosan and its isomers; mannosan and galactosan, measured in ambient samples collected at Pearse Street (February 2019).

The levoglucosan to organic carbon ratio was also examined (Figure 4.33). The ambient levoglucosan concentration measured was only a fraction of the total organic carbon measured. Using twenty-eight corresponding samples, the ratio was calculated as 0.065. Excellent correlation between the parameters was observed ( $r^2 = 0.88$ ). Correlation improved significantly, increasing to 0.94, when nighttime samples were isolated. Samples collected overnight (18:00 – 05:59) yielded a ratio of 0.066. Samples collected during the day had less levoglucosan content and the ratio between levoglucosan and organic carbon was reduced to 0.026. The correlation between the two parameters in these samples also reduced, to 0.80. Mean ambient concentrations of both levoglucosan and organic carbon were lower during the day in comparison to those measured at night. The variation in levoglucosan to OC ratios at different times of day was indicative of additional factors and components influencing the composition and absolute concentration of organic carbon measured, particularly during the day.

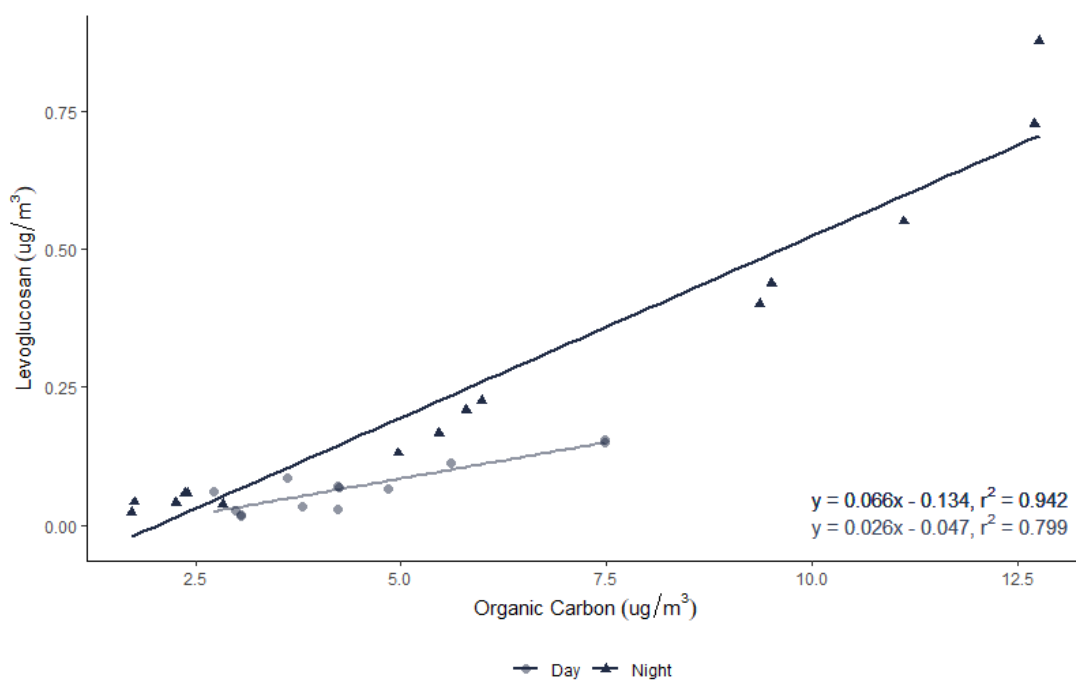


**Figure 4.33** Concentration of levoglucosan versus organic carbon measured during daytime and nighttime at Pearse Street (February 2019).

The measured levoglucosan concentrations were also compared with optically-determined equivalent black carbon concentrations (Figure 4.34). eBC measurements were averaged over the corresponding 12-hour sampling period of filter collection used for levoglucosan analysis. As anticipated due to the origins of levoglucosan, the greatest correlation was observed between levoglucosan and eBC attributed to solid fuel combustion related emissions ( $r^2 = 0.797$ ). A correlation between levoglucosan and black carbon attributed to traffic-related emissions could not be established.

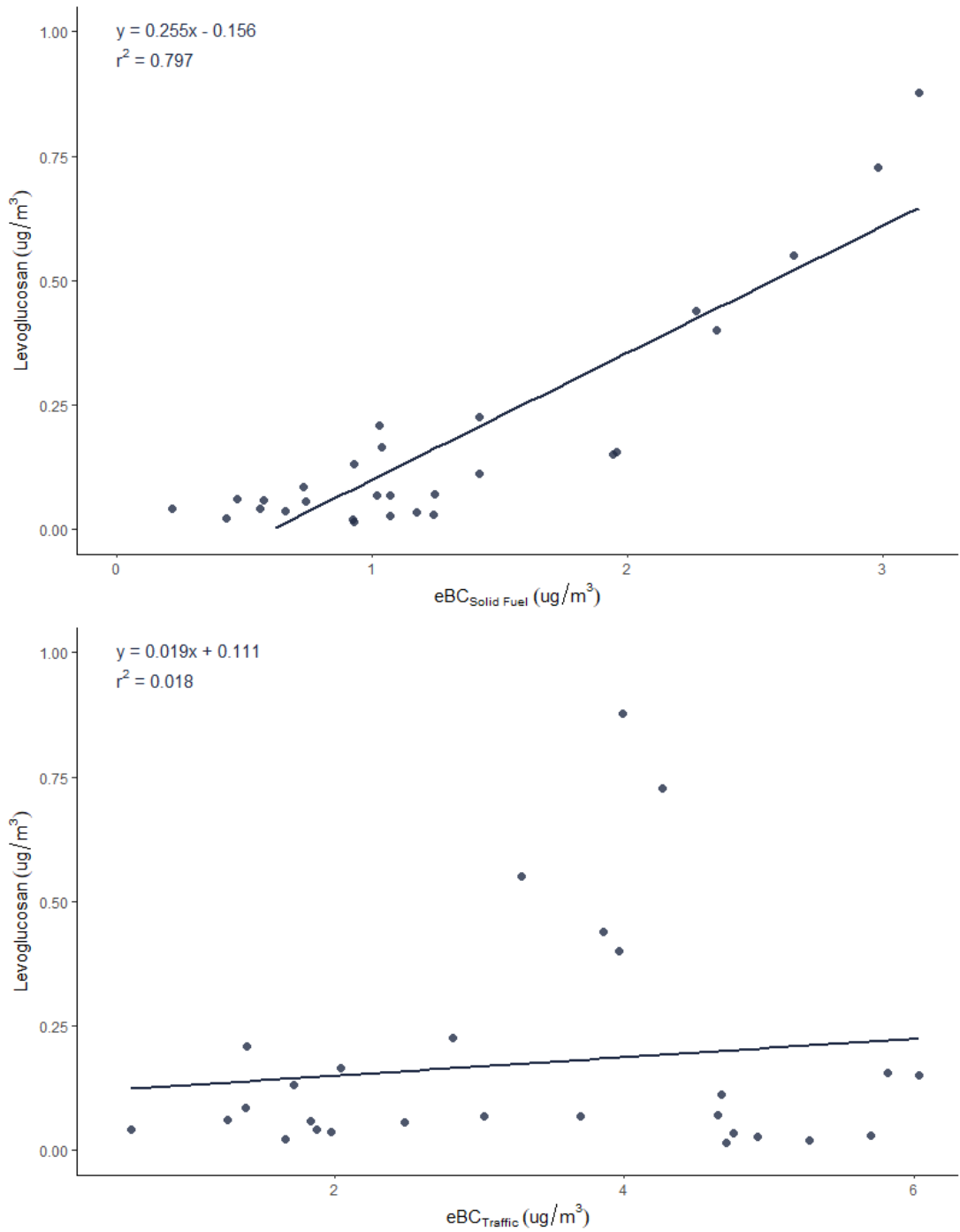


**Figure 4.34** Levoglucosan versus eBC<sub>SF</sub> and eBC<sub>Tr</sub> measured at Pearse Street during February 2019. eBC measurements were averaged over 12-hour periods to correspond with ambient filter samples.

#### 4.3.7 On-line Measurement of Carbon Content

The Total Carbon Analyzer operated continuously on a one-hour time basis from May 22 to August 21, 2019, when there was a power failure. During this time period there was excellent data capture (95.1%), with down time attributed to stoppages for quartz fibre filter changes and other routine maintenance. The TCA-08 relies on the output of optical measurements of eBC from the aethalometer to determine the equivalent elemental (eEC) and equivalent organic carbon (eOC) fractions. Due to interruption to AE33 sampling in June and July 2019, the corresponding eEC and eOC data was deemed invalid.

Total carbon analysis presented below is representative of 10, 30, 27 and 21 days sampling in May, June, July and August 2019, respectively (Figure 4.35). TC concentrations varied from hour to hour throughout the sampling period. Consequently, the EC and OC concentrations also varied significantly. Over the entire sampling period, the mean hourly total carbon concentration was  $3.99 \mu\text{g m}^{-3}$ , ranging from  $0.12 \mu\text{g m}^{-3}$  to  $22.31 \mu\text{g m}^{-3}$ . A summary of the hourly TC concentration measured between May and August 2019 is provided in Table 4.9.

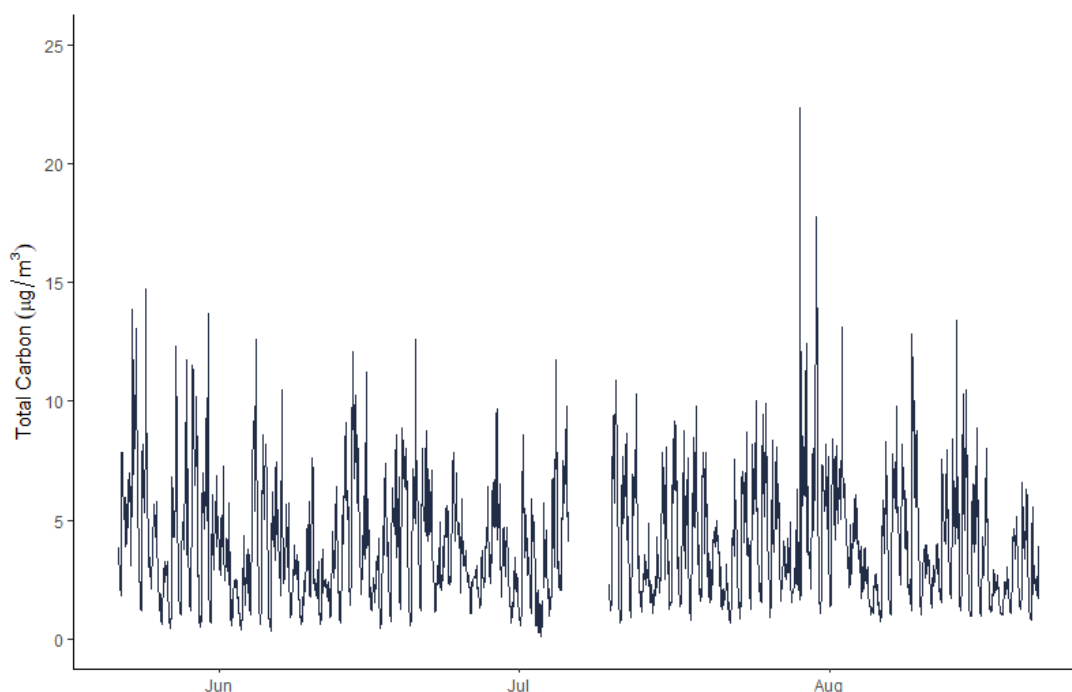


**Figure 4.35** Temporal profile of total carbon measured by the Total Carbon Analyzer (TCA-08, Magee Scientific) at Pearse Street (May - August 2019).

eEC and eOC analysis presented below is representative of 10, 20, 22 and 21 days sampling in May, June, July and August 2019, respectively (Table 4.9). Due to a lack of cross over in sampling periods, the EC and OC fractions determined by conventional thermal-optical methods cannot be accurately compared to the results from the Total Carbon Analyzer, however the OC/EC ratio can be investigated while accounting for the seasonal difference. Table 4.9 provides a mean monthly OC/EC ratio. The average OC/EC ratio determined using thermal-optical methods (EUSAAR\_2 protocol) of samples collected during February 2019, was 1.64; 1.21 in samples collected during the day and 2.04 in samples collected overnight. The mean eOC/eEC ratio recorded during the summer months using on-line methods was 2.11. Without corresponding filter samples for the summer period, it is difficult to determine whether the variation in ratio is due to seasonality or the use of an inaccurate  $b$  parameter for this site. Conventional thermal analysis of filter samples collected concurrently are required to calculate a site-specific  $b$  parameter in order to accurately estimate the equivalent elemental carbon concentration.

The diurnal profile of eEC and eOC is shown in Figure 4.36. Mean concentrations were quite low in the early hours of the morning. From approximately 06:00 onwards the mean eEC and eOC concentration increased. Simultaneously, the range of values recorded also increased. The mean recorded value of eEC is greater than that of eOC during the day, consistent with increased traffic emissions, while the eOC fraction dominates overnight. The diurnal variation is reflected in the diel profile of AAE measured simultaneously at the sampling site. Due to the season in which sampling took place, it is unlikely that this can be attributed to solid fuel burning, and thus supports the argument that traffic emissions enhanced secondary organic aerosol (SOA) formation, which subsequently led to higher organic carbon content.

It is also plausible that the use of an inappropriate value of the  $b$  parameter may have influenced results. The data output by the Total Carbon Analyzer is dependent on precise conversion from BC to eEC in order to accurately estimate eOC concentration.

**Table 4.9** Mean hourly average concentrations of organic and elemental black carbon measured by the Total Carbon Analyzer between May and August 2019.

	eOC ( $\mu\text{g m}^{-3}$ )		eEC ( $\mu\text{g m}^{-3}$ )		Total Carbon ( $\mu\text{g m}^{-3}$ )		eOC/eEC Ratio
	<i>Mean</i>	<i>Range</i>	<i>Mean</i>	<i>Range</i>	<i>Mean</i>	<i>Range</i>	<i>Mean</i>
<i>May 2019</i>	3.07	0.38 – 11.40	1.79	0.07 – 7.03	4.86	0.47 – 14.72	2.381
<i>Jun 2019</i>	2.85	0.29 – 11.33	0.84	0.04 – 3.79	3.66	0.36 – 12.61	4.242
<i>Jul 2019</i>	1.54	0.37 – 13.60	2.72	0.13 – 13.59	4.15	0.12 – 22.31	0.926
<i>Aug 2019</i>	1.39	-2.78 - 4.69	2.44	0.13 – 10.79	3.82	0.74 – 13.41	1.232
<i>Total</i>	2.06	-2.78 – 13.60	2.00	0.04 – 13.59	3.99	0.12 – 22.31	2.11

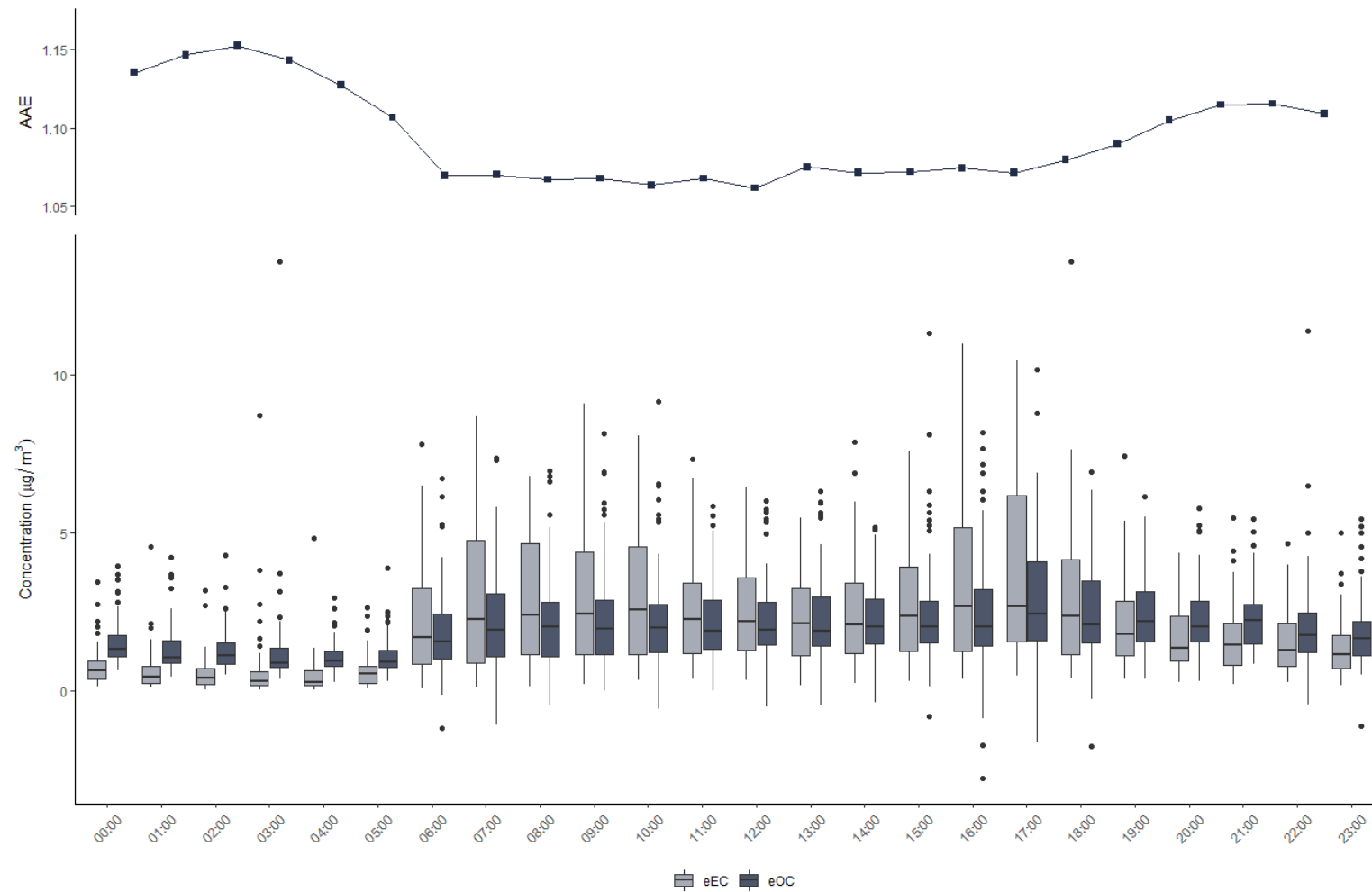


**Figure 4.36** Boxplot illustrating the diurnal pattern of eEC and eOC observed at Pearse Street over the entire sampling period (May – August 2019) with the corresponding AAE diurnal trend.

#### 4.4 CONCLUSIONS

---

A distinct seasonal and diurnal trend in eBC concentrations was identified at this high density traffic site on Pearse Street in Dublin city centre throughout the twelve month field campaign which ran from September 2018 to August 2019. Data output by the multi-wavelength aethalometer (AE33, Magee Scientific), which sampled continuously, indicated that the highest hourly average concentrations of eBC were measured in Autumn and Winter, with a maximum hourly average concentration of  $38.76 \mu\text{g m}^{-3}$  recorded in October 2018. eBC concentrations were significantly reduced during the summer months, however similar diurnal patterns were observed.

Repetition in the weekly variation of eBC was observed consistently throughout the entire sampling period. Two strong traffic-related peaks were observed Monday to Friday, inclusive, coinciding with rush hour when commuters were entering and exiting the city for work purposes, in the morning and evening. Calculated AAE confirmed the dominance of traffic-related emissions in spring ( $\bar{x} = 1.11$ ), summer ( $\bar{x} = 1.09$ ), autumn ( $\bar{x} = 1.11$ ) and winter ( $\bar{x} = 1.14$ ), respectively. Commuter traffic-related peaks did not exist at the weekend (Saturday and Sunday) during any season, and background levels of eBC persisted throughout the day. The levels of eBC observed at the weekend signify the extent of the possible improvement in air quality if a major reduction in traffic volume in the city centre occurred or with increased use of alternatively fuelled vehicles.

An interesting point to note is the apparently consistent contribution of solid fuel combustion emissions to the total eBC concentrations measured at Pearse Street, when Zotter values ( $\alpha_{\text{Tr}} = 0.9$  and  $\alpha_{\text{SF}} = 1.68$ ) were applied in source apportionment analysis. Hourly average measurements indicated that a mean value of 22.5% was attributed to solid fuel combustion, ranging from 18.3% (June 2019) to 27.6% (January 2019). Such a persistent contribution from solid fuel combustion throughout the year was unexpected; a significant decrease during the warmer summer months was anticipated, particularly at a sampling site located in the city centre with considerably high volumes of traffic of all vehicle types. On further investigation, diurnal trends illustrated an increase in eBC attributed to both solid fuel combustion and traffic-related emissions on two concurrent occasions during the day. This was anticipated in the eveningtime, specifically during the winter with the onset of domestic heating, however the

simultaneous increase during morning rush hour was unexpected. It is highly unlikely that solid fuel combustion played such an influential role in the condition of the ambient aerosol so early in the morning. Diurnal variation exhibited by eEC and eOC measured by the Total Carbon Analyzer echoed these findings during the summer months, when solid fuel burning is presumably at a minimum.

It is reasonable to assume that enhanced secondary organic aerosol production due to the substantial emission of SOA precursors by both petrol and diesel vehicles was observed at this urban roadside sampling site. Analysis of levoglucosan and thermally determined OC concentration provided further support for this hypothesis. Despite excellent correlation ( $r^2 = 0.88$ ) between the two parameters, a mean ratio of 0.065 was calculated. This indicated the limited influence of solid fuel combustion emissions on the total ambient organic carbon content and was suggestive of significant contribution from additional sources. Optimisation of the AAE values employed in the aethalometer model may improve the accuracy of source apportionment analysis. However, even with an optimised AAE pair, it may prove difficult to distinguish between natural SOA and enhanced SOA production caused by the fossil fuel combustion emissions of traffic.

The measurements recorded at Pearse Street were compared to measurements recorded a year previously at the urban residential monitoring site on the campus of University College Dublin (September 2017 – August 2018). The magnitude of concentrations observed at Pearse Street were greater than those recorded at University College Dublin, despite evidence of similar temporal trends at both locations. A larger distribution of concentrations was recorded at Pearse Street, particularly during autumn and winter. There was a markedly greater contribution from solid fuel combustion related emissions in the ambient aerosol sampled at University College Dublin which was anticipated in a predominantly residential area. The location and proximity to major sources of sampling inlets at both locations must be considered when comparing the sampling sites; while the inlet at Pearse Street was located at ground level, in close proximity to freshly emitted, dominant sources (traffic), the inlet at UCD was located on the roof of a building, approximately 20 m above ground level. This sampling site did not have any major sources directly in the vicinity allowing for greater dispersion and aerosol mixing.

## 5. CARBONACEOUS AEROSOL IN A SMALL TOWN IN RURAL IRELAND

---

<b>5.1</b>	<b><i>Aims</i></b> .....	<b>232</b>
<b>5.2</b>	<b><i>Methodology</i></b> .....	<b>234</b>
5.2.1	Sampling Site .....	234
5.2.2	Instrumentation and Analysis.....	237
<b>5.3</b>	<b><i>Results and Discussion</i></b> .....	<b>239</b>
5.3.1	Meteorological Data.....	239
5.3.2	Particulate Matter .....	243
5.3.3	Equivalent Black Carbon .....	247
5.3.3.1	Temporal Trends.....	248
5.3.3.2	Diurnal Trends .....	252
5.3.3.3	Source Contribution.....	254
5.3.4	Elemental Carbon (EC) and Organic Carbon (OC) .....	263
5.3.4.1	Calculation of Mass Absorption Cross Section .....	267
5.3.4.2	Fractions of EC and OC.....	269
5.3.5	On-line Measurement of Carbon Content .....	274
5.3.5.1	Determination of eEC and eOC .....	278
5.3.6	Comparison of Wintertime Air Quality in 2015, 2020 and 2021 .....	289
5.3.6.1	Meteorological Conditions .....	291
5.3.6.2	Particulate Matter and Equivalent Black Carbon .....	293
5.3.6.3	Elemental and Organic Carbon.....	297
<b>5.4</b>	<b><i>Conclusions</i></b> .....	<b>300</b>

## 5.1 AIMS

---

The principal aims of the work presented in this chapter are threefold: (1) to investigate the seasonal variability of ambient carbonaceous aerosol in the town of Enniscorthy, Co. Wexford and assess the contributions of fossil fuel and solid fuel combustion related emissions in a small town reliant on solid fuel for residential heating; (2) to estimate the accuracy of the newly developed ‘TC-BC’ method employed by the Total Carbon Analyzer (TCA-08, Magee Scientific) for the on-line determination of EC and OC in comparison to conventional thermal-optical methods when the EUSAAR\_2 protocol is used for samples collected in this environment, and (3) to compare the results with those recorded in the Source Apportionment of Particulate Matter in Urban and Rural Residential Areas of Ireland (SAPPHIRE) report (Wenger et al., 2020) which examined the dominant sources of PM<sub>2.5</sub> at the same location during winter 2015. The key instruments used for this work were the seven-wavelength dual-spot aethalometer (Drinovec et al., 2015) and the recently developed Total Carbon Analyzer (Rigler et al., 2020). Following the deployment of the aethalometer and Total Carbon Analyzer at the monitoring site, measurements began on December 1, 2019. The instruments ran continuously until January 20, 2021, however the analysis presented in this chapter will focus mainly on the time period from December 1, 2019 to November 30, 2020, inclusive; precisely a twelve month period.

The data collected during the campaigns will be used to assess the absolute concentrations and seasonal variability of black carbon in this rural town. The source apportionment model developed by Sandradewi, Prévôt, Szidat et al. (2008) will be used to ascertain the contributions made by solid fuel combustion and traffic-related emissions to total ambient black carbon, using the parameters ( $\alpha_{SF} = 1.68$  and  $\alpha_{Tr} = 0.9$ ) proposed by Zotter et al. (2017). These parameters were used previously during a wintertime monitoring campaign (SAPPHIRE) at the same location in 2015 (Buckley, 2019; Wenger et al., 2020). Comparison of measurements obtained in 2015, 2020 and 2021 will inform an assessment as to whether ambient conditions have improved, and if there has been a change in the dominant sources contributing the total mass concentration throughout the intervening period and following the extension of a ban on the sale of bituminous coal to include Enniscorthy from September 2020.

The new 'TC-BC' method recently proposed by Rigler et al. (2020) utilises the total carbon concentration, thermally derived by the Total Carbon Analyzer, and the black carbon (BC) concentration, optically derived by the AE33 aethalometer. Using a proportionality parameter,  $b$ , the BC is used to determine the equivalent elemental carbon (eEC). The equivalent organic carbon content (eOC) is subsequently estimated by subtracting the eEC from the total carbon measured. In February 2020, ambient aerosol samples were collected on quartz fibre filters using a high volume air sampler (DHA-80, DIGITEL) and the elemental and organic carbon content was measured using a conventional thermal-optical method; the EUSAAR\_2 protocol which is the current European standard (CEN EN 16909). The comparison of both methods will be used to evaluate the suitability of the 'TC-BC' method in this multi-fuel environment and to estimate a proportionality factor appropriate in the Irish context.

## 5.2 METHODOLOGY

---

### 5.2.1 Sampling Site

---

Ambient aerosol sampling took place on the grounds of the public library in the town of Enniscorthy, Co. Wexford (52° 30' 1.44" N, 6° 34' 13.12" W) in the south-east of Ireland, between December 1, 2019 and January 20, 2021. Instrumentation included a multi-wavelength aethalometer (AE33, Magee Scientific), a high volume air sampler (DHA-80, DIGITEL Elektronik GmbH), a Total Carbon Analyzer (TCA-08, Magee Scientific) provided by Aerosol d.o.o., and an ultraviolet (UV) fluorescence sulfur dioxide monitor (T100, Teledyne API). The instruments, with the exception of the high volume air sampler, were installed in a mobile container. The high volume air sampler stood independently at the same location. Results presented in this chapter are based on analysis of data collected during a twelve month period (01/12/2019 – 30/11/2020).

The town, which is situated in the valley of the River Slaney, has a population of just over 11,300 according to the census carried out by the Central Statistics Office in 2016 (CSO, 2016). The sampling site was located near the centre of the town, approximately 520 m south west of the train station. The M11, which connects Dublin and Wexford, is 3 km east of the monitoring site, while the N30, a national primary road, is approximately 3.5 km to the west. There were no major sources located in close proximity of the site.

It is worth noting two significant events that took place during the sampling period which may ultimately influence the results presented in this chapter; (1) the onset of the COVID-19 pandemic in Ireland in late February 2020 and (2) the extension of the ‘Smoky Coal’ ban, which limits the sale, distribution and marketing of bituminous coal, to include the town of Enniscorthy from September 2020 onwards. The intermittent implementation of stringent travel restrictions and mandatory ‘stay at home’ orders, aimed at curbing the spread of the coronavirus, presumably limited the contributions from traffic-related emissions and led to an increase in solid fuel usage for domestic heating as people spent the majority of their time at home.

Particulate matter (PM<sub>2.5</sub> and PM<sub>10</sub>) mass concentrations were measured concurrently at the monitoring site (FIDAS 200, Palas). The measurements were obtained from the Environmental Protection Agency (EPA) to inform supplementary analysis presented

in this chapter. Meteorological data was obtained from the Met Éireann weather station located on the grounds of Teagasc in Johnstown Castle, Wexford; 24 km south east of the sampling site (Figure 5.1). Meteorological parameters used in the analysis included rainfall (mm), temperature ( $^{\circ}\text{C}$ ), wind direction and wind speed ( $\text{m s}^{-1}$ ).



**Figure 5.1** Satellite image of the town of Enniscorthy, Co. Wexford with red marker indicating the location of the sampling site (left). The relative locations of the sampling site in Enniscorthy (red) and the weather station (blue) at Johnstown Castle, Co. Wexford (right).

### 5.2.2 Instrumentation and Analysis

---

A range of instruments were deployed during the monitoring campaign in Enniscorthy to measure the absolute concentrations, and subsequently identify the dominant sources contributing to the ambient carbonaceous aerosol. The principal instruments; the multi-wavelength aethalometer and the Total Carbon Analyzer, operated on a continuous basis with short stoppages for routine maintenance. Filter samples were collected throughout February 2020 for off-line thermal-optical analysis. The SO<sub>2</sub> monitor ran continuously between January 2020 and January 2021, inclusive. A summary of the dates of operation and percentage data capture is provided in Table 5.1.

The multi-wavelength dual-spot aethalometer (AE33, Magee Scientific) measured eBC concentrations continuously on a 60 second time basis with a flow rate of 5 L min<sup>-1</sup>. Default mass absorption cross section values were applied at each wavelength to calculate the instantaneous concentration of black carbon. Source apportionment of solid fuel combustion and traffic-related emissions was based on the aethalometer model proposed by Sandradewi, Prévôt, Szidat et al. (2008) and employed the Zotter parameters of 1.68 and 0.9, respectively.

The Total Carbon Analyzer ran continuously during the sampling period on an hourly basis. The instrument operated at a flow rate of 16.7 L min<sup>-1</sup>. The total carbon concentration was determined by flash heating the sample collected on a quartz fibre filter. The equivalent elemental and organic carbon concentrations were estimated using the optically-derived black carbon concentrations, measured by the co-located AE33 aethalometer (Eqn. 5.1).

$$OC = TC - b \cdot BC \quad \text{Eqn. 5.1}$$

The proportionality parameter,  $b$ , is used to determine the eEC content from the optically measured black carbon. The default value of 1 was applied in the initial analysis of the on-line data. A site-specific value of  $b$ , representative of the ambient wintertime conditions, was then calculated using the filter samples collected during

the corresponding period. An orthogonal regression model was used to investigate the linear relationship between the thermally-derived EC of the filter samples and the optically-derived black carbon concentrations. This analysis was performed using the ‘Deming’ function of the *MethComp* software package (Carstensen et al., 2020).

The high volume air sampler (DHA-80, DIGITEL Elektronik GmbH) collected ambient aerosol samples on quartz fibre filters between February 3 and 23, 2020. The instrument operated at a flow rate of 500 L min<sup>-1</sup> and sample collection was of eight hours duration, beginning at 07:00, 15:00 and 23:00, respectively. Filter samples were analysed off-line at the Environmental Radioactivity Laboratory (Institute of Nuclear and Radiological Science and Technology, NCSR ‘Demokritos’) in Athens, Greece using a Laboratory OCEC Aerosol Analyzer (Sunset Laboratory Inc.). The EUSAAR\_2 protocol was employed and analysis adhered to the CEN approved European standard for measurement of elemental and organic carbon collected on filters.

Additionally, the ambient concentration of sulfur dioxide (SO<sub>2</sub>) was measured continuously at 60 second intervals from January 2020 onwards using a UV fluorescence sulfur dioxide monitor (T100, Teledyne API). A detailed description of the instruments and analysis techniques employed is provided in Chapter 2.

**Table 5.1** Summary of instrumentation deployed at the Enniscorthy sampling site. Percentage data capture is representative of the sampling period between December 2019 and November 2020, inclusive.

		Dates of Operation	Data Capture
			%
<b>Aethalometer</b>	AE33	01/12/2019 – 20/01/2021	98.5
<b>Ambient Air Sampler</b>	DHA-80	03/02/2020 – 23/02/2020	93.7
<b>Total Carbon Analyzer</b>	TCA-08	01/12/2019 – 20/01/2021	88.3
<b>Sulfur Dioxide Monitor</b>	T100	17/01/2020 – 20/01/2021	92.9

## 5.3 RESULTS AND DISCUSSION

### 5.3.1 Meteorological Data

The meteorological data presented was obtained from the Met Éireann weather station located on the grounds of Johnstown Castle ( $52^{\circ} 17' 52.8''$  N,  $6^{\circ} 29' 49.2''$  W), approximately 23.5 km south east of the monitoring site and 62 m above sea level. A monthly summary of the meteorological parameters observed during the sampling period are provided in Table 5.2.

Maximum temperatures were recorded during the summer months, reaching a maximum of  $22.3^{\circ}\text{C}$  in both June and August 2020. February 2020 was the coldest month on average; temperatures ranged between  $0.2^{\circ}\text{C}$  and  $12.3^{\circ}\text{C}$  (Figure 5.3). Predominant winds originated in the south west throughout the sampling period, however strong north easterly winds were recorded in March and April 2020 (Figure 5.4). Lowest wind speeds were recorded during the summer months. A number of storms were recorded during the measurement period; Storms Atiyah and Elsa (December 2019), Storm Brendan (January 2020), Storms Ciara, Dennis and Jorge (February 2020) and Storms Ellen and Francis (August 2020).

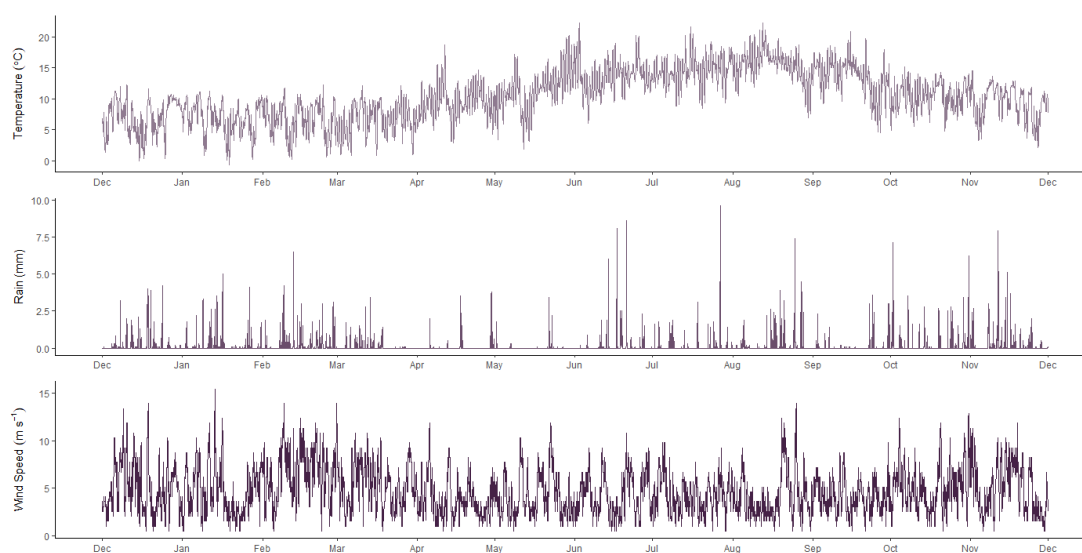


**Figure 5.2** Temporal profile of temperature, precipitation and wind speed recorded during the sampling period (December 2019 - November 2020).

*Table 5.2 Hourly meteorological parameters recorded at Johnstown Castle, Co. Wexford.*

	Precipitation (mm)		Temperature (°C)		Wind Speed (m s <sup>-1</sup> )	
	<i>Mean</i>	<i>Range</i>	<i>Mean</i>	<i>Range</i>	<i>Mean</i>	<i>Range</i>
<b>Dec 2019</b>	0.13	0 – 4.2	7.00	0.0 – 12.3	4.99	0 – 13.89
<b>Jan 2020</b>	0.14	0 – 5.0	6.81	-0.7 – 11.2	4.68	0 – 15.43
<b>Feb 2020</b>	0.22	0 – 6.5	6.64	0.2 – 12.3	6.68	0 – 13.89
<b>Mar 2020</b>	0.06	0 – 3.4	6.67	0.8 – 12.2	5.24	0 – 10.80
<b>Apr 2020</b>	0.07	0 – 3.8	9.55	2.9 – 18.7	3.78	0 – 11.83
<b>May 2020</b>	0.02	0 – 3.4	11.48	1.9 – 20.3	4.20	0 – 11.83
<b>Jun 2020</b>	0.13	0 – 8.6	13.64	6.0 – 22.3	4.32	0 – 10.80
<b>Jul 2020</b>	0.12	0 – 9.6	14.59	8.5 – 21.6	4.23	0 – 9.77
<b>Aug 2020</b>	0.17	0 – 7.4	15.46	7.0 – 22.3	4.15	0 – 13.89
<b>Sep 2020</b>	0.07	0 – 3.6	13.58	4.5 – 20.9	4.09	0 – 9.77
<b>Oct 2020</b>	0.18	0 – 7.1	10.52	4.8 – 15.2	5.08	0 – 12.86
<b>Nov 2020</b>	0.17	0 – 7.9	9.27	2.1 – 14.6	4.92	0 – 11.83

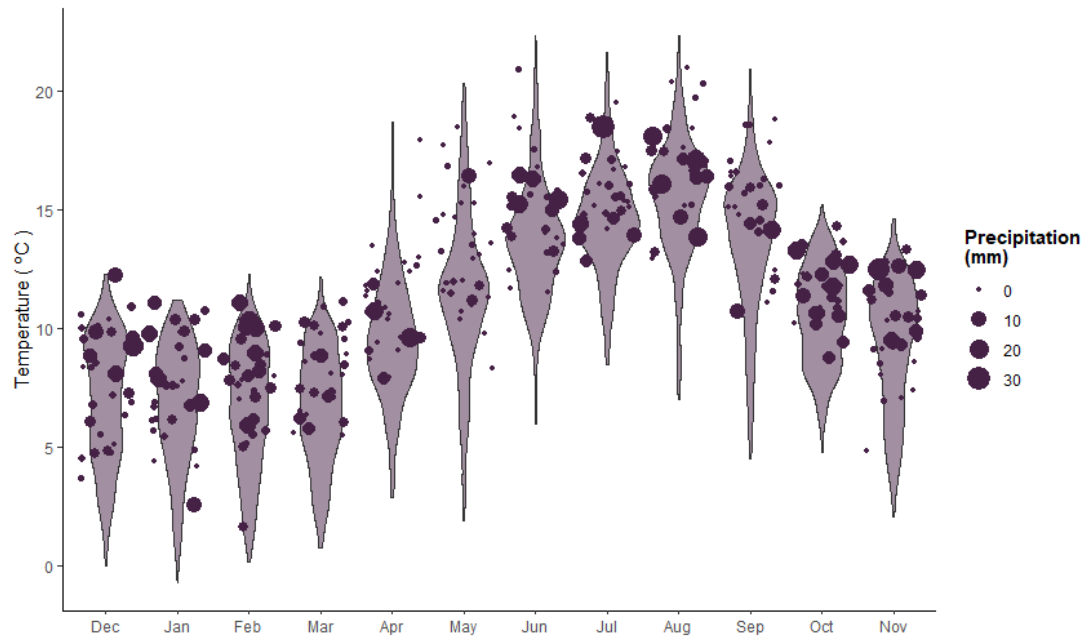


**Figure 5.3** Distribution of monthly temperatures and rainfall record at Johnstown Castle (December 2019 – November 2020).

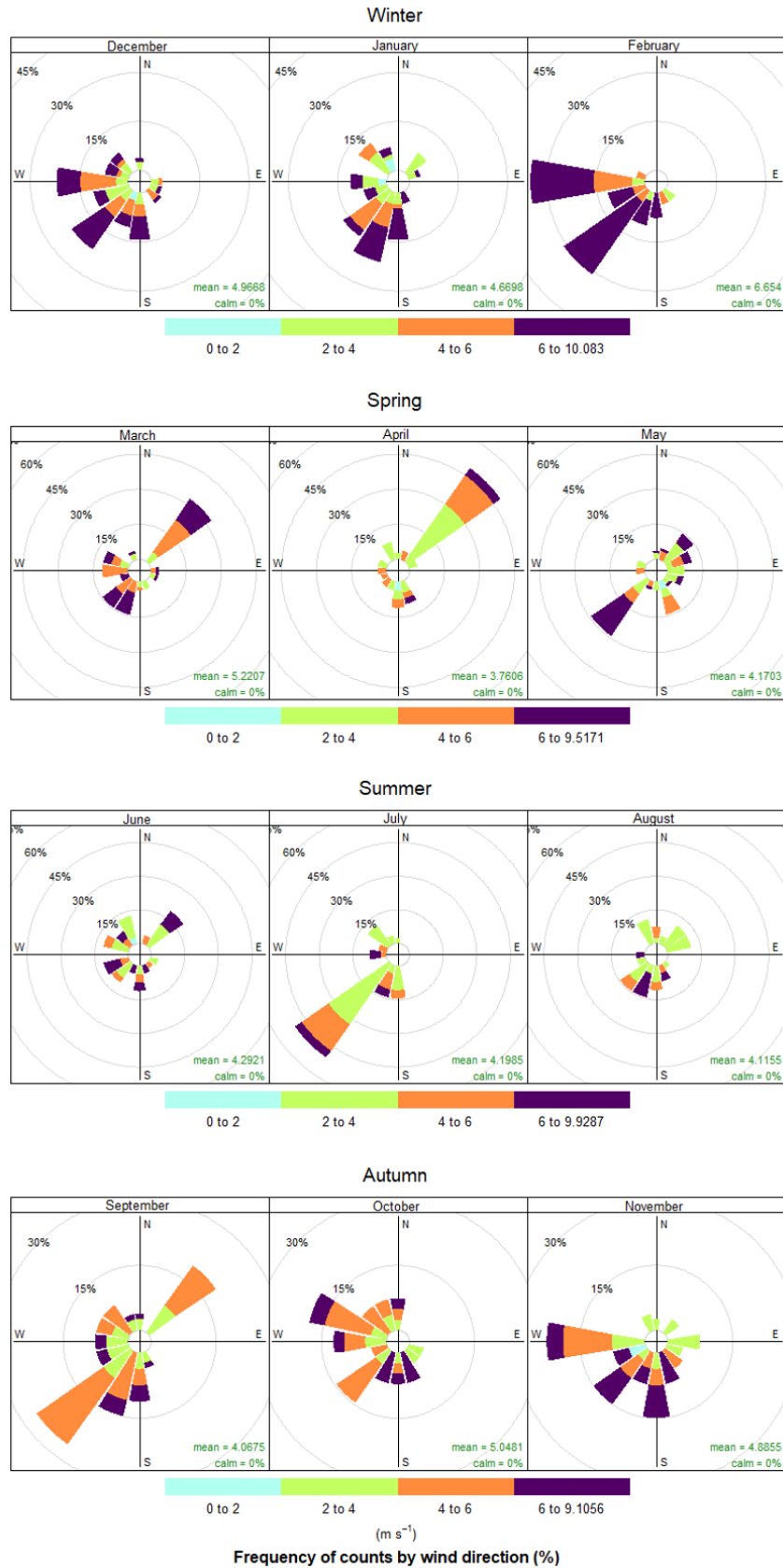


**Figure 5.4** Monthly wind rose plots for Enniscorthy during the measurement campaign (December 2019 - November 2020).

### 5.3.2 Particulate Matter

PM<sub>2.5</sub> and PM<sub>10</sub> mass concentration data was provided by the Environmental Protection Agency. The hourly concentrations varied with seasonality. Average concentrations were highest during winter (December 2019 – February 2020), while the lowest concentrations were recorded during the summer months (June – August 2020). This can be explained by the increased levels of solid fuel combustion, corresponding with lower ambient temperatures. A summary of the recorded mass concentrations is provided in Table 5.3.

Despite general adherence to EU legislation, a number of instances of exceedance of PM<sub>10</sub> 24-hour average concentration limits (50 µg m<sup>-3</sup>) were recorded in Enniscorthy between December 2019 and November 2020, as shown by the temporal profile in Figure 5.5. Maximum hourly concentrations of 350.3 µg m<sup>-3</sup> and 360.5 µg m<sup>-3</sup> were recorded for PM<sub>2.5</sub> and PM<sub>10</sub>, respectively, in January 2020. Annual average EU limits of both PM<sub>2.5</sub> (20 µg m<sup>-3</sup>) and PM<sub>10</sub> (40 µg m<sup>-3</sup>) were complied with over the twelve month sampling period. The stringent annual average guideline proposed by the WHO (at the time of sampling) of 20 µg m<sup>-3</sup> PM<sub>10</sub> was also adhered to, despite an exceedance of the recommended average level of PM<sub>2.5</sub> (10 µg m<sup>-3</sup>). The WHO guideline limits have subsequently been reduced further. As of 2021, the WHO recommends concentration limits of 15 µg m<sup>-3</sup> and 45 µg m<sup>-3</sup> for annual and 24-hour mean values of PM<sub>10</sub>, respectively. Stringent limits of 5 µg m<sup>-3</sup> and 15 µg m<sup>-3</sup> have been recommended for annual and 24-hour mean values for more damaging PM<sub>2.5</sub> particles

**Table 5.3** Summary of PM mass concentration recorded in Enniscorthy (December 2019 - November 2020).

	PM <sub>2.5</sub> (µg m <sup>-3</sup> )		PM <sub>10</sub> (µg m <sup>-3</sup> )	
	<i>Mean</i>	<i>Range</i>	<i>Mean</i>	<i>Range</i>
<i>Winter</i>	19.77	0.3 – 350.3	23.73	0.4 – 360.5
<i>Spring</i>	12.73	0.3 – 121.7	17.47	0.5 – 131.6
<i>Summer</i>	5.58	0.5 – 24.7	9.06	1.1 – 32.1
<i>Autumn</i>	13.14	0.3 – 209.0	17.35	0.8 – 217.7

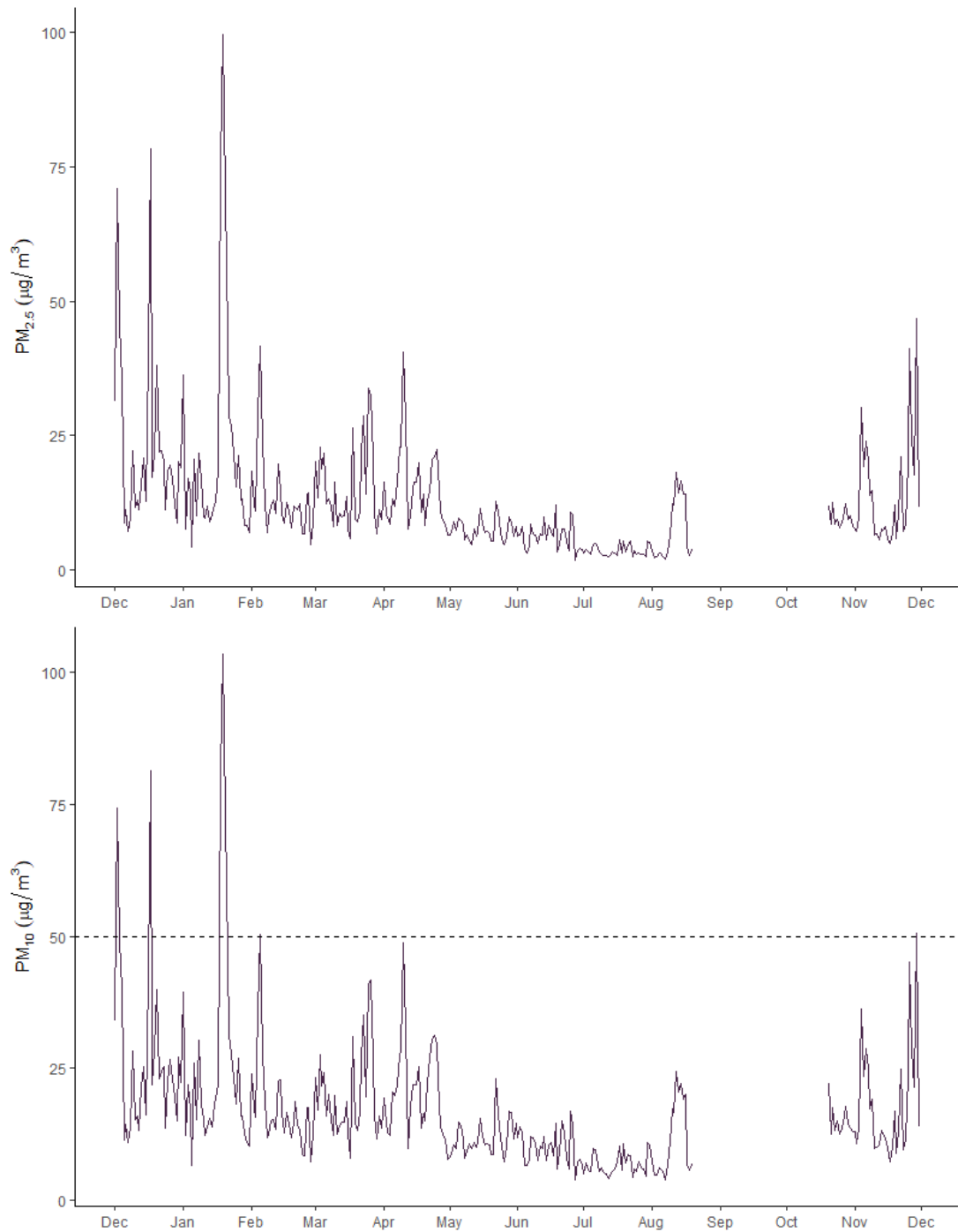


**Figure 5.5** Temporal profile of daily average  $PM_{2.5}$  and  $PM_{10}$  mass concentration measured in Enniscorthy (December 2019 - November 2020). The dashed line indicates the EU 24-hour average limit of  $50 \mu\text{g m}^{-3}$ .

Diurnal trends also varied with seasonality (Figure 5.6). A significant increase in  $PM_{2.5}$  concentrations was observed during the eveningtime in winter (December 2019 – February 2020). In general, mean concentrations peaked at 19:00. A number of outliers are illustrated by the boxplot showing the average diurnal profile. These outliers are

associated with periods when wind speeds were low, resulting in little pollution dispersion. However, the distance in location, between the monitoring site and the weather station, must be considered. The highest concentrations correspond with the time of day typical of domestic solid fuel burning. During the colder season, a temperature inversion is also likely at this time which can also lead to limited dispersion of emissions. Measured concentrations were significantly lower during the summer months and a more uniform diurnal profile was observed, with little variation throughout the day. This is indicative of a single dominant source, producing consistent concentrations of particulate matter throughout the day. Assuming traffic counts were similar in winter and summer, it was estimated that there was an increase of approximately 49% in morningtime  $PM_{2.5}$  concentrations in winter, most likely associated with lower temperatures. The emissions related to domestic heating were estimated by comparing the morningtime concentrations of  $PM_{2.5}$  with the significantly increased eveningtime levels. Assuming traffic volumes are comparable morning and evening, solid fuel combustion emissions account for an estimated 70% of the total mass concentration.

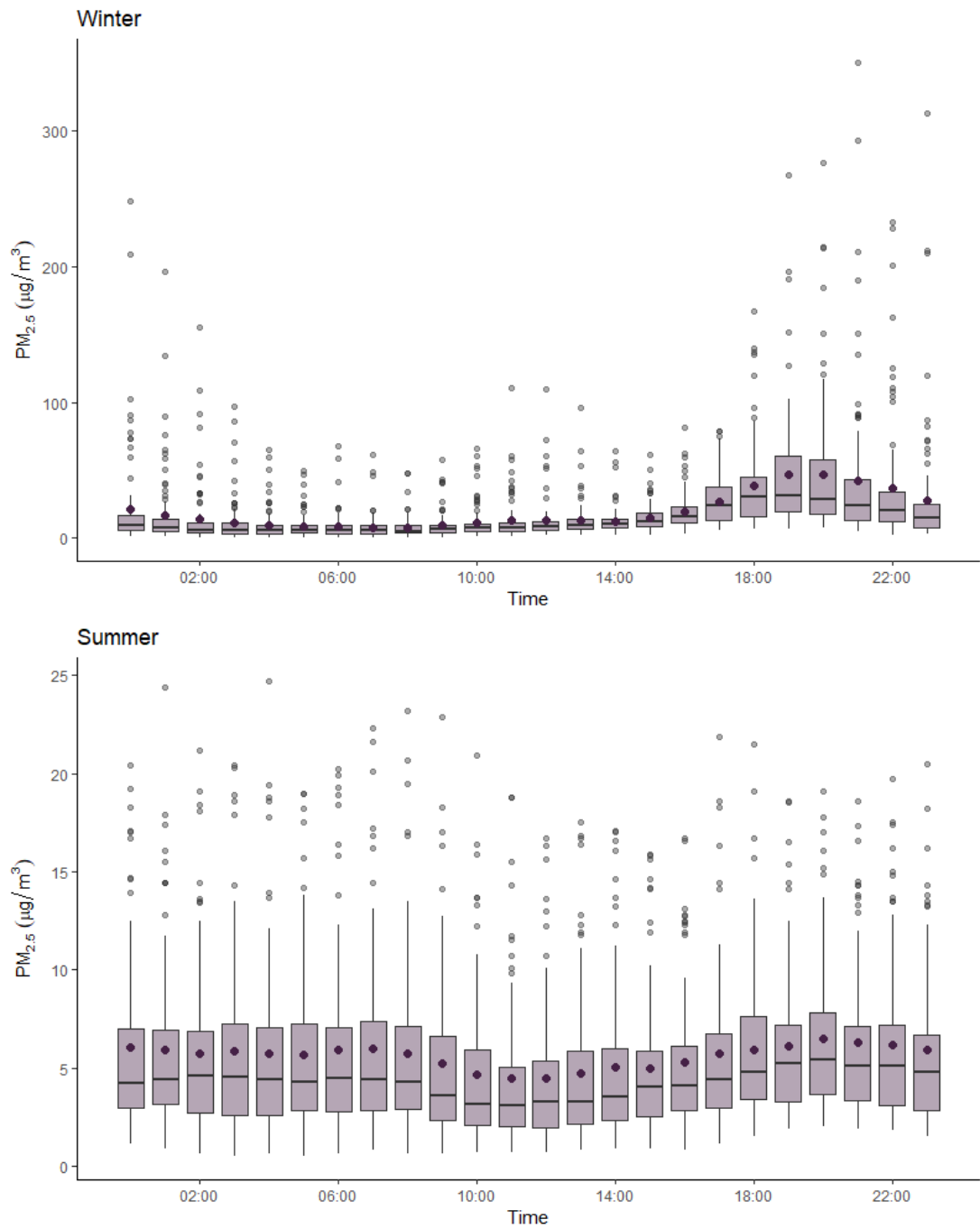


**Figure 5.6** Diurnal variation in mass concentration of PM<sub>2.5</sub> during winter (December 2019 - February 2020) and summer (June - August 2020) months in Enniscorthy.

### 5.3.3 Equivalent Black Carbon

The multi-wavelength aethalometer was employed in the assessment of black carbon concentration on a continuous basis between December 2019 and November 2020 in Enniscorthy. The data capture for the instrument over the duration of the sampling period was 98.5%. Absent data is due to instrument stoppages for the purposes of routine maintenance, such as filter tape changes and clean air tests.

A strong correlation ( $r^2 = 0.88$ ) was observed between the ambient eBC concentration and PM mass concentration at this monitoring site throughout the sampling period (Figure 5.7). Equivalent black carbon contributed a mean value of 8.5% to the total PM<sub>2.5</sub> mass concentration over the entire sampling period. This contribution fluctuated with seasonality. Equivalent black carbon accounted for 9.3%, 7.9%, 8.5% and 7.9% of PM<sub>2.5</sub> mass concentration during the winter, spring, summer and autumn seasons, respectively. It is interesting that the contribution of eBC to total mass concentration did not increase significantly during the winter months, when solid fuel burning was, presumably, at a maximum, comparative to the summer months. This observation suggests that other constituents of ambient particulate matter, including traffic-related emissions, must fluctuate correspondingly throughout the year.

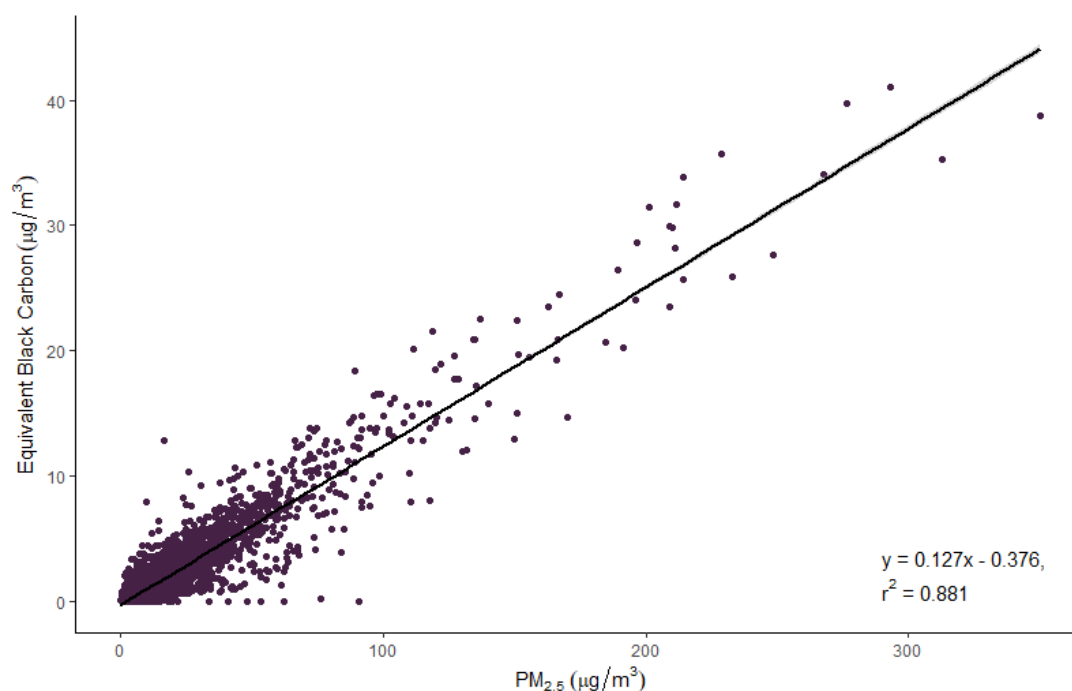


**Figure 5.7** Comparison of eBC and PM<sub>2.5</sub> mass concentration measured in Enniscorthy (December 2019 - November 2020).

### 5.3.3.1 Temporal Trends

The temporal profile of the measured equivalent black carbon is presented in Figure 5.8. The highest concentrations of eBC were measured during the colder, winter months. The concentration reduces dramatically in the summer months. A maximum hourly concentration of  $41.08 \mu\text{g m}^{-3}$  was recorded in December, 2019 at 21:00. This is higher than any hourly equivalent black carbon concentration recorded at the designated traffic site on Pearse Street in Dublin city centre the previous year (Chapter 4). In a rural location such as Enniscorthy, without access to a natural gas supply, the presence of eBC attributed to solid fuel combustion ( $\text{eBC}_{\text{SF}}$ ) is anticipated throughout the winter, regardless of daily ambient temperature. Therefore, a linear relationship between temperature and BC levels was not anticipated. However, there is a noticeable difference in the percentage contribution from solid fuel burning emissions when ambient temperatures are below 0 and above 9, decreasing from 87.4% to 61.0%, respectively. Ambient eBC concentrations declined substantially between June and August 2020, when a mean hourly average concentration of  $0.37 \mu\text{g m}^{-3}$  was recorded. During this period hourly average concentrations did not exceed  $3.5 \mu\text{g m}^{-3}$ . A summary of the hourly average measured equivalent black carbon is provided in Table 5.4.

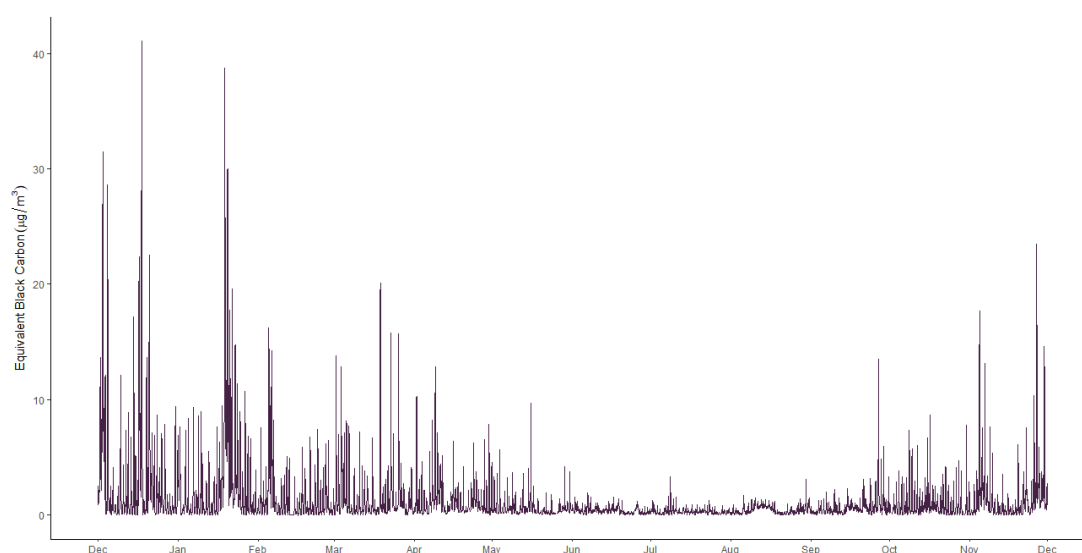


**Figure 5.8** Temporal profile of equivalent black carbon concentration (December 2019 - November 2020).

Wind speed had a distinct effect on ambient eBC concentration; in general, increased wind speeds resulted in decreased concentrations (Figure 5.9). Wind direction did not influence the measured concentrations to the same extent, as high concentrations of eBC originated in several directions relative to the sampling site in winter, spring and autumn, consistent with the surrounding residential areas. Wind direction appeared to impact the levels of eBC during the summer months. This was strongly influenced by one week of sustained high levels of eBC in August (09/08/2020 – 16/08/2020) when prevailing winds were northerly; however the overall low absolute concentrations must be considered. The distance between the sampling site and weather station must also be accounted for. Co-location of air quality sampling and meteorological data collection would have been preferable. The unique geography of the sampling site, situated in the valley of the River Slaney, may exaggerate ambient temperatures, but will have little, if any, effect, on the wind speed or direction.

**Table 5.4** Summary of hourly average eBC concentrations recorded in Enniscorthy between December 2019 and November 2020.

	Equivalent Black Carbon ( $\mu\text{g m}^{-3}$ )			eBC <sub>SF</sub>	eBC <sub>Tr</sub>
	<i>Mean ± SD</i>	<i>Minimum</i>	<i>Maximum</i>	%	%
<b>Dec 2019</b>	2.82 ± 4.82	0.02	41.08	74.16	25.84
<b>Jan 2020</b>	2.73 ± 4.78	0.01	38.75	69.95	30.05
<b>Feb 2020</b>	1.29 ± 2.10	0.00	16.23	70.42	29.58
<b>Mar 2020</b>	1.46 ± 2.33	0.01	20.08	69.50	30.50
<b>Apr 2020</b>	1.20 ± 1.48	0.01	12.87	60.25	39.75
<b>May 2020</b>	0.59 ± 0.76	0.04	9.69	48.29	51.71
<b>Jun 2020</b>	0.38 ± 0.28	0.01	1.90	38.38	61.62
<b>Jul 2020</b>	0.29 ± 0.24	0.00	3.32	35.40	64.60
<b>Aug 2020</b>	0.44 ± 0.35	0.00	3.12	32.70	67.30
<b>Sep 2020</b>	0.66 ± 1.00	0.01	13.50	43.65	56.35
<b>Oct 2020</b>	0.84 ± 1.09	0.01	8.66	61.90	38.10
<b>Nov 2020</b>	1.42 ± 2.43	0.00	23.48	71.30	28.70

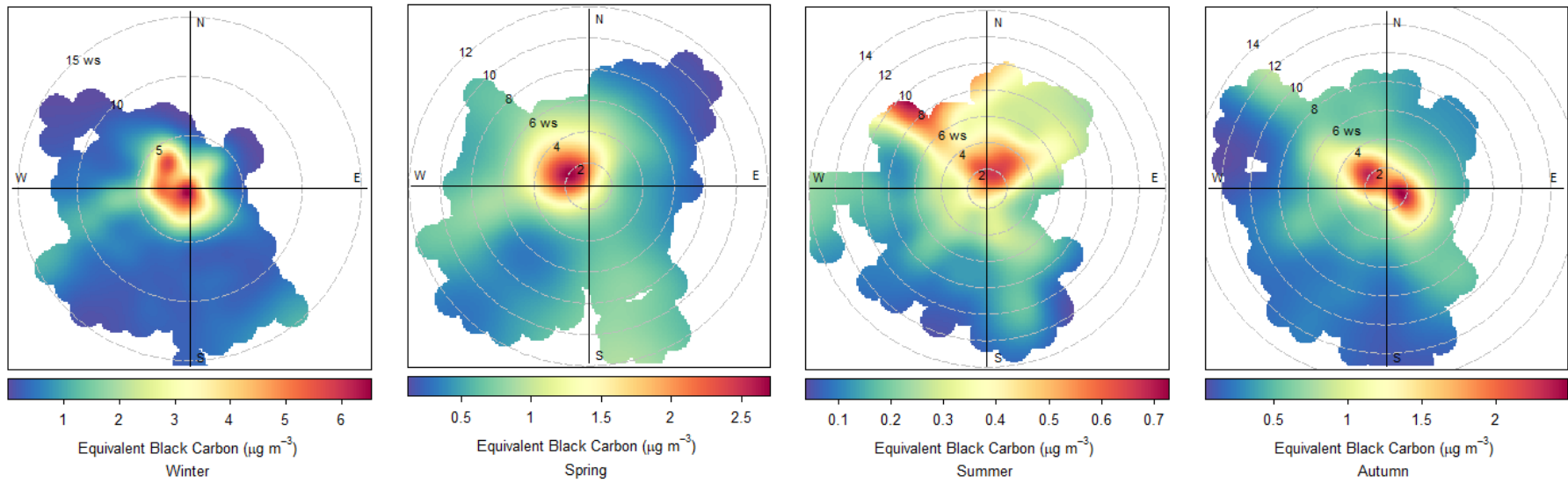


**Figure 5.9** Relationship between wind speed ( $m s^{-1}$ ), wind direction and eBC concentration measured in Enniscorthy (December 2019 – November 2020).

### 5.3.3.2 *Diurnal Trends*

---

Similar to PM mass concentrations, seasonality affected the diurnal pattern of measured eBC. As previously stated, the highest concentrations of eBC were recorded during the winter months. Concentrations decreased dramatically between June and August, before rising again in the autumn. The diurnal profile revealed a strong peak in the eveningtime during the winter, spring and autumn seasons. Concentrations began to rise sharply from approximately 15:00 onwards. Source apportionment analysis attributed this dramatic increase in ambient concentration exclusively to solid fuel combustion emissions (Figure 5.10), confirming the popularity of solid fuel as the preferred source of domestic heating during the colder months in this small town. Furthermore, it demonstrates the impact of solid fuel usage on the local air quality. When isolated, the diurnal profile of eBC<sub>Tr</sub> is reasonably constant throughout the year; seasonal variability had scarcely any impact. This implies that the poor air quality experienced by the town is caused almost exclusively by solid fuel combustion and could be drastically improved by implementing measures to curtail usage.

There is little diurnal variation during the summer months as concentrations of eBC are constant throughout the day. Despite a small contribution from UV absorbing species, the majority of the eBC is attributed to traffic-related emissions in June, July and August 2020.

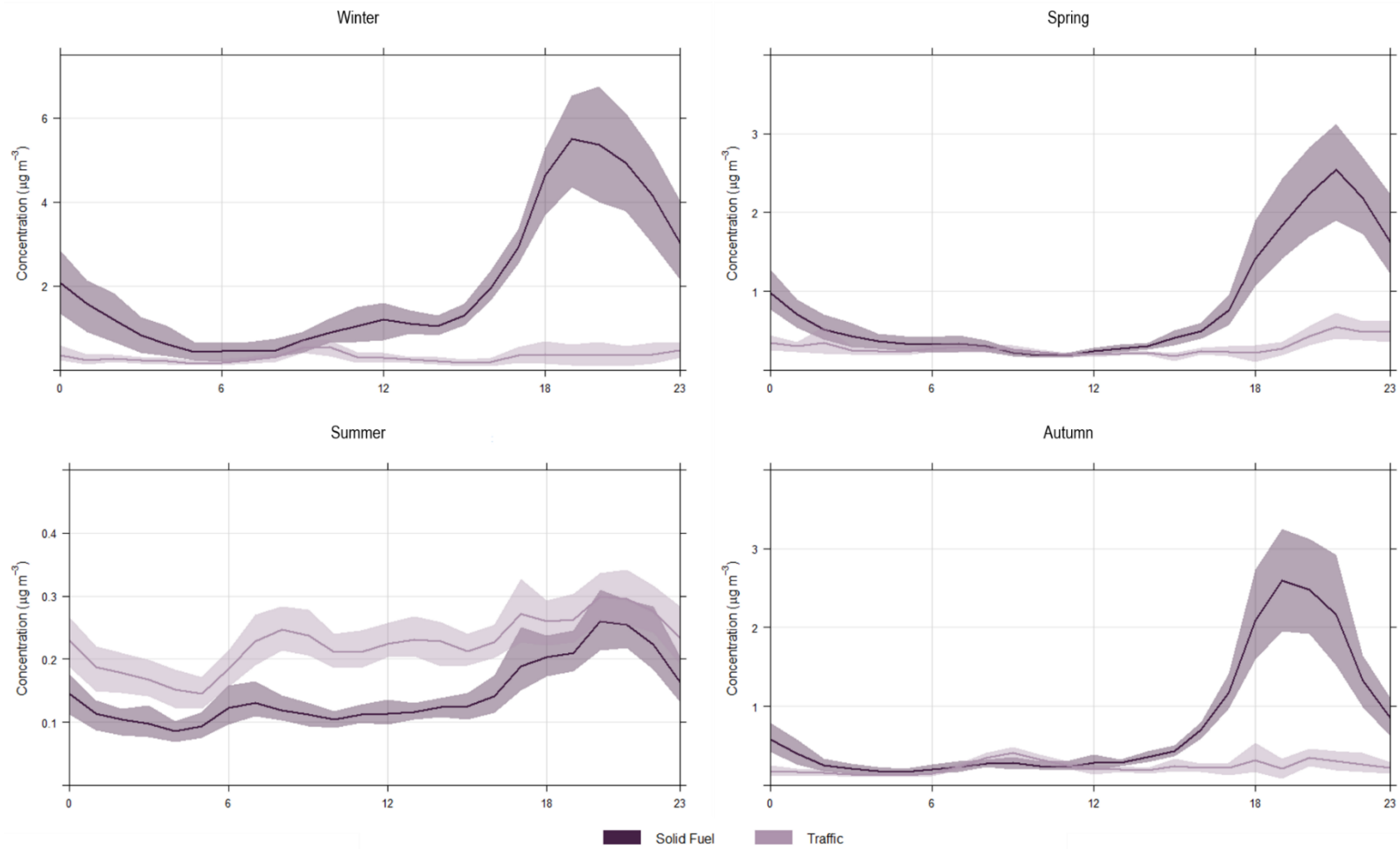


**Figure 5.10** Seasonal diurnal profiles of eBC attributed to solid fuel burning and traffic-related emissions in Enniscorthy (December 2019 – November 2020).

### 5.3.3.3 Source Contribution

---

As previously stated, the aethalometer model was applied, using AAE values of 1.68 and 0.9, to attribute eBC to solid fuel burning and traffic-related emissions, respectively. The contribution of solid fuel emissions varied with average ambient temperature, as illustrated by Figure 5.11. Accordingly, contributions from solid fuel combustion related emissions were at a maximum during the winter months (71.6%) when domestic solid fuel burning was most prevalent. This is consistent with the estimated contribution of solid fuel combustion emissions to total PM<sub>2.5</sub> mass concentration (70.4%). Contributions from traffic-related emissions were highest in June, July and August 2020; mean monthly percentage contributions were 61.6%, 64.6% and 67.3%, respectively, corresponding to a period when the absolute concentration of eBC was considerably reduced. However, it is interesting that eBC<sub>SF</sub> was not entirely eliminated at any stage throughout the year, and continued to impact the ambient conditions, albeit to a lesser extent, during the summer.

AAE ~1 is indicative of an environment dominated by fossil fuel combustion, such as designated traffic sites. The high frequency of AAE tending towards ~2 was suggestive of the presence of biomass or solid fuel combustion. The frequency distribution of AAE measured in Enniscorthy, shown in Figure 5.12, was well defined between 1 and 2, and the low kurtosis demonstrated indicates the absence of outlier data points. Percentage source contribution observations were consistent with the recorded AAE which was shifted towards higher values, indicative of a solid fuel dominated environment during the winter months ( $\bar{x} = 1.47$ ). The atmosphere was dominated by solid fuel combustion emissions to a lesser extent in the spring ( $\bar{x} = 1.39$ ) and autumn ( $\bar{x} = 1.38$ ), when ambient temperatures increased slightly, confirmed by comparable contributions from solid fuel related emissions during corresponding seasons, 59.3% and 58.9%, respectively, according to the aethalometer model output. Interestingly, both spring and autumn appeared to exhibit tri-modal distribution, suggestive of multiple sources contributing to increased absorption at lower wavelengths. If this was caused by multiple fuel types, it is interesting that a similar distribution was not observed during the winter, when solid fuel combustion is most prevalent. It is possible that the unique distribution is linked with biogenic sources or enhanced photochemical-induced oxidative processes associated with seasonal variability. Similar distribution during spring and autumn was also indicative of the dynamic

situation between summer and winter, when dominant sources influencing ambient aerosol alter.

The lowest mean AAE (1.23) and the lowest contribution attributed to solid fuel related emissions was recorded during the summer months. Similar to the mean percentage source contribution determined by the aethalometer, the average AAE suggested a minor influence from solid fuel burning emissions on the ambient atmosphere during this period. Although it was the lowest average value recorded at this sampling site, the AAE is higher than those measured at typical ‘traffic sites’. However, accounting for the significantly reduced absolute concentration, the sharp distribution indicates one dominant source of eBC.

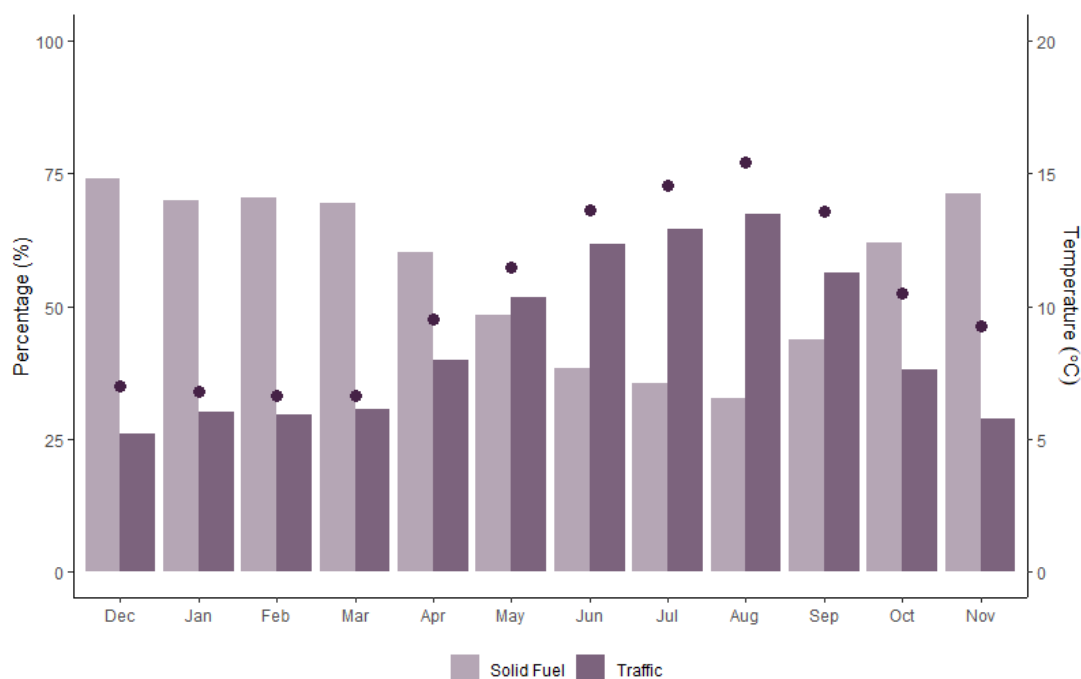


**Figure 5.11** Percentage contribution of solid fuel burning and traffic-related emissions (bar) and corresponding hourly average mean monthly temperature (point) (December 2019 - November 2020).

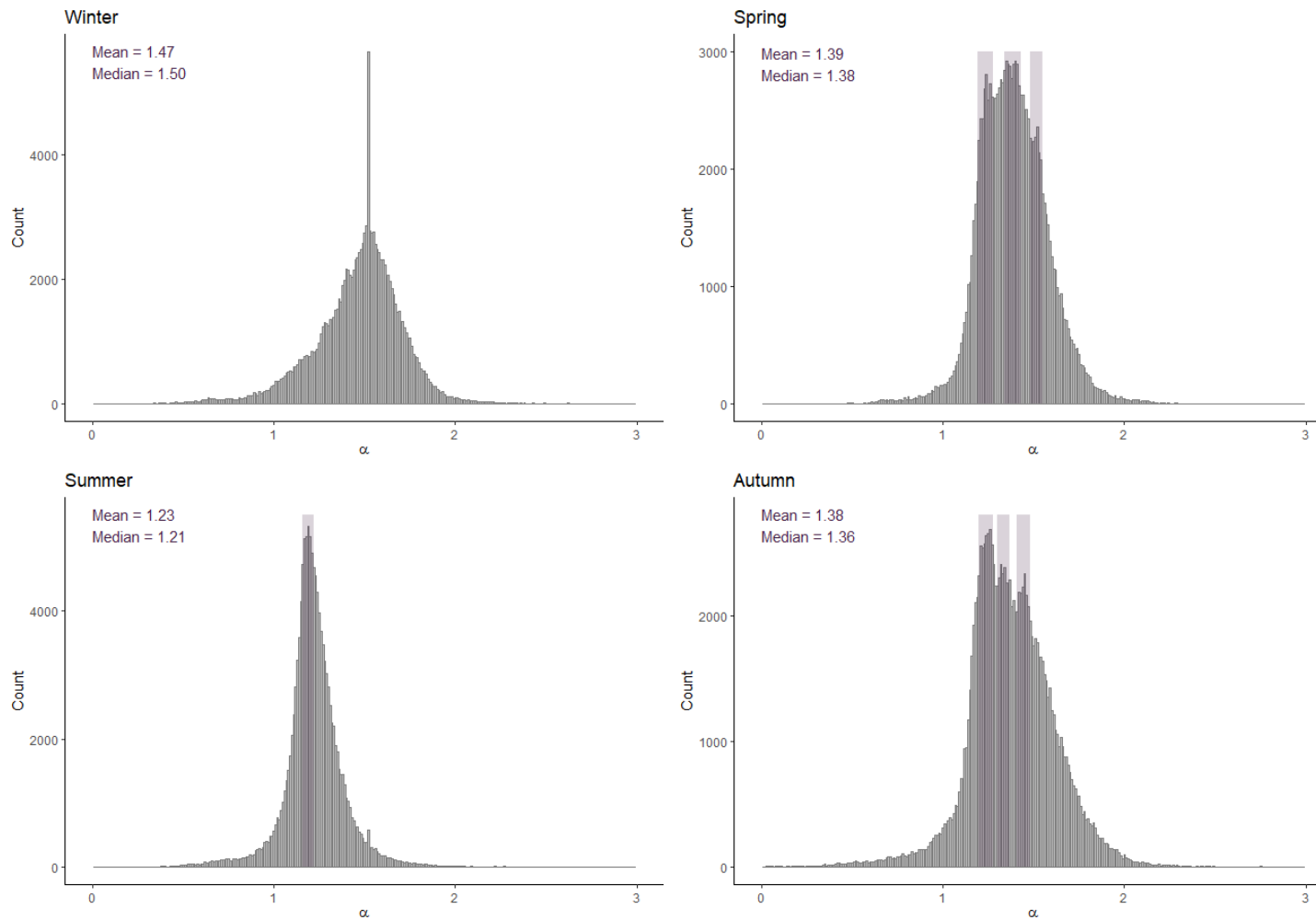


**Figure 5.12** Frequency distribution of AAE measured each season by the multi-wavelength aethalometer throughout the sampling period (December 2019 – November 2020).

The tri-modal distribution of AAE observed during spring and autumn was noteworthy and demonstrates the complex environment of Enniscorthy. The mean and median values were similar during both seasons, and the peaks appeared at similar AAE values (Figure 5.12). If this unique frequency distribution was caused solely by the variety of solid fuel types used for domestic heating, a similar distribution would be expected during the winter, when solid fuel combustion was prevalent. This, however, was not the case.

The observed peaks were isolated and the diurnal patterns of the identified AAE were investigated (Figure 5.13). Similar diurnal profiles were obtained in both Spring and Autumn. Low AAE values ( $1.19 \leq \alpha \leq 1.28$ ) were dominant in the morningtimes, possibly associated with traffic-related emissions, while higher AAE values ( $1.41 \leq \alpha \leq 1.55$ ) prevailed in the afternoon and eveningtime, corresponding with increased solid fuel burning. Secondary organic aerosol (SOA) formation from biogenic precursors is often enhanced by substantial levels of several anthropogenic pollutants, such as  $\text{NO}_x$ ,  $\text{SO}_2$  and  $\text{O}_3$ , in residential and urban areas (Minguillón et al., 2016). Anthropogenically-driven SOA formation, of biogenic origin, may subsequently amplify the observations made in spring and autumn. The diurnal profiles were also consistent with observations made by Lee et al. (2017) who noted the relationship between primary organic aerosol constituents and black carbon associated with traffic emissions during morning rush hour, while considerable formation of secondary organic aerosol (SOA) coatings on black carbon particles due to photochemistry was prevalent in the afternoon.

There did not appear to be an association between the periods in which the isolated AAE values were observed and the corresponding wind direction (Figure 5.14). However, the absence of a tri-modal distribution in winter may be explained by wind speeds. The highest wind speeds were recorded during the winter months, with a mean hourly wind speed of  $5.4 \text{ m s}^{-1}$ , reaching a maximum of  $15.4 \text{ m s}^{-1}$ . The high wind speeds potentially removed fresh emissions and, in addition to long range transportation, carried air masses containing aged particles to the environment. Such air masses, combined with black carbon particles attributed to solid fuel combustion, ubiquitous in the ambient aerosol in wintertime, may have obscured any interesting distribution frequency unique to this locality. If so, it is possible that the distribution frequency observed in spring and autumn is a true reflection of the fresh emissions

dominating the local ambient aerosol; the lower wind speeds recorded may have resulted in less pollution dispersion. Detailed chemical composition analysis, including a complete characterisation of organic and secondary organic aerosol, is required for further explanation.

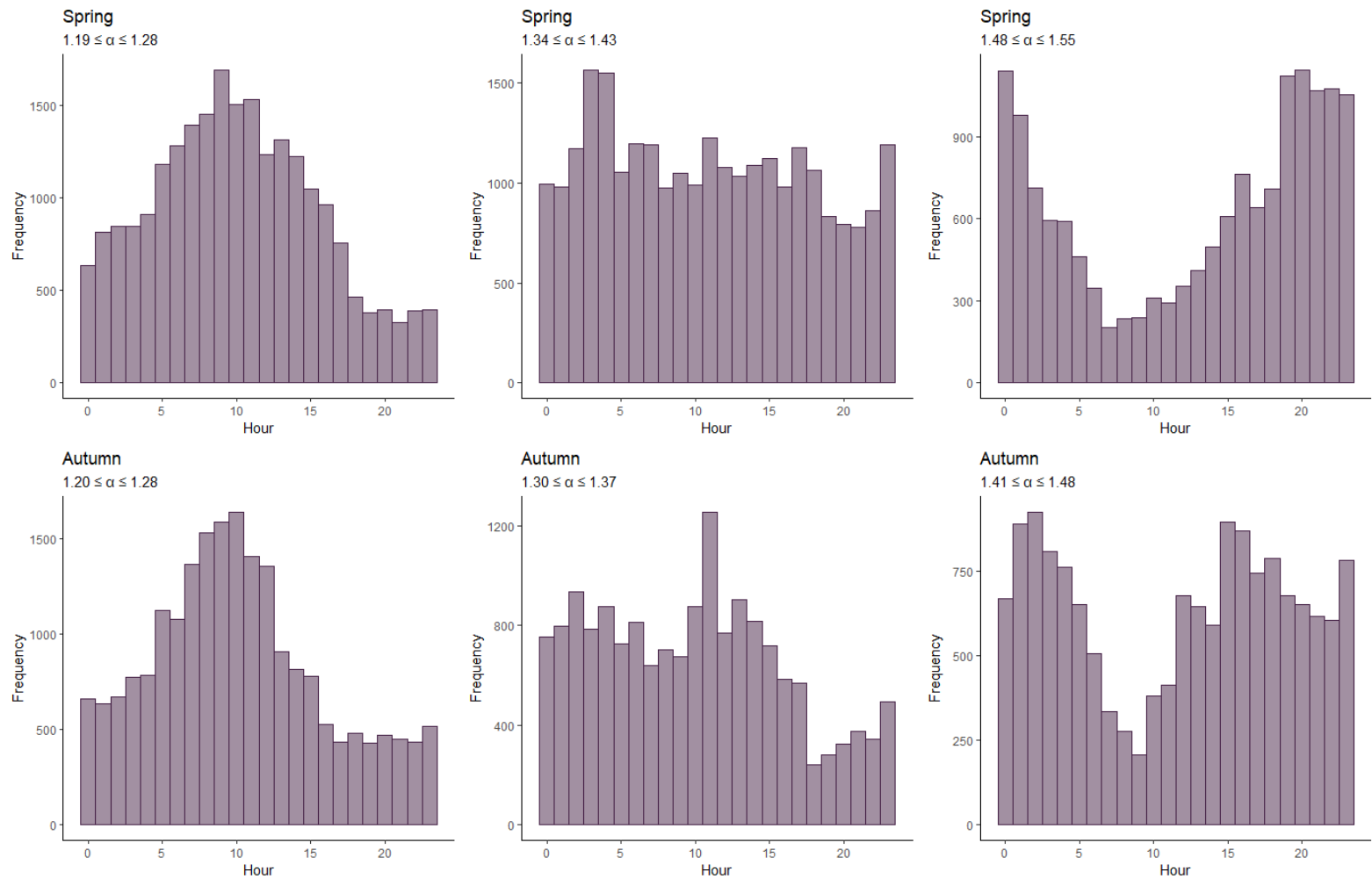


**Figure 5.13** Diurnal profile of isolated AAE contributing to overall tri-modal distribution observed during the spring (March – May 2020) and autumn (September – November 2020) seasons.

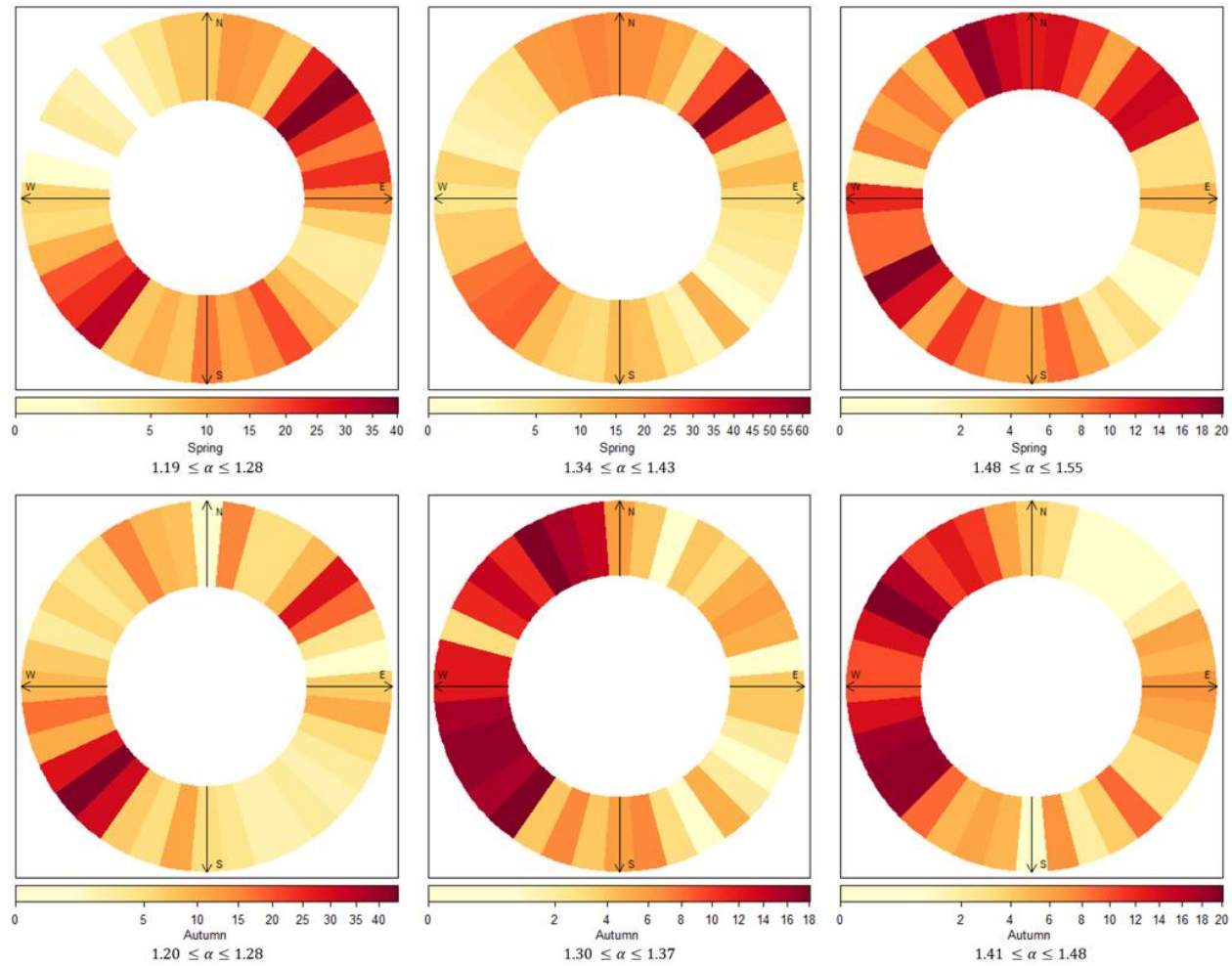


**Figure 5.14** Polar frequency plots illustrating frequency of tri-modal peaks of AAE and dependence on wind direction throughout spring (March - May 2020) and autumn (September - November 2020).

Figure 5.15 shows the linear relationship between hourly average measurements of sulfur dioxide (SO<sub>2</sub>) and eBC and PM<sub>2.5</sub> in January and February 2020. Both SO<sub>2</sub> and eBC are considered primary emissions and are associated with combustion. A good correlation was observed between the two parameters ( $r^2 = 0.62$ ). The correlation was improved significantly ( $r^2 = 0.77$ ) when both parameters were averaged over corresponding 24-hour periods. A correlation could not be established between the parameters during the summer months. However, extremely low concentrations of both species were observed during this time. Mean concentrations of 3.58  $\mu\text{g m}^{-3}$  and 0.37  $\mu\text{g m}^{-3}$  were recorded for SO<sub>2</sub> and equivalent black carbon, respectively (June – August 2020). Similar correlation was observed between SO<sub>2</sub> and PM<sub>2.5</sub> measured during the winter period ( $r^2 = 0.63$ ), despite significantly higher concentrations of PM<sub>2.5</sub>.

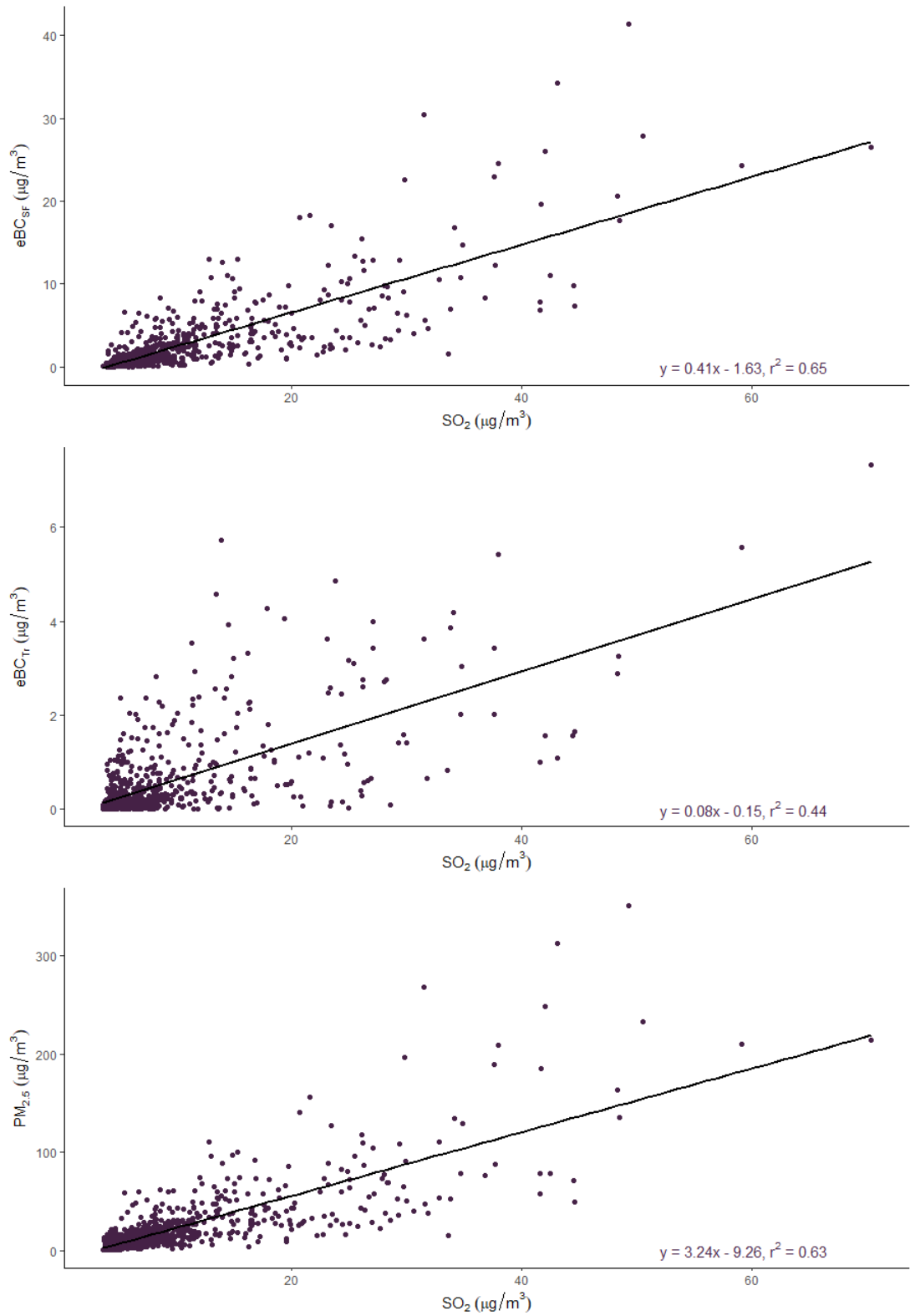


**Figure 5.15** Linear relationship of hourly average  $e\text{BC}_{\text{SF}}$  (top),  $e\text{BC}_{\text{Tr}}$  (middle) and  $\text{PM}_{2.5}$  (bottom) with corresponding  $\text{SO}_2$  concentration measured in Enniscorthy (January – February 2020).

#### 5.3.4 Elemental Carbon (EC) and Organic Carbon (OC)

---

Filter samples were collected using a high volume air sampler (DHA-80, DIGITEL Elektronik GmbH) throughout February 2020. The filter samples were collected at eight-hour time intervals, starting at 07:00 (morning), 15:00 (evening) and 23:00 (night), respectively. A total of 59 samples and 3 field blanks were collected. Following sample collection, the ambient concentration of elemental, organic and total carbon was measured by the thermal-optical analysis of filters, as outlined in Chapter 2. The samples collected were representative of typical wintertime conditions in the town of Enniscorthy.

The total carbon concentration measured on the field blanks had a mean value of  $0.27 \mu\text{g m}^{-3}$  and did not exceed  $0.40 \mu\text{g m}^{-3}$ . In the ambient samples collected, the total carbon content ranged between  $0.40 \mu\text{g m}^{-3}$  and  $35.26 \mu\text{g m}^{-3}$ . Mean total carbon concentrations of  $3.30 \mu\text{g m}^{-3}$ ,  $11.63 \mu\text{g m}^{-3}$  and  $3.05 \mu\text{g m}^{-3}$  were determined for the various sampling periods; morning, evening and nighttime, respectively. Total carbon concentrations were at a maximum in the evening (15:00 - 23:00), corresponding with the time of day when solid fuel burning for domestic heating was most prevalent. The mean concentration of ambient total carbon measured during morning and nighttime was comparable. Total carbon accounted for, on average, 34.5% of  $\text{PM}_{2.5}$  measured concurrently at the sampling site. Hourly  $\text{PM}_{2.5}$  measurements were averaged to match the corresponding filter sampling period. Excellent correlation between the two parameters was observed ( $r^2 > 0.94$ ).

The thermal-optical protocol (EUSAAR\_2) employed in the analysis of filter samples allowed for the determination of elemental (EC) and organic (OC) carbon content. Concentrations of EC and OC measured in Enniscorthy in February 2020 ranged between  $0.04 \mu\text{g m}^{-3}$  and  $7.57 \mu\text{g m}^{-3}$  ( $\bar{x} = 1.19 \mu\text{g m}^{-3}$ ), and  $0.40 \mu\text{g m}^{-3}$  and  $27.69 \mu\text{g m}^{-3}$  ( $\bar{x} = 4.95 \mu\text{g m}^{-3}$ ), respectively. Organic carbon accounted for the majority of the total carbon present in each sample, approximately 82.9%. The contribution of OC to the total carbon content was consistent throughout the day; morning (80.96%), evening (81.18%) and nighttime (86.77%), however absolute concentrations increased significantly in samples collected between 15:00 and 23:00 (Figure 5.16). During this time period, the mean concentration of OC was  $9.41 \mu\text{g m}^{-3}$ . Large concentrations of organic carbon were indicative of the strong influence of solid fuel burning in the

locality at this time of day. Shorter time intervals in filter collection would provide a clearer diurnal profile.

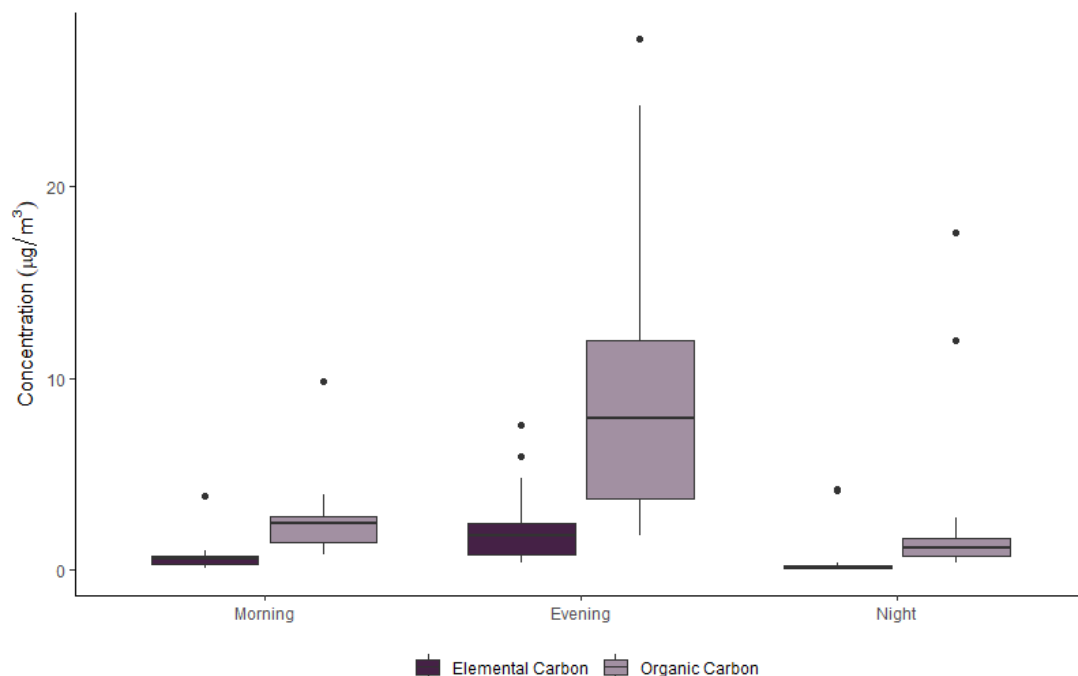


**Figure 5.16** Mean concentration of elemental and organic carbon measured during the morning, evening and night in Enniscorthy (February 2020).

Figure 5.17 illustrates the dominance of OC contribution to total carbon content throughout each sampling interval. Contributions from EC were at a minimum at nighttime, between 23:00 and 07:00, corresponding with periods when traffic counts in the locality were also at a minimum. Traffic count data were obtained from the Transport Infrastructure Ireland website (TII, 2021). The OC/EC ratio was also investigated. This ratio is often used to identify the dominant sources; solid fuel burning or traffic-related emissions, contributing to ambient carbonaceous aerosol. A mean OC/EC ratio of 5.31 was determined for Enniscorthy, ranging between 2.54 and 12.43. The ratio was lowest in the evening samples (15:00 – 23:00) when there were greater volumes of traffic present ( $\bar{x} = 4.36$ ). This increased to a mean value of 7.10 in samples collected at night. This is most likely explained by the significant reduction in traffic, in addition to the occurrence of aging processes throughout the night of the particles emitted during the combustion of solid fuels in the eveningtime. The OC/EC ratio is highest in samples with a high percentage contribution from organic carbon to

total carbon mass concentration; indicative of the strong influence of solid fuel, most likely wood and peat, combustion. In a study presented by Ni et al. (2018) OC/EC ratios of 5 and 2.38 were proposed as indicators of environments dominated by biomass and coal combustion, respectively. The ratios determined at this location are indicative of an environment strongly influenced by biomass burning emissions.

The relationship between organic carbon, elemental carbon and the source apportioned equivalent black carbon,  $eBC_{SF}$  and  $eBC_{Tr}$ , was examined. Poor correlation was observed between  $eBC_{Tr}$  and both organic and elemental carbon ( $r^2 < 0.4$ ), while the correlation between  $eBC_{SF}$  and organic and elemental carbon was much stronger;  $r^2$  values of 0.76 and 0.79, respectively, were obtained. The  $eBC$  data was averaged over an 8-hour period to correspond with the filter sample collection periods. Assuming correct apportionment of the equivalent black carbon, the strong correlation between  $eBC_{SF}$  and organic carbon was anticipated, particularly in an environment dominated by solid fuel combustion emissions. The strong correlation between  $eBC_{SF}$  and elemental carbon, comparable to that between  $eBC_{SF}$  and organic carbon, is interesting. It is possible that it is due to the use of coal, despite the OC/EC ratio suggestive of strong influences from biomass burning. It is also possible that volatile organic compounds associated with vehicular emissions contributed SOA formation and led to the artificial enhancement of  $eBC_{SF}$  concentration.



#### 5.3.4.1 Calculation of Mass Absorption Cross Section

---

Despite differing sampling periods and measurement techniques, a strong correlation was observed between optically-derived equivalent black carbon and thermally-derived elemental carbon ( $r^2=0.95$ ). In order to compare the measurements, equivalent black carbon, measured by the aethalometer, was averaged over the corresponding eight-hour sampling period used for quartz fibre filter sample collection.

The regression of the average absorption coefficient ( $b_{abs}$ ) from the aethalometer and the elemental carbon present on filter samples was investigated to determine a site-specific mass absorption cross section (MAC) value. The aethalometer employed default MAC values for each wavelength channel, as discussed in Chapter 2. The calculation of the site-specific MAC value allows for assessment of the appropriateness of the default MAC values in this environment. Figure 5.18 focuses on measurements at wavelengths of 660 nm and 880 nm, at which default MAC values of  $10.35 \text{ m}^2 \text{ g}^{-1}$  and  $7.77 \text{ m}^2 \text{ g}^{-1}$ , respectively, were applied in the aethalometer software. The slope of the regression line was indicative of the estimated average MAC value for this site;  $14.36 \text{ m}^2 \text{ g}^{-1}$  and  $9.48 \text{ m}^2 \text{ g}^{-1}$  at 660 nm and 880 nm, respectively. Both are marginally greater than default values. It is worth noting that the calculated site-specific MAC value is representative of wintertime only at this location, as filter samples were only collected during the month of February. The determined value can be affected by seasonality, primarily due to the variation in dominant sources throughout the year.

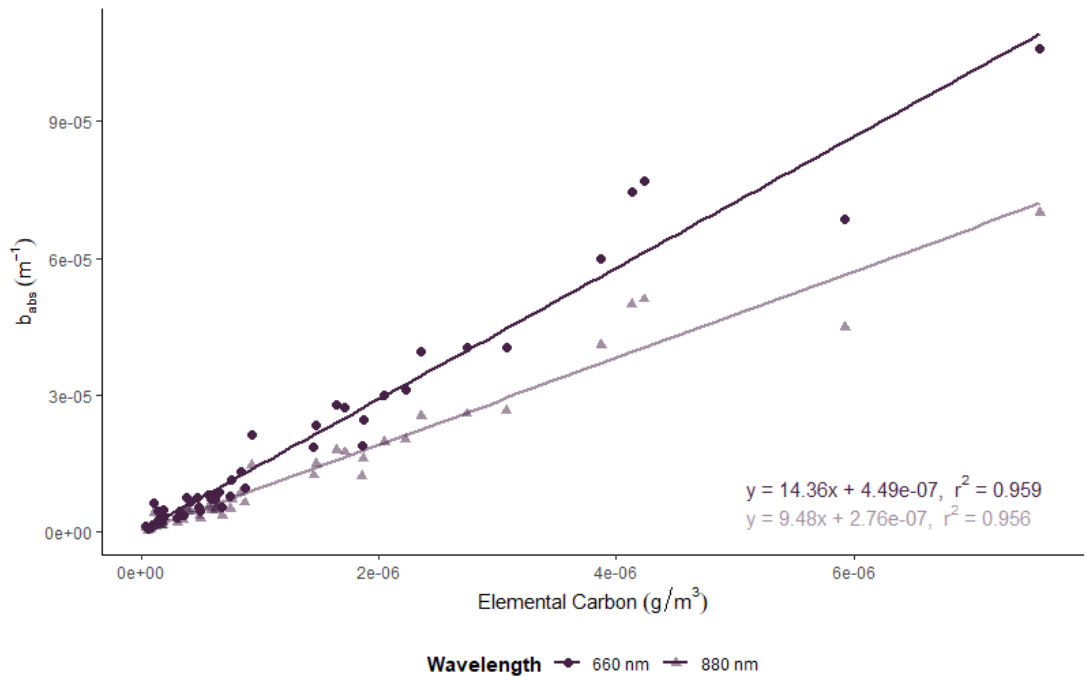


**Figure 5.18** Calculation of site-specific mass absorption cross section values at 660 nm and 880 nm in Enniscorthy. Samples used in the analysis were collected during February 2020.

#### 5.3.4.2 *Fractions of EC and OC*

---

To ensure consistent assessment of air quality across Europe, EU member states must employ standardised measurement techniques and procedures. The EUSAAR\_2 thermal-optical transmittance protocol is the current, recommended protocol for the measurement of elemental and organic carbon content collected on quartz fibre filters (European Committee for Standardization, 2017). This eight-step temperature protocol measures the optical properties of the sample throughout the analysis and incorporates a laser beam as a correction technique for pyrolysed carbon (PC). Pyrolytic carbon is formed when thermally unstable organic carbon (OC) chars under an inert atmosphere (He mode) and usually desorbs off the filter under an oxidising atmosphere (He/O<sub>2</sub> mode), similar to true elemental carbon (EC). Failing to correct for PC results in an underestimation of OC and an associated overestimation of EC (Cavalli et al., 2010). A further advantage of the conventional thermal-optical method of elemental and organic carbon determination is the evolution of carbon content at increasing temperatures under an inert and an oxidising environment, providing information about aerosol composition based on relative volatilities. This information can be indicative of the dominant sources contributing to the ambient aerosol and how fresh or aged the collected sample is.

The elemental and organic fractions correspond to the temperature protocol. A summary of the contributions of elemental and organic carbon fractions to total mass concentration is provided in Table 5.5. Organic carbon contributed approximately 28.5% of the total PM<sub>2.5</sub> concentration. In general, OC fractions, organic compounds that desorb in an inert environment, contribute more to ambient mass concentration than EC fractions. A temporal profile of the EC and OC fractions is visually represented by Figure 5.19.

**Table 5.5** Summary of contributions of elemental and organic carbon fractions to corresponding  $PM_{2.5}$  concentrations recorded in Enniscorthy (February 2020).

	Percentage Contribution (%)		
	<i>Mean</i>	<i>Minimum</i>	<i>Maximum</i>
<i>OC/PM<sub>2.5</sub></i>	28.48	5.87	52.01
<i>EC/PM<sub>2.5</sub></i>	6.37	0.60	16.53
<i>TC/PM<sub>2.5</sub></i>	34.85	6.47	68.54
<i>OC1/PM<sub>2.5</sub></i>	6.46	1.05	13.29
<i>OC2/PM<sub>2.5</sub></i>	7.69	1.51	15.65
<i>OC3/PM<sub>2.5</sub></i>	5.29	1.46	10.02
<i>OC4/PM<sub>2.5</sub></i>	4.02	1.22	8.27
<i>PC/PM<sub>2.5</sub></i>	5.00	-0.59	11.63
<i>EC1/PM<sub>2.5</sub></i>	2.16	-0.86	5.88
<i>EC2/PM<sub>2.5</sub></i>	4.01	0.20	11.65
<i>EC3/PM<sub>2.5</sub></i>	3.75	0.35	11.48
<i>EC4/PM<sub>2.5</sub></i>	1.46	0.19	5.56

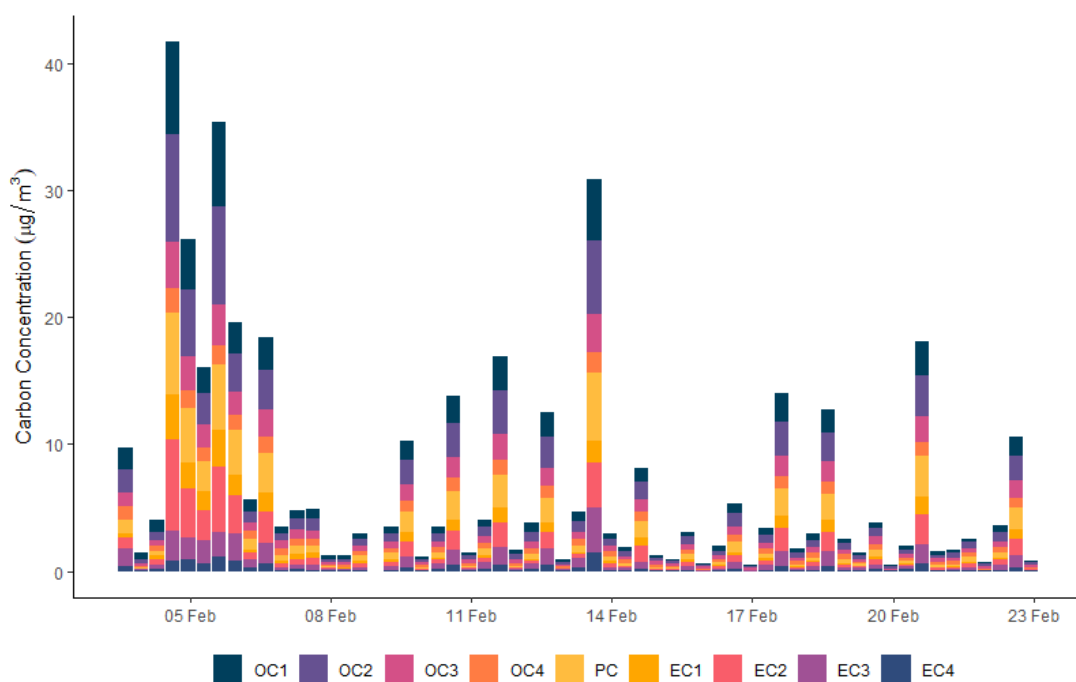


**Figure 5.19** Temporal profile of elemental and organic carbon fractions contained in samples collected in Enniscorthy (February 2020).

Because the analysis provided four different OC fractions and four different EC fractions, it is of interest to investigate whether the different fractions were associated with different temporal trends in a consistent way, i.e. it is useful to perform a form of factor analysis on the data matrix to examine whether common trends emerge for some species, or groups of species. To this aim, the OC/EC data was further analysed using the Positive Matrix Factorization (PMF) multi-variate factor analysis tool (Version 5.0.14), developed by the US EPA (Norris et al., 2014) based on the multi-linear engine developed by Paatero (1999).

Conceivably, it is a possibility to merge the data with other measured parameters, such as levoglucosan and gas-phase species like  $\text{NO}_x$  and  $\text{SO}_2$ , averaged to match the filter collection periods, but one major limitation of the dataset is the small number of samples, so including additional parameters would result in an unacceptably low sample to variable ratio for meaningful PMF analysis. Because of the low number of samples, it is not appropriate to carry out this analysis with a view to generating source contribution estimates, but the factors resulting can nevertheless potentially inform further discussion on the nature and character of the carbonaceous aerosol in the locality in terms of i) how many major sources appear to influence the aerosol levels?

and ii) what are their apparent temporal cycles? Results from the PMF analysis are presented in Figure 5.20. Factor analysis can provide several possible solutions. The optimal solution, best representing the real conditions, should be supported by quantitative indicators, including the evaluation of the Q-value; ‘a goodness of fit parameter’ (Belis et al., 2014 and references therein). It is important to monitor changes in the Q-value as additional factors are calculated. Once the appropriate number of factors are included in the fit, there will be no further improvements in the Q-value, indicating that the optimal solution has been determined. A solution with too few or too many factors may result in the combination or over-splitting, respectively, of important factors contributing to the sample. It is also important to bear in mind that the original number of variables is only nine, and the aim of PMF is to achieve a meaningful dimension reduction and extract plausible source profiles. Therefore a useful solution should contain more than two but less than nine factors. In this study, several solutions involving 3 to 5 factors were generated. Ultimately a three-factor solution was selected, and this solution potentially involves a split traffic factor, but the US EPA tool does not allow less than three factors to be extracted. Factor 1 appears to be dominated by organic carbon. Factor 2 has contributions from organic carbon, and the least volatile fractions of elemental carbon; EC3 and EC4. In contrast, elemental carbon compounds, particularly EC1 and EC2, dominate Factor 3, despite a similar temporal trend to Factor 1. Presumably Factor 3 is closely associated with traffic-related emissions and the combustion of fossil fuels. All three factors show peaks in the eveningtime, between 15:00 and 23:00. Conclusions regarding temporal trends of the factors are limited by low time resolution of filter sample collection. But the analysis does suggest that the sources influencing the character of the carbonaceous aerosol and the temporal trends of same, are limited to a very small number of categories, in line with the divide between fossil fuel and biomass sources.

High time resolution filter sample collection throughout the year would provide a comprehensive dataset, accounting for temporal and seasonal variability. Incorporation of detailed chemical composition data, and concurrent measurements of unique markers or specific compounds, as well as gas-phase species like  $\text{NO}_x$  and  $\text{SO}_2$ , could vastly improve the information value of the PMF output. Such a technique may also allow for discrimination between aged and fresh particles, providing further insights into the influence of local and regional sources.

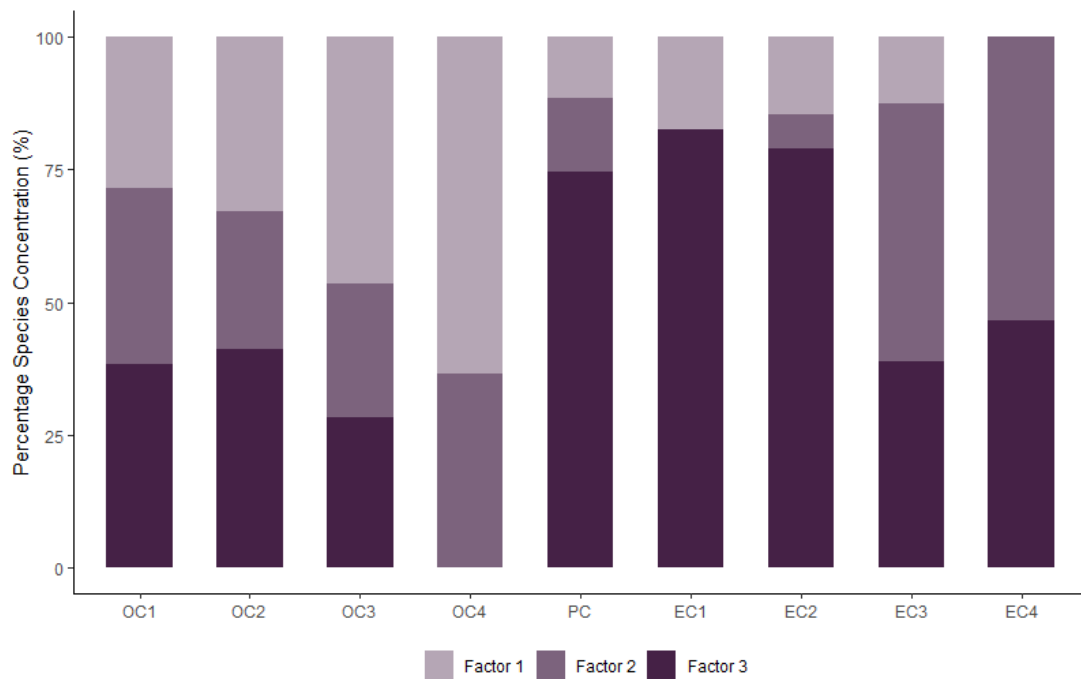


**Figure 5.20** Factor fingerprint of elemental and organic carbon fraction measurements from Enniscorthy (February 2020), as provided by PMF analysis.

### 5.3.5 On-line Measurement of Carbon Content

---

Measurements collected by the Total Carbon Analyzer (TCA-08, Magee Scientific) at the Enniscorthy monitoring site between December 2019 and November 2020 are provided. As outlined in Chapter 2, the instrument employed a thermal method to determine total ambient carbon concentration at a high time resolution (1 hour). The total carbon was subsequently separated into equivalent elemental carbon (eEC) and equivalent organic carbon (eOC) fractions, using the ‘TC-BC’ method (Rigler et al., 2020). This approach relied on the optical determination of black carbon by the aethalometer. Organic carbon is calculated as:

$$OC = TC - b \cdot BC \quad \text{Eqn. 5.1}$$

where the parameter,  $b$ , relates the optical measurement of black carbon (BC) to the thermal measurement of elemental carbon (EC). The default value of  $b$  is one, thus assuming the equivalence of optically measured black carbon and thermally derived elemental carbon. This parameter can vary with location and seasonality, and also depends on the thermal protocol employed to assess the elemental carbon content in conventional thermal methods.

The temporal profile of the on-line measurement of total carbon is shown in Figure 5.21. Similar to PM<sub>2.5</sub> and optically derived equivalent black carbon, the highest concentrations were observed during the winter months, where a maximum hourly concentration of 157.37  $\mu\text{g m}^{-3}$  was recorded in January 2020. The average total carbon concentration during the winter was 9.30  $\mu\text{g m}^{-3}$ . This decreased significantly during the summer months, when a mean value of 1.68  $\mu\text{g m}^{-3}$  was recorded (Table 5.6).

A strong diurnal trend in total carbon concentration was observed (Figure 5.22). Despite variation in absolute concentration, similar trends were observed throughout winter, spring and autumn. Concentrations increased in the eveningtime, from approximately 16:00 until a maximum was reached between 18:00 and 21:00, consistent with the PM and eBC patterns observed. There was little diurnal variation in carbon concentration detected during the summer months. Concentrations were

consistently low; exceeding  $10 \mu\text{g m}^{-3}$  only on three occasions. Measured TC was below  $5 \mu\text{g m}^{-3}$  over 99% of the sampling period during the summer months.

*Table 5.6 Summary of total carbon recorded hourly in Enniscorthy (December 2019 - November 2020).*

<b>Total Carbon Concentration (<math>\mu\text{g m}^{-3}</math>)</b>		
	<i>Mean (<math>\pm</math> SD)</i>	<i>Range</i>
<b>Winter</b>	9.30 ( $\pm$ 15.2)	0.0 – 157.37
<b>Spring</b>	5.34 ( $\pm$ 7.0)	0.11 – 65.53
<b>Summer</b>	1.68 ( $\pm$ 1.6)	0.14 – 48.07
<b>Autumn</b>	4.09 ( $\pm$ 6.8)	0.0 – 99.55

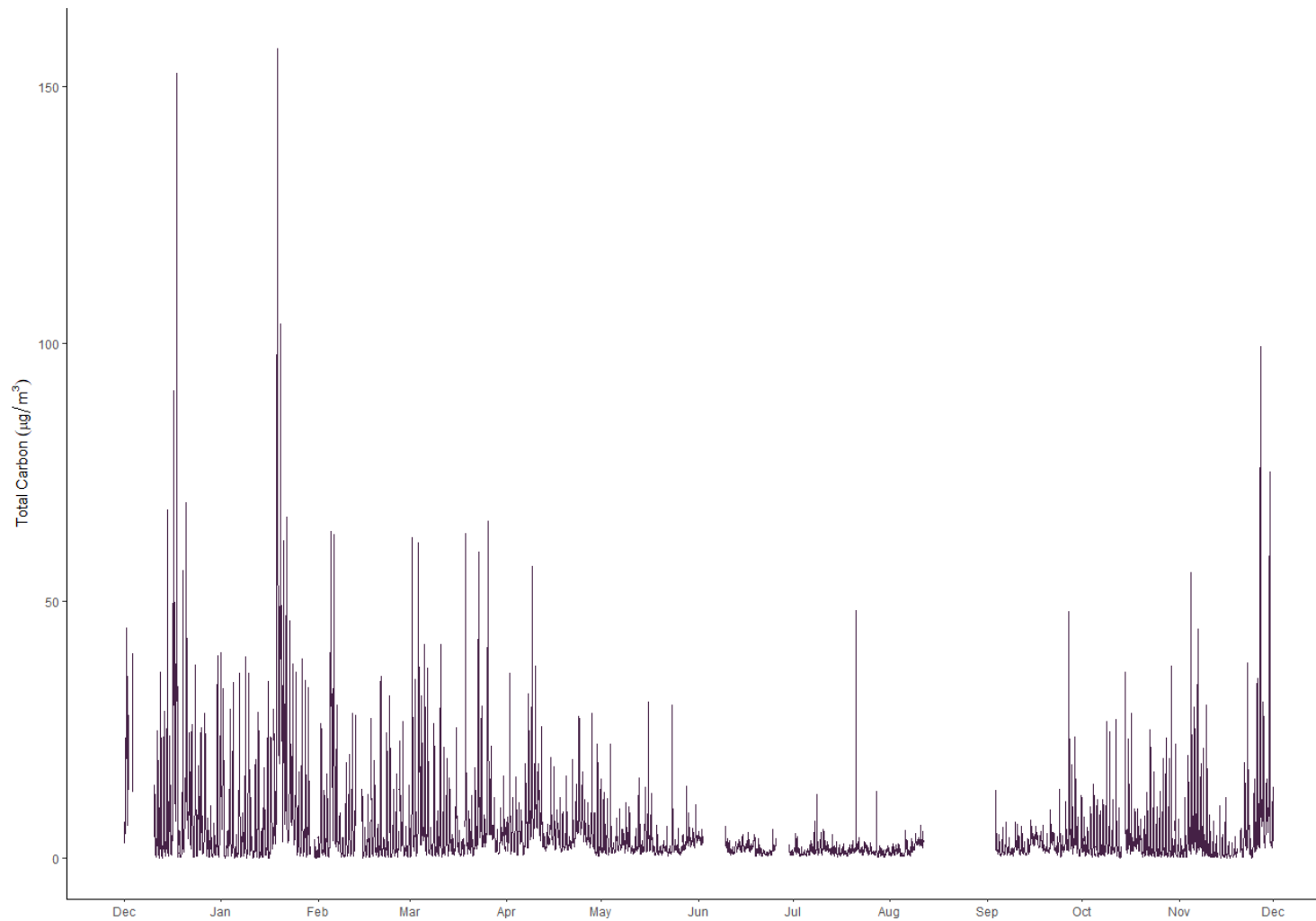


**Figure 5.21** Temporal profile of total carbon hourly concentration measured on-line by the Total Carbon Analyzer in Enniscorthy (December 2019 – November 2021).

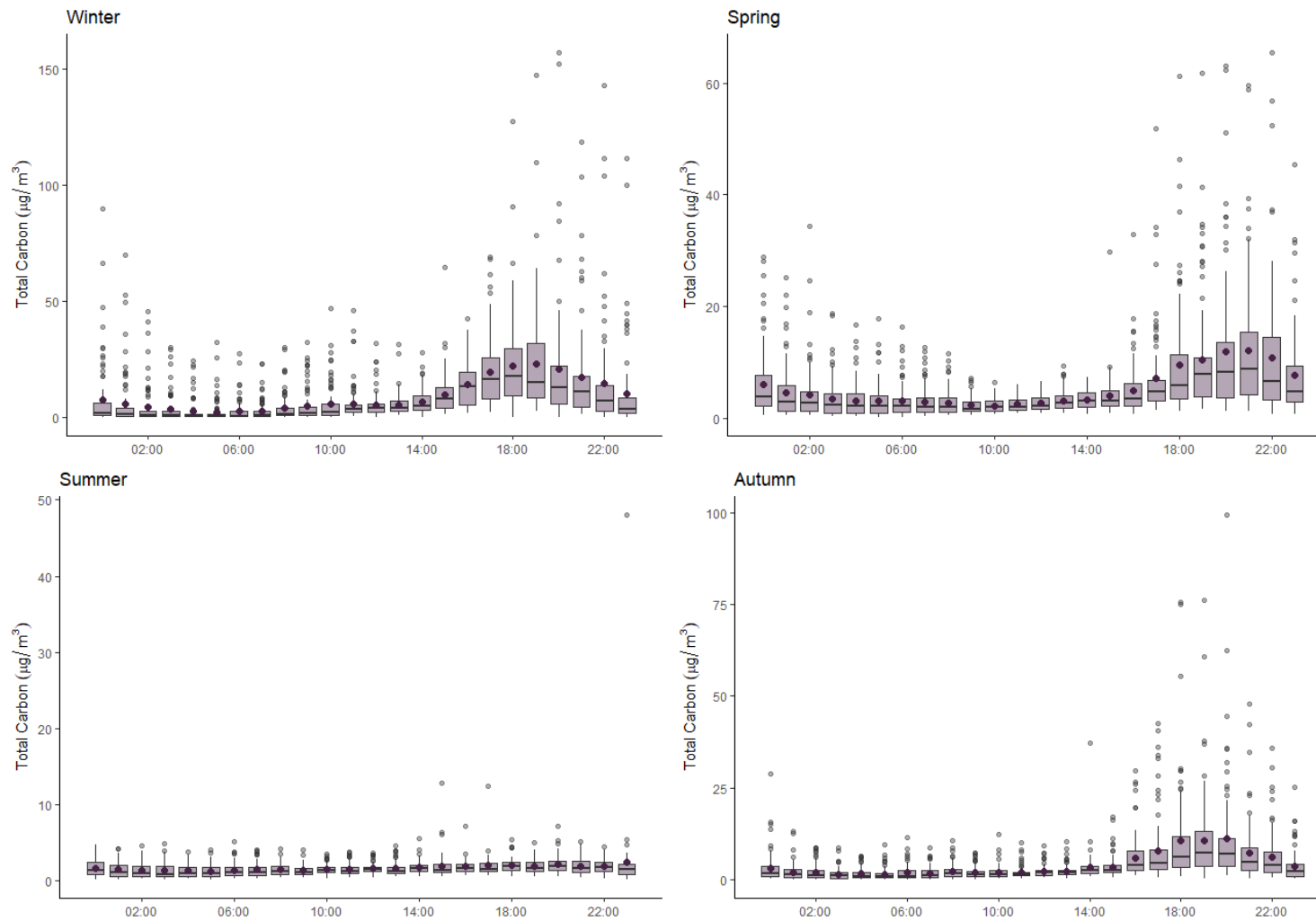


Figure 5.22 Diurnal profiles of hourly total carbon recorded in Enniscorthy (December 2019 - November 2020).

### 5.3.5.1 Determination of eEC and eOC

---

By applying the 'TC-BC' method, the eEC and eOC fractions were determined. This method assumed that the optically derived black carbon and thermally derived elemental carbon were equivalent. Table 5.7 provides a summary of the hourly concentrations of eEC and eOC recorded during the sampling period by the Total Carbon Analyzer in conjunction with the multi-wavelength aethalometer. Mean concentrations of both eEC and eOC were at a minimum during the summer months, when presumably there was significantly less contribution from solid fuel emissions. Simultaneously, the overall mean eOC/eEC ratio was at its highest, despite little variation in the diurnal profile of the eOC/eEC ratio from season to season (Figure 5.23). The increased eOC/eEC ratio during the summer months was unexpected. A greater eEC influence was anticipated due to reduced contribution from solid fuel combustion related emissions, and the resultant increased contribution from vehicular emissions during the summer season, as indicated by the aethalometer data (Figure 5.11). It is possible that the strong influence of OC during the summer months can be explained by secondary organic aerosol formation. Previous studies have noted the dominance of SOA in aerosol composition during the summer months, largely attributed to biogenic emissions (Aksoyoglu et al., 2011; Gelencsér et al., 2007; Zeng & Wang, 2011). It is also possible that employment of the default value of  $b$  resulted in an overestimation of the organic carbon content.

Measurements were made continuously on an hourly basis by the Total Carbon Analyzer, while filter samples were collected over an eight-hour period, starting at 07:00, 15:00 and 23:00, respectively. The continuous TCA measurements were averaged over the corresponding filter sampling period in order to compare the on-line and off-line methods of carbon content determination. Excellent correlation was observed between the two methods in the measurement of total, elemental and organic carbon concentration ( $r^2 > 0.9$ ) (Figure 5.24).

However, further investigation revealed the overestimation of TC, eEC and eOC content, by the TCA, in the majority of measurements, in comparison to results obtained by thermal-optical methods. The difference in sampling times, and manipulation of data to match the corresponding period, may have had a negative impact on the comparison. The proportionality parameter ( $b = 1$ ) employed to convert

eBC measurements to eEC may have also contributed to the discrepancy. Rigler et al. (2020) noted the effect that location and seasonality, in addition to the thermal protocol used for the determination of elemental and organic carbon content, have on the proportionality parameter. The calculation of a site- and season-specific  $b$  value would, perhaps, provide a more accurate on-line apportionment of equivalent organic and equivalent elemental carbon content.

**Table 5.7** Summary of monthly equivalent elemental (eEC) and organic (eOC) carbon measured in Enniscorthy using the 'TC-BC' method (December 2019 – November 2020).

	eEC ( $\mu\text{g m}^{-3}$ )		eOC ( $\mu\text{g m}^{-3}$ )		eOC/eEC
	<i>Mean</i>	<i>Range</i>	<i>Mean</i>	<i>Range</i>	<i>Mean</i>
<b>Dec 2019</b>	2.95	0.01 – 52.19	7.92	-0.03 – 100.38	3.42
<b>Jan 2020</b>	2.96	0.01 – 49.35	7.85	-3.85 – 108.02	3.82
<b>Feb 2020</b>	1.40	0.01 – 18.42	4.89	-0.06 – 47.28	4.83
<b>Mar 2020</b>	1.47	0.00 – 23.15	5.45	0.08 – 48.67	5.75
<b>Apr 2020</b>	1.21	0.02 – 13.34	4.93	0.23 – 46.77	5.61
<b>May 2020</b>	0.58	0.03 – 10.32	2.41	0.30 – 27.99	6.16
<b>Jun 2020</b>	0.36	0.00 – 1.61	1.51	0.31 – 5.63	5.84
<b>Jul 2020</b>	0.28	0.00 – 3.30	1.24	0.08 – 47.75	5.91
<b>Aug 2020</b>	0.40	0.02 – 1.63	1.41	0.25 – 5.18	5.28
<b>Sep 2020</b>	0.70	0.01 – 14.20	2.31	0.21 – 33.73	4.82
<b>Oct 2020</b>	0.85	0.01 – 9.27	2.61	-1.90 – 37.09	4.43
<b>Nov 2020</b>	1.48	0.01 – 28.48	4.31	-1.52 – 71.07	3.81

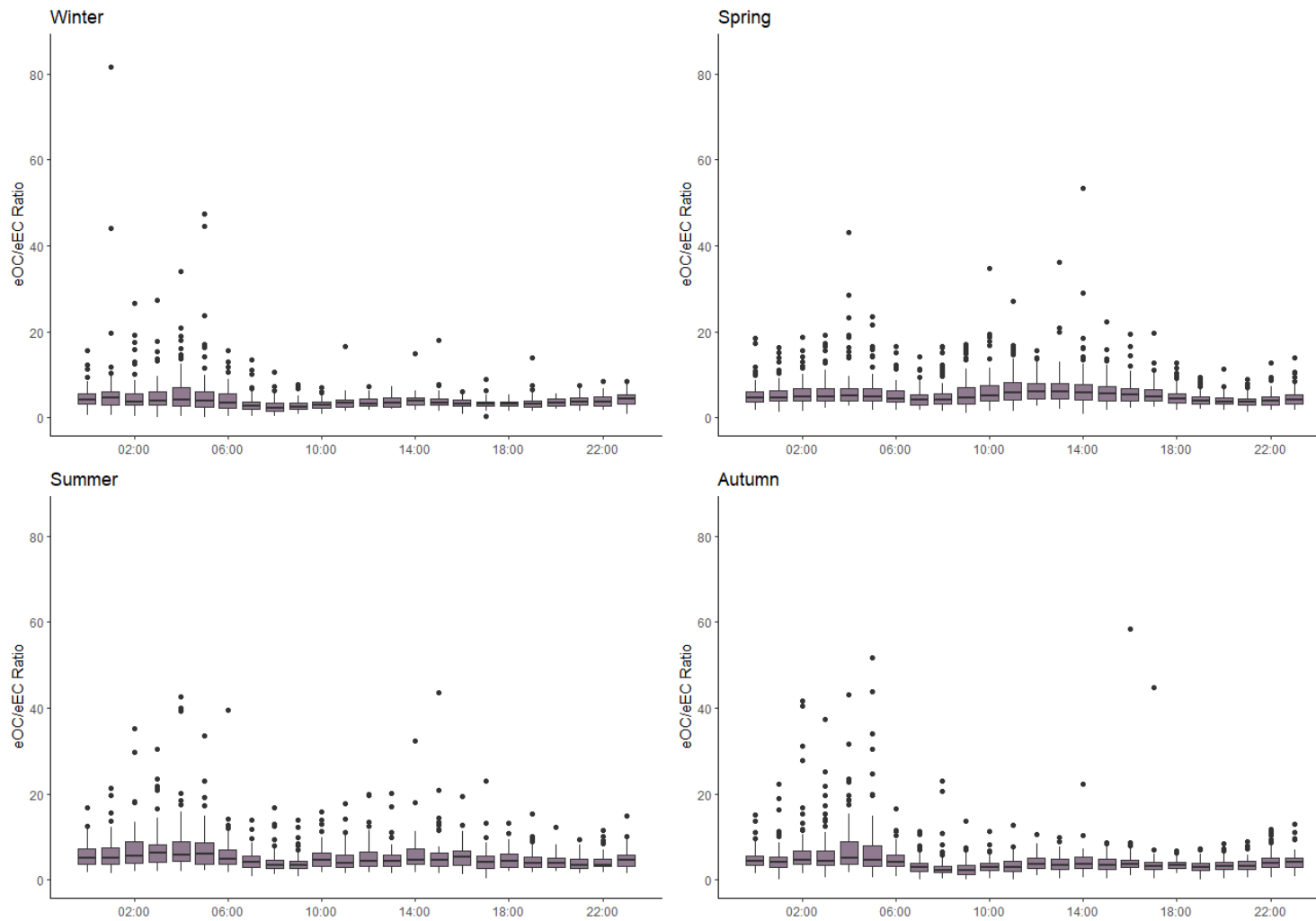
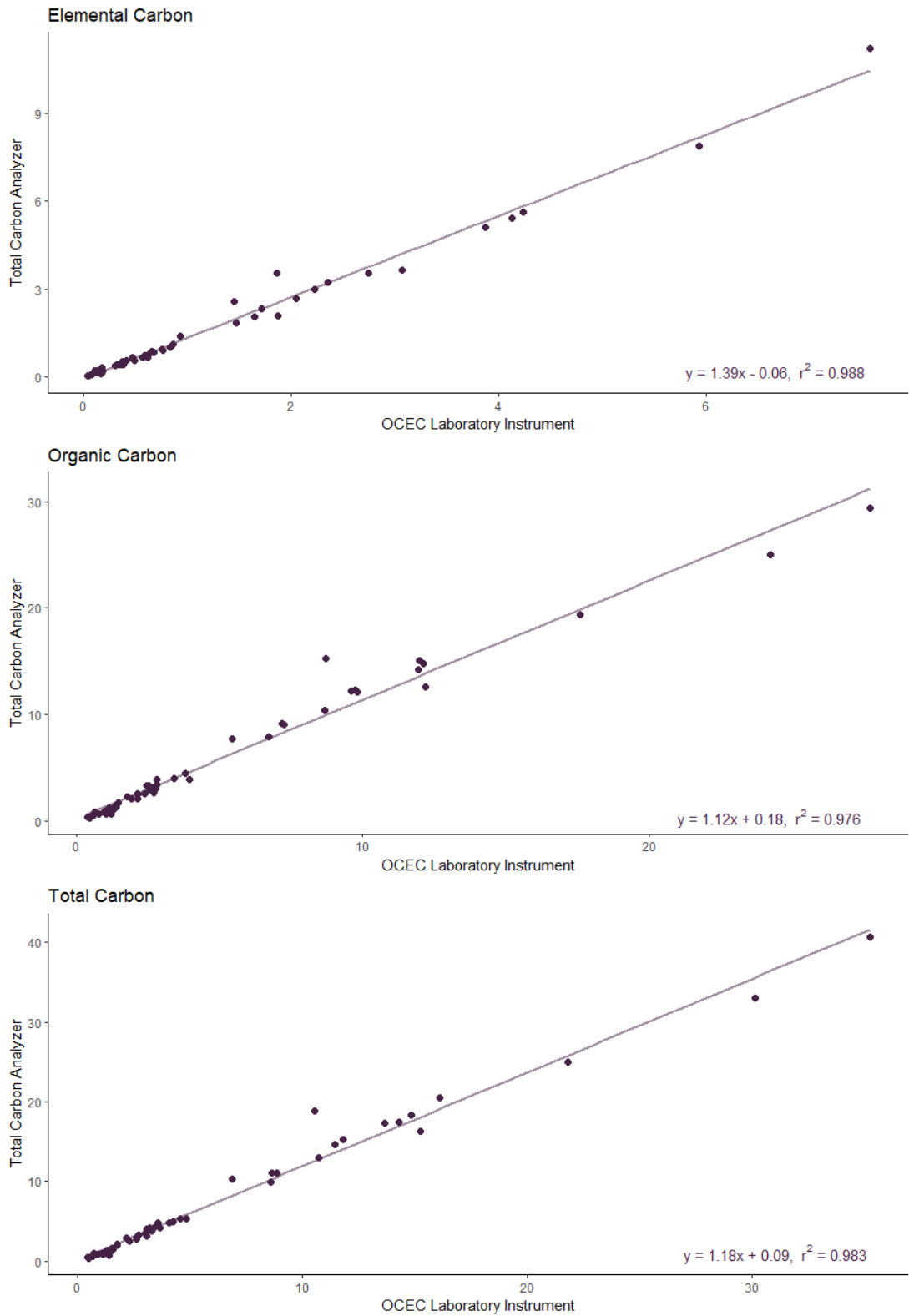
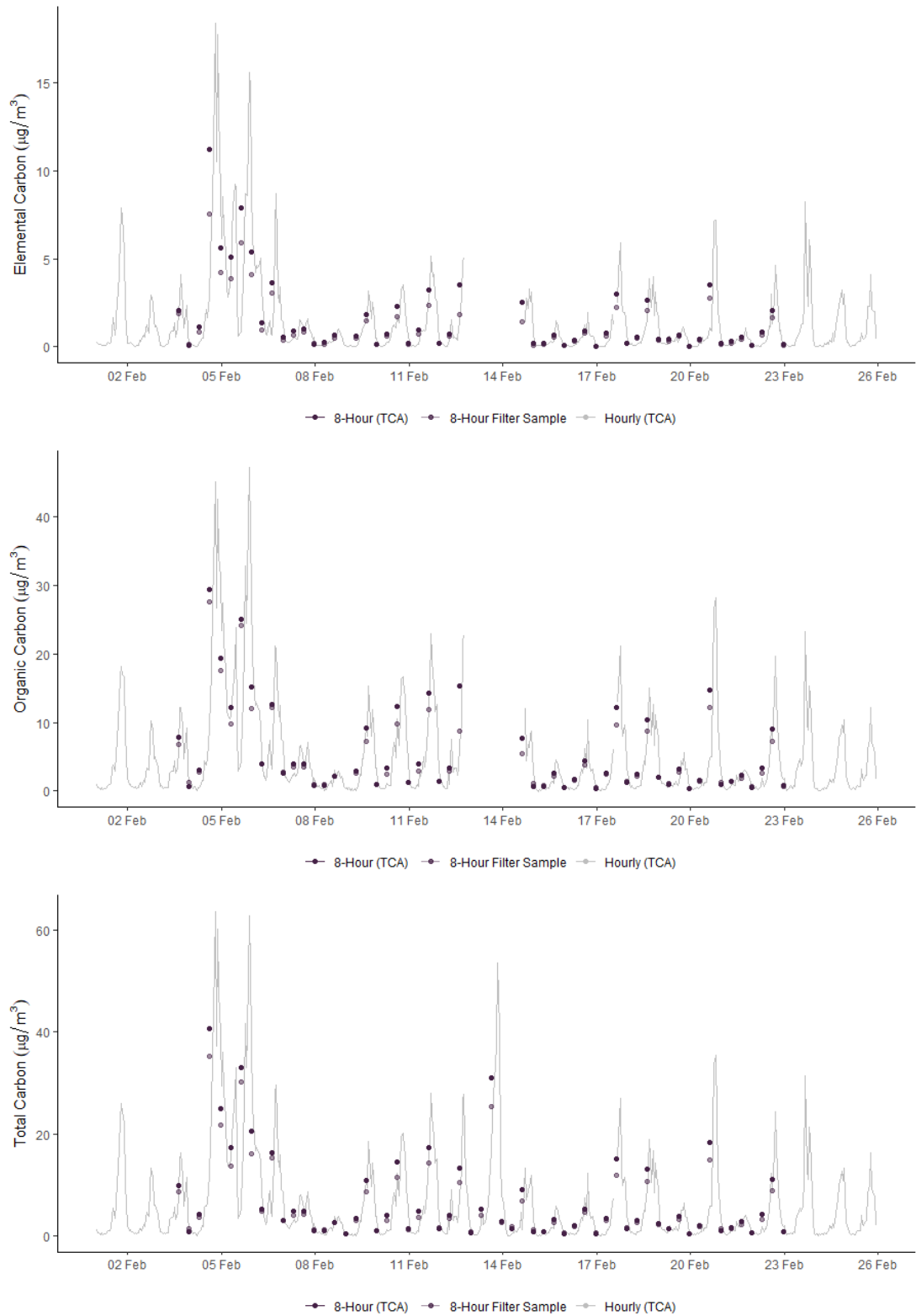


Figure 5.23 Seasonal diurnal profiles of eOC/eEC ratio measured in Enniscorthy by the TCA-08 (December 2019 - November 2020).



**Figure 5.24** Comparison of elemental, organic and total carbon measured by the Total Carbon Analyzer (TCA-08, Magee Scientific) and the OCEC Laboratory Instrument (Sunset Laboratory Inc.) in Enniscorthy (February 2020). TCA data was averaged over the corresponding filter sampling period.



**Figure 5.25** Temporal comparison of off-line results of carbon content derived from filter analysis to the hourly and 8-hour average on-line TCA-08 measurements.

The linear relationship between thermally derived elemental carbon (EC) and optically derived equivalent black carbon (eBC) is described as slope  $s$ , by applying an orthogonal regression model (Figure 5.26). This analysis employed the ‘*Deming*’ function of the *MethComp* R software package (Carstensen et al., 2020). The  $b$  parameter, used to relate the black carbon measured by the aethalometer to equivalent elemental carbon, is described in Eqn. 5.2. This proportionality parameter was determined as 0.71 for the samples used in the analysis. It is within the range of values determined for numerous background locations in Europe (0.44 – 1.23), which also employed the EUSAAR\_2 protocol for conventional thermal-optical off-line analysis of filter samples (Rigler et al., 2020).

$$b = \frac{1}{s} \quad \text{Eqn. 5.2}$$

Samples used in this analysis were collected in February 2020. Therefore, the  $b$  value of 0.71 is considered to be representative of the proportionality parameter appropriate for use in Enniscorthy during wintertime. Seasonality, and associated changes in source contributions, can influence the parameter. Filter samples collected throughout the year, at times representative of each season, would allow for more accurate determination of  $b$ . Employing the value of 0.71 for  $b$  improved the accuracy of the on-line measurement of equivalent elemental carbon, when compared with the off-line filter sample measurement of same. The reduction in eEC consequently increased the estimated eOC content, resulting in an even greater discrepancy between the two methods for measurement of organic carbon Figure 5.27.

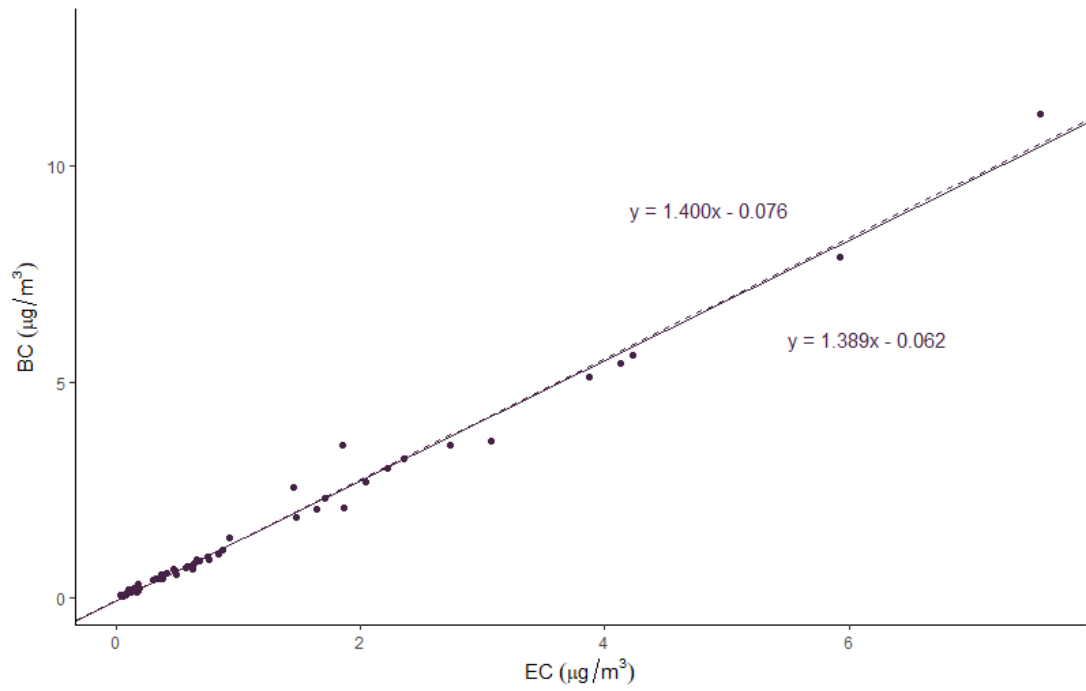


**Figure 5.26** Comparison of thermally-derived elemental carbon (EC) and optically-derived black carbon (BC) using linear (solid line) and orthogonal (dashed line) regression models.

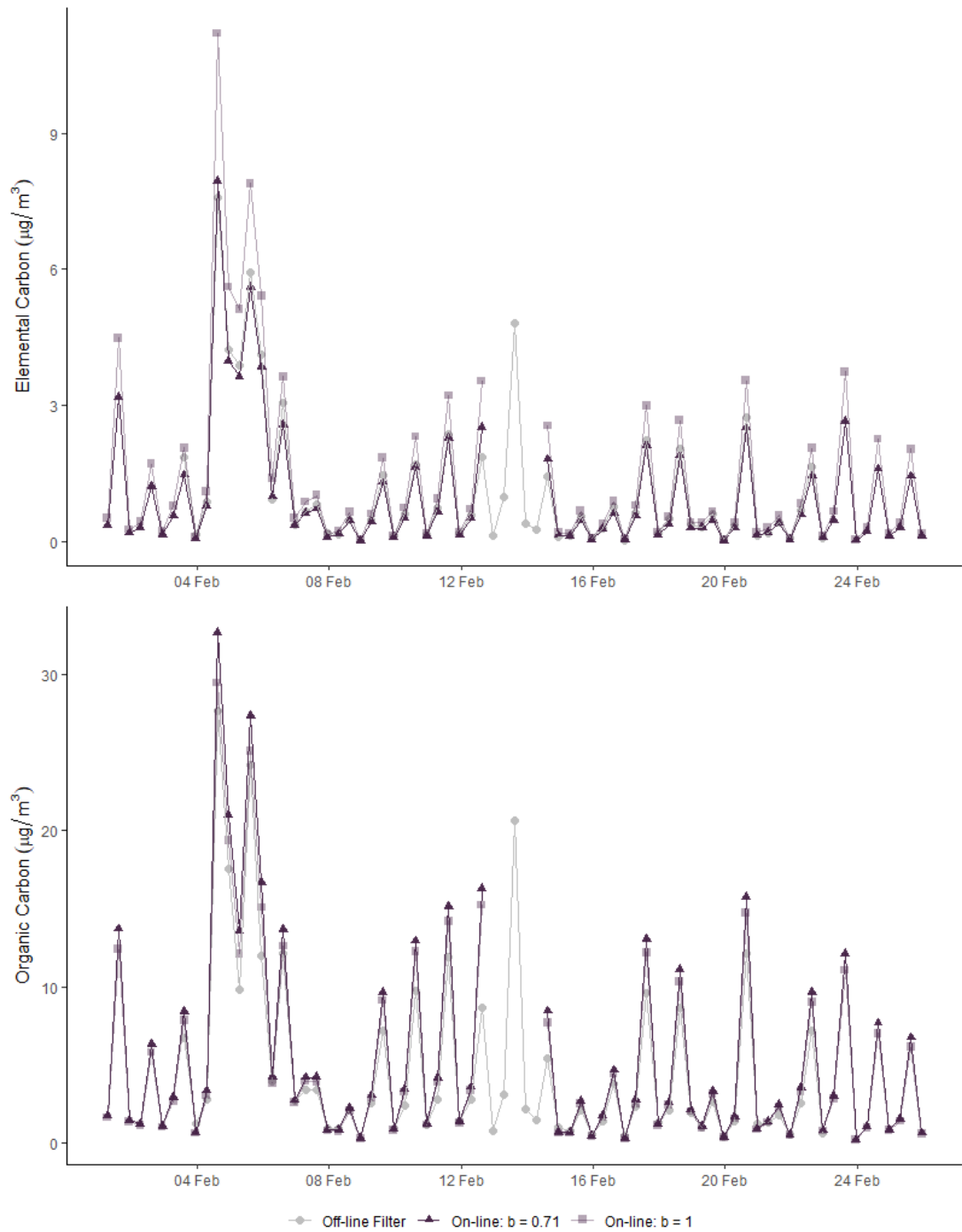


**Figure 5.27** Comparison of on-line estimation of eEC and eOC using two values for the proportionality factor,  $b$ ; 1 and 0.71. The estimation is also compared with conventional off-line determination of elemental and organic carbon.

The Total Carbon Analyzer can also be used for the determination of total carbon content of aerosol samples previously collected on quartz fibre filters. This thermal analysis of the samples can be carried out in the 'off-line' mode. The 'Cleaning Procedure' and 'Zero Verification' procedure were carried out prior to analysis to minimise contamination. A total carbon mass of below 0.5  $\mu\text{g}$  is acceptable in terms of reported carbon on a 'clean' filter following the 'Zero Verification' procedure. All 'Zero Verification' procedures carried out were deemed 'successful'. A punch (3.3  $\text{cm}^2$ ) of the previously collected filter sample was placed on the 'clean' filter and one thermal analysis cycle was performed. By providing the area of the punch, in  $\text{cm}^2$ , the TC content was calculated in  $\mu\text{g cm}^{-2}$ .

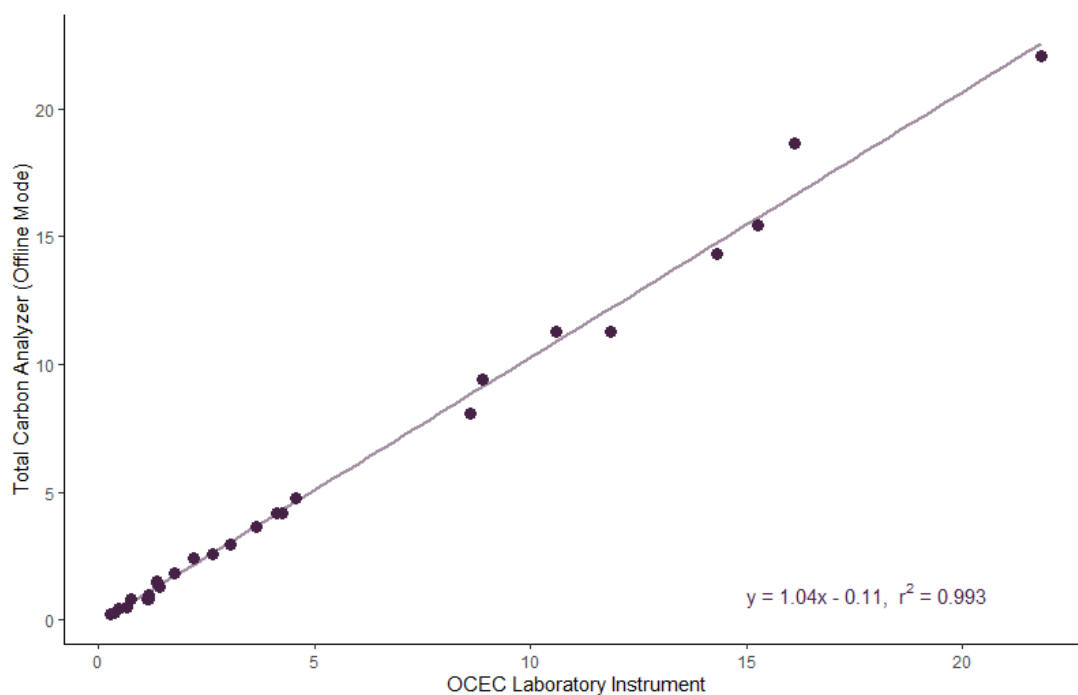


**Figure 5.28** Comparison of total carbon content determination ( $\mu\text{g cm}^{-2}$ ) using two off-line techniques; thermal-optical analysis (OCEC Laboratory Instrument, Sunset Laboratory Inc.) and thermal analysis (Total Carbon Analyzer, Magee Scientific).

The thermal analysis of filter samples in 'off-line' mode were compared with the conventional thermal-optical analysis which employed the EUSAAR\_2 protocol (Figure 5.28). Excellent correlation ( $r^2 > 0.99$ ) was observed between the two techniques. Assuming the thermal-optical analysis performed by the OCEC Laboratory Instrument (Sunset Laboratory Inc.) determined the most accurate TC

content, the percentage error in the TCA determination of TC ranged between 1.4% and 28.7%. Figure 5.29 shows that, in general, the on-line measurement of total carbon by the TCA is marginally greater than the off-line measurements, by the TCA (thermal analysis) and the OCEC Laboratory Instrument (thermal-optical analysis). The discrepancy is likely explained by the variable sampling periods; eight-hour filter sample collection versus hourly on-line sampling.

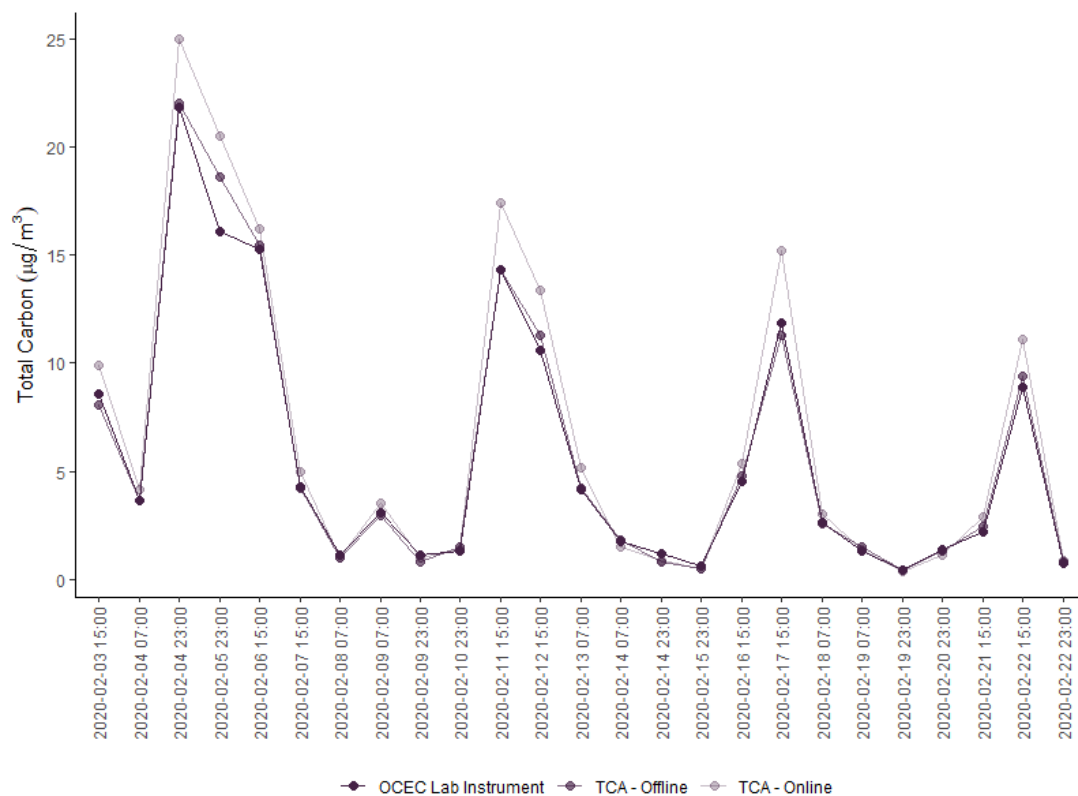


**Figure 5.29** Total carbon concentration determined using various thermal and thermal-optical methods of analysis; the OCEC Laboratory Instrument (Sunset Laboratory Inc.) and the Total Carbon Analyzer (TCA-08, Magee Scientific) in on-line and off-line modes.

### 5.3.6 Comparison of Wintertime Air Quality in 2015, 2020 and 2021

---

The Source Apportionment of Particulate Matter in Urban and Rural Residential Areas of Ireland (SAPPHIRE) project (2013-EH-MS-15) was commissioned by the Environmental Protection Agency with the aim of identifying sources of PM<sub>2.5</sub> in residential areas of small towns in Ireland. Research was carried out by members of the Centre for Research in Atmospheric Chemistry in University College Cork. Measurement campaigns were conducted during the winter months in three small towns in Ireland; Birr, Co. Offaly (November 2015 – January 2016), Enniscorthy, Co. Wexford (January – February 2015) and Killarney, Co. Kerry (November – December 2014). The towns were selected based on certain criteria; no access to natural gas supply, a population of < 15,000, and therefore outside areas subjected to the ‘Smoky Coal’ ban, and a location where residents are likely to use solid fuel as a main source of heating.

The project concluded that PM<sub>2.5</sub> concentrations increased significantly during the evening hours, often further exaggerated when wind speeds were low. PM<sub>2.5</sub> measurements were particularly high in Enniscorthy; an average of 29.2 µg m<sup>-3</sup> was recorded over a 38-day period, while the WHO 24-hour average guideline was exceeded on 42% of the days of the sampling period at this location (Wenger et al., 2020). Solid fuel combustion related emissions contributed the majority of PM<sub>2.5</sub> mass at each location, 60%, 82% and 72% in Birr, Enniscorthy and Killarney, respectively, while traffic emissions and sea spray had a minor influence on the total PM mass.

In recent years, numerous scientific, environmental and political campaigns have heightened awareness surrounding the adverse effects poor air quality, including increased levels of particulate matter, has on both human and planetary health. The need to reverse the severe damage incurred on the Earth, and its atmosphere, by humans is becoming increasingly obvious and urgent. A reduction in the emission of greenhouse gases and particulate matter will be advantageous for both planetary and human health. A number of studies have previously documented the positive impact of limiting the use of certain solid fuels and particulate matter emissions (Brimblecombe, 2006; Clancy et al., 2002; Goodman et al., 2009; Ma et al., 2019). Severe pollution events in Ireland throughout the 1980’s were attributed to cold temperatures and the increased use of solid fuel for domestic heating following the oil

crisis in the 1970's. Such severe episodes prompted the government to introduce a number of measures to reduce the use of solid fuels, particularly bituminous coals. The introduction of the '*Marketing, Sale, and Distribution of Fuels Regulation*' in Dublin in September 1990, colloquially known as the 'Smoky Coal' ban, resulted in a significant decrease in black smoke concentrations (Buckley, 2019). Clancy et al. (2002) reported a decrease in mortality associated with air pollution following the implementation of the ban on the sale of bituminous coal in Dublin in 1990, while Dockery et al. (2013) noted a reduction in hospital admissions consistent with the ban. The ban was extended to include several new areas, including Enniscorthy, in September 2020.

This section will focus on comparing the results of the SAPPHIRE project (January – February 2015) with the current measurement campaign (January – February 2020) and measurements made following the introduction of the 'Smoky Coal' ban in Enniscorthy (December 2020 – January 2021) to identify and quantify any improvements or deterioration in the ambient wintertime conditions (Table 5.8).

**Table 5.8** *Dates of sampling periods analysed for comparison of ambient wintertime conditions in Enniscorthy.*

<b>Year</b>	<b>Sampling Period</b>
2015	08/01/2015 – 14/02/2015
2020	08/01/2020 – 18/02/2020
2021	08/12/2020 – 20/01/2021

### 5.3.6.1 Meteorological Conditions

Similar meteorological conditions were recorded during all measurement periods. Figure 5.30 shows the daily maximum and minimum temperatures recorded during the 2015, 2020 and 2021 sampling periods. The daily-averaged wind speed is also provided.

A similar range of temperatures were recorded in 2015 and 2021, while ambient temperatures were slightly higher during the 2020 sampling period. However, there was little variation in the recorded wind speed across all three sampling periods ( $4.99 < \bar{x} < 5.36$ ), which is the most important meteorological factor in this context.

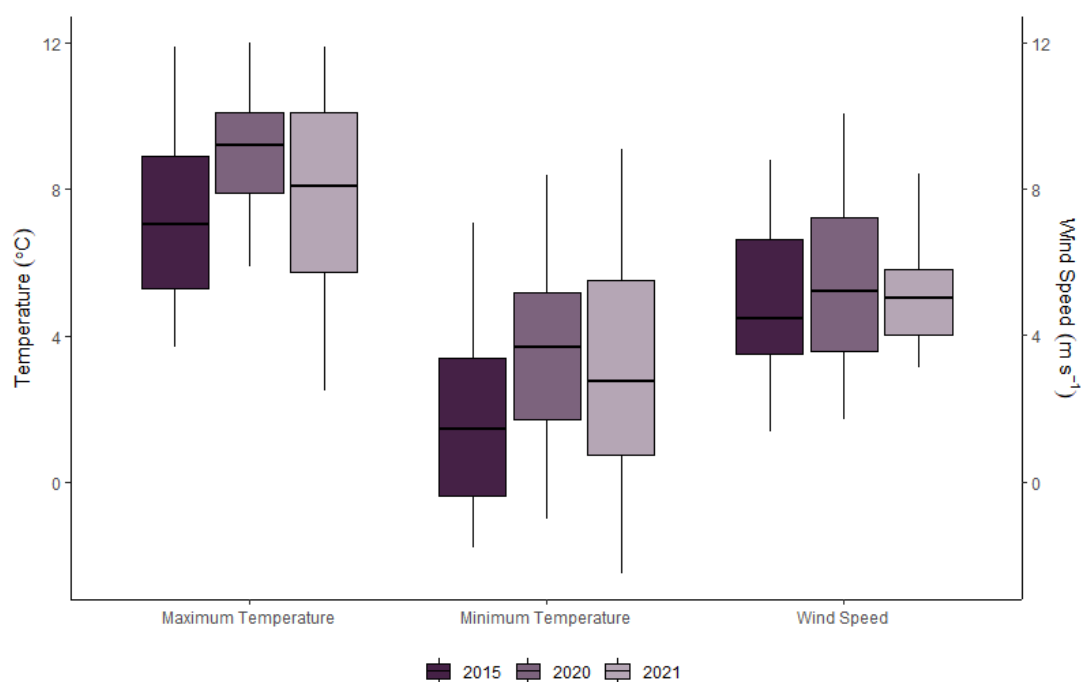


**Figure 5.30** Comparison of meteorological conditions during the 2015, 2020 and 2021 sampling periods in Enniscorthy. Meteorological parameters were obtained from the Met Éireann weather station located at Johnstown Castle, 24 km south east of the sampling site.

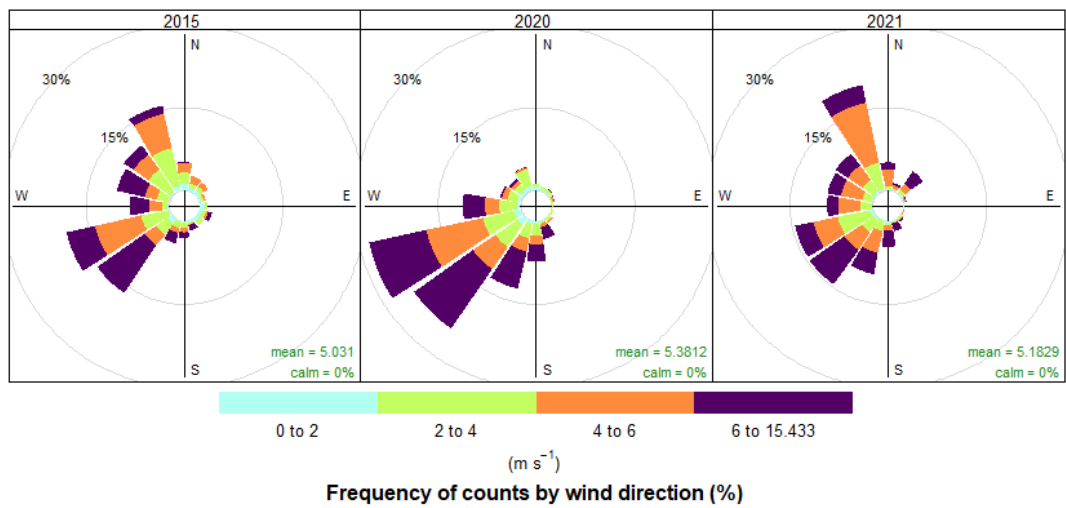


*Figure 5.31* Wind rose plot describing the wind speed and direction during the 2015, 2020 and 2021 sampling periods in Enniscorthy.

### 5.3.6.2 *Particulate Matter and Equivalent Black Carbon*

---

The PM<sub>2.5</sub> mass concentrations recorded in Enniscorthy decreased steadily since the sampling period in 2015 ( $\bar{x} = 29.2 \mu\text{g m}^{-3}$ ) to an hourly average of  $11.6 \mu\text{g m}^{-3}$  in 2021, as shown in Table 5.9. Variation in instrumentation employed in the measurement of mass concentration must be acknowledged; a TEOM was used during the 2015 SAPPHIRE project, while a FIDAS 200 was permanently installed prior to the 2020 and 2021 campaigns. The 2005 WHO guideline mean of  $25 \mu\text{g m}^{-3}$  over a 24-hour period was breached on 8 occasions in 2020 (19.1%) and on 2 occasions in 2021 (4.5%). This was a significant improvement on the number of exceedances in 2015 (42%). As in 2015, the highest concentrations of PM<sub>2.5</sub> coincided with periods of low wind speed. A considerable increase in PM mass concentration was observed in the eveningtimes, rising sharply from approximately 15:00 onwards. This diurnal trend was comparable to observations recorded in the SAPPHIRE report (Wenger et al., 2020), despite considerably lower concentrations in latter years, indicating initial benefits of solid fuel restrictions.

Black carbon, measured optically by the multi-wavelength aethalometer, was investigated. Despite a continuous decrease in the mean hourly-average concentration in equivalent black carbon between 2015 and 2021, similar maximum concentrations were observed during the 2015 and 2020 sampling periods;  $35.2 \mu\text{g m}^{-3}$  and  $38.8 \mu\text{g m}^{-3}$ , respectively. A substantially lower maximum level of eBC was recorded in 2021 ( $18.2 \mu\text{g m}^{-3}$ ). Similar to the PM mass concentration, strong diurnal variation was observed during all sampling periods; an intense evening peak attributed to solid fuel combustion for domestic heating (Figure 5.32). Despite an overall reduction in absolute concentrations, contribution from solid fuel related emissions to total eBC remained relatively consistent.

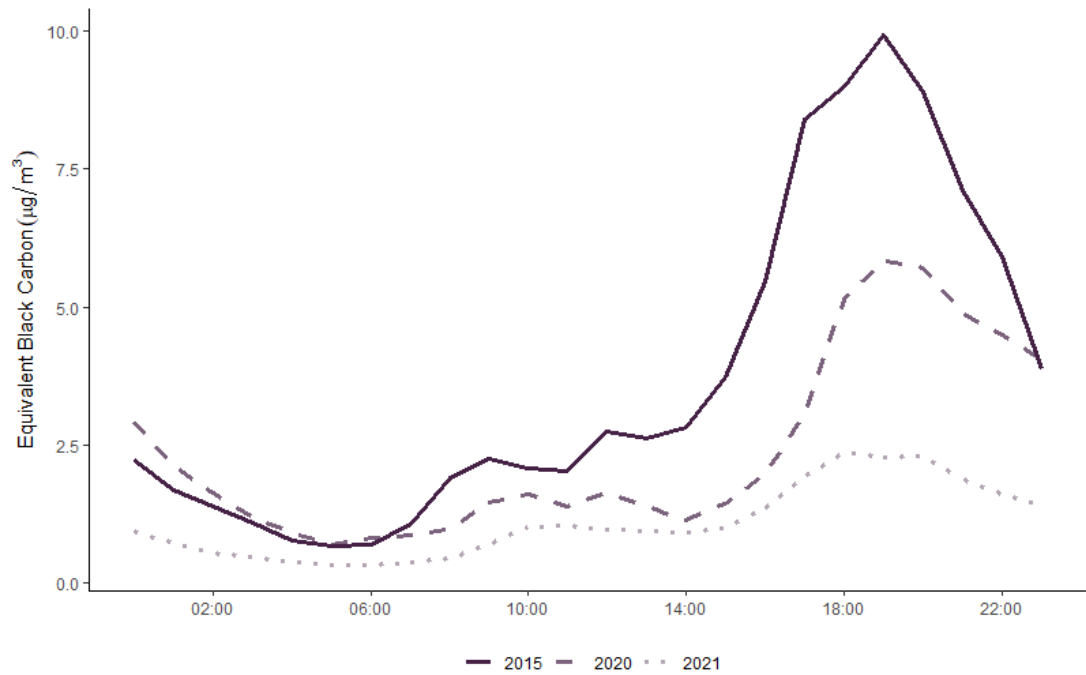


**Figure 5.32** Diurnal profile of eBC measured in Enniscorthy during the 2015, 2020 and 2021 sampling periods showing a strong peak in the eveningtime, attributed to emissions from solid fuel combustion.

A slight increase in eBC<sub>SF</sub> contributions to total eBC was observed between the 2020 (73%) and 2021 (83%) sampling periods. It is possible that it was caused by increased solid fuel usage due to extended combustion hours associated with COVID-19 ‘stay-at-home’ orders. However, it is also plausible that there was a reduction in bituminous coal burning. As previously discussed, due to the infrared (IR) absorbing material produced in coal combustion, these emissions may previously have been attributed to the ‘traffic’ portion of total eBC. Following the implementation of the ‘Smoky Coal’ ban in September 2020, the source apportionment aethalometer model may have, incorrectly, observed a reduction in ‘traffic’-related contributions.

The frequency distribution of the absorption Ångström exponent recorded in Enniscorthy during the 2015, 2020 and 2021 sampling periods are shown in Figure 5.33. Similar broad distributions were observed, with mean AAE values of 1.45, 1.47 and 1.54, respectively. The high frequency of AAE tending towards 2 indicated the presence of solid fuel related emissions in the ambient environment. The increased AAE recorded in 2021 suggests a stronger influence of UV-absorbing materials, as indicated by the source apportionment analysis output (Table 5.9), potentially due to a reduction in coal combustion emissions.

**Table 5.9** Hourly average eBC and PM<sub>2.5</sub> concentrations measured in Enniscorthy during winter sampling periods of 2015, 2020 and 2021.

	2015		2020		2021	
	<i>Mean (± SD)</i>	<i>Range</i>	<i>Mean (± SD)</i>	<i>Range</i>	<i>Mean (± SD)</i>	<i>Range</i>
<b>PM<sub>2.5</sub> (µg m<sup>-3</sup>)</b>	29.2 (± 31.9)	0.0 – 236.6	20.6 (± 31.8)	0.3 – 350.3	11.6 (± 13.2)	0.3 – 210.5
<b>eBC (µg m<sup>-3</sup>)</b>	3.6 (± 4.8)	0.01 – 35.2	2.4 (± 4.4)	0.0 – 38.8	1.1 (± 1.4)	0.0 – 18.2
<b>eBC/PM<sub>2.5</sub> (%)</b>	13.2		9.3		9.1	
<b>eBC<sub>SF</sub>/eBC<sub>Total</sub></b>	0.80		0.73		0.83	

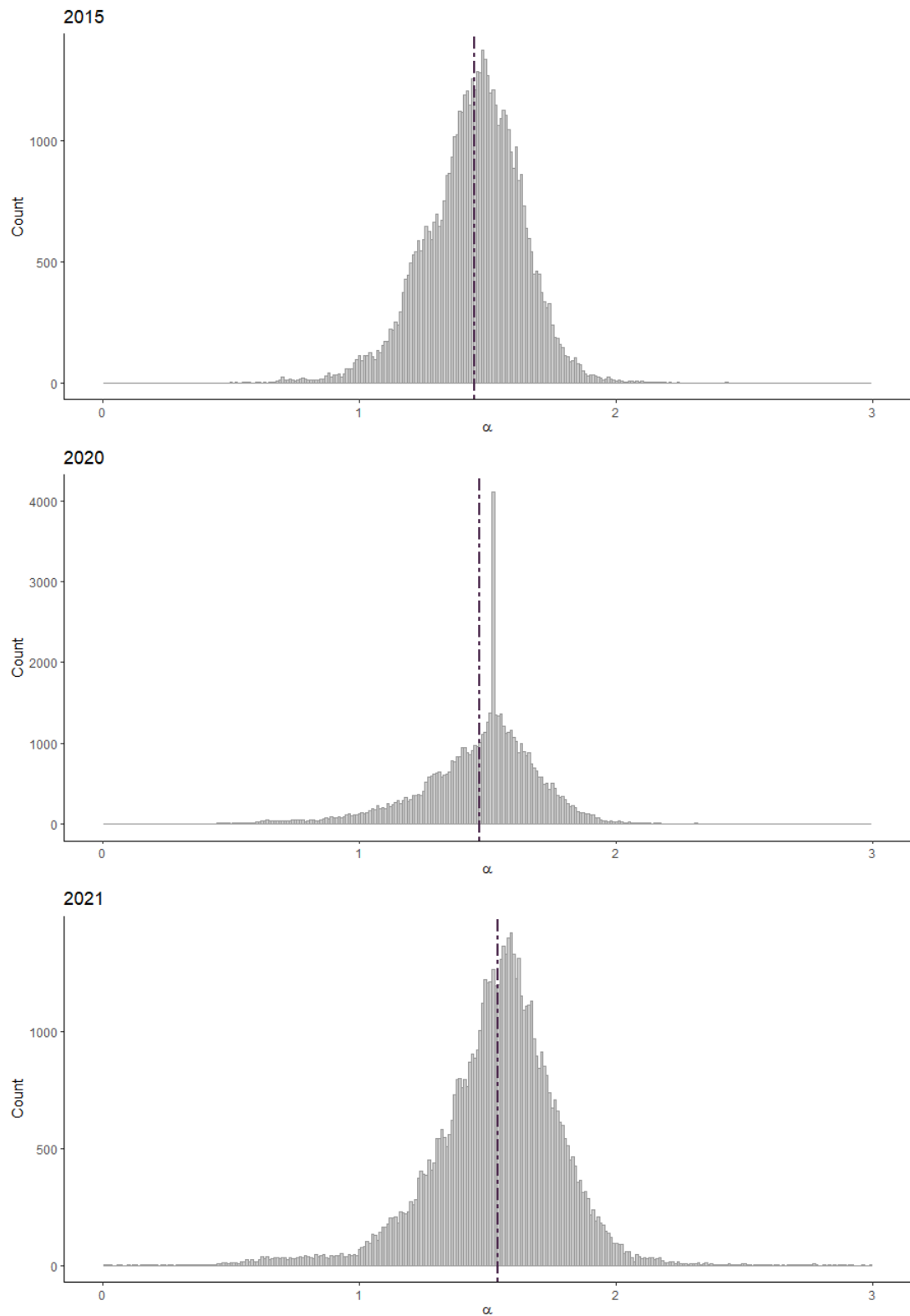


**Figure 5.33** Frequency distribution of the absorption Ångström exponent recorded in Enniscorthy during the 2015 (top), 2020 (middle) and 2021 (bottom) sampling periods.

### 5.3.6.3 *Elemental and Organic Carbon*

---

Ambient concentrations of organic, elemental and total carbon were assessed during the 2015, 2020 and 2021 sampling periods. A summary of results from each measurement campaign is provided in Table 5.10. Quartz fibre filter samples were used to determine ambient carbonaceous aerosol, however the instruments, time resolution and thermal protocols employed for analysis varied from year to year. During the SAPPHIRE campaign (2015) a Semi-Continuous OCEC Carbon Aerosol Analyzer (Sunset Laboratory Inc.) was used for filter sampling, 108 minute duration, followed by 12 minute analysis using a modified version of the National Institute for Occupation Safety and Health (NIOSH) 5040 protocol (Birch, 2003). This provided average concentrations of elemental and organic carbon on a two-hour basis. Collection and measurement of ambient samples during the 2020 campaign is outlined in Chapter 2. Briefly, ambient samples were collected on quartz fibre filters using a high volume air sampler (DHA-80, DIGITEL Elektronik GmbH) over an eight-hour period and were subsequently analysed using an Organic Carbon/Elemental Carbon (OCEC) Laboratory Instrument (Model 5L, Sunset Laboratory Inc.), which employed the EUSAAR\_2 protocol (Cavalli et al., 2010). Total carbon measurements were made on-line using the Total Carbon Analyzer (TCA-08, Magee Scientific) during the 2020 and 2021 sampling periods. The ‘TC-BC’ method was employed to subsequently determine the equivalent elemental and equivalent organic carbon fractions present in each sample. Previous studies have concluded that total carbon concentrations provided by common thermal protocols are comparable, however the quantification of organic and, to a greater extent, elemental carbon content is dependent on such protocols (Bautista et al., 2015; Karanasiou et al., 2015). This must be considered when comparing results from both measurement campaigns.

Although comparable in 2020 and 2021, concentrations of EC and OC have decreased significantly since 2015 (Table 5.10). Comparison of the mean OC/EC ratio during each sampling period is usually indicative of a change in the dominant sources contributing to the ambient carbonaceous aerosol. However, both elemental and organic carbon contributions to PM<sub>2.5</sub> mass concentrations appeared to remain relatively constant between 2015 and 2020. This indicates that despite the marked decrease in PM<sub>2.5</sub> concentration, the dominant sources have remained relatively unchanged. It is, therefore, likely that the inconsistency in OC/EC ratio is due to the

inequivalent assignment of OC and EC content by different protocols employed in analyses. However, comparison of thermal-optical analysis and thermal analysis employing the 'TC-BC' method exhibited variation (2020). The SAPPHIRE report concluded that ambient conditions were likely influenced by both biomass and coal burning in 2015. The higher OC/EC ratio obtained during the 2020 and 2021 sampling periods indicated that biomass has become the primary type of solid fuel used for domestic heating, suggesting general compliance with the recent legislation. This is further evidence of a change in the fuel mixture, consistent with the increased AAE values recorded in 2021 ( $\bar{x} = 1.54$ ), compared with 2015 ( $\bar{x} = 1.45$ ).

A significant reduction in the ambient concentration of each of PM<sub>10</sub>, PM<sub>2.5</sub> and eBC was observed in the comparison of winter periods 2015, 2020 and 2021. The dramatic decrease in ambient levels of pollutants following the curtailment of use of a single fuel type (bituminous coal) provides scope for further restrictions of other types of solid fuels to improve air quality. The dominance of solid fuel combustion emissions in the environment has been established. Further chemical analysis is required to discriminate between frequently used fuels and their respective contribution to total mass concentration. By identifying the prevalence of each individual fuel type (i.e. coal, wood and peat) the potential reduction in mass concentration can be estimated pending further fuel usage restrictions in future.

Further long term measurements at this sampling site are required to continuously monitor the impact of the ban on bituminous coal. Initial improvements in ambient air quality are encouraging. Ideally, local residents will experience associated health benefits similar to those reported by Clancy et al. (2002).

**Table 5.10** Organic and elemental carbon concentrations measured in Enniscorthy during the winter seasons of 2015, 2020 and 2021.

	2015		2020 <sup>§§§</sup>		2021	
	Mean ( $\pm$ SD)	Range	Mean ( $\pm$ SD)	Range	Mean ( $\pm$ SD)	Range
TC <sub>Sunset</sub> ( $\mu\text{g m}^{-3}$ )	-	-	6.1 ( $\pm$ 7.5)	0.5 – 35.3	-	-
TC <sub>TCA</sub> ( $\mu\text{g m}^{-3}$ )	-	-	7.0 ( $\pm$ 10.0)	0.0 – 63.6	5.9 ( $\pm$ 7.0)	0.0 – 87.0
OC ( $\mu\text{g m}^{-3}$ )	9.6 ( $\pm$ 12.2)	0.5 – 75.8	4.9 ( $\pm$ 6.0)	0.4 – 27.7	-	-
eOC ( $\mu\text{g m}^{-3}$ )	-	-	5.9 ( $\pm$ 8.3)	0.0 – 51.8	5.1 ( $\pm$ 6.0)	0.0 – 71.7
EC ( $\mu\text{g m}^{-3}$ )	2.9 ( $\pm$ 3.5)	0.0 - 22.1	1.2 ( $\pm$ 1.6)	0.0 – 7.6	-	-
eEC ( $\mu\text{g m}^{-3}$ )	-	-	1.1 ( $\pm$ 1.8)	0.0 – 13.1	0.8 ( $\pm$ 1.1)	0.0 – 15.3
OC/EC	4.0	0.5 – 71.1	5.3	2.5 – 12.4	-	-
eOC/eEC	-	-	7.7	-	7.3	-
PM <sub>2.5</sub> ( $\mu\text{g m}^{-3}$ )	29.5 ( $\pm$ 30.7)	0.7 – 205.2	14.6 ( $\pm$ 15.8)	0.4 – 117.4	11.6 ( $\pm$ 13.2)	0.3 – 210.5
OC/PM <sub>2.5</sub>	0.29	0.05 – 0.88	0.28	0.06 – 0.52	-	-
eOC/PM <sub>2.5</sub>	-	-	0.36	-	0.45	-
EC/PM <sub>2.5</sub>	0.08	0 – 0.48	0.06	0.01 – 0.17	-	-
eEC/PM <sub>2.5</sub>	-	-	0.06	-	0.10	-

<sup>§§§</sup> Analysis of ambient samples collected during February 2020 (03/02/2020 – 23/02/2020).

## 5.4 CONCLUSIONS

---

The temporal variability of particulate matter mass concentration, equivalent black carbon and the contribution of dominant sources to the ambient carbonaceous aerosol in the small town of Enniscorthy, Co. Wexford was investigated between December 2019 and November 2020. The measurements clearly exhibit a strong seasonal dependence. Although solid fuel burning emissions were never eliminated entirely at any point throughout the monitoring campaign, contributions were at a maximum during the colder, winter months.

PM mass concentration demonstrated significant temporal variation. Highest and lowest concentrations were recorded during the winter ( $\bar{x}_{\text{PM}_{10}} = 23.7 \mu\text{g m}^{-3}$ ,  $\bar{x}_{\text{PM}_{2.5}} = 19.8 \mu\text{g m}^{-3}$ ) and summer ( $\bar{x}_{\text{PM}_{10}} = 9.1 \mu\text{g m}^{-3}$ ,  $\bar{x}_{\text{PM}_{2.5}} = 5.6 \mu\text{g m}^{-3}$ ) months, respectively. Analysis of the data collected continuously by the multi-wavelength aethalometer between December 2019 and November 2020 provided strong evidence of the temporal variability associated with equivalent black carbon concentration and composition in Enniscorthy, Co. Wexford. The highest concentrations of eBC were observed during the winter months. A mean wintertime eBC concentration of  $2.30 \mu\text{g m}^{-3}$  was determined, while a maximum hourly average of  $41.08 \mu\text{g m}^{-3}$  was recorded in December 2019. A combination of the prevalent emissions from solid fuel combustion for residential heating purposes and low temperatures with the potential to cause temperature inversions, particularly in the eveningtime, gave rise to the considerable levels of eBC measured during the winter period. Pollution dispersion was limited during periods of low wind speed. In contrast, summertime concentrations were significantly reduced; with levels below  $3.5 \mu\text{g m}^{-3}$  between June and August 2020.

A discernible diurnal pattern was observed in the concentrations of both  $\text{PM}_{2.5}$  and eBC. A strong evening peak was observed during the winter, spring and autumn seasons, attributed largely to solid fuel combustion, following source apportionment analysis which employed absorption Ångström exponent values of 0.9 and 1.68 for traffic-related and solid fuel combustion emissions. Little diurnal variation was observed during the summer months when a low level of  $\text{PM}_{2.5}$  and eBC was present consistently throughout the day. The AAE recorded by the aethalometer software provided an indication of the ambient aerosol composition. The seasonality associated

with the distribution of AAE was recognised; a broad distribution between 1 and 2 was observed over the course of the winter, while a narrow distribution with a mean value of 1.23 was obtained during the summer months. The distribution of AAE values recorded throughout the spring and autumn seasons was perhaps one of the most interesting findings of this campaign. A tri-modal distribution, suggestive of multiple contributing sources, was observed in spring ( $\bar{x} = 1.39$ ,  $\tilde{x} = 1.38$ ) and autumn ( $\bar{x} = 1.38$ ,  $\tilde{x} = 1.36$ ). The influence of combustion of various fuel types (e.g. coal, peat, wood) on the ambient aerosol was initially thought to be central to the observation, however a similar pattern was not observed during winter when solid fuel combustion was most prevalent. It is possible that anthropogenic activity indirectly influenced this unique AAE distribution by enhancing SOA production of biogenic origin.

Quartz fibre filter samples, collected throughout February 2020, were analysed using thermal-optical methods for the determination of total carbon content ( $0.4 \mu\text{g m}^{-3}$  –  $35.26 \mu\text{g m}^{-3}$ ). TC accounted for an average of 34.5% of  $\text{PM}_{2.5}$  during the sampling period. TC concentration was highest in samples collected between 15:00 and 23:00, corresponding to the time of day when solid fuel combustion was widespread. The contribution of organic carbon to TC was relatively consistent throughout the day; 80.96%, 81.18% and 86.77% in the morning, evening and nighttime, respectively. A comparison between the EC fraction of filter samples and optical eBC measurements was used to derive a MAC value representative of this location ( $9.48 \text{ m}^2 \text{ g}^{-1}$  at 880 nm). A complete seasonal assessment of carbonaceous aerosol requires sample collection throughout the year, with shorter sample collection intervals, would provide a clearer diurnal profile. In addition, detailed chemical analysis would afford a comprehensive evaluation of the temporal variability of dominant sources and the atmospheric processes influencing the ambient aerosol composition.

The Total Carbon Analyzer was employed in the continuous measurement of ambient total carbon for the duration of the measurement campaign. Similar to other parameters measured, the on-line measurement of total carbon demonstrated distinct temporal variability. TC concentrations were at a maximum during the winter ( $\bar{x} = 9.30 \mu\text{g m}^{-3}$ ), while the lowest concentrations were recorded during the summer months ( $\bar{x} = 1.68 \mu\text{g m}^{-3}$ ). A strong diurnal trend in TC was also observed, particularly in winter when a pronounced evening peak was detected, consistent with  $\text{PM}_{2.5}$  and eBC measurements. Despite reduced concentrations of TC in comparison to winter, similar diurnal profiles

were recorded in spring and autumn, however there was little diurnal variation throughout the summer.

The new ‘TC-BC’ method, developed by Rigler et al. (2020), was evaluated in the unique environment, dominated by solid fuel combustion emissions, and compared to conventional thermal-optical methods of determining elemental and organic carbon content. The lowest mean concentrations of eEC and eOC were recorded during the summer months, coinciding with the period when the mean eOC/eEC ratio was at a maximum. It is possible that the organic portion of the ambient aerosol was strongly influenced by SOA during the summer, leading to an increase in the ratio. It is also possible that the application of an incorrect value for  $b$ , the proportionality parameter, caused an overestimation of the OC fraction. A site-specific  $b$  value (0.71) was derived using the EC concentration determined using off-line thermal-optical methods. Application of the updated  $b$  value improved the accuracy of the on-line measurement of eEC, and increased the average eOC/eEC ratio. On-line measurement of TC at a high time resolution is extremely beneficial. Precise distinction of the eEC and eOC fractions requires application of an accurate value of  $b$ . It is therefore recommended that filter samples, both spatially and temporally representative, are simultaneously collected and analysed using conventional thermal-optical methods. The use of an accurate proportionality parameter is essential, particularly in an environment with considerable temporal variability in carbonaceous aerosol composition.

The results obtained during the winter period of the measurement campaign were compared with measurements previously recorded as part of the SAPPHIRE campaign (2015) and were also used to evaluate the effectiveness of the bituminous coal ban recently introduced in Enniscorthy. Examination of quantitative and qualitative components indicated changes in carbonaceous aerosol concentration and composition in the intervening years. The mean hourly average  $PM_{2.5}$  concentration has reduced from  $29.2 \mu\text{g m}^{-3}$  to  $20.6 \mu\text{g m}^{-3}$  between 2015 and 2020, and decreased further to  $11.6 \mu\text{g m}^{-3}$  in 2021. A similar decrease in mean hourly average eBC concentration was observed; from  $3.6 \mu\text{g m}^{-3}$  (2015) to  $2.4 \mu\text{g m}^{-3}$  (2020), however a similar range in minimum and maximum absolute values was detected. A strong diurnal pattern in both  $PM_{2.5}$  and eBC was observed during each measurement campaign; a considerable increase in eveningtime concentrations was attributed to solid fuel combustion emissions. Despite a significant decrease in absolute concentration between 2015

(mean hourly eBC =  $3.6 \mu\text{g m}^{-3}$ ) and 2021 (mean hourly eBC =  $1.1 \mu\text{g m}^{-3}$ ), the overall average contribution of eBC<sub>SF</sub> to total eBC remained relatively stable (range: 73% - 83%). Elemental and organic carbon content was determined by thermal-optical methods (Sunset OCEC Laboratory Instrument, Sunset Laboratory Inc.) and thermal methods (Total Carbon Analyzer, Magee Scientific). The mean concentration of both species decreased between 2015 and 2020. The OC/EC ratio determined during each campaign was also compared. Wenger et al. (2020) concluded that the OC/EC ratio of 4.0 calculated in 2015 was indicative of aerosol influenced by biomass and coal burning. The higher ratios calculated in 2020 (5.3 using the conventional thermal-optical method and 7.7 using the 'TC-BC' method) and 2021 (7.3) were suggestive of aerosol increasingly influenced by biomass burning. However, in the absence of a detailed chemical composition profile, it is difficult to determine whether the cause of this shift is due to a change in predominant sources impacting the ambient aerosol, or the variation in temperature protocols and methods of analysis. Initial results highlight the considerable reduction in mass concentration observed in Enniscorthy over the duration of the three winter periods, providing early indications of the positive effect of the 'Smoky Coal' ban. In order to assess the long-term effectiveness of this ban, continuous measurements are required, alongside interrogation of local sales figures of various solid fuels.

## **6. EFFECT OF COVID-19 RESTRICTIONS ON AMBIENT AIR QUALITY**

---

<b>6.1</b>	<b><i>COVID-19 (SARS-CoV-2) Pandemic</i></b> .....	<b>305</b>
<b>6.2</b>	<b><i>Particulate Matter</i></b> .....	<b>309</b>
6.2.1	Equivalent Black Carbon .....	313
6.2.2	Carbonaceous Aerosol .....	318
<b>6.3</b>	<b><i>Conclusions</i></b> .....	<b>320</b>

## 6.1 COVID-19 (SARS-CoV-2) PANDEMIC

---

Early 2020 saw an unprecedented event on a global scale. On December 31, 2019 cases of ‘viral pneumonia’ with unknown causes were reported by the Wuhan Municipal Health Commission in the People’s Republic of China. One month later, on January 30, 2020 the director of the WHO declared the outbreak a public health emergency of international concern. The novel coronavirus, named COVID-19, which caused severe respiratory illness began rapidly spreading globally. The first case of COVID-19 in the Republic of Ireland was reported on February 29. By March 11, 2020 the WHO had characterised COVID-19 as a pandemic, following alarming levels of transmission and severity of the disease. On the same day, the first death from COVID-19 was announced in Ireland.

In an effort to control the spread of this deadly virus, a number of measures were put in place, resulting in a total societal and economic shutdown worldwide. Interruptions to economic and industrial activity resulted in rapid improvements in air quality, in addition to a reduction in greenhouse gas emissions and a decrease in water and noise pollution (Elsaid et al., 2021; Kroll et al., 2020; Rume & Islam, 2020). Such significant improvements in air quality meant that the Himalayan mountains were visible from the Indian state of Punjab for the first time in decades. The usually murky canals in Venice, Italy ran clear due to the lack of boat traffic.

A significant improvement in air quality, associated with lockdown measures, has been documented globally. Considerable reductions in levels of NO<sub>2</sub> and PM were observed compared with levels in previous years (European Environment Agency; Gualtieri et al., 2020; Menut et al., 2020; Wang et al., 2020), as large as 63% (Wuhan, China) and 61% (Berlin, Germany) (Habibi et al., 2020). Figure 6.1 illustrates that significant decrease in NO<sub>2</sub> concentrations in major cities in Europe, measured by the Copernicus Sentinel-5P satellite. Owing to the significant contributions of traffic emissions to ambient air pollution, a reduction in mass concentration was inevitable with such considerable reduction in the number of vehicles on the roads. In the UK there was a 69% reduction in overall traffic counts during lockdown periods. Reductions in NO<sub>2</sub> (38.3%) and PM<sub>2.5</sub> (16.5%) were identified from measurements at 129 monitoring stations compared with measurements from the same period in previous years (Jephcote et al., 2021). A decrease of up to 50% in traffic occurred in parts of

California, USA. Correspondingly, reduced concentrations of  $\text{NO}_2$  and  $\text{PM}_{2.5}$  were observed, compared with measurements recorded during the same period of the previous five years (Parker et al., 2020). Evangeliou et al. (2021) estimated an average 11% reduction in ambient BC concentration across Europe as a result of strict COVID-19 lockdowns, with countries most severely impacted by the disease experiencing the most dramatic decrease in BC levels, most notably in France (42%), Germany (21%) and UK (13%).

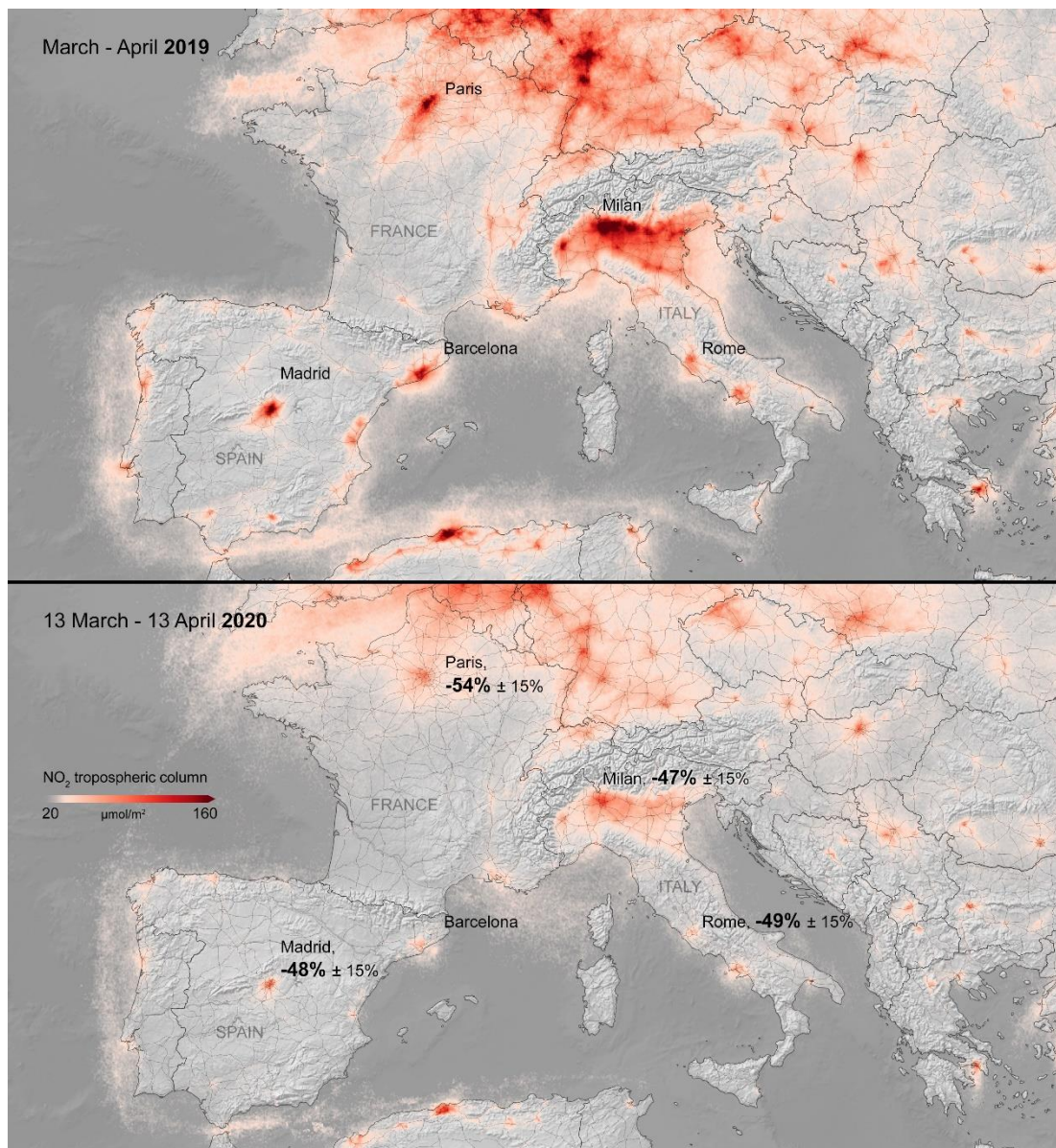


**Figure 6.1**  $\text{NO}_2$  concentration over major European cities. Image contains modified Copernicus Sentinel data (2019-20), processed by KNMI/ESA (ESA, 2020).

In order to limit the spread of the virus in Ireland, schools, colleges and childcare facilities were closed on March 12, and by March 27 the public was ordered to stay at home and travel was permitted within 2 km of homes, with the exception of essential workers (medical, supermarkets, transport). These public health restrictions remained in place until May 18, when the permitted radius from home was extended to 5 km. By June 2020, intercounty travel within the Republic of Ireland was reinstated. With case numbers rapidly increasing during the Autumn, nationwide restrictions were reintroduced, limiting travel to within 5 km of homes, on October 21 for a period of six weeks. Intercounty travel was allowed for the Christmas period from December 18. Large social gatherings, in addition to the evolution of the Alpha variant, first documented in the United Kingdom in September 2020 (World Health Organization, 2021a), led to a rapid increase in case numbers and forced public health experts to advise a nationwide ‘Level 5’ lockdown from December 24, 2020. The third wave of COVID-19 peaked in Ireland in January 2021, with the announcement of 8,248 new cases on January 8, as shown in Figure 6.2.

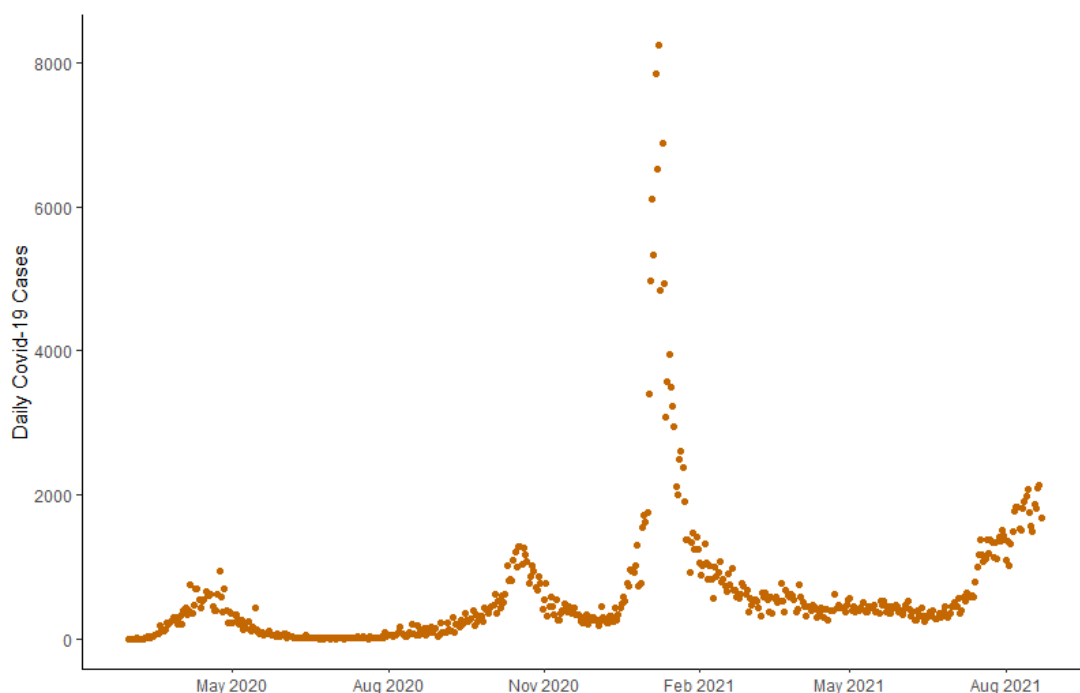


**Figure 6.2** Number of new COVID-19 cases reported daily in the Republic of Ireland by the Health Service Executive (February 2020 - August 2021). Data was obtained from the Health Protection Surveillance Centre (HPSC, 2021).

Public health advice to work from home where possible, in addition to the restrictions on travel limited to 2 km and 5 km, respectively, beyond the home, resulted in a considerable decrease in traffic volumes. Significant reductions in traffic volumes were observed on all major roadways during lockdown periods, including on the M11 (Enniscorthy), as shown in Figure 6.3, M50 (Dublin) and N40 (Cork). The most notable reduction was observed during the first lockdown (March 27 – May 18, 2020) as the pandemic took hold in Ireland. This open access data was obtained from the Transport Infrastructure Ireland (TII, 2021).

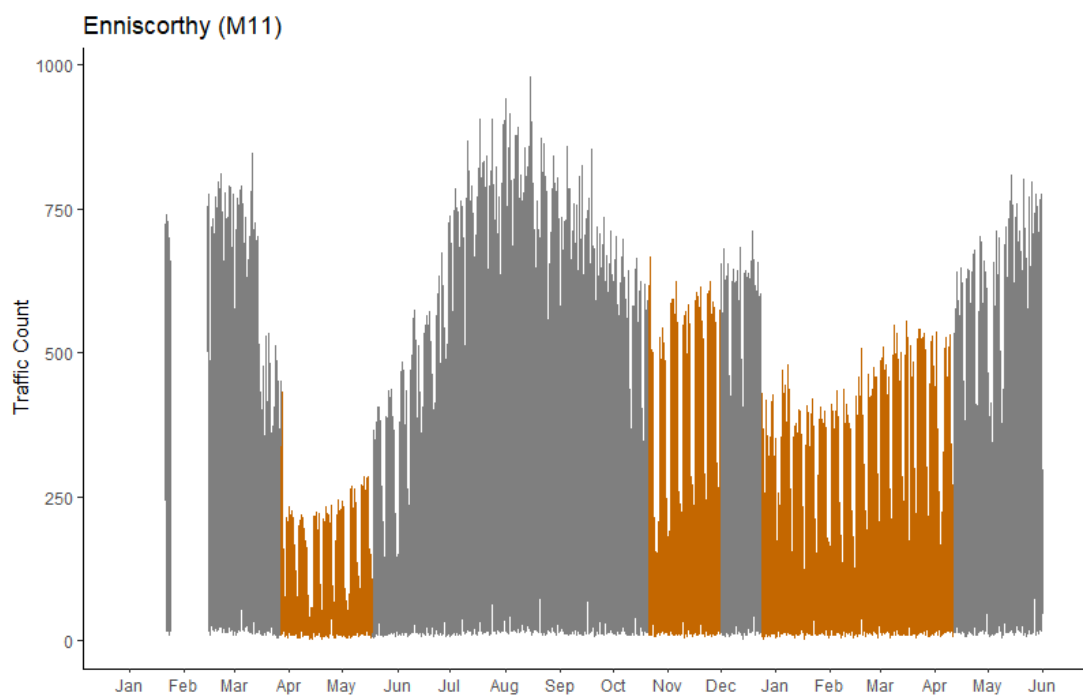


**Figure 6.3** Temporal profile of hourly traffic counts on the M11 (Enniscorthy) between January 2020 and May 2021. COVID-19 lockdown periods are highlighted in orange.

## 6.2 PARTICULATE MATTER

As outlined in Chapter 5, PM mass concentrations have been decreasing in Enniscorthy in the past number of years. It is difficult to determine whether any decrease in  $PM_{2.5}$  was due to a pattern of gradual decrease, the impact of restrictions introduced to reduce transmission of COVID-19 or following the extension of the ban on the sale of bituminous coal to include Enniscorthy in September 2020. Figure 6.4 shows the range and mean monthly concentrations of  $PM_{2.5}$  recorded in Enniscorthy between May 2018 and May 2021.

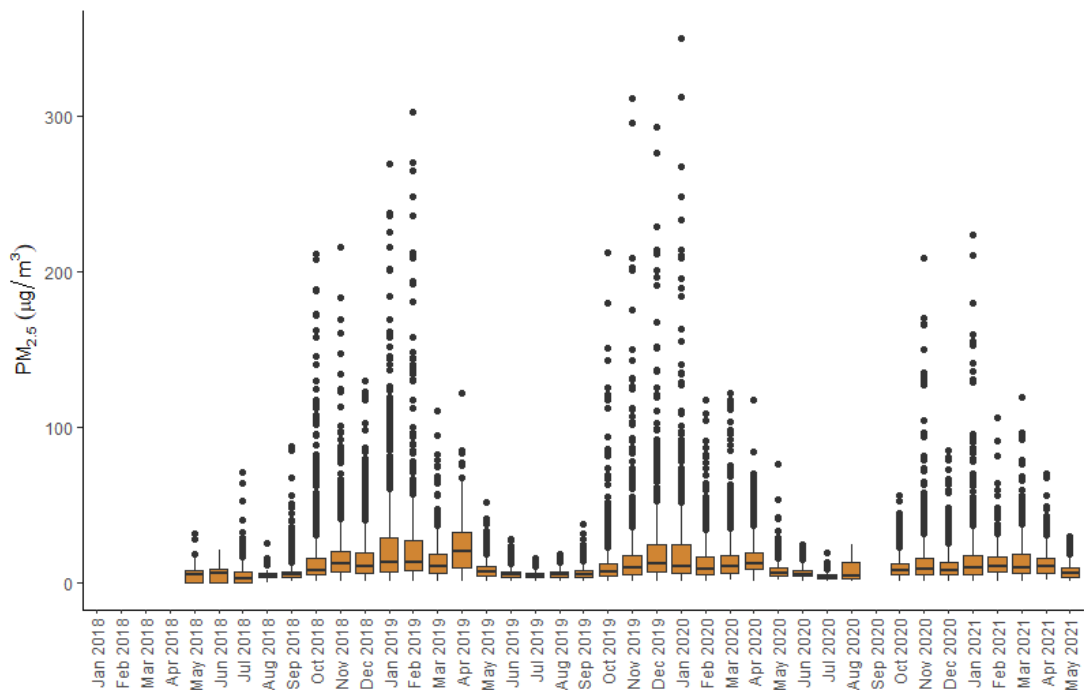


**Figure 6.4** Distribution of  $PM_{2.5}$  measured in Enniscorthy (May 2018 - May 2021).

A direct comparison of particulate matter from year to year does not take into account meteorological differences, which are known to have a major impact on air pollution. Therefore, weather normalisation was performed to accurately investigate the effect of the COVID-19 restrictions on ambient air quality. Measurements of  $PM_{2.5}$  recorded in Enniscorthy in 2018 and 2019 were used to train a random forest model. This model normalised data for meteorological conditions and subsequently predicted the daily concentration of  $PM_{2.5}$  in a business-as-usual scenario, i.e. if lockdown measures had not been implemented. The *rmweather* R package (version 0.1.51) was used for this

process (Grange & Carslaw, 2019; Grange et al., 2018). The predicted and observed concentrations were compared (Figure 6.6). Prior to the introduction of COVID-19 restrictions (01/01/2020 – 27/03/2020) the predicted and observed levels of PM<sub>2.5</sub> were in agreement. The observed concentrations deviated from the predictions following the implementation of public health restrictions. The severity of restrictions varied throughout 2020 and 2021. This was reflected in the inconsistency in predicted and observed concentrations of PM<sub>2.5</sub> in Enniscorthy. On average, the restrictions resulted in a significant reduction (37%) in PM<sub>2.5</sub> mass concentration during lockdown periods.

Calculating the cumulative sum (CUSUM), first described by Page (1954), is a sequential analysis technique, typically used in statistical quality control to monitor change detection. It allows for the detection of small shifts by calculating the cumulative sums of deviations from the target value. In this case, it is used to highlight the decrease in mass concentration from the predicted values as a consequence of the public health restrictions. The mean distribution of the cumulative difference between predicted versus observed concentrations of PM<sub>2.5</sub> prior to implementation of public health restrictions indicated that the model was a good fit (Figure 6.5). The bias was emphasised during lockdown periods, when observed concentrations varied from those predicted by the model. As the situation briefly returned to business-as-usual between the first and second lockdown periods, the curve exhibited a marked plateau. Similarly, a significant reduction in NO<sub>2</sub> in comparison to previous years, associated with traffic emissions, was observed at several monitoring stations in Ireland (EPA, 2021). Despite uncertainties associated with the overall reduction in acute hospital admissions during the period due to increased pressure on the health system and widespread fear of infection, Quintyne et al. (2021) concluded that the reduction in ambient NO<sub>2</sub> due to transport restrictions was associated with a reduction in hospital admissions for respiratory system diseases in Dublin city and county.



**Figure 6.5** Cumulative difference in predicted versus observed PM<sub>2.5</sub> concentrations in Enniscorthy during COVID-19 lockdown periods which are highlighted in orange.

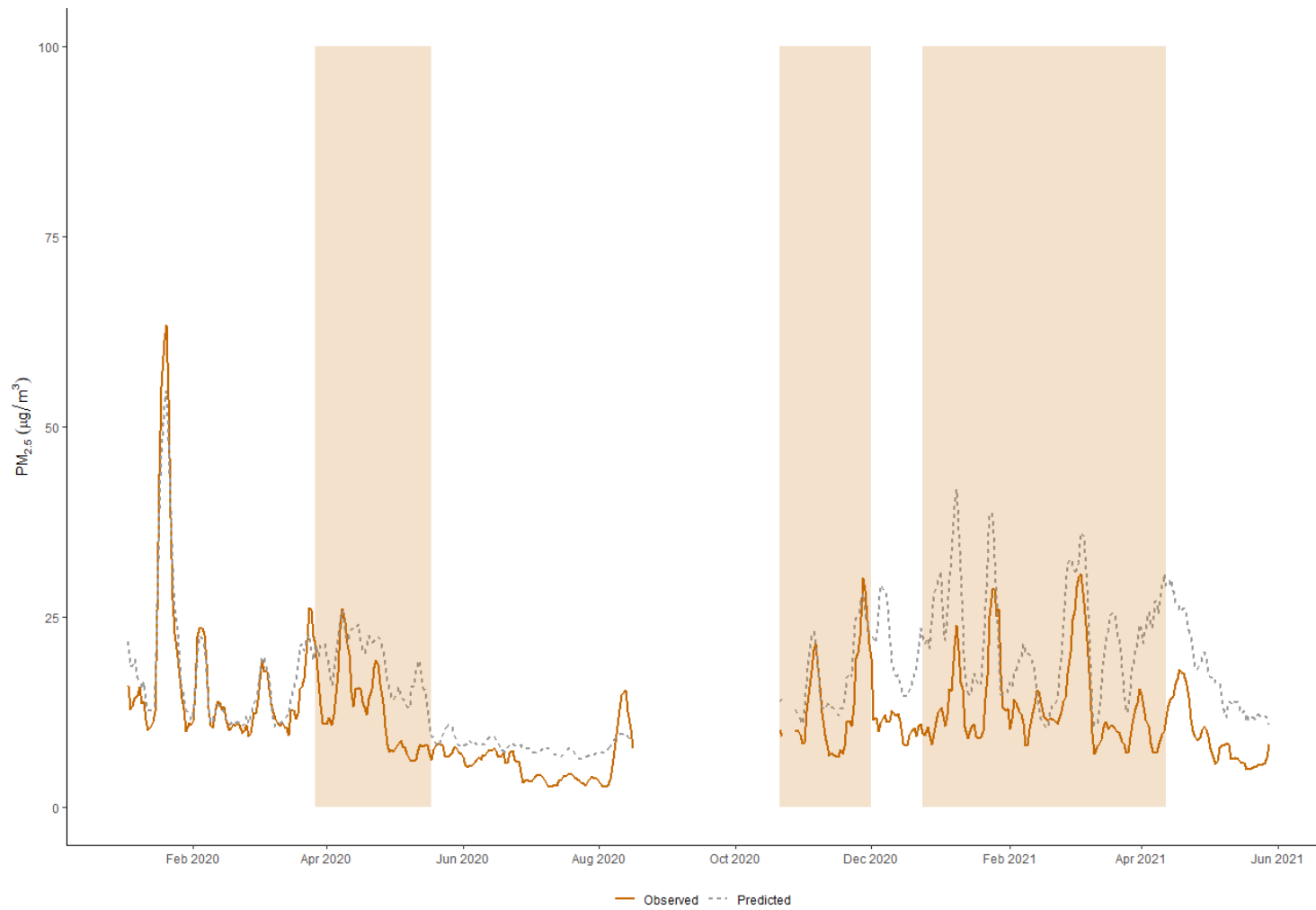


**Figure 6.6** Rolling average (5 days) of daily levels of PM<sub>2.5</sub> in Enniscorthy; predicted versus observed, between January 2020 and June 2021.

## 6.2.1 Equivalent Black Carbon

There was no obvious decrease in equivalent black carbon concentration measured in Enniscorthy following the introduction of COVID-19 restrictions. The levels appeared to follow a typical seasonal trend; decreasing equivalent black carbon concentrations in spring due to warmer weather, resulting in reduced demand for solid fuel burning in domestic heating. An increase in eBC was observed in autumn and winter, however these concentrations do not reach similar high levels observed the previous winter. It is difficult to determine whether this decrease is associated with the implementation of COVID-19 restrictions, the extension of the ‘Smoky Coal’ ban to include Enniscorthy, or an overall reduction in solid fuel combustion for domestic heating in the locality.

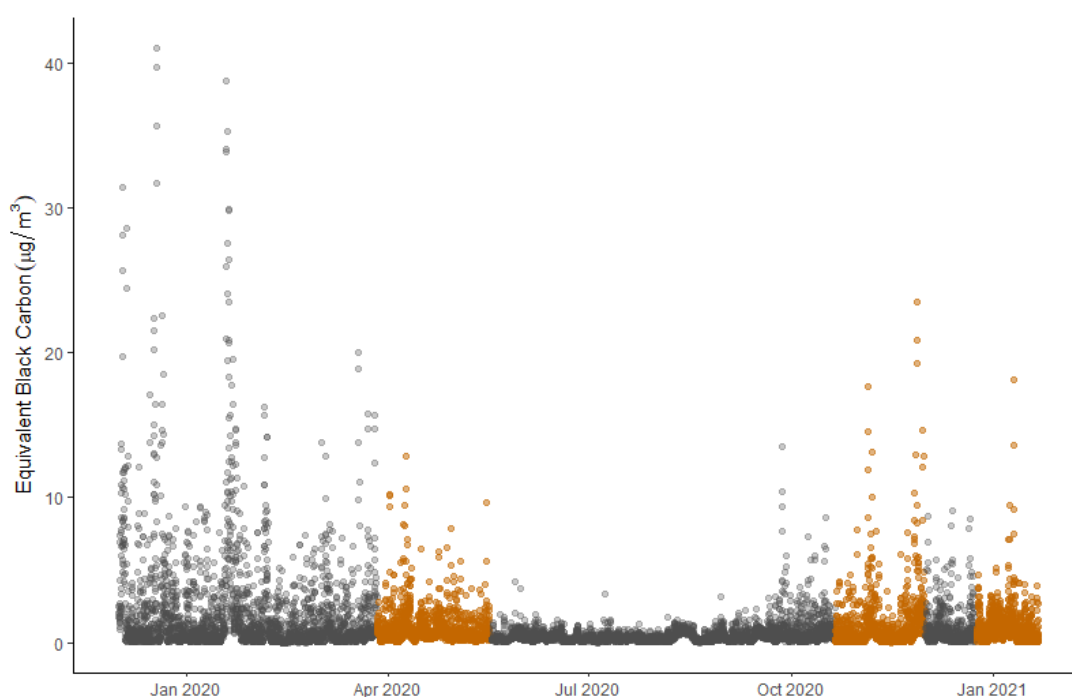


**Figure 6.7** Temporal profile of hourly average eBC concentration measured in Enniscorthy (December 2019 - January 2021). COVID-19 lockdown periods are highlighted in orange.

Application of the Zotter parameters,  $\alpha_{SF} = 1.68$  and  $\alpha_{Tr} = 0.9$ , allowed for the source apportionment of solid fuel combustion and traffic-related emissions of the total eBC measured. As anticipated, seasonal variation was observed in the contributions from each main fuel source; solid fuel burning related emissions were dominant during the winter months, while traffic-related emissions were the largest contributor during the

warmer, summer months (Figure 6.8). Seasonal variation in the source apportionment of eBC was likely, regardless of the implementation of COVID-19 restrictions. Without long term measurement of eBC at this monitoring site, the degree to which the contribution of each source was influenced by the imposed restrictions cannot be confirmed. However, an obvious interruption to the typical trend of decreasing contributions from eBC<sub>SF</sub> to total eBC between December and July was not detected. Similarly, there was no significant variation in contributions from traffic-related emissions to total eBC that can assuredly be attributed to the restrictions.

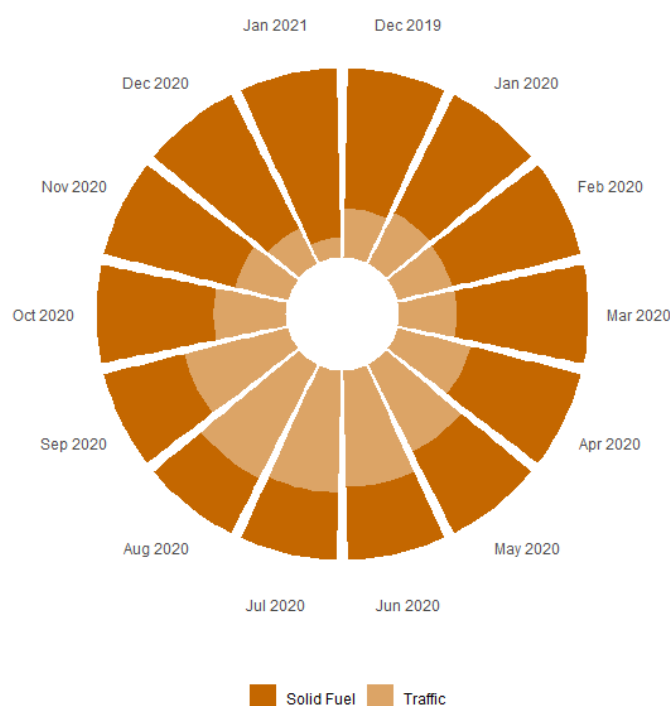


**Figure 6.8** Monthly source apportionment of total ambient eBC measured in Enniscorthy (December 2019 - January 2021).

The diurnal pattern of eBC<sub>Tr</sub> was investigated during periods with and without COVID-19 restrictions, showing little variation (Figure 6.9). Considering the dramatic reduction in traffic volume (Figure 6.3), the absence of significant changes to levels of eBC<sub>Tr</sub> is indicative of the minor role of traffic-related emissions in this environment. The AAE recorded in Enniscorthy was also examined for ‘normal’ periods during spring and autumn 2020 and when COVID-19 restrictions were in place. There was little variation in the mean AAE recorded which suggests that the restrictions did not

have a strong influence on the ambient aerosol composition. A narrow range of AAE values were observed during the spring lockdown (March 27 – May 17, 2020), in comparison to periods throughout the season without restrictions (March 1 – March 26 and May 18 – May 31, 2020). This was likely due to a decrease in solid fuel combustion for residential heating owing to the time of year. The opposite is true in autumn, when restrictions introduced in late autumn (October 21, 2020) presumably coincided with increased solid fuel burning as the ambient temperature decreased. These results further emphasise the strong impact of solid fuel combustion in the locality and the negative implications for ambient air quality.

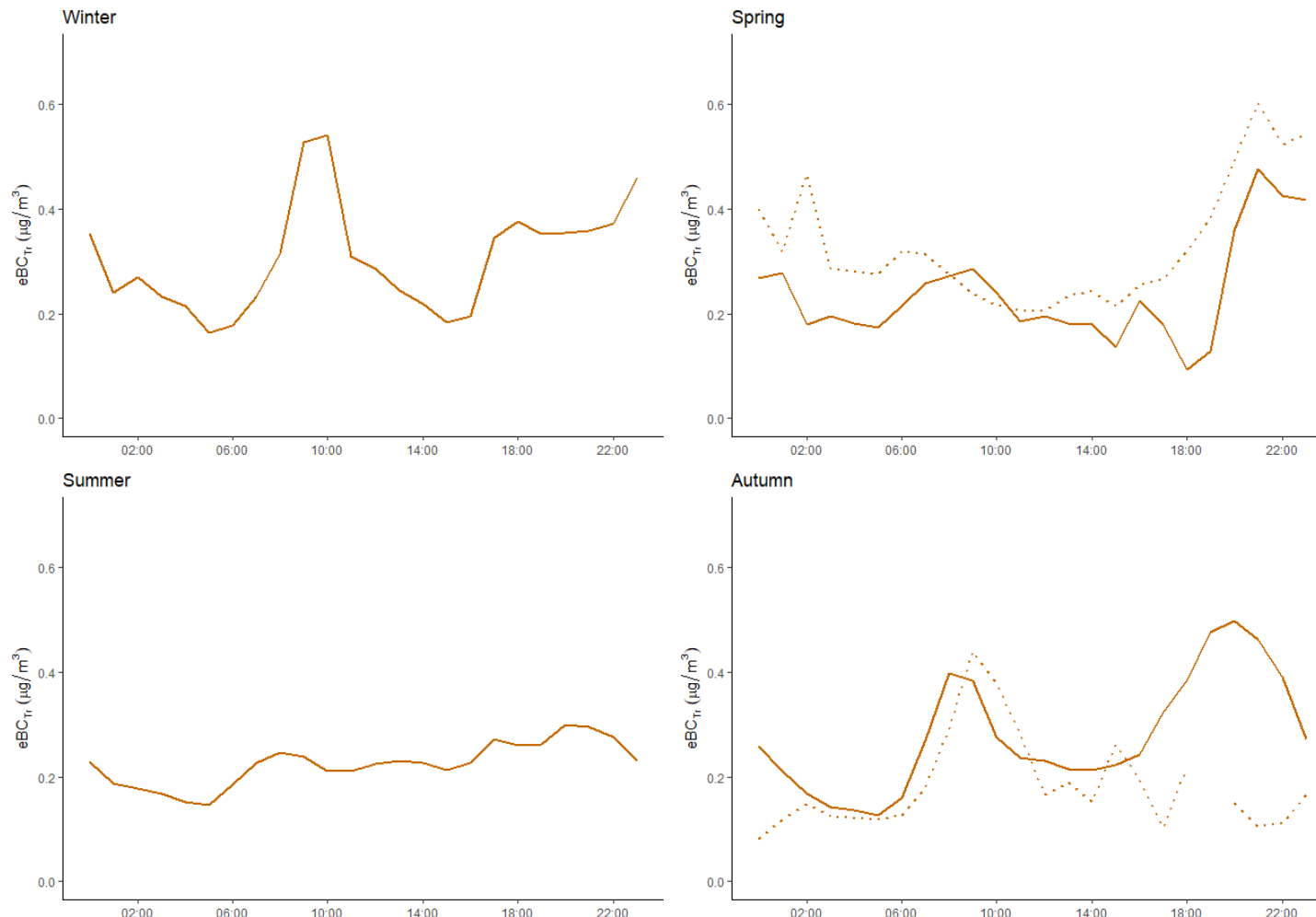


**Figure 6.9** Diurnal profiles of  $eBC_{Tr}$  recorded in Enniscorthy during lockdown (dashed line) and business as usual (solid line) scenarios (December 2019 - November 2020).

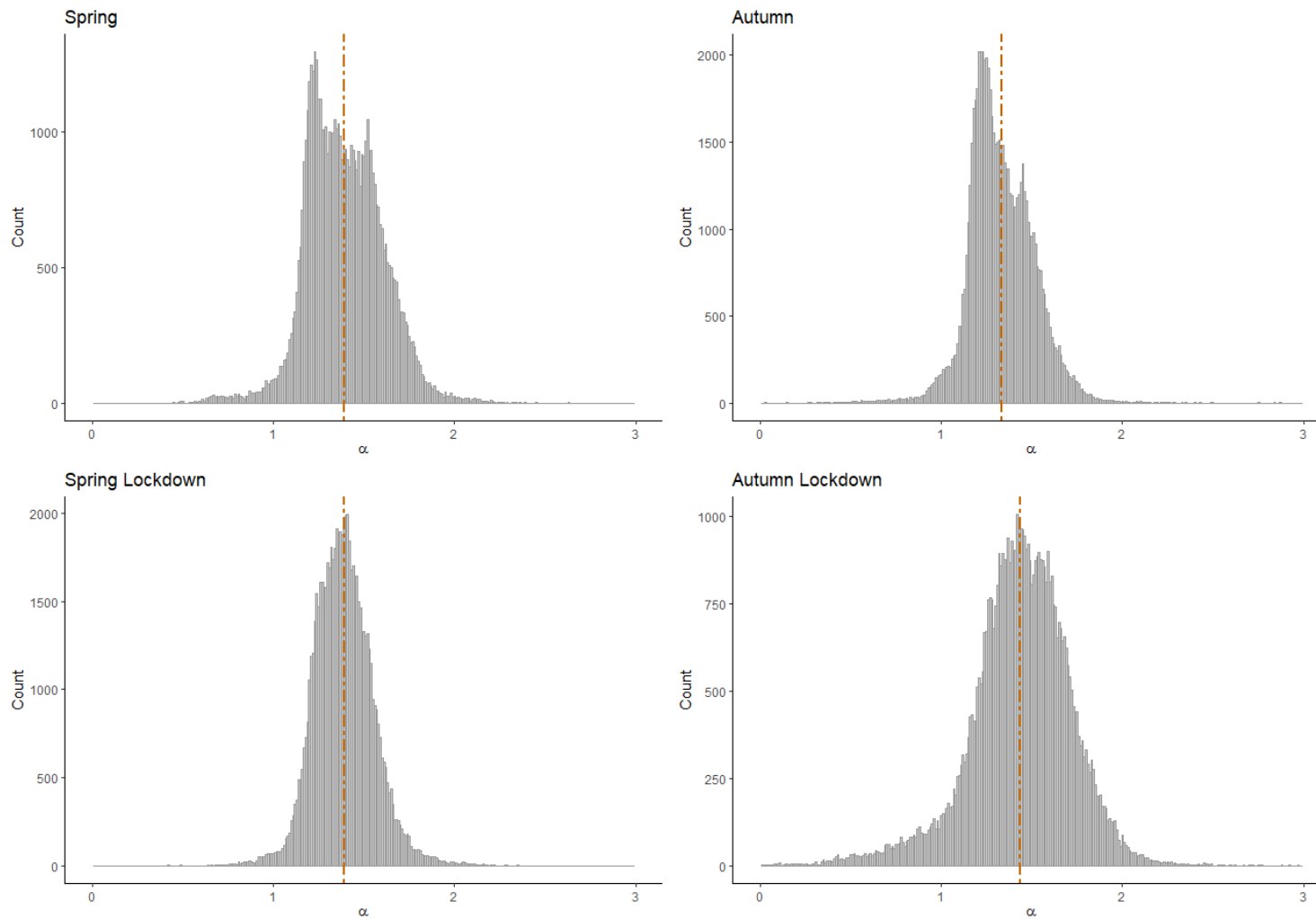


**Figure 6.10** Frequency distribution of AAE recorded in Enniscorthy in spring and autumn 2020, during normal and lockdown periods.

## 6.2.2 Carbonaceous Aerosol

Total carbon was measured in Enniscorthy throughout the various levels of restrictions using a Total Carbon Analyzer (TCA-08, Magee Scientific). Similar to the equivalent black carbon trends observed, the total ambient carbon appears to follow a typical seasonal trend in an environment dominated by solid fuel burning; maximum and minimum concentrations throughout winter and summer months, respectively.

Due to the longevity of the lockdown periods, it is difficult to compare the lockdown measurements with mean seasonal measurements without long term records of total carbon concentration at this monitoring site. Table 6.1 provides a summary of the mean concentrations of TC, eEC and eOC measured throughout each season (December 2019 – November 2020) and during each lockdown period. The ratio of organic to equivalent elemental carbon (eOC/eEC) is also included. Mean seasonal values obtained for spring and autumn include measurements recorded during the first (March 27 – May 17, 2020) and second (October 21 – December 1, 2020) lockdown periods. In general, there is little difference in mean values recorded during each lockdown period and the corresponding seasonal mean.

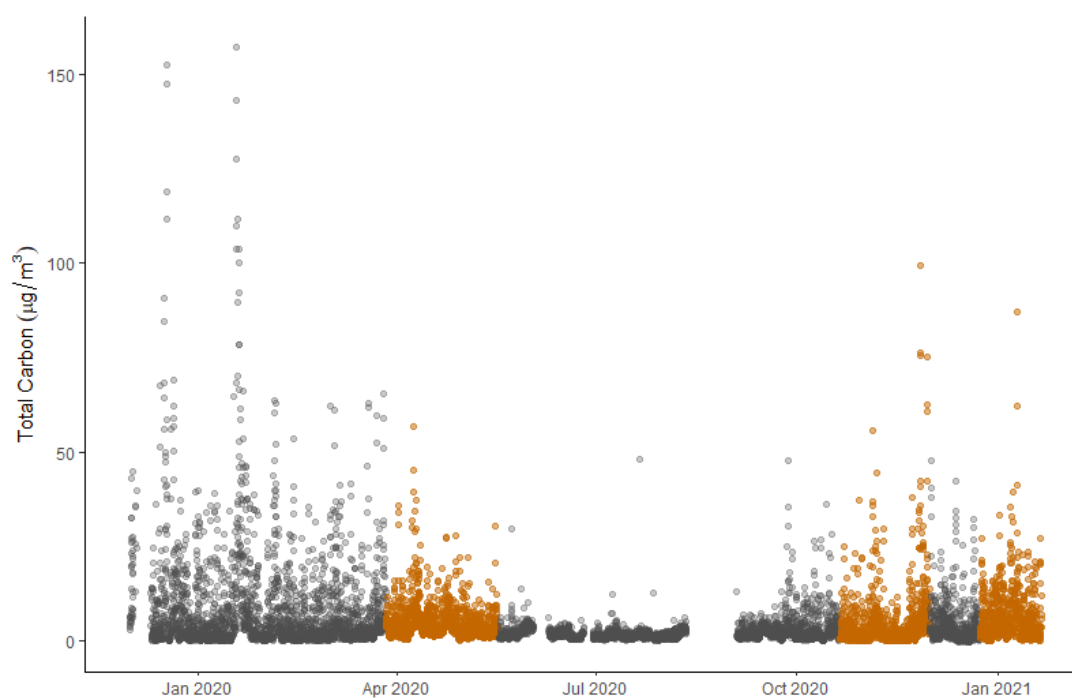


**Figure 6.11** Temporal profile of hourly TC concentration measured in Enniscorthy (December 2019 - January 2021). COVID-19 lockdown periods are highlighted in orange.

**Table 6.1** Comparison of mean seasonal TC, eEC and eOC concentration measured in Enniscorthy between December 2019 and November 2020 and during each lockdown period. Site-specific proportionality factor ( $b = 0.71$ ) was employed for eEC and eOC determination.

	Dates	TC ( $\mu\text{g m}^{-3}$ )	eEC ( $\mu\text{g m}^{-3}$ )	eOC ( $\mu\text{g m}^{-3}$ )	eOC/eEC
Winter	01/12/2019 – 29/02/2020	9.30	1.73	7.57	6.10
Spring	01/03/2020 – 31/05/2020	5.34	0.77	4.57	8.64
<b>Lockdown 1</b>	<b>27/03/2020 – 17/05/2020</b>	<b>5.06</b>	<b>0.72</b>	<b>4.34</b>	<b>8.83</b>
Summer	01/06/2020 – 31/08/2020	1.68	0.23	1.45	8.55
Autumn	01/09/2020 – 30/11/2020	4.09	0.72	3.37	6.53
<b>Lockdown 2</b>	<b>21/10/2020 – 30/11/2020</b>	<b>5.09</b>	<b>0.91</b>	<b>4.19</b>	<b>6.45</b>
<b>Lockdown 3</b>	<b>24/12/2020 – 20/01/2021</b>	<b>6.75</b>	<b>0.87</b>	<b>5.88</b>	<b>8.70</b>
<b>Lockdown 3</b>	<b>21/01/2021 – 12/04/2021</b>	<b>ND</b>	<b>ND</b>	<b>ND</b>	<b>ND</b>

### 6.3 CONCLUSIONS

---

Seasonal variance influenced pollutant concentrations throughout the sampling period in Enniscorthy, Co. Wexford. In line with studies carried out across the globe of several air pollutants, according to the model predicting levels based on previous years, the introduction of public health measures to limit the spread of COVID-19 resulted in a 37% reduction in concentration of PM<sub>2.5</sub>, on average, in Enniscorthy. Without long term measurements of equivalent black carbon or total carbon, it is difficult to assess the effect that the lockdown measures had on the ambient pollutant concentration by modelling a ‘business-as-usual’ scenario at this location. However, dramatic reductions in equivalent black carbon and total carbon coinciding with public health restrictions were not observed in Enniscorthy. Source apportionment analysis yielded predictable results, largely influenced by seasonal variation. Considering the dramatic reduction in traffic volumes in the locality, little change in total eBC and eBC<sub>Tr</sub> concentration was indicative of the prevalence of solid fuel combustion and the dominance of this source in its contribution to total ambient black carbon. Traffic-related emissions evidently have little impact on the ambient levels of equivalent black carbon in Enniscorthy compared to solid fuel burning for home heating.

## 7. SUMMARY AND PERSPECTIVES

---

<b>7.1</b>	<b><i>Summary</i></b> .....	<b>322</b>
7.1.1	Spatial Variability .....	322
7.1.2	Temporal Variability .....	327
<b>7.2</b>	<b><i>Perspectives</i></b> .....	<b>331</b>

## 7.1 SUMMARY

---

Long-term measurements of ambient carbonaceous aerosol were recorded at several unique monitoring locations around Ireland over the course of this research, including regional and urban background, coastal, residential and roadside sites. The multi-wavelength aethalometer provided real-time information concerning the optical properties of the ambient aerosol and allowed for the determination of equivalent black carbon concentration. Source apportionment analysis ensued with the application of absorption Ångström exponents ( $\alpha$ ) proposed by Zotter et al. (2017). In order to account for the complex, multi-fuel environment, the absorption exponents were used to discriminate between traffic and solid fuel combustion related emissions, rather than traffic and wood burning emissions, as is common in Europe. The source apportionment analysis resulted in the identification of major sources contributing to total equivalent black carbon concentrations at each location. Off-line techniques were used to analyse quartz filter samples collected as part of wintertime measurement campaigns. Thermal-optical methods were employed in the quantification of total, elemental and organic carbon content, while evaluation of the biomass burning tracer levoglucosan involved an anion-exchange chromatographic method.

Off-line measurements of elemental and organic carbon allowed for an estimation of site-specific OC/EC ratios, indicative of the influence of biomass and fossil fuel burning sources. Site-specific mass absorption cross-section values ( $\text{m}^2 \text{g}^{-1}$ ) were determined through the correlation of thermally derived elemental carbon and optically derived equivalent black carbon. The concentration of the molecular marker compound levoglucosan, primarily associated with biomass combustion, was assessed and compared with corresponding aethalometer measurements and source apportionment output.

### 7.1.1 Spatial Variability

---

A summary of the absolute concentrations of equivalent black carbon, elemental carbon, organic carbon and levoglucosan measured during winter (December, January and February) over the course of three years (2017 – 2020) at each monitoring site are provided in Table 7.1.

Measurements were made at three regional background sites; Carnsore Point (CP), Mace Head (MHD) and Malin Head (MLN), and an urban background site at University College Dublin (UCD), between December 2017 and February 2018, inclusive. The highest concentrations of each species measured were observed at UCD, located in a predominantly residential area of Dublin. Source apportionment of data analysis of eBC measurements collected by the aethalometer indicated that traffic-related emissions contributed a high percentage of the total equivalent black carbon concentration at Carnsore Point (83.6%), Malin Head (69.7%) and University College Dublin (59.5%) measured each month over the course of the wintertime field campaign.

Subsequent campaigns at Pearse Street, Dublin and Enniscorthy, Co. Wexford provided further insights into the spatial variability of ambient carbonaceous aerosol at urban roadside and rural town/residential locations, respectively. As anticipated, high levels of eBC were observed at Pearse Street, where instruments were deployed adjacent to a busy roadside that experienced a consistently high volume of traffic. Source apportionment analysis indicated that traffic-related emissions accounted for 74% of the total eBC, on average throughout the winter. In contrast, solid fuel combustion related emissions accounted for 72% of the total eBC recorded in Enniscorthy during the winter months. Over the course of the winter sampling period the absorption Ångström exponent recorded by the aethalometer varied with location. At regional background and predominantly residential urban sites, a broad bi-modal distribution was observed, indicative of multiple sources contributing to ambient aerosol. A narrow distribution, with mean and median values of 1.14 and 1.12 were observed at Pearse Street, confirming traffic-related emissions as the major source at this site.

Ambient elemental, organic and total carbon concentration was determined through thermal-optical analysis of quartz filter samples. Mean EC and OC concentrations were low at the regional background sites (CP, MHD, MLN). Highest average concentrations of EC and OC were recorded at Pearse Street ( $3.11 \mu\text{g m}^{-3}$ ) and Enniscorthy ( $4.95 \mu\text{g m}^{-3}$ ), respectively. Differing sampling periods must be considered when comparing the parameters. OC/EC ratios, indicative of the dominant fuel type, demonstrated spatial variability. The ratio determined for all sites, with the exception of Pearse Street, were suggestive of environments dominated by biomass

burning emissions. In general, thermally derived EC correlated well with the on-line measurement of eBC and allowed for determination of site-specific MAC values which ranged from 6.96 m<sup>2</sup> g<sup>-1</sup> (Mace Head) to 12.64 m<sup>2</sup> g<sup>-1</sup> (University College Dublin) at 880 nm. The spatial variability of the MAC value reflected the local characteristics of ambient aerosol. The thermal-optical method of determining EC concentration presumably provides the same value regardless of the molecular composition. Oftentimes EC consists of carbon ring structures which can incorporate impurities, and thus impact the absorption properties.

Ambient concentrations of levoglucosan, mannosan and galactosan were determined using anion-exchange chromatographic methods. High levels of levoglucosan recorded at each of the background sites, particularly Carnsore Point ( $\bar{x} = 40.3 \text{ ng m}^{-3}$ ) and Malin Head ( $\bar{x} = 43.4 \text{ ng m}^{-3}$ ), indicate significant solid fuel usage. The mean concentrations measured in central (Pearse Street) and suburban (University College Dublin) Dublin were comparable to mean concentrations recorded in London (Fuller et al., 2014). Levoglucosan concentrations were well correlated with eBC<sub>SF</sub> at most sites, particularly Carnsore Point, Malin Head and Pearse Street ( $r^2 \geq 0.8$ ).

In locations where absolute concentrations were extremely low (regional background sites, particularly Mace Head), it is difficult to assess the accuracy of the aethalometer model. Mean hourly average eBC concentrations of 0.27  $\mu\text{g m}^{-3}$ , 0.12  $\mu\text{g m}^{-3}$  and 0.28  $\mu\text{g m}^{-3}$  were measured at Carnsore Point, Mace Head and Malin Head, respectively, between December 2017 and February 2018. Source apportionment analysis employed an AAE pair of 0.9 and 1.68 for traffic and solid fuel combustion related emissions. The model estimated traffic-related contributions accounted for, on average, 84% and 70% of the total eBC measured at Carnsore Point and Malin Head, respectively. In such sparsely populated areas, it is unlikely that such a large portion of the total eBC should be attributed to traffic emissions. In coastal locations, there is the possibility of influence from shipping emissions, but more likely, is the impact of coal combustion on ambient conditions. Future research including detailed analysis of the aerosol composition, using instruments such as an ATOFMS or ACSM, would provide additional data required to accurately assess the appropriateness of the aethalometer model, and AAE values, in such environments.

The highest concentration of all species measured were recorded in populated locations; University College Dublin, Pearse Street and Enniscorthy. As reported by numerous previous studies, aerosol composition can vary widely from region to region. Within these populous areas, source contribution can vary; traffic-related emissions were the dominant source at both sampling sites in Dublin, while solid fuel combustion was the major contributor to ambient equivalent black carbon measured in Enniscorthy. This research has highlighted the spatial variability of carbonaceous aerosol, specifically black carbon, and the significant influence from anthropogenic activity, common to all locations.

**Table 7.1** Range and mean hourly average eBC concentrations recorded at each monitoring site during wintertime. Range and mean concentrations of TC and levoglucosan are also provided. The sampling period of the measurements are outlined in the relevant chapters.

		eBC ( $\mu\text{g m}^{-3}$ )		TC ( $\mu\text{g m}^{-3}$ )		Levoglucosan ( $\text{ng m}^{-3}$ )	
		<i>Mean</i>	<i>Range</i>	<i>Mean</i>	<i>Range</i>	<i>Mean</i>	<i>Range</i>
<b>Carnsore Point</b>	Regional background	0.27	0.0 - 5.36	1.38	0.26 – 4.78	40.3	2.6 - 149.3
<b>Mace Head</b>	Regional background	0.12	0.0 - 2.97	0.45	0.06 – 1.87	15.2	0.5 - 37.8
<b>Malin Head</b>	Regional background	0.28	0.0 - 4.10	1.99	0.18 – 5.55	43.4	0.8 - 151.7
<b>University College Dublin</b>	Urban background	0.80	0.0 - 17.18	3.54	0.87 – 16.64	149.3	33.1 - 1090.1
<b>Pearse Street</b>	Urban roadside	4.88	0.2 - 27.58	7.56	2.43 – 18.36	173.8	15.5 - 877.7
<b>Enniscorthy</b>	Rural town	2.30	0.0 - 41.08	6.14	0.45 – 35.26	-	-

### 7.1.2 Temporal Variability

---

Long-term monitoring campaigns at University College Dublin (September 2017 – August 2018), Pearse Street (September 2018 – August 2019) and Enniscorthy (December 2019 – November 2020) revealed a distinct temporal variability associated with equivalent black carbon concentrations. There was a substantial difference in eBC levels measured in summer and winter, particularly in locations strongly influenced by solid fuel combustion. Maximum hourly average concentrations of eBC were recorded during the winter at University College Dublin ( $17.18 \mu\text{g m}^{-3}$ ) and Enniscorthy ( $41.08 \mu\text{g m}^{-3}$ ), while the highest level of eBC at Pearse Street ( $38.76 \mu\text{g m}^{-3}$ ) was recorded during the autumn. The lowest mean concentrations were recorded during the summer at all three sampling sites. Concentrations were assumed to be exacerbated due to limited pollution dispersion caused by a low boundary layer during the winter months. Inefficient pollution dispersion was also observed during periods of low wind speed at each location. The mean concentrations of eBC measured in Enniscorthy ( $2.30 \mu\text{g m}^{-3}$ ), a small rural town, were significantly higher than those measured in a large suburban area of Dublin ( $0.78 \mu\text{g m}^{-3}$ ) over a similar time period during the winter months, likely due to enhanced emissions from solid fuel combustion for domestic heating. A summary of the seasonal eBC concentrations recorded is provided in Table 7.2.

Strong diurnal trends were observed at each location and exhibited seasonal variability. There was little diurnal variation in eBC concentrations during the summer months at sampling sites located at University College Dublin and Enniscorthy. Modest diurnal variation was observed on weekdays (Monday – Friday) at Pearse Street, where relatively low concentrations were recorded during the summer months ( $\bar{x} = 2.17 \mu\text{g m}^{-3}$ ). Levels of eBC began to increase from 06:00, consistent with morning rush hour, and remained reasonably constant throughout the day until 19:00, when concentrations began to decrease. However, little variation was detected in eBC concentration over the weekend (Saturday – Sunday) at this location throughout the summer period. There was relatively no difference between weekday and weekend diurnal profiles observed at University College Dublin and Enniscorthy during the summer months. In contrast, the wintertime measurements exhibited considerable diurnal variation at each sampling location. Strong morning and eveningtime peaks were observed and attributed to traffic and solid fuel combustion emissions, respectively, at

predominantly residential sites; University College Dublin and Enniscorthy. Compared to the average weekday profile, the morning 'traffic peak' is reduced and delayed at the weekend in both locations. The wintertime concentrations measured at Pearse Street follow a similar diurnal pattern, a strong morning and evening peak, however both peaks were largely attributed to increased volumes of traffic at these times. Although it is not considered a dominant source of black carbon at Pearse Street, there is undoubtedly some influence from background solid fuel combustion emissions.

Source apportionment analysis was used to evaluate the seasonal variability of dominant sources at each location. Traffic-related emissions accounted for 73%, 80% and 65% of total eBC measured at University College Dublin (urban background), Pearse Street (urban roadside) and Enniscorthy (small, rural town), respectively, during the summer months. Despite an overall reduction in percentage contribution, traffic remained the major contributor to ambient levels in the winter at University College Dublin (60%) and Pearse Street (74%), while solid fuel combustion emissions were identified as the dominant source of eBC in Enniscorthy during the winter (72%).

The AAE measured by the aethalometer were also indicative of aerosol composition and contributing sources. Little temporal variation was observed in the distribution of AAE recorded at Pearse Street. The narrow distribution was suggestive of a single dominant source and the relatively stable mean seasonal AAE ( $1.09 \leq \bar{x} \leq 1.14$ ) was consistent with traffic-related emissions. This confirmed the output of the source apportionment model which indicated that traffic accounted for 74%, 78%, 80% and 78% of total equivalent black carbon measured in winter, spring, summer and autumn, respectively, at this location. A broad range of AAE values, exhibiting bi- and tri-modal distribution, were observed throughout winter and autumn at University College Dublin, indicative of multiple contributing sources. The shift in AAE towards 2 during the winter months suggested that solid fuel combustion was a major contributor. During the summer months, a narrow distribution, with a mean of 1.17 was observed, consistent with considerable contributions from traffic during this period. The distribution of AAE recorded in Enniscorthy during the winter and summer were as anticipated; a broad distribution with a mean AAE of 1.47 indicative of significant contribution from solid fuel combustion emissions during the winter, and a narrower distribution with a reduced AAE ( $\bar{x} = 1.23$ ) during the summer when solid fuel burning

is considerably less prevalent. Spring and autumn yielded interesting results in the form of a broad, tri-modal distribution, which could be interpreted as multiple sources, including wood, peat and coal burning for domestic heating, contributing to the ambient aerosol. However, this tri-modal distribution was not observed during the winter, when solid fuel burning was most prevalent and, according to the aethalometer source apportionment model, accounted for over 70% of the ambient black carbon measured. Approximately 60% of eBC measured in spring and autumn at this location was attributed to solid fuel burning. It is possible that anthropogenic activity, including traffic emissions and significant contributions from solid fuel combustion, could enhance secondary organic aerosol formation of biogenic origin. Detailed chemical analysis of the aerosol composition is required to validate this hypothesis.

The results presented here demonstrate the significant temporal variability associated with concentration and composition of carbonaceous aerosol, particularly in locations with considerable contributions from solid fuel combustion during winter. They confirm the strong link between solid fuel combustion and poor air quality in residential locations. Average concentrations of eBC measured during the winter were more than double those recorded during the summer months at UCD and Pearse Street, while average hourly wintertime concentrations recorded in Enniscorthy were approximately 6 times larger than summertime measurements. While acknowledging the influence of natural factors, including meteorology, the significant decrease in eBC concentration in summer is an indicator of the improvement in air quality that could be attained if solid fuel usage was reduced.

*Table 7.2 Spatial and temporal comparison of eBC concentrations measured in three unique environments in Ireland.*

	<b>University College Dublin</b>		<b>Pearse Street</b>		<b>Enniscorthy</b>	
	September 2017 – August 2018		September 2018 – August 2019		December 2019 – November 2020	
	<i>Urban background</i>		<i>Urban roadside</i>		<i>Rural town</i>	
<b>Equivalent Black Carbon (<math>\mu\text{g m}^{-3}</math>)</b>						
	<i>Mean</i>	<i>Range</i>	<i>Mean</i>	<i>Range</i>	<i>Mean</i>	<i>Range</i>
<b>Winter</b>	0.78	0.00 - 17.18	4.88	0.22 - 27.58	2.30	0.00 - 41.08
<b>Spring</b>	0.68	0.00 - 10.78	3.02	0.07 - 12.77	1.08	0.01 - 20.08
<b>Summer</b>	0.37	0.00 - 5.68	2.17	0.04 - 14.09	0.37	0.00 - 3.32
<b>Autumn</b>	0.54	0.00 - 5.94	5.65	0.00 - 38.76	0.98	0.00 - 23.48

## 7.2 PERSPECTIVES

---

This work highlights the complexity of ambient carbonaceous aerosol and clearly demonstrates the strong influence of anthropogenic activity. In spite of occasional exacerbation due to meteorological conditions (e.g. low boundary layer, low wind speed), the spatial and temporal variability of carbonaceous aerosol is inherently linked with anthropogenic activity, particularly in relation to solid fuel combustion and traffic-related emissions. This was most evident in wintertime and especially in residential locations where solid fuel burning for domestic heating was most prevalent.

A reduction in black carbon emitted to the atmosphere would alleviate the associated negative implications on climate and human health. Black carbon is now widely recognised as a significant radiative forcing agent and is associated with various health problems, including cancer, respiratory and cardiovascular disease and birth defects. The effectiveness of the ‘Smoky Coal’ ban introduced in Dublin in 1990, and its extension to include other urban/populous areas in subsequent years, has been well documented (Clancy et al., 2002; Dockery et al., 2013; Goodman et al., 2009). The current study has demonstrated the persistent significant contribution from solid fuel burning to total ambient black carbon, accounting for over 40% and 70% in University College Dublin and Enniscorthy, respectively, during the winter heating season. The ban on the sale and consumption of bituminous coal is to be extended nationwide in September 2022, in combination with new restrictions to encompass smoke emission rates of any manufactured solid fuel and moisture content of commercially sold wood (Department of the Environment, Climate and Communications, 2021). Bituminous coal is easily controlled as it is imported and is exclusively available through commercial entities. However, regulating the use of peat and wood will be considerably more difficult to enforce as it can be harvested on private property. It is important that planned restrictions are accompanied by significant investment and incentives to promote the use of renewable and non-polluting methods of heating. Similarly, in order to successfully reduce the contribution from traffic-related emissions in urban areas, public transport networks must be upgraded and expanded to serve suburban and regional commuters, in combination with extension of pedestrian and cycling infrastructure with improved safety measures. In addition, an expansion of the national monitoring network to incorporate the aethalometer and

Total Carbon Analyzer is required in order to facilitate the accurate assessment of the efficacy of the proposed actions.

The work presented in this thesis includes results from several instruments deployed at six unique sampling locations over a three year period, for on- and off-line quantitative and qualitative analysis of the ambient carbonaceous aerosol. Central to each campaign was the aethalometer (AE33, Magee Scientific). This instrument provided quantitative data in real-time. Application of the source apportionment model developed by Sandradewi, Prévôt, Szidat et al. (2008) provided an indication of the dominant sources contributing to the total ambient black carbon measured. The AAE output by the aethalometer also provided information concerning aerosol composition based on optical properties. However, as discussed in relation to the interesting distribution of AAE values recorded in Enniscorthy in spring and autumn, additional instrumentation is required for a more detailed chemical analysis in order to confirm hypotheses. The employment of on-line and off-line techniques, including aerosol mass spectrometry (AMS) and gas chromatography/mass spectrometry, in future investigations would provide greater insight into local aerosol composition. This study has demonstrated the efficacy of the aethalometer. However in a complex, multi-fuel environment, further development of the source apportionment model is required for a more accurate determination of the contribution of all solid fuel types, rather than combining all fuel types into a collective ‘solid fuel’ category. The current aethalometer model is biased towards continental conditions which focuses mainly on wood burning and road traffic, without account for coal combustion or shipping emissions, relevant in the Irish context.

When coupled with the Total Carbon Analyzer (TCA-08, Magee Scientific) hourly measurements of equivalent elemental and organic carbon were obtained, through the application of the ‘TC-BC’ method (Rigler et al., 2020). This automated instrument renders conventional, thermal-optical methods of determining elemental, organic and total carbon redundant, if the purpose of the monitoring is, exclusively, to assess the carbon content of atmospheric aerosols in terms of absolute concentration. The Total Carbon Analyzer has the capacity to provide near real-time data, allowing the user to monitor diurnal changes in aerosol composition, which is not possible with 24-hour filter sample collection. The labour intensive maintenance and off-line analysis of filter samples, in addition to disadvantages associated with filter sample collection over

prolonged sampling periods, can be avoided by using the Total Carbon Analyzer. However, in doing so, data based on species volatility obtained during the stepwise temperature protocol used in conventional methods is lost, forfeiting the opportunity for further detailed investigation of aerosol composition.

Detailed chemical analysis is essential for the purposes of a quantitative and qualitative research campaign. It is advantageous to incorporate filter sampling collection in order to obtain a comprehensive evaluation of aerosol composition through off-line analytical techniques including thermal-optical methods to determine elemental and organic carbon content (stepwise fractions) and chromatographic methods for identification and quantification of organic tracers such as levoglucosan. Filter samples are also required for the determination of site-specific mass absorption cross-section value and proportionality factor ( $b$ ) employed in the 'TC-BC' method, both of which should be representative of the season in which measurements take place.

Despite the influential role of black carbon as a positive radiative forcing agent, it is not a specified air pollutant in Irish or European legislation and a dedicated monitoring network is yet to be established in Ireland. In order to inform models used for the predictions of future concentrations and to develop targeted mitigation strategies to limit emissions of black carbon, and carbonaceous aerosol in general, detailed information of the dominant sources is required. Targeting BC would target combustion emissions directly which account for a significant portion of total mass concentration. An extensive national network measuring particulate matter (PM<sub>10</sub> and PM<sub>2.5</sub>) is predominantly operated and maintained by the Environmental Protection Agency, in partnership with local authorities, state bodies and universities. Expansion of this monitoring network to include an aethalometer and a co-located Total Carbon Analyzer would have the capacity to perform source apportionment analysis of carbonaceous aerosol in real-time. There are several advantages to this combination of instruments, all of which would be highly beneficial to authorities tasked with air quality management. Both instruments require little maintenance following initial installation. They operate automatically and can recover from power outages. Remote monitoring of the operation of both instruments is possible and continuous operation allows for real-time measurement and source apportionment analysis of ambient black, elemental, organic and total carbon. Such data is crucial to accurately monitoring levels of harmful pollutants and associated dominant sources.

The substantial negative impact of anthropogenic activity on both air quality and climate is widely recognised. Various abatement targets, strategies and policies have been developed and ratified internationally to rectify the problem, however, to date, industrial and political willpower has been lacking, and thus the damaging situation persists. The planet is now at a point where major changes are required to dramatically reduce emissions in an effort to improve air quality and reverse the current climate crisis. The future of air quality management will rely heavily on models to predict concentrations of harmful pollutants on a local, regional and global scale, necessitating a substantial amount of accurate spatially and temporally representative data. In Ireland, long-term measurements of ambient levels of carbonaceous aerosol could be achieved through a national network with the ability to perform quantitative and qualitative analysis in real-time by incorporation of on-line instruments capable of characterising the carbonaceous fraction of ambient aerosols, such as those employed in this research and discussed above. On-line analysis of bulk properties inherent in the carbonaceous fraction of ambient aerosol would extend the capability of air quality monitoring networks by providing information on the sources of particulate pollution in near real-time.

## 8. REFERENCES

---

- Aas, W., Platt, S., & Yttri, K. E. (2017). EMEP/ACTRIS intensive measurement period - Winter 2018
- Ailshire, J. A., & Crimmins, E. M. (2014). Fine Particulate Matter Air Pollution and Cognitive Function Among Older US Adults. *American Journal of Epidemiology*, *180*(4), 359-366. <https://doi.org/10.1093/aje/kwu155>
- Aksoyoglu, S., Keller, J., Barmpadimos, I., Oderbolz, D., Lanz, V. A., Prévôt, A. S. H., & Baltensperger, U. (2011). Aerosol modelling in Europe with a focus on Switzerland during summer and winter episodes. *Atmospheric Chemistry & Physics*, *11*(14), 7355-7373
- Allen, G. A., Babich, P., & Poirot, R. L. (2004). Evaluation of a new approach for real time assessment of wood smoke PM. *Regional and global perspectives on haze: causes, consequences, and controversies, air and waste management association visibility specialty conference*, 25-29
- Amaral, S. S., De Carvalho, J. A., Costa, M. A. M., & Pinheiro, C. (2015). An overview of particulate matter measurement instruments. *Atmosphere*, *6*(9), 1327-1345
- Andreae, M. O., & Gelencsér, A. (2006). Black carbon or brown carbon? The nature of light-absorbing carbonaceous aerosols. *Atmospheric Chemistry & Physics*, *6*(10), 3131-3148. <https://doi.org/10.5194/acp-6-3131-2006>
- ApSimon, H. M., del Campo, M. T. G., & Adams, H. S. (2001). Modelling long-range transport of primary particulate material over Europe. *Atmospheric Environment*, *35*(2), 343-352
- Apte, J. S., Brauer, M., Cohen, A. J., Ezzati, M., & Pope, C. A. (2018). Ambient PM<sub>2.5</sub> Reduces Global and Regional Life Expectancy. *Environmental Science & Technology Letters*, *5*(9), 546-551. <https://doi.org/10.1021/acs.estlett.8b00360>
- Asmi, E., Backman, J., Servomaa, H., Virkkula, A., Gini, M. I., Eleftheriadis, K., Hyvärinen, A. (2021). Absorption instruments inter-comparison campaign at the Arctic Pallas station. *Atmospheric Measurement Techniques*, *14*(8), 5397-5413
- Backman, J., Schmeisser, L., Virkkula, A., Ogren, J. A., Asmi, E., Starkweather, S., Jefferson, A. (2017). On Aethalometer measurement uncertainties and an instrument correction factor for the Arctic. *Atmospheric Measurement Techniques*, *10*(12), 5039-5062
- Bakand, S., Hayes, A., & Dechsakulthorn, F. (2012). Nanoparticles: A review of particle toxicology following inhalation exposure. *Inhalation toxicology*, *24*(2), 125-135
- Baltensperger, U., Kalberer, M., Dommen, J., Paulsen, D., Alfarra, M. R., Coe, H., Nyeki, S. (2005). Secondary organic aerosols from anthropogenic and biogenic precursors. *Faraday Discussions*, *130*, 265-278
- Baltensperger, U., & Prévôt, A. S. H. (2008). Chemical analysis of atmospheric aerosols. *Analytical & Bioanalytical Chemistry*, *390*(1), 277-280
- Bautista, A. T., Pabroa, P. C. B., Santos, F. L., Quirrit, L. L., Asis, J. L. B., Dy, M. A. K., & Martinez, J. P. G. (2015). Intercomparison between NIOSH, IMPROVE\_A, and EUSAAR\_2 protocols: Finding an optimal thermal-optical protocol for Philippines OC/EC samples. *Atmospheric Pollution Research*, *6*(2), 334-342. <https://doi.org/https://doi.org/10.5094/APR.2015.037>

- Begum, B. A., Biswas, S. K., Markwitz, A., & Hopke, P. K. (2010). Identification of Sources of Fine and Coarse Particulate Matter in Dhaka, Bangladesh. *Aerosol & Air Quality Research*, *10*(4), 345-353. <https://doi.org/10.4209/aaqr.2009.12.0082>
- Belis, C. A., Larsen, B. R., Amato, F., El Haddad, I., Favez, O., Harrison, R. M., Prevot, A. (2014). European Guide on Air Pollution Source Apportionment with Receptor Models. *JRC reference reports EUR26080 EN*
- Bellouin, N., Quaas, J., Gryspeerdt, E., Kinne, S., Stier, P., Watson-Parris, D., Daniau, A. L. (2020). Bounding global aerosol radiative forcing of climate change. *Reviews of Geophysics*, *58*(1)
- Bergstrom, R. W., San Rafael, C., Ackerman, T. P., & Richards, L. W. (1982). Optical Properties of Particulate Elemental Carbon
- Birch, M. E. (2003). Monitoring of diesel particulate exhaust in the workplace. *NIOSH Manual of Analytical Methods (NMAM)*, 2154
- Birch, M. E., & Cary, R. A. (1996). Elemental Carbon-Based Method for Monitoring Occupational Exposures to Particulate Diesel Exhaust. *Aerosol Science & Technology*, *25*(3), 221-241. <https://doi.org/10.1080/02786829608965393>
- Bond, T. C., & Bergstrom, R. W. (2006). Light absorption by carbonaceous particles: An investigative review. *Aerosol Science & Technology*, *40*(1), 27-67. <https://doi.org/10.1080/02786820500421521>
- Bond, T. C., Doherty, S. J., Fahey, D. W., Forster, P. M., Berntsen, T., Deangelo, B. J., Zender, C. S. (2013). Bounding the role of black carbon in the climate system: A scientific assessment. *Journal of Geophysical Research Atmospheres*, *118*(11), 5380-5552. <https://doi.org/10.1002/jgrd.50171>
- Bové, H., Bongaerts, E., Slenders, E., Bijnens, E. M., Saenen, N. D., Gyselaers, W., Nawrot, T. S. (2019). Ambient black carbon particles reach the fetal side of human placenta. *Nature Communications*, *10*(1), Article 3866. <https://doi.org/10.1038/s41467-019-11654-3>
- Brauer, M., Lencar, C., Tamburic, L., Koehoorn, M., Demers, P., & Karr, C. (2008). A cohort study of traffic-related air pollution impacts on birth outcomes. *Environmental Health Perspectives*, *116*(5), 680-686. <https://doi.org/10.1289/ehp.10952>
- Breiman, L. (2001). Random Forests. *Machine Learning*, *45*(1), 5-32. <https://doi.org/10.1023/A:1010933404324>
- Briggs, N. L., & Long, C. M. (2016). Critical review of black carbon and elemental carbon source apportionment in Europe and the United States. *Atmospheric Environment*, *144*, 409-427. <https://doi.org/https://doi.org/10.1016/j.atmosenv.2016.09.002>
- Brimblecombe, P. (2006). The Clean Air Act after 50 years. *Weather*, *61*(11), 311-314
- Buckley, P. (2019). *Nature and Origin of Black Carbon in Ireland*, University College Cork
- Calvo, A. I., Alves, C., Castro, A., Pont, V., Vicente, A. M., & Fraile, R. (2013). Research on aerosol sources and chemical composition: Past, current and emerging issues. *Atmospheric Research*, *120-121*, 1-28. <https://doi.org/https://doi.org/10.1016/j.atmosres.2012.09.021>
- Carslaw, D., & Ropkins, K. (2012). Openair: An R package for air quality data analysis. *Environmental Modelling & Software*, *27*, 52-61

- Carslaw, D., & Taylor, P. (2009). Analysis of air pollution data at a mixed source location using boosted regression trees. *Atmospheric Environment*, 43(22-23), 3563-3570
- Carstensen, B., Gurrin, L., Ekstrøm, C., & Figurski, M. (2020). MethComp: Analysis of Agreement in Method Comparison Studies. R Package Version 1.30. 0.
- Cavalli, F., Alastuey, A., Areskou, H., Ceburnis, D., Čech, J., Genberg, J., Putaud, J. P. (2016). A European aerosol phenomenology -4: Harmonized concentrations of carbonaceous aerosol at 10 regional background sites across Europe. *Atmospheric Environment*, 144, 133-145. <https://doi.org/10.1016/j.atmosenv.2016.07.050>
- Cavalli, F., Viana, M., Yttri, K. E., Genberg, J., & Putaud, J. P. (2010). Toward a standardised thermal-optical protocol for measuring atmospheric organic and elemental carbon: The EUSAAR protocol. *Atmospheric Measurement Techniques*, 3(1), 79-89. <https://doi.org/10.5194/amt-3-79-2010>
- Ceburnis, D., Yin, J., Allen, A. G., Jennings, S. G., Harrison, R. M., Wright, E., Barry, E. (2006). Local and regional air pollution in Ireland during an intensive aerosol measurement campaign. *Journal of Environmental Monitoring*, 8(4), 479-487. <https://doi.org/10.1039/b516029d>
- Cesari, D., Merico, E., Dinoi, A., Marinoni, A., Bonasoni, P., & Contini, D. (2018). Seasonal variability of carbonaceous aerosols in an urban background area in Southern Italy. *Atmospheric Research*, 200, 97-108
- Chan, T. W., Meloche, E., Kubsh, J., Brezny, R., Rosenblatt, D., & Rideout, G. (2013). Impact of ambient temperature on gaseous and particle emissions from a direct injection gasoline vehicle and its implications on particle filtration. *SAE International Journal of Fuels & Lubricants*, 6(2), 350-371
- Chen, J., & Hoek, G. (2020). Long-term exposure to PM and all-cause and cause-specific mortality: A systematic review and meta-analysis. *Environment International*, 143, 105974
- Cheng, Y., Engling, G., He, K. B., Duan, F. K., Ma, Y. L., Du, Z. Y., Weber, R. J. (2013). Biomass burning contribution to Beijing aerosol. *Atmospheric Chemistry & Physics*, 13(15), 7765-7781. <https://doi.org/10.5194/acp-13-7765-2013>
- Cheng, Y., He, K.-b., Duan, F.-k., Zheng, M., Du, Z.-y., Ma, Y.-l., & Tan, J.-h. (2011). Ambient organic carbon to elemental carbon ratios: Influences of the measurement methods and implications. *Atmospheric Environment*, 45(12), 2060-2066
- Chow, J. C., Watson, J. G., Chen, L. W. A., Arnott, W. P., Moosmüller, H., & Fung, K. (2004). Equivalence of Elemental Carbon by Thermal/Optical Reflectance and Transmittance with Different Temperature Protocols. *Environmental Science & Technology*, 38(16), 4414-4422. <https://doi.org/10.1021/es034936u>
- Chow, J. C., Watson, J. G., Chen, L. W. A., Chang, M. C. O., Robinson, N. F., Trimble, D., & Kohl, S. (2007). The IMPROVE\_A Temperature Protocol for Thermal/Optical Carbon Analysis: Maintaining Consistency with a Long-Term Database. *Journal of the Air & Waste Management Association*, 57(9), 1014-1023. <https://doi.org/10.3155/1047-3289.57.9.1014>
- Chow, J. C., Watson, J. G., Pritchett, L. C., Pierson, W. R., Frazier, C. A., & Purcell, R. G. (1993). The DRI thermal/optical reflectance carbon analysis system: Description, evaluation and applications in U.S. Air quality studies. *Atmospheric Environment. Part A. General Topics*, 27(8), 1185-1201. [https://doi.org/https://doi.org/10.1016/0960-1686\(93\)90245-T](https://doi.org/https://doi.org/10.1016/0960-1686(93)90245-T)

- Clairotte, M., Adam, T. W., Zardini, A. A., Manfredi, U., Martini, G., Krasenbrink, A., Astorga, C. (2013). Effects of low temperature on the cold start gaseous emissions from light duty vehicles fuelled by ethanol-blended gasoline. *Applied Energy*, *102*, 44-54
- Clancy, L., Goodman, P., Sinclair, H., & Dockery, D. W. (2002). Effect of air-pollution control on death rates in Dublin, Ireland: An intervention study. *Lancet*, *360*(9341), 1210-1214. [https://doi.org/10.1016/S0140-6736\(02\)11281-5](https://doi.org/10.1016/S0140-6736(02)11281-5)
- Colette, A., & Tarasova, O. (2019). Progress in EMEP Activities in 2018-2019 and Future Work: Measurements and Modelling
- Comero, S., Capitani, L., & Gawlik, B. M. (2009). Positive Matrix Factorisation (PMF). *JRC Sci. Technol. Rep*, *59*, 3-59
- Contini, D., Vecchi, R., & Viana, M. (2018). Carbonaceous aerosols in the atmosphere. *Atmosphere*, *9*(5), Article 181. <https://doi.org/10.3390/atmos9050181>
- Coz, E., Gómez-Moreno, F. J., Pujadas, M., Casuccio, G. S., Lersch, T. L., & Artíñano, B. (2009). Individual particle characteristics of North African dust under different long-range transport scenarios. *Atmospheric Environment*, *43*(11), 1850-1863. <https://doi.org/https://doi.org/10.1016/j.atmosenv.2008.12.045>
- Crilley, L. R., Bloss, W. J., Yin, J., Beddows, D. C. S., Harrison, R. M., Allan, J. D., Mohr, C. (2015). Sources and contributions of wood smoke during winter in London: Assessing local and regional influences. *Atmospheric Chemistry & Physics*, *15*(6), 3149-3171. <https://doi.org/10.5194/acp-15-3149-2015>
- Crinnion, W. (2017). Particulate Matter is a Surprisingly Common Contributor to Disease. *Integrative Medicine (Encinitas, Calif.)*, *16*(4), 8-12
- CSO. (2016). *Census 2016*. Retrieved from <https://cso.maps.arcgis.com>
- Cuesta-Mosquera, A., Močnik, G., Drinovec, L., Müller, T., Pfeifer, S., Minguillón, M. C., Wiedensohler, A. (2020). Intercomparison and characterization of 23 Aethalometers under laboratory and ambient air conditions: Procedures and unit-to-unit variabilities. *Atmospheric Measurement Techniques Discussion*, *2020*, 1-34. <https://doi.org/10.5194/amt-2020-344>
- Dall'Osto, M., Ovadnevaite, J., Ceburnis, D., Martin, D., Healy, R. M., O'Connor, I. P., O'Dowd, C. (2013). Characterization of urban aerosol in Cork city (Ireland) using aerosol mass spectrometry. *Atmospheric Chemistry & Physics*, *13*(9), 4997-5015
- Department for Environment, Food & Rural Affairs. Retrieved 15/10/2021 from <https://uk-air.defra.gov.uk/networks/brief-history>
- Department of the Environment, Climate and Communications. (2021)
- Diapouli, E., Kalogridis, A. C., Markantonaki, C., Vratolis, S., Fetfatzis, P., Colombi, C., & Eleftheriadis, K. (2017). Annual variability of black carbon concentrations originating from biomass and fossil fuel combustion for the suburban aerosol in Athens, Greece. *Atmosphere*, *8*(12), Article 234. <https://doi.org/10.3390/atmos8120234>
- DIGITEL Elektronik GmbH. (2009). DIGITEL High Volume Aerosol Sampler Manual
- Dockery, D. W., Pope, C. A., Xu, X., Spengler, J. D., Ware, J. H., Fay, M. E., Speizer, F. E. (1993). An Association between Air Pollution and Mortality in Six U.S. Cities. *New England Journal of Medicine*, *329*(24), 1753-1759. <https://doi.org/10.1056/NEJM199312093292401>

- Dockery, D. W., Rich, D. Q., Goodman, P. G., Clancy, L., Ohman-Strickland, P., George, P., Committee, H. E. I. H. R. (2013). Effect of air pollution control on mortality and hospital admissions in Ireland. *Research report (Health Effects Institute)*(176), 3-109
- Draxler, R. R., & Hess, G. D. (1998). An overview of the HYSPLIT\_4 modelling system for trajectories. *Australian Meteorological Magazine*, 47(4), 295-308
- Drinovec, L., Močnik, G., Zotter, P., Prévôt, A. S. H., Ruckstuhl, C., Coz, E., Hansen, A. D. A. (2015). The "dual-spot" Aethalometer: An improved measurement of aerosol black carbon with real-time loading compensation. *Atmospheric Measurement Techniques*, 8(5), 1965-1979. <https://doi.org/10.5194/amt-8-1965-2015>
- Dublin Bus. (2021). Retrieved 18/05/2021 from <https://www.dublinbus.ie/About-Us/Dublin-Bus-Fleet/>
- Elsaid, K., Olabi, V., Sayed, E. T., Wilberforce, T., & Abdelkareem, M. A. (2021). Effects of COVID-19 on the environment: An overview on air, water, wastewater, and solid waste. *Journal of Environmental Management*, 292, 112694. <https://doi.org/https://doi.org/10.1016/j.jenvman.2021.112694>
- Engling, G., Carrico, C. M., Kreidenweis, S. M., Collett Jr, J. L., Day, D. E., Malm, W. C., Herrmann, H. (2006). Determination of levoglucosan in biomass combustion aerosol by high-performance anion-exchange chromatography with pulsed amperometric detection. *Atmospheric Environment*, 40, 299-311
- EPA. (2020). *Data obtained from EPA Ireland Air Quality Team*
- EPA. (2021). *Air Quality in Ireland 2020*
- ESA. (2020). Retrieved 10/01/2022 from [https://www.esa.int/Applications/Observing\\_the\\_Earth/Copernicus/Sentinel-5P/Coronavirus\\_lockdown\\_leading\\_to\\_drop\\_in\\_pollution\\_across\\_Europe](https://www.esa.int/Applications/Observing_the_Earth/Copernicus/Sentinel-5P/Coronavirus_lockdown_leading_to_drop_in_pollution_across_Europe)
- European Committee for Standardization. (2017). *Ambient air - Measurement of elemental carbon (EC) and organic carbon (OC) collected on filters* (EN 16909:2017 E)
- European Environment Agency. <https://www.eea.europa.eu/themes/air/air-quality-and-covid19/monitoring-covid-19-impacts-on>
- Evangelidou, N., Platt, S. M., Eckhardt, S., Lund Myhre, C., Laj, P., Alados-Arboledas, L., Stohl, A. (2021). Changes in black carbon emissions over Europe due to COVID-19 lockdowns. *Atmospheric Chemistry & Physics*, 21(4), 2675-2692. <https://doi.org/10.5194/acp-21-2675-2021>
- Fagerli, H., Tsyro, S., Jonson, J. E., Nyíri, Á., Gauss, M., Simpson, D., Mortier, A. (2019). Transboundary particulate matter, photo-oxidants, acidifying and eutrophying components. Meteorologisk Institutt Norwegian Meteorological Institute.
- Fajersztajn, L., Saldiva, P., Pereira, L. A. A., Leite, V. F., & Buehler, A. M. (2017). Short-term effects of fine particulate matter pollution on daily health events in Latin America: A systematic review and meta-analysis. *International Journal of Public Health*, 62(7), 729-738
- Favez, O., Cachier, H., Sciare, J., Sarda-Estève, R., & Martinon, L. (2009). Evidence for a significant contribution of wood burning aerosols to PM<sub>2.5</sub> during the winter season in Paris, France. *Atmospheric Environment*, 43(22-23), 3640-3644. <https://doi.org/10.1016/j.atmosenv.2009.04.035>

- Feng, Y., Ramanathan, V., & Kotamarthi, V. R. (2013). Brown carbon: A significant atmospheric absorber of solar radiation? *Atmospheric Chemistry & Physics*, 13(17), 8607-8621. <https://doi.org/10.5194/acp-13-8607-2013>
- Fine, P. M., Cass, G. R., & Simoneit, B. R. T. (2004a). Chemical Characterization of Fine Particle Emissions from the Fireplace Combustion of Wood Types Grown in the Midwestern and Western United States. *Environmental Engineering Science*, 21(3), 387-409. <https://doi.org/10.1089/109287504323067021>
- Fine, P. M., Cass, G. R., & Simoneit, B. R. T. (2004b). Chemical characterization of fine particle emissions from the wood stove combustion of prevalent united states tree species. *Environmental Engineering Science*, 21(6), 705-721. <https://doi.org/10.1089/ees.2004.21.705>
- Finlayson-Pitts, B. J., & Pitts, J. N. (2000). *Chemistry of the upper and lower atmosphere: Theory, experiments, and applications*. Academic Press
- Fuller, G. (2019). *The Invisible Killer: The Rising Global Threat of Air Pollution - and How We Can Fight Back*. Melville House
- Fuller, G. W., Tremper, A. H., Baker, T. D., Yttri, K. E., & Butterfield, D. (2014). Contribution of wood burning to PM<sub>10</sub> in London. *Atmospheric Environment*, 87, 87-94. <https://doi.org/10.1016/j.atmosenv.2013.12.037>
- Fuzzi, S., Andreae, M. O., Huebert, B. J., Kulmala, M., Bond, T. C., Boy, M., Kawamura, K. (2006). Critical assessment of the current state of scientific knowledge, terminology, and research needs concerning the role of organic aerosols in the atmosphere, climate, and global change. *Atmospheric Chemistry & Physics*, 6(7), 2017-2038
- Gelencsér, A., May, B., Simpson, D., Sánchez-Ochoa, A., Kasper-Giebl, A., Puxbaum, H., Legrand, M. (2007). Source apportionment of PM<sub>2.5</sub> organic aerosol over Europe: Primary/secondary, natural/anthropogenic, and fossil/biogenic origin. *Journal of Geophysical Research: Atmospheres*, 112(D23)
- Gentner, D. R., Jathar, S. H., Gordon, T. D., Bahreini, R., Day, D. A., El Haddad, I., Robinson, A. L. (2017). Review of Urban Secondary Organic Aerosol Formation from Gasoline and Diesel Motor Vehicle Emissions. *Environmental Science & Technology*, 51(3), 1074-1093. <https://doi.org/10.1021/acs.est.6b04509>
- Gilardoni, S., Vignati, E., Cavalli, F., Putaud, J. P., Larsen, B. R., Karl, M., Dentener, F. (2011). Better constraints on sources of carbonaceous aerosols using a combined <sup>14</sup>C-macro tracer analysis in a European rural background site. *Atmospheric Chemistry & Physics*, 11(12), 5685-5700. <https://doi.org/10.5194/acp-11-5685-2011>
- Glasius, M., Hansen, A. M. K., Claeys, M., Henzing, J. S., Jedynska, A. D., Kasper-Giebl, A., Yttri, K. E. (2018). Composition and sources of carbonaceous aerosols in Northern Europe during winter. *Atmospheric Environment*, 173, 127-141. <https://doi.org/https://doi.org/10.1016/j.atmosenv.2017.11.005>
- Goodman, P. G., Rich, D. Q., Zeka, A., Clancy, L., & Dockery, D. W. (2009). Effect of air pollution controls on black smoke and sulfur dioxide concentrations across Ireland. *Journal of the Air & Waste Management Association*, 59(2), 207-213. <https://doi.org/10.3155/1047-3289.59.2.207>

- Goosse, H., Barriat, P. Y., Lefebvre, W., Loutre, M. F., & Zunz, V. (2008-2010) *Introduction to climate dynamics and climate modeling*. Retrieved 10/09/2021 from <http://www.climate.be/textbook>
- Grange, S. (2018). rmweather: Tools to conduct meteorological normalisation on air quality data. *R package version 0.1.51*
- Grange, S., & Carslaw, D. (2019). Using meteorological normalisation to detect interventions in air quality time series. *Science of the Total Environment*, 653, 578-588. <https://doi.org/https://doi.org/10.1016/j.scitotenv.2018.10.344>
- Grange, S., Carslaw, D., Lewis, A., Boleti, E., & Hueglin, C. (2018). Random forest meteorological normalisation models for Swiss PM<sub>10</sub> trend analysis. *Atmospheric Chemistry & Physics*, 18(9), 6223-6239
- Grange, S., Lötscher, H., Fischer, A., Emmenegger, L., & Hueglin, C. (2020). Evaluation of equivalent black carbon source apportionment using observations from Switzerland between 2008 and 2018. *Atmospheric Measurement Techniques*, 13(4), 1867-1885. <https://doi.org/10.5194/amt-13-1867-2020>
- Grieshop, A. P., Logue, J. M., Donahue, N. M., & Robinson, A. L. (2009). Laboratory investigation of photochemical oxidation of organic aerosol from wood fires 1: Measurement and simulation of organic aerosol evolution. *Atmospheric Chemistry & Physics*, 9(4), 1263-1277. <https://doi.org/10.5194/acp-9-1263-2009>
- Grivas, G., Cheristanidis, S., & Chaloulakou, A. (2012). Elemental and organic carbon in the urban environment of Athens: Seasonal and diurnal variations and estimates of secondary organic carbon. *Science of the Total Environment*, 414, 535-545. <https://doi.org/https://doi.org/10.1016/j.scitotenv.2011.10.058>
- Gualtieri, G., Brillì, L., Carotenuto, F., Vagnoli, C., Zaldei, A., & Gioli, B. (2020). Quantifying road traffic impact on air quality in urban areas: A COVID19-induced lockdown analysis in Italy. *Environmental Pollution*, 267, 115682. <https://doi.org/https://doi.org/10.1016/j.envpol.2020.115682>
- Gustafsson, Ö., Kruså, M., Zencak, Z., Sheesley, R. J., Granat, L., Engström, E., Rodhe, H. (2009). Brown clouds over South Asia: Biomass or fossil fuel combustion? *Science*, 323(5913), 495-498. <https://doi.org/10.1126/science.1164857>
- Habibi, H., Awal, R., Fares, A., & Ghahremannejad, M. (2020). COVID-19 and the Improvement of the Global Air Quality: The Bright Side of a Pandemic. *Atmosphere*, 11(12). <https://doi.org/10.3390/atmos11121279>
- Haerter, J. O., Roeckner, E., Tomassini, L., & von Storch, J. S. (2009). Parametric uncertainty effects on aerosol radiative forcing. *Geophysical research letters*, 36(15)
- Hallquist, M., Wenger, J. C., Baltensperger, U., Rudich, Y., Simpson, D., Claeys, M., Goldstein, A. H. (2009). The formation, properties and impact of secondary organic aerosol: Current and emerging issues. *Atmospheric Chemistry & Physics*, 9(14), 5155-5236
- Hansen, A. D. A., Rosen, H., & Novakov, T. (1984). The aethalometer: An instrument for the real-time measurement of optical absorption by aerosol particles. *Science of the Total Environment*, 36, 191-196. [https://doi.org/https://doi.org/10.1016/0048-9697\(84\)90265-1](https://doi.org/https://doi.org/10.1016/0048-9697(84)90265-1)

- Haywood, J., & Boucher, O. (2000). Estimates of the direct and indirect radiative forcing due to tropospheric aerosols: A review. *Reviews of Geophysics*, 38(4), 513-543. <https://doi.org/10.1029/1999RG000078>
- Heal, M., & Quincey, P. (2012). The relationship between black carbon concentration and black smoke: A more general approach. *Atmospheric Environment*, 54, 538-544. <https://doi.org/https://doi.org/10.1016/j.atmosenv.2012.02.067>
- Heal, M. R., & Beverland, I. J. (2017). A chronology of ratios between black smoke and PM<sub>10</sub> and PM<sub>2.5</sub> in the context of comparison of air pollution epidemiology concentration-response functions. *Environmental Health*, 16(1), 44. <https://doi.org/10.1186/s12940-017-0252-2>
- Healy, R. M., Hellebust, S., Kourtchev, I., Allanic, A., O'Connor, I. P., Bell, J. M., Wenger, J. C. (2010). Source apportionment of PM<sub>2.5</sub> in Cork Harbour, Ireland using a combination of single particle mass spectrometry and quantitative semi-continuous measurements. *Atmospheric Chemistry & Physics*, 10(19), 9593-9613
- Healy, R. M., Sofowote, U., Su, Y., Debosz, J., Noble, M., Jeong, C. H., Doerksen, G. (2017). Ambient measurements and source apportionment of fossil fuel and biomass burning black carbon in Ontario. *Atmospheric Environment*, 161, 34-47
- Helin, A., Niemi, J. V., Virkkula, A., Pirjola, L., Teinilä, K., Backman, J., Timonen, H. (2018). Characteristics and source apportionment of black carbon in the Helsinki metropolitan area, Finland. *Atmospheric Environment*, 190, 87-98. <https://doi.org/https://doi.org/10.1016/j.atmosenv.2018.07.022>
- Herich, H., Hueglin, C., & Buchmann, B. (2011). A 2.5 year's source apportionment study of black carbon from wood burning and fossil fuel combustion at urban and rural sites in Switzerland. *Atmospheric Measurement Techniques*, 4(7), 1409-1420. <https://doi.org/10.5194/amt-4-1409-2011>
- Hidy, G. M. (2019). Atmospheric aerosols: Some highlights and highlighters, 1950 to 2018. *Aerosol Science & Engineering*, 3(1), 1-20
- HPSC. (2021). Retrieved 23/08/2021 from <https://covid-19.geohive.ie/search>
- Huntzicker, J. J., Johnson, R. L., Shah, J. J., & Cary, R. A. (1982). Analysis of organic and elemental carbon in ambient aerosols by a thermal-optical method. *Particulate Carbon* (79-88). Springer
- Iinuma, Y., Engling, G., Puxbaum, H., & Herrmann, H. (2009). A highly resolved anion-exchange chromatographic method for determination of saccharidic tracers for biomass combustion and primary bio-particles in atmospheric aerosol. *Atmospheric Environment*, 43(6), 1367-1371. <https://doi.org/10.1016/j.atmosenv.2008.11.020>
- IPCC. (2007a). Climate Change 2007: Synthesis Report. Contribution of Working Groups I, II and III to the Fourth Assessment Report of the Intergovernmental Panel on Climate Change. Geneva, Switzerland: IPCC
- IPCC. (2007b). Climate Change 2007: The Physical Science Basis. Contribution of Working Group I to the Fourth Assessment Report of the Intergovernmental Panel on Climate Change. Cambridge, United Kingdom and New York, NY, USA: Cambridge University Press
- IPCC. (2013). Climate Change 2013: The Physical Science Basis. Contribution of Working Group I to the Fifth Assessment Report of the Intergovernmental Panel

- on Climate Change. Cambridge, United Kingdom and New York, NY, USA: Cambridge University Press
- IPCC. (2014). Climate Change 2014: Synthesis Report. Contribution of Working groups I, II and III to the Fifth Assessment Report of the Intergovernmental Panel on Climate Change. Geneva, Switzerland: IPCC
- IPCC. (2021). Climate Change 2021: The Physical Science Basis. Contribution of Working Group I to the Sixth Assessment Report of the Intergovernmental Panel on Climate Change. Cambridge, United Kingdom and New York, NY, USA: Cambridge University Press
- Jafar, H. A., & Harrison, R. M. (2020). Spatial and temporal trends in carbonaceous aerosols in the United Kingdom. *Atmospheric Pollution Research*. <https://doi.org/10.1016/j.apr.2020.09.009>
- Jakubiak-Lasocka, J., Lasocki, J., & Badyda, A. J. (2014). The influence of particulate matter on respiratory morbidity and mortality in children and infants. *Environmental Biomedicine* (39-48). Springer
- Jeong, C.-H., Evans, G. J., Dann, T., Graham, M., Herod, D., Dabek-Zlotorzynska, E., Wang, D. (2008). Influence of biomass burning on wintertime fine particulate matter: Source contribution at a valley site in rural British Columbia. *Atmospheric Environment*, 42(16), 3684-3699. <https://doi.org/https://doi.org/10.1016/j.atmosenv.2008.01.006>
- Jephcote, C., Hansell, A. L., Adams, K., & Gulliver, J. (2021). Changes in air quality during COVID-19 'lockdown' in the United Kingdom. *Environmental Pollution*, 272, 116011. <https://doi.org/https://doi.org/10.1016/j.envpol.2020.116011>
- Jones, A. M., & Harrison, R. M. (2005). Interpretation of particulate elemental and organic carbon concentrations at rural, urban and kerbside sites. *Atmospheric Environment*, 39(37), 7114-7126
- Jung, J., Souri, A. H., Wong, D. C., Lee, S., Jeon, W., Kim, J., & Choi, Y. (2019). The impact of the direct effect of aerosols on meteorology and air quality using aerosol optical depth assimilation during the KORUS-AQ campaign. *Journal of Geophysical Research: Atmospheres*, 124(14), 8303-8319
- Karaca, F., Anil, I., & Alagha, O. (2009). Long-range potential source contributions of episodic aerosol events to PM<sub>10</sub> profile of a megacity. *Atmospheric Environment*, 43(36), 5713-5722. <https://doi.org/https://doi.org/10.1016/j.atmosenv.2009.08.005>
- Karanasiou, A., Minguillón, M. C., Viana, M., Alastuey, A., Putaud, J. P., Maenhaut, W., Kuhlbusch, T. A. J. (2015). Thermal-optical analysis for the measurement of elemental carbon (EC) and organic carbon (OC) in ambient air a literature review. *Atmospheric Measurement Techniques Discussion*, 2015, 9649-9712. <https://doi.org/10.5194/amtd-8-9649-2015>
- Karanasiou, A., Panteliadis, P., Perez, N., Minguillón, M. C., Pandolfi, M., Titos, G., Alastuey, A. (2020). Evaluation of the Semi-Continuous OCEC analyzer performance with the EUSAAR2 protocol. *Science of the Total Environment*, 747, Article 141266. <https://doi.org/10.1016/j.scitotenv.2020.141266>
- Kilian, J., & Kitazawa, M. (2018). The emerging risk of exposure to air pollution on cognitive decline and Alzheimer's disease – Evidence from epidemiological and

- animal studies. *Biomedical Journal*, 41(3), 141-162. <https://doi.org/https://doi.org/10.1016/j.bj.2018.06.001>
- Knox, A., Evans, G. J., Brook, J. R., Yao, X., Jeong, C. H., Godri, K. J., Slowik, J. G. (2009). Mass absorption cross-section of ambient black carbon aerosol in relation to chemical age. *Aerosol Science & Technology*, 43(6), 522-532. <https://doi.org/10.1080/02786820902777207>
- Kourtchev, I., Hellebust, S., Bell, J. M., O'Connor, I. P., Healy, R. M., Allanic, A., Sodeau, J. R. (2011). The use of polar organic compounds to estimate the contribution of domestic solid fuel combustion and biogenic sources to ambient levels of organic carbon and PM<sub>2.5</sub> in Cork Harbour, Ireland. *Science of the Total Environment*, 409(11), 2143-2155. <https://doi.org/https://doi.org/10.1016/j.scitotenv.2011.02.027>
- Kreyling, W. G., Hirn, S., & Schleh, C. (2010). Nanoparticles in the lung. *Nature Biotechnology*, 28(12), 1275-1276. <https://doi.org/10.1038/nbt.1735>
- Kreyling, W. G., Semmler-Behnke, M., & Möller, W. (2006). Health implications of nanoparticles. *Journal of Nanoparticle Research*, 8(5), 543-562
- Kroll, J. H., Heald, C. L., Cappa, C. D., Farmer, D. K., Fry, J. L., Murphy, J. G., & Steiner, A. L. (2020). The complex chemical effects of COVID-19 shutdowns on air quality. *Nature Chemistry*, 12(9), 777-779. <https://doi.org/10.1038/s41557-020-0535-z>
- Kuhlbusch, T., Borowiak, A., Gelenscer, A., Genberg, J., Gladtko, D., Maenhaut, W., Quincey, P. (2009). Measurement of elemental and organic carbon in Europe. *JRC Scientific & Technical Reports*
- Kutzner, R. D., von Schneidmesser, E., Kuik, F., Quedenau, J., Weatherhead, E. C., & Schmale, J. (2018). Long-term monitoring of black carbon across Germany. *Atmospheric Environment*, 185, 41-52. <https://doi.org/10.1016/j.atmosenv.2018.04.039>
- Laskin, A., Laskin, J., & Nizkorodov, S. A. (2015). Chemistry of Atmospheric Brown Carbon. *Chemical Reviews*, 115(10), 4335-4382. <https://doi.org/10.1021/cr5006167>
- Lee, A. K. Y., Chen, C.-L., Liu, J., Price, D. J., Betha, R., Russell, L. M., Cappa, C. D. (2017). Formation of secondary organic aerosol coating on black carbon particles near vehicular emissions. *Atmospheric Chemistry & Physics*, 17(24), 15055-15067
- Lee, J. H., Hopke, P. K., Holsen, T. M., & Polissar, A. V. (2005). Evaluation of continuous and filter-based methods for measuring PM<sub>2.5</sub> mass concentration. *Aerosol Science & Technology*, 39(4), 290-303
- Lelieveld, J., Evans, J. S., Fnais, M., Giannadaki, D., & Pozzer, A. (2015). The contribution of outdoor air pollution sources to premature mortality on a global scale. *Nature*, 525(7569), 367-371. <https://doi.org/10.1038/nature15371>
- Levy, H., Horowitz, L. W., Schwarzkopf, M. D., Ming, Y., Golaz, J. C., Naik, V., & Ramaswamy, V. (2013). The roles of aerosol direct and indirect effects in past and future climate change. *Journal of Geophysical Research: Atmospheres*, 118(10), 4521-4532
- Lin, C. (2019). Chemical nature and sources of particulate matter in urban areas

- Lin, C., Ceburnis, D., Hellebust, S., Buckley, P., Wenger, J., Canonaco, F., Ovadnevaite, J. (2017). Characterization of primary organic aerosol from domestic wood, peat, and coal burning in Ireland. *Environmental Science & Technology*, 51(18), 10624-10632
- Lin, C., Ceburnis, D., Xu, W., Heffernan, E., Hellebust, S., Gallagher, J., Ovadnevaite, J. (2020). The impact of traffic on air quality in Ireland: Insights from the simultaneous kerbside and suburban monitoring of submicron aerosols. *Atmospheric Chemistry & Physics*, 20(17), 10513-10529
- Lin, C., Huang, R.-J., Ceburnis, D., Buckley, P., Preissler, J., Wenger, J., Ovadnevaite, J. (2018). Extreme air pollution from residential solid fuel burning. *Nature Sustainability*, 1(9), 512-517
- Liu, B., Zhang, J., Wang, L., Liang, D., Cheng, Y., Wu, J., Yang, H. (2018). Characteristics and sources of the fine carbonaceous aerosols in Haikou, China. *Atmospheric Research*, 199, 103-112. <https://doi.org/https://doi.org/10.1016/j.atmosres.2017.08.022>
- Liu, D., He, C., Schwarz, J. P., & Wang, X. (2020). Lifecycle of light-absorbing carbonaceous aerosols in the atmosphere. *npj Climate & Atmospheric Science*, 3(1), 40. <https://doi.org/10.1038/s41612-020-00145-8>
- Liu, Y., Xu, J., Chen, D., Sun, P., & Ma, X. (2019). The association between air pollution and pre-term birth and low birth weight in Guangdong, China. *BMC Public Health*, 19(1), 3. <https://doi.org/10.1186/s12889-018-6307-7>
- Lohmann, U., Rotstajn, L., Storelvmo, T., Jones, A., Menon, S., Quaas, J., Ruedy, R. (2010). Total aerosol effect: Radiative forcing or radiative flux perturbation? *Atmospheric Chemistry & Physics*, 10(7), 3235-3246
- Ma, Z., Liu, R., Liu, Y., & Bi, J. (2019). Effects of air pollution control policies on PM<sub>2.5</sub> pollution improvement in China from 2005 to 2017: A satellite-based perspective. *Atmospheric Chemistry & Physics*, 19(10), 6861-6877
- Maenhaut, W., Vermeylen, R., Claeys, M., Vercauteren, J., & Roekens, E. (2016). Sources of the PM<sub>10</sub> aerosol in Flanders, Belgium, and re-assessment of the contribution from wood burning. *Science of the Total Environment*, 562, 550-560
- Magee Scientific. (2016). Aethalometer Model AE33 User Manual
- Magee Scientific. (2018). Total Carbon Analyzer TCA 08 User Manual
- Martinsson, J., Abdul Azeem, H., Sporre, M. K., Bergström, R., Ahlberg, E., Öström, E., Eriksson Stenström, K. (2017). Carbonaceous aerosol source apportionment using the Aethalometer model-evaluation by radiocarbon and levoglucosan analysis at a rural background site in southern Sweden. *Atmospheric Chemistry & Physics*, 17(6), 4265-4281. <https://doi.org/10.5194/acp-17-4265-2017>
- Mbengue, S., Fusek, M., Schwarz, J., Vodička, P., Šmejkalová, A. H., & Holoubek, I. (2018). Four years of highly time resolved measurements of elemental and organic carbon at a rural background site in Central Europe. *Atmospheric Environment*, 182, 335-346. <https://doi.org/10.1016/j.atmosenv.2018.03.056>
- Menut, L., Bessagnet, B., Siour, G., Mailler, S., Pennel, R., & Cholakian, A. (2020). Impact of lockdown measures to combat Covid-19 on air quality over western Europe. *Science of the Total Environment*, 741, 140426. <https://doi.org/https://doi.org/10.1016/j.scitotenv.2020.140426>

- Met Éireann. (2019). *Storm Emma: An Analysis of Storm Emma and the cold spell which struck Ireland between the 28th of February and the 4th of March 2018*.
- Mikhailov, E. F., Vlasenko, S. S., Podgorny, I. A., Ramanathan, V., & Corrigan, C. E. (2006). Optical properties of soot-water drop agglomerates: An experimental study. *Journal of Geophysical Research Atmospheres*, *111*(7), Article D07209. <https://doi.org/10.1029/2005JD006389>
- Minguillón, M. C., Pérez, N., Marchand, N., Bertrand, A., Temime-Roussel, B., Agrios, K., Alastuey, A. (2016). Secondary organic aerosol origin in an urban environment: Influence of biogenic and fuel combustion precursors. *Faraday Discussions*, *189*, 337-359
- Moise, T., Flores, J. M., & Rudich, Y. (2015). Optical Properties of Secondary Organic Aerosols and Their Changes by Chemical Processes. *Chemical Reviews*, *115*(10), 4400-4439. <https://doi.org/10.1021/cr5005259>
- Moosmüller, H., Chakrabarty, R. K., Ehlers, K. M., & Arnott, W. P. (2011). Absorption Ångström coefficient, brown carbon, and aerosols: Basic concepts, bulk matter, and spherical particles. *Atmospheric Chemistry & Physics*, *11*(3), 1217-1225. <https://doi.org/10.5194/acp-11-1217-2011>
- Mosley, S. (2009). 'A Network of Trust': Measuring and Monitoring Air Pollution in British Cities, 1912-1960. *Environment and History*, *15*(3), 273-302
- Moulton, P. V., & Yang, W. (2012). Air Pollution, Oxidative Stress, and Alzheimer's Disease. *Journal of Environmental & Public Health*, *2012*, 472751. <https://doi.org/10.1155/2012/472751>
- Mousavi, A., Sowlat, M. H., Hasheminassab, S., Polidori, A., & Sioutas, C. (2018). Spatio-temporal trends and source apportionment of fossil fuel and biomass burning black carbon (BC) in the Los Angeles Basin. *Science of the Total Environment*, *640-641*, 1231-1240. <https://doi.org/https://doi.org/10.1016/j.scitotenv.2018.06.022>
- Nam, E., Kishan, S., Baldauf, R. W., Fulper, C. R., Sabisch, M., & Warila, J. (2010). Temperature Effects on Particulate Matter Emissions from Light-Duty, Gasoline-Powered Motor Vehicles. *Environmental Science & Technology*, *44*(12), 4672-4677. <https://doi.org/10.1021/es100219q>
- Ni, H., Huang, R. J., Cao, J., Liu, W., Zhang, T., Wang, M., Dusek, U. (2018). Source apportionment of carbonaceous aerosols in Xi'an, China: Insights from a full year of measurements of radiocarbon and the stable isotope <sup>13</sup>C. *Atmospheric Chemistry & Physics*, *18*(22), 16363-16383. <https://doi.org/10.5194/acp-18-16363-2018>
- Nicolosi, E., Quincey, P., Font, A., & Fuller, G. W. (2018). Light attenuation versus evolved carbon (AVEC) – A new way to look at elemental and organic carbon analysis. *Atmospheric Environment*, *175*, 145-153. <https://doi.org/10.1016/j.atmosenv.2017.12.011>
- NIOSH. (1996). Elemental Carbon (Diesel Particulate): Method 5040. NIOSH Manual of Analytical Methods. *National Institute for Occupational Safety and Health: Cincinnati, OH, USA*, 2003-2154
- Norris, G., Duvall, R., Brown, S., & Bai, S. (2014). EPA positive matrix factorization (PMF) 5.0 fundamentals and user guide. *US Environmental Protection Agency EPA/600/R-14/108*, 1-136
- O'Connell, P. (2019). Diesel-powered vehicles continue to dominate the Irish market

- O'Dowd, C. D., Facchini, M. C., Cavalli, F., Ceburnis, D., Mircea, M., Decesari, S., Putaud, J.-P. (2004). Biogenically driven organic contribution to marine aerosol. *Nature*, *431*(7009), 676-680
- Oberdörster, G., Oberdörster, E., & Oberdörster, J. (2005). Nanotoxicology: An Emerging Discipline Evolving from Studies of Ultrafine Particles. *Environmental Health Perspectives*, *113*(7), 823-839. <https://doi.org/10.1289/ehp.7339>
- Orellano, P., Reynoso, J., Quaranta, N., Bardach, A., & Ciapponi, A. (2020). Short-term exposure to particulate matter (PM<sub>10</sub> and PM<sub>2.5</sub>), nitrogen dioxide (NO<sub>2</sub>), and ozone (O<sub>3</sub>) and all-cause and cause-specific mortality: Systematic review and meta-analysis. *Environment International*, *142*, 105876
- Oudin, A. (2020). Short review: Air pollution, noise and lack of greenness as risk factors for Alzheimer's disease - epidemiologic and experimental evidence. *Neurochemistry International*, *134*, 104646. <https://doi.org/https://doi.org/10.1016/j.neuint.2019.104646>
- Ovadnevaite, J., Lin, C., Rinaldi, M., Ceburnis, D., Buckley, P., Coleman, L., O'Dowd, C. (2021). *Air Pollution Sources in Ireland*. Environmental Protection Agency
- Owens, J. S. (1926). Measuring the smoke pollution of city air. *Analyst*, *51*(598), 2-18
- Paatero, P. (1997). Least squares formulation of robust non-negative factor analysis. *Chemometrics and intelligent laboratory systems*, *37*(1), 23-35
- Paatero, P. (1999). The multilinear engine - A table-driven, least squares program for solving multilinear problems, including the n-way parallel factor analysis model. *Journal of Computational and Graphical Statistics*, *8*(4), 854-888
- Paatero, P., & Tapper, U. (1994). Positive matrix factorization: A non-negative factor model with optimal utilization of error estimates of data values. *Environmetrics*, *5*(2), 111-126
- Page, E. (1954). Continuous inspection schemes. *Biometrika*, *41*, 100-115
- Pandolfi, M., Ripoll, A., Querol, X., & Alastuey, A. (2014). Climatology of aerosol optical properties and black carbon mass absorption cross section at a remote high-altitude site in the western Mediterranean Basin. *Atmospheric Chemistry & Physics*, *14*(12), 6443-6460. <https://doi.org/10.5194/acp-14-6443-2014>
- Park, S., Son, S.-C., & Lee, S. (2018). Characterization, sources, and light absorption of fine organic aerosols during summer and winter at an urban site. *Atmospheric Research*, *213*, 370-380. <https://doi.org/https://doi.org/10.1016/j.atmosres.2018.06.017>
- Parker, H. A., Hasheminassab, S., Crounse, J. D., Roehl, C. M., & Wennberg, P. O. (2020). Impacts of traffic reductions associated with COVID-19 on southern California air quality. *Geophysical Research Letters*, *47*(23)
- Pedersen, M., Giorgis-Allemand, L., Bernard, C., Aguilera, I., Andersen, A.-M. N., Ballester, F., Slama, R. (2013). Ambient air pollution and low birthweight: A European cohort study (ESCAPE). *The Lancet Respiratory Medicine*, *1*(9), 695-704. [https://doi.org/https://doi.org/10.1016/S2213-2600\(13\)70192-9](https://doi.org/https://doi.org/10.1016/S2213-2600(13)70192-9)
- Peralta, O., Ortíz-Alvarez, A., Basaldud, R., Santiago, N., Álvarez-Ospina, H., de la Cruz, K., Gavilán, A. (2019). Atmospheric black carbon concentrations in Mexico. *Atmospheric Research*, *230*, 104626. <https://doi.org/https://doi.org/10.1016/j.atmosres.2019.104626>

- Perrino, C., Tofful, L., Dalla Torre, S., Sargolini, T., & Canepari, S. (2019). Biomass burning contribution to PM10 concentration in Rome (Italy): Seasonal, daily and two-hourly variations. *Chemosphere*, 222, 839-848
- Petzold, A., Ogren, J. A., Fiebig, M., Laj, P., Li, S. M., Baltensperger, U., Sugimoto, N. (2013). Recommendations for reporting "black carbon" measurements. *Atmospheric Chemistry & Physics*, 13(16), 8365-8379
- Pio, C., Cerqueira, M., Harrison, R. M., Nunes, T., Mirante, F., Alves, C., Matos, M. (2011). OC/EC ratio observations in Europe: Re-thinking the approach for apportionment between primary and secondary organic carbon. *Atmospheric Environment*, 45(34), 6121-6132. <https://doi.org/10.1016/j.atmosenv.2011.08.045>
- Platt, S. M., El Haddad, I., Pieber, S. M., Zardini, A. A., Suarez-Bertoa, R., Clairotte, M., Prévôt, A. S. H. (2017). Gasoline cars produce more carbonaceous particulate matter than modern filter-equipped diesel cars. *Scientific Reports*, 7(1), 4926. <https://doi.org/10.1038/s41598-017-03714-9>
- Platt, S. M., Haddad, I. E., Zardini, A. A., Clairotte, M., Astorga, C., Wolf, R., Ježek, I. (2013). Secondary organic aerosol formation from gasoline vehicle emissions in a new mobile environmental reaction chamber. *Atmospheric Chemistry & Physics*, 13(18), 9141-9158
- Pope, C. A., & Dockery, D. W. (2006). Health effects of fine particulate air pollution: Lines that connect. *Journal of the Air & Waste Management Association*, 56(6), 709-742. <https://doi.org/10.1080/10473289.2006.10464485>
- Pope III, C. A., Burnett, R. T., Thun, M. J., Calle, E. E., Krewski, D., Ito, K., & Thurston, G. D. (2002). Lung cancer, cardiopulmonary mortality, and long-term exposure to fine particulate air pollution. *Journal of the American Medical Association*, 287(9), 1132-1141. <https://doi.org/10.1001/jama.287.9.1132>
- Praphawatvet, T., Peters, J. I., & Williams III, R. O. (2020). Inhaled nanoparticles - An updated review. *International Journal of Pharmaceutics*, 119671
- Prather, K. A., Hatch, C. D., & Grassian, V. H. (2008). Analysis of atmospheric aerosols. *Annual Review of Analytical Chemistry* (Vol. 1, 485-514)
- Putaud, J. P., Van Dingenen, R., Alastuey, A., Bauer, H., Birmili, W., Cyrys, J., Raes, F. (2010). A European aerosol phenomenology - 3: Physical and chemical characteristics of particulate matter from 60 rural, urban, and kerbside sites across Europe. *Atmospheric Environment*, 44(10), 1308-1320. <https://doi.org/10.1016/j.atmosenv.2009.12.011>
- Pöschl, U. (2005). Atmospheric aerosols: Composition, transformation, climate and health effects. *Angewandte Chemie - International Edition*, 44(46), 7520-7540. <https://doi.org/10.1002/anie.200501122>
- Quincey, P. (2007). A relationship between Black Smoke Index and Black Carbon concentration. *Atmospheric Environment*, 41(36), 7964-7968. <https://doi.org/https://doi.org/10.1016/j.atmosenv.2007.09.033>
- Quincey, P., Butterfield, D., Green, D., Coyle, M., & Cape, J. N. (2009). An evaluation of measurement methods for organic, elemental and black carbon in ambient air monitoring sites. *Atmospheric Environment*, 43(32), 5085-5091. <https://doi.org/https://doi.org/10.1016/j.atmosenv.2009.06.041>

- Quintyne, K. I., Kelly, C., Sheridan, A., Kenny, P., & O'Dwyer, M. (2021). COVID-19 transport restrictions in Ireland: Impact on air quality and respiratory hospital admissions. *Public Health*, *198*, 156-160
- Ramanathan, V., Crutzen, P. J., Kiehl, J. T., & Rosenfeld, D. (2001). Aerosols, climate, and the hydrological cycle. *Science*, *294*(5549), 2119-2124
- Ramanathan, V., Ramana, M. V., Roberts, G., Kim, D., Corrigan, C., Chung, C., & Winker, D. (2007). Warming trends in Asia amplified by brown cloud solar absorption. *Nature*, *448*(7153), 575-578. <https://doi.org/10.1038/nature06019>
- Ranjan, M., Presto, A. A., May, A. A., & Robinson, A. L. (2012). Temperature dependence of gas-particle partitioning of primary organic aerosol emissions from a small diesel engine. *Aerosol Science & Technology*, *46*(1), 13-21
- Rao, S., & Dey, S. (2020). Consistent signal of aerosol indirect and semi-direct effect on water clouds in the oceanic regions adjacent to the Indian subcontinent. *Atmospheric Research*, *232*, 104677. <https://doi.org/https://doi.org/10.1016/j.atmosres.2019.104677>
- Rattigan, O. V., Civerolo, K., Doraiswamy, P., Felton, H. D., & Hopke, P. K. (2013). Long term black carbon measurements at two urban locations in New York. *Aerosol & Air Quality Research*, *13*(4), 1181-1196
- Reisen, F., Meyer, C. P., & Keywood, M. D. (2013). Impact of biomass burning sources on seasonal aerosol air quality. *Atmospheric Environment*, *67*, 437-447. <https://doi.org/https://doi.org/10.1016/j.atmosenv.2012.11.004>
- Rigler, M., Drinovec, L., Lavric, G., Vlachou, A., Prevot, A. S. H., Jaffrezo, J. L., Mocnik, G. (2020). The new instrument using a TC-BC (total carbon-black carbon) method for the online measurement of carbonaceous aerosols. *Atmospheric Measurement Techniques*, *13*(8), 4333-4351. <https://doi.org/10.5194/amt-13-4333-2020>
- Rume, T., & Islam, S. M. D.-U. (2020). Environmental effects of COVID-19 pandemic and potential strategies of sustainability. *Heliyon*
- Saarikoski, S. K., Sillanpää, M. K., Saarnio, K. M., Hillamo, R. E., Pennanen, A. S., & Salonen, R. O. (2008). Impact of Biomass Combustion on Urban Fine Particulate Matter in Central and Northern Europe. *Water, Air, & Soil Pollution*, *191*(1), 265-277. <https://doi.org/10.1007/s11270-008-9623-1>
- Saffari, A., Daher, N., Samara, C., Voutsas, D., Kouras, A., Manoli, E., Sioutas, C. (2013). Increased Biomass Burning Due to the Economic Crisis in Greece and Its Adverse Impact on Wintertime Air Quality in Thessaloniki. *Environmental Science & Technology*, *47*(23), 13313-13320. <https://doi.org/10.1021/es403847h>
- Saleh, R., Robinson, E. S., Tkacik, D. S., Ahern, A. T., Liu, S., Aiken, A. C., Yokelson, R. J. (2014). Brownness of organics in aerosols from biomass burning linked to their black carbon content. *Nature Geoscience*, *7*(9), 647-650
- Salvador, P., Artíñano, B., Querol, X., Alastuey, A., & Costoya, M. (2007). Characterisation of local and external contributions of atmospheric particulate matter at a background coastal site. *Atmospheric Environment*, *41*(1), 1-17. <https://doi.org/https://doi.org/10.1016/j.atmosenv.2006.08.007>
- Sandradewi, J., Prévôt, A. S. H., Szidat, S., Perron, N., Alfarra, M. R., Lanz, V. A., Baltensperger, U. R. S. (2008). Using aerosol light absorption measurements for the quantitative determination of wood burning and traffic emission contribution

- to particulate matter. *Environmental Science & Technology*, 42(9), 3316-3323. <https://doi.org/10.1021/es702253m>
- Sandradewi, J., Prévôt, A. S. H., Weingartner, E., Schmidhauser, R., Gysel, M., & Baltensperger, U. (2008). A study of wood burning and traffic aerosols in an Alpine valley using a multi-wavelength Aethalometer. *Atmospheric Environment*, 42(1), 101-112. <https://doi.org/10.1016/j.atmosenv.2007.09.034>
- Sanyal, S., Rochereau, T., Maesano, C. N., Com-Ruelle, L., & Annesi-Maesano, I. (2018). Long-term effect of outdoor air pollution on mortality and morbidity: A 12-year follow-up study for metropolitan France. *International Journal of Environmental Research & Public Health*, 15(11), 2487
- Schauer, J. J., Mader, B. T., Deminter, J. T., Heidemann, G., Bae, M. S., Seinfeld, J. H., Huebert, B. J. (2003). ACE-Asia intercomparison of a thermal-optical method for the determination of particle-phase organic and elemental carbon. *Environmental Science & Technology*, 37(5), 993-1001
- Schmidl, C., Marr, I. L., Caseiro, A., Kotianová, P., Berner, A., Bauer, H., Puxbaum, H. (2008). Chemical characterisation of fine particle emissions from wood stove combustion of common woods growing in mid-European Alpine regions. *Atmospheric Environment*, 42(1), 126-141. <https://doi.org/10.1016/j.atmosenv.2007.09.028>
- Shehab, M. A., & Pope, F. D. (2019). Effects of short-term exposure to particulate matter air pollution on cognitive performance. *Scientific Reports*, 9(1), 8237. <https://doi.org/10.1038/s41598-019-44561-0>
- Simpson, D., Yttri, K. E., Klimont, Z., Kupiainen, K., Caseiro, A., Gelencsér, A., Legrand, M. (2007). Modeling carbonaceous aerosol over Europe: Analysis of the CARBOSOL and EMEP EC/OC campaigns. *Journal of Geophysical Research: Atmospheres*, 112(D23)
- Solomon, P. A., & Sioutas, C. (2008). Continuous and semicontinuous monitoring techniques for particulate matter mass and chemical components: A synthesis of findings from EPA's particulate matter supersites program and related studies. *Journal of the Air & Waste Management Association*, 58(2), 164-195
- Spada, N. J., & Hyslop, N. P. (2018). Comparison of elemental and organic carbon measurements between IMPROVE and CSN before and after method transitions. *Atmospheric Environment*, 178, 173-180. <https://doi.org/https://doi.org/10.1016/j.atmosenv.2018.01.043>
- Stein, A. F., Draxler, R. R., Rolph, G. D., Stunder, B. J. B., Cohen, M. D., & Ngan, F. (2015). NOAA's HYSPLIT atmospheric transport and dispersion modeling system. *Bulletin of the American Meteorological Society*, 96(12), 2059-2077
- Stevens, B. (2015). Rethinking the lower bound on aerosol radiative forcing. *Journal of Climate*, 28(12), 4794-4819
- Stockwell, C. E., Coggon, M. M., Gkatzelis, G. I., Ortega, J., McDonald, B. C., Peischl, J., Warneke, C. (2021). Volatile organic compound emissions from solvent- and water-borne coatings - compositional differences and tracer compound identifications. *Atmospheric Chemistry & Physics*, 21(8), 6005-6022
- Streets, D. G., Bond, T. C., Lee, T., & Jang, C. (2004). On the future of carbonaceous aerosol emissions. *Journal of Geophysical Research: Atmospheres*, 109(D24)

- Sullivan, A. P., Frank, N., Onstad, G., Simpson, C. D., & Collett Jr, J. L. (2011). Application of high-performance anion-exchange chromatography–pulsed amperometric detection for measuring carbohydrates in routine daily filter samples collected by a national network: 1. Determination of the impact of biomass burning in the upper Midwest. *Journal of Geophysical Research: Atmospheres*, *116*(D8)
- Sundvor, I., Balaguer, N. C., Viana, M., Querol, X., Reche, C., Amato, F., Guerreiro, C. (2012). Road traffic’s contribution to air quality in European cities. *ETC/ACM Technical Paper*, *14*, 74
- Sunset Laboratory Inc. Organic Carbon/Elemental Carbon (OCEC) Laboratory Instrument Manual - Model 5L. Sunset Laboratory Inc.
- Szidat, S., Ruff, M., Perron, N., Wacker, L., Synal, H. A., Hallquist, M., Simpson, D. (2009). Fossil and non-fossil sources of organic carbon (OC) and elemental carbon (EC) in Göteborg, Sweden. *Atmospheric Chemistry & Physics*, *9*(5), 1521-1535
- Thermo Scientific. (2015). Partisol 2025*i* Sequential Air Sampler/Partisol 2025*i*-D Dichotomous Sequential Air Sampler Instruction Manual. Thermo Scientific
- TII. (2021). Retrieved 23/06/2021 from <https://trafficdata.tii.ie/publicmultinodemap.asp>
- Titos, G., del Águila, A., Cazorla, A., Lyamani, H., Casquero-Vera, J. A., Colombi, C., Alados-Arboledas, L. (2017). Spatial and temporal variability of carbonaceous aerosols: Assessing the impact of biomass burning in the urban environment. *Science of the Total Environment*, *578*, 613-625. <https://doi.org/https://doi.org/10.1016/j.scitotenv.2016.11.007>
- Tomasi, C., Fuzzi, S., & Kokhanovsky, A. (2017). *Atmospheric aerosols: Life cycles and effects on air quality and climate*. John Wiley & Sons
- UNECE. (2020). *Economic Commission for Europe: Executive Body for the Convention on Long-range Transboundary Air Pollution - 2020 Joint Progress Report on Policy-Relevant Scientific Findings*. ECE/EB.AIR/GE.1/2020/3 – UNECE
- Viana, M., Pey, J., Querol, X., Alastuey, A., De Leeuw, F., & Lükewille, A. (2014). Natural sources of atmospheric aerosols influencing air quality across Europe. *Science of the Total Environment*, *472*, 825-833
- Viidanoja, J., Sillanpää, M., Laakia, J., Kerminen, V.-M., Hillamo, R., Aarnio, P., & Koskentalo, T. (2002). Organic and black carbon in PM<sub>2.5</sub> and PM<sub>10</sub>: 1 year of data from an urban site in Helsinki, Finland. *Atmospheric Environment*, *36*(19), 3183-3193. [https://doi.org/https://doi.org/10.1016/S1352-2310\(02\)00205-4](https://doi.org/https://doi.org/10.1016/S1352-2310(02)00205-4)
- Wang, L., Liu, Z., Sun, Y., Ji, D., & Wang, Y. (2015). Long-range transport and regional sources of PM<sub>2.5</sub> in Beijing based on long-term observations from 2005 to 2010. *Atmospheric Research*, *157*, 37-48. <https://doi.org/https://doi.org/10.1016/j.atmosres.2014.12.003>
- Wang, Y., Hopke, P. K., Rattigan, O. V., Chalupa, D. C., & Utell, M. J. (2012). Multiple-year black carbon measurements and source apportionment using Delta-C in Rochester, New York. *Journal of the Air & Waste Management Association*, *62*(8), 880-887
- Wang, Y., Yuan, Y., Wang, Q., Liu, C., Zhi, Q., & Cao, J. (2020). Changes in air quality related to the control of coronavirus in China: Implications for traffic and industrial emissions. *Science of the Total Environment*, *731*, 139133. <https://doi.org/https://doi.org/10.1016/j.scitotenv.2020.139133>

- Weingartner, E., Saathoff, H., Schnaiter, M., Streit, N., Bitnar, B., & Baltensperger, U. (2003). Absorption of light by soot particles: Determination of the absorption coefficient by means of aethalometers. *Journal of Aerosol Science*, 34(10), 1445-1463. [https://doi.org/10.1016/S0021-8502\(03\)00359-8](https://doi.org/10.1016/S0021-8502(03)00359-8)
- Wenger, J., Arndt, J., Buckley, P., Hellebust, S., McGillicuddy, E., O'Connor, I., Wilson, E. (2020). Source Apportionment of Particulate Matter in Urban and Rural Residential Areas of Ireland (SAPPHIRE). *EPA Research*(Report No. 318), 1-60
- WHO Regional Office for Europe. (2019). *Noncommunicable Diseases & Air Pollution*.
- Wild, C., Weiderpass, E., & Stewart, B. (2020). World Cancer Report: Cancer Research for Cancer Prevention. Lyon: International Agency for Research on Cancer.
- Wilson, W. E., Chow, J. C., Claiborn, C., Fusheng, W., Engelbrecht, J., & Watson, J. G. (2002). Monitoring of particulate matter outdoors. *Chemosphere*, 49(9), 1009-1043. [https://doi.org/https://doi.org/10.1016/S0045-6535\(02\)00270-9](https://doi.org/https://doi.org/10.1016/S0045-6535(02)00270-9)
- World Health Organization. (2019). *Healthy environments for healthier populations: Why do they matter, and what can we do?*
- World Health Organization. (2021a). Retrieved 24/08/2021 from <https://www.who.int/en/activities/tracking-SARS-CoV-2-variants/>
- World Health Organization. (2021b). Retrieved 06/09/2021 from <https://www.who.int/data/gho/map-gallery>
- World Health Organization. (2021c). *Ambient (outdoor) air pollution*. Retrieved 07/10/2021 from [https://www.who.int/news-room/fact-sheets/detail/ambient-\(outdoor\)-air-quality-and-health](https://www.who.int/news-room/fact-sheets/detail/ambient-(outdoor)-air-quality-and-health)
- World Health Organization. (2021d). *WHO global air quality guidelines: Particulate matter (PM<sub>2.5</sub> and PM<sub>10</sub>), ozone, nitrogen dioxide, sulfur dioxide and carbon monoxide*. World Health Organization
- Wu, C., Huang, X. H. H., Ng, W. M., Griffith, S. M., & Yu, J. Z. (2016). Inter-comparison of NIOSH and IMPROVE protocols for OC and EC determination: Implications for inter-protocol data conversion. *Atmospheric Measurement Techniques*, 9(9), 4547-4560. <https://doi.org/10.5194/amt-9-4547-2016>
- Yoon, Y. J., Ceburnis, D., Cavalli, F., Jourdan, O., Putaud, J. P., Facchini, M. C., Jennings, S. G. (2007). Seasonal characteristics of the physicochemical properties of North Atlantic marine atmospheric aerosols. *Journal of Geophysical Research: Atmospheres*, 112(D4)
- Yttri, K. E., Aas, W., Bjerke, A., Cape, J. N., Cavalli, F., Ceburnis, D., Tørseth, K. (2007). Elemental and organic carbon in PM<sub>10</sub>: A one year measurement campaign within the European Monitoring and Evaluation Programme EMEP. *Atmospheric Chemistry & Physics*. 7(22), 5711-5725. <https://doi.org/10.5194/acp-7-5711-2007>
- Yttri, K. E., Myhre, C. L., & Tørseth, K. (2009). The carbonaceous aerosol - A remaining challenge. *World Meteorological Organization (WMO) Bulletin*, 58(1), 54.
- Yttri, K. E., Simpson, D., Bergström, R., Kiss, G., Szidat, S., Ceburnis, D., Perrino, C. (2019). The EMEP Intensive Measurement Period campaign, 2008–2009: Characterizing carbonaceous aerosol at nine rural sites in Europe. *Atmospheric Chemistry & Physics*, 19(7), 4211-4233
- Yttri, K. E., Simpson, D., Stenström, K., Puxbaum, H., & Svendby, T. (2011). Source apportionment of the carbonaceous aerosol in Norway – quantitative estimates

- based on  $^{14}\text{C}$ , thermal-optical and organic tracer analysis. *Atmospheric Chemistry & Physics*, 11(17), 9375-9394. <https://doi.org/10.5194/acp-11-9375-2011>
- Yuan, J., Lewis Modini, R., Zanatta, M., Herber, A. B., Müller, T., Wehner, B., Gysel-Beer, M. (2021). Variability in the mass absorption cross section of black carbon (BC) aerosols is driven by BC internal mixing state at a central European background site (Melpitz, Germany) in winter. *Atmospheric Chemistry & Physics*, 21(2), 635-655, Article 32. <https://doi.org/10.5194/acp-21-635-2021>
- Yusuf, A. A., & Inambao, F. L. (2019). Effect of cold start emissions from gasoline-fueled engines of light-duty vehicles at low and high ambient temperatures: Recent trends. *Case Studies in Thermal Engineering*, 14, 100417
- Zanatta, M., Gysel, M., Bukowiecki, N., Müller, T., Weingartner, E., Areskoug, H., Laj, P. (2016). A European aerosol phenomenology-5: Climatology of black carbon optical properties at 9 regional background sites across Europe. *Atmospheric Environment*, 145, 346-364. <https://doi.org/10.1016/j.atmosenv.2016.09.035>
- Zeng, T., & Wang, Y. (2011). Nationwide summer peaks of OC/EC ratios in the contiguous United States. *Atmospheric Environment*, 45(3), 578-586
- Zhang, Q., Shen, Z., Ning, Z., Wang, Q., Cao, J., Lei, Y., Xu, H. (2018). Characteristics and source apportionment of winter black carbon aerosols in two Chinese megacities of Xi'an and Hong Kong. *Environmental Science & Pollution Research*, 25(33), 33783-33793. <https://doi.org/10.1007/s11356-018-3309-z>
- Zhang, Y., Albinet, A., Petit, J.-E., Jacob, V., Chevrier, F., Gille, G., Favez, O. (2020). Substantial brown carbon emissions from wintertime residential wood burning over France. *Science of the Total Environment*, 743, 140752. <https://doi.org/https://doi.org/10.1016/j.scitotenv.2020.140752>
- Zotter, P., Herich, H., Gysel, M., El-Haddad, I., Zhang, Y., Mocnik, G., Prévôt, A. S. H. (2017). Evaluation of the absorption Ångström exponents for traffic and wood burning in the Aethalometer-based source apportionment using radiocarbon measurements of ambient aerosol. *Atmospheric Chemistry & Physics*, 17(6), 4229-4249. <https://doi.org/10.5194/acp-17-4229-2017>